Yuansheng Gao

Biology of Vascular Smooth Muscle: Vasoconstriction and Dilatation

Springer

Biology of Vascular Smooth Muscle: Vasoconstriction and Dilatation

Yuansheng Gao

Biology of Vascular Smooth Muscle: Vasoconstriction and Dilatation

Springer

Yuansheng Gao
Department of Physiology and Pathophysiology
Peking University Health Science Center
Beijing, China

ISBN 978-981-10-4809-8 ISBN 978-981-10-4810-4 (eBook)
DOI 10.1007/978-981-10-4810-4

Library of Congress Control Number: 2017940986

Printed on acid-free paper

This Springer imprint is published by Springer Nature
The registered company is Springer Nature Singapore Pte Ltd.
The registered company address is: 152 Beach Road, #21-01/04 Gateway East, Singapore 189721, Singapore

To my dear mentor Professor Paul M. Vanhoutte.

Preface

The discovery that the vascular contractility is regulated by a potent diffusible factor derived from the endothelium made by Furchgott and Zawadzki in 1980 is an epoch-making milestone in vascular biology. For a long time, the endothelium has been largely considered as a selective permeable barrier between the circulating blood and the vascular smooth muscle. Intensive studies evoked by Furchgott and Zawadzki's work since then have firmly established that the endothelium-derived nitric oxide, prostanoids, endothelin, and endothelium-dependent hyperpolarization play a dominant role in the regulation of vascular activities both under physiological and pathophysiological conditions. Meanwhile, aided by the rapid advances in biology and medical science in particular advance in molecular biology, numerous progresses have been made on the mechanisms underlying the vascular motion, including STIM–Orai protein-mediated store-operated Ca^{2+} entry, RhoA-Rho kinase signaling, the regulation of myosin light chain phosphatase activity, the effect of mitochondria-derived reactive oxygen species, and redox modulation of protein activities. These progresses made in the last four decades not only have greatly enriched our knowledge of vascular activities but also have in many aspects fundamentally changed our views on how the activities of the vasculature are regulated.

This book is intended to provide a concise yet comprehensive updated information on the regulation of vascular constriction and dilatation. It is divided into four parts. The first part is related to the general properties of the vasculature, including the structural, electrical, mechanical, and metabolic properties of vascular smooth muscle as well as the functions of the endothelium. The second part discusses the regulation of vasoreactivity by neurotransmitters, endothelium-derived factors, local metabolic factors and shear stress as well as myogenic response, and blood flow autoregulation. The third part deals with the intracellular signaling related to vascular activity, including the intracellular Ca^{2+} regulation, regulation of myosin light chain phosphorylation, and cyclic AMP and cyclic GMP signaling. The last part is regarding the heterogeneity in vasoreactivity of the coronary, cerebral, and pulmonary vasculatures and the vascular reactivity under hypoxia and during aging.

For each topic, there are many excellent review articles with different perspective available in the literature. This book wishes to provide a cohesive summary of the diverse aspects of vascular contraction and dilatation.

I am indebted to many people, in particular, my mentor Professor Paul M. Vahoutte, for teaching me what I have tried to pass on to the readers of this book. I have spent 4 years for a PhD degree under Professor Vahoutte's guidance in Mayo Graduate School and 3 years for postdoctoral training in his laboratory in Baylor College of Medicine. Afterward, we have collaborated in vascular research until now since 2003 when he had moved to the University of Hong Kong and I was in Peking University. Professor Vahoutte has trained more than a hundred students and fellows and made everyone feel fully trusted and specially treated. When I was a fresh PhD student, I already found that his laboratory was run by a rule that I named it PMV Principle, that is, all members in the laboratory are equally important, fresh or senior; everyone is endowed with unalienable equal rights to access all lab resources, to have his/her own project, and to be the principal author of his/her scientific discovery. In his laboratory, every student or fellow is passionate in pursuing the truth of science and ready to help each other. The laboratory is a family to all. No matter how long or short a time a person has stayed in the laboratory, he/she becomes a lifetime friend of Professor Vahoutte and all other members. Professor Vahoutte has taught us not only science but more importantly to be a good person.

Finally, I wish to thank my wife, Xue Wang, for all her encouragement, support, and help, which are always available and heartwarming. I also like to acknowledge the partial financial support for writing this book by the National Natural Science Foundation of China Grants 81270341.

Beijing, China Yuansheng Gao

Contents

Part I
General Properties of Vasculature

Chapter 1
Architecture of the Blood Vessels

Abstract The blood vessels are tubular structured consisting of three layers: the tunica intima, the tunica media, and the tunica adventitia. The tunica intima is the innermost layer of the vessels mainly made up by one layer of endothelial cells. With the exception that the capillaries have only the tunica intima, the arteries and veins also possess the other two layers. The tunica media, i.e., the middle layer, is constituted of smooth muscle cells, elastic, and collagenous fibrils, while the tunica adventitia is the outermost layer of the vessel wall consisting of dense fibroelastic tissue. The mixtures of different tissue components including smooth muscle, elastic, and collagen fibers as well as the diameter and thickness of the vascular wall vary among different vessel types to serve their functions. In this chapter, the architectural characteristics of the arteries, capillaries, and veins will be discussed. Furthermore, the gap junctions that form intercellular connections and the vessels that provide nutrient to vessel walls as well as some cell types of functional importance including fibroblasts, stem/progenitor cells, and perivascular adipose tissue will be reviewed.

Keywords Artery • Vein • Capillary • Endothelial cell • Vascular smooth muscle cell • Pericyte • Gap junction • Vasa vasorum • Perivascular cells

1.1 Introduction

The vascular circuits are categorized as systemic and pulmonary circulation; each is made up of arteries, capillaries, and veins. In systemic circulation, the arteries carry the blood from the heart to the peripheral tissues, and the veins drain the blood from the peripheral tissues to the heart. The capillaries interposed between the arteries and veins are the place where the oxygen, nutrition, and signal molecules from the arteries are delivered to the cells, while the carbon dioxide, metabolic wastes, and signal molecules produced by the cells diffuse to the veins. In pulmonary circulation, the deoxygenated blood from the pulmonary artery is oxygenated at the capillaries where the carbon dioxide is removed. With the function of these circulatory systems, the cells in the body, no matter where they are located, are exposed to an environment that is appropriate for their survival. As the humoral and various bioactive molecules move through the circulatory systems, the interactions

Y. Gao, *Biology of Vascular Smooth Muscle: Vasoconstriction and Dilatation*,
DOI 10.1007/978-981-10-4810-4_1

among cells in different locations become possible or are greatly facilitated so that the whole circulation system can act coordinately to serve the body function.

The wall of blood vessels contains three layers: the tunica intima, the tunica media, and the tunica adventitia, with the exception that the capillaries do not have the latter two layers. The intima is the innermost layer of the vascular wall composing of one layer of endothelial cells (ECs) resting on a thin layer of connective tissue. The tunica media is made up of smooth muscle cells interspersed by a varied number of elastic sheets, bundles of collagenous fibrils, and a network of elastic fibrils. The tunica adventitia is the outermost layer of the vessel wall consisting of dense fibroelastic tissue, which renders the vascular wall a fair amount of stability. In this chapter, the architectural characteristics of the arteries, the veins, and the capillaries, the gap junctions that form homo- and hetero-intercellular connections, and the vasa vasorum, i.e., the vessels, that provide nutrient to blood vessels will be reviewed. In the adventitia, there are several different cell types including fibroblasts and stem/progenitor cells. The blood vessels are surrounded by adipose tissue. They exert important influence on vascular activities and hence will also be briefly discussed.

1.2 Architecture of the Arteries

The arteries can be classified by the characteristics of the tunica media into two categories, elastic and muscular. Those with large diameters such as the aorta, brachiocephalic trunk, subclavian artery, and carotid and iliac arteries that possess abundant elastic lamellae are referred to as elastic arteries. As the arterial tree extends toward the periphery and the diameters of the vessels decrease, the media is less elastic and the smooth muscle cells prevail. These vessels are termed as muscular arteries. As the vessels approach capillaries, their diameters reduce to 30–60 μm, and their media contains only 1–2 layers of smooth muscle. These vessels are known as arterioles (Rhodin 2014).

The tunica intima of the elastic arteries consists of a single layer of endothelial cells resting on a thin layer of fibrous tissue. The endothelial cells are elongated with their long axis parallel to that of the blood flow. These cells are connected by the tight, occluding junctions (zonulae occludentes) and communicating junctions (gap junctions). The subendothelial layer is made up of a three-dimensional network of collagenous bundles and elastic fibers. The tunica media consists of a varied number of fenestrated elastic laminae interspersed with smooth muscle cells. The elastic laminae are concentrically arranged, spaced equidistantly, and bound by a network of fine elastin fibers. There are 40–60 fenestrated elastic laminae in the human aorta but only 5 in the much smaller aorta of the mouse. The comparison of ten different mammalian aortae shows that the total number of the medial elastic laminae is nearly proportional to aortic diameter (Wolinsky and Glagov 1967a). In the inner part of the media, the smooth muscle cells are directed both longitudinally and circularly in canine aorta (Bunce 1974). The majority of smooth muscle cells in

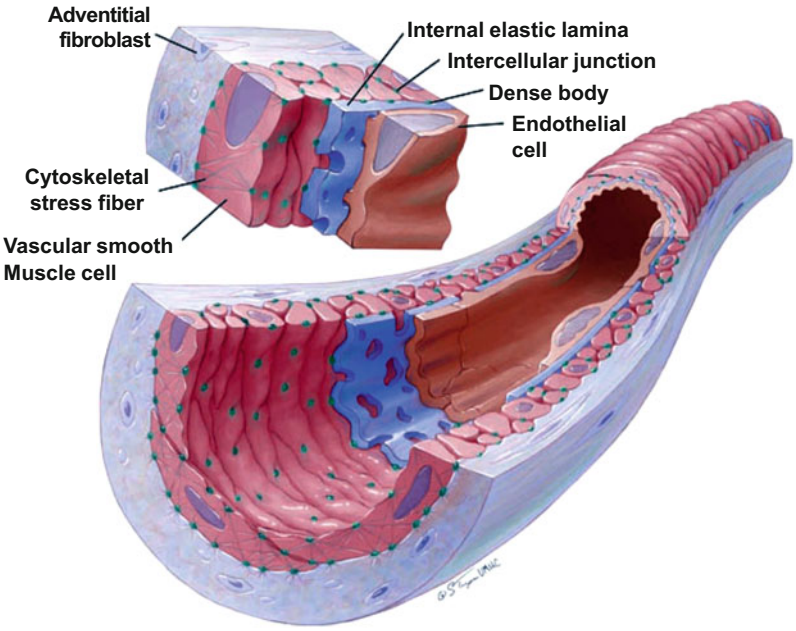

Fig. 1.1 Schematic illustration of an arteriole. The endothelial cells (ECs) run parallel to the longitudinal axis of the vessel sitting on a basement membrane apposed by an internal elastic lamina. Fenestrae in the internal elastic lamina allow ECs to make contact with vascular smooth muscles (VSMCs), which are spindled shaped and arranged transversal to the longitudinal axis of the vessel. The dense bodies of VSMCs are connected to cytoskeletal stress fibers within the smooth muscle cells for the transmission of forces in and out of the cell. The intercellular junctions allow cells to directly communicate with each other so that the activity of the vessel is synchronized. Within the adventitia, the fibroblasts are arranged mostly parallel to the longitudinal axis of the vessel (The figure is from Martinez-Lemus (2012), with permission)

the rest of the media are oriented at small angles between the concentric elastic laminae. The adventitia of elastic arteries is relatively thin, constituting only 10% of the vascular wall. Cells that exist in the adventitia are fibroblasts, occasional macrophages, and Schwann cells with associated nerve axons (Rhodin 2014).

The intima of most muscular arteries is thinner than in elastic arteries, with one layer of endothelial cells and a basal lamina. The intima and the media are separated by a very distinct and highly fenestrated internal elastic lamina. In larger muscular arteries, there are a varied number of intermediate, less well-defined elastic laminae present in the media. These laminae gradually disappear as the size of the vessels decreases toward the periphery. The tunica media is dominated by numerous concentric layers of spindle-shaped smooth muscle cells, circumferentially arranged, probably forming a spiral or helix with a low pitch. In larger vessels, the number of the concentric layers of smooth muscle cells ranges from 25 to 35, while in small arteries and arterioles, there are only 3–6 and 1–2 layers, respectively (Rhodin 2014; Martinez-Lemus 2012) (Fig. 1.1). Between the smooth

muscle cells, there are very limited collagenous fibrils. In the larger muscular arteries, a distinct external elastic lamina exists between the media and the adventitia, but it is less clear and may even be absent and replaced by longitudinally arranged elastic fibrils in small muscular arteries. The adventitia is wider in muscular arteries than in elastic arteries, often occupying half of the vascular wall (Rhodin 2014).

1.3 Capillaries and Microcirculation

Capillaries are the smallest blood vessels (internal diameter, 4–9 μm) consisting of a single layer of endothelial cells resting on a basement membrane and wrapped uncontinuously by contractile supporting cells termed pericytes. There are three types of capillaries: continuous, fenestrated, and sinusoidal. Continuous capillaries are made up of endothelial cells linked together by interendothelial junctions so that only smaller molecules such as water and ions are allowed to pass. The lipid-soluble molecules may passively diffuse through the endothelial cell membranes along concentration gradients. Fenestrated capillaries have pores in the endothelial cells (50–80 nm in diameter) that run completely through the cell, from the capillary lumen to the interstitial space. This type of capillaries is primarily located in tissues with large fluid and solute fluxes across the capillary walls (e.g., the intestine, choroid plexus, and renal glomeruli). Sinusoidal capillaries are characterized by wide gaps (30–40 μm) between adjacent endothelial cells and discontinuous basal lamina. Such an arrangement makes red and white blood cells (7.5–25-μm diameter) and various serum proteins pass through. Sinusoidal capillaries are primarily located in the liver, bone marrow, and spleen (Burton 1954; Boulpaep 2011).

Capillaries, precapillary arterioles, and postcapillary venules form the microcirculation. The precapillary arterioles give rise to a network of capillaries which converges on postcapillary venules. At microcirculatory level, the capillaries are the place where most material exchanges between the blood and the interstitial fluid occur, termed capillary exchange. There are about four billion capillaries with a total surface area estimated to be 500–700 m^2 in the whole body. It is rare that any single functional cell of the body is more than 20–30 μm away from a capillary. It is estimated that there are only about 25% of capillaries at any moment are open (Burton 1954). The operation of the capillaries is tightly controlled by the activities of the arterioles and the pericytes. The arterioles of varying sizes possess different sensitivities to metabolic, myogenic, neuronal, and humoral stimuli. It appears that the activities of the precapillary arterioles are in particular sensitive to metabolic factors (Muller et al. 1996; Beyer and Gutterman 2012). In mesentery microcirculation, it is believed that the opening and closing of the capillary are controlled by a special structure named precapillary sphincter, a ring-shaped smooth muscle fiber at the entrance point of the capillaries. In addition, a thoroughfare channel between

the arteriole and the venule named metarteriole is also believed to be involved in the regulation of the microcirculation. However, morphological and physiological evidence so far indicates that neither precapillary sphincters nor metarterioles exist in the microcirculation of the other organs and tissues. Thus, the precapillary sphincters and metarterioles are not universal components of the microcirculation but rather unique features of the mesenteric microcirculation (Sakai and Hosoyamada 2013). In addition to arterioles, the pericytes which encircle the capillaries may play a critical role in the regulation of microcirculation. A recent study suggests that, in cerebral circulation, an increased neuronal activity may cause the pericytes to relax their grip on cerebral capillaries via PGE_2 and nitric oxide (NO), which results in increased blood flow and enhanced oxygen supply to active neurons. The pericytes may transfer its relaxant signal via pericyte–endothelial gap junctions to endothelial cells and via pericyte–pericytal gap junctions to other pericytes, thus forming a functional syncytium (Armulik et al. 2011; Nees et al. 2012; Hall et al. 2014) (Fig. 1.2).

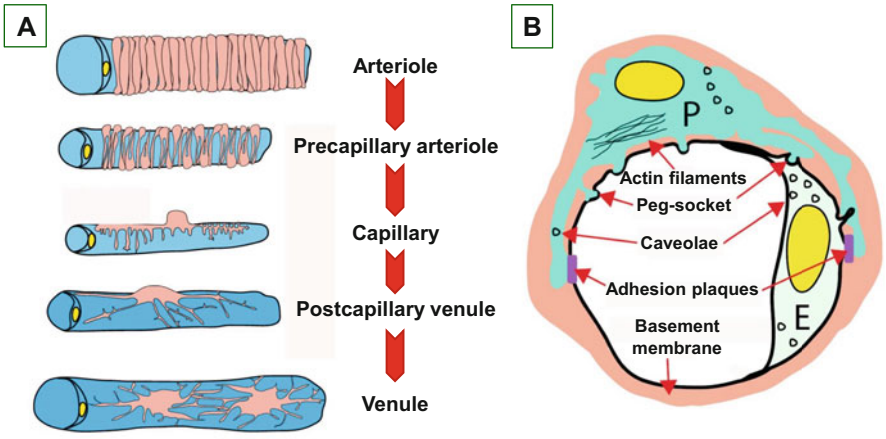

Fig. 1.2 Schematic illustration of pericytes. (**a**) The arterioles are more encircled by pericytes (in *brown color*) than precapillary arterioles. Pericytes that invest capillaries have a nearly rounded cell body giving rise to a few primary processes running on the endothelium in the length of the capillary, and the primary processes give rise to secondary perpendicular processes. On postcapillary venules and venules, the cell body of the pericyte flattens giving rise to many slender, branching processes. (**b**) Ultrastructural characteristics of pericytes (*P*) and their relation with endothelial cells (*E*). The mature capillary pericyte has a discoid nucleus (in *yellow color*) with microtubules stretching along the primary and secondary cytoplasmic extensions. Intermediate filaments are mostly concentrated within in the primary extensions. The outer, abluminal pericyte surface often has numerous caveolae. Despite being separated by the shared BM, pericytes and endothelial cells make numerous direct contacts of different types, such as peg–socket contacts and adhesion plaques (The figure is from Armulik et al. (2011), with permission)

1.4 Architecture of the Veins

Venous vessels are generally divided based on their sizes in diameters. The smallest are those originated from the capillary network, with diameter ranged from 10 to 100 μm, named venules. From the venules, the venous vessels sequentially merge to form small-, medium-, and large-sized veins on their way approaching the heart, with average diameters ranging from 100 μm to 1 mm, from 1 mm to 10 mm, and greater than 1 cm, respectively (Marieb and Hoehn 2015). Veins can also be classified in other ways, including pulmonary vs. systemic veins and superficial vs. deep veins. Superficial veins are those close to the surface of the body and without companion arteries, whereas deep veins are deeper in the body and almost always beside an artery with the same name. There are veins that directly connect superficial veins to deep veins, known as communicating or perforator veins. Except most veins in the head and neck, small- to medium-sized veins are equipped with a structure named valve inside the vessel to prevent the backflow of blood that would otherwise occur as the result of gravity. The valves are formed by loose, pocket-shaped folds of the tunica intima extended into the lumen (Marieb and Hoehn 2015).

Veins are recognized being made up of the intimal, the media, and the adventitia layer as the arteries. However, the boundaries between different layers are not very clear. In comparison with the arteries, the veins are generally thinner walled and larger in size, and the amount of smooth muscle fibers is much less abundant. In the media of venules and small veins, there are a small number of smooth muscle cells, separated by a greater number of collagen. The medium- and large-sized veins contain a few circularly arranged smooth muscle cells as well as some longitudinally arranged smooth muscle cells. In the humans, longitudinally oriented smooth muscle predominates in the veins of the thorax and abdomen, whereas circular smooth muscle occupies more than 50% of the wall in the leg veins (Rhodin 2014). In the vena cava of the squirrel monkey, the circularly arranged smooth muscle cells are found in the subendothelial area and the longitudinally arranged bundles of smooth muscle cells in the media–adventitia area. The connective tissues are more richly expressed in veins than in arteries. There is a network of mostly longitudinal elastic fibers within the media and adventitia of most veins. There are also abundant collagen fibers throughout the walls of veins, which are interspersed with smooth muscle. The adventitia of both medium-sized veins and large veins occupies between 60% and 75% of the vascular wall (Rhodin 2014).

1.5 Gap Junctions

Gap junctions are specialized intercellular connections, which allow bidirectional passage of current and small signaling molecules lower than 1 kDa between the cytoplasm of two adjacent cells. A gap-junction channel is made up of two

hemichannels termed connexons supplied by the opposing cells, one from each. Each connexon consists of six proteins called connexins (Cx) that form the pore. Currently there are four different connexins (Cx37, Cx40, Cx43, and Cx45) being identified in blood vessels. Among these connexins, Cx45 is expressed only in the smooth muscle cells, whereas the other three are present in both endothelial and smooth muscle cells, although Cx37 and Cx40 are located primarily in the endothelial cells and Cx43 is the most prominent gap-junction protein found in the smooth muscle cells (Figueroa and Duling 2009; Nielsen et al. 2012). In both large and small arteries, the gap junctions between ECs are abundantly expressed whereas those between SMCs are less often expressed. Transmission and scanning electron microscopy and immunohistochemistry reveal large gap-junction plaques between tightly sealed opposing plasma membranes of the adjacent ECs. In contrast, gap junctions between SMCs are usually found between small sections of plasma membrane (Sandow and Hill 2000; Brisset et al. 2009).

The gap junction between ECs and VSMCs is termed myoendothelial injunction (MEJ). MEJs may be derived from ECs, from SMCs, and from both and meet halfway. The MEJs have an appearance of bulbous or mushroomlike head on a thin stalk, usually ~100–150 nm in diameter and ~0.8 μm in length, either abutting the smooth muscle cell membrane or lying in indentations in the smooth muscle cell membrane, with the former more frequently observed. It is estimated that there are approximately two EMJs per smooth muscle cell at the level of the internal elastic lamina in the distal mesenteric artery and one endothelial cell could drive 15–18 smooth muscle cells (Sandow and Hill 2000; Sandow et al. 2012). MEJs have been identified in several species and from many vascular beds. They are more numerous in smaller than larger diameter arteries. The more abundant expression of MEJs would facilitate electronic signals to propagate between ECs and SMCs (Brisset et al. 2009; Sandow et al. 2012). In caudal and mesenteric arteries of the rat, the distance between MEJs and the homocellular endothelial gap junctions is noted being often within <2 μm (Sandow and Hill 2000; Sandow et al. 2012). Such an arrangement would facilitate the endothelium a favorable pathway for the transmission of electrical signals along blood vessels and facilitate the coordination of the response along vascular tree (Haas and Duling 1997).

1.6 Vasa Vasorum

The arteries of small size are directly nourished by diffusion from the lumen of the vessel. For arteries whose thickness of the vessel wall exceeds 0.5 mm, there are small arteries termed vasa vasorum (denoting “vessels of the vessels” in Latin) entering the vascular wall either from the abluminal surface or from the luminal surfaces and then arborizing to the outer media to supply the needs of the vessels. A venous vasculature termed venous vasa vasorum drains a network of capillaries/venules laid down around the outer media to the veins in close proximity to the arteries (Wolinsky and Glagov 1967b; Gössl et al. 2003). The vasa vasorum that

supply the ascending aorta come from the coronary and brachiocephalic arteries, those that supply the descending thoracic aorta arise from intercostal arteries, those that supply the abdominal aorta originate from the lumbar and mesenteric arteries, and those that supply large veins arise from branch points of arteries lying next to the vein (Williams and Heistad 1996). The first-order vasa vasorum originate from large vessels and run longitudinally between the adventitia and media of the main vessel, and those branches from the first-order vasa vasorum form circumferential arches around the vessel wall (Kwon et al. 1998). In comparison with the arteries, the venous vasa vasorum are larger in diameters and are more extensive, as vessels from the adventitia may penetrate up to the intima, probably because of the low venous pressure and the low oxygen tension (Brook 1977).

1.7 Adventitia and Perivascular Cells

The adventitia is predominantly made up of extracellular matrix (ECM), a dynamic and complex array of collagens, elastins, glycoproteins, glycosaminoglycans, and proteoglycans to provide structural and biochemical support to the vascular wall. In the structural frame provided by the ECM, various tissues such as vasa vasorum, lymphatic vessels, and nerves as well as many different cells including fibroblasts, immune cells, and vascular progenitor cells reside in the adventitia. Among the different cells, the fibroblast is the most abundant, which is the major cell type to synthesize the elements of the ECM and also produce the matrix metalloproteinases (MMPs), which degrade ECM, and the tissue inhibitors of MMPs (TIMPs). Thus, fibroblasts play a central role in the hemostasis of the ECM (Stenmark et al. 2013; Arpino et al. 2015). When exposed to hypoxia, ischemia, mechanical force, or certain biochemical stimuli, fibroblasts may release a complex mixture of growth factors, cytokines, chemokines, and reactive oxygen species (ROS), resulting in an altered ECM environment and profound changes in the activities of the residential cells (Stenmark et al. 2013).

The stem and progenitor cells, both of resident and circulating origins, are present in the intimal, medial, and adventitial layers, with the adventitia existing the most. These cells show a wide spectrum of potential to differentiate into various cell types including ECs, SMCs, pericytes, fibroblasts, myofibroblasts, and macrophages (Stenmark et al. 2013; Zhang et al. 2013). Studies demonstrate that the differentiation of vascular stem cells can be regulated by mechanical stress. Under physiological conditions, these cells are dormant and reside in "stem cell niches" of the vessel wall. When exposed to certain stimuli, these cells are activated, mobilized, and migrated to the areas where the stimuli originated. The laminar shear stress can stimulate these cells to differentiate toward endothelial lineage, whereas cyclic strain results in smooth muscle differentiation (Zhang et al. 2013). It appears that the microenvironments not only soluble factors but also mechanical characteristics of the ECM exert profound influence on the lineage specification of the stem and progenitor cells. Naive mesenchymal stem cells (MSCs) have been found to

specify lineage and commit to phenotypes in a manner extremely sensitivity to the elasticity of the ECM. Soft matrices favor MSCs to differentiate into neuronal-like cells, stiffer matrices promote myogenic differentiation, and a rigid matrix stimulates osteogenic differentiation (Engler et al. 2006).

The large vessels are directly surrounded by various amount of adipose tissue, known as perivascular adipose tissue (PVAT). In small vessels and microvessels, the adipocytes are present as an integral part of the adventitial layer. Like other adipose tissues, PVAT can secrete a wide range of bioactive molecules that influence vascular contractility, proliferation, and inflammation status of the blood vessels.

Several compounds released by PVAT have been shown to cause vasodilatation, including adiponectin, H_2S, NO, angiotensin I–VII, palmitic acid methyl ester, and prostacyclin, whereas electrical stimulation can cause vasocontraction via angiotensin II released by PVAT (Brown et al. 2014). PVAT may also affect the inflammatory state by the release of proinflammatory cytokines such as MCP-1, interleukin-8, and interleukin-6 as well as anti-inflammatory molecules such as adiponectin (Omar et al. 2014). Studies also show that PVAT affects vascular function differentially depending on its anatomical location. For instance, human pericoronary perivascular adipocytes exhibit a reduced state of adipogenic differentiation and a heightened proinflammatory state compared with adipocytes derived from other regional depots of the same subjects. This may render coronary arteries as being more venerable to develop certain vascular diseases (Omar et al. 2014; Gil-Ortega et al. 2015).

References

Armulik A, Genové G, Betsholtz C (2011) Pericytes: developmental, physiological, and pathological perspectives, problems, and promises. Dev Cell 21:193–215

Arpino V, Brock M, Gill SE (2015) The role of TIMPs in regulation of extracellular matrix proteolysis. Matrix Biol 44-46:247–254

Beyer AM, Gutterman DD (2012) Regulation of the human coronary microcirculation. J Mol Cell Cardiol 52:814–821

Boulpaep EL (2011) Arteries and veins. In: Boron WF, Boulpaep EL (eds) Medical physiology, 2e Updated edn. Saunders, Philadelphia, pp 467–481

Brisset AC, Isakson BE, Kwak BR (2009) Connexins in vascular physiology and pathology. Antioxid Redox Signal 11:267–282

Brook WH (1977) Vasa vasorum of veins in dog and man. Angiology 28:351–360

Brown NK, Zhou Z, Zhang J, Zeng R, Wu J, Eitzman DT, Chen YE, Chang L (2014) Perivascular adipose tissue in vascular function and disease: a review of current research and animal models. Arterioscler Thromb Vasc Biol 34:1621–1630

Bunce DF II (1974) Atlas of arterial histology. St. Louis, Green

Burton AC (1954) Relation of structure to function of the tissues of the wall of blood vessels. Physiol Rev 34:619–642

Engler AJ, Sen S, Sweeney HL, Discher DE (2006) Matrix elasticity directs stem cell lineage specification. Cell 126:677–689

Figueroa XF, Duling BR (2009) Gap junctions in the control of vascular function. Antioxid Redox Signal 11:251–266

Gil-Ortega M, Somoza B, Huang Y, Gollasch M, Fernández-Alfonso MS (2015) Regional differences in perivascular adipose tissue impacting vascular homeostasis. Trends Endocrinol Metab 26:367–375

Gössl M, Rosol M, Malyar NM, Fitzpatrick LA, Beighley PE, Zamir M, Ritman EL (2003) Functional anatomy and hemodynamic characteristics of vasa vasorum in the walls of porcine coronary arteries. Anat Rec A Discov Mol Cell Evol Biol 272:526–537

Haas TL, Duling BR (1997) Morphology favors an endothelial cell pathway for longitudinal conduction within arterioles. Microvasc Res 53:113–120

Hall CN, Reynell C, Gesslein B, Hamilton NB, Mishra A, Sutherland BA, O'Farrell FM, Buchan AM, Lauritzen M, Attwell D (2014) Capillary pericytes regulate cerebral blood flow in health and disease. Nature 508:55–60

Kwon HM, Sangiorgi G, Ritman EL, Lerman A, McKenna C, Virmani R, Edwards WD, Holmes DR, Schwartz RS (1998) Adventitial vasa vasorum in balloon-injured coronary arteries: visualization and quantitation by a microscopic three-dimensional computed tomography technique. J Am Coll Cardiol 32:2072–2079

Marieb EN, Hoehn KN (2015) Human anatomy and physiology, 10th edn. Pearson, Harlow

Martinez-Lemus LA (2012) The dynamic structure of arterioles. Basic Clin Pharmacol Toxicol 110:5–11

Muller JM, Davis MJ, Chilian WM (1996) Integrated regulation of pressure and flow in the coronary microcirculation. Cardiovasc Res 32:668–678

Nees S, Juchem G, Weiss DR, Partsch H (2012) Pathogenesis and therapy of chronic venous disease: new insights into structure and function of the leg venous system. Phlebologie 41:246–257

Nielsen MS, Axelsen LN, Sorgen PL, Verma V, Delmar M, Holstein-Rathlou N-H (2012) Gap junctions. Compr Physiol 2:1981–2035

Omar A, Chatterjee TK, Tang Y, Hui DY, Weintraub NL (2014) Proinflammatory phenotype of perivascular adipocytes. Arterioscler Thromb Vasc Biol 34:1631–1636

Rhodin JAG (2014) Architecture of the vessel wall. Compr Physiol, Supplement 7: Handbook of Physiology, The Cardiovascular System, Vascular Smooth Muscle, pp 1–31

Sakai T, Hosoyamada Y (2013) Are the precapillary sphincters and metarterioles universal components of the microcirculation? An historical review. J Physiol Sci 63:319–331

Sandow SL, Hill CE (2000) Incidence of myoendothelial gap junctions in the proximal and distal mesenteric arteries of the rat is suggestive of a role in endothelium-derived hyperpolarizing factor-mediated responses. Circ Res 86:341–346

Sandow SL, Senadheera S, Bertrand PP, Murphy TV, Tare M (2012) Myoendothelial contacts, gap junctions, and microdomains: anatomical links to function? Microcirculation 19:403–415

Stenmark KR, Yeager ME, El Kasmi KC, Nozik-Grayck E, Gerasimovskaya EV, Li M, Riddle SR, Frid MG (2013) The adventitia: essential regulator of vascular wall structure and function. Annu Rev Physiol 75:23–47

Williams JD, Heistad DD (1996) Structure and function of vasa vasorum. Trends Cardiovasc Med 6:53–57

Wolinsky H, Glagov S (1967a) A lamellar unit of aortic medial structure and function in mammals. Circ Res 20:99–111

Wolinsky H, Glagov S (1967b) Nature of species differences in the medial distribution of aortic vasa vasorum in mammals. Circ Res 20:409–421

Zhang C, Zeng L, Emanueli C, Xu Q (2013) Blood flow and stem cells in vascular disease. Cardiovasc Res 99:251–259

Chapter 2
Ultrastructure of Vascular Smooth Muscle

Abstract Vascular smooth muscle, which is located in the tunica media layer of the vascular wall, is the primary player to enable the blood vessel to constrict and dilate. This is fulfilled by the interaction of thin and thick filaments of the contractile apparatus. These filaments in the smooth muscle are organized differently from striated muscle, termed side polar geometry. Such an arrangement gives the blood vessel high adaptational capacity in contractility. Several cell organelles including sarcoplasmic reticulum, mitochondria, caveolae, and cytoskeleton are indispensable for the contractile functionality, which are involved in the regulation of cytosol calcium level, ATP generation, signal transduction, and cell shape adaptation in response to the contractile status. In this chapter, the current understanding of the ultrastructural characteristics of these cellular components of vascular smooth muscle will be reviewed.

Keywords Actin • Myosin • Sarcoplasmic reticulum • Mitochondria • Caveolae • Cytoskeleton

2.1 Introduction

Vascular smooth muscle cells (VSMCs) are the primary cells which endow the blood vessel with the ability to contract and to relax and thus the ability to regulate the blood pressure and blood distribution. When being immature, during pregnancy and exercise, after vascular injury, or under certain pathophysiological conditions, VSMCs do not exhibit contractility but synthesize large amounts of extracellular matrix (ECM) components and display marked proliferative and migratory activities. Thus, VASCs may have two different phenotypes, the contractile and synthetic. The contractile VSMCs fit for rapid regulation of the vessel diameter, whereas the synthetic phenotype is for long-term adaptation by changing cell number and connective tissue composition (Chamley et al. 1977; Rensen et al. 2007).

VSMCs in the contractile phenotype are spindle- or ribbon-shaped of ~100 μm in length and 5 μm in diameter with a sausage-shaped nucleus (Hill and Meininger 2012). This chapter will focus on the morphological characteristics of contractile VSMCs, including the thin and thick filaments which constitute the contractile

Y. Gao, *Biology of Vascular Smooth Muscle: Vasoconstriction and Dilatation*,
DOI 10.1007/978-981-10-4810-4_2

apparatus; sarcoplasmic reticulum, which functions as a calcium storage, release, and uptake site; mitochondria which serves as the primary site for ATP generation; caveolae which act as an important site for cell signaling; and cytoskeleton which provides the structural basis for cell morphology.

2.2 Thin Filaments

Smooth muscle contraction results from the interaction of thin and thick filaments. The thin filament is made up of a double helix of actin monomers, with monomers repeating every 5.9 nm and the helix completing one full turn every 74 nm consisting of 13 actin monomers. The filament is about 7 nm in width and averaged 4.5 μm in length, which is about 3 times of length of the thick filament. The architecture of the thin and thick filaments remains controversial (Marston and Smith 1985; Yamin and Morgan 2012; Liu et al. 2013). The thin filaments, while associated with myosin on one side, are connected by dense bodies inside the cytoplasm in a manner that they snake longitudinally along the length of the cell and to focal adhesion on cell membrane (Marston and Smith 1985; Yamin and Morgan 2012).

Actin is the building block protein of the thin filament. It is a single-chain globular protein of 374 amino acid residues of 42 kDa, with a diameter of 40–50 Å. It consists of a large and a small domain, separated by a cleft where the binding site for ATP or ADP is located. Cellular actin exists as two forms: monomeric globules termed G-actin and polymeric filaments termed F-actin. In addition to act as the thin filament of the contractile apparatus, F-actin is also an essential element of the eukaryotic cytoskeleton which controls cell shape and cell–cell communication during contraction and force maintenance (Lehman and Morgan 2012). There are four isoforms of actin related to smooth muscle: α- and γ-smooth muscle actin, β-nonmuscle actin, and γ-cytoplasmic actin. Both α- and γ-smooth muscle actin are concentrated in the contractile filaments, with the former predominantly exists in vascular smooth muscle whereas the latter mainly in enteric smooth muscles. The functions of β-nonmuscle actin and γ-cytoplasmic actin are less well defined. In VSMCs actin makes up to ~20% of total protein content. In ferret aorta, about 66% of total actin is α-smooth muscle isoform, followed by β-cytoplasmic and γ-smooth muscle, and nonmuscle actin, 21% and 13% of total actin, respectively (Kim et al. 2008).

There are several proteins associated with the F-actin filament, including tropomyosin (Tm), caldesmon (CaD), and calponin. Tm is a long rodlike molecule, with a length of about 410 Å and diameter of about 20 Å. It consists of two α-helical chains, each of 35 kDa, wound together to form a coiled coil along the grooves between the two actin helices. Tm acts as a gatekeeper for actin function by controlling the accessibility of other actin-binding proteins to actin filaments and

thereby regulating actin polymerization as well as the interaction of actin and myosin (Marston and El-Mezgueldi 2008). CaD is present as two isoforms: the smooth muscle h-CaD and the nonmuscle isoform I-CaD, with h-CaD dominant in VSMCs. Like Tm, h-CaD is an elongated molecule, 74 nm in length, about twice as long as Tm. Studies show that the N-terminal end of h-CaD binds to the neck (S2) region of myosin, while the C-terminal end of CaD binds to actin and inhibits the actomyosin ATPase activity. It is proposed that h-CaD tethers myosin filaments to actin filaments and, together with Tm, blocks actomyosin interactions in the resting state. When myosin is phosphorylated and the C-terminal domain of h-CaD is removed from its inhibitory position on actin allowing myosin binding and muscle contraction, the elongated shapes of CaD and Tm facilitate their binding to actin filaments. In the resting state, smooth muscle Tm lies in a position partially overlapping the myosin-binding site to prevent myosin to bind to actin. When CaD is activated by Ca^{2+}/calmodulin (CaM), myosin heads may move Tm to a position so that neighboring actin is activated (Wang 2008). Calponin is a heat-stable, basic, 34-kDa protein present in smooth muscle at the same molar concentration as Tm. Calponin exerts an inhibitory effect on the actin-activated MgATPase of fully phosphorylated or thiophosphorylated myosin. Calponin is phosphorylated by protein kinase C and Ca^{2+}/calmodulin-dependent protein kinase II, which results in the loss of its ability to inhibit the actomyosin ATPase (Winder et al. 1998; Roman et al. 2013).

2.3 Thick Filaments

Thick filaments of smooth muscle are formed by type 2 myosin (myosin II) molecules, a member of the myosin superfamily which has been shown to interact with actin, hydrolyze ATP, and produce movement. Myosin II is formed by two myosin heavy chains (MHCs), a pair of 17-kDa essential myosin light chains (MLCs) and a pair of 20-kDa regulatory MLCs. The two MHCs starting from the carboxyl termini are wound around each other to form a long double helical structure. At the amino termini, both chains are folded into separate globular structures to form the two heads. The long tail portion forms the backbone of the thick filament, and the heads protrude as cross-bridges toward the thin filament. MHC can be proteolytically cleaved into discrete functional domains. When myosin is treated with trypsin, a cleavage occurs in the middle of the tail yielding heavy meromyosin (HMM, 350 kDa) and light meromyosin (LMM, 150 kDa). HMM can be further split by proteolytic enzymes such as papain into a globular subfragment 1 (S1, 110 kDa) and subfragment 2 (S2). The S1 is composed of the motor domain which contains the binding sites for actin and nucleotides and the lever arm which contains the binding domains for the regulatory and essential MLCs as well as the

converter domain, the region of rotation for the lever arm relative to the motor domain. The phosphorylation of regulatory MLCs at serine 19 plays a primary role in the activation of myosin ATPase to promote the formation of cross-bridge by myosin head and actin and thus to allow contraction to begin. The role of the essential MLCs is less well understood and appears to be critical for myosin activation (Eddinger and Meer 2007; Taylor et al. 2014; Gao 2015) (Fig. 2.1).

There are multiple isoforms existed for myosin II. In smooth muscle cells, four unique MHC molecules are found being transcripted from a single gene via alternative splices. The presence or absence of a seven-amino acid insert at the 25- to 50-kDa junction in the S1 head region of the molecule is termed as SMB and SMA, respectively. Meanwhile, the presence or absence of a 34-amino acid insert in the tail portion is termed as SM1 and SM2, respectively (Eddinger and Meer 2007). Studies show that the ATPase activity of SMB MHC is about twofold greater than SMA and that the former isoform is preferentially expressed in phasic tissues while the latter in tonic tissues (Zhang et al. 2013).

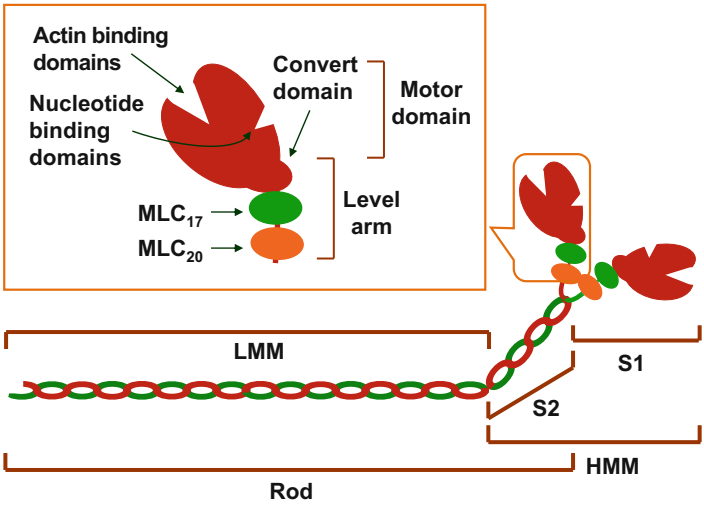

Fig. 2.1 Schematic of the smooth muscle myosin II molecule. The myosin contains two myosin heavy chains (MHCs) and two myosin light chains (MLCs), which form a double helical structure (*Rod*) and two globular structures (heads, S1). When treated with trypsin, the MHC is separated into heavy meromyosin (*HMM*) and light meromyosin (*LMM*). HMM can be further split by proteolytic enzymes into a globular subfragment 1 (*S1*) and subfragment 2 (*S2*). The S1 is made up of the motor domain which contains the binding sites for actin and nucleotides and the lever arm which contains the binding domains for the regulatory and essential MLCs (MLC_{17} and MLC_{20}, respectively) as well as the converter domain, the region of rotation for the lever arm relative to the motor domain. The phosphorylation of MLC_{20} plays a critical role in the activation of myosin ATPase to promote the myosin cross-bridge to bind to the actin filament and allow contraction to begin (The figure is from Gao (2015), with permission)

2.4 Organization of the Thin and Thick Filaments

In striated muscle, the thin and thick filaments are organized into sarcomeres, the basic functional units of the muscle structure, which are connected in a highly orderly manner giving them a striated appearance. The sarcomere shows overlapping arrays of thick and thin filaments. The thin filaments are anchored perpendicularly to the Z lines, which are located on the two sides of the longitudinal axis of the sarcomere. The thick filaments, with the myosin heads toward the Z

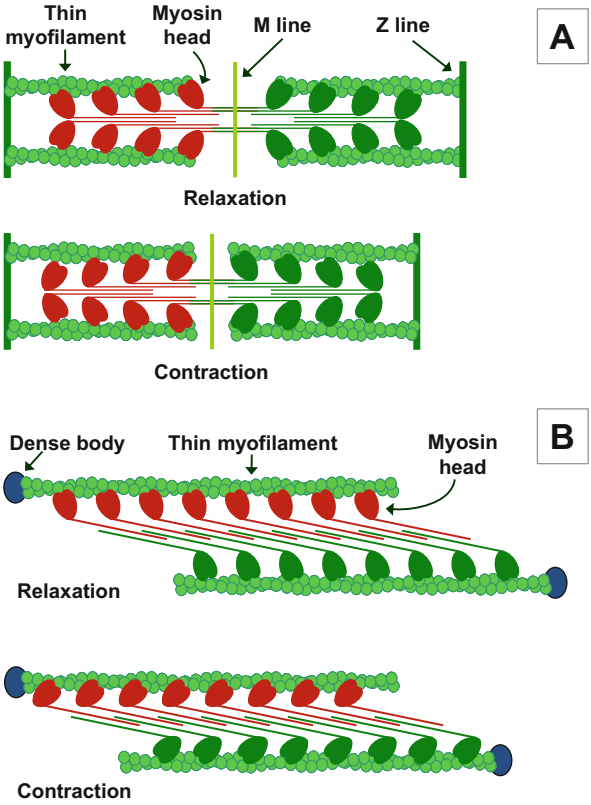

Fig. 2.2 Organization of the thin and thick filaments. In striated muscle (panel *A*), the thin and thick filaments are organized into sarcomeres. The thin filaments are anchored perpendicularly to the Z lines. The thick filaments arise from the both sides of the M line, which is at the center of the sarcomere. During contraction, the myosin heads form cross-bridges with actins and pull the thin filaments toward the M line. Such an arrangement is termed as bipolar geometry. In smooth muscle (panel *B*), the thin filaments are connected to the dense body. The myosin heads of the smooth muscle on one side of the thick filament face in one direction while those on the opposite side facing in the opposite direction. Such an arrangement, termed as side polar geometry, would enable a thin filament to slide unimpeded along a thick filament "side" until the end of the thin filament is reached (The figure is from Gao (2015), with permission)

lines, arise from the both sides of a perpendicular line, named M line, at the center of the sarcomere. During contraction, the myosin heads form cross-bridges with actins and pull the thin filaments toward the M line. Such an arrangement of the thick filaments is known as bipolar geometry. In smooth muscle, thin and thick filaments are arranged less orderly, so there is no clear appearance of the existence of sarcomere. The myosin heads of the smooth muscle on one side of the thick filament face in one direction with myosin heads on the opposite side facing in the opposite direction. Such an arrangement, termed side polar geometry, would enable a thin filament to slide unimpeded along a thick filament "side" until the end of the thin filament is reached. If the thick filament were bipolar, sliding would be inhibited when the thin filament encounters cross-bridges of opposite polarity. The side polar arrangement makes it possible for myosin to easily associate with and dissociate from the filament ends, consistent with assembly–disassembly processes thought to occur in some smooth muscles in different physiological states (Craig and Woodhead 2006; Thoresen et al. 2013) (Fig. 2.2). In the sarcomere of striated muscle, the lengths and diameters of both thin and thick filaments are stable. In contrast, the length of smooth muscle actin may change in response to certain stimuli via decreased depolymerization or increased actin filament nucleation, branching, and elongation (Seow 2005; Bednarek et al. 2011). The monomeric and dimeric statuses of smooth muscle are dynamically modulated. The length and the number of myosin head of smooth muscle thick filaments in a contractile unit are also variable in different physiological states that resulted from the assembly–disassembly processes. These flexible characteristics of the organization of thin and thick filaments may contribute to the high adaptational capacity of smooth muscle (Liu et al. 2013; Thoresen et al. 2013; Lan et al. 2015).

2.5 Sarcoplasmic Reticulum

The sarcoplasmic reticulum (SR) is a large, convoluted organelle formed by flattened sacs or tubules. It is a specialized smooth endoplasmic reticulum (ER) that existed in myocytes to function as the intracellular Ca^{2+} store. It is estimated that myofilaments and intermediate filaments along with associated dense bodies occupy up to 90% of the cell's volume of the smooth muscle cell. About 5% of the cell volume is accounted for by the SR in the aorta and pulmonary artery and ~2% for by the SR in the mesenteric vein and artery and portal vein in the rabbit (Devine et al. 1972). The cellular distribution of SR is not uniform. Studies of electron and confocal microscopy reveal that the SR can be more preferentially located in the plasma membrane, which is described as peripheral (or superficial). When SR is located away from plasma membrane, it is described as close to the central (or deep). The peripheral SR may have a close relationship with Ca^{2+} homeostasis, local Ca^{2+} release, and interactions with plasma membrane ion channels. For the central SR, it may be more involved in contraction by directly supplying Ca^{2+} to the myofilaments. There is evidence indicating that the peripheral

SR is more abundant in phasic smooth muscle such as portal veins, whereas the central SR is more dominant in tonic smooth muscle such as aortas (Wray and Burdyga 2010).

The Ca^{2+} concentration inside SR is ~100 μm, whereas the Ca^{2+} concentration in the cytosol is 0.1–0.2 μm under resting conditions and 0.3–1.5 μm during contraction. When the smooth muscle is stimulated, SR Ca^{2+} is released into the cytosol via ryanodine receptors (RyRs) and inositol 1,4,5-trisphosphate (IP_3) receptors (IP_3Rs)-gated Ca^{2+} release channels. After contraction, the cytosol Ca^{2+} is sequestered into SR via sarco-/endoplasmic reticulum Ca^{2+}–ATPase (SERCA) (Wray and Burdyga 2010). The ryanodine receptors (RyRs) are homotetrameric complexes of four ~565-kDa subunits, forming a square around a central Ca^{2+} pore. Because of its short and wide channel region, the RyRs are suitable for sudden and large release of Ca^{2+} from intracellular stores. RyR is a symmetrical mushroomlike structure with large N-terminal cytoplasmic domains that modulate the gating of the channel pore located in the C-terminus. The cytosolic domain consists of ~80% of the mass of the RyRs, which is the modulatory region of the molecule, containing binding sites for Ca^{2+}, adenine nucleotides, calmodulin, FK506-binding proteins (FKBPs), as well as phosphorylation sites. Three isoforms of RyR have been identified. RyR1 and RyR2 are predominantly expressed in the skeletal and cardiac muscle, respectively, while RyR3 is ubiquitously expressed. All three RyR isoforms have been found in vascular smooth muscles, with the type and the relative proportion of expression of each being tissue and species dependent (Wray and Burdyga 2010; Amador et al. 2013). In VSMCs, RyRs of the peripheral SR may be located in very close proximity to the Ca^{2+}-activated K^+ (BK) channels of the plasma membrane. Ca^{2+} sparks result from focal Ca^{2+} release into the cytosol from the SR by the opening of a cluster of RyRs may activate the BK channels, which leads to membrane hyperpolarization and reduced vasocontractility (Zhuge et al. 2002). In portal vein, the inhibition of either RyR1 or RyR2 but not RyR3 with antisense oligonucleotides abolishes Ca^{2+} sparks, suggesting RyR1 and RyR2 may colocalize to form Ca^{2+} spark sites (Mironneau et al. 2001). In pulmonary artery smooth muscle cells, RyR3 gene knockout inhibits hypoxia- but not noradrenaline-induced $Ca2^+$ and contractile responses (Zheng et al. 2005).

IP_3Rs are about half the size of RyRs, with a molecular mass of ~1.3 MDa for IP_3Rs and ~ 2.3 MDa for RyRs. Both are transmembrane proteins that share a high sequence homology in their ion-conducting pore. Genomic studies indicate that the two receptors have coevolved from a common ancestor in unicellular species (Amador et al. 2013). IP_3R protein can be divided into four functional regions: an IP3-binding region comprising ~600 residues at the N-terminus, a central modulatory region, a C-terminal channel-forming region (residues 2276–2589) containing six putative transmembrane domains, and the C-terminal tail including the last ~160 residues. Both the N- and C-termini are cytoplasmic and form a large portion of the IP3R channel that includes ~90% of the protein mass (Amador et al. 2013; Serysheva 2014). In mammals, IP_3Rs exist as three isoforms, IP_3R1, IP_3R2, and IP_3R3. They are ubiquitously expressed and have distinct cellular distribution patterns. In the thoracic aorta and mesenteric arteries, IP_3R1 is the only isoform

noted, while IP_3R1 and weak expression of IP_3R2 were found in basilar artery (Wray and Burdyga 2010; Narayanan et al. 2012).

The ion channel activity of IP_3Rs is regulated by coupled interplay between the binding of its primary ligands, IP_3 and Ca^{2+}. IP_3 is generated from phosphoinositide in response to various extracellular stimuli. The IP_3R shows a single high-affinity binding site to IP_3 with a K_D value of 80 nM. It is estimated that half-maximal release of Ca^{2+} from the SR requires 40 nM $InsP_3$. The K_D values of IP_3 for IP_3R1, IP_3R2, and IP_3R3 are 1.5, 2.5, and 40 nM, respectively. IP_3R activity is modulated by the cytosolic concentration of Ca^{2+}. IP_3R1 activity can be stimulated by Ca^{2+} at concentrations below 300 nM but inhibited at concentrations >300 nM (Wray and Burdyga 2010).

In a variety of smooth muscle cells, the cluster of RyR and/or IP_3R may be activated by a localized Ca^{2+} elevation so that a propagated and amplified Ca^{2+} wave with distinct spatial and temporal characteristics is generated, which is termed Ca^{2+}-induced Ca^{2+} release (CICR). CICR can be triggered by the entry of extracellular Ca^{2+} or the elevated Ca^{2+} concentration of the SR. The Ca^{2+} concentration of the SR may exert potent influence on the activity of RyR and IP_3R. The lowing of SR Ca^{2+} leads to a reduced activity of RyR and IP_3R (Chalmers et al. 2007). The decrease of SR Ca^{2+} can also activate store-operated Ca^{2+} entry (SOCE), which is sensed by stromal interaction molecule 1 (STIM1). Consequently, STIM1 aggregates and moves to areas where the SR comes close to the plasma membrane (within 25 nm) to interact with Orai channels and activate extracellular Ca^{2+} entry (Prakriya and Lewis 2015).

The Ca^{2+} concentration of the SR is maintained by both SOCE, which refill SR with extracellular Ca^{2+}, and by SERCA, which sequesters cytosolic Ca^{2+} into SR. The SERCA is a transmembrane ion transporter belonging to the P-type ATPase family. It comprises a single polypeptide chain (~110 kDa) and topologically has three parts: a cytoplasmic head, a stalk domain, and a transmembrane domain. The cytoplasmic head region encompasses the phosphorylation and nucleotide-binding domains, which form the catalytic site, and the actuator domain, which is involved in the transmission of major conformational changes. The transmembrane domain forms the channel through which Ca moves. There are two Ca^{2+}-binding sites in the transmembrane domain, with the two Ca^{2+} ions being 5.7A° apart. The Ca^{2+}-binding domains exist in either a high- or low-affinity form, known as E1 and E2 states, and allow access only from the cytosolic and luminal side, respectively. The SERCAs transport two Ca^{2+} into the SR for each ATP hydrolyzed, with two H^+ being transported out of the SR. The activity of SERCA is normally inhibited by a closely associated 52-amino acid homopentameric protein, known as phospholamban (PLB). When PLB is phosphorylated by cAMP-dependent protein kinase (PKA) or cGMP-dependent protein (PKG), PLB is dissociated from SERCA, and thus Ca^{2+} movement increases. Mammalian SERCA exists as three isoforms, namely, SERCA1, SERCA2, and SERCA3, which are encoded by three different genes. In addition, alternative splicing occurs giving rise to SERCA1a, SERCA1b, SERCA2a, and SERCA2b. In vascular smooth

muscle, the SERCA2 subtype has been identified, with the SERCA2b isoform being more abundant (Wray and Burdyga 2010; Bublitz et al. 2013).

2.6 Mitochondria

Mitochondria are the powerhouse of the cell as they generate most of the cell's supply of ATP. They are also involved in broad range of biological processes, including vasocontraction, cellular differentiation, and apoptosis. Mitochondria are composed of double membranes which divide the organelle into four distinct parts: the outer membrane, the intermembrane space (the space between the outer and inner membranes), the inner membrane, and the matrix. The outer membrane contains large numbers of integral membrane proteins which permit free diffusion of molecules. The intermembrane space contains proteins (e.g., cytochrome c) that are critical for mitochondrial energetics and apoptosis. In contrast to the outer membrane, the inner membrane is highly impermeable, and most ions and molecules require transporters to cross. The inner membrane is inwardly folded into numerous cristae, which expand the surface area of the membrane. The inner membrane contains various proteins, such as the enzymes of oxidative phosphorylation, ATP synthase, and transporters for carrying proteins into the matrix. The matrix contains about two-thirds of the total protein in a mitochondrion, including most of the enzymes that are responsible for the citric acid cycle reactions. In native VSMCs, mitochondria are ovoid- or rod-shaped organelles sized 0.5–10 μm and are stably positioned in cytosol. In cultured VSMCs, however, mitochondria exist as long filamentous entities, loops, and networks. Mitochondria appearance changes due to extension, retraction, wriggling, Brownian motion, and large directed movements. These movements may be involved in the organelles' turnover, localized ATP provision, or cell proliferation. Fission and fusion are also widely observed in cultured cells but are infrequent events in native cells, which have been linked to apoptosis and mitochondrial quality control via autophagy (mitophagy) (McCarron et al. 2013).

2.7 Caveolae

Caveolae are cholesterol- and glycosphingolipid-rich, flask-shaped, small (50–100 nm) invaginations of the plasma membrane. These organelles are present in most mammalian cell types and particularly abundant in adipocytes and endothelial and muscle cells. The organization and function of caveolae are mediated by coat proteins (caveolins (Cav)) and support or adapter proteins (cavins). Cav is a family of 22–24-kDa proteins existed as three isoforms, Cav-1, Cav-2, and Cav-3. All these isoforms share a common topology: cytoplasmic N-terminus with scaffolding domain, long hairpin transmembrane domain, and cytoplasmic C-terminus.

Cav-1 and Cav-2 are ubiquitously expressed, while Cav-3 is expressed primarily in the cardiac and skeletal muscle. Cavins, which act as a regulator of caveolar function and organization, are present in mammals with four isoforms, cavins 1–4. Cavins 1–3 are broadly expressed, and cavin-4 is cardiac and skeletal muscle-specific. Studies show that genetic deletion of Cav-1 results in the almost complete loss of caveolae through decreased availability of caveolin proteins. Evidence also indicates that cavin-2 is required for the stable expression levels of both Cav-1 and cavin-1 proteins (Chidlow and Sessa 2010).

Caveolae are originally considered being involved in cholesterol transport, endocytosis, and potocytosis. However, later studies have revealed that these morphologically distinct structures play a critical role in cell signaling, mostly due to their ability to concentrate and compartmentalize various signaling molecules, such as receptor tyrosine kinase, G-protein-coupled receptors, transforming growth factor-β (TGF-β) type I and II receptors, endothelial nitric oxide synthase (eNOS), and calcium channels (e.g., TRPC1 and TRPC4, TRPV4) (Sowa 2012). Substantial evidence suggests that caveolae play a pivotal role in the regulation of vascular contractility. In vascular endothelial cells under resting conditions, eNOS is bound to Cav-1 which renders the enzyme inactive. An increase in the cytosolic Ca^{2+} concentration leads to the activation of calmodulin, the displacement of eNOS from Cav-1, and followed by the deinhibition of eNOS, increase in NO generation, and vasodilatation. A cell-permeable peptide containing Cav-1 scaffolding domain with a single mutation (F92A) named cavnoxin, which blocked a specific interaction between Cav-1 and eNOS, results in eNOS hyperactivation, increased NO release, and lowered blood pressure in WT but not in eNOS knockout mice (Bernatchez et al. 2011). In vascular smooth muscle, RhoA–Rho kinase and PKC signalings are the primary mechanisms for the sensitization of the filaments to Ca^{2+} which leads to enhanced contractility. The Ca^{2+} sensitization requires a redistribution of RhoA, ROK, and PKC from the cytoplasm to caveolae (Hardin and Vallejo 2006).

2.8 Cytoskeleton

Cytoskeleton gives the cell shape and mechanical resistance to deformation, provides a scaffold to organize the intracellular contents, and moves the vesicles and organelles within the cell. It is also involved in many other cellular activities such as endocytosis, cell migration, and cellular division. The cytoskeleton can be classified into three types, microfilaments, intermediate filaments, and microtubules. Microfilaments are the thinnest filaments in the cytoskeleton. They are composed of linear polymers of G-actin subunits. In VSMCs, microfilaments are ~4 nm in diameter. They are connected with each other with dense bodies and attached to the focal adhesions of the cell membrane to form a network structure inside the cell. Among the four isoforms of actin identified in smooth muscle cells, α-smooth

muscle actin is the major isoform concentrated in the contractile filaments in VSMCs. In general, large arteries contain about 60% α-smooth muscle actin, 20% β-actin, and about 20% γ-smooth muscle and γ-nonmuscle actin. Studies have shown that γ-nonmuscle actin is mainly localized in the cell cortex, while α-smooth muscle actin filaments snake longitudinally down the length of the cell and β-actins are associated with dense bodies and focal adhesions (Yamin and Morgan 2012).

Intermediate filaments average 10 nm in diameter. They are more stable (strongly bound) than microfilaments and heterogeneous constituents of the cytoskeleton. They organize the internal tridimensional structure of the cell, anchoring organelles and serving as structural components of the nuclear lamina. They also participate in some cell–cell and cell–matrix junctions. Intermediate filaments have more than 60 different building block proteins. In smooth muscle, vimentin and desmin are predominant constituents of the intermediate filament network. A gradient in the vimentin/desmin expression ratio is found in human and some animal arteries from proximal to distal, with larger arteries containing a high ratio. Microtubules are hollow cylinders with an outside diameter ~23 nm (lumen ~15 nm in diameter), most commonly comprising 13 protofilaments that, in turn, are polymers of alpha and beta tubulin. In addition to maintain the cell shape, microtubules play key roles in intracellular transport (Tang 2008;Yamin and Morgan 2012).

The cytoskeletal architecture provides the structural basis for cell morphology. The cytoskeletal structure is not static but rather in a constantly reorganizing process to coordinate the cellular activities including the contractile activities. An increased actin polymerization in the cell cortex occurs during vasoconstriction. The inhibition of actin polymerization with latrunculins or cytochalasins leads to reduced contractility. The contraction-induced actin polymerization may serve to strengthen the membrane for the transmission of force generated by the contractile apparatus to the extracellular matrix and to enable the adaptation of smooth muscle cells to mechanical stresses (Gunst and Zhang 2008;Tang 2008;Yamin and Morgan 2012).

References

Amador FJ, Stathopulos PB, Enomoto M, Ikura M (2013) Ryanodine receptor calcium release channels: lessons from structure-function studies. FEBS J 280:5456–5470

Bednarek ML, Speich JE, Miner AS, Ratz PH (2011) Active tension adaptation at a shortened arterial muscle length: inhibition by cytochalasin-D. Am J Physiol Heart Circ Physiol 300: H1166–H1173

Bernatchez P, Sharma A, Bauer PM, Marin E, SessaWC (2011) A noninhibitory mutant of the caveolin-1scaffolding domain enhances NOS-derived NO synthesis and vasodilation in mice. J Clin Invest 121: 3747–3755

Bublitz M, Musgaard M, Poulsen H, Thøgersen L, Olesen C, Schiøtt B, Morth JP, Møller JV, Nissen P (2013) Ion pathways in the sarcoplasmic reticulum Ca^{2+}-ATPase. J Biol Chem 288:10759–10765

Chalmers S, Olson ML, MacMillan D, Rainbow RD, McCarron JG (2007) Ion channels in smooth muscle: regulation by the sarcoplasmic reticulum and mitochondria. Cell Calcium 42:447–466

Chamley JH, Campbell GR, McConnell JD, Gröschel-Stewart U (1977) Comparison of vascular smooth muscle cells from adult human, monkey and rabbit in primary culture and in subculture. Cell Tissue Res 177:503–522

Chidlow JH Jr, Sessa WC (2010) Caveolae, caveolins, and cavins: complex control of cellular signalling and inflammation. Cardiovasc Res 86:219–225

Craig R, Woodhead JL (2006) Structure and function of myosin filaments. Curr Opin Struct Biol 16:204–212

Devine CE, Somlyo AV, Somlyo AP (1972) Sarcoplasmic reticulum and excitation-contraction coupling in mammalian smooth muscles. J Cell Bio 52:690–718

Eddinger TJ, Meer DP (2007) Myosin II isoforms in smooth muscle: heterogeneity and function. Am J Physiol Cell Physiol 293:C493–C508

Gao Y (2015) Vascular smooth muscle (Chapter 3). In: Dong E, Zhang Y (eds) Vascular biology, 2nd edn. Peking University Medical Press, Beijing, pp p28–p42. in Chinese

Gunst SJ, Zhang W (2008) Actin cytoskeletal dynamics in smooth muscle: a new paradigm for the regulation of smooth muscle contraction. Am J Physiol Cell Physiol 295:C576–C587

Hardin CD, Vallejo J (2006) Caveolins in vascular smooth muscle: form organizing function. Cardiovasc Res 69:808–815

Hill MA, Meininger GA (2012) Arteriolar vascular smooth muscle cells: mechanotransducers in a complex environment. Int J Biochem Cell Biol 44:1505–1510

Kim HR, Gallant C, Leavis PC, Gunst SJ, Morgan KG (2008) Cytoskeletal remodeling in differentiated vascular smooth muscle is actin isoform dependent and stimulus dependent. Am J Physiol Cell Physiol 295:C768–C778

Lan B, Deng L, Donovan GM, Chin LY, Syyong HT, Wang L, Zhang J, Pascoe CD, Norris BA, Liu JC, Swyngedouw NE, Banaem SM, Paré PD, Seow CY (2015) Force maintenance and myosin filament assembly regulated by Rho-kinase in airway smooth muscle. Am J Physiol Lung Cell Mol Physiol 308:L1–L10

Lehman W, Morgan KG (2012) Structure and dynamics of the actin-based smooth muscle contractile and cytoskeletal apparatus. J Muscle Res Cell Motil 33:461–469

Liu JC, Rottler J, Wang L, Zhang J, Pascoe CD, Lan B, Norris BA, Herrera AM, Paré PD, Seow CY (2013) Myosin filaments in smooth muscle cells do not have a constant length. J Physiol 591:5867–5878

Marston S, El-Mezgueldi M (2008) Role of Tropomyosin in the regulation of contraction in smooth muscle. Adv Exp Med Biol 644:110–123

Marston SB, Smith CW (1985) The thin filaments of smooth muscles. J Muscle Res Cell Motil 6:669–708

McCarron JG, Wilson C, Sandison ME, Olson ML, Girkin JM, Saunter C, Chalmers S (2013) From structure to function: mitochondrial morphology, motion and shaping in vascular smooth muscle. J Vasc Res 50:357–371

Mironneau J, Coussin F, Jeyakumar LH, Fleischer S, Mironneau C, Macrez N (2001) Contribution of ryanodine receptor subtype 3 to Ca^{2+}- responses in Ca^{2+} -overloaded cultured rat portal vein myocytes. J Biol Chem 276:11257–11264

Narayanan D, Adebiyi A, Jaggar JH (2012) Inositol trisphosphate receptors in smooth muscle cells. Am J Physiol Heart Circ Physiol 302:H2190–H2210

Prakriya M, Lewis RS (2015) Store-operated calcium channels. Physiol Rev 95:1383–1436

Rensen SS, Doevendans PA, van Eys GJ (2007) Regulation and characteristics of vascular smooth muscle cell phenotypic diversity. Neth Heart J 15:100–108

Roman HN, Zitouni NB, Kachmar L, Ijpma G, Hilbert L, Matusovsky O, Benedetti A, Sobieszek A, Lauzon AM (2013) Unphosphorylated calponin enhances the binding force of unphosphorylated myosin to actin. Biochim Biophys Acta 1830:4634–4641

Seow CY (2005) Myosin filament assembly in an ever-changing myofilament lattice of smooth muscle. Am J Physiol Cell Physiol 289:C1363–C1368

Serysheva II (2014) Toward a high-resolution structure of IP_3R channel. Cell Calcium 56:125–132

Sowa G (2012) Caveolae, caveolins, cavins, and endothelial cell function: new insights. Front Physiol 2:120

Tang DD (2008) Intermediate filaments in smooth muscle. Am J Physiol Cell Physiol 294:C869–C878

Taylor KA, Feig M, Brooks CL 3rd, Fagnant PM, Lowey S, Trybus KM (2014) Role of the essential light chain in the activation of smooth muscle myosin by regulatory light chain phosphorylation. J Struct Biol 185:375–382

Thoresen T, Lenz M, Gardel ML (2013) Thick filament length and isoform composition determine self-organized contractile units in actomyosin bundles. Biophys J 104:655–665

Wang CL (2008) Caldesmon and the regulation of cytoskeletal functions. Adv Exp Med Biol 644:250–272

Winder SJ, Allen BG, Clément-Chomienne O, Walsh MP (1998) Regulation of smooth muscle actin-myosin interaction and force by calponin. Acta Physiol Scand 164:415–426

Wray S, Burdyga T (2010) Sarcoplasmic reticulum function in smooth muscle. Physiol Rev 90:113–178

Yamin R, Morgan KG (2012) Deciphering actin cytoskeletal function in the contractile vascular smooth muscle cell. J Physiol 590:4145–4154

Zhang Y, Hermanson ME, Eddinger TJ (2013) Tonic and phasic smooth muscle contraction is not regulated by the PKCα - CPI-17 pathway in swine stomach antrum and fundus. PLoS One 8: e74608

Zheng YM, Wang QS, Rathore R, Zhang WH, Mazurkiewicz JE, Sorrentino V, Singer HA, Kotlikoff MI, Wang YX (2005) Type-3 ryanodine receptors mediate hypoxia-, but not neurotransmitter-induced calcium release and contraction in pulmonary artery smooth muscle cells. J Gen Physiol 125:427–440

Zhuge R, Fogarty KE, Tuft RA, Walsh JV Jr (2002) Spontaneous transient outward currents arise from microdomains where BK channels are exposed to a mean Ca^{2+} concentration on the order of 10 microM during a Ca^{2+} spark. J Gen Physiol 120:15–27

Chapter 3
Vascular Endothelium

Abstract The endothelium is strategically located at the interface between the blood flow and the vascular smooth muscle and other components of the vessel wall and thus is endowed with a broad range of capacities in the regulation of various vascular activities. It acts as a selective barrier to regulate the movement of small and macromolecules through the paracellular and transcellular routes. Thus, the endothelium exerts important effects on the exchange of metabolites and bioactive agents between the blood and the vascular wall. The endothelium also serves as a pathway for circulating leukocytes to be recruited to the extravascular sites where injuries or inflammation occurs. The interaction between the endothelium and the leukocytes may affect the immune reactivities. Under physiological conditions, the endothelium plays a critical role in maintaining the fluidity of blood flow through its inhibitory actions on platelet aggregation and coagulation and its facilitating effect on fibrinolysis. These effects are mainly mediated by the endothelium-derived molecules such as nitric oxide, prostaglandin I_2, thrombomodulin, heparan sulfate proteoglycan, and tissue factor pathway inhibitor. However, under physiological conditions, the endothelium may adversely affect the hemostatic balance through certain molecules such as von Willebrand factor, tissue factor, and plasminogen activator inhibitor-1. The endothelium also plays a central role in the de novo formation of blood vessels and the expansion of the existing vasculature, which are critical for the development of circulatory system as well as tissue repair. The above aspects will be reviewed in this chapter with a focus on the recent progress.

Keywords Endothelial cell • Interendothelial junctions • Transcytosis • Leukocyte trafficking • Coagulation • Vasculogenesis • Angiogenesis

3.1 Introduction

The endothelium is the innermost layer of blood vessels. In the adult, it consists of approximately 60 trillion endothelial cells (ECs), forming an almost 1 kg "organ" with the total area of the blood/endothelium interface ~350 m^2. The shape of ECs varies across the vascular tree. They are typically flat. The arterial ECs are generally thicker than those in veins, with the exception of ECs of high endothelial venules of secondary lymphoid organs, which have been described as plump and cuboidal.

Y. Gao, *Biology of Vascular Smooth Muscle: Vasoconstriction and Dilatation*,
DOI 10.1007/978-981-10-4810-4_3

ECs are aligned in the direction of blood flow. Arterial ECs are long and narrow or ellipsoidal. Venous ECs are short and wide. The difference in their shapes may be a reflection of the blood flow they encountered. Physiological arterial and venous shear stress levels are typically 10–40 dynes/cm^2 and 1–5 dynes/cm^2, respectively (Pries et al. 2000; Aird 2007a, b; dela Paz and D'Amore 2009).

The endothelium plays an important role in a broad range of physiological functions, including the regulation of vasomotor tone, acting as a selective permeable barrier characterized by tight junctions and vesicular carriers, leukocyte trafficking, hemostatic balance, and blood vessel formation (Claesson-Welsh 2015; Sukriti et al. 2014; Vestweber 2015; Yau et al. 2015; Versteeg et al. 2013; Heinke et al. 2012). The current understanding of the above aspects will be reviewed in this chapter, with the exception of the role of the endothelium in vasoreactivity, which will be discussed in detail in Chap. 8.

3.2 Permeability Activity: The Paracellular Route

The endothelium exists as a selective barrier for the flux of material between the blood and underlying interstitium. Small molecules such as glucose, water, and ions may move passively across the barrier via the paracellular route. Molecules larger than 3 nm, such as albumin, IgG, and other macromolecules, are transported in membrane-bound vesicular carriers, including caveolae and vesiculo-vacuolar organelles (VVOs), known as transcytosis. (Mehta and Malik 2006; Aird 2007a, b; Sukriti et al. 2014; Claesson-Welsh 2015). Vesicles and vacuoles that make up the VVO were originally thought arising from the fusion of individual caveolae. In mice deficient in caveolin-1, the main component of caveolae, the vasculature was found still containing VVOs. It suggests that VVO may be also originated from other structures presently not clear (Chang et al. 2009). The activities of the paracellular diffusion and transcellular transport vary greatly along vascular tree and among vascular beds. The arteries and veins are both lined by continuous nonfenestrated endothelium. However, the arterial endothelium has more tight junctions and thus acts as a more restrictive barrier as compared with that of the veins. The capillary permeability varies profoundly in different tissues and organs. In the muscle, lung, skin, and brain, the capillaries are formed by nonfenestrated endothelium and possess a much limited permeability than those formed by fenestrated endothelium in tissues such as the kidney glomerulus and gastrointestinal tract. In the liver and marrow sinus, the capillaries are formed by discontinuous endothelium and thus display much greater permeability. ECs of postcapillary venules are rich in VVOs. Postcapillary venules have been found being the primary site of permeability for leukocyte trafficking and permeability in inflammation (Aird 2007a, b).

The movement of small molecule of Stokes radius (refer to the radius of a hard sphere that diffuses at the same rate as that solute named after George Stokes) < 3 nm in diameter across the interendothelial cleft is a process of diffusion and convection.

The overall flux of solute molecules can be estimated by Kedem–Katchalsky equation (Kedem and Katchalsky 1958)

$$J_s = J_v(1 - \sigma)\, C_s + PS\, (\Delta C) \tag{3.1}$$

where J_s is transmembrane solute flux (mg/min); J_v is volume flux of fluid (ml/min); σ is osmotic reflection coefficient of the membrane that ranged from 0 to 1 with 0 represents fully permeable and 1 totally impermeable to transported molecular species; C_s is mean concentration of the solute within the interendothelial junctions; P is permeability (cm/s); S is surface area of the membrane; and ΔC is the difference in solute concentration across the membrane. For J_v, it depends on the net balance of Starling forces across the endothelium according to the relationship

$$J_v = \left(L_pS\right)[(P_c\text{-}P_i) - \sigma(\Pi_c - \Pi_i)] \tag{3.2}$$

where L_p is hydraulic conductivity ($cm \cdot min^{-1} \cdot mmHg^{-1}$); Pc and P_i are capillary and interstitial fluid hydrostatic pressures, respectively (mmHg); Π_c and Π_i are capillary and interstitial oncotic pressures, respectively (mmHg); and J_v, S, and, σ are the same terms used in Eq. 3.1 (Mehta and Malik 2006).

The interendothelial junctions are composed of adherens and tight junctions. The adherens junction (AJ) is a homophilic complex formed by vascular endothelial cadherin (VE-cadherin) of the contiguous endothelial cells in a calcium-dependent manner. VE-cadherin is a transmembrane protein. Its cytoplasmic domains interact with three armadillo family proteins known as β-catenin, plakoglobin (γ-catenin), and p-120 catenin. β-Catenin via α-catenin and plakoglobin is linked to actin cytoskeleton to maintain junctional stability [Giannotta et al. 2013; Sukriti et al. 2014). AJs can be weakened by a number of bioactive agents, including vascular endothelial growth factors (VEGFs), histamine, and bradykinin. These agents cause hyperphosphorylated and internalized VE-cadherin, followed by extravasation of macromolecules. Under physiological conditions, the dissolution of AJs is transient. VE-cadherins are soon recycled and reappeared on the cell surface and the junctions close again. Under pathological conditions, the regulation of junction dynamics is lost and the junctions remain open, which result in chronic and excess vascular permeability (Claesson-Welsh 2015).

AJs have a prominent role regulating endothelial barrier function. Neutralization of VE-cadherin with specific antibody induces endothelial barrier leak. Truncation of the β-catenin binding site at the cytosolic domain of VE-cadherin results in lethality in mice due to the disruption of endothelial junctions (Sukriti et al. 2014). In addition to AJs, the other important component of the interendothelial cleft is the tight junction (TJ). TJs are composed of claudin, occludin, and junctional adhesion molecule (JAM). These TJ proteins interact with zona occludens-1 (ZO-1) in cytoplasm, which in turn associates with actin cytoskeleton and stabilizes the barrier function (Sukriti et al. 2014). Several members of the Ras superfamily, a protein superfamily of small GTPases, such as Ras homolog gene family, member A (RhoA), Ras-related C3 botulinum toxin substrate 1 (Rac1), cell division control

protein 42 homolog (Cdc42), and Ras-related protein-1 small GTPase (Rap1), are involved in the fine-tuning of vascular permeability. Rac1 and Cdc42 may suppress the internalization of VE-cadherin to strength barrier function. RhoA may promote the formation of stress fibers, which impairs barrier integrity (Komarova and Malik 2010; Sukriti et al. 2014).

The vascular endothelium is composed of not only ECs but also subcellular extracellular matrix (ECM). Therefore, the permeability of the endothelium is also affected by the properties of the ECM. Studies of quantifying the contributions of cell–cell and cell–ECM adhesion to endothelial permeability by measuring the electrical resistance of confluent endothelial monolayers and the underlying ECM suggest that the ECM contributes ~50% of the total barrier function. Besides, the integrin receptors binding to the ECM also contribute to the barrier function by stabilizing the closed configuration of the interendothelial junctions (Mehta and Malik 2006). It is known that the luminal surface of the endothelium is lined with a glycocalyx, which is composed of a negatively charged network of proteoglycans, glycoproteins, and glycolipids with an estimated thickness up to 1 μm thick. Such an endothelial surface layer would have substantial impact on the permeability of the endothelial layer. For instance, studies demonstrated that permeation into the layer for neutral tracers with molecular weights ranging from 0.4 to 40 kDa was much faster than anionic tracers in the same range (Pries et al. 2000). It is of worth noting that although water is diffused mainly through the interendothelial junctions, a significant amount of water (up to 40% of the total hydraulic pathway) crosses the barrier through a transcellular route via the aquaporin water channels (Michel and Curry 1999). Recent evidence indicates that aquaporin-mediated water diffusion is involved in cell volume regulation. The aquaporin channels may also be permeable to some other molecules such as glycerol and H_2O_2 and thus contribute to triglyceride cycling and redox hemostasis (Day et al. 2014).

3.3 Permeability Activity: The Transcellular Route

The movement of macromolecular solute of Stokes radius >3 μm across the endothelium is through transcytosis. Transcytosis is mediated by specialized structures, including caveolae, vesiculo-vacuolar organelles (VVOs), and transendothelial channels. Caveolae are caveolin-1-positive vesicles and are abundant in ECs, composing up to ~15% of the total endothelial cell volume (~10,000–30,000 caveolae/cell). Caveolae exist as either flask-shaped cell surface invaginations or as free vesicles of 50–100 nm in diameter in the cytoplasm. The openings of caveolae frequently display a stomatal diaphragm composed of radial fibrils anchored at the rim and interwoven in a central knob. The component of these fibrils is the 60-kDa plasmalemmal vesicle-1 (PV-1) protein glycoprotein, selectively expressed by most endothelial cells except for the endothelium of the blood–brain barrier (Hallmann et al. 1995). It is believed that the stomatal diaphragms may function as a structural feature to control the access of plasma proteins into the

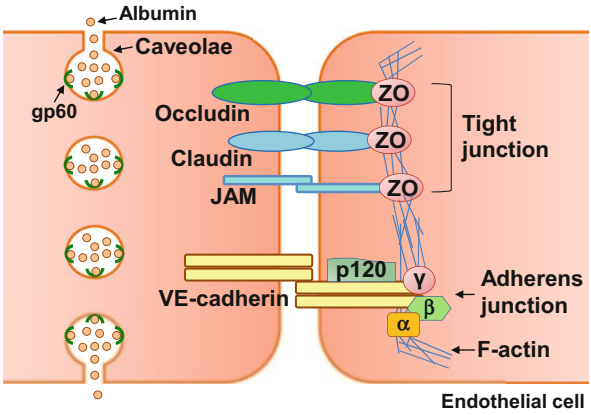

Fig. 3.1 Schematic diagram of the transcellular and paracellular pathways for molecules to cross the endothelium. The movement of macromolecular solute of Stokes radius >3 μm across the endothelium is mediated by caveolae, vesiculo-vacuolar organelles (VVOs), and transendothelial channels. The latter two are not shown in the figure. Here in the figure, albumin in the plasma is loaded into the caveolae by binding the albumin-binding glycoprotein (gp60) in the inner surface of the caveolae followed by the fluid-phase component of albumin loading. The fluid-phase component constitutes the majority of albumin loaded. Small molecules (Stokes radius <3 μm) move across the endothelium mainly through the interendothelial junctions, which include the tight junction and adherens junction. The tight junction is composed of claudin, occludin, and junctional adhesion molecule (JAM). These junctional proteins interact with zona occludens-1 (ZO-1) in cytoplasm, which is associated with F-actin to stabilize the barrier function. The adherens junction is composed of vascular endothelial cadherin (VE-cadherin). The cytoplasmic domains of VE-cadherin interact with β-catenin (β), plakoglobin (γ), and p-120 catenin. β-Catenin via α-catenin (α) and plakoglobin is directly linked to actin cytoskeleton to maintain junctional stability

caveolar cavity. Caveolae can fuse with large vacuoles to form VVOs or fuse into transendothelial channels either open on both fronts of the cell or isolated in the cytosol. Studies show that caveolae represent >95% of the whole vesicular population of the ECs. VVOs, which are most commonly observed in venular endothelium, are grapelike clusters of interconnected vesicles and vacuoles. Their sizes vary from 80 to 140 nm in diameter consisting of 79–362 vesicles or vacuoles that are 1–2 μm at their longest dimension and occupy 16–18% of the venular endothelial cytoplasm. VVOs can assemble into transcellular membranous channels with openings at the luminal, abluminal, and lateral endothelial cell surface (Mehta and Malik 2006; Predescu et al. 2007) (Fig. 3.1). The volume density of endothelial vesicles varies among different vascular segments, about 200 vesicles/μm^3 in arterioles, 900 vesicles/μm^3 in the capillaries, 600 vesicles/ μm^3 in postcapillary venules, and 1200 vesicles/μm^3 in the venules (Simionescu and Simionescu 1984). The endothelium of cerebral vessels has the lowest frequency of transcytotic vesicles, which may contribute to the high restrictiveness of the blood–brain barrier (Stewart 2000).

Transcytosis involves macromolecule loading into the caveolae, formation of a sealed vesicle by membrane fission, movement of vesicle across the cell, fusion of vesicle membrane with the plasmalemma on the opposite front of the cell, and discharge of vesicular content into the extracellular medium. These processes are best exemplified by the transportation of albumin. Albumin in the plasma is loaded into the caveolae via both receptor-mediated processes and fluid phase. The loading is initiated by the binding of albumin to the 60-kDa albumin-binding glycoprotein (gp60) in the inner surface of the caveolae followed by the fluid-phase component of albumin loading. Specific binding of albumin to localized gp60 is a saturable process, and ~98% of the albumin internalized is free within vesicles. The binding of albumin to gp60 induces the receptor clustering and its interaction with caveolin-1. The latter leads to $G_{\alpha i}$ activation, dissociation of $G\beta\gamma$, and c-Src activation. Activated Src phosphorylates dynamin and caveolin-1, which leads to the formation of dynamin into a spiral around the neck of caveolae. Once the spiral is in place, it extends lengthwise and constricts through GTP hydrolysis and results in the release of caveolae into the cytosol. Free caveolae then move to the target membrane for exocytosis in a Rab GTPase-dependent manner, possibly mediated by actin/microtubules. The fusion of the caveolae with the membrane and albumin exocytosis is mediated by soluble N-ethylmaleimide-sensitive factor attachment protein receptor (SNARE) machinery. SNAREs consist of pairs of proteins known as v-SNAREs (VAMP) localized on caveolae and t-SNAREs (syntaxin- and synaptosome-associated protein of 25-kDa (SNAP25) family members) localized on the target membrane (Mehta and Malik 2006; Komarova and Malik 2010). Transport of albumin is exclusive to caveolae. Mice deficient in caveolin-1, the key structural protein of caveolae, show a loss of caveolae and of vesicular albumin transport (Schubert et al. 2001). Albumin is the most abundant plasma protein crucial for the homeostasis of the protein oncotic pressure and fluid balance across capillaries. Albumin is also involved in the cotransport of cholesterol, hormones, fatty acids, and amino acids, and its function extends beyond endothelial physiology (Mehta and Malik 2006).

3.4 Leukocyte Transendothelial Migration

The transendothelial migration of leukocyte constitutes a critical part of the innate and adaptive immune responses. When ECs are activated by cytokines, chemokines, and lipid mediator released from the nearby abluminal infectious and injurious tissues, a number of cell adhesion molecules such as E-selectin, P-selectin, intercellular adhesion molecule 1 (ICAM1), and vascular cell adhesion molecule 1 (VCAM1) are induced on the surface of ECs. E- and P-selectin mediate the capture of circulating leukocytes, the rolling of leukocytes on EC surface, and the activation of leukocyte integrins. The binding of activated integrins to ICAM1 and VCAM1 leads to firm adhesion and crawling of leukocytes on EC surface to the sites suitable for transmigration. Leukocyte transendothelial migration occurs

predominantly through the EC junctions, whereas through the endothelial cell body, it may occur up to 10% of the time outside of the central nervous system (Vestweber 2015; Muller 2015; Gerhardt and Ley 2015).

At the beginning of the transmigration, ICAM1 and VCAM1 are clustered at the apical surface of ECs nearing the junction. These adhesion molecules interact with their integrin counter-receptors of the leukocyte, which leads to activations of myosin light chain kinase and Rho kinase resulting in the contraction of the ECs and leads to cellular Src kinase (c-Src)-mediated phosphorylation of VE-cadherin resulting in the weakening of adherens junctions (Gerhardt and Ley 2015). Another important mechanism for the leukocyte transmigration involves the lateral border recycling compartment (LBRC), which is a reticulum of tubulovesicle-like membrane that is continuous with the plasmalemma at the lateral EC borders. It contains all of the membrane proteins known to play a positive role in the transmigration including platelet endothelial cell adhesion molecule 1 (PECAM1), CD99, CD155, and JAMs. During the transmigration, the homophilic interaction of PECAM between ECs and leukocytes triggers extensive recycling of LBRC to the site of transmigration. Thus, the migrating leukocyte is supplied with sufficient surface area and unligated receptors for the process to continue (Muller 2015).

The diameter of a leukocyte is >10 μm, and the thickness of the EC at the junction is ≤ 0.5 μm (Muller 2015; Vestweber 2015). In the transmigratory process, the leukocytes rearrange their cytoskeletal structures and change their shape by establishing distinct subcellular structures. The leading edge (pseudopod) of the leukocyte is characterized by membrane sheets (lamellipodia) formed by Rac-mediated actin polymerization that push the cell forward. The trailing edge (uropod) is enriched in Rho GTPases and related molecules needed for actomyosin fibers to contract which leads to detachment of the trailing edge from the substratum. Between the leading and trailing edge is the middle region of the cell, which is characterized by a microtubule lattice that facilitates the dynamic delivery of intracellular molecules to the front and back domains (Mócsai et al. 2015). The transmigration through the endothelial barrier takes about 2–3 min., whereas leukocytes take up to 15–20 min. to overcome the basement membrane to reach the extravascular tissues (Vestweber 2015). Leukocyte transendothelial migration is generally observed in postcapillary venules. The fact that postcapillary venules have a lower flow rate, thinner walls, and fewer tight junctions than arterial vessels would make them suitable for leukocyte trafficking. (dela Paz and D'Amore 2009).

3.5 Modulation of Coagulation and Fibrinolysis

The endothelium plays an indispensable role in maintaining undisturbed blood fluidity in the body through suppressing platelet aggregation, inhibiting coagulation, and facilitating fibrinolysis (Wu and Thiagarajan 1996; Versteeg et al. 2013; Yau et al. 2015). The inhibitory action on platelet aggregation is mainly through the

actions of NO and prostacyclin (PGI_2), which are released from ECs under basal conditions and in response to various stimuli such as shear stress, thrombin, and ADP. PGI_2 is also released from vascular smooth muscle cell and other cell types to a less extent. The effect of NO and PGI_2 on platelets is mediated by cGMP/PKG and cAMP/PKA pathways, respectively. These two pathways often converge at the level of substrate proteins, which can be broadly grouped into two main categories: signaling regulators and actin-binding proteins (ABPs). The former include Rap1B, Gα13, inositol 1,4,5-trisphosphate receptor, IRAG, and TRPC6, and the latter include vasodilator-stimulated phosphoprotein (VASP), Lim and SH3 domain protein (LASP), and heat-shock protein 27 (HSP27). The endothelial surface expresses an enzyme termed ecto-adenosine diphosphatase (Ecto-ADPase), which can also attenuate platelet activity resulting from the degradation of ADP. ADP is an important mediator released from activated platelets for recruiting and amplifying platelet aggregation (Smolenski 2012).

The anticoagulant effect of ECs is primarily implemented through thrombomodulin, heparan sulfate proteoglycan (HSPG), tissue factor pathway inhibitor (TFPI), and the related bioactive molecules (Wu and Thiagarajan 1996; Versteeg et al. 2013; Yau et al. 2015). Thrombomodulin is a 60-kDa transmembrane type 1 glycoprotein expressed on the lumenal surface of ECs at a density of ~50,000–100,000 molecules per cell (Suzuki et al. 1988). The binding of thrombomodulin to thrombin, which is formed in coagulation, leads to activate protein C that is bound to nearby endothelial protein C receptor (EPCR). Protein C is a 419-amino acid anticoagulant factor synthesized by the liver. Activated protein C (APC) may form a complex with its cofactor protein S (PS), a 635-amino acid synthesized by ECs as well as by the liver and megakaryocytes. The APC–PS complex exerts its anticoagulation effect by cleaving activated coagulation factor V and VIII (fVa and fVIIIa, respectively). It has been found that APC only inactivates fVa when the thrombin-generating surface is provided by ECs but not from platelets, suggesting that APC does not function to switch off coagulation but rather to prevent clotting reactions on healthy, uninjured vessels (Versteeg et al. 2013). TFPI is a peptide with relative molecular mass of 34,000–40,000. There are two major TFPI isoforms, TFPIα and TFPIβ. Both isoforms are present in ECs, with TFPIβ predominant. TFPI is the primary inhibitor of the initiation of blood coagulation. It binds to FXa or the tissue factor (TF)-activated coagulation factor VII (fVIIa)-fXa complex to suppress coagulation function. Protein S may additionally bind to TFPIα to further inhibit fXa activity (Versteeg et al. 2013; Wood et al. 2014; Yau et al. 2015). Another mechanism for the endothelium involved in anticoagulation is related to HSPG, which is expressed on the surface of most eukaryotic cells including ECs and in the extracellular matrix. HSPG exerts its anticoagulation effect by activating antithrombin, which is a glycoprotein consisting of 432 amino acids produced by the liver and is considered one of the most important inhibitors of thrombin generation and function through the degradation thrombin and the activated coagulation factor IX, X, XI, and XII (fIXa, fXa, fXIa, and fXIIa, respectively) (Olson et al. 2010).

The endothelium plays a key role in the regulation of fibrinolysis via tissue plasminogen activator (t-PA). t-PA is a 70-kDa protein that converts plasminogen, a plasma protein synthesized in the liver, to plasmin. Plasmin proteolytically cleaves fibrin into fibrin degradation products that inhibit excessive fibrin formation. t-PA is predominantly synthesized in endothelial cells. It is released into the blood very slowly by the damaged endothelium such that after several days, the clot is broken down (Kim et al. 2015). An increased release of t-PA occurs when ECs encounter various stimuli such as shear stress, increased venous pressure, thrombin, acidosis, and hypoxia. The conversion of plasminogen to plasmin by t-PA is through cleaving the zymogen plasminogen at its Arg561–Val562 peptide bond. t-PA is inefficient in activating plasminogen in solution but becomes effective when t-PA and plasminogen form a complex on the surface of fibrin. Receptors for plasminogen and t-PA are identified on the endothelial cell surface (Wu and Thiagarajan 1996;Yau et al. 2015).

The endothelium also promotes platelet aggregation and coagulation as well as suppresses fibrinolysis. These effects are often manifested in facing vascular injury and inflammation. Von Willebrand factor (vWF), a pivotal player in hemostasis and thrombosis, is mainly a product of the endothelium. It is a large multimeric glycoprotein consisting of over 80 subunits of 250 kDa each stored in the Weibel–Palade bodies inside ECs (Sadler 1998; Yau et al. 2015). Under basal conditions, vWF is secreted via the interaction of Gα12 with soluble N-ethylmaleimide-sensitive fusion factor attachment protein α (α-SNAP). On thrombin stimulation, the rate of vWF secretion is augmented by Gαq-dependent and Ca^{2+}-induced activation of α-SNAP and by an enhanced Gα12-RhoA-actin signaling (Rusu et al. 2014). When the endothelial layer is disrupted and the underneath collagen is exposed, vWF acts as a bridge molecule binding concurrently to both collagen and platelet receptor Ib-V-IX, which results in the activation and aggregation of the platelet. vWF also binds to platelet receptor IIb–IIIa to further support platelet aggregation (Sadler 1998; Yau et al. 2015). The endothelium has recently been found to be the primary source for fVIII (Everett et al. 2014). When released fVIII forms a stable noncovalent complex with vWF. Upon activation by thrombin, it dissociates from the complex to interact with FIXa in the coagulation cascade, which leads to activation of fX. The activated fX in turn, with its cofactor fVa, activates more thrombin and consequently the conversion of cleaved fibrinogen into fibrin which polymerizes and cross-links into a blood clot (Yau et al. 2015). Endothelial cells do not express TF except when they are exposed to inflammatory molecules such as tumor necrosis factor-α (TNF-α). Thus, under certain disease conditions, the endothelium-derived TF may contribute to blood clotting by triggering the coagulation through the tissue factor pathway by activating coagulation factor VII and then form a complex with the activated factor VII (Versteeg et al. 2013; Yau et al. 2015). ECs are also the major producer of plasminogen activator inhibitor-1 (PAI-1),which inhibits fibrinolysis by acting on t-PA. PAI-1 is present in increased levels in various disease states such as obesity, metabolic syndrome, and atherosclerosis (Wu and Thiagarajan 1996; De Taeye et al. 2005) (Fig. 3.2).

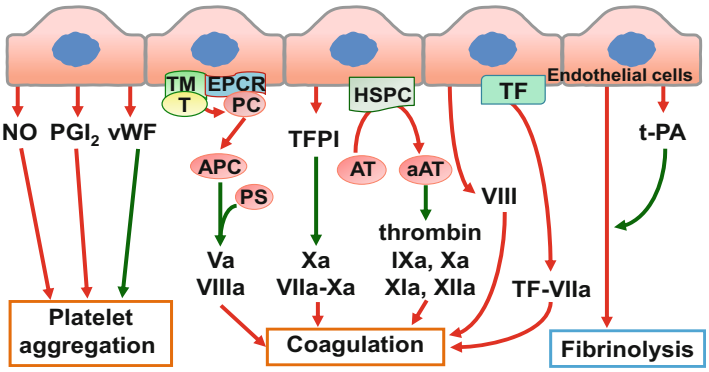

Fig. 3.2 Mechanism underlying the role of the endothelium in the hemostasis system. The endothelium may inhibit the platelet aggregation through nitric oxide (NO) and PGI_2 and promote platelet aggregation through von Willebrand factor (vWF). When blood vessels are injured and the underneath collagen is exposed, vWF binds to both collagen and platelets and consequently leads to platelet aggregation. The endothelium may inhibit coagulation through thrombomodulin (TM), heparan sulfate proteoglycan (HSPG), and tissue factor pathway inhibitor (TFPI). TM is expressed on the lumenal surface of the endothelial cells (ECs). Following the binding of TM to thrombin (T), protein C (PC) that is bound to nearby endothelial protein C receptor (EPCR) is activated. Activated protein C (APC) then forms a complex with its cofactor protein S (PS), resulting in the inactivation of activated coagulation factor V and VIII (Va and VIIIa, respectively). TFPI binds to activated coagulation factor X (Xa) or the tissue factor (TF)-activated coagulation factor VII (VIIa)–Xa complex to inhibit coagulation. Heparan sulfate proteoglycan (HSPG) is expressed on the lumenal surface of the endothelial cells (ECs). It may activate antithrombin (AT). The activated AT (aAT) can degrade thrombin and the activated coagulation factor IX, X, XI, and XII (IXa, Xa, XIa, and XIIa, respectively). The procoagulation effects of the endothelium are through the release of coagulation factor VIII and the exposure of TF, which occurs when stimulated with certain inflammatory molecules. TF can initiate coagulation through the tissue factor pathway by activating coagulation factor VII and then form a complex with the activated factor VII (TF-VIIa). ECs are the major producer of tissue plasminogen activator (t-PA) and plasminogen activator inhibitor-1 (PAI-1). t-PA promotes fibrinolysis by converting plasminogen to plasmin. The effect of t-PA is inhibited by PAI-1. The release of PAI-1 is increased in various disease states

3.6 Vasculogenesis and Angiogenesis

Blood vessels form either by vasculogenesis or angiogenesis. Vasculogenesis is the de novo formation of blood vessels. In the embryo, a subset of mesodermal cells differentiates into hemangioblasts, which further develop into angioblast, the precursors of endothelial cells. Vasculogenesis involves the differentiation, proliferation, and migration of the EC precursors to form a primitive vascular plexus, followed by arterial-venous differentiation (Heinke et al. 2012; Marcelo et al. 2013; Charpentier and Conlon 2014). Angiogenesis is the formation of blood vessels from the existing vasculature. It has two forms: sprouting angiogenesis (SA) and intussusceptive angiogenesis (IA). In SA, tip ECs project into the extracellular matrix through a disrupted basement membrane, followed by EC

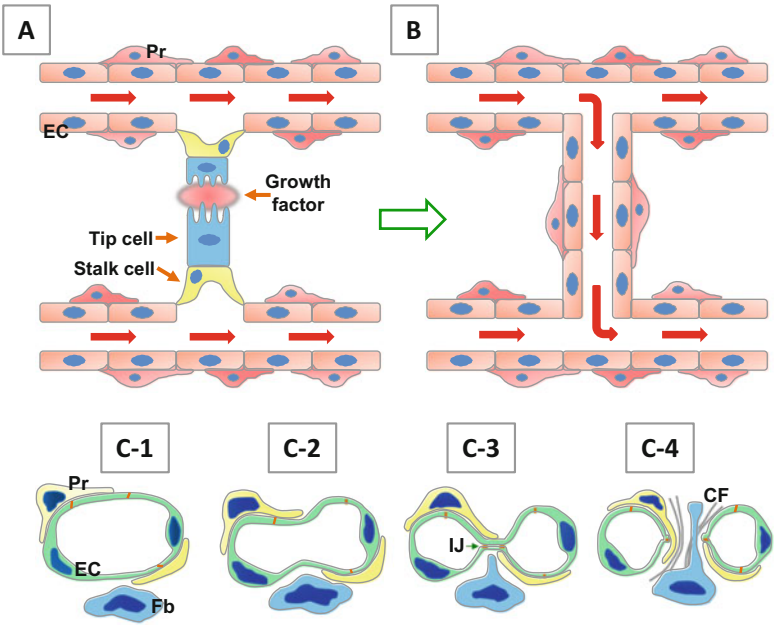

Fig. 3.3 Mechanisms of sprouting angiogenesis (*A* and *B*) and intussusceptive angiogenesis (*C-1–C-4*). *A* and *B*, under the stimuli of growth factors such as vascular endothelial growth factors A (VEGF-A), VEGF-C, and angiopoietin 2 (ANG2); a tip endothelial cell (EC) projects into the extracellular matrix through a disrupted basement membrane. The tip cell senses the angiogenic cues in microenvironment with its filopodial extensions. The cell trailing behind the tip cell is termed stalk cell, which exhibits a high proliferation rate, accompanied by lumenization and basement membrane formation. The sprouting continues until the tip cells of the adjacent vessels connect and form a continuous lumen. Meanwhile, the nascent vasculature is wrapped by pericytes (Pr) or vascular smooth muscle cells. This process is needed for the maturation and stabilization of the newly formed vasculature. *C-1–C-4*, the generation of new vascular segments by intussusceptive angiogenesis begins with the protrusion of opposing capillary walls into the vessel lumen (*C-1* and *C-2*) until they contact with each other and the formation of interendothelial junctions (IJ) (*C-3*).The endothelial bilayer is then perforated centrally, and the newly formed hole enlarges after being invaded by fibroblasts (Fb) and pericytes (Pr), which lay down collagen fibrils (CD) (*C-4*) (Figure *A* and *B* are modified from Herbert and Stainier (2011) with permission. Figure *C* is modified from Djonov et al. (2003) with permission)

elongation, vascular lumen formation, branching, and anastomosis (Herbert and Stainier 2011). In IA, the ECs on the opposite sides of a capillary or a small vessel protrude into its lumen to contact with each other; thereafter, the endothelial bilayer is perforated centrally, ECs retract, the newly formed hole increases in girth after being invaded by fibroblasts and pericytes, and thus the existing blood vessel is split into two (Djonov et al. 2003; Gianni-Barrera et al. 2014) (Fig. 3.3). Vasculogenesis occurs predominantly during embryonic period although may also occur postnatally such as in revascularization following trauma, tumor growth, and endometriosis by

circulating and residential endothelial progenitor cells (Luo et al. 2011). Angiogenesis is the primary way of new blood vessel formation whenever there is an existing vasculature both under physiological and pathophysiological conditions. In the angiogenic processes, the initial network is often formed through SA, and IA gradually takes over. SA is purely responsible for vascular growth, whereas IA also involves vascular remodeling through pruning of excessive blood vessels. IA allows a vast increase in the number of capillaries without a corresponding increase in the number of ECs. In comparison with SA, IA causes less interference with the local environments as endothelial migration and proliferation are kept to a minimum, which results in a relatively lower metabolic cost (De Spiegelaere et al. 2012).

The formation of new blood vessels is orchestrated by a plethora of molecular signals that carry communication between ECs and other cell types in a spatially and temporally defined pattern. In the embryonic stage, the differentiation of EC progenitors from the mesodermal precursors is regulated by fibroblast growth factor 2 (FGF-β), bone morphogenetic protein 4 (BMP4), and Indian hedgehog (IHH). Once endothelial cells are differentiated and coalesce into a vascular plexus, they are proliferated to form a circulatory network. This process is regulated by VEGF-A and its receptor VEGFR-1 (Flt-1) (Marcelo et al. 2013). In the process of SA, a single tip cell located at the apex of the sprout is formed under stimuli of exogenous growth factors such as VEGF-A, VEGF-C, and angiopoietin 2 (ANG2). The tip cell acts as a guide for the sprout by sensing the angiogenic cues in microenvironment with its filopodial extensions. The sprouting behavior of tip cell is facilitated by the VE-cadherin-mediated loosening of interendothelial junctions, the degradation of extracellular matrix by matrix metalloproteinase, and the detachment of pericytes. Meanwhile, adjacent ECs are prevented to transform into tip cells by Delta-like 4–Notch signaling. Those trailings behind the tip cell are termed stalk cells. These cells exhibit a high proliferation rate, accompanied by lumenization, and the formation of the capillary basement membrane. The EC sprouting continues until the tip cells connect with adjacent vessels and undergoes anastomosis to form a continuous lumen. The nascent vasculature is further wrapped by mural cells (pericytes and vascular smooth muscle cells). This process is critical for the maturation and stabilization of the new vascular networks and regulated by platelet-derived growth factor B (PDGFB) and transforming growth factor-β1 (TGFβ1) (Herbert and Stainier 2011; De Spiegelaere et al. 2012). Compared with SA, the mechanisms underlying IA are less well understood. Studies show that a surge in flow rate by 50–60% for 15–45 min induces IA within the areas of altered hemodynamics. The rapid response indicates that the alternation of gene expression is not involved. Data suggest that IA is also regulated by growth factors, particularly by VEGF (Gianni-Barrera et al. 2014).

References

Aird WC (2007a) Phenotypic heterogeneity of the endothelium: I. Structure, function, and mechanisms. Circ Res 100:158–173

Aird WC (2007b) Phenotypic heterogeneity of the endothelium: II. Representative vascular beds. Circ Res 100:174–190

Chang SH, Feng D, Nagy JA, Sciuto TE, Dvorak AM, Dvorak HF (2009) Vascular permeability and pathological angiogenesis in caveolin-1-null mice. Am J Pathol 175:1768–1776

Charpentier MS, Conlon FL (2014) Cellular and molecular mechanisms underlying blood vessel lumen formation. BioEssays 36:251–259

Claesson-Welsh L (2015) Vascular permeability-the essentials. Ups J Med Sci 120:135–143

Day RE, Kitchen P, Owen DS, Bland C, Marshall L, Conner AC, Bill RM, Conner MT (2014) Human aquaporins: regulators of transcellular water flow. Biochim Biophys Acta 1840:1492–1506

dela Paz NG, D'Amore PA (2009) Arterial versus venous endothelial cells. Cell Tissue Res 335:5–16

De Spiegelaere W, Casteleyn C, Van den Broeck W, Plendl J, Bahramsoltani M, Simoens P, Djonov V, Cornillie P (2012) Intussusceptive angiogenesis: a biologically relevant form of angiogenesis. J Vasc Res 49:390–404

De Taeye B, Smith LH, Vaughan DE (2005) Plasminogen activator inhibitor-1: a common denominator in obesity, diabetes and cardiovascular disease. Curr Opin Pharmacol 5:149–154

Djonov V, Baum O, Burri PH (2003) Vascular remodeling by intussusceptive angiogenesis. Cell Tissue Res 314:107–117

Everett LA, Cleuren AC, Khoriaty RN, Ginsburg D (2014) Murine coagulation factor VIII is synthesized in endothelial cells. Blood 123:3697–3705

Gerhardt T, Ley K (2015) Monocyte trafficking across the vessel wall. Cardiovasc Res 107:321–330

Gianni-Barrera R, Bartolomeo M, Vollmar B, Djonov V, Banfi A (2014) Split for the cure: VEGF, PDGF-BB and intussusception in therapeutic angiogenesis. Biochem Soc Trans 42:1637–1642

Giannotta M, Trani M, Dejana E (2013) VE-cadherin and endothelial adherens junctions: active guardians of vascular integrity. Dev Cell 26:441–454

Hallmann R, Mayer DN, Berg EL, Broermann R, Butcher EC (1995) Novel mouse endothelial cell surface marker is suppressed during differentiation of the blood brain barrier. Dev Dyn 202:325–332

Heinke J, Patterson C, Moser M (2012) Life is a pattern: vascular assembly within the embryo. Front Biosci (Elite Ed) 4:2269–2288

Herbert SP, Stainier DY (2011) Molecular control of endothelial cell behaviour during blood vessel morphogenesis. Nat Rev Mol Cell Biol 12:551–564

Kedem O, Katchalsky A (1958) Thermodynamic analysis of the permeability of biological membranes to non-electrolytes. Biochim Biophys Acta 27:229–246

Kim DY, Cho SH, Takabayashi T, Schleimer RP (2015) Chronic Rhinosinusitis and the coagulation system. Allergy Asthma Immunol Res 7:421–430

Komarova Y, Malik AB (2010) Regulation of endothelial permeability via paracellular and transcellular transport pathways. Annu Rev Physiol 72:463–493

Luo Z, Wang G, Wang W, Xiao Q, Xu Q (2011) Signalling pathways that regulate endothelial differentiation from stem cells. Front Biosci (Landmark Ed) 16:472–485

Marcelo KL, Goldie LC, Hirschi KK (2013) Regulation of endothelial cell differentiation and specification. Circ Res 112:1272–1287

Mehta D, Malik AB (2006) Signaling mechanisms regulating endothelial permeability. Physiol Rev 86:279–367

Michel CC, Curry FE (1999) Microvascular permeability. Physiol Rev 79:703–761

Mócsai A, Walzog B, Lowell CA (2015) Intracellular signalling during neutrophil recruitment. Cardiovasc Res 107:373–385

Muller WA (2015) The regulation of transendothelial migration: new knowledge and new questions. Cardiovasc Res 107:310–320

Olson ST, Richard B, Izaguirre G, Schedin-Weiss S, Gettins PG (2010) Molecular mechanisms of antithrombin-heparin regulation of blood clotting proteinases. A paradigm for understanding proteinase regulation by serpin family protein proteinase inhibitors. Biochimie 92:1587–1596

Predescu SA, Predescu DN, Malik AB (2007) Molecular determinants of endothelial transcytosis and their role in endothelial permeability. Am J Physiol Lung Cell Mol Physiol 293:L823–L842

Pries AR, Secomb TW, Gaehtgens P (2000) The endothelial surface layer. Pflugers Arch 440:653–666

Rusu L, Andreeva A, Visintine DJ, Kim K, Vogel SM, Stojanovic-Terpo A, Chernaya O, Liu G, Bakhshi FR, Haberichter SL, Iwanari H, Kusano-Arai O, Suzuki N, Hamakubo T, Kozasa T, Cho J, Du X, Minshall RD (2014) G protein-dependent basal and evoked endothelial cell vWF secretion. Blood 123:442–450

Sadler JE (1998) Biochemistry and genetics of von Willebrand factor. Annu Rev Biochem 67:395–424

Schubert W, Frank PG, Razani B, Park DS, Chow CW, Lisanti MP (2001) Caveolae-deficient endothelial cells show defects in the uptake and transport of albumin in vivo. J Biol Chem 276:48619–48622

Simionescu M, Simionescu N (1984) Ultrastructure of the microvascular wall: functional correlations. In: Handbook of physiology. American Physiological Society, Bethesda, pp 78–91

Smolenski A (2012) Novel roles of cAMP/cGMP-dependent signaling in platelets. J Thromb Haemost 10:167–176

Stewart PA (2000) Endothelial vesicles in the blood-brain barrier: are they related to permeability? Cell Mol Neurobiol 20:149–163

Sukriti S, Tauseef M, Yazbeck P, Mehta D (2014) Mechanisms regulating endothelial permeability. Pulm Circ 4:535–551

Suzuki K, Nichioka J, Hayaoni T, Kosaka Y (1988) Functionally active thrombomodulin is present in human platelets. J Biochem 104:628–632

Versteeg HH, Heemskerk JW, Levi M, Reitsma PH (2013) New fundamentals in hemostasis. Physiol Rev 93:327–358

Vestweber D (2015) How leukocytes cross the vascular endothelium. Nat Rev Immunol 15:692–704

Wood JP, Ellery PE, Maroney SA, Mast AE (2014) Biology of tissue factor pathway inhibitor. Blood 123:2934–2943

Wu KK, Thiagarajan P (1996) Role of endothelium in thrombosis and hemostasis. Annu Rev Med 47:315–331

Yau JW, Teoh H, Verma S (2015) Endothelial cell control of thrombosis. BMC Cardiovasc Disord 15:130

Chapter 4
Electrical and Mechanical Properties of Vascular Smooth Muscle

Abstract Vascular smooth muscle (VSM) manifests unique electrical and mechanical properties which impart profound influences on vascular contractility. The resting membrane potentials of VSM cells, although being mainly determined by the equilibrium potential of K^+, are markedly affected by a high concentration of intracellular Cl^-. The changes in membrane potentials associated with vasoconstriction are often graded depolarization rather than in action potentials, insensitive to blockade of Na^+ channels, and related to the activities of Cl^-, K^+, and voltage-dependent Ca^{2+} channels. These features help the vasculatures to response to various stimuli in a level-controlled manner. The mechanical activity of a muscle can be described based on tension, length, and velocity, which is mainly determined by the number of cross-bridge formed and the activity of actomyosin ATPase. VSM displays a high plasticity in the tension development when its length is altered and in the shortening speed when its load is changed. This is ascribed to a dynamic process of formation of cross-bridge by myosins and actins and lends VSM marked flexibility to meet different physiological needs. The above topic will be discussed in this chapter.

Keywords Membrane potential • Action potential • Slow waves • Ionic channels • Length • Tension • Velocity

4.1 Introduction

The electrical and mechanical properties are of fundamental importance in determining the responses of vascular smooth muscle (VSM). In striated muscle, action potentials are essential to initiate the release of Ca^{2+} from the sarcoplasmic reticulum that triggers contraction. In smooth muscle including VSM, the action potentials are not indispensible for the changes in cytosolic Ca^{2+} concentration needed for contraction, since the intracellular Ca^{2+} levels could be elevated not only by depolarization-induced activation of voltage-dependent Ca^{2+} channels (VDCCs) but also by receptor-mediated activation of phospholipase C (PLC) resulting in

Y. Gao, *Biology of Vascular Smooth Muscle: Vasoconstriction and Dilatation*,
DOI 10.1007/978-981-10-4810-4_4

inositol 1,4,5-trisphosphate (IP_3) receptor (IP_3R)-mediated Ca^{2+} release from the sarcoplasmic reticulum. However, the contraction of VSM is often a sustained activity and depends critically on the Ca^{2+} entry through VDCCs. Therefore, graded changes in membrane potentials regulated by Cl^-, K^+, and transient receptor potential (TRP) channels rather than action potentials constitute an important mechanism in the regulation of vasoactivities (Thorneloe and Nelson 2005; Kuo and Ehrlich 2015; Hübner et al. 2015; Earley and Brayden 2015). While the electrical properties have their effects mainly on the early steps of VSM response, the mechanical properties affect the outcome of VSM characterized by high plasticity. The basic contractile unit, the sarcomere, of striated muscle has a stable organization, and the force developed is constant under defined length of the muscle. By contrast, smooth muscles including VSM do not have definite basic contractile unit, and the number and arrangement of cross-bridge formed by actins and myosins could adjust under altered physiological states. Such a dynamic process provides VSM with remarkable capacity in the tension development under varying fiber lengths and shortening velocity under different loads (Ratz 2015). In the following section, the electrical properties of VSM, including the resting potentials, action potentials, and slow waves as well as their ionic basis, will be analyzed. The mechanical properties to be discussed will focus on the length–tension and force–velocity relationships of VSM.

4.2 Electrical Properties of Vascular Smooth Muscle

Due to a high cytosolic concentration of Cl^-, the resting membrane potential of VSM cells (VSMCs) is more positive than the equilibrium potential of K^+ compared with non-smooth muscle cells (Chipperfield and Harper 2000; Hübner et al. 2015). In VSMCs, the Na^+ influx is not important for the generation of action potential, which is in sharp contrast to those of skeletal and cardiac muscles. The action potential is often observed being associated with phasic vasoconstriction. However, a common electrical activity that occurred in vasoconstriction is graded depolarization without action potential (Holman et al. 1968; Johansson and Somlyo 1980). The depolarization is mediated by the activity of Cl^- channels and TRP channels. K^+ channels act as hyperpolarizing ion channels that provide a negative feedback on excitation (Thorneloe and Nelson 2005). In VSM, the contraction-dependent Ca^{2+} is predominantly derived from the voltage-dependent Ca^{2+} channels. By contrast, the sarcoplasmic reticulum is the major source of Ca^{2+} for contraction of striated muscle (Holman et al. 1968; Johansson and Somlyo 1980; Thorneloe and Nelson 2005). These distinct characteristics of the electrical properties exert a profound influence on the responsiveness of smooth muscle (Holman et al. 1968; Johansson and Somlyo 1980; Thorneloe and Nelson 2005; Kuo and Ehrlich 2015; Hübner et al. 2015).

4.2.1 Resting Membrane Potential

The resting membrane potential of mammalian cell is primarily determined by the concentration gradient of K^+, Na^+, and Cl^- across cell membrane and the permeability of the membrane. For each individual ion, if fully permeable, its contribution to the resting membrane potential can be calculated by the Nernst equation:

$$V_{Eq} = \frac{RT}{zF} \cdot \ln\left(\frac{[Ion]_{out}}{[Ion]_{in}}\right) \tag{4.1}$$

where V_{Eq} is the equilibrium potential (Nernst potential) for a particular ion when its diffusion across cell membrane driven by the concentration gradient is balanced by the electric gradient created by the concentration gradient. Note that the unit of V_{Eq} is the volt but typically reported in millivolts (mV). R is the universal gas constant (8.314 Joules per Kelvin per mole). T is the temperature in Kelvin (K = °C + 273.15). z is the valence of the ionic species. F is the Faraday's constant (96,485 Coulombs per mole). The subscripts "out" and "in" of the ion in square brackets are the extracellular and intracellular concentration for the ion, respectively. Assuming the intra- and extracellular concentrations of K^+ in VSMCs are 150 and 5.9 mM, respectively, V_{Eq} for K^+ (E_K) is −86 mV at 37 °C. The concentrations of Na^+ and Cl^- are more concentrated in the extracellular medium (145 mM and 125 mM, respectively) than intracellularly (10 mM and 35 mM, respectively). The V_{Eq} for Na^+ (E_{Na}) is +61 and while that for Cl^- (E_{Cl}) is −34 mV (Johansson and Somlyo 1980; Layton and Edwards 2014; Hübner et al. 2015). It is worth to note that it is generally believed that Cl^- is passively distributed across cell and that the V_{Eq} value for Cl^- is similar to that of K^+. However, in smooth muscle cells, E_{Cl} is substantially more positive than E_K due to a high intracellular concentrations of Cl^-, which results from Cl^-/HCO_3 exchange, (Na + K + Cl) cotransport, and probably pump III activity (Chipperfield and Harper 2000; Hübner et al. 2015).

The resting membrane potential is affected by the V_{Eq} of K^+, Na^+, and Cl^- as well as cellular permeabilities of these ions. It can be calculated by using the Goldman–Hodgkin–Katz equation (GHK equation):

$$V_m = \frac{RT}{F} \cdot \ln\left(\frac{pK \cdot [K^+]_{out} + pNa \cdot [Na^+]_{out} + pCl \cdot [Cl^-]_{in}}{pK \cdot [K^+]_{in} + pNa \cdot [Na^+]_{in} + pCl \cdot [Cl^-]_{out}}\right) \tag{4.2}$$

where V_m is the membrane potential and pK, pNa, and pCl are the relative cellular permeabilities for K^+, Na^+, and Cl^-, respectively. In VASCs, they are approximately 1, 0.1, and 1, respectively (with pK as 1 because in most cells at rest pK is larger than pNa and pCl) (Johansson and Somlyo 1980). R, T, F, and the subscripted "out" and "in" are the same terms used in Eq. 4.1. Using the values of intra- and extracellular concentrations of K^+, Na^+, and Cl^- as well as the cellular permeabilities of these ions aforementioned, the resting membrane potential yielded by GHK equation is −43 mV. The resting membrane potentials of smooth muscle cells in

arteries and arterioles measured in vitro are between −40 and −70 mV (Holman and Surprenant 1980; Nelson and Quayle 1995) and measured in vivo are in the range of −40 to −55 mV (Nelson and Quayle 1995). The membrane potential is considerably more positive than the E_K (~ −86 mV). This may be ascribed to rather high E_{Cl} (−34 mV) that resulted from a high concentration of intracellular Cl^- (Chipperfield and Harper 2000; Hübner et al. 2015). The heterogeneity in resting membrane potential between different VSMCs may also result from the variance in Na^+/K^+ pump activity (Johansson and Somlyo 1980).

4.2.2 Action Potentials

Action potentials have been recorded in a variety of blood vessels with different configurations, such as a single spike or spike bursts; they may have a more prolonged time course and may resemble cardiac action potentials with an early rapid component followed by a plateau. The action potentials of VSM cells differ in many aspects from those in the nerve and skeletal muscle. For instance, the action potentials in portal–mesenteric veins are insensitive to tetrodotoxin, a blocker of voltage-gated sodium channels, and insensitive to reduction in the concentration of extracellular Na^+. Instead, they are blocked by the removal of extracellular Ca^{2+} and the blocker of L-type voltage-gated Ca^{2+} channels. Hence, the current carried by Ca^{2+} rather than Na^+ through voltage-gated Ca^{2+} channels plays a major role in the generation of action potentials (Holman et al. 1968; Johansson and Somlyo 1980; Gokina et al. 1996). Although action potentials often lead to the development of vessel tension, vasoconstriction of various blood vessels often occurs with only membrane depolarization, with moderate change in membrane potential, or even without change in membrane potential (Su et al. 1964; Holman et al. 1968; Johansson and Somlyo 1980; Bolton et al. 1984; Gokina et al. 1996). For instance, the contractile response of rabbit pulmonary arteries elicited by sympathetic nerve stimulation and norepinephrine shows no change in membrane potential (Su et al. 1964). In guinea-pig mesenteric arteries, the increase in tension caused by norepinephrine is associated with a substantially less depolarization as compared with that caused by high potassium (Bolton et al. 1984). It is generally accepted that, while vasoconstriction to high potassium results mainly from depolarization-elicited Ca^{2+} entry, vasoconstriction to neurotransmitters and humoral agents is mediated by both receptor-mediated Ca^{2+} release of sarcoplasmic reticulum and by the entry of extracellular Ca^{2+} as well as the sensitization of myofilaments to Ca^{2+} (Thorneloe and Nelson 2005; Kuo and Ehrlich 2015).

4.2.3 Roles of Ionic Channels

The membrane potential and changes in membrane potential including action potentials reflect the activities of ionic channels. In VSMCs, the ionic channels

closely associated with the electric activities are K^+, Ca^{2+}, Cl^-, and TRP channels. With more than 78 genes encoding pore-forming subunits in the human genome, K^+ channels constitute the largest ion channel family. In vascular smooth muscle, five major types of K^+ channels have been identified as modulators of membrane potential and contractility, which are voltage-gated (Kv), large-conductance Ca^{2+}-activated (BK), inward rectifier (Kir), ATP-sensitive (K_{ATP}), and two-pore-domain (K2P) K^+ channels (Nelson and Quayle 1995; Feliciangeli et al. 2015). The K2P K^+ channels are open at all voltages and thought to underlie many background K currents. K2P6.1, a member of the K2P K^+ channel family, is highly expressed in the vascular system. The resting membrane potential of freshly dispersed VSMCs depolarizes by ~17 mV in mice lacking K2P6.1 channels compared with wild-type littermates, indicating a critical role of this K2P K^+ subunit in the maintenance of the resting membrane potential (Lloyd et al. 2011). Among the other types of K^+ channels, Kv channels are activated by membrane potential depolarization with activation thresholds in the range of −50 to −30 mV. BK channels are activated by membrane depolarization and/or elevation of intracellular Ca^{2+}. These two types of K^+ channels function in a negative feedback mechanism to limit depolarization and Ca^{2+} entry. The K_{IR} channel is more active at negative membrane potentials and is therefore involved in regulating the membrane potential of VSMCs in the absence of extrinsic influences that depolarize. When extracellular K^+ is increased (up to 15 mM), conditions that occur physiologically during hypoxia, ischemia, or hypoglycemia, K^+ equilibrium potential becomes less negative. This leads to an increased outward current through K_{IR} channels, membrane hyperpolarization, and vasodilation. K_{ATP} channels are members of the inward rectifier family and are voltage-independent. They are inhibited by cytoplasmic ATP and activated with ATP depletion during hypoxia or metabolic inhibition (Nelson and Quayle 1995; Thorneloe and Nelson 2005).

The VDCCs can be grouped into the high-voltage-activated dihydropyridine-sensitive (L-type, CaV1.1–1.4) and -insensitive (P-, Q-, R-, N-type, Cav2.1–2.3) channels as well as the low-voltage-activated (T-type, CaV3.1–3.3) channels. In vascular smooth muscle, dihydropyridine-sensitive L-type Ca^{2+} channels provide the major source of contractile Ca^{2+}; the expression pattern and current density of other VDCC types may differ among different vasculatures (Thorneloe and Nelson 2005). In addition to the VDCCs, the membrane depolarization and Ca^{2+} influx can also mediated by the TRP channels. Mammalian genomes encode 28 distinct TRP protein subunits, which comprise a large number of nonselective cation channels with a variable degree of Ca^{2+} permeability. These TRP channels are grouped into six subfamilies: canonical, vanilloid, melastatin, ankyrin, polycystic, and mucolipin TRPs. Unlike VDCCs, TRP channels are not sensitive to voltage changes. Instead they can sense a variety of other stimuli including pressure, shear stress, mechanical stretch, oxidative stress, lipid environment alterations, hypertrophic signals, and inflammation products (Earley and Brayden 2015; Yue et al. 2015). In blood vessels, stretch of the plasma membrane of smooth muscle cell may activate G-protein-coupled receptors (GPCRs) and leads to generation of diacyl glycerol (DAG) and inositol 1,4,5-trisphosphate (IP_3),

resulting in DAG-mediated TRPC6 activation and extracellular Ca^{2+} influx and IP_3-induced Ca^{2+} release from the sarcoplasmic reticulum. The localized increase in Ca^{2+} triggers Ca^{2+}-induced Ca^{2+} release and activating TRPM4. Currents through TRPC6 and TRPM4 depolarize the plasma membrane, activate VDCCs, and lead to vasoconstriction (Hill-Eubanks et al. 2014).

In VSMCs the cytosolic Cl^- concentration is normally ranged from 28 to 44 mM. Thus, the estimated E_{Cl} will be between −40 and −28 mV, which is above resting membrane potential in the majority of smooth muscles. Hence, opening of Cl^- channels in the plasma membrane of VSMCs causes a depolarizing Cl^- efflux, which results in the activation of VDCCs, elevation of cytosol Ca^{2+}, and vasoconstriction (Hübner et al. 2015). Cl^- channels identified in VSMCs include Ca^{2+}-activated Cl^- channels (Cl_{Ca}), cGMP-dependent Cl_{Ca} channels, cAMP-regulated cystic fibrosis transmembrane conductance regulator (CFTR), and volume-regulated Cl^- channels (VRACs). The Cl_{Ca} channels in VSMCs are largely generated by the dimerization of the transmembrane member 16A (TMEM16A), while expression of TMEM16B appeared to be very low. Gating of TMEM16A is both voltage and Ca^{2+} dependent, and Ca^{2+} exerts its effect by directly binding to the channel protein. Activation of TMEM16A by localized increase in cytosolic Ca^{2+} may be critically involved in the stretch-regulated Cl^- current in the myogenic response, which helps to maintain blood flow constant in the face of fluctuations of perfusion pressure (Hübner et al. 2015; Tykocki and Nelson 2015). A Cl_{Ca} activity distinct from that of TMEM16A Cl_{Ca} has also been observed in vascular smooth muscle that requires the presence of cGMP to function. Its molecular identity is unclear, but bestrophins, a family of four proteins (1 through 4), have been considered as the candidate (Bulley and Jaggar 2014). Activation of CFTR occurs at membrane potentials positive to E_{Cl}, hence causing Cl^- influx, hyperpolarization, and vasodilatation. Such a mechanism may not take place in all types of VSMCs, as the expression of CFTR varies considerably along the vascular tree (Bulley and Jaggar 2014; Hübner et al. 2015). VRAC may be important for VSMC proliferation. Its molecular identity in vasculatures is proposed to be Cl^- channel-3 (ClC-3), a member of the ClCn gene family (Bulley and Jaggar 2014).

4.2.4 Slow Waves and Vasomotion

In small resistance vessels of the microcirculation as well as in larger arteries and veins, the cell membrane potential may oscillate with a non-perfect sine wave appearance know as slow wave. The slow wave may occur spontaneously or in response to pressure, stretch, and vasoconstrictors and often precede rhythmic vasocontraction, which is termed vasomotion (Aalkjaer and Nilsson 2005; Haddock and Hill 2005; Seppey et al. 2010) (Fig. 4.1). The slow wave is generally recognized being caused by the cyclic changes in the cytosolic Ca^{2+} concentrations ($[Ca^{2+}]_i$) due to the release of Ca^{2+} from the sarcoplasmic reticulum through inositol trisphosphate (IP_3)- and/or ryanodine-activated Ca^{2+} channels. In iris arterioles,

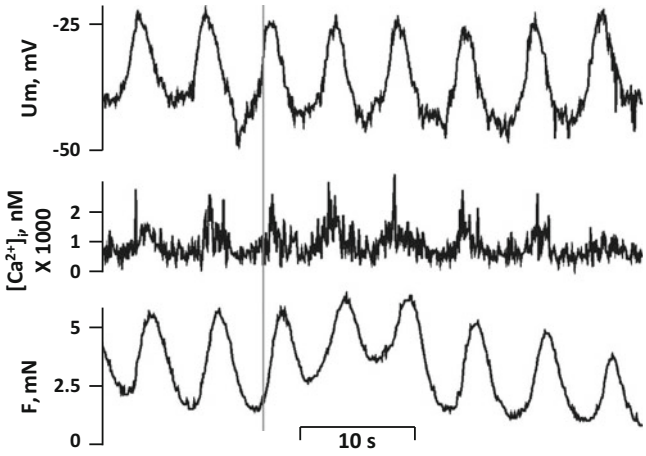

Fig. 4.1 Simultaneous measurements of membrane potential (upper panel), intracellular Ca^{2+} level ($[Ca^{2+}]_i$ middle panel), and isometric force (lower panel) in an isolated rat mesenteric small artery. As is shown, the membrane potential oscillations precede $[Ca^{2+}]_i$ oscillations, and the $[Ca^{2+}]_i$ oscillations precede cyclic change in isometric force (The figure is from Aalkjaer and Nilsson (2005), with permission)

the IP_3-evoked cyclical release of calcium is activated by cross talk between the phospholipase C and phospholipase A2 pathways. The Ca^{2+} oscillations are coincident with cyclical depolarizations. Synchronization the Ca^{2+} waves through gap junctions results in vasomotion. Interestingly, the vasomotion is insensitive to inhibitors of VDCCs and voltage clamp, suggesting that vasomotion of iris arterioles is independent of the slow waves of the cell membrane (Haddock et al. 2002). Although the release of Ca^{2+} from IP_3 and/or ryanodine stores and a regenerative mechanism of Ca^{2+}-induced Ca^{2+} release may be sufficient to lead to rhythmic vasocontraction in some vessels, most often, Ca^{2+} entry through VDCCs results from cyclical depolarizations of the membrane is essential for the synchronization of the Ca^{2+} waves. Indeed, in most vasculatures studied, inhibitors of VDCCs reduce or eliminate slow waves, desynchronize Ca^{2+} waves, and abolish vasomotion (Haddock and Hill 2005).

In rat mesenteric small arteries, the oscillations in membrane potential, $[Ca^{2+}]_i$, and tone disappear with ionic thiocyanate (SCN^-, a Cl^- substitute). Whole-cell patch-clamp experiments on rat mesenteric small artery VSMC show that Cl^- conductances are suppressed. These results implicate that Cl_{Ca} channels may be critically involved in the formation of slow wave formation and cyclic vasocontraction (Boedtkjer et al. 2008). An important role for Cl_{Ca} channels, both cGMP dependent and independent, in the activities of slow waves and vasomotion has been implicated in a number of arteries (Haddock and Hill 2005). While Cl_{Ca} channels may contribute to the depolarization portion of slow waves, evidence suggests that the microdomains formed by ryanodine receptors (RyRs) of sarcoplasmic reticulum and BK channels of the adjacent plasma membrane may be

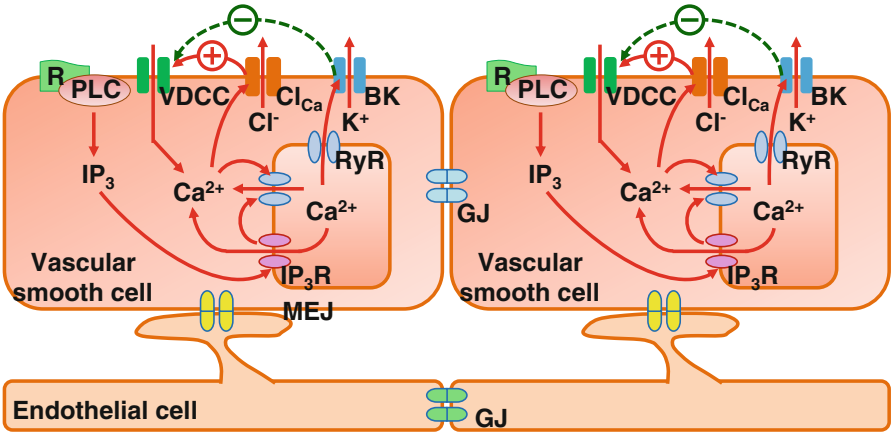

Fig. 4.2 Possible mechanisms for the generation and synchronization of the slow wave. The slow wave is initiated by the oscillation of intracellular Ca^{2+} levels $[Ca^{2+}]_i$, which results from Ca^{2+} release of sarcoplasmic reticulum (SR) through inositol 1,4,5-trisphosphate (IP_3) receptor (IP_3R) and ryanodine receptors (RyRs). An elevated IP_3 level occurs when the G-protein-coupled receptors are stimulated followed by the activation of phospholipase C (PLC); in some arteries, a constitutive activity of PLC may exist. The elevated $[Ca^{2+}]_i$ could activate Ca^{2+}-dependent chloride channels (Cl_{Ca}), which leads to increased outflow of intracellular Cl^- and the membrane depolarization, followed by the opening of voltage-dependent Ca^{2+} channels (VDCC) and extracellular Ca^{2+} influx. This Ca^{2+} influx causes Ca^{2+}-induced Ca^{2+} release (CICR) through RyRs. CICR can also be stimulated by Ca^{2+} released from IP_3Rs, and both RyR- and IP_3R-mediated Ca^{2+} releases are suppressed by high $[Ca^{2+}]_i$. While the Cl_{Ca}-mediated membrane depolarization contributes to the upper rising of slow waves, the opening of Ca^{2+}-activated K^+ channels (BK) by Ca^{2+} released from RyRs of the SR adjacent to cell membrane causes hyperpolarization and closing of the VDCCs. The synchronization of slow waves and the $[Ca^{2+}]_i$ oscillations between adjacent smooth muscle cells may occur through electrical coupling via the gap junctions (GP) between neighboring vascular smooth muscle cells (VSMCs) as well as via the myoendothelial junctions (MEJ) and GPs between the endothelial cells (ECs). The MEJs and GPs between ECs are more abundant than GPs between VSMCs. The MEJ- and GP-mediated cross talks through transfer of Ca^{2+} and IP_3 may be also involved. The *solid line arrow*: stimulatory. The *dotted line arrows*: inhibitory

related to the opening of BK channels by RyR-mediated Ca^{2+} sparks (Tykocki and Nelson 2015). Vasomotion is generated by the synchronization of the cyclic Ca^{2+} waves among sufficient smooth muscle cells. This may be achieved by the intercellular spread of membrane potential oscillations as well as Ca^{2+} and/or IP_3 signalings through gap junctions. Alternatively, these signalings may communicate between VSMCs through the myoendothelial junctions (MEJs). Studies show that MEJs are more abundant in the gap junctions between smooth muscles. The endothelium may act as a favorable pathway for the signal transmission along blood vessels (Haas and Duling 1997; Haddock and Hill 2005; Gao et al. 2016) (Fig. 4.2).

4.3 Mechanical Properties of Vascular Smooth Muscle

The study of the mechanical properties of vascular smooth muscle is of fundamental importance to understand the circulatory functions. Unlike many biochemical and molecular studies, the techniques available currently make it possible the real-time measurements and analyses of mechanical response of the vasculature with high precision, sensitivity, and reproducibility (Ratz 2015). In the following sections, the basic mechanical properties of vascular smooth muscle, i.e., the length–tension relationship, the force–velocity relationship, and the functions of elastic and collagenous fibers, will be discussed.

4.3.1 Length–Tension Relationship

Muscle contractions are manifested as changes in tension and length. When tension changes without changes in muscle length, the contraction is termed as isometric. When the isometric tensions are measured following each stepwise stretch of the muscle, with and without stimulation, a length–tension relationship of the muscle can be constructed. The tension observed under no stimulation, known as passive tension, results from the stretch of the elastic components of the muscle. The increase in tension caused by stimulation is termed active tension. As the length of the muscle increases from its unstretched status, both the passive tension and the stimulation-induced active tension increase. While the passive tension continually increases with the stretch, the active tension will reach a plateau, and further stretch will lead to declined active tension. The muscle length that the maximal active tension is obtained is known as the optimal length, which occurs when the most cross-bridges are formed by actins and myosins (Herlihy and Murphy 1973; Zhang et al. 2007; Bednarek et al. 2011; Ratz 2015) (Fig. 4.3). The active length–tension curves generated by striated muscles are acutely static, adapting only slowly after alternated gene transcription and translation of specific sarcomeric proteins (Willis et al. 2009; Bednarek et al. 2011). By contrast, the active length–tension curves of smooth muscle display a longer working length range and broader optimal length range and can adapt acutely, causing shifts in the length–tension curve along the length axis (Tuna et al. 2012). In rabbit carotid artery, the setting of the vessel length to 67% or 133% of the optimal length decreases active tensions to ~75% and ~93% of maximal contraction, respectively. After an adaptation period of 27 min during which the muscle is stimulated at the same lengths once every 5 min, the active tensions are recovered to ~85% and ~98% of maximal contraction, respectively (Seow 2000). A leftward shift in the length–tension relationship has also been observed by incubation of the small mesenteric artery with vasoconstrictor endothelin (Tuna et al. 2013). These adaptational changes in active tension may result from actin polymerization, involved in both the formation of cross-bridges and reorganization of cytoskeletons (Tuna et al. 2012). Studies show that the active

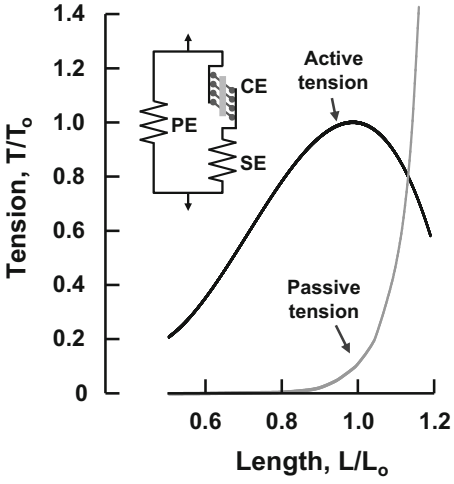

Fig. 4.3 Length–tension relationship of isolated arteries. Left panel, active and passive tension of porcine carotid arterial strips under different lengths. Based on the Hill's muscle model, which is composed of a contractile element (CE), an elastic elements in series (SE), and an elastic elements in parallel (PE) with the CE, the active tension is generated by the contractile response of the artery, which is at maximum (T_o) when the artery is stretched to the optimal length (L_o). Tension (T) and length (L) of the arteries are expressed as the ratio to T_o and L_o, respectively (The figures is modified from Herlihy and Murphy (1973), with permissions)

tension adaptation of the artery rabbit femoral artery is prevented by the inhibition of actin polymerization with cytochalasin-D (Bednarek et al. 2011). Apart from actins, myosin filaments in smooth muscles also undergo assembly and disassembly in a dynamic equilibrium (Black et al. 2009; Milton et al. 2011). It is likely that a dynamic remodeling of cross-bridges is critically involved in the adaptation of tension generation when encountered with length changes.

The length–tension characteristics of a muscle are contributed by both active and passive tension component. The muscle mechanical response can be represented by the Hill's muscle model, which is composed of a contractile element, and two elastic elements, one in series and one in parallel. The contractile element refers to the actin and myosin machinery. The parallel elastic element represents the passive tension evoked by stretch of the connective tissues surrounding the contractile filaments. The serial elastic element represents the intrinsic elastic tension of the myofilaments (Fig. 4.3) (Martins et al. 1998). During isometric contractions, the serial elastic component is under tension and therefore is stretched. Since the muscle length is kept constant, the stretching of the serial element occurs due to an equal shortening of the contractile element. Therefore, the tension generated by the contractile element (T_C) is equal to that of the serial elastic element (T_S). The total tension is the sum of that generated by the contractile element (T_C) and that generated by the parallel elastic element (TP). Meanwhile, the muscle length (L) is

equal to the length of the parallel elastic element (LP), which is also equal to the length of the contractile element (LC) plus the length of the serial elastic element (Roach and Burton 1957; Ratz 2015).

4.3.2 Functions of Elastic and Collagenous Fibers

The passive tension evoked by stretch is primarily derived from elastic and collagenous fibers. Elastic fibers are complex structures that contain elastin as well as microfibrils. Microfibrils are 10- to 15-nm filaments that are believed to facilitate elastin assembly and provide overall structure to the growing elastic fiber. Elastin is the major protein that imparts the property of elasticity. It is an insoluble polymeric protein formed through lysine-mediated cross-linking of its soluble monomeric precursor tropoelastin, a protein encoded by a single gene ELN (Wagenseil and Mecham 2009; Ratz 2015). More than 28 types of collagen have been identified. Among them, 17 different collagen types are present in the vasculature, with types I and III being mainly responsible for imparting strength to the vessel wall. Collagenous fibers are made up of collagen fibrils, which are formed by multiple tropocollagen molecules through hydroxylysine and lysine-mediated cross-links. Collagen may be attached to cell membranes via several types of protein, including fibronectin and integrin (Wagenseil and Mecham 2009). Elastic fibers are highly elastic, with an elastic modulus, which is the force per cross-sectional area required to stretch the material to twice its initial length, of ~$3 \cdot 10^6$ dyne/cm^2. By contrast, collagenous fibers are much harder to be stretched with high elastic modulus of ~$1 \cdot 10^9$ dyne/cm^2 (Burton 1954). Elastic fibers are relatively straight at rest and act as an efficient spring that stores mechanical energy, assisting in shape recovery upon shortening. Arterial collagenous fibers are tortuous and not tensioned at short tissue lengths. As the stretch is increased, collagenous fibers begin to straighten, and collagenous fibers of different lengths are sequentially recruited as load-bearing structures (Ratz 2015). The relative contribution of elastic fibers to collagenous fibers to passive tension has been studied in arteries by comparing the tension vs. circumference of preparations before and after digestion of collagen by formic acid and digestion of elastin by trypsin (containing an elastase). These studies suggest that the resistance to stretch at low pressures is almost entirely due to elastic fibers and that at physiological pressures is due to both collagenous and elastic fibers. At high pressures, the tension in the wall would rise rapidly with little further deformation, almost entirely due to collagenous fibers (Roach and Burton 1957).

The elastic and collagenous fibers provide the necessary maintenance tension, without the expenditure of energy, to withstand the stress of pressures across the wall of the blood vessel. In arteries, they are a medium for pressure wave propagation to help blood flow. They would have the function of producing stability of the wall of the blood vessel by making possible a graded constriction or dilation under vasomotor tone. Assuming there is only smooth muscle that is present in the wall of

the blood vessel, an increased tension caused by vasoconstriction would naturally decrease the radius of the vessel. According to the law of Laplace, $T = P \cdot r$, where T is the total tangential tension, in dynes per centimeter length of the vessel; P is the pressure in dynes per square centimeter (1 mm. Hg = 1330 dynes/cm^2); and r is the radius in centimeters. The decreased vessel radius will require a smaller tension to be held in equilibrium rather than an increased tension. Thus, the higher vessel tension under vasoconstriction would overwhelm and make the vessel to constrict further until it completed closed. Conversely, if the vessel tension were to decrease caused by vasodilators and began to "lose" in the struggle with the pressure, it would continue to lose and "blowout" would occur. Hence, to maintain the stability of the wall of a blood vessel, there must be an elastic tension in the wall, depending on stretch, which automatically changes as the vessel changes its size, so that Laplace's law is satisfied. Clearly, the elastic tissue in the blood vessel wall, acting in cooperation with the smooth muscle, is essential to make possible stable-graded contraction (Burton 1954; Ratz 2015).

4.3.3 Force–Velocity Relationship

When a muscle contracts isotonically, an increase in the load of the muscle, which means an increased force generated, is associated with a declined shortening speed of the muscle. When the load of the muscle is zero, its shortening speed reaches the maximum (V_o); conversely, the maximum force (f_o) generated by the muscle occurs when its shortening speed is at zero. The force–velocity relationship for a particular muscle can be empirically determined. The muscle is first stimulated isometrically at its optimal length. During the rising phase of the contraction at a force value that is a fraction of f_o, the muscle is load-clamped quickly and permitted to shorten isotonically. These steps are repeated with the muscle load-clamped at various fractional f_o values so that a plot of force vs. velocity is curve fitted and extrapolation of the curve to zero load provides an estimate of V_o. The force–velocity curve can be expressed as a rectangular hyperbola Hill's equation: $V = \beta \cdot (f_o - f)/(f + \alpha)$, where V is velocity, f is force, and α and β are force and velocity asymptotes, respectively. The mechanical work (power) is the product of force and velocity, as shown in the figure; the optimal shortening velocity for power generation is approximately one-third of maximum shortening velocity (Fig. 4.4) (Hill 1938; Herlihy and Murphy 1974).

The isotonic shortening velocity of a muscle reflects cross-bridge cycling rates, and the V_o is probably the best index of average cross-bridge cycling rate (Hai and Murphy 1989; Ratz 2015). The shortening velocity of vascular smooth muscle is distinctively different from those of striated muscles, which may be primarily ascribed to the difference in the isoforms of myosins (Canepari et al. 2010; Reho et al. 2014). Moreover, in striated muscle, the sarcomere has a constant length, and the numbers of myosins and actins are stable. In smooth muscle including VSM, thin and thick filament mass can be added during contraction. Doubling the number of filaments acting in series would double velocity, while doubling the number of

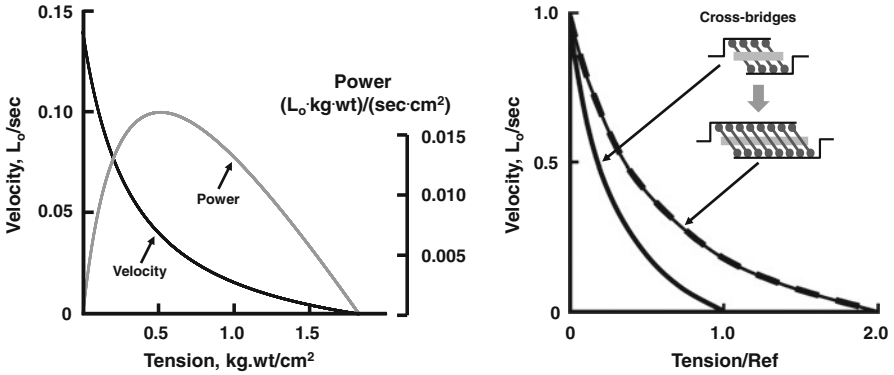

Fig. 4.4 Force–velocity relationship of isolated arteries. *Left panel*, force–velocity (*solid line*) and power output (*gray line*) curves for porcine carotid strips. The force–velocity curve is expressed as a rectangular hyperbola Hill's equation: $V = \beta \cdot (f_o - f)/(f + \alpha)$, where V is velocity and f and f_o are isometric tension with f_o measured at the optimal length. α and β are determined by plotting $(1-f/f_o)/V$ against f/f_o to obtain a linearized form of the Hill's equation, with the slope that is $1/\beta$ and the intercept at the abscissa that is $-\alpha/f_o$. The maximum velocity of shortening (V_{max}) under conditions of zero after load is to be obtained from the ordinate intercept and equals $f_o \cdot \beta/\alpha$. The power output curve is the product of velocity and tension. *Right panel* shows that the tension generated by smooth muscle may double without affecting the maximal velocity when the number of cross-bridges is doubled. Note the tension is expressed as ratio of control conditions (The figure in the *left panel* is modified from Herlihy and Murphy (1974) and that in the *right panel* from Ford (2005), with permissions)

filaments acting in parallel would double tension (Ratz et al. 1989; Ford 2005) (Fig. 4.4). Arterioles from hamster cheek pouch with higher myogenic tone is found with higher V_0 than those with lower myogenic tone, and increased V_o also occurs when stimulated with norepinephrine (Davis and Davidson 2002).An increased shortening speed is also observed in caudal arteries of the spontaneously hypertensive rats (SHRs) as compared with those of the normotensive Wistar Kyoto (WKY) rats (Packer and Stephens 1985).

References

Aalkjaer C, Nilsson H (2005) Vasomotion: cellular background for the oscillator and for the synchronization of smooth muscle cells. Br J Pharmacol 144:605–616

Bednarek ML, Speich JE, Miner AS, Ratz PH (2011) Active tension adaptation at a shortened arterial muscle length: inhibition by cytochalasin-D. Am J Physiol Heart Circ Physiol 300: H1166–H1173

Black J, Dykes A, Thatcher S, Brown D, Bryda EC, Wright GL (2009) FRET analysis of actin-myosin interaction in contracting rat aortic smooth muscle. Can J Physiol Pharmacol 87:327–336

Boedtkjer DM, Matchkov VV, Boedtkjer E, Nilsson H, Aalkjaer C (2008) Vasomotion has chloride-dependency in rat mesenteric small arteries. Pflugers Arch 457:389–404
Bolton TB, Lang RJ, Takewaki T (1984) Mechanisms of action of noradrenaline and carbachol on smooth muscle of guinea-pig anterior mesenteric artery. J Physiol 351:549–572
Bulley S, Jaggar JH (2014) Cl^-channels in smooth muscle cells. Pflugers Arch 466:861–872
Burton AC (1954) Relation of structure to function of the tissues of the wall of blood vessels. Physiol Rev 34:619–642
Canepari M, Pellegrino MA, D'Antona G, Bottinelli R (2010) Skeletal muscle fibre diversity and the underlying mechanisms. Acta Physiol (Oxf) 199:465–476
Chipperfield AR, Harper AA (2000) Chloride in smooth muscle. Prog Biophys Mol Biol 74:175–221
Davis MJ, Davidson J (2002) Force-velocity relationship of myogenically active arterioles. Am J Physiol Heart Circ Physiol 282:H165–H174
Earley S, Brayden JE (2015) Transient receptor potential channels in the vasculature. Physiol Rev 95:645–690
Feliciangeli S, Chatelain FC, Bichet D, Lesage F (2015) The family of K2P channels: salient structural and functional properties. J Physiol 593:2587–2603
Ford LE (2005) Plasticity in airway smooth muscle: an update. Can J Physiol Pharmacol 83:841–850
Gao Y, Chen T, Raj JU (2016) Endothelial and smooth muscle cell interactions in the pathobiology of pulmonary hypertension. Am J Respir Cell Mol Biol 54:451–460
Gokina NI, Bevan RD, Walters CL, Bevan JA (1996) Electrical activity underlying rhythmic contraction in human pial arteries. Circ Res 78:148–153
Haas TL, Duling BR (1997) Morphology favors an endothelial cell pathway for longitudinal conduction within arterioles. Microvasc Res 53:113–120
Haddock RE, Hill CE (2005) Rhythmicity in arterial smooth muscle. J Physiol 566:645–656
Haddock RE, Hirst GD, Hill CE (2002) Voltage independence of vasomotion in isolated irideal arterioles of the rat. J Physiol 540:219–229
Hai CM, Murphy RA (1989) Ca^{2+}, crossbridge phosphorylation, and contraction. Annu Rev Physiol 51:285–298
Herlihy JT, Murphy RA (1973) Length-tension relationship of smooth muscle of the hog carotid artery. Circ Res 33:275–283
Herlihy JT, Murphy RA (1974) Force-velocity and series elastic characteristics of smooth muscle from the hog carotid artery. Circ Res 34:461–466
Hill AV (1938) The heat of shortening and the dynamic constants of muscle. Proc R Soc Lond B 126:136–195
Hill-Eubanks DC, Gonzales AL, Sonkusare SK, Nelson MT (2014) Vascular TRP channels: performing under pressure and going with the flow. Physiology (Bethesda) 29:343–360
Holman ME, Surprenant A (1980) An electrophysiological analysis of the effects of noradrenaline and alpha-receptor antagonists on neuromuscular transmission in mammalian muscular arteries. Br J Pharmacol 71:651–661
Holman ME, Kasby CB, Suthers MB, Wilson JA (1968) Some properties of the smooth muscle of rabbit portal vein. J Physiol 196:111–132
Hübner CA, Schroeder BC, Ehmke H (2015) Regulation of vascular tone and arterial blood pressure: role of chloride transport in vascular smooth muscle. Pflugers Arch 467:605–614
Johansson B, Somlyo AP (1980) Electrophysiology and excitation-contraction coupling (Chapter 12). In: Bohr DF, Somlyo AP, Sparks HV (eds) Handbook of physiology, The Cardiovascular System II. American Physiological Society, Baltimore, pp p301–p323
Kuo IY, Ehrlich BE (2015) Signaling in muscle contraction. Cold Spring Harb Perspect Biol 7: a006023
Layton AT, Edwards A (2014) Electrophysiology of renal vascular smooth muscle cells (Chapter 6). In: Mathematical modeling in renal Physiology. Springer, Berlin/Heidelberg, pp p107–p140

Lloyd EE, Crossland RF, Phillips SC, Marrelli SP, Reddy AK, Taffet GE, Hartley CJ, Bryan RM Jr (2011) Disruption of $K_{2P}6.1$ produces vascular dysfunction and hypertension in mice. Hypertension 58:672–678

Martins JAC, Pires EB, Salvado R, Dinis PB (1998) Numerical model of passive and active behavior of skeletal muscles. Comput Methods Appl Mech Eng 151:419–433

Milton DL, Schneck AN, Ziech DA, Ba M, Facemyer KC, Halayko AJ, Baker JE, Gerthoffer WT, Cremo CR (2011) Direct evidence for functional smooth muscle myosin II in the 10S self-inhibited monomeric conformation in airway smooth muscle cells. Proc Natl Acad Sci U S A 108:1421–1426

Nelson MT, Quayle JM (1995) Physiological roles and properties of potassium channels in arterial smooth muscle. Am J Phys 268:C799–C822

Packer CS, Stephens NL (1985) Force-velocity relationships in hypertensive arterial smooth muscle. Can J Physiol Pharmacol 63:669–674

Ratz PH (2015) Mechanics of vascular smooth muscle. Compr Physiol 6:111–168

Ratz PH, Hai CM, Murphy RA (1989) Dependence of stress on cross-bridge phosphorylation in vascular smooth muscle. Am J Phys 256:C96–C100

Reho JJ, Zheng X, Fisher SA (2014) Smooth muscle contractile diversity in the control of regional circulations. Am J Physiol Heart Circ Physiol 306:H163–H172

Roach MR, Burton AC (1957) The reason for the shape of the distensibility curves of arteries. Can J Biochem Physiol 35:681–690

Seow CY (2000) Response of arterial smooth muscle to length perturbation. J Appl Physiol 89:2065–2072

Seppey D, Sauser R, Koenigsberger M, Bény JL, Meister JJ (2010) Intercellular calcium waves are associated with the propagation of vasomotion along arterial strips. Am J Physiol Heart Circ Physiol 298:H488–H496

Su C, Bevan JA, Ursillo RC (1964) Electrical quiescence of pulmonary artery smooth muscle during sympathomimetic stimulation. Circ Res 15:26–27

Thorneloe KS, Nelson MT (2005) Ion channels in smooth muscle: regulators of intracellular calcium and contractility. Can J Physiol Pharmacol 83:215–242

Tuna BG, Bakker EN, VanBavel E (2012) Smooth muscle biomechanics and plasticity: relevance for vascular calibre and remodelling. Basic Clin Pharmacol Toxicol 110:35–41

Tuna BG, Schoorl MJ, Bakker EN, de Vos J, VanBavel E (2013) Smooth muscle contractile plasticity in rat mesenteric small arteries: sensitivity to specific vasoconstrictors, distension and inflammatory cytokines. J Vasc Res 50:249–262

Tykocki NR, Nelson MT (2015) Location, Location, Location: juxtaposed calcium-signaling microdomains as a novel model of the vascular smooth muscle myogenic response. J Gen Physiol 146:129–132

Wagenseil JE, Mecham RP (2009) Vascular extracellular matrix and arterial mechanics. Physiol Rev 89:957–989

Willis MS, Schisler JC, Portbury AL, Patterson C (2009) Build it up-tear it down: protein quality control in the cardiac sarcomere. Cardiovasc Res 81:439–448

Yue Z, Xie J, Yu AS, Stock J, Du J, Yue L (2015) Role of TRP channels in the cardiovascular system. Am J Physiol Heart Circ Physiol 308:H157–H182

Zhang RZ, Gashev AA, Zawieja DC, Davis MJ (2007) Length-tension relationships of small arteries, veins, and lymphatics from the rat mesenteric microcirculation. Am J Physiol Heart Circ Physiol 292:H1943–H1952

Chapter 5
Biochemistry of the Contractile Proteins of Smooth Muscle

Abstract Muscle contraction at the molecular level is a process named cross-bridge cycle or actomyosin ATPase cycle resulting from the interaction of myosin and actin. The conformational changes of myosin head after bound to actin transfer the chemical energy stored in ATP into the force or tension through the swing of myosin head on the actin filaments. The specific myosin heavy chain isoforms are the key determinants of the unique characteristics of cross-bridge cycle of smooth muscle including vascular smooth muscle. Differing from the striated muscle, the cross-bridge cycle and thus the force generation are mainly regulated by the phosphorylation of the regulatory myosin light chain (MLC_{20}). The MLC_{20} isoforms as well as the latch state may contribute to different contractile responses between the tonic and phasic arteries.

Keywords Cross-bridge cycle • ATP • Myosin heavy chain • Myosin light chain • Latch state

5.1 Introduction

The sliding filament theory, developed by Andrew Huxley and Rolf Niedergerke and by Hugh Huxley and Jean Hanson in 1954, lays down the foundation of our understanding of muscle contraction (Huxley and Niedergerke 1954; Huxley and Hanson 1954). According to this theory, the contraction is a cycle of repetitive events caused by the swing of myosin head on the thin filament driven by ATP, known as cross-bridge cycle or actomyosin ATPase cycle. In this process the myosin is the molecular that converts the chemical energy to mechanical force and movement. The myosin family consists of at least 31 different classes, which are involved in a broad range of bioactivities such as muscle contraction, intracellular transport, sensory functions, and cell division and differentiation (Odronitz and Kollmar 2007; Sebé-Pedrós et al. 2014). Among them, class II myosins (myosins II) are responsible for the contraction of skeletal, cardiac, and smooth muscles. For these muscle types, various isoforms for both myosin heavy chains and light chains have been identified, which endow the different muscle types with distinct characteristics including differing ATPase activity, unloaded shortening velocity, and contractile force (Reggiani et al. 2000; Bloemink and Geeves 2011;

Y. Gao, *Biology of Vascular Smooth Muscle: Vasoconstriction and Dilatation*,
DOI 10.1007/978-981-10-4810-4_5

Reho et al. 2014; Miller et al. 2015). In this chapter the current understandings of the cross-bridge cycle mechanisms, the myosin heavy chain (MHC) isoforms, and myosin light chain (MLC) that are critical for the unique characteristics of smooth muscle in particular vascular smooth muscle related to the cross-bridge cycle and the latch hypothesis of smooth muscle contractile activities will be discussed.

5.2 The Structural Basis of the Myosin Motor Activity

The globular head of the myosin protein, also termed subfragment-1 (S1), is the molecular motor that performs mechanical work in the cross-bridge cycle. In each cycle, the myosin motor undergoes a head swing of the myosin, termed power

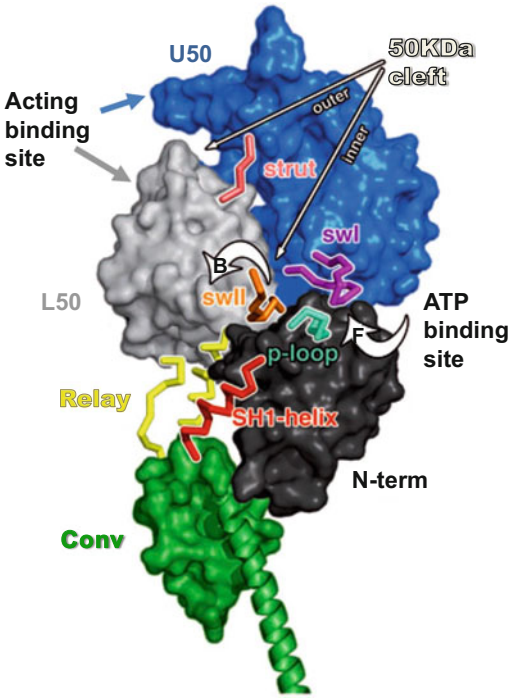

Fig. 5.1 Structural features of the myosin motor. The structure of the myosin II motor domain is composed of four subdomains: the upper 50 kDa (U50, *blue*), lower 50 kDa (L50, *light gray*), N-terminal (N-term, *dark gray*), and converter (Conv, *green*). The subdomains are linked by highly flexible joints including the "strut" (*pink*), switch II (SwII, *orange*), the relay connector (Relay, *yellow*), and the SH1-helix (*red*). The U50 and L50 constitute the actin-binding interface. Between the two subdomains, there is a 50-kDa long cleft. The nucleotide binding site is composed of the P-loop (*cyan*), switch I (SwI, *magenta*), and SwII (*orange*). The *white arrows* marked with "F" and "B" represent the front door and back door that allow entering of ATP and Pi release from the active site, respectively (The figure is from Llinas et al. (2009), with permission)

stroke. It is triggered by the binding to actin and displayed as axial tilting of its light chain domain (LCD) with respect to the thick filament backbone, thereby generating a force drugging the interdigitating thin filaments (Houdusse and Sweeney 2001; Málnási-Csizmadia and Kovács 2010; Sweeney and Houdusse 2010; Llinas et al. 2015).

The motor domain of the myosin (myosin head) is comprised of four subdomains (Fig. 5.1): the upper 50 kDa (U50), lower 50 kDa (L50), N-terminal, and converter. The U50 and L50 subdomains are primarily composed of flexible loops and constitute the actin-binding interface. Between these two subdomains, there is a 50-kDa long cleft. When the cross-bridge forms, the actin is initially weakly bound to the L50 followed by the closure of the cleft and further interaction of the U50 with actin, leading to strong actin binding. At the interface between the U50 and the N-terminal subdomains, the nucleotide-binding pocket is located. Three elements contribute to nucleotide binding: the P-loop grasps the phosphates of the nucleotide, switch I is essential for Mg^{2+} coordination, and switch II is a sensor for the γ-phosphate. Conformational changes of switch II control the closure and opening of the so-called back door in myosin near the γ-phosphate. Closure is essential for the hydrolysis of ATP, whereas reopening likely controls P_i release. The C-terminal converter is the smallest, most mobile subdomain and is directly linked to the myosin lever arm. The converter interacts strongly with the relay connector, an extension of the L50 subdomain, whereas the SH1 helix connects it to the N-terminal subdomain. Thus, the conformational information at the actin- or the nucleotide-binding site may propagate to the converter via the relay and SH1 helix and control the position of the converter and thus the lever arm (Málnási-Csizmadia and Kovács 2010; Llinas et al. 2009).

5.3 The Cross-Bridge Cycle

Muscle contraction at the molecular level results from an ATP-dependent repeated process of the formation of cross-bridge by actin and myosin, the swing of myosin head, and the detachment of actin. The myosins may be classified as processive or nonprocessive depending on whether the myosin head (motor domain) moves several steps or only one step along actin filaments before detaching. For instance, the nonmuscular myosin V, which is involved in vesicle and organelle transport, is a processive motor. This type of molecular motor is characterized by a slow detachment from the actin filament and coordinated actions of its two head domains so that it is possible to move processively several steps along the actin track (Mehta 2001; Månsson et al. 2015). By contrast, the myosin II (from now on referred to as myosin) is considered as nonprocessive. In a cross-bridge cycle, each myosin motor domain spends most time detached from actin, and a myosin motor takes only one single step along the actin filament before detaching. Therefore, the operation of muscle relies on a large assembly of myosin motors working together

asynchronously between different motors for a smooth shortening and force development (Månsson et al. 2015).

Prior to the formation of cross-bridge, ATP is hydrolyzed, and MgADP and P_i are trapped within the nucleotide pocket of motor domain of myosin. The myosin is initially bound to actin via electrostatic interactions with loop 2 and likely other flexible surface loops, such as the HCM loop. The binding of actin triggers P_i release by inducing the transition to the more strongly and stereo-specifically bound state. It is likely that P_i is released through a "back door" created by a movement of the switch II without disturbing the elements that keep the coordination of the ADP and the Mg^{2+}. P_i release is also proposed through a "side door" formed by a rearrangement of switch I relative to the P-loop. However, this presumption cannot explain how actin, after triggering release of P_i by moving switch I, would subsequently maintain MgADP binding before triggering its release. Another possible route for P_i release is the "front door" that the nucleotide enters. Since P_i is released before MgADP, this exit route is blocked by the MgADP (Llinas et al. 2015).

It is currently less clear how to relate the release of P_i and structural events occurred after actin binding to power stroke (Månsson et al. 2015). Based on the hypothesis purposed by Houdusse and colleagues (Sweeney and Houdusse 2010; Llinas et al. 2015), the release of P_i and the followed isomerization of the actin-binding interface to a state of strong actin binding lead to a rotational movement of the lower 50-K domain and the closure of the cleft, which generate a torsional strain on the β4-strand of the central β-sheet via the W-helix forcing the molecule to subsequently straighten the relay helix. The distal end of the relay helix is in close contact with the converter. As the relay moves, the converter moves with it, and the lever arm amplifies the movement to a 5–10-nm translation of the myosin tail (Månsson et al. 2015; Bloemink et al. 2016).

Following the power stroke, Mg^{2+} and ADP are released from actomyosin, which occurs following an isomerization reaction resulting in opening of the nucleotide-binding pocket and may be accompanied by a second swing of the lever arm in the absence of load. The ADP release step is highly strain dependent, and thus load can increase the duty ratio of the myosin. The duty ratio is the ratio of the occupancy of the strong actin-binding (force-generating) states to the occupancy of the weak + dissociated + strong states (De La Cruz and Ostap 2004). Under intermediate loads that are not sufficiently high to prevent or even reverse the power stroke, the lever arm swing associated with ADP release can be slowed, prolonging the time of strong attachment to actin. For smooth muscle, this would increase the economy of isometric force generation (Sweeney and Houdusse 2010; Månsson et al. 2015; Bloemink et al. 2016).

The release of Mg^{2+} and ADP is closely followed by the binding of Mg^{2+}-ATP, which induces a closing of switch I and subsequent formation of a salt bridge between switch I and switch II. These rearrangements caused by Mg^{2+}-ATP binding are coupled to the distortion of the seven-stranded β-sheet, which drives the upper 50-kDa subdomain to undergo a large movement, resulting in reduced contact area and weakened affinity to actin. Consequently, the cleft is open, and actin is dissociated from myosin. The dissociated state is accompanied with the

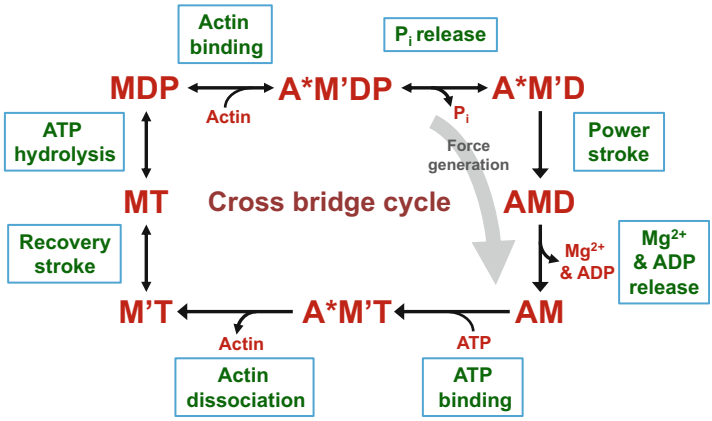

Fig. 5.2 Cross-bridge cycle. Prior to the binding of myosin to actin, the myosin is pocketed with ADP and P_i. The initial weak binding of myosin to actin triggers the release of P_i and a strong actin-binding state, followed by the power stroke, i.e., the force generation swing of the myosin head. Thereafter, Mg^{2+} and ADP are released. In accompanying with the ADP release, a second swing of the lever arm may occur in the absence of load. ATP is then bound to the myosin and the recovery of stroke (repriming of the lever arm). Following the hydrolysis of ATP, the next cross-bridge cycle is ready to be initiated by acting binding. A, actin; D, ADP; M, myosin; P, P_i; T, ATP. AM, AMD, AMDP, and AMT refer to actomyosin alone, bound to ADP, bound to ADP and P_i, and bound to ATP, respectively. A*M'DP or A*M'D refers to a weak actin-binding state. MT refers to myosin with ATP bound, while M'T refers to myosin with ATP bound prior to recovery stroke, i.e., prior to the lever arm is reprimed

closing of switch II, which is not only necessary for the hydrolysis of ATP but also leads to a partial unwinding of the relay helix and a kink. Since the tip of the relay helix is connected with the converter, the relatively small movement of switch II is amplified to a 65° rotation of the converter and a swinging of the lever arm from the initial down to the up position. This transition is known as the recovery stroke, which is immediately followed by the hydrolysis of ATP enabling the myosin to rebind to actin for another round of cross-bridge cycle (Llinas et al. 2009; Månsson et al. 2015; Bloemink et al. 2016) (Fig. 5.2).

5.4 Heterogeneous Activities of Myosin Heavy Chain Isoforms

Multiple isoforms of the myosin heavy chain (MHC) are present in the muscle lineages (striated and smooth muscle), which act as the primary determinants of the properties of the cross-bridge cycle and thus the contractile properties of the muscle (Reho et al. 2014; Miller et al. 2015; Bloemink et al. 2016). In adult human skeletal muscle fibers, three major MHC isoforms have been identified: MHC-I, MHC-IIA, and MHC-IIX, with MHC-I predominantly expressed in slow-twitch muscle while

MHC-IIA and MHC-IIX mainly expressed in fast-twitch fatigue-resistant and fast-twitch fatigable muscle, respectively (Schiaffino and Reggiani 2011). The expressed and purified myosin heads from human MHC isoforms demonstrate that contractile velocity increases (I < IIA < IIX) as the time myosin spends bound to actin decreases (I > IIA > IIX), resulting from quicker release of ADP (Miller et al. 2015). Mammalian hearts express α- and β-MHCs. The ratio of expressed isoforms varies at different stages of development and between atrium and ventricle (Weiss and Leinwand 1996). Healthy human heart ventricles express the α-isoforms in a ratio of about 1:9 to the β-isoform, while failing human hearts express no detectable α-MHC (Miyata et al. 2000). Studies with recombinant human α- and β-MHC motor domains reveal that the α-subfragment 1 (S1) is more similar to adult fast skeletal muscle myosin isoforms than to the slow β-isoform. The ATP hydrolysis rate of α-S1 is ~tenfold faster than β-S1, and the ADP release for α-S1 is >tenfold faster than for β-S1 (Deacon et al. 2012).

The MHC isoforms of smooth muscle are produced by alternative splicing of a single gene. They are classified as SMl and SM2 based on the presence or absence of a 34-amino acid insert in the tail portion and classified as SMA and SMB based on the absence or presence of a 7-amino acid insert at the NH_2-terminal region close to the ATP binding site near the 25- to 50-kDa junction. Expression of SMB has been found associated with a higher actin-activated Mg-ATPase activity and faster maximum shortening velocity. SMB is primarily expressed in phasic or fast rhythmic contracting smooth muscle, while SMA is mainly expressed in tonic or slow-sustained contracting smooth muscle (Eddinger and Meer 2007; Reho et al. 2014). In rabbit vascular tissues, the abdominal aorta contains almost entirely of SMA mRNA, and the distributing arteries (femoral and saphenous) begin to show SMB mRNA. The femoral/iliac artery contains >50% SMB mRNA, whereas the more distal saphenous artery contains >80% SMB mRNA. The actin-activated ATPase activity of myosin of saphenous artery is 1.7-fold higher than that of the aorta, accompanied by about twofold increase in the maximum shortening velocity of the saphenous artery compared with that of the aorta (DiSanto et al. 1997). In rat cardiac vessels, SMB is detected in smooth muscle cells of precapillary arterioles but not in larger vessels or aorta (Wetzel et al. 1998). Interestingly, the expression of SMB of cardiac precapillary arterioles is significantly reduced in spontaneously hypertensive rats but not in hypertensive rats induced by occlusion of renal artery, which is known to activate the renin angiotensin system, and chronic infusion of the vasoconstrictor angiotensin II compared with normotensive controls, suggesting that the downregulation of SMB in spontaneously hypertensive rats is of genetic origin rather than an adaptive response to chronically enhanced blood pressure and cardiac hypertrophy (Wetzel et al. 2003). In comparison with the isoforms SMA and SMB, the biological role of SMl and SM2 of smooth muscle MHC is less well understood. The muscle strips of the bladder and aorta from mice deficient in SM2 show augmented contractile response, suggesting that SM2 may negatively modulate force development during smooth muscle contraction (Chi et al. 2008).

5.5 Myosin Light Chain Phosphorylation

In striated muscle, the interaction of myosin with actin is sterically blocked by troponin and tropomyosin. Upon elevation of the cytosolic Ca^{2+} and the binding of Ca^{2+} to the troponin C, a conformational change in the troponin complex moves the troponin I away from the actin/tropomyosin filament followed by the moving of tropomyosin away from the myosin binding site on the actin so that the myosin head can interact with actin. The myosin ATPase activity of the striated muscle is constitutively high. The cross-bridge cycle can begin as soon as the tropomyosin is moved out of the way (El-Mezgueldi 2014). Although troponin has been detected in vasculature (Moran et al. 2008), it is likely that troponin does not play a major role in the regulation of contractile activity. Rather, the ATPase activity of smooth muscle is regulated by the phosphorylation of the regulatory myosin light chain (RLC) at Ser19. In the unphosphorylated state, the myosin has low actin-activated MgATPase activity due to an asymmetric interaction between its two heads. Phosphorylation of RLC at Ser19 disrupts the head–head interaction producing a conformation with the heads extended away from each other on opposite sides of the elongated coiled-coil rod, thereby allowing the myosin heads to interact with actin. This results in a marked increase in the MgATPase activity, which correlates with the unloaded shortening velocity of smooth muscle tissue (Taylor et al. 2014). The phosphorylation domain (PD) is located in the N-terminal segment of RLC. In the unphosphorylated state, PD is bent onto the surface of the C-terminal lobe, stabilized by interdomain salt bridges. In the phosphorylated state, PD is more helical and straight, is further from the C-terminal lobe, and is stabilized by an intradomain salt bridge. The phosphorylation of RLC accelerates the rate of P_i release from the active site when myosin is bound to actin, and the rate of this step in the cycle is likely limited by a preceding isomerization from a weak-binding to strong-binding actomyosin ADP.P_i state (Wu et al. 1999; Wendt et al. 2001; Walsh 2011; Ni et al. 2012).

Smooth muscle contraction is activated primarily by the phosphorylation RLC of Ser19 stimulated by Ca^{2+}/calmodulin-dependent myosin light chain kinase (MLCK). The neighboring T18 residue in RLC has been shown being phosphorylated by MLCK, but at very high concentrations of MLCK, and occurs much slowly than at Ser19 (Ikebe et al. 1986). In vascular smooth muscle, the diphosphorylation of RLC at Ser19 and Thr18 can also occur in a Ca^{2+}-independent manner with the stimulation of integrin-linked kinase (ILK), Rho-associated kinase (ROCK), and zipper-interacting protein kinase (ZIPK) (Walsh 2011). In rat caudal arterial smooth muscle, phosphorylation at Thr18 decreases the rates of RLC dephosphorylation and smooth muscle relaxation compared with phosphorylated exclusively at Ser19. It is possible that the diphosphorylation may underlie the hypercontractility observed in response to certain physiological contractile stimuli and under pathological conditions such as cerebral and coronary arterial vasospasm (Sutherland and Walsh 2012).

Both the RLC and the essential myosin light chain (ELC) are noncovalently linked to the IQ motifs of the lever arm of the myosin. Fast skeletal muscle has two ELC isoforms, A1 and A2, which differ primarily by an additional domain of 40–45 residues at the N-terminus of A1. Slow skeletal muscle and heart contain only the A1 isoform. In smooth muscle and nonmuscle myosins, only the A2 isoforms are present (Petzhold et al. 2014; Taylor et al. 2014; Guhathakurta et al. 2015). A study using time-resolved fluorescence resonance energy transfer reveals that, in skeletal muscle, the amplitude of the power stroke is much larger in myosin expressing A1 than A2 isoform (Guhathakurta et al. 2015). Two varieties of ELC are expressed in the heart, designated ALC1 and VLC1 for atrial and ventricular ELC. Studies suggest that the utmost N-terminal domains 1–15 of ALC1 and VLC1 specifically bind to actin, and the binding to actin slows down shortening velocity of cardiomyocytes, probably by reducing the rate of ADP release. It has been found that the affinity of human ALC-1 to actin is significantly lower compared with that of VLC-1. The difference is likely to be related to three amino acid residues in the N-terminal domains 1–15 (Petzhold et al. 2014).In smooth muscle site, directed mutagenesis shows that interactions between the phosphorylated N-terminus of the RLC and helix-A of the ELC are required for phosphorylation to activate myosin (Taylor et al. 2014).

5.6 The Latch State

In tonic smooth muscle, many stimuli can induce a sustained increase in tension while the myosin phosphorylation rise and then rapidly fall to low levels. Steady-state stress maintenance with reduced levels of myosin phosphorylation and cross-bridge cycling rates is termed the “latch state” (Dillon et al. 1981). It implies the ability to “hold” stress at high levels for prolonged periods without paying the energetic cost of rapidly cycling cross-bridges (Ratz 2015). Hai and Murphy proposed that a latch-bridge configuration, i.e., myosin unphosphorylated but attached to actin, is populated after the cross-bridge (myosin phosphorylated and attached to actin) forms. It is postulated that, if the kinetic constant for the detachment of actin from the unphosphorylated myosin is sufficient low, the latch state would be extended, which leads to a reduced rate of ATP hydrolysis while maintained muscle tension (Hai and Murphy 1988; Murphy and Rembold 2005; Ratz 2015). The detachment of actin from the unphosphorylated myosin in tonic artery is substantially slower than that in phasic artery. This would in part explain why tonic arteries such as carotid, femoral, and renal arteries possess a sustained contractility (Singer and Murphy 1987; Ratz 2015) (Fig. 5.3), while phasic arteries such as the saphenous artery and much smaller muscular feed arteries and arterioles exhibit a nonstable contractility (Han et al. 2006; Call et al. 2006; Ratz 2015).

In the latch-bridge model proposed by Hai and Murphy (Fig. 5.3), the phosphorylation of myosin in actin unattached and attached configurations is Ca^{2+}-dependent and phosphorylated by MLC kinase. The dephosphorylation of phosphorylated

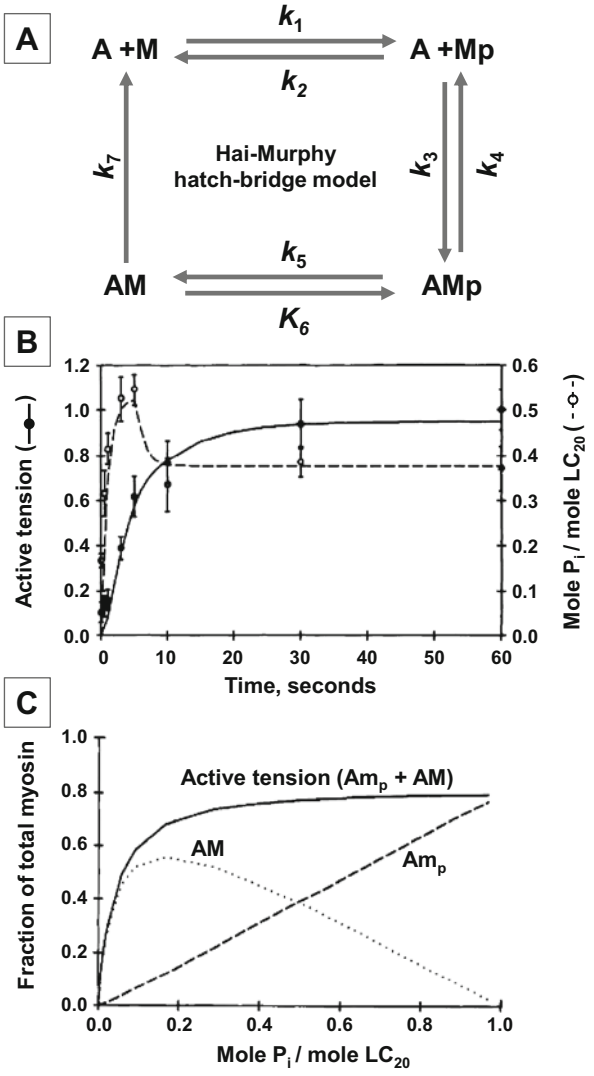

Fig. 5.3 Possible mechanism based on Hai–Murphy latch-bridge model for the contraction of tonic artery. (**a**) The Hai–Murphy latch-bridge model is composed of four kinetic states: actin (A) plus myosin (M), actin (A) plus phosphorylated M (Mp), a phosphorylated cross-bridge species (AMp), and a dephosphorylated cross-bridge species, the latch bridge (AM). *k* values represent rate constants. Based on the results of Singer and Murphy (1987; Circ Res 60:438–445) obtained from porcine carotid smooth muscle, the rate constants (in s^{-1}) are K_1 and $K_6 = 0.55$ for 5 s followed by 0.3; K_2 and $K_5 = 0.5$; $K_3 = 0.4$; $K_4 = 0.1$; $K_7 = 0.01$. The slow detachment of actin from the latch bridge (k_7) appears to be responsible for the tonic characteristics of the contraction (the latch state). (**b**) Fitting of Singer and Murphy's data (Singer and Murphy (1987) on phosphorylation of 20-kDa myosin light chain (MLC_{20}) and active tension stress. (**c**) Steady-state relationship between active tension (AM_p + AM), attached phosphorylated cross-bridges (AM_P), latch bridges (AM), and phosphorylation of 20-kDa myosin light chain based on Singer and Murphy's data (Singer and Murphy 1987) (Figures (**b** and **c**) are from Hai and Murphy (1988), with permission)

myosin in actin unattached and attached configurations is regulated by MLC phosphatases. The mechanism for the slow kinetic constant for the detachment of actin from the unphosphorylated myosin of tonic smooth muscle may in part be due to their predominant expression of SMA myosin isoform, the so called slow isoforms. By contrast, the dominant myosin isoform in phasic smooth muscle is the "fast" SMB myosin isoform (Reho et al. 2014). At the cross-bridge cycle level, a lower rate of ADP release from the myosin may be involved in the latch state (Ratz 2015). It is of interest to note that there is evidence that suggests the steady-state phosphorylated MLC (MLC-p) and tension development relationship as nearly a step function. To support full steady contraction from a passive state, MLC-p increase from ~15% to 20% to ~30% would be sufficient. It appears that MLC-p level in the range of 30–60% affects the contractility by regulating the maximum velocity of muscle shortening (Walker et al. 2000; Ratz 2015).

References

Bloemink MJ, Geeves MA (2011) Shaking the myosin family tree: biochemical kinetics defines four types of myosin motor. Semin Cell Dev Biol 22:961–967

Bloemink MJ, Melkani GC, Bernstein SI, Geeves MA (2016) The relay/converter interface influences hydrolysis of ATP by skeletal muscle myosin II. J Biol Chem 291:1763–1773

Call C, Han S, Speich JE, Eddinger TJ, Ratz PH (2006) Resistance to pressure-induced dilatation in femoral but not saphenous artery: physiological role of latch? Am J Physiol Heart Circ Physiol 291:H1513–H1520

Chi M, Zhou Y, Vedamoorthyrao S, Babu GJ, Periasamy M (2008) Ablation of smooth muscle myosin heavy chain SM2 increases smooth muscle contraction and results in postnatal death in mice. Proc Natl Acad Sci U S A 105:18614–18618

Deacon JC, Bloemink MJ, Rezavandi H, Geeves MA, Leinwand LA (2012) Identification of functional differences between recombinant human α and β cardiac myosin motors. Cell Mol Life Sci 69:2261–2277

De La Cruz EM, Ostap EM (2004) Relating biochemistry and function in the myosin superfamily. Curr Opin Cell Biol 16:61–67

Dillon PF, Aksoy MO, Driska SP, Murphy RA (1981) Myosin phosphorylation and the cross-bridge cycle in arterial smooth muscle. Science 211:495–497

DiSanto ME, Cox RH, Wang Z, Chacko S (1997) NH_2-terminal-inserted myosin II heavy chain is expressed in smooth muscle of small muscular arteries. Am J Physiol Cell Physiol 272:C1532–C1542

Eddinger TJ, Meer DP (2007) Myosin II isoforms in smooth muscle: heterogeneity and function. Am J Physiol Cell Physiol 293:C493–C508

El-Mezgueldi M (2014) Tropomyosin dynamics. J Muscle Res Cell Motil 35:203–210

Guhathakurta P, Prochniewicz E, Thomas DD (2015) Amplitude of the actomyosin power stroke depends strongly on the isoform of the myosin essential light chain. Proc Natl Acad Sci U S A 112:4660–4665

Hai CM, Murphy RA (1988) Cross-bridge phosphorylation and regulation of latch state in smooth muscle. Am J Phys 254:C99–C106

Han S, Speich JE, Eddinger TJ, Berg KM, Miner AS, Call C, Ratz PH (2006) Evidence for absence of latch-bridge formation in muscular saphenous arteries. Am J Physiol Heart Circ Physiol 291: H138–H146

Houdusse A, Sweeney HL (2001) Myosin motors: missing structures and hidden springs. Curr Opin Struct Biol 11:182–194
Huxley H, Hanson J (1954) Changes in the cross-striations of muscle during contraction and stretch and their structural interpretation. Nature 173:973–976
Huxley AF, Niedergerke R (1954) Structural changes in muscle during contraction: interference microscopy of living muscle Fibres. Nature 173:971–973
Ikebe M, Hartshorne DJ, Elzinga M (1986) Identification, phosphorylation, and dephosphorylation of a second site for myosin light chain kinase on the 20,000-Dalton light chain of smooth muscle myosin. J Biol Chem 261:36–39
Llinas P, Pylypenko O, Isabet T, Mukherjea M, Sweeney HL, Houdusse AM (2009) How myosin motors power cellular functions: an exciting journey from structure to function: based on a lecture delivered at the 34th FEBS congress in Prague, Czech Republic, July 2009. FEBS J 279:551–562
Llinas P, Isabet T, Song L, Ropars V, Zong B, Benisty H, Sirigu S, Morris C, Kikuti C, Safer D, Sweeney HL, Houdusse A (2015) How actin initiates the motor activity of myosin. Dev Cell 33:401–412
Málnási-Csizmadia A, Kovács M (2010) Emerging complex pathways of the actomyosin power stroke. Trends Biochem Sci 35:684–690
Månsson A, Rassier D, Tsiavaliaris G (2015) Poorly understood aspects of striated muscle contraction. Biomed Res Int 2015:245154
Mehta A (2001) Myosin learns to walk. J Cell Sci 114:1981–1998
Miller MS, Bedrin NG, Ades PA, Palmer BM, Toth MJ (2015) Molecular determinants of force production in human skeletal muscle fibers: effects of myosin isoform expression and cross-sectional area. Am J Physiol Cell Physiol 308:C473–C484
Miyata S, Minobe W, Bristow MR, Leinwand LA (2000) Myosin heavy chain isoform expression in the failing and nonfailing human heart. Circ Res 86:386–390
Moran CM, Garriock RJ, Miller MK, Heimark RL, Gregorio CC, Krieg PA (2008) Expression of the fast twitch troponin complex, fTnT, fTnI and fTnC, in vascular smooth muscle. Cell Motil Cytoskeleton 65:652–661
Murphy RA, Rembold CM (2005) The latch-bridge hypothesis of smooth muscle contraction. Can J Physiol Pharmacol 83:857–864
Ni S, Hong F, Haldeman BD, Baker JE, Facemyer KC, Cremo CR (2012) Modification of interface between regulatory and essential light chains hampers phosphorylation-dependent activation of smooth muscle myosin. J Biol Chem 287:22068–22079
Odronitz F, Kollmar M (2007) Drawing the tree of eukaryotic life based on the analysis of 2,269 manually annotated myosins from 328 species. Genome Biol 8:R196
Petzhold D, Simsek B, Meißner R, Mahmoodzadeh S, Morano I (2014) Distinct interactions between actin and essential myosin light chain isoforms. Biochem Biophys Res Commun 449:284–288
Ratz PH (2015) Mechanics of vascular smooth muscle. Compr Physiol 6:111–168
Reggiani C, Bottinelli R, Stienen GJ (2000) Sarcomeric myosin isoforms: fine tuning of a molecular motor. News Physiol Sci 15:26–33
Reho JJ, Zheng X, Fisher SA (2014) Smooth muscle contractile diversity in the control of regional circulations. Am J Physiol Heart Circ Physiol 306:H163–H172
Schiaffino S, Reggiani C (2011) Fiber types in mammalian skeletal muscles. Physiol Rev 91:1447–1531
Sebé-Pedrós A, Grau-Bové X, Richards TA, Ruiz-Trillo I (2014) Evolution and classification of myosins, a paneukaryotic whole-genome approach. Genome Biol Evol 6:290–305
Singer HA, Murphy RA (1987) Maximal rates of activation in electrically stimulated swine carotid media. Circ Res 60:438–445
Sutherland C, Walsh MP (2012) Myosin regulatory light chain diphosphorylation slows relaxation of arterial smooth muscle. J Biol Chem 287:24064–24076

Sweeney HL, Houdusse A (2010) Structural and functional insights into the myosin motor mechanism. Annu Rev Biophys 39:539–557

Taylor KA, Feig M, Brooks CL 3rd, Fagnant PM, Lowey S, Trybus KM (2014) Role of the essential light chain in the activation of smooth muscle myosin by regulatory light chain phosphorylation. J Struct Biol 185:375–382

Walker JS, Walker LA, Etter EF, Murphy RA (2000) A dilution immunoassay to measure myosin regulatory light chain phosphorylation. Anal Biochem 284:173–182

Walsh MP (2011) Vascular smooth muscle myosin light chain diphosphorylation: mechanism, function, and pathological implications. IUBMB Life 63:987–1000

Weiss A, Leinwand LA (1996) The mammalian myosin heavy chain gene family. Annu Rev Cell Dev Biol 12:417–439

Wendt T, Taylor D, Trybus KM, Taylor K (2001) Three dimensional image reconstruction of dephosphorylated smooth muscle heavy meromyosin reveals asymmetry in the interaction between myosin heads and placement of subfragment 2. Proc Natl Acad Sci U S A 98:4361–4366

Wetzel U, Lutsch G, Haase H, Ganten U, Morano I (1998) Expression of smooth muscle myosin heavy chain B in cardiac vessels of normotensive and hypertensive rats. Circ Res 83:204–209

Wetzel K, Baltatu O, Nafz B, Persson PB, Haase H, Morano I (2003) Expression of smooth muscle MyHC B in blood vessels of hypertrophied heart in experimentally hypertensive rats. Am J Physiol Regul Integr Comp Physiol 284:R607–R610

Wu X, Clack BA, Zhi G, Stull JT, Cremo CR (1999) Phosphorylation-dependent structural changes in the regulatory light chain domain of smooth muscle heavy meromyosin. J Biol Chem 274:20328–20335

Chapter 6
Metabolism of Vascular Smooth Muscle

Abstract Metabolism refers to chemical reactions that occur in living organisms necessary to maintain its structure and activities, to respond to environment changes, and to grow and reproduce. In this chapter we focus on the metabolism related to energy supply for the contractility of vascular smooth muscle (VSM), including the characteristics of energy consumption and the metabolites of glucose, lipids, and amino acids that are critical for VSM contractile activities. Many of these metabolites are actively involved in the regulation of vascular activities, such as nicotinamide adenine dinucleotide phosphate generated from the pentose phosphate pathway, and metabolites of L-arginine, heme, and cysteine. The current understandings of these subjects are discussed.

Keywords Energetics • Glycolysis • Lipid • L-arginine • Heme • Cysteine

6.1 Introduction

Vascular smooth muscle (VSM) consumes remarkably less energy to generate and to sustain its contractile activity, largely due to its unique characteristics of cross-bridge cycle that is discussed in Chap. 5 (Ratz 2015). The energy requirement of VSM activity mainly depends on ATP generated from lipid metabolism. However, VSM displays a substantially large portion glycolytic activity even under aerobic conditions as compared with striated muscle. Moreover, the glycolytic activity is functionally divided as two compartments, one is associated with the Na^+/K^+ pump activity of cell membrane and the other is linked to myofilament contractility (Paul 1989; Barron et al. 2000). Under hypoxic conditions the energy needed for vasocontractility is predominantly from glycolysis (Furchgott 1966). It appears that the pentose phosphate pathway of glucose metabolism plays a pivotal role in the differential responses between systemic and pulmonary arteries to hypoxia (Gupte et al. 2002; Gupte and Wolin 2006; Gupte et al. 2010; Dou et al. 2013). Comparing with those of lipids and glucose, the metabolites of amino acids have a minor role as energy suppliers. However, many of these metabolites such as L-arginine and its methylated product asymmetric dimethyl-L-arginine (ADMA) (Caplin and Leiper 2012), heme and its degradation product CO (Kim et al. 2011), and cysteine and its metabolites such as H_2S, sulfur dioxide (SO_2), and taurine

Y. Gao, *Biology of Vascular Smooth Muscle: Vasoconstriction and Dilatation*,
DOI 10.1007/978-981-10-4810-4_6

(Li et al. 2009; Nagpure and Bian 2016; Huang et al. 2016; Yao et al. 2016; Abebe and Mozaffari 2011) have profound effect on vascular activities. These aspects will be discussed in this chapter.

6.2 Energy Metabolism

The energy needed for muscle contraction is supplied by ATP. During contraction ATP is hydrolyzed into ADP and Pi. ADP is then recycled to ATP with a concomitant conversion of phosphocreatine (PCr) to creatine by creatine kinase (CK). Thereafter, PCr is regenerated from creatine at the expense of ATP, which is produced from oxidative phosphorylation and glycolysis (Barclay 2015). The energy consumption of smooth muscle is remarkably low comparing with that of striated muscle. For instance, the contracted frog sartorius utilizes ATP about 100-fold faster than the rate of its aerobic synthesis of ATP. Although the sartorius muscle has a sizable (15–30 μmol/g tissue) pool of PCr, the concentration of the high-energy phosphate rapidly decreased during contraction. VSM consumes ATP at rates ~0.5–1 μmol/min/g tissue and has relatively low levels of PCr (1–3 μmol/g). When stimulated at optimal lengths (L_o), the rate of ATP utilization (J_{ATP}) arises to three times of the unstimulated rate, followed by a decrease to steady-state rates of approximately twice the unstimulated rate. There is no appreciable change in the ATP + PCr content since the ATP breakdown can be matched by the rate of its aerobic resynthesis (Paul 1989). The ratio of PCr to ATP (PCr/ATP) is often used as an index of cellular energy level. Studies show that the (PCr)/(ATP) ratio is high (1.4–1.7) in fast phasic smooth muscles such as guinea-pig taenia caeci and pig urinary bladder but is low (0.5–0.7) in tonic smooth muscles such as pig carotid artery and sheep aorta (Nakayama and Clark 2003).

When smooth muscle contracts at fixed lengths, either the intact smooth muscle or skinned smooth muscle, the utilization of ATP is linearly dependent on the level of the active tension. It implies that the energy is mainly consumed in the cross-bridge cycle (Paul 1989). The contractile activity of smooth muscle is regulated by the phosphorylation/dephosphorylation of myosin light chain (MLC) (Walsh 2011; Taylor et al. 2014). The utilization of ATP of skinned smooth muscle is similar in the presence and absence of ATPγS, which causes nearly irreversibly phosphorylation of MLC. Hence, ATP is mainly consumed by the actin-activated ATPase of myosin rather than the phosphorylation/dephosphorylation of MLC (Hellstrand and Arner 1985).

In a shortening contraction of striated muscle, the consumption of energy is greater than that of isometric contraction, known as Fenn effect (Fenn 1923; Loiselle et al. 2008; Ortega et al. 2015). A similar phenomenon has also been observed in smooth muscle (Butler et al. 1983; Paul 1989). The “Fenn effect” can be quantitatively described as the energy liberated equals to the energy cost of isometric force production plus the work done. The work is defined as the product of force production and change in muscle length. Interestingly, the efficiency of

smooth muscle, in contrast to its high economy of force maintenance, seems to be significantly lower than skeletal muscle. Efficiency is the fraction of energy used by a muscle that appears as external work. It can be expressed as work produced per mole of the high-energy phosphagen consumed. In various skeletal muscles, this value is about 20 kJ/mol, while a few available studies of smooth muscle report this value is in the range of 5 kJ/mol (Butler et al. 1983; Paul 1989). The mechanism underlying the relatively low efficiency of smooth muscle compared to that of skeletal muscle is not clear. The contraction of smooth muscle is regulated by the phosphorylation/dephosphorylation of MLC. If this process constitutes a sizable fraction of ATP utilization associated with the contractile activity, it could account for the low efficiency of smooth muscle relative to skeletal muscle. Whether or not this is the case, it remains to be determined (Butler et al. 1983; Paul 1989).

6.3 Glucose Metabolism

The glucose metabolism of VSM is characterized by a substantial high glycolytic activity even under fully oxygenated conditions. The glycolytic cascade exists in two compartments. One is oxygen-independent production of ATP to meet the need of the Na^+/K^+ pump activity of cell membrane. The lactate production resulted from this pathway is inhibited by ouabain. The other compartmented pathway is linked to the entry of pyruvate into the mitochondria, and the ATP generated is associated with the myofilament contractility (Paul et al. 1989; Barron et al. 2000). Studies using a ^{13}C-labeled isotopomer analysis of glutamate reveal that exogenous glucose is the predominate substrate oxidized by VSM and glycogen oxidation contributes minimally to substrate oxidation. Moreover, exogenous pyruvate reduces glucose utilization but has no effect on glycogen utilization, while provision of acetate has no effect on glucose utilization but augments utilization. This differential regulation of glycolysis and glycogenolysis implies that these pathways are compartmentalized (Allen and Hardin 2000; Hardin and Roberts 1997).

Under normoxic conditions the contraction of rabbit aorta to epinephrine is decreased by less than 15% when glucose is absent, indicating that the energy needed for vasoconstriction depends on non-glycolytic activity. The contraction of the aorta caused by epinephrine is reduced by ~34% under anoxic compared under normoxic conditions in the presence of glucose. In anoxia and in the absence of glucose, the aortic contraction is depressed by more than 80%, suggesting that glycolysis is the predominant energy source for contraction of anoxic VSM (Furchgott 1966). The effect of glucose removal affects vasoconstriction differently depending on the type of vasoconstrictors. In rabbit aortas, epinephrine, angiotensin, and especially histamine appear to require a continuous supply of exogenous glucose to maintain their potential contractile effects. In contrast, potassium is less vulnerable to the glucose-free treatment. The results may indicate that different vasoactive stimulants may utilize glucose at a different level for generation of the energy required for contraction of vascular muscle (Altura and Altura 1970). There

are multiple energy-dependent reactions that may occur in a contractile response. The involvement of these events differs depending on the constrictor encountered. For instance, the energy consumption of contraction of rabbit aorta evoked by high K^+ mainly results from the phosphorylation of MLC and ATP hydrolysis in the cross-bridge cycle. In the same preparation, the contraction caused by norepinephrine may also involve other ATP-dependent events upstream to MLC phosphorylation (Coburn et al. 1992).

In addition to being converted to pyruvate by glycolysis pathway, glucose can also be converted to reduced nicotinamide adenine dinucleotide phosphate (NADPH), pentoses, and ribose 5-phosphate through the pentose phosphate pathway (PPP). Of these products, NADPH plays a key role in the maintenance of the redox hemostasis of the cell. The intracellular content of NADPH is produced primarily via the PPP with glucose-6-phosphate dehydrogenase (G6PD) being the rate-limiting enzyme. The activity of G6PD is regulated by the oxidized nicotinamide adenine dinucleotide phosphate ($NADP^+$)/NADPH ratio so that as the ratio increases, G6PD activity increases, and more NADPHs are generated. Indeed, when the cell is exposed to extracellular oxidants, $NADP^+$/NADPH ratio increases, and G6PD is activated (Stanton 2012). Hypoxia causes bovine pulmonary arteries to contract accompanied by increased G6PD activity and elevated cytosolic level of NADPH; in contrast, hypoxia causes bovine coronary arteries to relax accompanied by decreased G6PD activity and diminished cytosolic level of NADPH (Gupte et al. 2002, 2010; Gupte and Wolin 2006). The regression analysis shows a positive linear relationship between G6PD activity and NADPH/$NADP^+$ ratio to hypoxic pulmonary vasoconstriction. Furthermore the inhibition of G6PD decreases Ca^{2+} sensitivity to the myofilaments and attenuates MLC phosphorylation and pulmonary vasoconstriction induced by hypoxia (Gupte et al. 2010). The results suggest that a change in $NADP^+$/NADPH ratio is casually related to vasocontractility. A possible mechanism for NADPH-associated change in the contractile response of the vasculature may result from the altered dimerization status of soluble guanylyl cyclase (sGC). sGC is a key enzyme for nitric oxide (NO)-mediated vasodilatation, and the heterodimeric structure of sGC is obligatory for its catalytic activity. A decreased $NADP^+$/NADPH ratio would shift the redox status being more reduced, and thus sGC is less dimerized and the arteries are more prone to contraction; conversely, an increased $NADP^+$/NADPH ratio would shift the redox status being more oxidized, and thus sGC is more dimerized and the arteries are more prone to dilatation (Nagahara 2011; Dou et al. 2013). Such a postulation is consistent with the observation that hypoxia attenuates the dimerization of sGC of pulmonary arteries along with reduced sGC activity and diminished NO-induced relaxation (Ye et al. 2012). In contrast, hypoxia promotes the dimerization of sGC of coronary arteries, enhances sGC activity, and augments NO-induced relaxation (Zheng et al. 2011) (Fig. 6.1).

Under anoxic conditions a maximum of 8 ATP can be generated through glycolysis from one molecule of glucose. When sufficient oxygen is supplied, an additional maximum of 30 ATP could be yield from the two pyruvates produced by glycolysis of glucose after being transported into the mitochondria via pyruvate

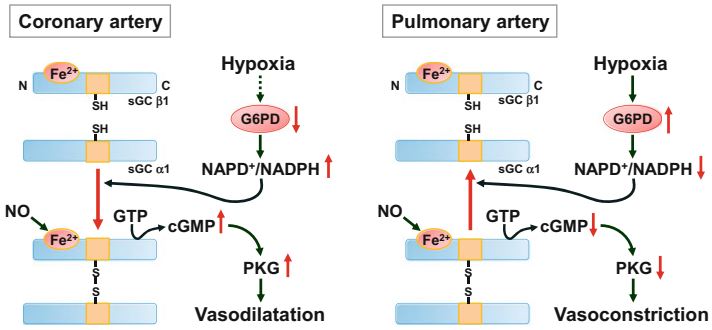

Fig. 6.1 Possible mechanisms for the dimerization of soluble guanylyl cyclase (sGC) in the hypoxic responses of coronary and pulmonary arteries. sGC is a heterodimer composed of α- and β-subunits, with $\alpha_1\beta_1$ dimer being the dominant isoform in vasculature. It is activated when nitric oxide (NO) binds to the reduced heme (Fe^{2+}) of sGC β-subunit, resulting in increased formation of cGMP from GTP. The increased cGMP level leads to the activation of cGMP-dependent protein kinase (PKG) and vasodilatation. The heterodimeric structure of sGC is obligatory for its catalytic activity. The dimerization of sGC is mediated by the formation of disulfide bonds of the cysteine residues between the two subunits of sGC. The balance between the monomeric and the dimeric status of sGC is redox modulated. In coronary artery (*left panel*), hypoxia inhibits the activity of glucose-6-phosphate dehydrogenase (G6PD), resulting in an increased ratio of oxidized to reduced nicotinamide adenine dinucleotide phosphate ($NADP^+$/NADPH) ratio. Such a more oxidized local environment promotes the dimerization of sGC, consequently increased sGC activity and elevated cGMP, PKG activation, and vasodilatation. In contrast, in pulmonary artery (*right panel*), hypoxia stimulates G6PD and thus decreased $NADP^+$/NADPH ratio. This leads to a more reduced local environment, decreased sGC dimerization, reduced sGC activity, diminished cGMP level and PKG activity, and vasoconstriction. The solid and dashed arrow lines denote stimulatory and inhibitory effects, respectively. *N* amino terminal, *C* carboxyl terminal, *SH* sulfhydryl, *S–S* disulfide bond (The figure is modified from Dou et al. (2013), with permission)

dehydrogenase. Pyruvate dehydrogenase is the rate-limiting enzyme of aerobic oxidation of glucose, and its activity can be inhibited by pyruvate dehydrogenase kinase (PDK)-mediated phosphorylation (Patel et al. 2014). It has been found that, compared with that of pulmonary VSM, the mitochondria of systemic VSM are under a more "hypoxic" state. This leads to a high level of hypoxia-inducible factor-1 (HIF-1). HIF-1 may inhibit pyruvate dehydrogenase activity by upregulating the expression of PDK, resulting in a more limited entry of pyruvate into the Krebs cycle and a higher glycolytic activity of systemic vs. pulmonary arteries (Michelakis and Weir 2008). A higher glycolytic activity may also result from AMP-activated protein kinase (AMPK)-dependent activation of 6-phosphofructo-2-kinase/fructose-6-phosphatase, isoform 3 (PFKFB3) (Bolaños et al. 2008). AMPK is activated when cellular energy status is compromised such as when exposed to sustained hypoxia (Wang et al. 2012). Some glycolytic enzymes could be upregulated by HIF-1 in pulmonary arterial hypertension, leading to exaggerated aerobic glycolytic rates, augmented pulmonary VSM proliferation, and diminished VSM apoptosis (Tuder et al. 2012).

6.4 Lipid Metabolism

The arterial wall possesses all the enzymes necessary for lipid synthesis and degradation. Triglyceride synthesis from glucose or fatty acid precursors is quite active in the arterial wall and is enhanced when treated with insulin. The artery contains a hormone-sensitive lipase which hydrolyzes triglycerides and whose activity is suppressed by insulin. The metabolic pathways involved in the synthesis and catabolism of phospholipids also exist in the arterial wall, and most of the phospholipids are locally synthesized. Synthesis of cholesterol has been observed in the arteries in several animals and humans. However, the cholesterol synthesis rate in vitro is very slow (Stout 1976). Under normoxic conditions, although there is significant glycolytic activity, the energy needed for vascular contractility is predominantly supplied by lipid metabolism (Furchgott 1966; Barron et al. 1997). In rabbit aortic strip depleted of substrate by exposure to epinephrine in a substrate-free bath for 2 hr, the diminished contraction is recovered by butyrate and oleate, acetoacetate, and beta hydroxybutyrate, suggesting that fatty acids (FAs) and ketone bodies are utilized to provide the energy needed for vascular contraction (Coe et al. 1968). A study using ^{3}H-labeled substrates revealed that, during the initial period of contraction of porcine carotid arteries to high K^{+}, intracellular pyruvate derived from extracellular glucose is the primary oxidative substrate and is preferred even over exogenous fatty acid; however, as stable, steady-state isometric force is achieved, and exogenous fatty acid substrates such as acetate or octanoate serve as the primary oxidative energy fuels (Barron et al. 1997).

With the exception of the adipose tissues, the excessive accumulation of FAs impairs insulin signaling, inhibits glucose uptake, and causes metabolic dysfunction (Samuel and Shulman 2012; Hagberg et al. 2013). Like other nonadipose tissues, the blood vessels depend on extracellular FAs as their main source for energy production. The lipids derived from dietary are mainly FAs with aliphatic tails 13 to 21 carbons, i.e., long-chain FAs (LCFAs). While medium-chain (with 6–12 carbons) and short-chain FAs (with <6 carbons) can passively diffuse into the cytosol of the cell, the transfer of the LCFAs across biological membranes is an active process. In the circulating blood, the LCFAs are transported as part of lipoproteins or bound to albumin. On the luminal side of the endothelium, the LCFAs are hydrolyzed by the lipoprotein lipase or dissociated from albumin, yielding free FAs. The transendothelial FA transport is through the isoforms 3 and 4 of the FA transporter proteins (FATPs), while the FA uptake of VSMs is mediated by the isoforms 1 and 4 of FATPs (Kazantzis and Stahl 2012; Hagberg et al. 2013). The uptake and β-oxidation of LCFAs are tightly regulated by a coordinated process of endothelial and VSM cells. The expression of FATPs is regulated by vascular endothelial growth factor B (VEGF-B), while VEGF-B is regulated by peroxisome proliferator-activated receptor gamma coactivator 1α (PGC1α), a key player in the regulation of energy metabolism (Villena 2015). In VSMs the activity of PGC1α is connected with the lipid supply to mitochondria and thereby maintains metabolic

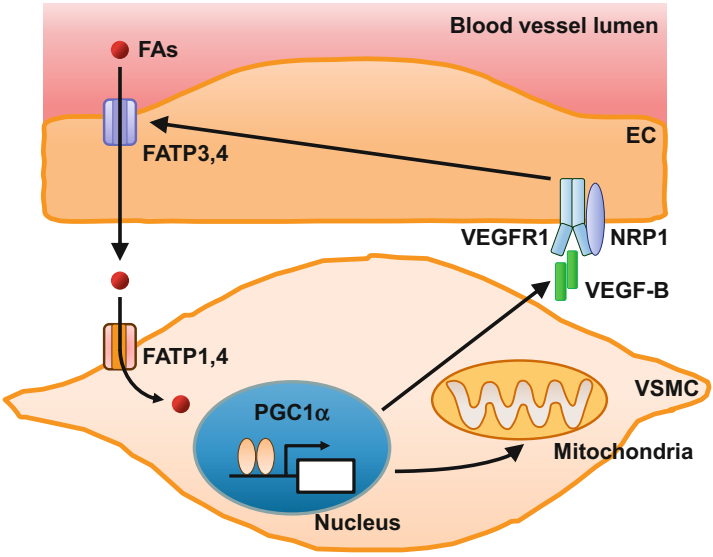

Fig. 6.2 Possible mechanism underlying the transendothelial transport of fatty acids (FAs). Under normal conditions the activity of peroxisome proliferator-activated receptor gamma coactivator 1α (PGC1α, a key player in the regulation of energy metabolism) connects lipid supply to mitochondrial biogenesis and thereby maintains metabolic balance. The expression of vascular endothelial growth factor B (VEGF-B) is regulated by PGC1α and coordinated with the expression of mitochondrial proteins. VEGF-B is secreted from vascular smooth muscle cells (VSMCs) and bound to receptor VEGFR1 and to the common co-receptor neuropilin-1 (NRP1) on endothelial cells (ECs). The stimulation of ECs with VEGF-B upregulates the expression of vascular FA transporter protein FATP3,4 and induces subsequent transport of FAs in the blood across the EC layer into VSMCs

balance (Fig. 6.2). VSMs can also regulate LCFA uptake via lipoprotein lipase, which is produced by the myocytes and subsequently transported through and anchored at the endothelium (Olivecrona and Olivecrona 2010; Hagberg et al. 2013).

In addition to serve as fuel substrates, various lipids have been shown to affect vascular reactivity via signaling modulation. In freshly isolated VSMs of rabbit pulmonary artery, single-channel current recording reveals that the activity of large-conductance Ca^{2+}-activated K^+ channel is directly stimulated by negatively charged lipids that have a sufficiently long alkyl chain with carbons ≥ 8 but inhibited by positively charged lipids that have a alkyl chain with carbons ≥ 8. Neutral and short-chain lipids have no effect (Clarke et al. 2002). Under certain pathological conditions including ischemia, hypoxia, and trauma, the levels of tissue-free FAs increase accompanied with an increased production of reactive oxygen species (ROS). FAs, in particular mono- and polyunsaturated long-chain FAs, could stimulate ROS generation through the inhibition of mitochondrial oxidative phosphorylation and activation of plasma-membrane NADPH oxidase

(Schönfeld and Wojtczak 2008). Lipids can also affect vascular activity by acting on the production and signaling of nitric oxide (NO). Docosahexaenoic acid (DHA), a 22-carbon chain and 6-*cis* double-bond omega-3 fatty acid, has been found to augment the activity endothelial NO synthase (eNOS) by modifying membrane lipid composition and by changing distribution of major structural proteins (Li et al. 2007). Omega-3 FAs may cause endothelium-derived NO-mediated vasodilatation through the stimulation of eNOS via the activation of PI3-kinase/Akt and MAPK pathways (Zgheel et al. 2014). Studies also suggest that eNOS activity and NO-mediated vasodilatation are impaired by hypertriglyceride (Török et al. 2007) and oxidized low-density lipoprotein (LDL), while high-density lipoprotein (HDL) acts oppositely (Everson and Smart 2001; Mineo and Shaul 2013).

6.5 Amino Acid Metabolism

It appears that amino acid metabolism is not an important energy source for VSMs both under basal conditions and during contraction (Chace and Odessey 1981; Odessey and Chace 1982; Barron et al. 1994). However, some amino acids and their metabolites are critically involved in the regulation of various vascular activities. For instance, L-arginine is the substrate of NO synthesis, and it is well recognized that NO plays a pivotal role in a broad range of cardiovascular function such as vasodilation, the inhibition of VSM proliferation, and platelet aggregation (Gao 2010). In addition to those related to L-arginine metabolism, several other amino acid metabolites are important in the regulation of vascular function, including heme and its degradation product carbon monoxide (CO) and cysteine and its metabolites (Leffler et al. 2011; Derbyshire and Marletta 2012; Winterbourn and Hampton 2008; Dou et al. 2013).

In human the plasma concentration of L-arginine normally is ~100 μmol/L, which may be reduced under pathological conditions but rarely falls below 60 μmol/L. L-arginine is transported into the endothelial cells where it is converted to NO by eNOS. The intracellular concentration of L-arginine of the endothelial cells may be as high as up to tenfold of that in the plasma, and the *K*m of eNOS for L-arginine is ~3 μmol/L. Since arginases can compete with eNOS for substrate, a relative L-arginine deficiency for eNOS may occur when arginase becomes overactive. This would explain at least partially the effectiveness of L-arginine supplementation in the improvement of endothelial dysfunction in hypercholesterolemia and hypertension (Förstermann and Sessa 2012).

The activity of eNOS can also be inhibited by ADMA, which is formed when intracellular arginine is methylated by methyltransferases that are widely distributed throughout the body. The inhibitory effect of ADMA can be neutralized by being converted to L-citrulline by dimethylarginine dimethylaminohydrolase (DDAH). DDAH exists as two subtypes, with the type 2 isoform (DDAH-2)

being dominant in vascular endothelium. An elevated circulating ADMA level is often observed in various vascular diseases characterized by endothelial dysfunction. A diminished expression and activity of DDAH is ascribed to the altered ADMA level and eNOS dysfunction (Caplin and Leiper 2012).

Heme is synthesized using glycine and the Krebs cycle metabolites succinyl-coenzyme. It is an essential cofactor for a variety of enzymes critical to vascular functions such as hemoglobin, peroxidase, cytochrome c oxidase, and sGC. Carbon monoxide (CO), a product of heme degradation, has profound effects on the intracellular signaling processes, such as anti-inflammatory, antiproliferative, and antiapoptotic effects (Kim et al. 2011). Both CO and YC-1, a chemical agent, are weak stimulants of sGC. In the presence of CO, the activity of sGC can be increased several hundredfold by YC-1 compared to 2–4-fold in the absence of CO. Considering that the stimulatory effect of CO on purified sGC is weaker than its effect in intact tissue, it is possible that there is an endogenous substances which may act synergistically with CO in vivo (Friebe et al. 1996; Purohit et al. 2014). Heme is degraded by heme oxygenase (HO). There are two subtypes of HO identified, HO-1 the inducible and HO-2 the constitutive. HO-1 is a stress protein. It is upregulated under pathophysiological conditions to exert various protective effects on cardiovascular and other tissues (Kim et al. 2011).

Cysteine is a sulfur-containing amino acid. Due to its ability to form disulfide bonds, cysteine plays a crucial role in protein structure and in protein-folding pathways. Evidence indicates that redox-dependent formation of disulfide bond within the protein molecule or between intermolecular certain thiol group of cysteine residues may act as a key mechanism in the regulation of cardiovascular function (Winterbourn and Hampton 2008; Dou et al. 2013). Cysteine is the substrate for the production of antioxidant glutathione and gas signaling molecule hydrogen sulfide (H_2S). H_2S is generated from cysteine either by cystathionine γ-lyase (CSE) or by cystathionine β-synthase (CBS) (Li et al. 2009). H_2S at low concentration ($< 100\,\mu M$) acts as a vasoconstrictor via inhibiting eNOS and cAMP signaling. At high concentration ($> 100\,\mu M$), H_2S acts as a potent vasodilator by activating K_{ATP} and K_V channels, downregulating ATP levels and cellular metabolism, regulating intracellular pH, and stimulating the release of endothelium-derived hyperpolarizing factor (EDHF) (Nagpure and Bian 2016). SO_2 is another vasoactive product of cysteine metabolism via the actions of cysteine dioxygenase (CDO) and amino acid transaminase (AAT). SO_2 may cause vasodilatation by stimulating K_{ATP} channel, inhibiting L-type Ca^{2+} channel, and promoting the dimerization of sGC and cGMP-dependent protein kinase (PKG) (Huang et al. 2016; Yao et al. 2016). Cysteine can also be converted to taurine by CDO and cysteinesulfinate decarboxylase (CSD). Taurine has been shown to reduce blood pressure in a number of animal models of hypertension. This effect may result from increased ROS scavenging, enhanced nitric oxide bioavailability, and activated K^+ channels (Abebe and Mozaffari 2011).

References

Abebe W, Mozaffari MS (2011) Role of taurine in the vasculature: an overview of experimental and human studies. Am J Cardiovasc Dis 1:293–311

Allen TJ, Hardin CD (2000) Influence of glycogen storage on vascular smooth muscle metabolism. Am J Physiol Heart Circ Physiol 278:H1993–H2002

Altura BM, Altura BT (1970) Differential effects of substrate depletion on drug-induced contractions of rabbit aorta. Am J Phys 219:1698–1705

Barclay CJ (2015) Energetics of contraction. Compr Physiol 5:961–595

Barron JT, Kopp SJ, Tow J, Parrillo JE (1994) Fatty acid, tricarboxylic acid cycle metabolites, and energy metabolism in vascular smooth muscle. Am J Phys 267:H764–H769

Barron JT, Bárány M, Gu L, Parrillo JE (1997) Oxidation of acetate and octanoate and its relation to glucose metabolism in contracting porcine carotid artery. Biochim Biophys Acta 1322:208–220

Barron JT, Gu L, Parrillo JE (2000) NADH/NAD redox state of cytoplasmic glycolytic compartments in vascular smooth muscle. Am J Physiol Heart Circ Physiol 279:H2872–H2878

Bolaños JP, Delgado-Esteban M, Herrero-Mendez A, Fernandez-Fernandez S, Almeida A (2008) Regulation of glycolysis and pentose-phosphate pathway by nitric oxide: impact on neuronal survival. Biochim Biophys Acta 1777:789–793

Butler TM, Siegman MJ, Mooers SU (1983) Chemical energy usage during shortening and work production in mammalian smooth muscle. Am J Phys 244:C234–C242

Caplin B, Leiper J (2012) Endogenous nitric oxide synthase inhibitors in the biology of disease: markers, mediators, and regulators? Arterioscler Thromb Vasc Biol 32:1343–1353

Chace KV, Odessey R (1981) The utilization by rabbit aorta of carbohydrates, fatty acids, ketone bodies, and amino acids as substrates for energy production. Circ Res 48:850–858

Clarke AL, Petrou S, Walsh JV Jr, Singer JJ (2002) Modulation of BK_{Ca} channel activity by fatty acids: structural requirements and mechanism of action. Am J Phys Cell Physiol 283:C1441–C1453

Coburn RF, Moreland S, Moreland RS, Baron CB (1992) Rate-limiting energy-dependent steps controlling oxidative metabolism-contraction coupling in rabbit aorta. J Physiol 448:473–492

Coe J, Detar R, Bohr DF (1968) Substrates and vascular smooth muscle contraction. Am J Phys 214:245–250

Derbyshire ER, Marletta MA (2012) Structure and regulation of soluble guanylate cyclase. Annu Rev Biochem 81:533–559

Dou D, Zheng X, Ying L, Ye L, Gao Y (2013) Sulfhydryl-dependent dimerization and cGMP-mediated vasodilatation. J Cardiovasc Pharmacol 62:1–5

Everson WV, Smart EJ (2001) Influence of caveolin, cholesterol, and lipoproteins on nitric oxide synthase: implications for vascular disease. Trends Cardiovasc Med 11:246–250

Fenn WO (1923) A quantitative comparison between the energy liberated and the work performed by the isolated sartorius muscle of the frog. J Physiol 58:175–203

Förstermann U, Sessa WC (2012) Nitric oxide synthases: regulation and function. Eur Heart J 33:829–837. 837a-837d

Friebe A, Schultz G, Koesling D (1996) Sensitizing soluble guanylyl cyclase to become a highly CO-sensitive enzyme. EMBO J 15:6863–6868

Furchgott RF (1966) Metabolic factors that influence contractility of vascular smooth muscle. Bull N Y Acad Med 42:996–1006

Gao Y (2010) The multiple actions of NO. Pflügers Archiv-Eur J Physiol 459:829–839

Gupte SA, Wolin MS (2006) Hypoxia promotes relaxation of bovine coronary arteries through lowering cytosolic NADPH. Am J Physiol Heart Circ Physiol 290:H2228–H2238

Gupte SA, Li KX, Okada T, Sato K, Oka M (2002) Inhibitors of pentose phosphate pathway cause vasodilation: involvement of voltage-gated potassium channels. J Pharmacol Exp Ther 301:299–305

Gupte RS, Rawat DK, Chettimada S, Cioffi DL, Wolin MS, Gerthoffer WT, McMurtry IF, Gupte SA (2010) Activation of glucose-6-phosphate dehydrogenase promotes acute hypoxic pulmonary artery contraction. J Biol Chem 285:19561–19571

Hagberg C, Mehlem A, Falkevall A, Muhl L, Eriksson U (2013) Endothelial fatty acid transport: role of vascular endothelial growth factor B. Physiology (Bethesda) 28:125–134

Hardin CD, Roberts TM (1997) Differential regulation of glucose and glycogen metabolism in vascular smooth muscle by exogenous substrates. J Mol Cell Cardiol 29:1207–1216

Hellstrand P, Arner A (1985) Myosin light chain phosphorylation and the cross-bridge cycle at low substrate concentration in chemically skinned guinea pig Taenia coli. Pflugers Arch 405:323–328

Huang Y, Tang C, Du J, Jin H (2016) Endogenous sulfur dioxide: a new member of gasotransmitter family in the cardiovascular system. Oxidative Med Cell Longev 2016:8961951

Kazantzis M, Stahl A (2012) Fatty acid transport proteins, implications in physiology and disease. Biochim Biophys Acta 1821:852–857

Kim YM, Pae HO, Park JE, Lee YC, Woo JM, Kim NH, Choi YK, Lee BS, Kim SR, Chung HT (2011) Heme oxygenase in the regulation of vascular biology: from molecular mechanisms to therapeutic opportunities. Antioxid Redox Signal 14:137–167

Leffler CW, Parfenova H, Jaggar JH (2011) Carbon monoxide as an endogenous vascular modulator. Am J Physiol Heart Circ Physiol 301:H1–H11

Li Q, Zhang Q, Wang M, Liu F, Zhao S, Ma J, Luo N, Li N, Li Y, Xu G, Li J (2007) Docosahexaenoic acid affects endothelial nitric oxide synthase in caveolae. Arch Biochem Biophys 466:250–259

Li X, Bazer FW, Gao H, Jobgen W, Johnson GA, Li P, McKnight JR, Satterfield MC, Spencer TE, Wu G (2009) Amino acids and gaseous signaling. Amino Acids 37:65–78

Loiselle DS, Crampin EJ, Niederer SA, Smith NP, Barclay CJ (2008) Energetic consequences of mechanical loads. Prog Biophys Mol Biol 97:348–366

Michelakis ED, Weir EK (2008) The metabolic basis of vascular oxygen sensing: diversity, compartmentalization, and lessons from cancer. Am J Physiol Heart Circ Physiol 295:H928–H930

Mineo C, Shaul PW (2013) Regulation of signal transduction by HDL. J Lipid Res 54:2315–2324

Nagahara N (2011) Intermolecular disulfide bond to modulate protein function as a redox-sensing switch. Amino Acids 41:59–72

Nagpure BV, Bian JS (2016) Interaction of hydrogen sulfide with nitric oxide in the cardiovascular system. Oxidative Med Cell Longev 2016:6904327

Nakayama S, Clark JF (2003) Smooth muscle and NMR review: an overview of smooth muscle metabolism. Mol Cell Biochem 244:17–30

Odessey R, Chace KV (1982) Utilization of endogenous lipid, glycogen, and protein by rabbit aorta. Am J Phys 243:H128–H132

Olivecrona G, Olivecrona T (2010) Triglyceride lipases and atherosclerosis. Curr Opin Lipidol 21:409–415

Ortega JO, Lindstedt SL, Nelson FE, Jubrias SA, Kushmerick MJ, Conley KE (2015) Muscle force, work and cost: a novel technique to revisit the Fenn effect. J Exp Biol 218:2075–2082

Patel MS, Nemeria NS, Furey W, Jordan F (2014) The pyruvate dehydrogenase complexes: structure-based function and regulation. J Biol Chem 289:16615–16623

Paul RJ (1989) Smooth muscle energetics. Annu Rev Physiol 51:331–349

Purohit R, Fritz BG, The J, Issaian A, Weichsel A, David CL, Campbell E, Hausrath AC, Rassouli-Taylor L, Garcin ED, Gage MJ, Montfort WR (2014) YC-1 binding to the β subunit of soluble guanylyl cyclase overcomes allosteric inhibition by the α subunit. Biochemistry 53:101–114

Ratz PH (2015) Mechanics of vascular smooth muscle. Compr Physiol 6:111–168

Samuel VT, Shulman GI (2012) Mechanisms for insulin resistance: common threads and missing links. Cell 148:852–871

Schönfeld P, Wojtczak L (2008) Fatty acids as modulators of the cellular production of reactive oxygen species. Free Radic Biol Med 45:231–241

Stanton RC (2012) Glucose-6-phosphate dehydrogenase, NADPH, and cell survival. IUBMB Life 64:362–369

Stout RW (1976) The lipid metabolism of the arterial wall and its abnormalities in diabetes. Acta Diabetol Lat 13:87–92

Taylor KA, Feig M, Brooks CL 3rd, Fagnant PM, Lowey S, Trybus KM (2014) Role of the essential light chain in the activation of smooth muscle myosin by regulatory light chain phosphorylation. J Struct Biol 185:375–382

Török J, L'upták I, Matúsková J, Pechánová O, Zicha J, Kunes J, Simko F (2007) Comparison of the effect of simvastatin, spironolactone and L-arginine on endothelial function of aorta in hereditary hypertriglyceridemic rats. Physiol Res 56(Suppl 2):S33–S40

Tuder RM, Davis LA, Graham BB (2012) Targeting energetic metabolism: a new frontier in the pathogenesis and treatment of pulmonary hypertension. Am J Respir Crit Care Med 185:260–266

Villena JA (2015) New insights into PGC-1 coactivators: redefining their role in the regulation of mitochondrial function and beyond. FEBS J 282:647–672

Walsh MP (2011) Vascular smooth muscle myosin light chain diphosphorylation: mechanism, function, and pathological implications. IUBMB Life 63:987–1000

Wang S, Song P, Zou MH (2012) AMP-activated protein kinase, stress responses and cardiovascular diseases. Clin Sci (Lond) 122:555–573

Winterbourn CC, Hampton MB (2008) Thiol chemistry and specificity in redox signaling. Free Radic Biol Med 45:549–561

Yao Q, Huang Y, Liu AD, Zhu M, Liu J, Yan H, Zhang Q, Geng B, Gao Y, Du S, Huang P, Tang C, Du J, Jin H (2016) The vasodilatory effect of sulfur dioxide via sGC/cGMP/PKG pathway in association with sulfhydryl-dependent dimerization. Am J Physiol Regul Integr Comp Physiol 310:R1073–R1080

Ye L, Liu J, Liu H, Ying L, Dou D, Chen Z, Xu X, Raj JU, Gao Y (2012) Sulfhydryl-dependent dimerization of soluble guanylyl cyclase modulates relaxation of porcine pulmonary vessels to nitric oxide. Pflügers Archiv Eur J Physiol 463:257–268

Zgheel F, Alhosin M, Rashid S, Burban M, Auger C, Schini-Kerth VB (2014) Redox-sensitive induction of src/PI3-kinase/akt and MAPKs pathways activate eNOS in response to EPA:DHA 6:1. PLoS One 9:e105102

Zheng X, Ying L, Liu J, Dou D, He Q, Leung SWS, Man RYK, Vanhoutte PM, Gao Y (2011) Role of sulfhydryl-dependent dimerization of soluble guanylyl cyclase in relaxation of porcine coronary artery to nitric oxide. Cardiovasc Res 90:565–572

Part II
Regulators of Vasoreactivity

Chapter 7
Neurotransmitters

Abstract The activities of vasculature are regulated by neurotransmitters released from the nerve terminals in the wall of the blood vessels, which include the sympathetic, parasympathetic, and sensory-motor nerves. These neurotransmitters exert their effects mostly by binding to the G-protein-coupled receptors (GPCRs), which trigger the dissociation of the α-subunit of the G-protein from the βγ-subunits followed by the activation of their downstream effectors. The α-subunits exist as multiple isoforms. The diversity of the α-subunits in combination with increasing revealed βγ-subunit functions thus endows vascular smooth muscle and endothelial cells to respond to different neurotransmitters in a manner suitable to intricate physiological changes. The neurotransmitters are co-released from the nerve terminals. These neurotransmitters include norepinephrine, acetylcholine, ATP, neuropeptide Y, vasoactive intestinal peptide, nitric oxide, calcitonin gene-related peptide, substance P, and others. Some of them are vasoconstrictors and some are vasodilators. The balance of the activities of these neurotransmitters is critical for the integrity of vascular function.

Keywords Sympathetic nerves • Parasympathetic nerves • Sensory-motor nerves • G-protein-coupled receptor • Adrenoceptors • Muscarinic receptor • Purinergic receptor • Neuropeptide receptor

7.1 Introduction

The vascular activities are regulated by the autonomic nervous system in a moment-to-moment fashion to ensure the local blood supply is distributed according to the global physiological purpose. Such a regulation is predominantly realized by sympathetic innervation. However, parasympathetic innervation may be of importance for some vasculature such as cerebral blood vessels. The activity of sensory-motor nerves may also affect vasoactivity. Autonomic nervous system exerts their effects by releasing various neurotransmitters, and the actions of the majority of these neurotransmitters are mediated by G-protein-coupled receptors (GPCRs), which exist as multiple isoforms. Thus, the responses of vascular smooth muscle cells (VSMCs) and endothelial cells induced by agonist binding are diversified and complicated. In this chapter the current understandings of the innervation of the

Y. Gao, *Biology of Vascular Smooth Muscle: Vasoconstriction and Dilatation*,
DOI 10.1007/978-981-10-4810-4_7

blood vessels, the general profiles of GPCR activation, and the signaling mechanisms of adrenergic, muscarinic, purinergic, and neuropeptide agonists will be discussed.

7.2 Innervation

The blood vessels are innervated by sympathetic, parasympathetic, and sensory-motor nerves (Hirst and Edwards 1989; Burnstock and Ralevic 2013). Sympathetic nerves account for the largest proportion of innervation in the resistance arteries and have been found in nearly every vascular bed studied across animal species. The axons of sympathetic nerves often run along with the pathways of arterial tree, split into finer bundles of axons, and give rise to the terminal axons lying in the adventitia. The terminal region of the sympathetic axon has a varicose appearance. Varicosities are ~2 μm long and 1 μm across, separated by short lengths (5–10 μm) of fine axon. The terminal branches of each individual fiber bear several hundred varicosities. The diffusion distances between sites of neurotransmitter release and adjacent SMCs are ~100 nm for resistance arteries with diameter <150 μm and several hundred nanometers for large arteries. Such an arrangement makes the release of neurotransmitter from varicosities in an en passant mode (Hirst and Edwards 1989; Westcott and Segal 2013). Several transmitters are synthesized in sympathetic nerves, mainly norepinephrine, ATP, and neuropeptide Y (NPY). When sympathetic nerves are activated norepinephrine and ATP are co-released in varying proportions, depending on the parameters of stimulation. Short bursts at low frequency favor the purinergic component, while longer periods of stimulation favor the adrenergic component. The release of NPY occurs more often with higher stimulation frequencies. NPY acts a direct vasoconstrictor and also potentiates the postjunctional action of norepinephrine and ATP (Hirsch and Zukowska 2012; Burnstock and Ralevic 2013).

The parasympathetic innervation of the blood vessels is poorly defined relative to those of sympathetic or sensory-motor nerves. In cerebral vasculature, the activation of parasympathetic nerves causes vasodilatation. In some other vascular beds, however, parasympathetic nerves have little influence on the vascular tone (Burnstock 1980; Westcott and Segal 2013). Acetylcholine (ACh), vasoactive intestinal polypeptide (VIP), ATP, and NO are co-transmitters for parasympathetic nerves. The relative functional importance of these co-transmitters varies depending on different tissues and species. NO has been found being the major co-transmitter in cerebral vasodilation whereas VIP being a more important co-transmitter in vasodilation in the pancreas (Burnstock 2009).

Many blood vessels are innervated by sensory-motor nerves, both unmyelinated C fibers and myelinated Aδ fibers. The terminal axons of these nerves in the vascular walls can release of neurotransmitters when an impulses travels antidromically up and then down to collateral fibers. The principal neurotransmitter in perivascular sensory-motor nerves is calcitonin gene-related peptide (CGRP),

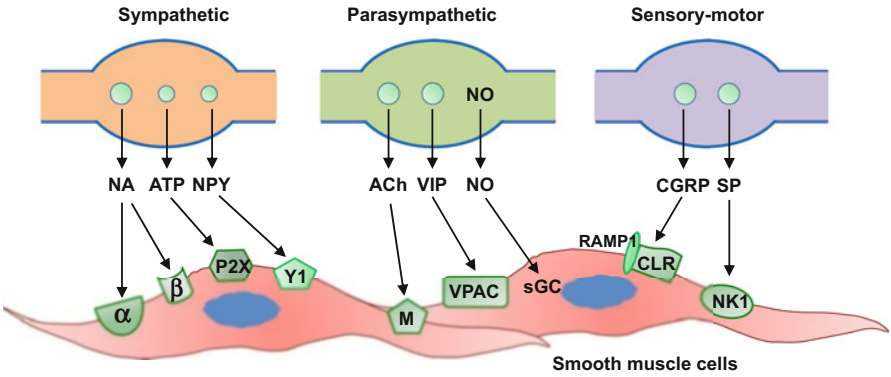

Fig. 7.1 Neurotransmitters co-released from sympathetic, parasympathetic, and sensory-motor nerve varicosities toward to smooth muscle cells. These neurotransmitters include norepinephrine (NA), neuropeptide Y (NPY), acetylcholine (ACh), vasoactive intestinal peptide (VIP), nitric oxide (NO), calcitonin gene-related peptide (CGRP), and substance P. They primarily act the following receptors on smooth muscle cells as the arrow-line pointed: α-adrenergic receptors (α), β-adrenergic receptors (β), P2X purinoceptors (P2X), NPY receptors Y1 (Y1), muscarinic receptors (M), VPAC receptors, soluble guanylyl cyclase (sGC), CGRP receptor consisting of calcitonin receptor-like receptor (CLR) linked to an essential receptor activity modifying protein 1 (RAMP1), and tachykinin receptor 1 (NK1)

which mediates vasorelaxation. There was early evidence that ATP can be released during antidromic stimulation of sensory-motor nerves in the rabbit ear artery causing vasodilation. In many unmyelinated, capsaicin-sensitive nerve terminals substance P (SP) and CGRP are co-transmitters, which often coexist in the same large granular vesicles. In a subpopulation of sensory terminals that mediate nociceptive signals ATP and glutamate are co-transmitters (Burnstock 2009; Westcott and Segal 2013) (Fig. 7.1).

7.3 G-Protein-Coupled Receptor

The majority of the neurotransmitters released from the nerves in the blood vessels act to bind to GPCRs (Hirst and Edwards 1989; Burnstock and Ralevic 2013; Westcott and Segal 2013; Foord et al. 2005). These receptors are structurally featured by a seven-alpha-helix transmembrane span topology, with the amino terminus and three transmembrane connecting loops positioned extracellularly and the carboxy-terminus and another three transmembrane connecting loops located intracellularly. GPCRs are defined by conserved sequence elements located primarily in the receptor transmembrane region. Overall, these receptors are divided into canonical (family A-C) and noncanonical groups. Family A is defined by homology with the visual receptor rhodopsin and the β_2-adrenergic receptor (β_2AR). Family B is defined by sequence homology to secretin and glucagon

receptors and is localized predominantly to gastrointestinal and neuronal tissue. Family C receptors are neuromodulatory metabotropic glutamate and $GABA_B$ receptors. Noncanonical receptors such as the frizzled family that recognize Wnt ligands and the hedgehog co-receptor Smoothened. These receptors exert their effect through G-protein-independent mechanisms (Foord et al. 2005; Black et al. 2016; Hodavance et al. 2016).

The G-protein is composed of a heterotrimers with the α-subunit tightly associated with the βγ-subunit dimer. Under nonstimulated status, the α-subunit is bound to GDP. When GPCR is activated by the agonist, GDP is exchanged for GTP on the α-subunit. This results in the dissociation of the α-subunit from the βγ-subunits. The dissociated α·GTP then bind to and activate their downstream signaling effectors. Based on the difference in their downstream effectors, G-proteins are divided into four subclasses: G-proteins that stimulate (G_s) and inhibit (G_i) adenylyl cyclase, respectively; G-proteins that activate phospholipase C-β enzymes (G_q proteins); and G-proteins that activate guanine nucleotide exchange factors (GEFs) for the RhoA small GTP-binding protein ($G_{12/13}$). In addition to the α-subunit, the unbound βγ-subunits can also bind to and activate their own effectors, such as G-protein-regulated inward rectifying K^+ (GIRK) channels and GPCR kinase 2 (GRK2) (Fig. 7.2). The α-subunit possesses an intrinsic GTPase that hydrolyzes GTP to GDP, which causes the α-subunit to dissociate from its effectors and reassociates with βγ-subunits and thus terminates the signaling. This process can be accelerated by some GTPase-activating proteins, such as regulator of G-protein signaling (RGS) family accessory proteins (Black et al. 2016; Hodavance et al. 2016).

When a GPCR is persistently over-activated, its intracellular domain may be phosphorylated by GPCR kinases (GRKs), which promote the binding of arrestins to the receptor, and consequently further G-protein-mediated signaling is blocked. Arrestins promote GPCR signal termination by two distinct mechanisms. Firstly, the binding of arrestins directly inhibits GPCR-G-protein coupling. Secondly, arrestin binding promotes receptor internalization. After mediating GPCR internalization, arrestins may either dissociate or remain bound to a receptor depending on arrestin affinity for the phospho-receptor. Early dissociation of arrestin from a weak-binding GPCR makes the endocytosed GPCR to quickly return to the cell surface in an activatable state. Otherwise the GPCR is faced with either receptor degradation or delayed receptor recycling (Black et al. 2016; Hodavance et al. 2016).

In addition to GPCR signal termination, arrestins and GRKs also serve as molecular scaffolds for various protein kinases, transcription factors, and bioactive molecules and thus alter their signaling activities. For instance, arrestins may scaffold with and activate mitogen-activated protein kinases (MAPKs), phosphatidylinositol 3-kinase (PI3K) and Akt, tyrosine kinase Src, diacyl glycerol kinases (DGKs), phosphodiesterase 4D (PDE4D), and Ca^{2+}/calmodulin kinase II (CaMKII). The arrestin family has four proteins, arrestins1–4. Arrestin 1 and 4 are largely confined to photoreceptors, whereas arrestins 2 and 3 (named also β-arrestin 1 and 2) are ubiquitously expressed. The GRK family consists of seven isoforms. While GRK1 and GRK2 are mainly expressed to the retinal tissue and GRK4 is

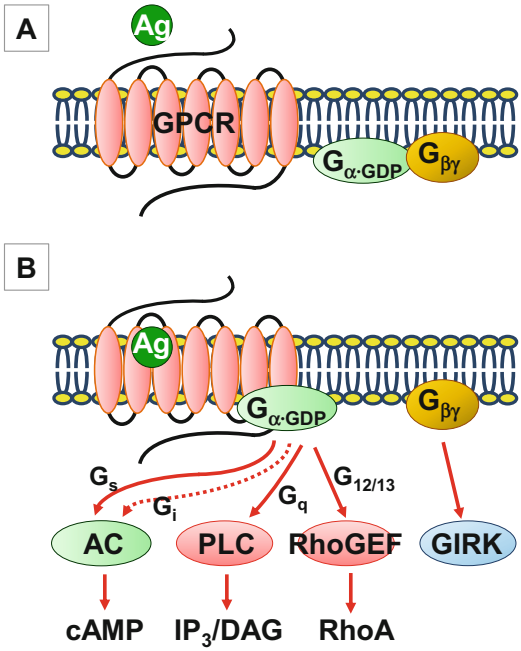

Fig. 7.2 A general mechanism for G-protein-coupled receptor (GPCR) signaling. (**a**) Under inactive state G-proteins exist as heterotrimeric G-protein complexes, consisting of a α-subunit bound to GDP and a stable dimeric complex made up by β- and γ-subunits. (**b**) Upon the binding of the cognate agonist (Ag), the GPCR is activated, which leads to GDP/GTP exchange on the α-subunit followed by the dissociation of activated α·GTP from the βγ-subunits. G_s and G_i proteins, respectively, stimulate and inhibit adenylyl cyclase (AC), resulting in increased and decreased formation of cAMP. G_q proteins activate phospholipase C (PLC), which increases intracellular inositol trisphosphate (IP_3) and diacyl glycerol (DAG). $G_{12/13}$ proteins increase the RhoA activity via guanine nucleotide exchange factors for the RhoA (RhoGEFs). The dissociated βγ-subunits can bind to and activate their own effectors, such as G-protein-regulated inward rectifying K^+ (GIRK). The *solid line arrow*: stimulatory. The *dotted line arrows*: inhibitory (The figure is modified from Black et al. (2016), with permission)

predominantly confined to the testes, the other members are widely expressed and involved in the modulation of diverse signaling pathways through GPCR-dependent and -independent mechanisms (Patel et al. 2010; Watari et al. 2014; Black et al. 2016).

In the classic model of GPCR activation, agonist binding activates both G-protein signaling as well as GRK and arrestin-mediated activites. However, certain ligands, termed biased ligands, have been found to be able to stabilize distinct conformations of the GPCR leading to the selective activation of either a G-protein or arrestin signaling pathway. The position of a GPCR where its endogenous ligand binds is known as the orthosteric site. Some ligands bind at a site different from the orthosteric site, resulting in a conformational change of the receptor that activates a specific subset of receptor-mediated pathways. Moreover,

the allosteric ligand may interact with the orthostatic site ligand and activate a specific subset of downstream signaling (Khajehali et al. 2015). Angiotensin II type 1 receptor (AT_1R) is a G-protein-coupled receptor. Studies suggest that mechanical stretch induces a conformational change of the AT_1R that results in the selectively activation of signaling pathway downstream to β-arrestin (Rakesh et al. 2010; Tang et al. 2014).

It should be noted that agonists can be are classified according to their effect on GPCR activity. A full agonist causes a maximal GPCR activation as compared to the endogenous ligand. A partial agonist even at the highest concentrations causes a submaximal activation of the receptor, while an antagonist inhibits the activation of the receptor. Many GPCRs displays a ligand-independent spontaneous activity. Such a constitutive activity is explained by a two-state receptor model in which GPCRs exist in a dynamic equilibrium between active and inactive states. A ligand that suppresses the basal constitutive activity of a GPCR through preventing spontaneous transitions to active states is termed as inverse or negative agonist. Meanwhile an agent that inhibits agonist-induced GPCR activation without affecting the basal constitutive activity of a GPCR is known as a neutral antagonist (Parra and Bond 2007; Walker et al. 2011; Black et al. 2016).

7.4 Adrenergic Signaling

The vascular effects of norepinephrine released from sympathetic nerve varicosities as well as epinephrine from the circulation are mediated by G-protein-coupled adrenoceptors (ARs). ARs are classified into three main subtypes: α_1-, α_2-, and β-ARs. The α_1 subtype comprises three members, α_{1A}, $\alpha_{1B,}$ and α_{1D}. These subtypes are activated by norepinephrine and epinephrine with equal potency, and their signaling is predominantly via $G_{q/11}$ but α_1-ARs also couple to $G_{i/o}$, G_s, and $G_{12/13}$. There are also differences between these subtypes in coupling efficiency to different pathways. The coupling efficiency to Ca^{2+} signaling is $\alpha_{1A} > \alpha_{1B} > \alpha_{1D}$ but for MAPK signaling is $\alpha_{1D} > \alpha_{1A} > \alpha_{1B}$. The α_2 subtype contains three members, α_{2A}, $\alpha_{2B,}$ and α_{2C}. The α_2-ARs have a relative potency of epinephrine > norepinephrine, and their signaling is mainly via $G_{i/o}$. β-ARs consist of three members, β_1, β_2, and β_3. The β_1 subtype is more sensitive to norepinephrine than to epinephrine, while the β_2 subtype is the reverse. The β_3 subtype is equally sensitive to the two endogenous agonists. All β-ARs are coupled to G_s protein, but they may also activate other G-proteins, particularly MAPKs (Alexander et al. 2011).

Activation of α_1-ARs causes vasoconstriction resulted from G_q-mediated stimulation of phospholipase C (PLC). PLC in turn hydrolyzes phosphatidylinositol 4,5-bisphosphate (PIP_2) to inositol 1,4,5-trisphosphate (IP_3) and diacyl glycerol (DAG). IP_3 triggers the release of Ca^{2+} from the sacoplasmic reticulum (SR) and thus elevates the intracellular concentration of Ca^{2+}, followed by Ca^{2+}-calmodulin-dependent activation of myosin light chain kinase (MLCK), phosphorylation of myosin light chain (MLC), and contraction. Meanwhile protein kinase C (PKC) is

activated by DAG, which leads to diminished activity of MLC phosphatase (MLCP), increased phosphorylation of MLC, and augmented contraction (Somlyo and Somlyo 2003; Alexander et al. 2011; Docherty 2010; Sánchez-Fernández et al. 2014). α_2-ARs are predominantly located on the prejunctional sympathetic terminal to inhibit neurotransmitter release and provide negative feedback (Giovannitti et al. 2015). α_2-ARs may be also present on vascular smooth muscle cells (VSMCs) and participated in contractile activities, via G_i-mediated inhibition of adenylyl cyclase. For instance, epicardial conduit vessel constriction of dogs and humans is largely mediated by α_1-ARs, but the constriction of the resistive microcirculation is largely by α_2-ARs, although α_1-ARs are also involved (Heusch 2011). α-ARs are present not only on VSMCs but also on endothelial, adventitial, and nerve cells (McGrath 2015). Studies show that the aortic endothelium possesses all three α_1-adrenoceptor subtypes as well as, the α_2-adrenoceptor. All appear to be involved in the release of endothelial relaxant factors (Miller and Vanhoutte 1985; Angus et al. 1986; Figueroa et al. 2001; McGrath 2015).

All three subtypes of β-ARs are present on VSMCs and endothelial cells (Gao et al. 1991; Tanaka et al. 2005; Figueroa et al. 2009; Feng et al. 2012). β-ARs cause vasodilatation via G_s protein-mediated activation of adenylyl cyclase and elevation in intracellular cAMP. Cyclic AMP exerts its effect by activating a select range of intracellular effector proteins including cAMP-dependent protein kinase (PKA), cAMP-responsive ion channels, and exchange protein activated by cAMP (EPAC) (Alexander et al. 2011; Morgado et al. 2012). PKA may reduce the cytosolic Ca^{2+} level by inhibiting the Ca^{2+} entry via the activation of K^+ channels on the cell membrane and by stimulating the Ca^{2+} uptake of the SRs, which resulting in decreased Ca^{2+}-dependent MLCK activity. Meanwhile, an enhanced activity of MLCP occurs resulting from direct PKA stimulation and from EPAC-mediated inhibition of Rho kinase (ROCK). Consequently, the decreased MLCK activity and enhanced MLCP activity lead to reduced MLC phosphorylation and vasodilatation (Zieba et al. 2011; Morgado et al. 2012). All three subtypes of β-ARs can also induce vasodilatation by stimulating endothelial nitric oxide synthase (eNOS) (Figueroa et al. 2009). Interestingly, nebivolol, a selective antagonist of β_1-AR, causes vasodilatation in part through the activation of β_3-AR and eNOS (Gao et al. 1991; Feng et al. 2012).

The G_s protein-cAMP signaling could be modulated by arrestins. When β_2-AR is activated, arrestin scaffolds with PDE4D and thus translocates it to the plasma membrane, resulting in increased degradation of cAMP (Black et al. 2016). Arrestins may also affect cAMP signaling by serving as a scaffold for MAPKs (Brown and Sacks 2009). In rat aortas, the relaxation caused by β-AR stimulation with isoproterenol is associated with an increased ERK1/2 activation. The relaxation is augmented by the inhibition of ERK1/2, implying the possibility that an interaction between arrestins and MAPK may exert a negative influence on β-AR-mediated vasodilation (Perez-Aso et al. 2014). As discussed previously, persistent over-activation of GPCRs leads to phosphorylation of its intracellular domain by GRKs and arrestin-mediated receptor desensitization and internalization. In contrast to β_1- and β_2-ARs, the β_3-AR lacks the phosphorylation sites in its

intracellular domain. This would explain the phenomenon that the downregulation of β_3-AR at the protein level has rarely been reported (Cernecka et al. 2014).

7.5 Muscarinic Signaling

ACh is the primary endogenous agonist release from parasympathetic nerves. The effect of acetylcholine is mediated by G-protein-coupled muscarinic receptors, which comprise five subtypes, $M_{1–5}$. M_1, M_3, and M_5 receptors couple to G_q proteins while M_2 and M_4 receptors couple to G_i proteins (Harvey 2012). In most blood vessels, except cerebral vessels, M_3 receptor seems to be the major subtype in mediating the relaxation of vessels with endothelium and contraction of those without endothelium induced by ACh (Eglen and Whiting 1990; Walch et al. 2001; Yamada et al. 2001; Attinà et al. 2008; Gericke et al. 2011). In cerebral vessels from humans, cows, and mice the M_5 receptor appears the major subtype responsible for cholinergic responses (Elhusseiny and Hamel 2000; Yamada et al. 2001). The M_1 receptor has also been reported in mediating both contractile and relaxing responses evoked by cholinergic agonists (Eglen and Whiting 1990; Walch et al. 2001).

The activation of M_1, M_3, or M_5 receptors exerts their effect via G_q protein coupled to activation of PLC and subsequent production of DAG and IP_3 (Harvey 2012). In endothelial cells the IP_3 generated by the activation of $M_{3/5}$ receptors leads to increased Ca^{2+} release from the SR. The resulting elevation in cytosolic Ca^{2+} activates eNOS via a calmodulin-dependent mechanism, which leads to the production of NO. NO can readily diffuse into the underlying VSMCs, followed by the activation of cGMP signaling pathway and vasodilatation. Besides NO, the activation of the endothelial muscarinic receptors also causes vasodilation through prostacyclin (PGI_2) and endothelium-dependent hyperpolarizing responses. Generally speaking NO plays a larger role in the endothelium-dependent vasodilatation (Vanhoutte et al. 2015). When ACh binds directly to $M_{1/3}$ receptors on VSMCs a contractile response ensues, resulting from the activation of G_q protein and the subsequent IP_3-induced Ca^{2+} release from the SR and DAG-dependent activation of PKC (Somlyo and Somlyo 2003; Harvey 2012). In healthy blood vessels, the relaxant effect of ACh overwhelms contractile effect. When the endothelium is damaged, the contractile effect prevails (Furchgott and Vanhoutte 1989).

Although exogenous ACh and mimetics are potent endothelium-dependent vasodilators, parasympathetic stimulation elicits limited influence on most blood vessels (Furchgott and Vanhoutte 1989; Eglen and Whiting 1990). However, the cerebral circulation is a notable exception to this generalization. In mice deficient in

M_5 receptors, the dilatator response induced by ACh is virtually lost in cerebral arteries and arterioles but remains unaltered in extracerebral arteries (Yamada et al. 2001). NO generated by neuronal NO synthase (nNOS) has been demonstrated to be released for vasodilatation from parasympathetic postganglionic (nitrergic) nerve fibers innervating pial arteries and intracerebral arterioles, in which nNOS

is activated by elevated Ca^{2+} level through stimulation of N-methyl-D-aspartate (NMDA) receptors (Toda et al. 2009). In addition to acting on endothelial cells and VSMCs, parasympathetic stimulation inhibits sympathetic neurotransmitter release. Depending whether the prevailing ARs on VSMCs is α- or β-subtype, the effect may be an attenuated or augmented vasoconstriction (Vanhoutte and Shepherd 1983; Cohen et al. 1984; Eglen and Whiting 1990).

7.6 Purinergic Signaling

Purinergic signaling refers to the signaling mediated by purine nucleotides and nucleosides. The purine nucleotides such as ATP and ADP exert their effect through binding to G-protein-coupled P_{2Y} receptors, while ATP can also act through binding to the ionotropic P_{2X} receptors. P_{2Y} receptors comprise eight subtypes, with $P2Y_1$, $P2Y_2$, $P2Y_4$, $P2Y_6$, $P2Y_{14}$ coupled to $G_{q/11}$ protein, $P2Y_{10}$ coupled to $G_s/G_{q/11}$ protein, and $P2Y_{12}$ and $P2Y_{13}$ coupled to G_i protein. The P2X receptors are nonselective cation channels composed of seven subtypes, denoted as $P2X_1$ to $P2X_7$ (Alexander et al. 2011; Coddou et al. 2011; Burnstock and Ralevic 2013; Ralevic and Dunn 2015). The nucleoside adenosine exerts its effect through the activation of G-protein-coupled adenosine receptors, which comprise four subtypes, with A_1 and A_3 coupled to G_i protein while A_{2A} and A_{2B} coupled to Gs protein. (Alexander et al. 2011; Layland et al. 2014).

ATP is released from sympathetic varicosities as a co-transmitter by vesicular exocytosis. It acts at VSMC $P2X_1$ receptors to cause vasoconstriction through eliciting Ca^{2+} influx, which resulting in depolarization and further entry of Ca^{2+} via voltage-gated calcium channels. The released ATP can act prejunctionally at inhibitory P2Y receptors. ATP is hydrolyzed via ectonucleotidase 5′-triphosphohydrolases (ENTPDase) to produce AMP, and ecto-5′-nucleotidase (CD73) further hydrolyzes AMP to adenosine. Both ENTPDase and CD73 are located on the cell surface of VSMCs. Adenosine can act prejunctionally at A_1 adenosine receptors to inhibit the neurotransmission. Inside the blood vessel, nucleotides (ATP, ADP, and UTP) can be released from the endothelium by shear stress and hypoxia. ATP and ADP can also be released from erythrocytes by shear stress, hypoxia, and low pH. These nucleotides act at endothelial $P2X_4$ and P2Y receptors to cause the release of NO, prostacyclin, and endothelium-derived hyperporlarizing factor (EDHF) leading to vasodilatation. Under the actions of cell surface ENTPDase and CD73, ATP and ADP are converted to adenosine, which acts at A_{2A} and A_{2B} adenosine receptors of endothelial cells and VSMCs to cause vasodilatation (Burnstock and Ralevic 2013; Layland et al. 2014; Ralevic and Dunn 2015).

7.7 Signalings via Neuropeptides

A number of neuropeptides are important neurotransmitters related to the regulation of vascular activities, which include NPY in sympathetic nerves, VIP in parasympathetic nerves, and CGRP and SP in sensory-motor nerves (Burnstock 1980; Westcott and Segal 2013). Among them, NPY coexists in postganglionic sympathetic nerves with norepinephrine and ATP. While ATP is stored with norepinephrine in a larger pool of small dense-core vesicles, NPY is contained with norepinephrine in a smaller population of large dense-core vesicles. ATP is released primarily when the nerves are exposed to very low-frequency stimuli, and NPY is released predominately during bursts of intense and prolonged high-frequency sympathetic activation. For norepinephrine, it is released throughout a wide range of nerve activities. The effects of NPY are mediated by G_i protein-coupled NPY receptors comprising five subtypes, Y1, Y2, Y4, Y5, and Y6. Among these receptors Y6 is nonfunctional in humans. NPY causes vasocontraction through the activation of its Y1 receptor on VSMCs. The contractile response is slow onset, but long lasting even in the midst of α-AR desensitization when norepinephrine is no longer effective. The activation of Y1 receptor on VSMCs also enhances the effects of ATP and norepinephrine. NPY also acts presynaptically via the Y2 receptors to inhibit sympathetic activation leading to reduced release of sympathetic transmitters. Hence, it seems that the postsynaptic actions of NPY are to maximize the amplitude and duration of the response evoked following activation of the nerve, while the presynaptic effect of this peptide is to protect against depletion of their stores. $NPY_{3–36}$, an endogenous product converted from NPY by the enzyme dipeptidyl peptidase 4, promotes angiogenesis via Y2 and Y5 receptors on endothelial cells and VSMCs (Hirsch and Zukowska 2012; Saraf et al. 2016).

In parasympathetic nerves, VIP and ACh are stored in separate vesicles and released differentially depending on stimulation conditions. In cat salivary gland, the stimulation of parasympathetic nerves at low-frequency ACh is released, resulting in minor vasodilatation. At high stimulation frequencies, VIP is released leading to marked vasodilatation. VIP also acts prejunctionally on the nerve varicosities to enhance the release of ACh while ACh exerts an inhibitory action on the release of VIP (Burnstock 2009). VIP exerts its effect through G_s protein-coupled VIP and pituitary adenylate cyclase-activating peptide (VIP/PACAP) receptors. These receptors are divided into three subtypes, VPAC1, VPAC2, and PAC1, and the former two exhibit affinity $\geq$100-fold for VIP than PAC1 (Harmar et al. 2012). In cerebral arteries of the rat, all three VIP/PACAP receptors have been detected on VSMCs but not endothelial cells by immunohistochemistry and Western blotting. Agonist potency profile of functional studies suggests that the dilatation of the cerebral arteries induced by VIP is mediated by VPAC1 and/or VPAC2 receptors on VSMCs (Erdling et al. 2013).

CGRP is primarily localized to C and Aδ sensory-motor nerves, which show an extensive perivascular distribution. CGRP exists as two major forms, α and β. They

are synthesized from two distinct genes, share >90% homology, and share similar biological actions. After synthesis, CGRP is stored in large, dense-core vesicles within the sensory nerve terminal and is released from the terminal by exocytosis upon depolarization. CGRP is a highly potent vasodilator. It acts through CGRP receptors, which consist of calcitonin receptor-like receptor (CLR) linked to an essential receptor activity modifying protein 1 (RAMP1) that is necessary for full functionality. The activation of CGRP receptors results in G_s protein-mediated cAMP elevation and relaxation of VSMCs as well as cAMP-PKA mediated activation of eNOS and thus increased NO production in the endothelial cells (Russell et al. 2014). Evidence also indicates that CGRP can attenuate vasoconstriction evoked by ET-1 by promoting the dissociation of ET-1/ETA receptor complexes via G-protein βγ-subunits (Meens et al. 2012). In addition, CGRP is also released from the central projections of the dorsal root ganglion neurons where it may play a role in the central sensitization (Russell et al. 2014).

SP is another principal neurotransmitter exists in sensory-motor nerves. The majority of SP-containing sensory-motor nerves are located around the blood vessels. In many unmyelinated, capsaicin-sensitive nerve terminals, SP and CGRP often coexist in the same large granular vesicles. The effect of SP is mediated by the $G_{q/11}$ protein-coupled neurokinin receptor 1(NK1) receptors. These receptors have been identified in VSMCs and endothelial cells of most arteries, arterioles, capillaries, and post-capillary venules. SP exerts a dilator effect by stimulating the endothelium to release NO, prostacyclin, and EDHF. SP released from the sensory-motor nerves may also act directly on VSMCs causing constriction. Under normal physiological conditions, vasodilation is the dominant action of SP, although the removal of endothelium or the inhibition of eNOS may reveals its direct vasoconstrictor effects (Burnstock 2009; Westcott and Segal 2013; Mistrova et al. 2015; Vanhoutte et al. 2015).

References

Alexander SPH, Mathie A, Peters JA (2011) Guide to Receptors and Channels (GRAC), 5th edn. Br J Pharmacol 164(Suppl. 1):S1–S324

Angus JA, Cocks TM, Satoh K (1986) The alpha adrenoceptors on endothelial cells. Fed Proc 45:2355–2359

Attinà TM, Oliver JJ, Malatino LS, Webb DJ (2008) Contribution of the M3 muscarinic receptors to the vasodilator response to acetylcholine in the human forearm vascular bed. Br J Clin Pharmacol 66:300–303

Black JB, Premont RT, Daaka Y (2016) Feedback regulation of G protein-coupled receptor signaling by GRKs and arrestins. Semin Cell Dev Biol 50:95–104

Brown MD, Sacks DB (2009) Protein scaffolds in MAP kinase signalling. Cell Signal 21:462–469

Burnstock G (1980) Cholinergic and purinergic regulation of blood vessels. In: Handbook of physiology. The cardiovascular system. Am Physiol Soc, Bethesda, sect. 2, vol II, chapter 19, pp 567–612

Burnstock G (2009) Autonomic neurotransmission: 60 years since sir Henry Dale. Annu Rev Pharmacol Toxicol 49:1–30

Burnstock G, Ralevic V (2013) Purinergic signaling and blood vessels in health and disease. Pharmacol Rev 66:102–192

Cernecka H, Sand C, Michel MC (2014) The odd sibling: features of β3-adrenoceptor pharmacology. Mol Pharmacol 86:479–484

Coddou C, Yan Z, Obsil T, Huidobro-Toro JP, Stojilkovic SS (2011) Activation and regulation of purinergic P2X receptor channels. Pharmacol Rev 63:641–683

Cohen RA, Shepherd JT, Vanhoutte PM (1984) Neurogenic cholinergic prejunctional inhibition of sympathetic beta adrenergic relaxation in the canine coronary artery. J Pharmacol Exp Ther 229:417–421

Docherty JR (2010) Subtypes of functional alpha1-adrenoceptor. Cell Mol Life Sci 67:405–417

Eglen RM, Whiting RL (1990) Heterogeneity of vascular muscarinic receptors. J Auton Pharmacol 10:233–245

Elhusseiny A, Hamel E (2000) Muscarinic- but not nicotinic-acetylcholine receptors mediate a nitric oxide-dependent dilation in brain cortical arterioles: a possible role for the M5 receptor subtype. J Cereb Blood Flow Metab 20:298–305

Erdling A, Sheykhzade M, Maddahi A, Bari F, Edvinsson L (2013) VIP/PACAP receptors in cerebral arteries of rat: characterization, localization and relation to intracellular calcium. Neuropeptides 47:85–92

Feng MG, Prieto MC, Navar LG (2012) Nebivolol-induced vasodilation of renal afferent arterioles involves β3-adrenergic receptor and nitric oxide synthase activation. Am J Physiol Ren Physiol 303:F775–F782

Figueroa XF, Poblete MI, Boric MP, Mendizabal VE, Adler-Graschinsky E, Huidobro-Toro JP (2001) Clonidine-induced nitric oxide dependent vasorelaxation mediated by endothelial α_2-adrenoceptor activation. Br J Pharmacol 134:957–968

Figueroa XF, Poblete I, Fernández R, Pedemonte C, Cortés V, Huidobro-Toro JP (2009) NO production and eNOS phosphorylation induced by epinephrine through the activation of beta-adrenoceptors. Am J Physiol Heart Circ Physiol 297:H134–H143

Foord SM, Bonner TI, Neubig RR, Rosser EM, Pin JP, Davenport AP, Spedding M, Harmar AJ (2005) International Union of Pharmacology. XLVI. G protein-coupled receptor list. Pharmacol Rev 57:279–288

Furchgott RF, Vanhoutte PM (1989) Endothelium-derived relaxing and contracting factors. FASEB J 3:2007–2018

Gao Y, Nagao T, Bond RA, Janssens WJ, Vanhoutte PM (1991) Nebivolol induces endothelium-dependent relaxations of canine coronary arteries. J Cardiovasc Pharmacol 17:964–969

Gericke A, Sniatecki JJ, Mayer VG, Goloborodko E, Patzak A, Wess J, Pfeiffer N (2011) Role of M1, M3, and M5 muscarinic acetylcholine receptors in cholinergic dilation of small arteries studied with gene-targeted mice. Am J Physiol Heart Circ Physiol 300:H1602–H1608

Giovannitti JA Jr, Thoms SM, Crawford JJ (2015) Alpha-2 adrenergic receptor agonists: a review of current clinical applications. Anesth Prog 62:31–39

Harmar AJ, Fahrenkrug J, Gozes I, Laburthe M, May V, Pisegna JR, Vaudry D, Vaudry H, Waschek JA, Said SI (2012) Pharmacology and functions of receptors for vasoactive intestinal peptide and pituitary adenylate cyclase-activating polypeptide: IUPHAR review 1. Br J Pharmacol 166:4–17

Harvey RD (2012) Muscarinic receptor agonists and antagonists: effects on cardiovascular function. Handb Exp Pharmacol 208:299–316

Heusch G (2011) The paradox of α-adrenergic coronary vasoconstriction revisited. J Mol Cell Cardiol 51:16–23

Hirsch D, Zukowska Z (2012) NPY and stress 30 years later: the peripheral view. Cell Mol Neurobiol 32:645–659

Hirst GDS, Edwards FR (1989) Sympathetic neuroeffector transmission in arteries and arterioles. Physiol Rev 69:546–604

Hodavance SY, Gareri C, Torok RD, Rockman HA (2016) G protein-coupled receptor biased agonism. J Cardiovasc Pharmacol 67:193–202

Khajehali E, Malone DT, Glass M, Sexton PM, Christopoulos A, Leach K (2015) Biased agonism and biased allosteric modulation at the CB1 cannabinoid receptor. Mol Pharmacol 88:368–379
Layland J, Carrick D, Lee M, Oldroyd K, Berry C (2014) Adenosine: physiology, pharmacology, and clinical applications. JACC Cardiovasc Interv 7(6):581–591
McGrath JC (2015) Localization of α-adrenoceptors: JR Vane Medal Lecture. Br J Pharmacol 172:1179–1194
Meens MJ, Mattheij NJ, van Loenen PB, Spijkers LJ, Lemkens P, Nelissen J, Compeer MG, Alewijnse AE, De Mey JG (2012) G-protein βγ subunits in vasorelaxing and anti-endothelinergic effects of calcitonin gene-related peptide. Br J Pharmacol 166:297–308
Miller VM, Vanhoutte PM (1985) Endothelial α_2-adrenoceptors in canine pulmonary and systemic blood vessels. Eur J Pharmacol 118:123–129
Mistrova E, Kruzliak P, Chottova Dvorakova M (2015) Role of substance P in the cardiovascular system. Neuropeptides. pii S0143-4179(15):00225–00225
Morgado M, Cairrão E, Santos-Silva AJ, Verde I (2012) Cyclic nucleotide-dependent relaxation pathways in vascular smooth muscle. Cell Mol Life Sci 69:247–266
Parra S, Bond RA (2007) Inverse agonism: from curiosity to accepted dogma, but is it clinically relevant? Curr Opin Pharmacol 7:146–150
Patel CB, Noor N, Rockman HA (2010) Functional selectivity in adrenergic and angiotensin signaling systems. Mol Pharmacol 78:983–992
Perez-Aso M, Flacco N, Carpena N, Montesinos MC, D'Ocon P, Ivorra MD (2014) β-adrenoceptors differentially regulate vascular tone and angiogenesis of rat aorta via ERK1/2 and p 38. Vasc Pharmacol 61:80–89
Rakesh K, Yoo B, Kim IM, Salazar N, Kim KS, Rockman HA (2010) β-arrestin-biased agonism of the angiotensin receptor induced by mechanical stress. Sci Signal 3:ra46
Ralevic V, Dunn WR (2015) Purinergic transmission in blood vessels. Auton Neurosci 191:48–66
Russell FA, King R, Smillie SJ, Kodji X, Brain SD (2014) Calcitonin gene-related peptide: physiology and pathophysiology. Physiol Rev 94:1099–1142
Sánchez-Fernández G, Cabezudo S, García-Hoz C, Benincá C, Aragay AM, Mayor F Jr, Ribas C (2014) Gαq signalling: the new and the old. Cell Signal 26:833–848
Saraf R, Mahmood F, Amir R, Matyal R (2016) Neuropeptide Y is an angiogenic factor in cardiovascular regeneration. Eur J Pharmacol 776:64–70
Somlyo AP, Somlyo AV (2003) Ca^{2+} sensitivity of smooth muscle and nonmuscle myosin II: modulated by G proteins, kinases, and myosin phosphatase. Physiol Rev 83:1325–1358
Tanaka Y, Horinouchi T, Koike K (2005) New insights into beta-adrenoceptors in smooth muscle: distribution of receptor subtypes and molecular mechanisms triggering muscle relaxation. Clin Exp Pharmacol Physiol 32:503–514
Tang W, Strachan RT, Lefkowitz RJ, Rockman HA (2014) Allosteric modulation of β-arrestin-biased angiotensin II type 1 receptor signaling by membrane stretch. J Biol Chem 289:28271–28283
Toda N, Ayajiki K, Okamura T (2009) Cerebral blood flow regulation by nitric oxide: recent advances. Pharmacol Rev 61:62–97
Vanhoutte PM, Shepherd JT (1983) Muscarinic and beta-adrenergic prejunctional modulation of adrenergic neurotransmission in the blood vessel wall. Gen Pharmacol 14:35–37
Vanhoutte PM, Shimokawa H, Feletou M, Tang EH (2015) Endothelial dysfunction and vascular disease - a thirthieth anniversary update. Acta Physiol (Oxford). doi:10.1111/apha.12646
Walch L, Brink C, Norel X (2001) The muscarinic receptor subtypes in human blood vessels. Therapie 56:223–226
Walker JK, Penn RB, Hanania NA, Dickey BF, Bond RA (2011) New perspectives regarding β_2-adrenoceptor ligands in the treatment of asthma. Br J Pharmacol 163:18–28
Watari K, Nakaya M, Kurose H (2014) Multiple functions of G protein-coupled receptor kinases. J Mol Signal 9:1
Westcott EB, Segal SS (2013) Perivascular innervation: a multiplicity of roles in vasomotor control and myoendothelial signaling. Microcirculation 20:217–238

Yamada M, Lamping KG, Duttaroy A, Zhang W, Cui Y, Bymaster FP, McKinzie DL, Felder CC, Deng CX, Faraci FM, Wess J (2001) Cholinergic dilation of cerebral blood vessels is abolished in M(5) muscarinic acetylcholine receptor knockout mice. Proc Natl Acad Sci U S A 98:14096–14101

Zieba BJ, Artamonov MV, Jin L, Momotani K, Ho R, Franke AS, Neppl RL, Stevenson AS, Khromov AS, Chrzanowska-Wodnicka M, Somlyo AV (2011) The cAMP-responsive Rap1 guanine nucleotide exchange factor, Epac, induces smooth muscle relaxation by down-regulation of RhoA activity. J Biol Chem 286:16681–16692

Chapter 8
Endothelium-Derived Factors

Abstract The endothelium-dependent regulation of vascular tone is predominantly by four major players: nitric oxide (NO), prostaglandin I_2 (PGI_2), endothelium-derived hyperpolarizing factor (EDHF), and endothelin-1 (ET-1). The former three are vasodilators, while ET-1 is a potent vasoconstrictor. NO and PGI_2 exert their effects primarily by activating, respectively, cGMP–cGMP-dependent protein kinase (PKG) and cAMP–cAMP-dependent pathways, which result in decreased Ca^{2+} influx, suppressed Ca^{2+} release from the sarcoplasmic reticulum, reduced sensitivity of myofilament to Ca^{2+}, and consequently vasodilatation. Unlike NO and PGI_2, the identity of EDHF differs depending on vessel sizes and types as well as species. The better known two EDHFs are epoxyeicosatrienoic acids (EETs) and H_2O_2. All EDHFs cause vasodilatation mainly by activation of K^+ channels, leading to membrane hyperpolarization and decreased Ca^{2+} influx. Among these vasodilators, NO is the dominant player, PGI_2 often has a complementary role, and EDHFs are more important in resistant arteries where NO is less crucial. The vasodilatory effects of these agents are counteracted by various vasoconstrictors in particular ET-1, which exerts its effect by stimulating Ca^{2+} influx, promoting Ca^{2+} release from the sarcoplasmic reticulum, and enhancing Ca^{2+} sensitivity of myofilament. ET-1 has delicate and complicated interactions with endothelium-derived NO as well as other vasodilators. The balance between the constrictor actions and dilator actions is essential for vascular hemostasis.

Keywords Nitric oxide • eNOS • Prostaglandin I2 • Hyperpolarization • Endothelin-1 • Vascular smooth muscle

8.1 Introduction

Vascular endothelium is composed of mainly a monolayer of endothelial cells (ECs) and located between circulating blood and vascular smooth muscle cells (VSMCs) and other structures of the wall of blood vessels. By occupying such a strategic position, the endothelium is uniquely fit and rightly endowed with the power to regulate vasomotor tone in a manner suitable for organ perfusion (Aird 2007). The endothelium affects the activities of blood vessels primarily through nitric oxide (NO), prostaglandin I_2 (PGI_2), endothelium-derived hyperpolarizing

Y. Gao, *Biology of Vascular Smooth Muscle: Vasoconstriction and Dilatation*,
DOI 10.1007/978-981-10-4810-4_8

factor (EDHF), and endothelin-1 (ET-1). The former three cause vasodilatation through reducing the cytosolic Ca^{2+} level and decreasing the sensitivity of myofilaments to Ca^{2+}. In contrast, ET-1 causes vasoconstriction by counteracting the effects of vasodilators (Moncada 2006; Edwards et al. 2010; Vanhoutte et al. 2017; Davenport et al. 2016). The actions and related mechanisms of these vasoactive agents are the focus of this chapter.

8.2 Endothelium-Derived NO

Endothelium-derived NO (EDNO) is a major player in cardiovascular homeostasis essential for the regulation of vascular tone, cellular proliferation, leukocyte adhesion, and platelet aggregation (Förstermann and Sessa 2012; Vanhoutte et al. 2017). EDNO is generated by NO synthase (NOS) that is mostly located in the endothelial cells, termed endothelial NOS (eNOS) or NOS-3. This enzyme is also detected in cardiac myocytes, platelets, certain neurons of the brain, in syncytiotrophoblasts of the human placenta, and in LLC-PK1 kidney tubular epithelial cells. There are two other NOS isoforms existed: neuronal (nNOS or NOS-1) and cytokine-inducible (iNOS or NOS-2). The former is mainly located in the nervous system and the latter predominantly in immune system. Inside the cell, eNOS is membrane-associated, while iNOS and nNOS are found in the cytosol (Förstermann et al. 1994).

NOS exists as homodimers. Each monomer is sized 134 kD comprising a C-terminal reductase domain with binding sites for nicotinamide adenine dinucleotide phosphate (NADPH), flavin adenine dinucleotide (FAD), flavin mononucleotide (FMN), and an N-terminal oxygenase domain with binding sites for heme group, zinc, tetrahydrobiopterin (BH_4), and the substrate L-arginine. These two domains are linked by a calmodulin (CaM)-binding sequence. In eNOS and nNOS, there is an autoinhibitory loop in the FMN-binding domains which may exert an inhibitory action on the binding of CaM. In all NOS isoforms, there is also an autoinhibitory loop in the C-terminal tail that curls back to interact with the flavin domain so that electron transfer is attenuated in a CaM-independent manner (Daff 2010; Fleming 2010). In the process of NO synthesis, electrons are transferred from NADPH, via the flavins FAD and FMN in the reductase domain to the heme in the oxygenase domain of the opposite monomer. The FMN domain first transfers an electron to the ferric heme to form a ferric heme-superoxy species (species I), which can receive an electron from tetrahydrobiopterin (H_4B) resulting in a heme-peroxo species (species II). When H_4B is insufficient, superoxide rather than species II is generated; otherwise species II may be protonated to form a heme iron-oxo species (species III), which may hydroxylate L-arginine or react with N^{ω}-hydroxy-L-arginine (NOHA). NOHA is an enzyme-bound intermediate during the synthesis of NO prior to being further oxidized to L-citrulline and NO. For each NO synthesized, one L-arginine, one and a half NADPH, and two O_2 are consumed (Stuehr et al. 2004; Förstermann and Sessa 2012) (Fig. 8.1).

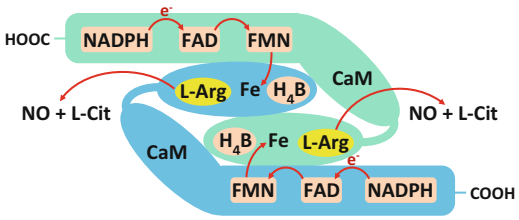

Fig. 8.1 Catalytic mechanisms of endothelial nitric oxide (eNOS). A functional eNOS is homodimer. Each monomer comprises a reductase domain containing binding sites for NADPH, FAD, FMN, and calmodulin (CaM) and an oxygenase domain with an iron heme group (Fe) and binding sites for L-arginine (L-Arg) and BH4. In the catalytic process, an electron from NADPH is transferred to FAD and FMN and then to the ferric heme of the opposite monomer. CaM regulates electron flow between the reductase and oxygenase domain. BH4 is essential to donate electrons to the heme group in order to oxidize L-arginine (L-Arg), resulting in the formation of nitric oxide (NO) and a by-product L-citrulline (L-Cit). *FAD* flavin adenine dinucleotide, *FMN* flavin mononucleotide, *H_4B* tetrahydrobiopterin, *NADPH* reduced nicotinamide adenine dinucleotide phosphate

The dimeric status is obligatory for the functionality of NOS. The heme-deficient NOSs exist only as a monomer. It preserves most of the structural elements found in the dimeric holoenzyme and is properly folded but is unable to bind the cofactor BH_4 or the substrate L-arginine and cannot produce NO, indicating that the prosthetic heme group of NOSs is requisite for dimerization of enzyme subunits (Klatt et al. 1996; List et al. 1997). All NOSs contain a Zn^{2+} coordinated in a tetrahedral conformation with pairs of Cys-(X)4-Cys motifs at the dimer interface (Förstermann and Sessa 2012). Evidence reveals that a Zn^{2+} bound to Cys94 and Cys99 from each monomer of eNOS. Such a Zn^{2+}-cysteine complex catalyzes proper dimer formation. The Zn^{2+}-binding cysteines are vulnerable to redox-modifications, particularly by peroxynitrite, resulting in disulfide-bond formation between Cys94 and Cys99 in each monomer, followed by release of Zn^{2+}, formation of free monomers, and loss of enzyme activity (Pace and Weerapana 2014).

Under basal conditions, eNOS is bound to caveolin-1 (Cav-1) of plasma membrane caveolae and tonically suppressed by Cav-1. In response to a broad range of stimuli, eNOS is bound to CaM, being phosphorylated and displaced from Cav-1. CaM binds to eNOS is evoked by stimuli-induced increase in the cytosolic concentration of Ca^{2+} ($[Ca^{2+}]_i$). The elevated Ca^{2+} forms a complex with CaM and bound to eNOS, resulting in a greatly accelerated transfer of electrons from NADPH of the reductase domain to the heme of oxygenase domain and stimulated production of NO (Förstermann and Sessa 2012; Ramadoss et al. 2013). In addition to the CaM action, the phosphorylation also serves as a major mechanism in regulating eNOS activity. eNOS can be phosphorylated on serine, threonine, and tyrosine residues. Among them the best studied and probably most important are Ser1177 and Thr495 (human eNOS sequence). Phosphorylation of Ser1177 may disable the autoinhibitory loop in the C-terminal tail and thus enhance electron flux through the oxygenase domain as well as increase Ca^{2+} sensitivity of eNOS.

Ser1177 can be phosphorylated by shear stress via Akt and PKA, vascular endothelial growth factor (VEGF), insulin, estrogen via Akt, bradykinin, and Ca^{2+} elevation via Ca^{2+}/CaM-dependent protein kinase II (CaMKII). Thr495 is constitutively phosphorylated, and its phosphorylation is associated with a decreased enzyme activity, resulting from interference with the binding of CaM to the CaM-binding domain. Thr495 is dephosphorylated by stimuli that elevate $[Ca^{2+}]_i$ such as bradykinin, histamine, and Ca^{2+} ionophores, resulting in an increase in eNOS activity by 10- to 20-fold over basal levels. Under such circumstances, phosphorylation of Ser1177 may also occur (Daff 2010; Fleming 2010).

The intracellular concentrations of the substrates and cofactors including L-arginine, O_2, NADPH, and BH_4 (Chen and Popel 2006; Kar and Kavdia 2011) are normally sufficient for NO synthesis by eNOS. In human ECs, the intracellular concentration of L-arginine could be as high as 1 mM, and the K_m of eNOS for L-arginine is ~3 μmol. Since arginases can compete with eNOS for substrate, a relative L-arginine deficiency for eNOS may occur when arginase becomes overactive, which could occur in patients with hypercholesterolaemia and hypertension (Förstermann and Sessa 2012). L-arginine can be methylated by methyltransferases to form asymmetric dimethyl-L-arginine (ADMA), which is an endogenous inhibitor of eNOS. In ECs ADMA is converted to L-citrulline by the type 2 isoform dimethylarginine dimethylaminohydrolase (DDAH-2). An elevated circulating ADMA level and/or a diminished expression and activity of DDAH are often observed in various vascular diseases characterized by eNOS dysfunction [Caplin and Leiper 2012]. The K_m of eNOS for O_2, another essential substrate of the enzyme, is ~4 μM, which implies that the concentrations of O_2 even under most hypoxic conditions would not be a limiting factor for NO synthesis (Stuehr et al. 2004; Ho et al. 2012). The intracellular concentration of BH_4, a critical cofactor of eNOS, is ~3.6 μM, and the EC_{50} of BH_4 for eNOS is ~0.05–0.22 μM. Thus, it appears that the availability of BH_4 would not constitute a factor to affect eNOS activity (Chen and Popel 2006). However, under oxidative stress, the oxidization of BH_4 to dihydrobiopterin (BH_2) is accelerated, but the reduction of BH_2 to BH_4 by dihydrofolate reductase could be suppressed, resulting in a decreased ratio of BH_4 to BH_2. BH_2 and BH_4 bind eNOS with equal affinity, and BH_2 can efficiently replace BH_4 from eNOS, which renders eNOS to generate superoxide rather NO, a situation termed eNOS uncoupling. The increased superoxide can rapidly interact with NO to form peroxidenitrite, which is a potent oxidant and can stimulate further eNOS uncoupling (Fleming 2010; Robinson et al. 2011).

Several proteins are also involved in the regulation of eNOS activity. Heat-shock protein 90 (Hsp90), a constitutively expressed molecular chaperone, has been found being involved in maturation of nNOS, iNOS, and highly likely eNOS by interacting with the apoenzymes and driving heme insertion in an ATP-dependent manner. Heme insertion is obligatory for NOSs to form a homodimers and become active for NO generation (Billecke et al. 2002; Ghosh et al. 2011; Chen et al. 2014). Hsp90 can also act as a scaffolding protein for eNOS signaling. It is rapidly recruited to the eNOS complex by agonists that stimulate NO production such as VEGF, histamine, and fluid shear stress (García-Cardeña et al. 1998). Studies show

that Hsp90 recruits activated Akt in the eNOS complex and maintains Akt activity by preventing proteosomal degradation of upstream phosphatidylinositide 3-kinases and by inhibiting dephosphorylation of Akt by phosphatase 2A (Balligand et al. 2009). Dynamin is a GTPase principally related in the scission of vesicles from the membranes of the cells and cellular organelles during endocytosis and prior to vesicle transportation (Durieux et al. 2010). Inhibition of dynamin-2 has been found to suppress bradykinin- stimulated NO generation by ECs, suggesting that dynamin-dependent vesicle trafficking pathways are involved in eNOS activity (Chatterjee et al. 2003). Studies also show that the interaction of dynamin-2 with the reductase domain of eNOS augments activity of the enzyme, at least in part, by potentiating electron transfer between FAD and FMN (Cao et al. 2003). The activity of eNOS is also regulated at the transcriptional and posttranscriptional (modifications of the primary transcript, mRNA stability, subcellular localization, and nucleo-cytoplasmatic transport) levels, in particular in response to more sustained stimuli. The expression of eNOS can be upregulated by stimuli such as shear stress, transforming growth factor-β1, lysophosphatidylcholine, and cell growth. In contrast, mRNA levels of eNOS can be downregulated by stimuli such as tumor necrosis factor-α, hypoxia, lipopolysaccaride, and oxidized LDL (Searles 2006). In combination with posttranslational modifications which include fatty acid acylation, protein–protein interactions, substrate and cofactor availability, and phosphorylation, the activity of eNOS and thus the production of NO are modulated in a delicate manner (Qian and Fulton 2013).

8.3 PGI_2

PGI_2 is a potent vasodilator as well as a potent inhibitor of platelet aggregation (Moncada 2006). It is synthesized from arachidonic acid (AA) released from membrane phospholipids following activation of phospholipase A2 (PLA2). There are three forms of PLA2 being identified: the Ca^{2+}-independent phospholipase $iPLA_2$, the Ca^{2+}-dependent cytosolic phospholipase $cPLA_2$, and the secretory phospholipase $sPLA_2$. Among them, $iPLA_2$ is primarily related to cell membrane remodeling and does not induce AA release. $cPLA_2$ is the dominant phospholipase involved in liberation of AA in response to stimuli-evoked increase in $[Ca^{2+}]_i$. When exposed to enduring and intense stimuli, $sPLA_2$ is activated leading to an enhanced and sustained AA release. Upon release, AA is converted to PGG_2 through a cyclooxygenase reaction by cyclooxygenases (COX) and then to PGH_2 through a peroxidase reaction also by COX, followed by further conversion to prostaglandins (PGs) and thromboxanes (TXs) by their respective synthases (Fitzpatrick and Soberman 2001). COXs are the rate-limiting enzymes for the production of prostanoids, i.e., PGs and TXs. The enzymes exist as constitutive and inducible, termed COX-1 and COX-2, respectively. Although the expression of COX-2 is induced by inflammatory factors, it has been found to be constitutively expressed in certain cells and organs such as the epithelium, neurons, brain, and

kidney. In vasculature, COX-1 is the dominant isoform (Flavahan 2007; Tang and Vanhoutte 2008).

PGI_2 is the main product of AA in vascular tissues, reflecting the fact that the expression of PGI_2 synthase (PGIS) is the most abundant as compared with the synthases for other prostanoids (Tang and Vanhoutte 2008). In the wall of blood vessels, the ability of the large vessel wall to synthesize PGI_2 is greatest at the intimal layer and progressively decreases toward the adventitia. Among cultured vascular cells, endothelial cells (ECs) are the most active PGI_2 producer (Zou 2007). The vascular effects of PGI_2 are mediated through IP receptors (Alexander et al. 2011), which are mainly localized on vascular smooth muscle cells (VSMCs). PGI_2 may also directly bind to nuclear receptors, which include peroxisome proliferator activated receptor (PPAR) -α, −γ, and -δ. PGI_2/IP couples primarily to G_s to activate adenylyl cyclase, leading to the activation of cAMP–cAMP-dependent protein kinase (PKA) signaling, leading to decreased $[Ca^{2+}]_i$ and diminished Ca^{2+} sensitivity of myofilament and thus vasodilatation. PGI_2 through IP receptor and in a cAMP-dependent and cAMP-independent manner can also activate K^+ channels, including large-conductance Ca^{2+}-dependent K^+ channel (BK_{Ca}), small-conductance SK_{Ca}, ATP-sensitive (K_{ATP}), voltage-gated (K_V), inward-rectifier (K_{IR}), and two-pore-domain K^+ channel (K2P), resulting in membrane hyperpolarization, reduced Ca^{2+} influx through voltage-gated Ca^{2+} channels, and vasodilatation. Intracrine PGI_2 binding to perinuclear PPARs causes translocation of PPAR, which leads to genomic effects related to cell proliferation and differentiation (Majed and Khalil 2012).

Mice deficient in eNOS with mean blood pressure 35% higher than control animals exhibit a hypertensive phenotype (Huang et al. 1995). By contrast, mice lacking the PGI_2 receptor (IP) are normotensive although having an increased tendency to thrombosis when the endothelium is damaged (Murata et al. 1997). Hence, PGI_2 seems to play a less important role in regulating vascular activities. However, when NO availability or action is impaired, a compensatory increase in the role of endothelium-derived PGI_2 may occur. For instance, PGI_2 show a more prominent role in modulating vascular tone in rat mesenteric arteries and dog coronary arteries after prolonged inhibition of NO synthesis (Puybasset et al. 1996; Henrion et al. 1997; Majed and Khalil 2012). Moreover, the PGI_2-dependent and NO-dependent signalings often act in a synergistic manner. In porcine pulmonary artery, the relaxation induced by PGI_2 is augmented by the basal release of EDNO, probably resulting from reduced degradation of cAMP by the type 3 phosphodiesterase, which is inhibited by cGMP generated by soluble guanylyl cyclase activated by EDNO (Zellers et al. 2000). Relaxation of canine pulmonary artery induced by bradykinin involves both endothelium-derived NO and PGI_2 components. Quantitative analysis shows that a synergistic interaction occurs between these two components with cAMP-activated ATP-sensitive K^+ channels being involved (Gambone et al. 1997).

In rat aorta contracted with norepinephrine, the relaxation induced by PGI_2 at higher concentrations is less than that induced at lower concentrations. The smaller relaxant response is prevented by SQ29548, an antagonist of receptors for TX (TP receptors), suggesting that PGI_2 at higher concentrations may bind to TP

receptors to cause vasoconstriction (Williams et al. 1994). In a spontaneously hypertensive rat (SHR), acetylcholine evokes endothelium-dependent contraction of the aorta, which is blocked by preferential inhibitors of COX-1 but not affected by the inhibition of TX synthase. The contraction is associated with a markedly increased production of PGI_2 in an amount that is 10–100 times greater than that of the other prostanoids. In these SHR, aortae PGI_2 causes contraction, implicating that this prostanoid may act as an endothelium-derived contracting factor (EDCF) (Gluais et al. 2005; Tang and Vanhoutte 2008; Félétou et al. 2011; Vanhoutte et al. 2017). The PGI_2-mediated vasoconstriction is augmented by an exaggerated production of reactive oxygen species (ROS) which is commonly observed in atherosclerosis, diabetes, and hypertension. In the rat aorta, ROS may potentiate EDCF response by stimulating COX activity, depolarizing vascular smooth muscle cells by inhibiting various potassium channels, and causing Ca^{2+} sensitization by activating Rho kinase (Tang and Vanhoutte 2009; Félétou et al. 2011; Vanhoutte et al. 2017).

8.4 EDH

EDH is defined as endothelium-dependent hyperpolarization of VSMCs. It may result from K^+ efflux through the small and intermediate conductance, Ca^{2+}-sensitive K^+ (SK_{Ca} and IK_{Ca}, respectively) channels of ECs followed by the activation of myocyte K_{IR} channels and Na^+/K^+-ATPases. The ensuing hyperpolarization of myocyte leads to decreased Ca^{2+} influx and thus vasodilatation (Edwards et al. 2010). Alternatively, ECs may release a diffusible substance(s) such as epoxyeicosatrienoic acids (EETs), which cause vasodilatation predominantly by activating myocyte K^+ channels or by activating endothelial SK_{Ca} and IK_{Ca} channels (Campbell and Fleming 2010). In vascular tree, generally speaking, the role of EDNO decreases as the vessels size is reduced, whereas the role of EDH increases as the vessel size decreases. Such a phenomenon is well preserved from rodents to humans. Thus, EDH may play an important role in small arteries and arterioles where organ perfusion is finely regulated (Shimokawa and Godo 2016).

The activation of endothelial SK_{Ca} and IK_{Ca} channels is a key feature of the classic EDH phenomenon. SK_{Ca} channels are located in the caveolae that are spread over the entire EC surface. When ECs are stimulated by various agonists, Ca^{2+}-released from IP_3 channels of the sarcoplasmic reticulum (SR) activates the SK_{Ca} channels located in caveolae, which leads to increased K^+ enflux into caveolae and sensed by the K_{IR} channels that are also localized in caveolae, resulting in further K^+ enflux. The elevated K^+ may diffuse out of the caveolae to activate K_{IR} channels and/or Na^+/K^+-ATPases of VSMCs, with resultant hyperpolarization. IK_{Ca} channels are not located in caveolae but concentrated within the endothelial cell projections that pass through the internal elastic lamina (IEL) and form myoendothelial junctions (MEJs) with VSMCs. When IP_3 channels are activated the Ca^{2+} released from SR within the EC projections stimulates IK_{Ca} channels and an increased K^+ efflux occurs, followed by the activation of Na^+/K^+-

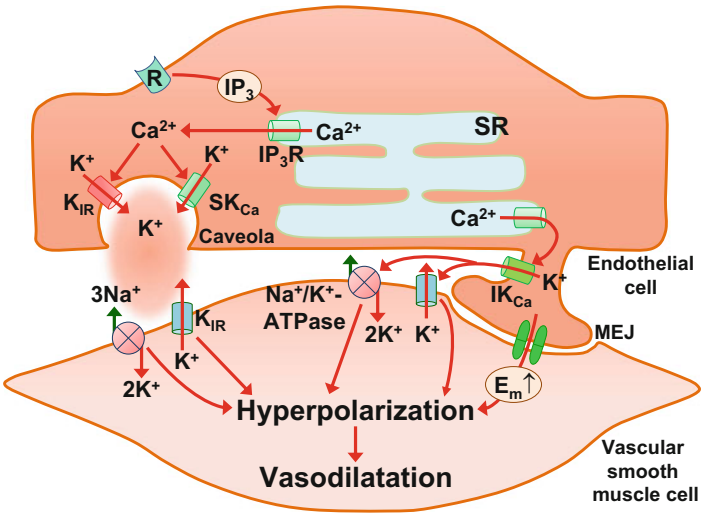

Fig. 8.2 Mechanism underlying endothelium-dependent hyperpolarization. When the receptor (R) is activated, an increased intracellular concentration of Ca^{2+} occurs resulting from inositol 1,4,5-trisphosphate (IP_3)-induced Ca^{2+} release through IP_3 receptor (IP_3R) from the sarcoplasmic reticulum (SR). The elevated Ca^{2+} can activate the small-conductance, Ca^{2+}-sensitive K^+ (SK_{Ca}) channels that are located in caveolae. This leads to an increased K^+ efflux into caveolae and causes further K^+ efflux through inward-rectifier (K_{IR}) channels that are also localized in caveolae. These events create a high K^+ microenvironment which may activate the K_{IR} channels and/or Na^+/K^+-ATPases of vascular smooth muscle cell (VSMCs), resulting in membrane hyperpolarization and vasodilatation. IK_{Ca} channels are concentrated within the endothelial cell projections that form myoendothelial junctions (MEJs) with VSMCs. The Ca^{2+} released from SR within the endothelial cell projections stimulates IK_{Ca} channels with resultant increased K^+ efflux, which can active Na^+/K^+-ATPases and/or K_{IR} channels and thus hyperpolarization of VSMCs. The efflux of K^+ may also hyperpolarize endothelial projections, and resultant hyperpolarization of ECs may be transferred electronically to the myocytes via MEJs and contribute to hyperpolarization and vasodilatation of VSMCs. E_m membrane potential

ATPases and/or and K_{IR} channels and thus hyperpolarization of VSMCs. The effluxing K^+ may also hyperpolarize endothelial projections. The hyperpolarization of ECs can also be transferred electronically to the myocytes via MEJs (Edwards et al. 2010) (Fig. 8.2). The ensuing hyperpolarization of myocyte radially spreads through the different layers of the vessel media via homocellular VSMC gap junctions, leading to decreased Ca^{2+} influx and vasodilatation. The homocellular EC gap junctions are abundantly expressed. Hence, the endothelial hyperpolarization may spread longitudinally via EC gap junctions and then influence the vascular activity through MEJs (Haas and Duling 1997; Sandow et al. 2012).

In some arteries including bovine, porcine, canine and human large coronary arteries and rodents, rabbit, and human mesenteric arteries epoxyeicosatrienoic acids (EETs) may take part in EDH-mediated relaxations. EETs are synthesized from AA by cytochrome P450 (CYP) epoxygenases. These nonclassic eicosanoids are generally short-lived, being rapidly converted to less active or inactive

dihydroxy-eicosatrienoic acids (diHETrEs) by soluble epoxide hydrolase (sEH), which is also termed epoxide hydrolase 2. Due to their short half-life, EETs act locally as autocrine agents to regulate the activity of the cells that produce them or as paracrine agents to regulate the activity of nearby cells. In the vascular wall, EETs are predominantly derived from ECs. In ECs two CYP epoxygenases, the CYP2C and CYP2J isozymes, have been identified. These isozymes produce mainly 14,15-EET and with lesser amounts of 11,12-EET. It appears that, these EETs are released when stimulated by acetylcholine, bradykinin, and shear stress (Campbell and Fleming 2010). EETs exert their action through binding to putative endothelial Gs-coupled EET receptors, which lead to a cAMP-PKA-dependent translocation of TRPC3/C6 (TRP) channels from the perinuclear Golgi apparatus, followed by increased Ca^{2+} influx, activation of SK_{Ca} and IK_{Ca} channels, and elevated K^+ concentration in the intracellular space between ECs and VSMCs. This results in the activation of K_{IR} channels and/or Na^+/K^+-ATPase in VSMCs and thus membrane hyperpolarization and vasodilatation. EETs may also act on VSMCs to activate the large-conductance, Ca^{2+}-sensitive K^+ (BK_{Ca}) channels, resulting in increased K^+ efflux, membrane hyperpolarization, and relaxation (Campbell and Fleming 2010; Frömel and Fleming 2015). The mechanism of BK_{Ca} activation by EETs may involve activation of TRPV4, which results in an increased Ca^{2+} entry, Ca^{2+}-induced Ca^{2+} release from SR via ryanodine-sensitive Ca^{2+}channels, and the subsequent activation of local BK_{Ca} channels (Edwards et al. 2010).

H_2O_2 is also believed to be an endothelium-derived hyperpolarizing factor (EDCF) with an action primarily on the pre-arterioles and arterioles where EDH-mediated relaxation becomes more important than EDNO (Shimokawa 2010; Shimokawa and Godo 2016). In porcine coronary microvessels, bradykinin causes relaxations and hyperpolarizations in the presence of inhibitors of eNOS and COX, which are prevented by catalase, the scavenger of H_2O_2. Coronary vasodilatation and hyperpolarization can also be obtained with exogenous H_2O_2 at micromolar concentrations. Studies using electron spin resonance imaging reveals that production of endothelial H_2O_2 is stimulated by bradykinin, indicating that H_2O_2 act as an EDCF (Matoba et al. 2003). It appears that endothelium-derived H_2O_2 can be generated from various sources in ECs, including nicotinamide adenine dinucleotide phosphate oxidase oxidase, mitochondrial electron transport chain, xanthine oxidase, lipoxygenase, and eNOS (Shimokawa and Godo 2016). The primary mechanism by which H_2O_2 hyperpolarizes the underlying vascular smooth muscle involves the activation of BK_{Ca} channels (Liu et al. 2011; Shimokawa and Godo 2016). The effect of H_2O_2 may in part be mediated by the type 1α cGMP-dependent protein kinase (PKG Iα). H_2O_2 can promote the dimerization of PKG Iα, resulting in enhanced activity of the kinase and subsequent activation of BK_{Ca} channels (Zhang et al. 2012; Burgoyne et al. 2013). In mice, knockin of the mutant Cys42Ser PKG1α renders VSMCs insensitive to H_2O_2-induced dimerization, due to the absence of redox-sensitive thiols. Consequently, the vasodilatory effect of H_2O_2 on resistance vessels is diminished, and the animals are hypertensive (Prysyazhna et al. 2012).

8.5 ET-1

ET-1 is the most potent vasoconstrictor identified to date. It is synthesized predominantly by ECs. ET-1 is derived from a larger 203-amino acid precursor peptide named preproendothelin, which is cleaved to a smaller 38-amino acid peptide, big-ET-1 by furin convertase, and then the bioactive 21-amino acid peptide ET-1 by endothelin-converting enzyme. Under physiological conditions, ET-1 is continuously shuttled from the trans-Golgi network to the cell surface in secretory vesicles and released, which contributes to basal vascular tone. ET-1 is also stored in Weibel–Palade bodies and released by exocytosis in response to Ca^{2+} elevation caused by stimuli such as mechanical stretch, hypoxia, growth factors, cytokines, and adhesion molecules (Davenport et al. 2016).

ET-1 is released mainly (~80%) toward the abluminal side of the endothelium (Wagner et al. 1992). Upon release, ET-1 may bind to two G-protein-coupled receptors (GPCRs), ET_A and ET_B, with the former predominantly located on VSMCs and the latter mainly on ECs. The activation of ET_A receptors leads to a potent and long lasting vasoconstriction, in part due to a slow dissociation of ET-1 from ET_A receptors (Blandin et al. 2000). Vasoconstriction mediated by ET_A results from an increase in intracellular Ca^{2+} concentration and sensitization of myofilaments to Ca^{2+}. Activation of ET_A receptors also results in mitogenic events mediated by phospholipase C-diacylglycerol mitogen-activated protein kinases cascade, RhoA/Rho kinase pathway, and phosphatidylinositol-3 kinase pathway (Thorin and Webb 2010; Sandoval et al. 2014; Davenport et al. 2016). The activation on ET_B receptors stimulates ECs to synthesize and release NO and PGI_2. ET_B receptors also possess "clearance" functions: once ET-1 binds to the receptors, the ligand-occupied receptors are internalized and subjected to degradation by endosomes/lysosomes (Bremnes et al. 2000; Oksche et al. 2000). Ablation of ET_B receptors exclusively from endothelial cells results in a significant rise in circulating ET-1 (Bagnall et al. 2006). In humans, the lungs (Dupuis et al. 1996), liver (Gandhi et al. 1996), and kidney (Saito et al. 1991) are the major sites for ET-1 clearance, reflecting the abundant expression of ET_B in these organs. Under physiological conditions, the vasoconstrictive effect of ET_A activation is counteracted and counter-regulated by vasodilatation effect of ET_B activity at several levels so that vascular hemostasis is maintained (Vanhoutte et al. 2017; Gao et al. 2016). The mRNA expression of ET-1 and the secretion of the peptide by ECs are inhibited by NO (Boulanger and Luscher 1990; Brunner et al. 1995; Mitsutomi et al. 1999; Smith et al. 2002; Lowenstein et al. 2005). In VSMCs, NO may attenuate ET-1-induced contraction by the inhibition of Ca^{2+} influx and Ca^{2+} release from the SR and by the interference with RhoA-Rho kinase (ROCK) signaling in a cGMP–PKG-dependent manner (Gao et al. 2007, 2008). ET-1-induced mitogenic and hypertrophic responses are also suppressed by NO-induced generation of cGMP (Bouallegue et al. 2007) (Fig. 8.3). Under in vivo conditions, the vasocontractile activity mediated by ET_A seems also being balanced by ET_B-mediated, NO-dependent vasodilation activity. In healthy humans, the systemic inhibition of

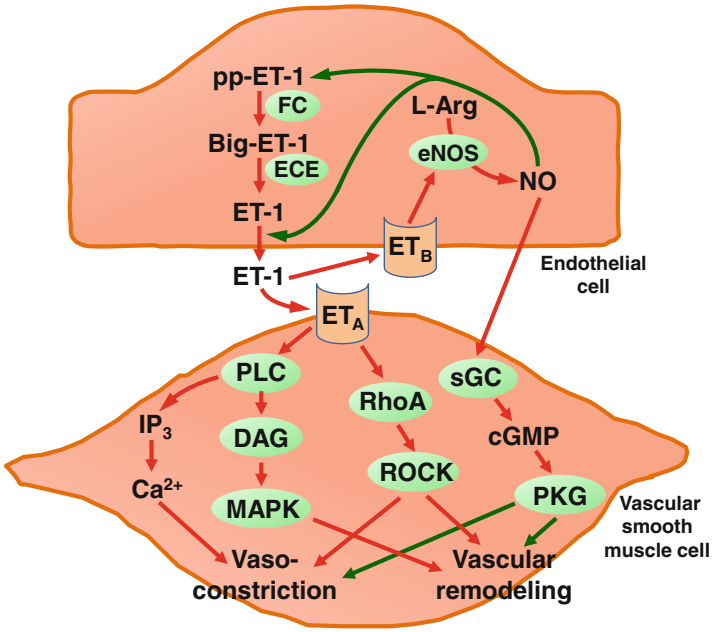

Fig. 8.3 Interaction between endothelin-1 (ET-1) and nitric oxide (NO) signaling pathways in endothelial cells (ECs) and vascular smooth muscle cells (VSMCs). ET-1 is synthesized as preproendothelin (pp-ET-1), which is cleaved to a smaller 38-amino acid peptide, big-ET-1 by furin convertase (FC), and then the bioactive 21-amino acid peptide ET-1 by endothelin-converting enzyme (ECE). After release ET-1 exerts its actions on VSMCs via ET_A to cause vasoconstriction by increasing intracellular Ca^{2+} concentration via inositol 1,4,5-trisphosphate (IP_3)-induced Ca^{2+} release from the sarcoplasmic reticulum and by sensitizing the myofilaments to Ca^{2+} through RhoA/Rho kinase (ROCK) pathway. It also stimulates vascular remodeling through phospholipase C (PLC)-diacylglycerol (DAG)-mitogen-activated protein kinases (MAPK) pathway. ET-1 stimulates the release of NO from ECs via ET_B receptors. The formation and release of ET-1 is suppressed by NO. NO can also counteract the vasoconstriction and vascular remodeling effects caused by ET-1 via cGMP–cGMP-dependent protein kinase (PKG) signaling. *L-Arg* L-arginine, *R* receptor, *sGC* soluble guanylyl cyclase. The *red* and *green arrow lines* denote stimulatory and inhibitory effect, respectively

ET_B increases peripheral resistance (Strachan et al. 1999). Under certain pathological conditions such as pulmonary arterial hypertension, gene expression and protein levels of ET_B may be downregulated (Sauvageau et al. 2009). Moreover, ET_B receptors on pulmonary artery endothelial cells can be inactivated by oxidative modification of cysteinyl thiols in the eNOS-activating region of ET_B (Maron et al. 2012). All these changes result in decreased NO production and consequently exaggerated vasoconstriction and vessel remodeling (Guignabert and Dorfmuller 2013).

References

Aird WC (2007) Phenotypic heterogeneity of the endothelium: I. Structure, function, and mechanisms. Circ Res 100:158–173

Alexander SPH, Mathie A, Peters JA (2011) Guide to Receptors and Channels (GRAC), 5th edn. Br J Pharmacol 164(Suppl. 1):S1–S324

Bagnall AJ, Kelland NF, Gulliver-Sloan F, Davenport AP, Gray GA, Yanagisawa M, Webb DJ, Kotelevtsev YV (2006) Deletion of endothelial cell endothelin b receptors does not affect blood pressure or sensitivity to salt. Hypertension 48:286–293

Balligand JL, Feron O, Dessy C (2009) eNOS activation by physical forces: from short-term regulation of contraction to chronic remodeling of cardiovascular tissues. Physiol Rev 89:481–534

Billecke SS, Bender AT, Kanelakis KC, Murphy PJ, Lowe ER, Kamada Y, Pratt WB, Osawa Y (2002) hsp90 is required for heme binding and activation of apo-neuronal nitric-oxide synthase: geldanamycin-mediated oxidant generation is unrelated to any action of hsp90. J Biol Chem 277:20504–20509

Blandin V, Vigne P, Breittmayer JP, Frelin C (2000) Allosteric inhibition of endothelin ETA receptors by 3, 5-dibromosalicylic acid. Mol Pharmacol 58:1461–1469

Bouallegue A, Daou GB, Srivastava AK (2007) Nitric oxide attenuates endothelin-1-induced activation of erk1/2, pkb, and PYK2 in vascular smooth muscle cells by a cGMP-dependent pathway. Am J Physiol Heart Circ Physiol 293:H2072–H2079

Boulanger C, Luscher TF (1990) Release of endothelin from the porcine aorta. Inhibition by endothelium-derived nitric oxide. J Clin Invest 85:587–590

Bremnes T, Paasche JD, Mehlum A, Sandberg C, Bremnes B, Attramadal H (2000) Regulation and intracellular trafficking pathways of the endothelin receptors. J Biol Chem 275:17596–17604

Brunner F, Stessel H, Kukovetz WR (1995) Novel guanylyl cyclase inhibitor, odq reveals role of nitric oxide, but not of cyclic gmp in endothelin-1 secretion. FEBS Lett 376:262–266

Burgoyne JR, Oka S, Ale-Agha N, Eaton P (2013) Hydrogen peroxide sensing and signaling by protein kinases in the cardiovascular system. Antioxid Redox Signal 18:1042–1052

Campbell WB, Fleming I (2010) Epoxyeicosatrienoic acids and endothelium-dependent responses. Pflugers Arch 459:881–895

Cao S, Yao J, Shah V (2003) The proline-rich domain of dynamin-2 is responsible for dynamin-dependent in vitro potentiation of endothelial nitric-oxide synthase activity via selective effects on reductase domain function. J Biol Chem 278:5894–5901

Caplin B, Leiper J (2012) Endogenous nitric oxide synthase inhibitors in the biology of disease: markers, mediators, and regulators? Arterioscler Thromb Vasc Biol 32:1343–1353

Chatterjee S, Cao S, Peterson TE, Simari RD, Shah V (2003) Inhibition of GTP-dependent vesicle trafficking impairs internalization of plasmalemmal eNOS and cellular nitric oxide production. J Cell Sci 116:3645–3655

Chen K, Popel AS (2006) Theoretical analysis of biochemical pathways of nitric oxide release from vascular endothelial cells. Free Radic Biol Med 41:668–680

Chen W, Xiao H, Rizzo AN, Zhang W, Mai Y, Ye M (2014) Endothelial nitric oxide synthase dimerization is regulated by heat shock protein 90 rather than by phosphorylation. PLoS One 9: e105479

Daff S (2010) NO synthase: structures and mechanisms. Nitric Oxide 23:1–11

Davenport AP, Hyndman KA, Dhaun N, Southan C, Kohan DE, Pollock JS, Pollock DM, Webb DJ, Maguire JJ (2016) Endothelin. Pharmacol Rev 68:357–418

Dupuis J, Stewart DJ, Cernacek P, Gosselin G (1996) Human pulmonary circulation is an important site for both clearance and production of endothelin-1. Circulation 94:1578–1584

Durieux AC, Prudhon B, Guicheney P, Bitoun M (2010) Dynamin 2 and human diseases. J Mol Med (Berl) 88:339–350

Edwards G, Félétou M, Weston AH (2010) Endothelium-derived hyperpolarising factors and associated pathways: a synopsis. Pflugers Arch 459:863–879

Félétou M, Huang Y, Vanhoutte PM (2011) Endothelium-mediated control of vascular tone: COX-1 and COX-2 products. Br J Pharmacol 164:894–912

Fitzpatrick FA, Soberman R (2001) Regulated formation of eicosanoids. J Clin Invest 107:1347–1351

Flavahan NA (2007) Balancing prostanoid activity in the human vascular system. Trends Pharmacol Sci 28:106–110

Fleming I (2010) Molecular mechanisms underlying the activation of eNOS. Pflugers Arch 459:793–806

Förstermann U, Sessa WC (2012) Nitric oxide synthases: regulation and function. Eur Heart J 33:829–837. 837a–837d

Förstermann U, Closs EI, Pollock JS, Nakane M, Schwarz P, Gath I, Kleinert H (1994) Nitric oxide synthase isozymes. Characterization, purification, molecular cloning, and functions. Hypertension 23:1121–1131

Frömel T, Fleming I (2015) Whatever happened to the epoxyeicosatrienoic acid-like endothelium-derived hyperpolarizing factor? The identification of novel classes of lipid mediators and their role in vascular homeostasis. Antioxid Redox Signal 22:1273–1292

Gambone LM, Murray PA, Flavahan NA (1997) Synergistic interaction between endothelium-derived NO and prostacyclin in pulmonary artery: potential role for KATP channels. Br J Pharmacol 121:271–279

Gandhi CR, Kang Y, De Wolf A, Madariaga J, Aggarwal S, Scott V, Fung J (1996) Altered endothelin homeostasis in patients undergoing liver transplantation. Liver Transpl Surg 2:362–369

Gao Y, Portugal AD, Negash S, Zhou W, Longo LD, Usha Raj J (2007) Role of rho kinases in pkg-mediated relaxation of pulmonary arteries of fetal lambs exposed to chronic high altitude hypoxia. Am J Phys Lung Cell Mol Phys 292:L678–L684

Gao Y, Portugal AD, Liu J, Negash S, Zhou W, Tian J, Xiang R, Longo LD, Raj JU (2008) Preservation of cgmp-induced relaxation of pulmonary veins of fetal lambs exposed to chronic high altitude hypoxia: role of PKG and Rho kinase. Am J Phys Lung Cell Mol Phys 295:L889–L896

Gao Y, Chen T, Raj JU (2016) Endothelial and smooth muscle cell interactions in the pathobiology of pulmonary hypertension. Am J Respir Cell Mol Biol 54:451–460

García-Cardeña G, Fan R, Shah V, Sorrentino R, Cirino G, Papapetropoulos A, Sessa WC (1998) Dynamic activation of endothelial nitric oxide synthase by Hsp90. Nature 392:821–824

Ghosh A, Chawla-Sarkar M, Stuehr DJ (2011) Hsp90 interacts with inducible NO synthase client protein in its heme-free state and then drives heme insertion by an ATP-dependent process. FASEB J 25:2049–2060

Gluais P, Lonchampt M, Morrow JD, Vanhoutte PM, Feletou M (2005) Molecular mechanisms underlying the activation of eNOS. Br J Pharmacol 146:834–845

Guignabert C, Dorfmuller P (2013) Pathology and pathobiology of pulmonary hypertension. Semin Respir Crit Care Med 34:551–559

Haas TL, Duling BR (1997) Morphology favors an endothelial cell pathway for longitudinal conduction within arterioles. Microvasc Res 53:113–120

Henrion D, Dechaux E, Dowell FJ, Maclour J, Samuel JL, Lévy BI, Michel JB (1997) Alteration of flow-induced dilatation in mesenteric resistance arteries of L-NAME treated rats and its partial association with induction of cyclo-oxygenase-2. Br J Pharmacol 121:83–90

Ho JJ, Man HS, Marsden PA (2012) Nitric oxide signaling in hypoxia. J Mol Med (Berl) 90:217–231

Huang PL, Huang Z, Mashimo H, Bloch KD, Moskowitz MA, Bevan JA, Fishman MC (1995) Hypertension in mice lacking the gene for endothelial nitric oxide synthase. Nature 377:239–242

Kar S, Kavdia M (2011) Modeling of biopterin-dependent pathways of eNOS for nitric oxide and superoxide production. Free Radic Biol Med 51:1411–1427

Klatt P, Pfeiffer S, List BM, Lehner D, Glatter O, Bächinger HP, Werner ER, Schmidt K, Mayer B (1996) Characterization of heme-deficient neuronal nitric-oxide synthase reveals a role for heme in subunit dimerization and binding of the amino acid substrate and tetrahydrobiopterin. J Biol Chem 271:7336–7342

List BM, Klosch B, Volker C, Gorren AC, Sessa WC, Werner ER, Kukovetz WR, Schmidt K, Mayer B (1997) Characterization of bovine endothelial nitric oxide synthase as a homodimer with down-regulated uncoupled NADPH oxidase activity: tetrahydrobiopterin binding kinetics and role of haem in dimerization. Biochem J 323:159–165

Liu Y, Bubolz AH, Mendoza S, Zhang DX, Gutterman DD (2011) H_2O_2 is the transferrable factor mediating flow-induced dilation in human coronary arterioles. Circ Res 108:566–573

Lowenstein CJ, Morrell CN, Yamakuchi M (2005) Regulation of weibel-palade body exocytosis. Trends Cardiovasc Med 15:302–308

Majed BH, Khalil RA (2012) Molecular mechanisms regulating the vascular prostacyclin pathways and their adaptation during pregnancy and in the newborn. Pharmacol Rev 64:540–582

Maron BA, Zhang YY, White K, Chan SY, Handy DE, Mahoney CE, Loscalzo J, Leopold JA (2012) Aldosterone inactivates the endothelin-B receptor via a cysteinyl thiol redox switch to decrease pulmonary endothelial nitric oxide levels and modulate pulmonary arterial hypertension. Circulation 126:963–974

Matoba T, Shimokawa H, Morikawa K, Kubota H, Kunihiro I, Urakami-Harasawa L, Mukai Y, Hirakawa Y, Akaike T, Takeshita A (2003) Electron spin resonance detection of hydrogen peroxide as an endothelium-derived hyperpolarizing factor in porcine coronary microvessels. Arterioscler Thromb Vasc Biol 23:1224–1230

Mitsutomi N, Akashi C, Odagiri J, Matsumura Y (1999) Effects of endogenous and exogenous nitric oxide on endothelin-1 production in cultured vascular endothelial cells. Eur J Pharmacol 364:65–73

Moncada S (2006) Adventures in vascular biology: a tale of two mediators. Philos Trans R Soc Lond Ser B Biol Sci 361:735–759

Murata T, Ushikubi F, Matsuoka T, Hirata M, Yamasaki A, Sugimoto Y, Ichikawa A, Aze Y, Tanaka T, Yoshida N, Ueno A, Oh-ishi S, Narumiya S (1997) Altered pain perception and inflammatory response in mice lacking prostacyclin receptor. Nature 388:678–682

Oksche A, Boese G, Horstmeyer A, Furkert J, Beyermann M, Bienert M, Rosenthal W (2000) Late endosomal/lysosomal targeting and lack of recycling of the ligand-occupied endothelin B receptor. Mol Pharmacol 57:1104–1113

Pace NJ, Weerapana E (2014) Zinc-binding cysteines: diverse functions and structural motifs. Biomolecules 4:419–434

Prysyazhna O, Rudyk O, Eaton P (2012) Single atom substitution in mouse protein kinase G eliminates oxidant sensing to cause hypertension. Nat Med 18:286–290

Puybasset L, Béa ML, Ghaleb B, Giudicelli JF, Berdeaux A (1996) Coronary and systemic hemodynamic effects of sustained inhibition of nitric oxide synthesis in conscious dogs. Evidence for cross talk between nitric oxide and cyclooxygenase in coronary vessels. Circ Res 79:343–357

Qian J, Fulton D (2013) Post-translational regulation of endothelial nitric oxide synthase in vascular endothelium. Front Physiol 4:347

Ramadoss J, Pastore MB, Magness RR (2013) Endothelial caveolar subcellular domain regulation of endothelial nitric oxide synthase. Clin Exp Pharmacol Physiol 40:753–764

Robinson MA, Baumgardner JE, Otto CM (2011) Oxygen-dependent regulation of nitric oxide production by inducible nitric oxide synthase. Free Radic Biol Med 51:1952–1965

Saito Y, Kazuwa N, Shirakami G, Mukoyama M, Arai H, Hosoda K, Suga S, Ogawa Y, Imura H (1991) Endothelin in patients with chronic renal failure. J Cardiovasc Pharmacol 17(Suppl 7): S437–S439

Sandoval YH, Atef ME, Levesque LO, Li Y, Anand-Srivastava MB (2014) Endothelin-1 signaling in vascular physiology and pathophysiology. Curr Vasc Pharmacol 12:202–214

Sandow SL, Senadheera S, Bertrand PP, Murphy TV, Tare M (2012) Myoendothelial contacts, gap junctions, and microdomains: anatomical links to function? Microcirculation 19:403–415

Sauvageau S, Thorin E, Villeneuve L, Dupuis J (2009) Change in pharmacological effect of endothelin receptor antagonists in rats with pulmonary hypertension: role of etb-receptor expression levels. Pulm Pharmacol Ther 22:311–317

Searles CD (2006) Transcriptional and posttranscriptional regulation of endothelial nitric oxide synthase expression. Am J Phys Cell Physiol 291:C803–C816

Shimokawa H (2010) Hydrogen peroxide as an endothelium-derived hyperpolarizing factor. Pflugers Arch 459:915–922

Shimokawa H, Godo S (2016) Diverse functions of endothelial NO synthases system: NO and EDH. J Cardiovasc Pharmacol 67:361–366

Smith AP, Demoncheaux EA, Higenbottam TW (2002) Nitric oxide gas decreases endothelin-1 mrna in cultured pulmonary artery endothelial cells. Nitric Oxide 6:153–159

Strachan FE, Spratt JC, Wilkinson IB, Johnston NR, Gray GA, Webb DJ (1999) Systemic blockade of the endothelin-B receptor increases peripheral vascular resistance in healthy men. Hypertension 33:581–585

Stuehr DJ, Santolini J, Wang ZQ, Wei CC, Adak S (2004) Update on mechanism and catalytic regulation in the NO synthases. J Biol Chem 279:36167–36170

Tang EH, Vanhoutte PM (2008) Gene expression changes of prostanoid synthases in endothelial cells and prostanoid receptors in vascular smooth muscle cells caused by aging and hypertension. Physiol Genomics 32:409–418

Tang EH, Vanhoutte PM (2009) Prostanoids and reactive oxygen species: team players in endothelium-dependent contractions. Pharmacol Ther 122:140–149

Thorin E, Webb DJ (2010) Endothelium-derived endothelin-1. Pflugers Arch 459:951–958

Vanhoutte PM, Shimokawa H, Feletou M, Tang EH (2017) Endothelial dysfunction and vascular disease – a 30th anniversary update. Acta Physiol (Oxford) 219:22–96

Wagner OF, Christ G, Wojta J, Vierhapper H, Parzer S, Nowotny PJ, Schneider B, Waldhausl W, Binder BR (1992) Polar secretion of endothelin-1 by cultured endothelial cells. J Biol Chem 267:16066–16068

Williams SP, Dorn GW 2nd, Rapoport RM (1994) Prostaglandin I_2 mediates contraction and relaxation of vascular smooth muscle. Am J Phys 267:H796–H803

Zellers TM, YQ W, McCormick J, Vanhoutte PM (2000) Prostacyclin-induced relaxations of small porcine pulmonary arteries are enhanced by the basal release of endothelium-derived nitric oxide through an effect on cyclic GMP-inhibited cyclic AMP phosphodiesterase. Acta Pharmacol Sin 21:131–138

Zhang DX, Borbouse L, Gebremedhin D, Mendoza SA, Zinkevich NS, Li R, Gutterman DD (2012) H_2O_2-induced dilation in human coronary arterioles: role of protein kinase G dimerization and large-conductance Ca^{2+}-activated K^+ channel activation. Circ Res 110:471–480

Zou MH (2007) Peroxynitrite and protein tyrosine nitration of prostacyclin synthase. Prostaglandins Other Lipid Mediat 82:119–127

Chapter 9
Local Metabolic Factors and Vasoactivity

Abstract The regulation of vasoreactivity by local metabolites is a key mechanism to ensure adequate blood flow so that adequate O_2 are supplied for the needed tissues and metabolic wastes are timely removed. Many metabolic factors may participate in the regulation of vascular activity such as local Po_2, Pco_2, pH, K^+, adenosine, and lactate. These metabolic factors affect vasoactivity either by directly acting on vascular smooth muscle cells (VSMCs) or by acting on the endothelial cells, resulting in altered cytosolic Ca^{2+} level and Ca^{2+} sensitivity of myofilaments in VSMCs and thus altered vasoactivity. For a metabolic factor to be involved, it must be released in a sufficient amount from the tissues and diffuse to the nearby vasculature. Since the formation and release profile of metabolic factors vary under different conditions, their relative importance in affecting vasoactivity varies under different conditions. Under most conditions there appears no single factor that is indispensable for the metabolic regulation of vasoactivity. More likely this process is regulated by multiple factors in a redundant manner. Such a concept is exemplified in exercise-induced vasodilatation in skeletal muscle.

Keywords Oxygen • Carbon dioxide • pH • Potassium • Adenosine • Lactate • Exercise

9.1 Introduction

The coupling of blood flow and thus oxygen delivery to the oxygen demand are fundamentally important for the homeostasis of the metabolism and functions of the tissues. Logically, local metabolic factors should be suitable messengers for the adjustment of vasoactivity so that blood flow is matched with tissue oxygen consumption. In 1963 Berne (Berne 1963) and Gerlach et al. (Gerlach et al. 1963) proposed that adenosine induced by hypoxia may be an important metabolic regulator of coronary blood flow. Subsequent studies suggest that under physiological conditions the level of myocardial oxygenation is largely unchanged and that adenosine is unlikely to be critically involved in the metabolic vasodilatation of the heart (Deussen et al. 2012). In skeletal muscle the interstitial adenosine is markedly elevated during strenuous physical exercise. However, no evidence indicates that adenosine is crucial for the skeletal muscle blood flow responses (Ballard 2014;

Y. Gao, *Biology of Vascular Smooth Muscle: Vasoconstriction and Dilatation*,
DOI 10.1007/978-981-10-4810-4_9

Joyner and Casey 2015). Adenosine is a potent vasodilator (Berwick et al. 2010; Lamb and Murrant 2015). The reason that it is not obligatory during metabolic vasodilatation even its local concentration is sufficiently high is, at least in partial, due to that there are many other dilators that also come into play. In fact, the metabolic regulation of vasoactivity is safeguarded by rather redundant mechanisms, and no single signaling molecule is indispensable (Sarelius and Pohl 2010; Joyner and Casey 2015). With this notion in mind, the role of a number of metabolic factors including Po_2, Pco_2, pH, K^+, adenosine, and lactate in the regulation of vasoactivity will be discussed in this chapter. The mechanism underlying the metabolic vasodilatation in skeletal muscle and myocardium will also be discussed.

9.2 O_2 Tension

Oxygen (O_2) is the most common oxidizing agent used in metabolism of nutrients to generate ATP, the energy source for the majority of cellular functions including vascular activity. Hence, it is natural to assume that O_2 tension under a critical level would inhibit vasoactivity due to suppressed oxidative phosphorylation and thus limited energy supply. Such an assumption is in line with the observations that lowering O_2 tension causes vasodilatation of various systemic arteries in an O_2 tension-dependent manner and that the relaxation is reversed upon reoxygenation (Detar and Bohr 1968). In porcine carotid artery strips, the tension development is found being related to the limitation of diffusion of O_2 to the core of the tissue. There is strong correlation between the square of one-half strip thickness and the critical Po_2, i.e., Po_2 at which the first observable fall in active tension occurs, indicating that the diffusion distance is the primary factor influencing critical Po_2 (Fig. 9.1) (Pittman and Duling 1973; Sparks 2011). The distance of diffusion for O_2 is proportional to its concentration gradient. Since O_2 has a relatively low solubility (α) in tissue ($\sim 3 \times 10^{-5}$ cm^3 $O_2 \cdot cm^{-3} \cdot Torr^{-1}$), diffusion is only effective over short distances. At a typical tissue Po_2 of 30 Torr, the concentration of O_2 (c) is $\sim 10^{-3}$ $cm^3 \cdot O_2 \cdot cm^3$ or 45 μM ($c = \alpha \cdot Po_2$). The maximum diffusion distance (d_t) of O_2 from blood into tissue can be estimated by a simple one-dimensional analysis:

$$d_t = (2D\alpha Po_2 / M_0)^{1/2}$$

where D is the diffusivity ($\sim 1.5 \times 10^{-5}$ cm^2/s), Po_2 is oxygen partial pressure in blood, and M_0 is the O_2 consumption rate. Therefore, for typical M_0 between 0.01 and 0.3 cm^3 $O_2 \cdot$ $cm^{-3} \cdot min^{-1}$ and Po_2 in blood between 30 and 100 Torr, the diffusion distance of O_2·is in the range between about 20 and 200 μm (Pries and Secomb 2014). In Fig. 9.1 the intercept of the least-squares regression line with the critical Po_2 axis is at ~1.8 mmHg (1 mmHg ≈ 1 Torr) (Pittman and Duling 1973), which is close to Po_2 for the half maximal activity of oxidative metabolism in isolated mitochondria (Gnaiger 2001). It indicates that oxidative phosphorylation is

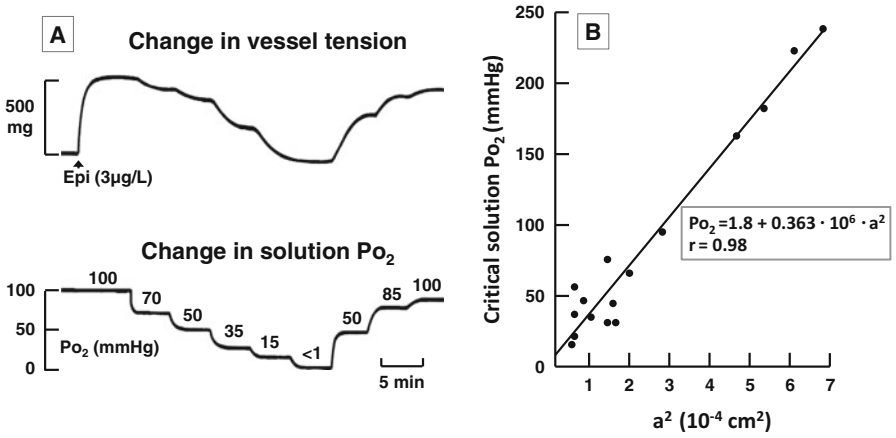

Fig. 9.1 Relationship between solution Po_2 and contraction of isolated artery preparations. (**a**) The rabbit aortic strip is suspended in a buffer solution and contracted with epinephrine (Epi). When the solution Po_2 is reduced (the *lower* panel), the vessel tension is decreased in a manner depending on the oxygen concentrations (From Detar and Bohr (1968), with permission). (**b**) A linear relationship exists between the square of one-half rabbit aortic strip thickness (a^2) and the critical Po_2, i.e., Po_2 at which the first observable fall in active tension occurs, suggesting that the diffusion distance is the primary factor influencing critical Po_2. Each point represents one experiment. Equation for least-squares regression line and the correlation coefficient are shown in the box (From Pittman and Duling (1973), with permission)

a critical factor involved in the O_2-sensitive vasocontractility (Jones 1986). It should be pointed out that, while ATP is primarily derived from mitochondrial oxidative phosphorylation for vascular smooth muscle under normoxia, glycolysis may provide substantial portion of the energy needed during hypoxia. For example, the contraction of rabbit aorta evoked by epinephrine is reduced by about one-third under anoxic in the presence of glucose but reduced by more than 80% in the absence of glucose compared with that under normoxic conditions in the presence of glucose (Furchgott 1966).

Effect of change in Po_2 on vasoactivity may differ depending on vasoconstrictors used. In rabbit aorta the reduction of Po_2 to 30 mmHg causes a markedly greater relaxation of vessels contracted with noradrenaline than with KCl. Hypoxia has a similar effect on the rates of decrease of phosphocreatine or ATP in all vessels. However, the level of myosin light chain (MLC) phosphorylation following hypoxic treatment is suppressed in vessels contracted with noradrenaline but not those contracted with KCl. Hence, the differential effects of hypoxia may result from altered signaling upstream to MLC phosphorylation that is specific to noradrenaline (Coburn et al. 1992). In permeabilized porcine coronary artery, smooth muscle hypoxia decreased force and MLC phosphorylation despite fixed Ca^{2+}. Such a Ca^{2+}-desensitizing hypoxic relaxation is attenuated by the inhibition of Rho kinase (ROCK). In situ assay shows that ROCK activity can be abolished by hypoxia, suggesting that hypoxia may directly inhibit ROCK-dependent MLC

and thereby leads to the vasodilatation (Wardle et al. 2007). In addition to Ca^{2+}-desensitizing, hypoxia may cause vasodilatation through the inhibition of Ca^{2+} channel activity (Smani et al. 2002), inhibition of Ca^{2+} channel-induced Ca^{2+} release from the sarcoplasmic reticulum (SR) (Calderón-Sánchez et al. 2009), and activation of several types of K^+ channels including voltage-gated K^+ (K_V) channel (Hedegaard et al. 2014), Ca^{2+}-activated K^+ channel (Gebremedhin et al. 2008), and ATP-sensitive K^+ (K_{ATP}) channels (Ngo et al. 2013). Most often, lowering Po_2 causes vasodilatation of systemic arteries but vasoconstriction of pulmonary arteries. The dilatation of systemic arteries improves the perfusion of hypoxic tissues, while constriction of pulmonary arteries diverts blood toward better-ventilated alveoli to optimize ventilation-to-perfusion matching (Sylvester et al. 2012). The underlying mechanisms for the opposite responses are not well understood. It appears that the differences in energy state (Leach et al. 2000), K^+ channel activity (Weir and Archer 2010), production of reactive oxygen species (Schumacker 2011), and redox status may be involved (Neo et al. 2010; Dou et al. 2013).

9.3 CO_2 and pH

CO_2 is generated from the formation of acetyl CoA from decarboxylation reaction in the citric acid cycle. Its production is proportional to O_2 consumption as defined as the respiratory exchange ratio, i.e., the ratio between the amount of CO_2 produced in metabolism and O_2 used. After being generated CO_2 diffuses down its concentration gradient from the cell into the extracellular space, then into the circulating blood, and finally being expired into ambient air. Under conditions such as blood flow is impaired and thus less CO_2 is carried away, the increased tissue concentration of CO_2 results in an increase of H^+ concentration ($CO_2 + H_2O \leftrightarrow H^+ + HCO_3^-$) by the action of carbonic anhydrase, which is expressed virtually in all cells and tissues. Meanwhile, the reduced blood flow and thus the lack of O_2 decrease the consumption of pyruvate by the citric acid cycle, promote the formation of lactate, and result in decreased intracellular pH (pH_i) (Occhipinti and Boron 2015). pH_i is affected by extracellular pH ($[pH]_o$) in the same direction. Typically a new steady-state pH_i is reached within a few minutes, and the change in steady-state pH_i is 50–75% of the imposed change in pH_o, with pH_i being more sensitive to respiratory (i.e., hyper or hypocapnic) than to metabolic (i.e., normocapnic) disturbances (Boedtkjer and Aalkjaer 2012).

A change in pH_i is damped by the buffer systems in particular the CO_2/HCO_3^- buffer system. The homeostasis of intracellular pH, ultimately, is regulated by the activities of acid extruders and acid loaders. In mammalian cells the acid extruders include the Na-H exchangers (NHEs, members of the SLC9 family of solute carriers), the electrogenic Na/HCO_3 cotransporters (NBCe1, NBCe2 in the SLC4 family of solute carriers), the electroneutral Na/HCO_3 cotransporters (NBCn1, NBCn2 in the SLC4 family), the Na^+-driven $Cl\text{-}HCO_3$ exchanger (NDCBE in the SLC4 family), V-type H^+ pumps, and the voltage-gated H^+ channel. The acid

loaders include passive fluxes ("leak") of H^+, HCO_3^- and weak base (e.g., NH_4^+), the electrogenic Na^+/HCO_3^- cotransporter (NBCe1, NBCe2), the Cl^-/HCO_3^- exchangers (AE1–3 in the SLC4 family), and the proton-driven transporters (Aalkjaer et al. 2014; Occhipinti and Boron 2015). In vascular smooth muscle cells (VSMCs), the acid extrusion is mediated exclusively by Na^+, HCO_3^- cotransport, and Na^+/H^+ exchange. The electroneutral Na^+, HCO_3^- cotransporter NBCn1 is identified in VSMCs and endothelial cells (ECs) of mouse mesenteric, renal, and cerebral arteries and veins (Boedtkjer et al. 2008) as well as rat aorta, small mesenteric and renal arteries, and the capillaries of the heart ventricles, spleen, and salivary glands (Damkier et al. 2006). NBCn1 has been found to be responsible for the Na^+,HCO_3^- cotransport activity in VSMCs and ECs of mouse mesenteric arteries during intracellular acidification (Boedtkjer et al. 2011). Na^+/H^+ exchanger NHE1 (SLC9A1) is expressed in resistance arteries and cerebrovascular tissue. The Na^+/H^+ exchange activity of NHE1 has been demonstrated in VSMCs of isolated mesenteric resistance arteries during intracellular acidification using knockout mice (Boedtkjer et al. 2006). Studies show that the individual contribution from NBCn1 and NHE1 to net acid extrusion in pHi ranging from 6.5 to 6.8 appears to be of similar magnitude. In the near-physiological pHi range, however, NBCn1 is the dominating mediator of net acid extrusion from resting VSMCs, whereas NHE1 appears to be a major acid extruder at low pHi (Boedtkjer and Aalkjaer 2012). The acid loaders of VSMCs have not been well studied. The Cl^-/HCO_3^- exchangers AE2 (SLC4A2) and AE3 (SLC4A3) are expressed in rat VSMC, aorta, and renal microvessels (Brosius et al. 1997). In rat mesenteric resistance arteries, the activity of Cl^-/HCO_3^- exchange appears to play an important role for pH_i recovery from intracellular alkalinization (Aalkjaer and Hughes 1991).

Changes in pH may affect cell functions through altering the protonation state of amino acids resulting in changes in the charge distribution, conformation, and function of proteins. Certain proteins are highly pH-sensitive, which include some ion channels (e.g., acid-sensing ion channels, L-type Ca^{2+} channels, Ca^{2+}-activated K^+ channels, and Twik-related acid-sensitive K^+ channel 1 and 3 (TASK1/TASK3)), G-protein-coupled receptors (e.g., GPR4, OGR1, G2A, and TDAG8), and enzymes (e.g., phosphofructokinase (PFK)-1, endothelial nitric oxide synthase (eNOS), and endothelin-converting enzyme) (Boedtkjer and Aalkjaer 2012; Buckler 2015). In mice deficient in Na/HCO_3 cotransporter NBCn1, relaxation of mesenteric artery induced by acetylcholine is attenuated in a manner sensitive to the inhibition of eNOS, which is associated with a lower steady-state pH_i and reduced production of nitric oxide (NO) production in response to acetylcholine (Boedtkjer et al. 2006). Similar results are also obtained in mesenteric artery of NHE1 knockout mice (Boedtkjer et al. 2012). These data are in line with the study showing that the stimulated eNOS activity of microsomal preparations of ECs is reduced by a third when pH is reduced from 7.0 to 6.7 (Fleming et al. 1994). Acidosis has also been found to attenuate while alkalosis augments endothelium-dependent contractions in mouse carotid arteries, resulting from alteration of the sensitivity of the thromboxane prostanoid (TP) receptor of vascular smooth muscle

(Baretella et al. 2014). In mesenteric artery from NBCn1 knockout mice (Boedtkjer et al. 2006) or from NHE1 knockout mice (Boedtkjer et al. 2012), intracellular acidification reduces VSMC Ca^{2+} sensitivity. In mesenteric artery from NBCn1 knockout mice, the phosphorylation of myosin phosphatase targeting subunit at Thr-850 is reduced. Moreover, in vitro assay shows that Rho kinase (ROCK) activity is reduced at low pH, indicating that lowering pH_i may inhibit vasoconstriction through desensitization of myofilaments to Ca^{2+} by the inhibition of ROCK (Boedtkjer et al. 2006).

9.4 Potassium

Studies of exercise hyperemia using K^+-sensitive electrodes and microdialysis show that the interstitial K^+ concentration of skeletal muscle rises sharply from the onset of contraction, reaching a peak within 5–10 s and attaining concentrations of up to 10 mM. The changes in the interstitial K^+ levels are associated arteriolar dilatation, which is attenuated in the presence of inhibitors of voltage-sensitive K^+ (K_v) channels, inwardly rectifying K^+ (K_{IR}) channels or Na^+-K^+ ATPase. Moreover, when the vascular smooth muscle is depolarized with high-K^+ solution, the rapid dilatation occurred at the early phase of skeletal muscle contraction is abolished. These observations suggest that the release of potassium ions from skeletal muscle cells may cause arteriolar dilatation via activation of K_v channels, K_{IR} channels, and Na^+-K^+ ATPase. Studies also show a close correlation between interstitial and venous concentrations of K^+ and the magnitude of exercise hyperemia, implying the possibility that K^+ contributes to the maintained phase. The hyperpolarization at early phase induced by K^+ in VSMCs and ECs may facilitate the action of dilators such as adenosine and prostaglandins (PGs) that are released later. Also, dilatation can be conducted from distal to upstream vessels by cell-to-cell conduction of hyperpolarization (Sarelius and Pohl 2010; Marshall and Ray 2012).

9.5 Adenosine

The interstitial concentration of adenosine in human skeletal muscle is about 0.1–0.5 μM at rest. It increases to 1.5–2.0 μM during moderate to high-intensity exercise. The blockade of adenosine receptors attenuates local vasodilation that accompanies muscle contractions by 14–29% in humans and 40% in cats, but no effect in dogs running on a treadmill. The infusion of adenosine deaminase, which converts adenosine to non-vasoactive metabolites, or infusion of α, β-methylene adenosine diphosphate, which inhibits the extracellular formation of adenosine, reduces vasodilation associated with muscle contractions by 40% in dogs and 20% in cats during 2-Hz contractions but no effect at contraction frequencies $\leq$0.5 Hz. These results suggest that interstitial adenosine may be involved in exercise-

induced vasodilation, predominantly at high-intensity and/or long-duration muscle activities (Ballard 2014). In canine heart the interstitial adenosine concentrations show no significant increase during exercise (Tune et al. 2000). In healthy adult human subjects and the pigs, the blockade of adenosine receptors causes coronary vasoconstriction that was similar at rest and during exercise (Edlund et al. 1989; Merkus et al. 2003). However, the extracellular adenosine level is markedly elevated in response to hypoxia in the heart of guinea pigs and dogs (Stowe 1981; Wang et al. 1994). Studies of the inhibition of adenosine receptors in dogs and the knockout of adenosine receptors in mice demonstrate that hypoxia-induced elevation of adenosine is causally related to ischemia dilatation of coronary arteries (Berwick et al. 2010; Sharifi et al. 2013). Therefore, adenosine seems not to be obligatory for coronary vasodilatation in exercise but has an important role when oxygen supply below oxygen consumption of the tissues (Duncker and Bache 2008; Deussen et al. 2012).

The extracellular adenosine is derived either from the external transport of intracellularly generated adenosine or formed from the hydrolysis of extracellular nucleotides, particularly ATP and ADP. ATP or ADP is first converted to AMP by ectonucleoside triphosphate diphosphohydrolase 1 (ENTPD1; also known as CD39), followed by AMP hydrolysis to adenosine by ecto-5′-nucleotidase (NT5E; also known as CD73) (Chen et al. 2013). In skeletal muscle at least 70% of the interstitial adenosine is formed extracellularly by the action of NT5E. The adenosine formed is not quickly degraded due to that there is no significant adenosine kinase or adenosine deaminase activity in the interstitial compartment. The extracellularly adenosine is cleared by cellular uptake, which is a relatively slow process (Ballard 2014). The formation of adenosine is elevated when muscle cells are stimulated, resulting from an increased affinity of NT5E for AMP at low pH (Cheng et al. 2000), from the translocation of additional NT5E from an intracellular pool to the membrane (Hellsten 1999), and, more importantly, from the increased concentration of AMP in the interstitial space during muscle contractions (Mortensen et al. 2009). In the heart the increased interstitial adenosine during myocardial hypoxia and ischemia is likely to be formed predominantly extracellularly by the action of NT5E (Deussen et al. 2012), while the adenosine concentration in the coronary artery wall is not affected by hypoxia (Frøbert et al. 2006).

There exist four subtypes of adenosine receptors, namely, A_1, A_{2A}, A_{2B}, and A_3 receptors. They have all been identified on the endothelium and vascular smooth muscle (Lynge and Hellsten 2000). Studies using selective antagonists of adenosine receptors suggest that the adenosine component of exercise hyperemia of skeletal muscle and of hypoxic coronary vasodilatation is mainly mediated by A_{2A} receptors, and additional vasodilation may result from activation of A_{2B} receptors (Sanjani et al. 2011; Deussen et al. 2012; Marshall and Ray 2012). Adenosine may cause vasodilatation by stimulating the release NO and prostacyclin from the endothelium (Nyberg et al. 2010) as well as by increasing cAMP to open K_{ATP} and K_V channels acting on VSMCs or ECs (Heaps and Bowles 2002; Deussen et al. 2012; Marshall and Ray 2012; Lamb and Murrant 2015). In mice the coronary reactive hyperemia is eliminated by the inhibitor of A_{2A} receptors, the H_2O_2

scavenger catalase, and the inhibitor of K_{ATP} channels. The coronary reactive hyperemia is augmented in mice deficient in A_1 but not in A_3 receptors, suggesting that A_1 but not A_3 adenosine receptors negatively modulates coronary reactive hyperemia via counteracting A_{2A}-mediated H_2O_2 production and K_{ATP} channel activity (Zhou et al. 2013).

9.6 Lactate

Lactate is formed from pyruvate, the product of glycolysis, coupled with the oxidation of NADH by lactate dehydrogenase. It has long been believed that lactate accumulation indicates accelerated glycolysis. However, there is neither an increase in content of lactate in the contracting muscle nor in lactate release from the muscle when exercise is at 40% of maximal O_2 uptake ($Vo_{2\cdot max}$). With the onset of heavy exercise, there is an increase in interstitial and venous concentrations of lactate. The increased lactate release is not due to a lack of cellular oxygen but rather resulted from the accelerated glycolytic activity that outpaces the oxidative activity of mitochondria. Studies show that during low exercise intensities (up to 50% $Vo_{2\cdot max}$), relatively large increase occurs in pyruvate while only small increases in lactate. At higher exercise intensities, pyruvate level remains fairly constant, whereas lactate content markedly increases. The increase in muscle lactate coincides with an increase in NADH, implying an increased stress on aerobic metabolism (Katz and Sahlin 1988). It is worthy of noting that lipid oxidation is greatest at exercise power outputs eliciting 45–50% of $Vo_{2\cdot max}$, but carbohydrate oxidation is increased more than lipid oxidation with greater exercise intensities. Exercise under hypoxic conditions is associated with greater glycolytic activity and lactate production than does the same effort under normoxia. These changes are further augmented under hypoxia by the effect of hypoxia on sympathetic nervous system activity (Brooks 2016).

Lactate is released into extracellular space via monocarboxylate transporters (MCTs), which are facilitated transporters characterized by saturation, stereospecificity, and dependent on the pH gradient. Among the four isoforms of MCTs (MCT1–MCT4), MCT1 is most ubiquitously expressed, MCT2 is little expressed in human tissues, MCT2 is confined to the retinal pigment epithelium and choroid, and MCT4 is quite widely expressed, especially so in tissues that rely on glycolysis. Indeed, highly glycolytic muscle fibers express more MCT4, whereas highly oxidative fibers express more MCT1 (Halestrap 2012).

Though lactate has been shown to act principally as a vasodilator, no correlation has been found between regional blood flow and regional lactate either at rest or during exercise hyperemia. While lactate seems not to be critical for mediating exercise hyperemia, it may contribute to blood flow responses during higher-intensity exercise and under conditions such as hypoxia where an enhanced release of lactate occurs (Sarelius and Pohl 2010; Joyner and Casey 2015). Lactate production occurs concurrently with the formation of H^+. Relaxation of isolated rat

cremaster skeletal muscle arterioles caused by neutralized lactic acid (lactate) but not relaxation caused by the acidification of the Krebs buffer is attenuated by the inhibition of soluble guanylyl cyclase (sGC), suggesting that the vasodilator effect of lactate is mediated by sGC in a manner different from acidification (Chen et al. 1996). In the isolated rat heart, lactate is found to cause coronary vasodilatation via endothelial nitric oxide (NO) (Montoya et al. 2011).

9.7 Redundant Regulation of Exercise-Induced Vasodilatation

At rest, for a young healthy male weighing 70 kg (from now on referred to as reference man), his cardiac output is typically ~5 l/min achieved by a heart rate of ~70 beat/min and a stroke volume of ~70 ml/beat. Of the 5 l cardiac output, ~80% is directed to the brain, heart, kidneys, and liver, while ~20% is sufficient to support the resting metabolism of all other tissues including skeletal muscle. During maximal exercise the cardiac output of the reference man can reach ~20 l/min achieved by a heart rate of ~200 beat/min and a stroke volume of ~100 ml/beat. The blood flow directed to skeletal muscle may increase by up to 20-fold and blood flow directed to the heart may increase by up to fivefold. The absolute value of cerebral blood flow shows no significant change or perhaps increases slightly, while renal and splanchnic blood flow can fall to ~25% of resting values (Deussen et al. 2012; Joyner and Casey 2015). The strikingly increased blood flow in skeletal muscle is accompanied by increased O_2 extraction. In resting muscle, O_2 extraction is in the range of 20–40% but may increase to a range of 70–80% with increasing intensity of exercise (Sarelius and Pohl 2010). In the heart 70–80% of the arterially delivered O_2 is extracted even at rest. During exercise ~80% of the O_2 needed for the heart is provided by increased blood flow, while ~20% of the O_2 needed results from enhanced O_2 extraction (Duncker and Bache 2008).

During exercise there is a linear relationship between exercise intensity and the blood flow in skeletal muscle, indicating a close association of muscle metabolic demand and exercise hyperemia. The metabolic regulation of blood flow results from combined actions of different mechanisms. It is safeguarded by rather redundant mechanisms, and no single signaling molecule is indispensable (Sarelius and Pohl 2010; Joyner and Casey 2015). In healthy young adults, the forearm blood flow increases by more than twofold by moderate rhythmic forearm exercise. Such a change is moderately reduced by N^G-nitro-L-arginine methyl ester (L-NAME, an inhibitor of endothelial NO synthase (eNOS)), transiently and moderately reduced by ketorolac (an inhibitor of cyclooxygenase (COX), respectively), and not affected by glibenclamide (an inhibitor of ATP-sensitive K^+ (K_{ATP}) channel). However, in the presence of glibenclamide, the administration of L-NAME plus ketorolac causes a marked reduction in blood flow, followed by a compensatory hyperemic response, and returns to steady-state values. Similar response is also obtained by

adding glibenclamide in the presence of L-NAME plus ketorolac (Schrage et al. 2004, 2006) (Fig. 9.2). The moderate or no effect of these inhibitors when each of them used alone indicates that there are multiple rather than single signaling pathways involved in the exercise hyperemia. Thus, when one or two of these pathways are blocked, the response becomes more dependent on the unblocked. For instance, when the synthesis of NO and prostaglandin (PG) is blocked, the blood flow response may become more dependent on K_{ATP} channels; thus, the blood flow falls dramatically when glibenclamide was administered, which causes a mismatch

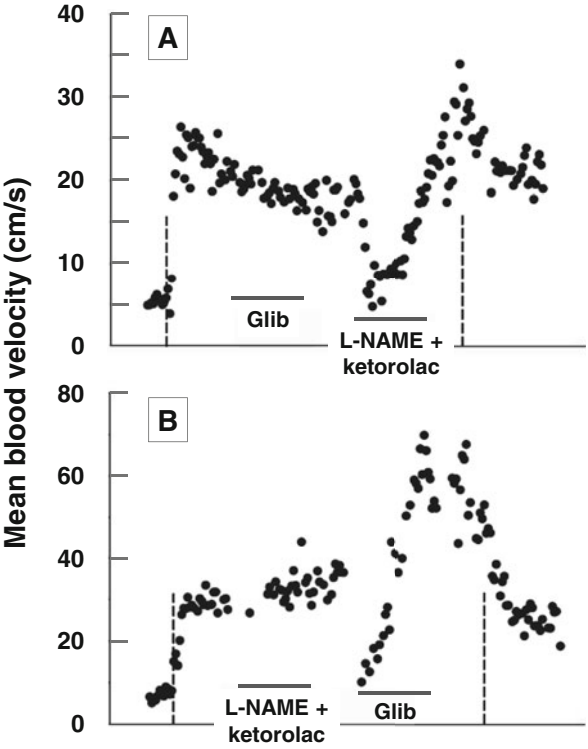

Fig. 9.2 Effects of glibenclamide (Glib, an inhibitor of ATP-sensitive K^+ (K_{ATP}) channel) and N^G-nitro-L-arginine methyl ester (L-NAME, an inhibitor of endothelial NO synthase) plus ketorolac (an inhibitor of cyclooxygenase) on the mean forearm blood flow velocity of healthy young adults during a moderate dynamic forearm exercise. Vertical dashed lines indicate the beginning and end of exercise. In panel A, Glib is infused during min 5–10 of exercise. Two min later L-NAME plus ketorolac is infused for 5 min. In panel B, L-NAME plus ketorolac is infused first for 5 min. Two min late, Glib is infused for 5 min. As is shown in panel A, Glib alone has no effect on the mean blood velocity. In the presence of Glib, the administration of L-NAME plus ketorolac causes a marked decrease, followed by a striking increase, and then returns to steady-state blood velocity. In panel B, L-NAME plus ketorolac causes a moderate reduction of the blood velocity. In the presence of these inhibitors, the administration of Glib results in a striking decrease, followed by a marked increase, and then returns to steady-state value of the blood velocity (The figure is from Schrage et al. (2006), with permission)

between oxygen delivery and metabolism in the contracting muscles that evoked the release of other mediators such as adenosine. This causes a brief hyperemic response above the normal blood flow value associated with contractions and then return toward the steady-state value seen prior to any intervention (Sarelius and Pohl 2010; Joyner and Casey 2015). It appears that the molecules and mechanisms involved in exercise hyperemia differ depending on exercise intensity and duration as well as local environment. Moreover, the local work load and hence oxygen demands are unlikely to be homogeneously distributed. Consequently the generation of the local metabolic signals will be nonhomogeneous throughout the muscle, leading to differences in the effectiveness of each of these signaling pathways at different vasculature locations (Sarelius and Pohl 2010).

The coronary blood flow is also closely tied to the oxygen requirements of the myocardium. The coronary venous Po_2 is maintained at around 20 mmHg even during strenuous physical exercise, indicating no signs of underperfusion. Under physiological conditions it appears that, among various metabolic factors, CO_2 and H_2O_2 are importantly involved in the match of O_2 consumption to O_2 delivery of the myocardium. Increased concentrations of CO_2 result in an increase of the proton concentration, which may cause coronary vasodilation through the activation of K_{ATP} channel (Deussen et al. 2012). In an in vivo study, the myocardium concentrations of H_2O_2 of the dog have been found to be proportionate to myocardial oxygen consumption and tightly correlated to coronary blood flow. Intracoronary infusion of catalase, a scavenger of H_2O_2, reduces the levels of the peroxide as well as coronary flow. These results suggest that H_2O_2 may act as a mediator for exercise hyperemia of myocardium. Furthermore, the in vitro study indicates that the myocardium H_2O_2 is derived from the mitochondria. When myocardial oxygen consumption is increased, there is an increased leak of electrons from mitochondrial complexes I and III resulting in increased generation of superoxide ($O_2^{\cdot -}$). Superoxide is rapidly converted to H_2O_2 by the actions of mitochondrial superoxide dismutase (SOD) (Saitoh et al. 2006). H_2O_2 may mediate exercise-induced coronary vasodilatation via the activation of voltage-gated K^+ (K_V) channel, K_{ATP} channel, and large-conductance voltage- and Ca^{2+}-activated K^+ (BK) channel (Duncker and Bache 2008; Deussen et al. 2012).

References

Aalkjaer C, Hughes A (1991) Chloride and bicarbonate transport in rat resistance arteries. J Physiol 436:57–73

Aalkjaer C, Boedtkjer E, Choi I, Lee S (2014) Cation-coupled bicarbonate transporters. Compr Physiol 4:1605–1637

Ballard HJ (2014) ATP and adenosine in the regulation of skeletal muscle blood flow during exercise. Sheng Li Xue Bao 66:67–78

Baretella O, Xu A, Vanhoutte PM (2014) Acidosis prevents and alkalosis augments endothelium-dependent contractions in mouse arteries. Pflugers Arch 466:295–305

Berne RM (1963) Cardiac nucleotides in hypoxia: possible role in regulation of coronary blood flow. Am J Phys 204:317–322

Berwick ZC, Payne GA, Lynch B, Dick GM, Sturek M, Tune JD (2010) Contribution of adenosine A_{2A} and A_{2B} receptors to ischemic coronary dilation: role of K_V and K_{ATP} channels. Microcirculation 17:600–607

Boedtkjer E, Aalkjaer C (2012) Intracellular pH in the resistance vasculature: regulation and functional implications. J Vasc Res 49:479–496

Boedtkjer E, Praetorius J, Aalkjaer C (2006) NBCn1 (slc4a7) mediates the na^+-dependent bicarbonate transport important for regulation of intracellular pH in mouse vascular smooth muscle cells. Circ Res 98:515–523

Boedtkjer E, Praetorius J, Fuchtbauer EM, Aalkjaer C (2008) Antibody-independent localization of the electroneutral Na^+-HCO_3^- cotransporter NBCn1 (slc4a7) in mice. Am J Phys Cell Physiol 294:C591–C603

Boedtkjer E, Praetorius J, Matchkov VV, Stankevicius E, Mogensen S, Füchtbauer AC, Simonsen U, Füchtbauer EM, Aalkjaer C (2011) Disruption of Na^+,HCO_3^- cotransporter NBCn1 (slc4a7) inhibits NO-mediated vasorelaxation, smooth muscle Ca^{2+} sensitivity, and hypertension development in mice. Circulation 124:1819–1829

Boedtkjer E, Damkier HH, Aalkjaer C (2012) NHE1 knockout reduces blood pressure and arterial media/lumen ratio with no effect on resting pH_i in the vascular wall. J Physiol 590:1895–1906

Brooks GA (2016) Energy flux, lactate shuttling, mitochondrial dynamics, and hypoxia. Adv Exp Med Biol 903:439–455

Brosius FC III, Pisoni RL, Cao X, Deshmukh G, Yannoukakos D, Stuart-Tilley AK, Haller C, Alper SL (1997) AE anion exchanger mRNA and protein expression in vascular smooth muscle cells, aorta, and renal microvessels. Am J Phys 273:F1039–F1047

Buckler KJ (2015) TASK channels in arterial chemoreceptors and their role in oxygen and acid sensing. Pflugers Arch 467:101310–101325

Calderón-Sánchez E, Fernández-Tenorio M, Ordóñez A, López-Barneo J, Ureña J (2009) Hypoxia inhibits vasoconstriction induced by metabotropic Ca^{2+} channel-induced Ca^{2+} release in mammalian coronary arteries. Cardiovasc Res 82:115–124

Chen YL, Wolin MS, Messina EJ (1996) Evidence for cGMP mediation of skeletal muscle arteriolar dilation to lactate. J Appl Physiol 81:349–354

Chen JF, Eltzschig HK, Fredholm BB (2013) Adenosine receptors as drug targets--what are the challenges? Nat Rev Drug Discov 12:265–286

Cheng B, Essackjee HC, Ballard HJ (2000) Evidence for control of adenosine metabolism in rat oxidative skeletal muscle by changes in pH. J Physiol 522:467–477

Coburn RF, Moreland S, Moreland RS, Baron CB (1992) Rate-limiting energy-dependent steps controlling oxidative metabolism-contraction coupling in rabbit aorta. J Physiol 448:473–492

Damkier HH, Nielsen S, Praetorius J (2006) An anti-NH2-terminal antibody localizes NBCn1 to heart endothelia and skeletal and vascular smooth muscle cells. Am J Physiol Heart Circ Physiol 290:H172–H180

Detar R, Bohr DF (1968) Oxygen and vascular smooth muscle contraction. Am J Phys 214:241–244

Deussen A, Ohanyan V, Jannasch A, Yin L, Chilian W (2012) Mechanisms of metabolic coronary flow regulation. J Mol Cell Cardiol 52:794–801

Dou D, Zheng X, Ying L, Ye L, Gao Y (2013) Sulfhydryl-dependent dimerization and cGMP-mediated vasodilatation. J Cardiovasc Pharmacol 62:1–5

Duncker DJ, Bache RJ (2008) Regulation of coronary blood flow during exercise. Physiol Rev 88:1009–1086

Edlund A, Sollevi A, Wennmalm A (1989) The role of adenosine and prostacyclin in coronary flow regulation in healthy man. Acta Physiol Scand 135:39–46

Fleming I, Hecker M, Busse R (1994) Intracellular alkalinization induced by bradykinin sustains activation of the constitutive nitric oxide synthase in endothelial cells. Circ Res 74:1220–1226

Frøbert O, Haink G, Simonsen U, Gravholt CH, Levin M, Deussen A (2006) Adenosine concentration in the porcine coronary artery wall and A2A receptor involvement in hypoxia-induced vasodilatation. J Physiol 570:375–384

Furchgott RF (1966) Metabolic factors that influence contractility of vascular smooth muscle. Bull N Y Acad Med 42:996–1006

Gebremedhin D, Yamaura K, Harder DR (2008) Role of 20-HETE in the hypoxia-induced activation of Ca^{2+}-activated K^+ channel currents in rat cerebral arterial muscle cells. Am J Physiol Heart Circ Physiol 294:H107–H120

Gerlach E, Deuticke B, Dreisbach RH (1963) Der Nucleotid-Abbau im Herzmuskel bei Sauerstoffmangel und seine mögliche Bedeutung für die Coronardurchblutung. Naturwissenschaften 50:228–229

Gnaiger E (2001) Bioenergetics at low oxygen: dependence of respiration and phosphorylation on oxygen and adenosine diphosphate supply. Respir Physiol 128:277–297

Halestrap AP (2012) The monocarboxylate transporter family-structure and functional characterization. IUBMB Life 64:1–9

Heaps CL, Bowles DK (2002) Gender-specific K^+-channel contribution to adenosine-induced relaxation in coronary arterioles. J Appl Physiol 92:550–558

Hedegaard ER, Nielsen BD, Kun A, Hughes AD, Krøigaard C, Mogensen S, Matchkov VV, Fröbert O, Simonsen U (2014) K_V7 channels are involved in hypoxia-induced vasodilatation of porcine coronary arteries. Br J Pharmacol 171:69–82

Hellsten Y (1999) The effect of muscle contraction on the regulation of adenosine formation in rat skeletal muscle cells. J Physiol 518:761–768

Jones DP (1986) Intracellular diffusion gradients of O_2 and ATP. Am J Phys Cell Physiol 250: C663–C675

Joyner MJ, Casey DP (2015) Regulation of increased blood flow (hyperemia) to muscles during exercise: a hierarchy of competing physiological needs. Physiol Rev 95:549–601

Katz A, Sahlin K (1988) Regulation of lactic acid production during exercise. J Appl Physiol 65:509–518

Lamb IR, Murrant CL (2015) Potassium inhibits nitric oxide and adenosine arteriolar vasodilatation via K_{IR} and Na^+/K^+ ATPase: implications for redundancy in active hyperaemia. J Physiol 593:5111–5126

Leach RM, Sheehan DW, Chacko VP, Sylvester JT (2000) Energy state, pH, and vasomotor tone during hypoxia in precontracted pulmonary and femoral arteries. Am J Phys Lung Cell Mol Phys 278:L294–L304

Lynge J, Hellsten Y (2000) Distribution of adenosine A1, A2A and A2B receptors in human skeletal muscle. Acta Physiol Scand 169:283–290

Marshall JM, Ray CJ (2012) Contribution of non-endothelium-dependent substances to exercise hyperaemia: are they O_2 dependent? J Physiol 590:6307–6320

Merkus D, Haitsma DB, Fung TY, Assen YJ, Verdouw PD, Duncker DJ (2003) Coronary blood flow regulation in exercising swine involves parallel rather than redundant vasodilator pathways. Am J Physiol Heart Circ Physiol 285:H424–H433

Montoya JJ, Fernández N, Monge L, Diéguez G, Villalón AL (2011) Nitric oxide-mediated relaxation to lactate of coronary circulation in the isolated perfused rat heart. J Cardiovasc Pharmacol 58:392–398

Mortensen SP, Gonzalez-Alonso J, Nielsen JJ, Saltin B, Hellsten Y (2009) Muscle interstitial ATP and norepinenphrine concentrations in the human leg during exercise and ATP infusion. J Appl Physiol 107:1757–1762

Neo BH, Kandhi S, Ahmad M, Wolin MS (2010) Redox regulation of guanylate cyclase and protein kinase G in vascular responses to hypoxia. Respir Physiol Neurobiol 174:259–264

Ngo AT, Riemann M, Holstein-Rathlou NH, Torp-Pedersen C, Jensen LJ (2013) Significance of K_{ATP} channels, L-type Ca^{2+} channels and CYP450-4A enzymes in oxygen sensing in mouse cremaster muscle arterioles in vivo. BMC Physiol 13:8

Nyberg M, Mortensen SP, Thaning P, Saltin B, Hellsten Y (2010) Interstitial and plasma adenosine stimulate nitric oxide and prostacyclin formation in human skeletal muscle. Hypertension 56:1102–1108

Occhipinti R, Boron WF (2015) Mathematical modeling of acid-base physiology. Prog Biophys Mol Biol 117(1):43–58

Pittman RN, Duling BR (1973) Oxygen sensitivity of vascular smooth muscle. Microvasc Res 6:202–211

Pries AR, Secomb TW (2014) Making microvascular networks work: angiogenesis, remodeling, and pruning. Physiology (Bethesda) 29:446–455

Saitoh S, Zhang C, Tune JD, Potter B, Kiyooka T, Rogers PA, Knudson JD, Dick GM, Swafford A, Chilian WM (2006) Hydrogen peroxide: a feed-forward dilator that couples myocardial metabolism to coronary blood flow. Arterioscler Thromb Vasc Biol 26:2614–2621

Sanjani MS, Teng B, Krahn T, Tilley S, Ledent C, Mustafa SJ (2011) Contributions of A_{2A} and A_{2B} adenosine receptors in coronary flow responses in relation to the K_{ATP} channel using A_{2B} and $A_{2A/2B}$ double-knockout mice. Am J Physiol Heart Circ Physiol 301:H2322–H2333

Sarelius I, Pohl U (2010) Control of muscle blood flow during exercise: local factors and integrative mechanisms. Acta Physiol (Oxford) 199:349–365

Schrage WG, Joyner MJ, Dinenno FA (2004) Local inhibition of nitric oxide and prostaglandins independently reduce forearm exercise hyperaemia in humans. J Physiol 557:599–611

Schrage WG, Dietz NM, Joyner MJ (2006) Effects of combined inhibition of ATP-sensitive potassium channels, nitric oxide, and prostaglandins on hyperemia during moderate exercise. J Appl Physiol 100:1506–1512

Schumacker PT (2011) Lung cell hypoxia: role of mitochondrial reactive oxygen species signaling in triggering responses. Proc Am Thorac Soc 8:477–484

Sharifi SM, Zhou X, Asano S, Tilley SL, Ledent C, Teng B, Dick GM, Mustafa SJ (2013) Interactions between A_{2A} adenosine receptors, hydrogen peroxide, and KATP channels in coronary reactive hyperemia. Am J Physiol Heart Circ Physiol 304:H1294–H1301

Smani T, Hernandez A, Urena J, Castellano AG, Franco-Obregon A, Ordonez A, López-Barneo J (2002) Reduction of Ca^{2+} channel activity by hypoxia in human and porcine coronary myocytes. Cardiovasc Res 53:97–104

Sparks HV (2011) Effect of local metabolic factors on vascular smooth muscle. Compr Physiol Supplement 7: Handbook of Physiology, The Cardiovascular System, Vascular Smooth Muscle, pp 475–513

Stowe DF (1981) Heart bioassay of effluent of isolated, perfused guinea pig hearts to examine the role of metabolites regulating coronary flow during hypoxia. Basic Res Cardiol 76:359–364

Sylvester JT, Shimoda LA, Aaronson PI, Ward JP (2012) Hypoxic pulmonary vasoconstriction. Physiol Rev 92:367–520

Tune JD, Richmond KN, Gorman MW, Feigl EO (2000) Role of nitric oxide and adenosine in control of coronary blood flow in exercising dogs. Circulation 101:2942–2948

Wang T, Sodhi J, Mentzer RM Jr, Van Wylen DG (1994) Changes in interstitial adenosine during hypoxia: relationship to oxygen supply: demand imbalance, and effects of adenosine deaminase. Cardiovasc Res 28:1320–1325

Wardle RL, Gu M, Ishida Y, Paul RJ (2007) Rho kinase is an effector underlying Ca^{2+}-desensitizing hypoxic relaxation in porcine coronary artery. Am J Physiol Heart Circ Physiol 293:H23–H29

Weir EK, Archer SL (2010) The role of redox changes in oxygen sensing. Respir Physiol Neurobiol 174:182–191

Zhou X, Teng B, Tilley S, Mustafa SJ (2013) A_1 adenosine receptor negatively modulates coronary reactive hyperemia via counteracting A_{2A}-mediated H_2O_2 production and K_{ATP} opening in isolated mouse hearts. Am J Physiol Heart Circ Physiol 305:H1668–H1679

Chapter 10
Shear Stress, Myogenic Response, and Blood Flow Autoregulation

Abstract The vascular activity is tonically regulated by two major hemodynamic variations: a force parallel to the vessel wall generated by blood flow brushing against the endothelial layer termed as shear stress and a force perpendicular to the vessel wall resulted from blood pressure termed as tensile stress. Shear stress is sensed by various types of ion channels and membrane receptors as well as adhesion proteins, glycocalyx, and primary cilia on the cell surface. The acute activation of these mechanosensory receptors leads to altered vascular activity, while chronic change in shear stress results in adaptive structural remodeling of the blood vessels. An increase in blood pressure causes increased stretch of vascular smooth muscle cells (VSMCs) and vasoconstriction, while a decrease in blood pressure causes vasodilatation. This phenomenon is known as myogenic response. Vascular myogenic response is initiated by the opening of mechanosensitive ion channels such as TRPC6 channel, TRPM4 channel, and probably a heteromultimeric channel complex formed by the β and γ subunits of epithelial sodium channels and the subunit 2 of acid-sensing ion channel. Myogenic response is of fundamental importance for providing organ a relatively stable blood flow when exposed to changes in blood pressure, a phenomenon named as blood flow autoregulation. In renal circulation the autoregulation is achieved largely by the myogenic response and the macula densa–tubuloglomerular feedback response.

Keywords Shear stress • Myogenic response • Mechanoreceptor • Blood flow autoregulation • Renal

10.1 Introduction

The circulating blood constantly imposes mechanical forces on the blood vessel wall, which can be categorized into two major components: one is parallel to the vessel wall, defined as shear stress, corresponding to the frictional force exerted by blood flow on the endothelial layer; the other is perpendicular to the vessel wall, defined as tensile stress, associated with the intravascular blood pressure. Shear stress is applied mainly to the vascular endothelium, while the tensile stress raised from blood pressure is transferred to all layers of the vessel wall (Hill-Eubanks et al. 2014). A dilatation of the artery in response to increments in blood flow, i.e.,

Y. Gao, *Biology of Vascular Smooth Muscle: Vasoconstriction and Dilatation*,
DOI 10.1007/978-981-10-4810-4_10

increases in shear stress, is first reported by Schretzenmayr in 1933 (Davies et al. 2005), and it is now well established that shear stress exerts both acute and chronic influence on vascular tone and remodeling through endothelium-derived substances including nitric oxide (NO), prostaglandin I_2, and endothelium-derived hyperpolarizing factor (EDHF) (Holtz et al. 1984; Rubanyi et al. 1986; Busse and Fleming 2006; Chiu and Chien 2011; Baeyens et al. 2016). An increase in blood pressure causes vasoconstriction, whereas a reduction in blood pressure causes vasodilatation. This phenomenon, named as myogenic response, is first reported by Bayliss in 1902 (Bayliss 1902). Myogenic response constitutes the basic mechanism for maintaining the blood flow at a relative stable level within physiological range of blood pressure, termed as blood flow autoregulation. In combination with metabolic regulation or other mechanism, the autoregulation activity is essential for tissue perfusion and functionality (Hall 2015; Carlström et al. 2015). In this chapter the current understanding of the role of shear stress, myogenic response, and blood flow autoregulation in the regulation of vascular activities will be discussed.

10.2 Shear Stress

In blood vessels shear stress is defined as the tangential force of blood flow that acts on endothelium. The magnitude of shear stress (τ) in straight vessels can be estimated by using the formula: $\tau = 4\ \mu Q/\pi r^3$, where μ is the blood viscosity, Q the blood flow, π the ratio of a circle's circumference to its diameter, and r the radius of the blood vessel. Under physiological conditions shear stress in the human ranges from 10 to 70 dyn/cm^2 in arteries and from 1 to 6 dyn/cm^2 in the venous system (Papaioannou and Stefanadis 2005; Davies 2009). Results from a study show that the shear stress of infrarenal aorta of mice and rats is markedly greater compared with humans (87.6, 70.5, and 4.8 dyn/cm^2, respectively). Such a difference, at least partially, is likely to be due to that the radius of infrarenal aortas of mice and rats (~3.5 and 8.5 mm, respectively) is much smaller than that of humans (~65 mm). As is known that shear stress is inversely proportional to the cube of the arterial radius (Greve et al. 2006). It is likely that an optimum value or set point of shear stress exists for each distinct segment of the blood vessel and that deviation from the set point rather than the absolute level of shear stress activates vascular response (Baeyens et al. 2015).

The mechanotransduction for shear-induced vascular responses may occur through various types of ion channels and membrane receptors, which include K^+, Cl^-, and Ca^{2+} channels, transient receptor potential channels, G-protein-coupled receptors (GPCRs), and tyrosine kinase receptors (TKRs). Various adhesion proteins such as integrins, platelet endothelial cell adhesion molecule (PECAM-1, CD31), and vascular endothelial cadherin (VE-cadherin, CD144) are also known to be involved in shear stress resulting in the activation of downstream signal transduction pathways. Changes in shear stress affect the conformation of the glycocalyx, a glycoprotein-polysaccharide covering that surrounds the cell

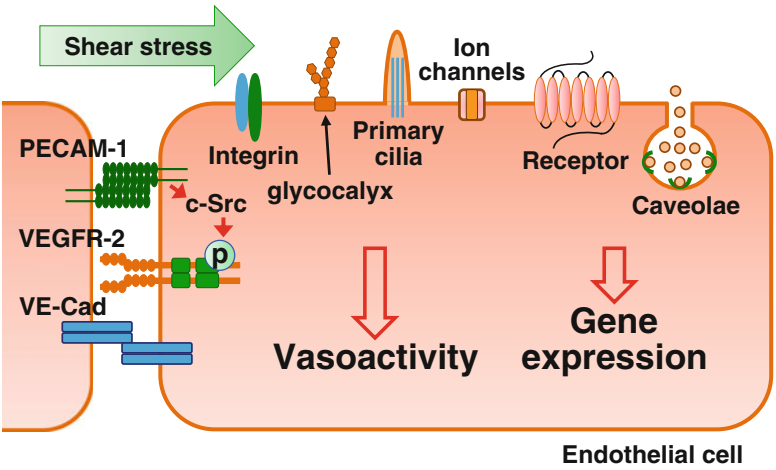

Fig. 10.1 Possible sensors for shear stress-induced changes in vasoactivity and gene expression. Platelet endothelial cell adhesion molecule (PECAM-1), vascular endothelial growth factor receptor-2 (VEGFR-2), and vascular endothelial cadherin (VE-cadherin) form a mechanosensory complex. PECAM-1 directly transmits mechanical force, resulting in the activation of c-Src phosphorylation of VEGFR-2, which in turn activates the downstream signaling pathway, while VE-cadherin serves as an adaptor. The mechanical force generated by shear stress may be transferred through integrins, glycocalyx, and primary cilia, which are connected intracellularly to cytoskeleton. Cytoskeleton may further transfer the signaling to subcellular sites distant from the luminal surface (not shown). Certain ion channels and membrane receptors are shear stress responsive. The ion channels include some K^+, Cl_2, and Ca^{2+} channels as well as transient receptor potential channels. The receptors include tyrosine kinase receptors and G-protein-coupled receptors. Caveolae have also been found being involved in shear stress sensing and response mechanisms. Moreover, the plasma membrane itself may directly act as a shear stress sensor

membranes. The signal is transmitted to the intracellular domain of the glycocalyx. Shear stress also causes deflection of the primary cilia, which are membrane-covered rodlike organelles that protrude from the surface of cells. The bending of primary cilia may activate a cation channel localized in the cilia and lead to Ca^{2+} influx. Both adhesion proteins, glycocalyx, and primary cilia are connected intracellularly to cytoskeleton, which not only stabilizes the structure and shape of the cell but also transfer shear-mediated signaling to subcellular sites distant from the luminal surface. Caveolae, the flask-shaped small (50–100 nm) plasma membrane invaginations, are also implicated in mediating shear stress signaling. Moreover, the plasma membrane itself may function as a shear stress sensor (Ando and Yamamoto 2013; Ye et al. 2014; Zhou et al. 2014) (Fig. 10.1).

Integrins are transmembrane glycoproteins consisting of α- and β-subunits. The extracellular domains of the subunits bind directly to extracellular matrix proteins, while the cytoplasmic domains interact with focal adhesion proteins. In mice lacking the gene encoding for α_1 integrins, the nitric oxide (NO)-mediated dilatation response of mesenteric resistance arteries induced by shear stress is diminished, which is associated with reduced phosphorylation of phosphatidylinositol

3-kinase (PI3-kinase) and protein kinase B (Akt) (Loufrani et al. 2008). The cellular Src kinase (c-Src) in the focal adhesions is rapidly activated by shear stress. When the integrins are subject to shear stress, the activation of c-Src/PI3-kinase/Akt cascade may stimulate the activity of endothelial NO synthase (eNOS) and consequently lead to NO-dependent vasodilatation (Loufrani et al. 2008; Ando and Yamamoto 2013). PECAM-1, another adhesion protein, is concentrated in the region of intercellular junctions and has been shown to form a mechanosensory complex with VE-cadherin and vascular endothelial growth factor receptor-2 (VEGFR-2) in which PECAM-1 directly transmits mechanical force, VE-cadherin serves as an adaptor, and VEGFR-2 activates PI3-kinase. The tension exerted by shear stress on PECAM-1 activates c-Src resulting in ligand-independent transactivation of VEGFR-2, followed by activation of Akt, phosphorylation of serine 1177 (S1177) of eNOS, and production of NO. Activation of VEGFR-2 can also cause S1177 phosphorylation via cAMP-dependent protein kinase (PKA). Heat shock protein 90 (Hsp90), a constitutively expressed molecular chaperone, when associated with eNOS, can recruit Akt into the eNOS complex and maintains Akt activity (Tzima et al. 2005; Davies 2009; Ando and Yamamoto 2013; Baeyens et al. 2016).

In straight segments of arteries, the endothelium is subjected to shear stress generated by a unidirectional laminar flow. Acute changes in shear stress regulate vascular tone through the release of endothelial-derived factors such as NO, prostaglandins, and hyperpolarizing factors. Chronic changes of local hemodynamics promote adaptive structural remodeling of the vessel wall through endothelium-dependent regulation of gene and protein expression (Davies 2009). However, at arterial branches and bifurcations as well as curvatures (e.g., the aortic arch), the blood flow is characterized by low average shear stress, constantly changing gradients of shear stress, oscillatory flow due to flow reversal, and multifrequency, multidirectional, secondary flows. A flow with such a pattern is termed disturbed flow. Straight segments of arteries are protected from atherosclerosis due to anti-inflammatory, antioxidative, and antithrombotic genes induced by unidirectional laminar shear stress, in particular the flow-dependent transcription factors Krüppel-like factor 2 (KLF2) and nuclear factor (erythroid-derived 2)-like 2 (NRF2). In contrast, regions of arteries exposed to disturbed flow exhibit low, chronic inflammation even under control conditions, rendering the vessels more susceptible to atherosclerosis (Davies 2009; Chiu and Chien 2011; Baeyens et al. 2016).

10.3 Myogenic Response

The blood vessels react to an increase in intraluminal pressure by contraction and react to a reduction in intraluminal pressure by relaxation. This phenomenon known as myogenic response is most pronounced in arterioles but can also be observed in arteries, venules, veins, and even lymphatic vessels (Hall 2015). It is generally recognized that the myogenic response is an intrinsic property of vascular smooth

muscle cells (VSMCs). It is initiated by pressure-induced vessel wall stretch and thus the VSMC stretch. In turn, VSMC stretch initiates a depolarization event, which activates voltage-gated Ca^{2+} channels, followed by increased Ca^{2+} influx. Stretch may also cause increased Ca^{2+} release from the sarcoplasmic reticulum, increased Ca^{2+} sensitivity of myofilaments, and consequently vasoconstriction. Overwhelming evidence supports the notion that myogenic response plays an pivotal role in the setting of vascular resistance, local control of microvascular blood flow through autoregulation, and in the control of capillary hydrostatic pressure (Drummond et al. 2008; Hill and Meininger 2012; Kauffenstein et al. 2012).

A variety of mechanisms have been proposed for the transduction of VSMC stretch into a cellular signaling, which include mechanical deformations in the cell membrane leading to the opening of mechanosensitive ion channels, activation of ion channels by force transferred from the tethered extracellular matrix or cytoskeleton, and second messengers generated by force-sensitive receptors and enzymes (Drummond et al. 2008; Hill and Meininger 2012; Liu and Montell 2015).

The mammalian transient receptor potential (TRP) superfamily consists of 28 nonselective cation channels, which are grouped into six subfamilies: canonical, vanilloid, melastatin, ankyrin, polycystic, and mucolipin TRPs (TRPC, TRPV, TRPM, TRPA, TRPP, and TRPML, respectively). TRP channels do not exhibit a typical voltage sensor but can sense a variety of other stimuli including pressure, shear stress, and mechanical stretch (Earley and Brayden 2015; Yue et al. 2015). In isolated middle cerebral arteries, suppression of TRPC6 or TRPM4 expression using antisense oligonucleotides abolishes pressure-induced depolarization and constriction, indicating a critical role in myogenic vasoconstriction for these TRP channels (Welsh et al. 2002; Earley et al. 2004). Studies show that stretch of the cell membrane causes membrane thinning and a conformational change in the TRPC6 channel, resulting in its open state. Alternatively, when G-protein-coupled receptor is activated, the large charged inositol 1,4,5-trisphosphate (IP_3) head group of phosphatidylinositol 4,5-bisphosphate (PIP_2) located in the vicinity of the TRPC6 channels is cleaved out by phospholipase C (PLC) to produce the small uncharged head group on diacyl glycerol (DAG), resulting in drastic change in lipid geometry and consequently stress and/or exposure of the TRPC6 channels and its opening (Spassova et al. 2006). In cerebral artery smooth muscle cells, Ca^{2+} influx evoked by the activation of TRPC6 channels due to either stretch-dependent generation of DAG or direct mechanical stimulation augments IP_3-dependent Ca^{2+} release from the sarcoplasmic reticulum, which then activates nearby TRPM4 channels. TRPM4 channels, in turn, promote Na^+ influx and cell depolarization, followed by increased Ca^{2+} influx through voltage-gated Ca^{2+} channels and vasoconstriction (Earley and Brayden 2015). In cerebral parenchymal arterioles, myogenic tone development has also been found being resulted from mechanoactivation of purinergic receptors, followed by Rho kinase (ROCK)-mediated enhancement of Na^+ influx through TRPM4 channels and ROCK-mediated enhancement of Ca^{2+} sensitivity of myofilaments (Li et al. 2014; Li and Brayden 2017).

In renal interlobar, renal afferent arterioles, and middle cerebral arteries, the epithelial sodium channel (ENaC) proteins and closely related acid-sensing ion channel (ASIC) have been proposed to form an ion channel (ENaC–ASIC) to act as a mechanosensor participating in the vascular myogenic response (Drummond et al. 2008; Drummond 2015). Both ASICs and ENaCs are members of the ENaC/DEG (degenerin) family of amiloride-sensitive Na^+ channels. All ENaC/DEG family members share a common membrane topology, with two transmembrane segments, intracellular N- and C-termini, and a large extracellular loop that represents more than half of the mass of the channel protein. There are five currently known subunits for EnaCs (α, β, γ, δ, and ε) and six subunits for ASICs (1a, 1b, 2a, 2b, 3, and 4). Based on the crystal structure of ASIC1, it is predicted that both ASICs and EnaCs are trimers (Drummond et al. 2008; Kellenberger and Schild 2015; Boscardin et al. 2016).

In VSMCs the βENaC and γENaC subunits are the predominant ENaC proteins expressed, whereas the αENaC subunit is rare. Considering that (1) βENaC, γENaC, and ASIC2 are expressed in similar VSMC populations (2), γENaC biochemically interacts with ASIC2 in other systems, and (3) the loss of ASIC2, βENaC, and γENaC generates the same phenotype (loss of pressure-induced vasoconstriction), it is proposed by Drummond and colleagues that these proteins form a heterotrimeric mechanosensitive channel. Based on a universal mechanotransducer model developed in the nematode for related DEG proteins, they hypothesize that the ENaC/ASIC channels in VSMCs are likely to be a large heteromultimeric channel complex containing extracellular matrix proteins and linking proteins, pore-forming channels, intracellular linking proteins, and cytoskeleton proteins. A mechanical force is transduced through the extracellular matrix to gate the channel, and the cytoskeleton may also participate in transduction of the applied force as well as stabilize the pore at the cell surface. When the channel is gated open, Na^+ and possibly Ca^{2+} entry leads to membrane depolarization and subsequent vasoconstriction (Drummond et al. 2008).

In isolated mouse renal interlobar arteries, the inhibition of ENaC channels with low concentrations of amiloride and benzamil attenuates pressure-induced vasoconstriction and increases in cytosolic Ca^{2+} and Na^+ without affecting vasoconstriction induced by phenylephrine (Jernigan and Drummond 2005). In the same preparations, pressure-induced vasoconstriction is also suppressed by specific knockdown of βENaC or γENaC using dominant-negative or small-interference RNA molecules (Jernigan and Drummond 2006). A critical role for ENaC channels in myogenic vasoconstriction has also been demonstrated in afferent arterioles of the mice and rat as well as rat posterior cerebral arteries (Guan et al. 2009; Ge et al. 2012; Kim et al. 2013). As aforementioned, ENaC and ASIC may form a functional complex to mediate myogenic vasoconstriction. Consistent with this postulation, the myogenic constriction in renal interlobar arteries is impaired in ASIC2(+/−) and ASIC2(−/−) mice (Gannon et al. 2015).

10.4 Blood Flow Autoregulation

In most tissues of the body, the blood flow is kept within a narrow range despite large fluctuations in systemic arterial pressure. When subject to an acute increase in arterial pressure, the blood flow rises immediately but returns almost to the normal level within less than a minute, even though the arterial pressure is kept elevated. This phenomenon is termed blood flow autoregulation. The autoregulation is largely independent of extrinsic nerves or circulating hormones. It is regulated locally predominantly by myogenic and metabolic mechanisms. The response is initiated by vessel wall stretch. Since the mechanical sensing mechanism detects circumferential stretch of the vessel wall rather than blood flow, it is unlikely to serve as the major factor to maintain the blood flow relatively stable. More likely, metabolic factors may override the myogenic mechanism to make the flow to match the metabolic demands of the tissues. Autoregulation is essential to keeping the blood supply adequate in the physiological range of blood pressure and preventing the transmission of pressure waves to small, fragile microvasculature. When perfusion pressure is increased, autoregulation avoids a waste of perfusion in the tissue where the flow is already sufficient. When perfusion pressure is decreased, autoregulation maintains capillary pressure and capillary flow, which is particularly important to certain organs which are sensitive to ischemia and hypoxia (Hall 2015). The autoregulation has been more extensively in the regulation of coronary, cerebral, and renal blood flow. The related contents for the former two will be discussed in Chaps. 15 and 16, respectively. The autoregulation of renal blood flow is discussed in the following paragraphs.

The renal blood flow (RBF) normally accounts for ~22% of cardiac output. This is expected since the kidney serves the body as a natural filter of the blood to remove water-soluble wastes and maintain the homeostasis of electrolytes and fluid. To fulfill this function, the maintenance of a constant glomerular filtration rate (GFR) is essential. This requires stable renal blood flow when exposed to variable blood pressure, a mission naturally suitable for blood flow autoregulation. Indeed, the renal autoregulation is capable of upholding the blood flow relatively stable across a broad range of blood pressure as low as 75 mmHg and as high as 160 mmHg. Renal autoregulation is intrinsic to the kidney and independent of extrinsic nerves or circulating hormones. It is achieved largely by the coordinating actions of the myogenic response and the macula densa–tubuloglomerular feedback (MD–TGF) response. The myogenic response normally contributes ~50%, MD–TGF ~35%, and a poorly characterized third mechanism modulated by connecting tubuloglomerular feedback system ~10–20% to renal autoregulation assessed by the magnitude and kinetics of the response. The myogenic response acts promptly by contracting the afferent arterioles to an increase and by relaxing the afferent arterioles to a decrease in perfusion pressure. The more delayed MD–TGF response is regulated by increased or decreased NaCl absorption of the macula densa cells resulting from altered GFR, which leads the release of vasoactive agents and thus

constriction or dilatation of the adjacent afferent arteriole (Burke et al. 2014; Carlström et al. 2015; Hall 2015).

The MD–TGF response depends on special anatomical arrangements of the juxtaglomerular complex where the macula densa cell acts as the sensor of GFR by using NaCl in the tubular fluid as an indicator and the nearby renal afferent arterioles as the effector. When NaCl concentration in the distal convoluted tubule is increased due to excessive filtration at the glomerulus evoked by high perfusion pressure, there is more sodium being transported into the macula densa cells, primarily through a luminal $Na^+/K^+/2Cl^-$ type 2 (NKCC2) cotransporter. The increased cytosolic concentration NaCl of macula densa cells results in the elevation of intracellular Ca^{2+}, and ATP is released though a basolateral nonselective Maxi-anion channel. The ATP is subsequently converted to adenosine by ecto-5′-nucleotidase. Adenosine constricts the afferent arteriole via the adenosine A_1 receptor (A_1ARs). The blockade of A_1ARs largely abolishes MD–TGF-induced reductions of single nephron GFR and glomerular capillary pressure in the rat. Similar phenomenon is also found in mice deficient in A_1ARs, suggesting that adenosine is the primary mediator for the MD–TGF response (Bell et al. 2003; Schnermann and Briggs 2008; Carlström et al. 2015). In addition to adenosine, there is compelling evidence suggesting that at least ten and probably more vasoactive agents are affected by NaCl at the macula densa/thick ascending limb sensing site and that all of them in varying degrees contribute to vasoactivity of the MD–TGF response. These agents include those with constrictor property and those with dilator property. The former include 20-hydroxyeicosatetraenoic acid (20-HETE), angiotensin II, thromboxane, superoxide, and ATP as well as renal nerves, while the latter include NO, carbon monoxide, kinins, and adenosine (acting via adenosine A_2 receptor). Undoubtedly multiple vasoactive agents participate in the MD–TGF response. The magnitude of the response represents the sum effect of these agents with constrictor effects exceeding that of the dilator effects (Schnermann 2015).

References

Ando J, Yamamoto K (2013) Flow detection and calcium signalling in vascular endothelial cells. Cardiovasc Res 99:260–268

Baeyens N, Bandyopadhyay C, Coon BG, Yun S, Schwartz MA (2016) Endothelial fluid shear stress sensing in vascular health and disease. J Clin Invest 126:821–828

Baeyens N, Nicoli S, Coon BG, Ross TD, Van den Dries K, Han J, Lauridsen HM, Mejean CO, Eichmann A, Thomas JL, Humphrey JD, Schwartz MA (2015) Vascular remodeling is governed by a VEGFR3-dependent fluid shear stress set point. Elife 4:e04645

Bayliss WM (1902) On the local reactions of the arterial wall to changes of internal pressure. J Physiol 28:220–231

Bell PD, Lapointe JY, Peti-Peterdi J (2003) Macula densa cell signaling. Annu Rev Physiol 65:481–500

Boscardin E, Alijevic O, Hummler E, Frateschi S, Kellenberger S (2016) The function and regulation of acid-sensing ion channels (ASICs) and the epithelial Na+channel (ENaC): IUPHAR review 19. Br J Pharmacol 173(18):2671–2701

Burke M, Pabbidi MR, Farley J, Roman RJ (2014) Molecular mechanisms of renal blood flow autoregulation. Curr Vasc Pharmacol 12:845–858

Busse R, Fleming I (2006) Vascular endothelium and blood flow. Handb Exp Pharmacol 176:43–78

Carlström M, Wilcox CS, Arendshorst WJ (2015) Renal autoregulation in health and disease. Physiol Rev 95:405–511

Chiu JJ, Chien S (2011) Effects of disturbed flow on vascular endothelium: pathophysiological basis and clinical perspectives. Physiol Rev 91:327–387

Davies PF (2009) Hemodynamic shear stress and the endothelium in cardiovascular pathophysiology. Nat Clin Pract Cardiovasc Med 6:16–26

Davies PF, Spaan JA, Krams R (2005) Shear stress biology of the endothelium. Ann Biomed Eng 33:1714–1718

Drummond HA (2015) Nontubular epithelial Na^+ channel proteins in cardiovascular regulation. Physiol Rep 3.pii:e12404

Drummond HA, Jernigan NL, Grifoni SC (2008) Sensing tension: epithelial sodium channel/acid-sensing ion channel proteins in cardiovascular homeostasis. Hypertension 51:1265–1271

Earley S, Brayden JE (2015) Transient receptor potential channels in the vasculature. Physiol Rev 95:645–690

Earley S, Waldron BJ, Brayden JE (2004) Critical role for transient receptor potential channel TRPM4 in myogenic constriction of cerebral arteries. Circ Res 95:922–929

Gannon KP, McKey SE, Stec DE, Drummond HA (2015) Altered myogenic vasoconstriction and regulation of whole kidney blood flow in the ASIC2 knockout mouse. Am J Physiol Renal Physiol 308:F339–F348

Ge Y, Gannon K, Gousset M, Liu R, Murphey B, Drummond HA (2012) Impaired myogenic constriction of the renal afferent arteriole in a mouse model of reduced βENaC expression. Am J Physiol Renal Physiol 302:F1486–F1493

Greve JM, Les AS, Tang BT, Draney Blomme MT, Wilson NM, Dalman RL, Pelc NJ, Taylor CA (2006) Allometric scaling of wall shear stress from mice to humans: quantification using cine phase-contrast MRI and computational fluid dynamics. Am J Physiol Heart Circ Physiol 291: H1700–H1708

Guan Z, Pollock JS, Cook AK, Hobbs JL, Inscho EW (2009) Effect of epithelial sodium channel blockade on the myogenic response of rat juxtamedullary afferent arterioles. Hypertension 54:1062–1069

Hall JE (2015) Guyton and Hall textbook of medical physiology, 13th edn. Elservier, Philadelphia

Hill MA, Meininger GA (2012) Arteriolar vascular smooth muscle cells: mechanotransducers in a complex environment. Int J Biochem Cell Biol 44:1505–1510

Hill-Eubanks DC, Gonzales AL, Sonkusare SK, Nelson MT (2014) Vascular TRP channels: performing under pressure and going with the flow. Physiology (Bethesda) 29:343–360

Holtz J, Förstermann U, Pohl U, Giesler M, Bassenge E (1984) Flow-dependent, endothelium-mediated dilation of epicardial coronary arteries in conscious dogs: effects of cyclooxygenase inhibition. J Cardiovasc Pharmacol 6:1161–1169

Jernigan NL, Drummond HA (2005) Vascular ENaC proteins are required for renal myogenic constriction. Am J Physiol Renal Physiol 289:F891–F901

Jernigan NL, Drummond HA (2006) Myogenic vasoconstriction in mouse renal interlobar arteries: role of endogenous β and γENaC. Am J Physiol Renal Physiol 291:F1184–F1191

Kauffenstein G, Laher I, Matrougui K, Guérineau NC, Henrion D (2012) Emerging role of G protein-coupled receptors in microvascular myogenic tone. Cardiovasc Res 95:223–232

Kellenberger S, Schild L (2015) International Union of Basic and Clinical Pharmacology. XCI. Structure, function, and pharmacology of acid-sensing ion channels and the epithelial Na^+ channel. Pharmacol Rev 67:1–35

Kim EC, Choi SK, Lim M, Yeon SI, Lee YH (2013) Role of endogenous ENaC and TRP channels in the myogenic response of rat posterior cerebral arteries. PLoS One 8:e84194

Li Y, Baylie RL, Tavares MJ, Brayden JE (2014) TRPM4 channels couple purinergic receptor mechanoactivation and myogenic tone development in cerebral parenchymal arterioles. J Cereb Blood Flow Metab 34:1706–1714

Li Y, Brayden JE (2017) Rho kinase activity governs arteriolar myogenic depolarization. J Cereb Blood Flow Metab 37:140–152

Liu C, Montell C (2015) Forcing open TRP channels: mechanical gating as a unifying activation mechanism. Biochem Biophys Res Commun 460:22–25

Loufrani L, Retailleau K, Bocquet A, Dumont O, Danker K, Louis H, Lacolley P, Henrion D (2008) Key role of $\alpha_1\beta_1$-integrin in the activation of PI3-kinase-Akt by flow (shear stress) in resistance arteries. Am J Physiol Heart Circ Physiol 294:H1906–H1913

Papaioannou TG, Stefanadis C (2005) Vascular wall shear stress: basic principles and methods. Hell J Cardiol 46:9–15

Rubanyi GM, Romero JC, Vanhoutte PM (1986) Flow-induced release of endothelium-derived relaxing factor. Am J Phys 250:H1145–H1149

Schnermann J (2015) Concurrent activation of multiple vasoactive signaling pathways in vasoconstriction caused by tubuloglomerular feedback: a quantitative assessment. Annu Rev Physiol 77:301–322

Schnermann J, Briggs JP (2008) Tubuloglomerular feedback: mechanistic insights from gene-manipulated mice. Kidney Int 74:418–426

Spassova MA, Hewavitharana T, Xu W, Soboloff J, Gill DL (2006) A common mechanism underlies stretch activation and receptor activation of TRPC6 channels. Proc Natl Acad Sci U S A 103:16586–16591

Tzima E, Irani-Tehrani M, Kiosses WB, Dejana E, Schultz DA, Engelhardt B, Cao G, DeLisser H, Schwartz MA (2005) A mechanosensory complex that mediates the endothelial cell response to fluid shear stress. Nature 437:426–431

Welsh DG, Morielli AD, Nelson MT, Brayden JE (2002) Transient receptor potential channels regulate myogenic tone of resistance arteries. Circ Res 90:248–250

Ye GJ, Nesmith AP, Parker KK (2014) The role of mechanotransduction on vascular smooth muscle myocytes' [corrected] cytoskeleton and contractile function. Anat Rec (Hoboken) 297:1758–1769

Yue Z, Xie J, Yu AS, Stock J, Du J, Yue L (2015) Role of TRP channels in the cardiovascular system. Am J Physiol Heart Circ Physiol 308:H157–H182

Zhou J, Li YS, Chien S (2014) Shear stress-initiated signaling and its regulation of endothelial function. Arterioscler Thromb Vasc Biol 34:2191–2198

Part III
Intracellular Signalings

Chapter 11
Intracellular Ca^{2+} Regulation

Abstract A plethora of cellular functions including vasoconstriction and vasodilatation are regulated by calcium (Ca^{2+}) ion and the cytosolic Ca^{2+} homeostasis and, therefore, are controlled by various complex yet coordinated mechanisms, in particular considering the marked difference in the concentrations across the cell membrane and across the membrane of the intracellular Ca^{2+} sarcoplasmic reticulum (SR). The major mechanisms for lowering the cytosolic Ca^{2+} concentrations ($[Ca^{2+}]_i$) are mediated by plasma membrane calcium ATPase, sodium–calcium exchanger, and sarco-/endoplasmic reticulum Ca^{2+}ATPase, while the primary mechanisms for elevating $[Ca^{2+}]_i$ are mediated by voltage-gated calcium channels, inositol 1,4,5-trisphosphate receptors, and ryanodine receptors. In addition, the replenishment of depleted SR Ca^{2+} is through store-operated calcium channels. In this chapter the above mechanisms and their physiological relevance to vascular activities are discussed.

Keywords Voltage-gated Ca^{2+} channels • Calcium ATPases • Sarcoplasmic reticulum • Store-operated Ca^{2+} entry • Ca^{2+} wave

11.1 Introduction

Calcium ion (Ca^{2+}) is an indispensable intracellular signal molecule in a broad range of cellular functions including muscle contraction, cellular motility, and cell proliferation and differentiation. Under basal conditions the intracellular Ca^{2+} ($[Ca^{2+}]_i$) concentration of vascular smooth muscle cells (VSMCs) is ~100–300 nM, which is about 10,000-fold lower than the extracellular Ca^{2+} concentration (Karaki 2004; Marchand et al. 2012; Billaud et al. 2014; Zheng et al. 2015). The remarkably low $[Ca^{2+}]_i$ concentration is maintained through active extrusion of Ca^{2+} from the cell by plasma membrane calcium ATPases (PMCAs) (Little et al. 2016) and by sodium-calcium exchangers (NCXs) (Hilge 2012) as well as sequestration of cytosolic Ca^{2+} into the sarcoplasmic reticulum (SR) by the sarco/endoplasmic reticulum Ca^{2+}ATPase (SERCA) (Wray and Burdyga 2010). When stimulated the $[Ca^{2+}]_i$ concentrations is rapidly increased by several folds to more than tenfold, resulting in the activation of various signaling cascades and vasoactivities (Karaki 2004). The increase in $[Ca^{2+}]_i$ is achieved through the

Y. Gao, *Biology of Vascular Smooth Muscle: Vasoconstriction and Dilatation*,
DOI 10.1007/978-981-10-4810-4_11

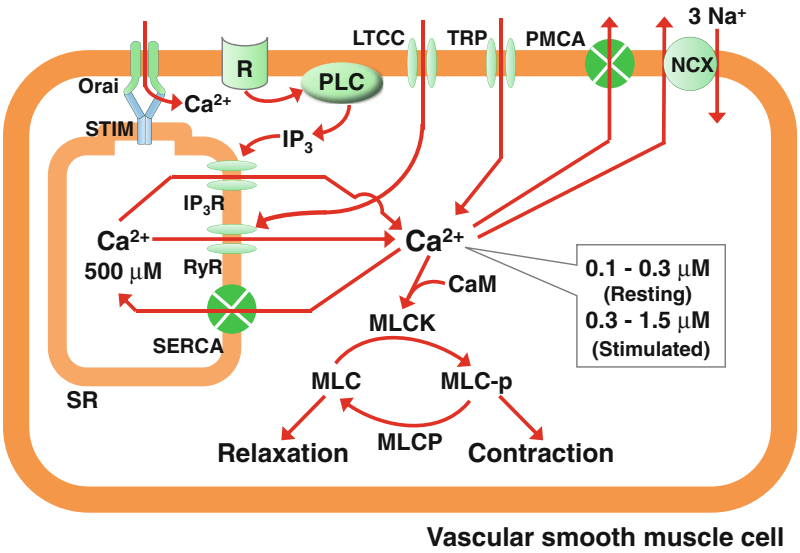

Fig. 11.1 The regulation of intracellular calcium (Ca^{2+}) concentration $[Ca^{2+}]_i$ of vascular smooth muscle cells (VSMCs). Under basal conditions, $[Ca^{2+}]_i$ is maintained at low and stable levels (0.1–0.3 μM) against very high extracellular concentration of Ca^{2+} (~1.2 mM ionized and ~2.4 mM ionized, complexed to small molecules, and protein bound). This is achieved mainly by extrusion of cytosolic Ca^{2+} by plasma membrane calcium ATPases (PMCAs) and by sodium–calcium exchangers (NCXs) and by sequestration of cytosolic Ca^{2+} into sarcoplasmic reticulum (SR) by the sarco/endoplasmic reticulum Ca^{2+} ATPase (SERCA). The SRs act as intracellular Ca^{2+} stores with a concentration of this ion at ~500 μM. When VSMCs are exposed to external stimuli, the $[Ca^{2+}]_i$ concentrations are rapidly elevated by several to more than tenfold. The increased $[Ca^{2+}]_i$, after bound to calmodulin (CaM), stimulates myosin light chain kinase (MLCK), resulting in increased phosphorylation of myosin light chain (MLC), consequently vasoconstriction. This reaction can be reversed by myosin light chain phosphatase (MLCP). The increase in $[Ca^{2+}]_i$ is achieved through extracellular Ca^{2+} influx through the opening of L-type voltage-gated calcium channels (LTCC) and the transient receptor potential (TRP) channels. Meanwhile, the release of SR Ca^{2+} is stimulated by the opening of inositol 1,4,5-trisphosphate (IP_3) receptors (IP_3Rs) and ryanodine receptors (RyRs). IP_3Rs are stimulated by IP_3 that is elevated by the action of phospholipase C (PLC) upon the activation of various receptors (R). RyRs are stimulated by increased $[Ca^{2+}]_i$. The activity of IP_3Rs and RyRs can also be further stimulated by the Ca^{2+} released from the nearby IP_3Rs and RyRs. During the stimulation the reduced Ca^{2+} content of the SR is sensed by the stromal interaction molecule (STIM). Through the direct interaction of STIM with Orai, a Ca^{2+} channel located in the plasma membrane, the extracellular Ca^{2+} influxes into the cytosol channels, and the SR Ca^{2+} are replenished. This process is known as store-operated Ca^{2+} entry

activation of voltage-gated calcium channels (VGCC, Atlas 2014) and receptor-activated cation channels (Hill-Eubanks et al. 2011) and through the release of Ca^{2+} from SR resulting from the opening of inositol 1,4,5-trisphosphate (IP_3) receptors (IP_3Rs) and ryanodine receptors (RyRs) (Wray and Burdyga 2010). The depleted Ca^{2+} levels inside the SR are replenished through store-operated calcium channels

(Prakriya and Lewis 2015). When the stimulation ends, the cytosolic Ca^{2+} level quickly returns to the basal levels due to the termination of the activities of $[Ca^{2+}]_i$ elevation occurred during stimulation and the reactivation of the activities of $[Ca^{2+}]_i$ reduction occurred during basal conditions. The above mechanisms are operated in a complicated and coordinated manner so that the changes in $[Ca^{2+}]_I$ vary both temporally and spatially depending on the stimulations and cellular conditions (Hill-Eubanks et al. 2011; Amberg and Navedo 2013) (Fig. 11.1).

11.2 The Maintenance of Basal Cytosolic Ca^{2+} Levels

Under basal conditions the very low cytosolic levels of Ca^{2+} ions of VSMCs are predominantly maintained by PMCAs (Little et al. 2016) and NCXs (Hilge 2012; Giladi et al. 2016) located in the plasma member and the SERCAs of the SR (Wray and Burdyga 2010). In culture VSMCs the basal Ca^{2+} leak into the cell is estimated about 1.45×10^9 $Ca^{2+} \cdot cell^{-1} \cdot min^{-1}$, mainly due to a basal open probability of excitable Ca^{2+} channels (Poburko et al. 2004). Such a fact indicates the necessity of Ca^{2+} extrusion for the hemostasis of this critical signaling molecule.

11.2.1 PMCA

PMCA is an ATP-dependent pump that expels Ca^{2+} from the cytosol to extracellular space. The pump operates with high Ca^{2+} affinity and low transport capacity, with a 1:1 Ca^{2+}/ATP stoichiometry. The equilibrium binding constant (K_d) of the pump for Ca^{2+} is ~0.2–0.5 μM under optimally activated conditions, enabling it to fine-tune the Ca^{2+} concentration of the region where the pumps are located. PMCA contains ten transmembrane (TM) domains with both NH_2- and COOH-terminals being intracellular. The loop between TM domains 2 and 3 is involved in calcium pore function, the loop between TM domains 4 and 5 is the site of ATP binding, and the long COOH-terminal tail contains the calmodulin (CaM)-binding domain (CaM-BD). In the absence of CaM, the CaM-BD binds to the main body of the pump to keep it autoinhibited. The inhibition is released upon binding of calmodulin to the CaM-BD. CaM interacts CaM-BD with high affinity, reducing the K_m of the pump for Ca^{2+} to submicromolar values. Mammalian PMCAs consist of four isoforms each encoded by its respective gene. Among them PMCA 2 and 3 are mainly present in neurons, while PMCA 1 and 4 are ubiquitously expressed including VSMCs (Brini and Carafoli 2009; Lopreiato et al. 2014; Little et al. 2016). In porcine aortas the endothelium expressed predominantly PMCA1, while smooth muscle expresses a higher level of PMCA4, indicating that the expression of PMCA isoforms are tissue specific (Pande et al. 2006).

11.2.2 NCX

NCX is an antiporter membrane protein of ten TM helices with a large cytosolic regulatory loop (f-loop) between TM5 and TM6. This loop contains regulatory domains such as the XIP (exchanger inhibitory peptide, involved in Na^+-dependent inactivation) region and the Ca^{2+}-binding domains (CBD1 and CBD2). Binding of Ca^{2+} to CBD domains activates the exchanger and removes the Na^+-dependent inactivation. In mammalian NCX exists in three isoforms: NCX1 is universally distributed, NCX2 is present in the brain and spinal cord, and NCX3 is present in the brain and skeletal muscles. In VSMCs NCX1 is the only isoform expressed, which is restricted to plasma membrane microdomains that overlie the junctional SR where the Ca^{2+} concentration is presumably higher (~2 μM) (Zhang 2013; Giladi et al. 2016; Spinelli and Trebak 2016).

NCX uses the energy stored in the electrochemical gradient of Na^+ by allowing Na^+ to flow down its gradient across the plasma membrane in exchange for the countertransport of Ca^{2+} (Carafoli et al. 2001; Giladi et al. 2016). The NCX expels a single Ca^{2+} ion in exchange for the import of three Na^+ ions. The NCX has a low affinity for Ca^{2+} (K_m, 1–10 μM or more) but has a high capacity (transporting up to 5000 Ca^{2+} ions per second). Hence, NCX is more effective to expel large amounts of Ca^{2+} in a short time, as is needed after a contractile activity is terminated (Hilgemann 1990; Hilgemann et al. 1991). NCX is a bidirectional transporter of Na^+ and Ca^{2+} depending on the electrochemical gradient of the substrate ions. When the intracellular levels of Na^+ is greater than that of the extracellular levels, which occurs under pathophysiological conditions, the NCX begins importing Ca^{2+} resulting in Ca^{2+} overload. Knockout of NCX1 in smooth muscle attenuates vascular myogenic reactivity and vasoconstriction and lowers blood pressure, while the increased expression and activity of VSMC NCX contribute to contractile dysfunction in spontaneously hypertensive rats. These data suggest that the NCX is importantly involved in the regulation of vasoactivity both under physiological and pathophysiological conditions (Zhang 2013).

11.2.3 SERCA

SERCA is a calcium ATPase of 110 kDa and the primary enzyme responsible for sequestration of Ca^{2+} from the cytosol into the SR. It transports two Ca^{2+} for every ATP hydrolyzed. Inside the SR the Ca^{2+}-binding proteins, namely, calsequestrin and calreticulin, enable this process to continue. With a free ionized Ca^{2+} content of ~500 μM in the lumen of the SR, calsequestrin and calreticulin exhibit a high capacity (25–50 mol/mol) but a low affinity (1–4 mM) for Ca^{2+} so that the Ca^{2+} stored can be easily released into the cytosol from the SR when needed (Laporte et al. 2004; Rossi and Dirksen 2006; Wray and Burdyga 2010).

SERCA exists in three isoforms known as SERCA1, SERCA2, or SERCA3. In VSMCs SERCA2b predominates, whereas SERCA2a and SERCA3 are present in much smaller amounts (Wu et al. 2001). SERCA is composed of three cytoplasmic domains (actuator, nucleotide-binding, and phosphorylation domains), ten transmembrane helices, and small luminal loops. The actuator domain is involved in the regulation of Ca^{2+} binding and release, whereas ATP hydrolysis occurs at the interface between the nucleotide and the phosphorylation domains. For each ATP consumed, two Ca^{2+} ions are pumped into the SR lumen. The Ca^{2+}-binding sites are in the transmembrane domain, with two Ca^{2+} ions being 5.7 Å apart. The two Ca^{2+}-binding sites exist in either a high- or low-affinity form, known as E1 and E2 states with K_d values 10^{-7} and 10^{-3} M, respectively. The Ca^{2+} ions are actively transported across membranes by interconverting between E1 and E2 ion-affinity states. The rate at which SERCA moves Ca^{2+} across the SR membrane is regulated by phospholamban (PLB), a single-span membrane protein of 52 amino acids. SERCA is normally under inhibition of PLB, with which it is closely associated. PLB can be phosphorylated by cAMP-dependent protein kinase (PKA) and cGMP-dependent protein kinase (PKG) at Ser-16 and by Ca/calmodulin-dependent protein kinase II (CaM kinase II) at Thr-17. Upon phosphorylation the association between SERCA and PLB is reduced, and Ca^{2+} movement increases (Wray and Burdyga 2010; Stammers et al. 2015). Studies show that the time course of the decline in Ca^{2+} upon removal of vasoconstrictor is substantially faster in the aorta of mice deficient in PLB than that of the wild type, which is likely to be due to the enhanced ability of the SR to remove Ca^{2+} from the cytosol resulting from the removal of inhibitory effect of PLB on SERCA. However, the blood pressure of PLB knockout mice is similar to that of the wild type, implying that the role of PLB at global level is limited or a mechanism to compensate the loss of PLB may have developed in the knockout mice (Lalli et al. 1997; Lalli et al. 1999; Wray and Burdyga 2010; Stammers et al. 2015).

11.3 Ca^{2+} Entry Through Plasma Member Channels Upon Membrane Depolarization

The influx of extracellular Ca^{2+} occurred during membrane depolarization is mediated primarily by L-type VGCCs with contributions from other channels such as T-type VGCCs, Ca^{2+}-permeable members of the transient receptor potential (TRP) channels, and Ca^{2+}-permeable ligand-gated cation channels (Hill-Eubanks et al. 2011; Amberg and Navedo 2013). VGCCs are formed by the pore-forming Cavα1 subunit alone or by co-assembly of Cavα1 with several ancillary subunits: Cavβ, Cavα2δ, and Cavγ. Cavα1 alone bestows the low voltage-activated (LVA) phenotype, i.e., the channels are activated by relatively smaller membrane depolarizations. The co-assembly of Cavα1 with Cavβ and Cavα2δ (and Cavγ in skeletal muscles) renders the channels being the high voltage-activated (HVA) phenotype,

i.e., activated by large depolarizations (Frolov and Weckström 2016). VGCCs are grouped into three families: the HVA dihydropyridine-sensitive (Cav 1) channels, the HVA dihydropyridine-insensitive (Cav 2) channels, and the LVA (Cav 3) channels (Alexander et al. 2015). Among the three families, Cav1 and Cav3 channels are implicated in vascular activities. The Cav1 channels, also known as L-type calcium channels (LTCCs), have four subtypes (Cav 1.1–Cav 1.4), of which Cav 1.2 is the major subtype expressed in VSMCs and the principle calcium channels responsible for stimulated-evoked Ca^{2+} influx. An action potential is not required for the activation of Cav 1.2 channels in VSMCs. Rather, a graded membrane depolarization would activate these channels leading to cell-wide increases in global $[Ca^{2+}]_i$ that triggers the contractile response. LTCCs activate relatively slowly at a relatively high threshold and also inactivate slowly. There are two types of inactivation, voltage-dependent inactivation (VDI) and calcium-dependent inactivation (CDI), are recognized. The former reflexes an intrinsic channel property, while the latter depends on activation of the Cav-associated calmodulin by the local increase in Ca^{2+} concentration near the inner mouth of the pore (Navedo and Santana 2013; Frolov and Weckström 2016).

The Cav3 channels, also known as T-type calcium channels (TTCCs), consist of three subtypes (Cav 3.1–Cav 3.3). In vasculature Cav 3.1and Cav3.2 are most commonly expressed. Generally speaking TTCCs are low voltage-activated, fast-activating, and fast-inactivating channels. The majority of electrophysiological studies conducted on VSMCs have failed to demonstrate the existence of a low-voltage-activated calcium current. By contrast, studies on smooth muscle cells from the mesenteric artery and vessels of the cerebral circulation show that a high-voltage-activated calcium current remains after blockade of LTCCs. These currents have time constants for activation, inactivation, and closure that are more similar to T-type channels and are blocked by several TTCC antagonists. These properties may result from vascular-specific expression of splice variants of Cav 3 genes. Recent studies suggest that TTCCs may play a role in vascular tone of small arterioles. The function of these channels is upregulated following the decrease in nitric oxide (NO) bioavailability and increase in oxidative stress, indicating that a more important role could be played by TTCCs in pathophysiological situations (Marchand et al. 2012; Kuo et al. 2014; Frolov and Weckström 2016).

The influx of extracellular Ca^{2+} during stimulation may result from the activation of the transient receptor potential (TRP) channels. There are 28 TRP channels being identified in mammalian, which are grouped into six subfamilies based on amino acid sequence homology. They are designated as canonical (TRPC), vanilloid (TRPV), melastatin (TRPM), ankyrin (TRPA), mucolipin (TRPML), and polycystin (TRPP) channels. TRP channels are described as "nonselective cation channels." This definition, however, is less informative and rather imprecise, since there are great differences in cation permeability among them. For instance, TRPV5 and TRPV6 channels are highly selective for Ca^{2+}, with relative permeability of Ca^{2+} vs. Na^+ of ~100:1. In contrast, TRPM4 and TRPM5 channels are selective for monovalent cations (Na^+ and K^+) and are essentially impermeant to Ca^{2+} and other divalent cations (Earley and Brayden 2015; Yue et al. 2015). In

vasculature the activation of TRP channels may affect the Ca^{2+} influx by directly opening the channels and letting the Ca^{2+} ions pass through. Ca^{2+} sparklets are distinct Ca^{2+} microdomains produced by plasmalemmal Ca^{2+}-permeable channels. In cerebral artery myocytes, the opening of TRPV4 channels generates a large Ca^{2+} sparklets. The total Ca^{2+} influx during a TRPV4 sparklet is ~100 times that of during a CaV 1.2 sparklet, although the overall activity of CaV 1.2 channels is much higher than that of TRPV4 channels (Mercado et al. 2014).

TRP channels also promote Ca^{2+} influx by activating LTCCs through membrane depolarization. Study results from cerebral artery smooth muscle suggest that the activation of TRPM4 channels stimulates the influx of extracellular Na^+, followed by membrane depolarization and thus the activation of VGCCs, increased Ca^{2+} influx, and vasoconstriction (Gonzales et al. 2014). In endothelial cells (ECs), TRPV4 Ca^{2+} influx from the extracellular space through as few as 3–4 channels may activate Ca^{2+}-activated K^+ (K_{Ca}) channels resulting in increased K^+ efflux and membrane hyperpolarization. The hyperpolarized EC membrane directly hyperpolarizes smooth muscle cells via gap junctions located within myoendothelial junctions and consequently leads to vasodilatation (Sullivan and Earley 2013).

Extracellular Ca^{2+} may also enter the cell through ligand-gated ion channels (LGICs). LGICs are integral membrane proteins containing a pore allowing selected ions across the plasma membrane. They are gated by the binding of a neurotransmitter to an orthosteric site(s) that triggers a conformational change resulting in the conducting state (Alexander et al. 2015). Among these channels the ATP-gated P2X receptor (P2XR) is better understood. The activation of $P2X_1$ receptor causes more abundant Na^+ influx; however, Ca^{2+} influx is substantial. In mice mesentery artery smooth muscle adjacent to the perivascular nerves, the activation of $P2X_1$ receptor is associated with an optically identifiable Ca^{2+} signal. It appears that Ca^{2+} that enters the cells through $P2X_1$ receptors is involved in the initial rapid component of the sympathetic neurogenic vasoconstriction (Lamont et al. 2006).

11.4 Stimulated Ca^{2+} Release from Sarcoplasmic Reticulum

Under physiological conditions the elevation of cytosolic Ca^{2+} that occurred during vasoconstriction is an integrated process driven by Ca^{2+} release from the SR through IP_3R and RyR channels and the influx of extracellular Ca^{2+} through VGCCs. The Ca^{2+} release from the SR is further augmented by the elevated level of cytosolic Ca^{2+}, termed Ca^{2+}-induced Ca^{2+} release (CICR). The depleted Ca^{2+} of the SRs is refilled through store-operated Ca^{2+} entry (SOCE) (Lopez et al. 2016).

11.4.1 Ca^{2+} Release from IP_3Rs of the SR

IP_3R is a membrane glycoprotein complex acting as a Ca^{2+} channel activated by inositol trisphosphate (IP_3). It is composed of four subunits of ~2700 amino acid residues each. For each subunit it can be subdivided into four functional regions: an IP_3-binding region of ~600 residues at the NH_2-terminus, a central modulatory region containing sites for interaction with regulatory molecules, a region (residues 2276–2589) containing six transmembrane domains (TMs) with the pore-forming loops between TM5 and TM6, and a relatively short COOH terminus of ~160 residues where the structural requirements for tetramerization reside. The COOH-terminal tail has been shown to interact with several proteins and to enhance the apparent sensitivity of the channel to IP_3. Both the NH_2- and COOH-termini are cytosolic, and ~90% of the protein mass is located in the cytosol (Foskett et al. 2007; Serysheva 2014). In mammals the IP_3R exists as three isoforms (IP_3R1-3) coded by separated genes and their splice variants. They assemble into homo- and heterotetrameric structures to form functional IP_3Rs. In VSMCs IP3R1 is the predominant isoform expressed. Studies indicate that IP3R isoform expression in VSMCs shifts during ontogeny and proliferation. IP_3R1 protein is lower, and IP_3R3 is higher in SMCs of aorta and portal vein of the neonatal rats as compared with those in juvenile rats. IP_3R2 and IP_3R3 levels have been found higher in proliferating, cultured aortic SMCs than in fresh isolated aorta (Wray and Burdyga 2010; Narayanan et al. 2012).

Activation of IP_3Rs is initiated by IP_3 binding to the IP_3-binding core (IBC, residues 224–604) of each subunit, which occurs when the formation of IP_3 is increased by phospholipase C (PLC) upon the activation of G-protein-coupled receptors (GPCRs) or receptor tyrosine kinases (RTKs) by extracellular stimuli. Studies show that all four IBC sites within the tetrameric IP_3R must bind IP_3 before the channel can open (Taylor and Konieczny 2016). The NH_2-terminal of the IP_3R (residues 1–223), termed the suppressor domain (SD), substantially reduces the affinity of the IBC for IP_3. An IP_3R without SDs binds IP_3 with high affinity, but the channel cannot open, implying important roles for SD not only in modulating IP_3 binding but also in coordinating the opening of the channels (Taylor et al. 2014). The IP_3R channels are primarily regulated by coupled interplay between the binding of its primary ligands, IP_3 and Ca^{2+}. For each subunit of the IP_3R, there is a single high-affinity binding site for IP_3 and several distinct binding sites for Ca^{2+}. Studies show that the activity of IP_3R is concentration dependently activated by IP_3, with an estimated K_d of ~1 μM. The activity of IP_3R is also enhanced by the cytosolic Ca^{2+} at the concentrations up to 300 nM. This property allows Ca^{2+} release activated by the IP_3R to be further modulated by Ca^{2+}, i.e., CICR. When the concentration of cytosolic Ca^{2+} is greater than 300 nM, the activity of IP_3R is inhibited. The sensitivity of IP_3R is also influenced by the SR luminal Ca^{2+} content. Depletion of SR Ca^{2+} abolishes IP_3R-mediated Ca^{2+} release in SMCs. Although IP_3R can be

regulated by both luminal and cytosolic Ca^{2+}, the cytoplasmic aspect of the channel appears being more important (Wray and Burdyga 2010).

The activity of IP_3R is also regulated by ATP and various protein kinases and molecules. In permeabilized portal vein smooth muscle cells (SMCs), ATP concentration-dependently increases IP_3-induced Ca^{2+} release with a maximal effect at 0.5 mM ATP. Considering that the cytoplasm contains 5–10 mM MgATP, ATP may not exert a major effect on IP_3R activity under normal conditions (Foskett et al. 2007; Narayanan et al. 2012). PKA and PKG inhibit SMC IP_3Rs via phosphorylation to regulation of IP_3 binding, resulting in reduced Ca^{2+} release. Consensus sequences for PKA- and PKG-mediated IP_3R phosphorylation are located in the regulatory domain at serine 1589 and serine 1755, respectively. In rat aortas phosphorylation of IP_3R induced by cAMP-elevating agent forskolin is inhibited by the inhibition of PKG, suggesting that both cAMP and cGMP can phosphorylate IP_3R via PKG in VSMCs (Narayanan et al. 2012).

11.4.2 Ca^{2+} Release from RyRs of the SR

RyRs are the largest ion channels known so far with molecular masses exceeding 2.2 MDa, which is about twice the size of IP_3Rs. RyRs are made of four homologous subunits, each ~5000 amino acid residues. For each subunit it can be subdivided into four regions: the NH_2-terminal domain (NTD) of ~559 residues, a central regulatory domain containing sites for interaction with diverse ligands ranging from ions to proteins (residues 560–4559), a region comprised of six TMs (residues 4560–4934) enclosing a pore-forming residues, and the COOH-terminal tail (CTT, residues 3935–5037). Both the N- and C-termini are cytosolic, and more than 80% of the RyR protein is folded into the cytoplasmic assembly. In mammals there exist three RyR isoforms (RyR1-3), which share about 70% sequence identity. RyR1 is primarily expressed in skeletal muscles, RyR2 is mainly expressed in cardiac muscles, and RyR3 is ubiquitously expressed. In VSMCs all three isoforms are present, with the type and the relative proportion of expression of each being tissue and species dependent. RyRs share considerable sequence similarity with the IP_3R. It is believed that RyRs and IP_3Rs have coevolved from a common ancestor in unicellular species. RyRs and IP_3Rs share ~17% sequence identity overall; however, the identity increases to ~35% within their predicted transmembrane regions (Wray and Burdyga 2010; Amador et al. 2013; Van Petegem 2015; Wei et al. 2016).

RyRs are large ion pores, with an estimated single unitary current of 0.5 pA under quasi physiological conditions. RyRs are activated by cytosolic Ca^{2+} from nano-molar to micromolar level in a concentration-dependent manner by Ca^{2+} entry through plasma membrane Ca^{2+} channels or by Ca^{2+} released from adjacent IP3Rs or RyRs, a mechanism known as CICR. RyRs are maximally activated at 10–100 μM Ca^{2+}. When Ca^{2+} concentration is greater than 100 μM, RyRs are inhibited, and the maximal inhibition occurs when Ca^{2+} is at mM concentrations. The bell-shaped relationship of the activation of RyRs to cytosolic Ca^{2+}

concentrations is likely to be due to that there are multiple Ca^{2+}-binding sites with different affinities and binding kinetics of the RyRs. In addition to be regulated by cytosolic Ca^{2+}, RyRs can sense the Ca^{2+} concentrations in the lumen of the SR. For instance, under conditions whereby the SR is overloaded with Ca^{2+}, RyRs can also open spontaneously in a process known as store overload-induced Ca^{2+} release (SOICR) (Dabertrand et al. 2013; Van Petegem 2015). In VSMCs local, rapid, and transient Ca^{2+} release from the opening of a cluster of RyRs of the SR located near the plasma membrane, termed Ca^{2+} sparks, may activate the large-conductance Ca^{2+}-dependent K^+ (BK_{Ca}) channels, resulting in membrane hyperpolarization and vasodilatation. This represents a negative feedback mechanism during vasoconstriction (Essin and Gollasch 2009).

RyRs are regulated by diverse ligands including multiple kinases. Each RyR1 subunit contains 15 sites, and there may be as many as 35 per RyR2 subunit for phosphorylation (Van Petegem 2015). In rat aortic SMCs PKCα is co-immunoprecipitated with RyRs, indicating that they directly interact. Application of the PKC inhibitor causes Ca^{2+} transients which are abolished after inhibition of RyRs with ryanodine. Thus, PKC may exert an inhibitory effect on the gating activity of RyRs in the SR (Peng et al. 2010). In rat cerebral arteries, NO-evoked hyperpolarization is implicated being resulted from activation of BK_{Ca} channels via RyRs. NO may act directly at RYRs or via PKG. RyRs are also activated by NO-independent mechanisms including those related to store filling via SERCA (Yuill et al. 2010).

11.5 Store-Operated Ca^{2+} Entry

When Ca^{2+} is depleted from the SR, the Ca^{2+} release-activated calcium channels (CRACs) are activated to let the extracellular Ca^{2+} to diffuse into the cytosol, a phenomenon known as SOCE. The reduction of Ca^{2+} content within the lumen of the SR is sensed by the stromal interaction molecules (STIMs), while Orai proteins of the plasma membrane (PM) act as the Ca^{2+} channels. The interaction between STIMs and Orai channels leads to the opening of the channels (Prakriya and Lewis 2015; Spinelli and Trebak 2016).

STIMs exist in mammals as two isoforms, STIM1 (77 kDa) and STIM2 (84 kDa). These two isoforms have ~74% sequence similarity (54% sequence identity). Both isoforms are widely expressed in tissues, with STIM1 usually presented at higher levels than STIM2 except in brain or liver. Also, both isoforms can be expressed in the same cell. STIMs can be divided into the luminal NH_2-terminal region, a single-pass transmembrane motif that is highly conserved in all STIM proteins, and the cytoplasmic COOH-terminal region. In the NH_2-terminal region, the EF-hand domain serves as a Ca^{2+} sensor to detect changes in Ca^{2+} concentration inside the SR. STIM isoforms become activated when Ca^{2+} bound to the EF-hand domain is released as a result of decreased Ca^{2+} levels inside the SR. STIM2 protein has a lower Ca^{2+}sensitivity than STIM1 (Prakriya and Lewis

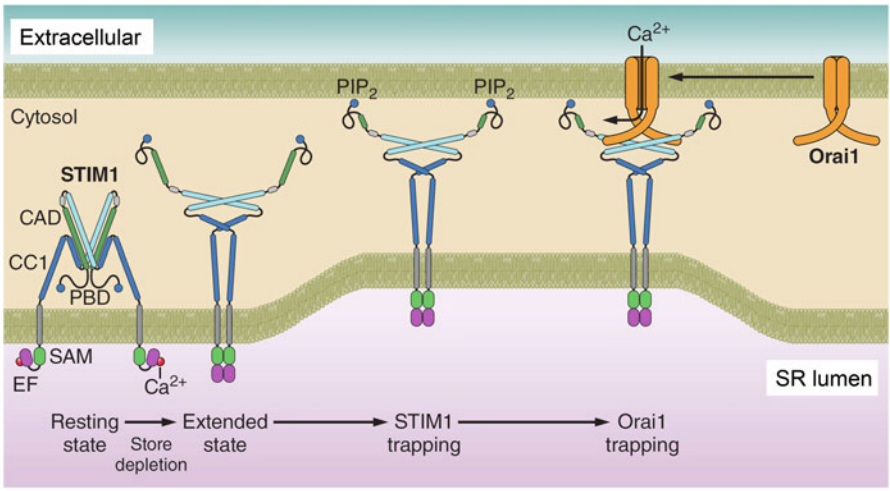

Fig. 11.2 A possible mechanism for store-operated Ca^{2+} entry (SOCE). The Ca^{2+} content inside the lumen of the sarcoplasmic reticulum (SR) is sensed by the stromal interaction molecule 1 (STIM1). Under resting conditions STIM1 is bound to Ca^{2+} and freely diffusing in the SR membrane as a dimer. During vasoconstriction the SR Ca^{2+} level is decreased resulting in the release of Ca^{2+} from the EF-hand domain (EF) followed by a conformational change of the cytosolic domains of STIM1 that leads to the polybasic domain (PBD) to bind to phosphatidylinositol 4,5-bisphosphate (PIP_2) in the plasma membrane (PM). The binding traps STIM1 at the SR-PM junction where SR and PM are in close vicinity. Subsequently, the Ca^{2+} release-activated calcium channel (CRAC) activation domain (CAD) of STIM1 is bound to the COOH-termini of Orai1 Ca^{2+} channels. The direct interaction of STIM1 and Oril1 results in the influx of extracellular Ca^{2+}. Although only a dimer of STIM1 is shown, the binding of multiple STIM1 dimers to Orai1 hexamers is required for full activity of SOCE. CC1, coiled-coil domain 1. SAM, sterile alpha motif. CC1 and SAM are involved in the maintenance and the stability of the resting state of STIM1 (This figure is from Prakriya and Lewis (2015), with permission)

2015; Spinelli and Trebak 2016). Evidence indicates that STIM2 could act as a regulator that stabilizes basal cytosolic and SR Ca^{2+} levels (Brandman et al. 2007). When cells are under resting conditions, STIM1 is bound to Ca^{2+} and freely diffusing in the SR membrane. Store depletion and Ca^{2+} release from the EF-hand domain trigger a conformational change of the cytosolic domains that promotes the polybasic domain (PBD) to bind to phosphatidylinositol 4,5-bisphosphate (PIP_2) in the PM, trapping STIM1 at the SR-PM junction, a specialized site where SR and PM are in close vicinity. Meanwhile, the coiled-coil domain 2 (CC2) helices in STIM1 move into an antiparallel configuration, and the coiled-coil domain 3 (CC3) helix disengages from CC2 to form a binding interface for the Orai COOH-termini. The binding of STIM1 activates the Orai1 channels resulting in the influx of extracellular Ca^{2+}. It seems that higher-order STIM1 oligomers are formed after store depletion and that the binding of multiple STIM1 dimers to Orai hexamers is required for full activity (Prakriya and Lewis 2015) (Fig. 11.2).

In mammalian three Orai isoforms (Orai1-3) have been identified encoded by independent genes. These isoforms are highly homologous to each other (~62% overall identity, increasing to ~92% in the TM domains); however, they exhibit negligible sequence similarity to other known ion channels. All three Orai homologs are ubiquitously expressed, including expression in VSMCs. The Orai protein contains four TM domains (TMD1–4), with its NH_2- and COOH-terminal domains located in the cytosol. The NH2-terminus contains a calmodulin-binding region, which is involved in Ca^{2+}-dependent inhibition (CDI) of Orai channels. The TMD1 and the extracellular loops between TMD1 and TMD2 contain a highly conserved pore region with a conserved glutamic acid residue representing the selectivity filter. The intracellular loop contains residues 153–157 that may mediate fast Ca^{2+}-dependent inhibition. The coiled-coil domain of the COOH-terminal region is essential for STIM1 binding and gating of Orai channels. The conserved COOH-terminal glutamate residues (three in Orai2/Orai3 and two in Orai1) determine more enhanced fast Ca^{2+}-dependent inactivation of Orai2/Orai3 than Orai1. Studies show that SOCE is inhibited by knockdown of STIM1 or Orai1 but not by knockdown of Orai2 or Orai3 in a number of mammalian cells. Hence, native SOCE is likely to be primarily mediated by STIM1 and Orai1 (Prakriya and Lewis 2015; Spinelli and Trebak 2016).

In addition to forming CRACs, STIM and Orai proteins also contribute to store-independent Ca^{2+} entry that is activated by receptor-mediated production of arachidonic acid (AA) or its metabolite leukotriene C_4 (LTC_4). The channels that operate by this mechanism are named ARC channels for **A**rachidonate-**R**egulated **C**a^{2+} channels. In contrast to the CRAC channel pore that is formed from a tetramer of Orai1 subunits, the ARC channel pore is formed from a pentameric assembly of three Orai 1 subunits and two Orai 3 subunits. When stimulated by AA or LTC_4, the STIM1 resident in the plasma membrane interacts with the Orai pentamer, resulting in extracellular Ca^{2+} entry. The conductances carried by ARC and CRAC are not additive in the same cell, indicating that they are mediated by physically distinct channels. The ARC and CRAC often coexist in the same cells, suggesting that they control distinct cellular functions (Shuttleworth 2012; Spinelli and Trebak 2016).

11.6 Ca^{2+} Dynamics in VSMCs

The profiles of Ca^{2+} signals evoked by various stimuli differ with respect to their mechanisms of generation, temporal properties, and spatial distributions. Accordingly, they can be categorized as Ca^{2+} waves, Ca^{2+} sparks, Ca^{2+} puffs, Ca^{2+} sparklets, and junctional Ca^{2+} transients (Table 11.1) (Amberg and Navedo 2013). Ca^{2+} waves are generated by Ca^{2+} release via IP_3Rs and RyRs from the SR. Ca^{2+} waves inherently require a regenerative Ca^{2+} release to promote the propagation of the wavefront by CICR mechanism between adjacent IP_3Rs and/or RyRs. The occurrence of Ca^{2+} waves in isolated vascular tissues is minimal to moderate in the absence of stimulation. When stimulated the elevation of cytosol

Table 11.1 Characteristics of vascular smooth muscle subcellular Ca^{2+} signals

	Ca^{2+} waves	Ca^{2+} sparks	Ca^{2+} puffs	Ca^{2+} sparklets	Junctional Ca^{2+} transients
Area (μm^2)	~50 (full width, half maximum)	~15	NA	~1	~25
Duration ($t_{0.5}$, ms)	NA	~50	NA	$\tau 1$ ~ 35 $\tau 2$ ~ 150	~150
Generated by	Ca^{2+} release from the SR via IP_3Rs and RyRs	Ca^{2+} microdomains generated by the opening of RyRs	Ca^{2+} microdomains generated by the opening of IP_3Rs	Ca^{2+} microdomains generated by plasmalemmal Ca^{2+}-permeable channels	Neural stimulation

Values are from Amberg and Navedo (2013). *NA* not available. $t_{0.5}$, halftime of duration. $\tau 1$ and $\tau 2$ are the fast and slow time constant of Ca^{2+} signal

Ca^{2+} during the Ca^{2+} waves contributes to global Ca^{2+} thus promoting contraction (Hill-Eubanks et al. 2011; Amberg and Navedo 2013).

While Ca^{2+} waves are more widespread, the localized Ca^{2+} microdomains generated by the opening of RyRs and IP_3Rs are defined as Ca^{2+} sparks and Ca^{2+} puffs, respectively. Ca^{2+} sparks are formed by the coordinated opening of a cluster of RyRs on the SR of smooth muscle cells. Ca^{2+} sparks have minimal direct effect on global $[Ca^{2+}]_i$ due to their restricted spatial spread. However, the SRs are often found in close vicinity to the plasma membrane (~10–20 nm), and the local Ca^{2+} concentrations caused by Ca^{2+} sparks at these region can be sufficient to active plasmalemmal ion channels so that the global membrane potential is altered. In VSMCs the BK_{Ca} channels can be activated by Ca^{2+} sparks resulting in a stereotypical temporal pattern of hyperpolarizing K^+ currents termed spontaneous transient outward currents (STOCs). Consequently, the vascular tension is inhibited due to membrane hyperpolarization. Ca^{2+} sparks have also been found to activate simultaneously of a number Ca^{2+}-activated Cl^- (Ca_{Cl}) channels, which underlies the spontaneous transient inward currents (STICs) and leads to membrane depolarization and enhanced vasocontractility. STOCs and STICs may represent the mechanisms by which the vascular tone is regulated in a negative and positive feedback manner, respectively (Jaggar et al. 2000; Hill-Eubanks et al. 2011; Amberg and Navedo 2013).

Ca^{2+} puffs are localized Ca^{2+} transient events produced by the opening of a cluster of IP_3Rs of the SRs. In cerebral artery SMCs, the sustained transient inward cation currents (TICCs) are inhibited by the replacement of extracellular Na^+, by the blockers of the melastatin transient receptor potential channel TRPM4, and by selectively silence of TRPM4 expression with siRNA. The TICCs do not depend on Ca^{2+} influx and RyR activity but are suppressed by the blockade of IP_3Rs. These findings suggest that Ca^{2+} puffs generated by IP_3Rs may promote the opening of the

Ca^{2+}-activated, Na^{+}-permeable TRPM4 channels, which causes arterial smooth muscle membrane depolarization, opening of VGCCs, Ca^{2+} influx, and eventually vasocontraction (Gonzales and Earley 2013; Amberg and Navedo 2013).

Ca^{2+} sparklets are Ca^{2+} microdomains generated by Ca^{2+} influx through plasmalemmal ion channels. Depending on the ion channels involved, Ca^{2+} sparklets can be named by preceding "sparklets" with the name of the underlying channel (e.g., L-type Ca^{2+} channel sparklets). Studies using a combinatorial approach of electrophysiology and the total internal reflection fluorescence (TIRF) microscopy reveal that in VSMCs brief stochastic opening of single L-type Ca^{2+} channels produces low-activity Ca^{2+} sparklet site, whereas prolonged opening of clustered L-type Ca^{2+} channels produces high-activity Ca^{2+} sparklet site. Both low- and high-activity Ca^{2+} sparklet sites contribute to global $[Ca^{2+}]_i$ resulting in vasocontraction (Amberg and Navedo 2013; Navedo and Santana 2013).

Ca^{2+} influx caused by neural (i.e., sympathetic) stimulation of VSMCs is defined as junctional Ca^{2+} transients. When perivascular sympathetic nerves are stimulated, the bindings of the released neurotransmitters such as norepinephrine and ATP to the postjunctional α_1 adrenergic receptors and $P2X_1$ purinergic receptors result in Ca^{2+} influx. The activation of α_1 adrenergic receptors leads to increased production of IP_3 by phospholipase C (PLC) followed by the opening of IP_3Rs, propagated Ca^{2+} release, and augmented vasoconstriction. $P2X_1$ receptors are ligand-gated Ca^{2+}-permeable nonselective cation channels. The activation of $P2X_1$ receptors increases Ca^{2+} influx. The membrane depolarization caused by $P2X_1$ receptor activation also stimulates Ca^{2+} influx through L-type Ca^{2+} channels (Wier et al. 2009; Amberg and Navedo 2013).

References

Alexander SPH, Catterall WA, Kelly E, Marrion N, Peters JA, Benson HE, Faccenda E, Pawson AJ, Sharman JL, Southan C, Davies JA, Collaborators CGTP (2015) The concise guide to pharmacology 2015/16: voltage-gated ion channels. Br J Pharmacol 172:5904–5941

Amador FJ, Stathopulos PB, Enomoto M, Ikura M (2013) Ryanodine receptor calcium release channels: lessons from structure-function studies. FEBS J 280:5456–5470

Amberg GC, Navedo MF (2013) Calcium dynamics in vascular smooth muscle. Microcirculation 20:281–289

Atlas D (2014) Voltage-gated calcium channels function as Ca^{2+}-activated signaling receptors. Trends Biochem Sci 39:45–52

Billaud M, Lohman AW, Johnstone SR, Biwer LA, Mutchler S, Isakson BE (2014) Regulation of cellular communication by signaling microdomains in the blood vessel wall. Pharmacol Rev 66:513–569

Brandman O, Liou J, Park WS, Meyer T (2007) STIM2 is a feedback regulator that stabilizes basal cytosolic and endoplasmic reticulum Ca^{2+} levels. Cell 131:1327–1339

Brini M, Carafoli E (2009) Calcium pumps in health and disease. Physiol Rev 89:1341–1378

Carafoli E, Santella L, Branca D, Brini M (2001) Generation, control, and processing of cellular calcium signals. Crit Rev Biochem Mol Biol 36:107–260

Dabertrand F, Nelson MT, Brayden JE (2013) Ryanodine receptors, calcium signaling, and regulation of vascular tone in the cerebral parenchymal microcirculation. Microcirculation 20:307–316

Earley S, Brayden JE (2015) Transient receptor potential channels in the vasculature. Physiol Rev 95:645–690

Essin K, Gollasch M (2009) Role of ryanodine receptor subtypes in initiation and formation of calcium sparks in arterial smooth muscle: comparison with striated muscle. J Biomed Biotechnol 2009:135249

Foskett JK, White C, Cheung KH, Mak DO (2007) Inositol trisphosphate receptor Ca2+ release channels. Physiol Rev 87:593–658

Frolov RV, Weckström M (2016) Harnessing the flow of excitation: TRP, voltage-gated Na^+, and voltage-gated Ca^{2+} channels in contemporary medicine. Adv Protein Chem Struct Biol 103:25–95

Giladi M, Tal I, Khananshvili D (2016) Structural features of ion transport and allosteric regulation in sodium-calcium exchanger (NCX) proteins. Front Physiol 7:30

Gonzales AL, Earley S (2013) Regulation of cerebral artery smooth muscle membrane potential by Ca^{2+}-activated cation channels. Microcirculation 20:337–347

Gonzales AL, Yang Y, Sullivan MN, Sanders L, Dabertrand F, Hill-Eubanks DC, Nelson MT, Earley S (2014) A PLCγ1-dependent, force-sensitive signaling network in the myogenic constriction of cerebral arteries. Sci Signal 7:ra49

Hilge M (2012) Ca^{2+} regulation of ion transport in the Na^+/Ca^{2+} exchanger. J Biol Chem 287:31641–31649

Hilgemann DW (1990) Regulation and deregulation of cardiac Na^+-Ca^{2+} exchange in giant excised sarcolemmal membrane patches. Nature 344:242–245

Hilgemann DW, Nicoll DA, Philipson KD (1991) Charge movement during Na^+ translocation by native and cloned cardiac Na^+/Ca^{2+} exchanger. Nature 352:715–718

Hill-Eubanks DC, Werner ME, Heppner TJ, Nelson MT (2011) Calcium signaling in smooth muscle. Cold Spring Harb Perspect Biol 3:a004549

Jaggar JH, Porter VA, Lederer WJ, Nelson MT (2000) Calcium sparks in smooth muscle. Am J Physiol Cell Physiol 278:C235–C256

Karaki H (2004) Historical techniques: cytosolic Ca^{2+} and contraction in smooth muscle. Trends Pharmacol Sci 25:388–393

Kuo IY, Howitt L, Sandow SL, McFarlane A, Hansen PB, Hill CE (2014) Role of T-type channels in vasomotor function: team player or chameleon? Pflugers Arch 466:767–779

Lalli J, Harrer JM, Luo W, Kranias EG, Paul RJ (1997) Targeted ablation of the phospholamban gene is associated with a marked decrease in sensitivity in aortic smooth muscle. Circ Res 80:506–513

Lalli MJ, Shimizu S, Sutliff RL, Kranias EG, Paul RJ (1999) $[Ca^{2+}]_i$ homeostasis and cyclic nucleotide relaxation in aorta of phospholamban-deficient mice. Am J Phys 277:H963–H970

Lamont C, Vial C, Evans RJ, Wier WG (2006) P2X1 receptors mediate sympathetic postjunctional Ca2+ transients in mesenteric small arteries. Am J Physiol Heart Circ Physiol 291:H3106–H3113

Laporte R, Hui A, Laher I (2004) Pharmacological modulation of sarcoplasmic reticulum function in smooth muscle. Pharmacol Rev 56:439–513

Little R, Cartwright EJ, Neyses L, Austin C (2016) Plasma membrane calcium ATPases (PMCAs) as potential targets for the treatment of essential hypertension. Pharmacol Ther 159:23–34

Lopez JJ, Albarran L, Gómez LJ, Smani T, Salido GM, Rosado JA (2016) Molecular modulators of store-operated calcium entry. Biochim Biophys Acta 1863:2037–2043

Lopreiato R, Giacomello M, Carafoli E (2014) The plasma membrane calcium pump: new ways to look at an old enzyme. J Biol Chem 289:10261–10268

Marchand A, Abi-Gerges A, Saliba Y, Merlet E, Lompré AM (2012) Calcium signaling in vascular smooth muscle cells: from physiology to pathology. Adv Exp Med Biol 740:795–810

Mercado J, Baylie R, Navedo MF, Yuan C, Scott JD, Nelson MT, Brayden JE, Santana LF (2014) Local control of TRPV4 channels by AKAP150-targeted PKC in arterial smooth muscle. J Gen Physiol 143:559–575

Narayanan D, Adebiyi A, Jaggar JH (2012) Inositol trisphosphate receptors in smooth muscle cells. Am J Physiol Heart Circ Physiol 302:H2190–H2210

Navedo MF, Santana LF (2013) $CaV_{1.2}$ sparklets in heart and vascular smooth muscle. J Mol Cell Cardiol 58:67–76

Pande J, Mallhi KK, Sawh A, Szewczyk MM, Simpson F, Grover AK (2006) Aortic smooth muscle and endothelial plasma membrane Ca^{2+} pump isoforms are inhibited differently by the extracellular inhibitor caloxin 1b1. Am J Physiol Cell Physiol 290:C1341–C1349

Peng H, Yaney GC, Kirber MT (2010) Modulation of Ca^{2+} release through ryanodine receptors in vascular smooth muscle by protein kinase Cα. Pflugers Arch 460:791–802

Poburko D, Lhote P, Szado T, Behra T, Rahimian R, McManus B, van Breemen C, Ruegg UT (2004) Basal calcium entry in vascular smooth muscle. Eur J Pharmacol 505:19–29

Prakriya M, Lewis RS (2015) Store-operated calcium channels. Physiol Rev 95:1383–1436

Rossi AE, Dirksen RT (2006) Sarcoplasmic reticulum: the dynamic calcium governor of muscle. Muscle Nerve 33:715–731

Serysheva II (2014) Toward a high-resolution structure of IP_3R channel. Cell Calcium 56:125–132

Shuttleworth TJ (2012) STIM and Orai proteins and the non-capacitative ARC channels. Front Biosci (Landmark Ed) 17:847–860

Spinelli AM, Trebak M (2016) Orai channel-mediated Ca^{2+} signals in vascular and airway smooth muscle. Am J Physiol Cell Physiol 310:C402–C413

Stammers AN, Susser SE, Hamm NC, Hlynsky MW, Kimber DE, Kehler DS, Duhamel TA (2015) The regulation of sarco(endo)plasmic reticulum calcium-ATPases (SERCA). Can J Physiol Pharmacol 93:843–854

Sullivan MN, Earley S (2013) TRP channel Ca^{2+} sparklets: fundamental signals underlying endothelium-dependent hyperpolarization. Am J Physiol Cell Physiol 305:C999–C1008

Taylor CW, Konieczny V (2016) IP_3 receptors: take four IP_3 to open. Sci Signal 9:pe1

Taylor CW, Tovey SC, Rossi AM, Lopez Sanjurjo CI, Prole DL, Rahman T (2014) Structural organization of signalling to and from IP3 receptors. Biochem Soc Trans 42:63–70

Van Petegem F (2015) Ryanodine receptors: allosteric ion channel giants. J Mol Biol 427:31–53

Wei R, Wang X, Zhang Y, Mukherjee S, Zhang L, Chen Q, Huang X, Jing S, Liu C, Li S, Wang G, Xu Y, Zhu S, Williams AJ, Sun F, Yin CC (2016) Structural insights into Ca^{2+}-activated long-range allosteric channel gating of RyR1. Cell Res 26:977–994

Wier WG, Zang WJ, Lamont C, Raina H (2009) Sympathetic neurogenic Ca^{2+} signalling in rat arteries: ATP, noradrenaline and neuropeptide Y. Exp Physiol 94:31–37

Wray S, Burdyga T (2010) Sarcoplasmic reticulum function in smooth muscle. Physiol Rev 90:113–178

Wu KD, Bungard D, Lytton J (2001) Regulation of SERCA Ca^{2+} pump expression by cytoplasmic Ca^{2+} in vascular smooth muscle cells. Am J Physiol Cell Physiol 280:C843–C851

Yue Z, Xie J, Yu AS, Stock J, Du J, Yue L (2015) Role of TRP channels in the cardiovascular system. Am J Physiol Heart Circ Physiol 308:H157–H182

Yuill KH, McNeish AJ, Kansui Y, Garland CJ, Dora KA (2010) Nitric oxide suppresses cerebral vasomotion by sGC-independent effects on ryanodine receptors and voltage-gated calcium channels. J Vasc Res 47:93–107

Zhang J (2013) New insights into the contribution of arterial NCX to the regulation of myogenic tone and blood pressure. Adv Exp Med Biol 961:329–343

Zheng J, Zeng XH, Wang SQ (2015) Calcium ion as cellular messenger. Sci China Life Sci 58:1–5

Chapter 12
Regulation of Myosin Light Chain Phosphorylation

Abstract The interaction of myosin and actin constitutes the basic mechanism of muscle contractile activity. In smooth muscle cells (SMCs) including vascular smooth muscle cells, this interaction is predominantly regulated by the phosphorylation of the regulatory light chain (RLC) of myosin. The RLC is phosphorylated by myosin light chain kinase (MLCK) and dephosphorylated by myosin light chain phosphatase (MLCP). Therefore, the contractility of SMCs is determined by the relative ratio of the activity of MLCK vs. that of MLCP. During a contractile response, MLCK is activated by calmodulin-bound Ca^{2+}. Meanwhile the activity of MLCP is suppressed by protein kinase C (PKC) through the 17-kDa PKC-potentiated inhibitor protein (CPI-17) and by Rho kinase (ROCK). The varied activities of these major signaling pathways endow SMCs with different contractile profiles such as phasic and tonic contractions to meet the diversified physiological requirements.

Keywords MLCK • MLCP • MYPT1 • PKC • CPI-17 • RhoA • Rho kinase

12.1 Introduction

The contractile activity of smooth muscle cells (SMCs) results from the interaction of myosin and actin. The myosin molecule is composed of two myosin heavy chains, a pair of regulatory light chains (RLCs) each sized of 20 kDa and a pair of essential light chains (ELCs) each sized of 17 kDa. Both RLCs and ELCs are bound to the lever arms of the myosin. Although a role of ELCs is implicated in modulating myosin activity, the phosphorylation of RLCs is the primary regulatory mechanism for the contractile activity of SMCs (Pfitzer 2001; Eddinger and Meer 2007; Brozovich et al. 2016; Heissler and Sellers 2016). RLCs are phosphorylated by myosin light chain kinase (MLCK) in a Ca^{2+}/calmodulin (CaM)-dependent manner. The phosphorylation of RLCs leads to a conformation change of the myosin, which results in the binding of the myosin head to actin and the swing of the lever arm of myosin, and subsequently the shortening of myofilaments (Kamm and Stull 2011). RLC is dephosphorylated by myosin light chain phosphatase (MLCP). Therefore, the level of MLC phosphorylation and consequently the SMC tone is not only determined by the activity of MLCK but also by the activity of MLCP.

Y. Gao, *Biology of Vascular Smooth Muscle: Vasoconstriction and Dilatation*,
DOI 10.1007/978-981-10-4810-4_12

Since MLCP is inhibited by protein kinase C (PKC) via the 17-kDa PKC-potentiated inhibitor protein (CPI-17) and by Rho kinase (ROCK), the activation of theses kinases causes a reduced MLCP activity and augmented SMC contraction (Butler et al. 2013; Reho et al. 2014; Shimokawa et al. 2016). In this chapter the current understanding of RLC phosphorylation and SMC contraction, in particular vascular SMC (VSMC) contraction, and their regulation by MLCK, PKC, and ROCK signaling pathways are discussed.

12.2 Myosin Light Chain Phosphorylation

The contraction of smooth muscle cells (SMCs), like skeletal and cardiac muscle, is caused by repeatedly binding of myosin head to the actin, swinging of myosin head known as power stroke, and detaching from the actin filament, resulting in thick filament moves or slides along the thin filament. In striated muscle the myosin-actin interaction is blocked by the troponin-tropomyosin complex in resting state. The blockade is removed by a conformational change of the troponin-tropomyosin complex triggered by the binding of elevated Ca^{2+} to troponin C, consequently contractile action ensues (Sun and Irving 2010; Månsson et al. 2015). The contraction of SMCs is primarily regulated by phosphorylation of the RLC. Under unphosphorylated conditions and in the presence of ATP, the two heads of myosin heavy chain assume an asymmetric conformation. The actin-binding site of one myosin head is positioned in the middle of the other head near the converter domain, preventing its interaction with actin. Such a position prevents the domain motion of the adjacent head, which is required for the opening of the myosin's back door for phosphate release, an essential step for the occurrence of power stroke. Thus, the unphosphorylated two myosin heads are in an autoinhibition state. In addition, the tail of the myosin folds back upon itself in two places to form a compact conformation that inhibits myosin II filament formation (Wendt et al. 1999; Brozovich et al. 2016; Heissler and Sellers 2016).

In SMCs the phosphorylation of myosin RLC at Ser-19 serves as an on/off switch of the actin-activated myosin ATPase activity. The SMC myosin is enzymatically inactive in the absence of RLC phosphorylation. RLC phosphorylation at Ser-19 leads to a conformation with the two myosin heads extended away from each other on opposite sides of the elongated coiled-coil rod of the heavy chains, a structure which is competent for filament assembly. Such a change is accompanied by up to 1000-fold increases in myosin ATPase activity and the formation of filaments. RLC can also be phosphorylated at Thr-18. Thr-18 phosphorylation alone does not affect contractile force. Dephosphorylation of the RLC at both Thr-18 and Ser-19 may sustain contractile force by reducing the rate of RLC20 dephosphorylation (Pfitzer 2001; Butler et al. 2013; Taylor et al. 2014; Heissler and Sellers 2016). The functional significance of ELC, which binds the IQ1 motif closest to the motor domain than RLC, is not well understood. Studies suggest that the interaction

between the phosphorylated helix-A of the ELC and NH_2-terminus of the RLC is required for phosphorylation to activate smooth muscle myosin (Taylor et al. 2014).

12.3 MLCK

Phosphorylation of myosin RLC is mainly mediated by myosin light chain kinase (MLCK), a Ca^{2+}/CaM-activated serine/threonine-specific protein kinase.

MLCK exists as four isoforms encoded by three different genes. The nonmuscle and smooth muscle isoforms are encoded by the same mylk1 gene but different promoters, with the former expressed predominantly in embryonic tissues and in epithelial, endothelial, and other kinds of nonmuscle cells, while the latter is ubiquitously expressed. The other two isoforms are separately encoded by different genes: one is encoded by mylk2 and exclusively located in skeletal muscle; the other one is encoded by mylk3 gene and exclusively located in cardiac muscle (Fisher and Ikebe 1995; Takashima 2009; Hong et al. 2011).

The smooth muscle MLCK (smMLCK, from now on referred as MLCK) is an elongated and potentially flexible molecule sized ~130–150 kDa. It has an actin-binding site localized to the first 114 residues at the NH_2-terminus, a catalytic core that binds MgATP and RLC, a regulatory segment composed of autoinhibitory and CaM-binding sequences, and a myosin-binding site at the COOH-terminus. The autoinhibitory motif extends from the COOH-terminus of the catalytic core and folds back to prevent RLC but not ATP binding in the absence of Ca^{2+}/CaM. When Ca^{2+}/CaM binds to the CaM-binding sequence, the regulatory segment of the kinase is displaced from the catalytic site, and the catalytic site is exposed, allowing the kinase to bind to RLC and phosphorylation of RLC (Gallagher et al. 1997; Kamm and Stull 2011). CaM is a small, highly conserved protein sized 16.7 KDa. It has two approximately symmetrical globular domains each containing a pair of EF-hand motifs (the NH_2- and COOH-domain) separated by a flexible linker region for a total of four Ca^{2+}-binding sites. The EF-hand motifs of the COOH-terminal lobe have higher Ca^{2+} affinity. It is estimated that 50–80% of these sites are occupied by Ca^{2+} in resting cells resulting in CaM bound to MLCK. However, the activation of MLCK would not occur until Ca^{2+} binds to the lower affinity Ca^{2+}-binding EF-hand motifs in the NH_2-terminal lobe. The activity of MLCK is maximally activated (~1000-fold) at 1 μmol of $[Ca^{2+}]_i$ (Gallagher et al. 1997; Takashima 2009; Hong et al. 2011).

In SMCs, the concentration of MLCK is only ~10–13% of the concentration of its substrate RLC. K_m value and V_{max} of MLCK is 3–5 μmol and 10–20/s, respectively. With these kinetics, RLC is totally phosphorylated within 1–2 s (Takashima 2009). Considering that one statically bound MLCK can only phosphorylate at most eight local myosin heads, the abundance of MLCK would be insufficient to explain the phosphorylation levels of RLCs in vivo. A study using total internal reflection fluorescence microscopy reveals that unphosphorylated myosin exhibits higher affinity toward MLCK than phosphorylated myosin.

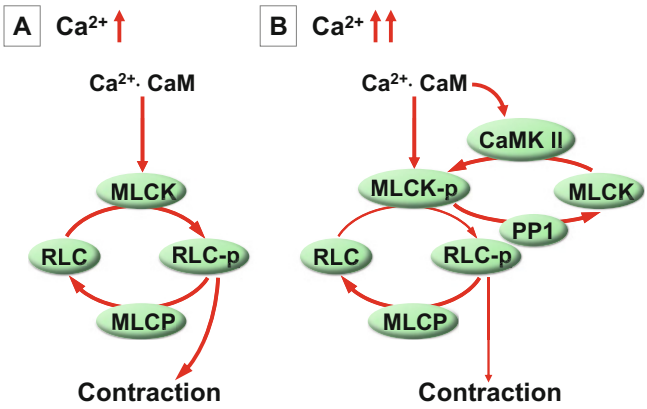

Fig. 12.1 The influence of cytosolic Ca^{2+} levels on the activity of myosin light chain kinase (MLCK) and vascular contractility. Panel A, a moderate increase in the concentration of cytosolic Ca^{2+} level activates MLCK after Ca^{2+} bound to calmodulin (CaM). MLCK promotes the phosphorylation of the regulatory light chain (RLC) of myosin, leading to increased contraction of vascular smooth muscle (VSM). The phosphorylation of RLC is reversed by myosin light chain phosphatase (MLCP), resulting in reduced contraction. Panel B, a marked increase in the concentration of cytosolic Ca^{2+} level, after bound to CaM, activates Ca^{2+}/CaM-dependent protein kinase II (CaMK II). CaMK II causes MLCK phosphorylation. The Ca^{2+} concentrations required for half-maximal RLC phosphorylation are ~400 nM vs. 170 nM when MLCK is phosphorylated compared with when MLCK is not phosphorylated. This results in reduced RLC phosphorylation and reduced contraction. The phosphorylated MLCK is dephosphorylated by phosphatase PP1. The thinner line indicates weaker action

Hence, MLCK would not get stuck on myosins that have already been phosphorylated. Such a mechanism may in part responsible for the high efficiency of RLC phosphorylation achieved by limited MLCK (Hong et al. 2015). In mice a 50% decrease in MLCK content has no effect on RLC phosphorylation or contractile response of urinary bladder smooth muscle evoked by KCL; however, both RLC phosphorylation and contraction of the aorta are significantly reduced. Meanwhile a 90% decrease of MLCK profoundly inhibits RLC phosphorylation and contractile responses of both muscle types. Since aortic tissue contains <50% MLCK compared with bladder, the difference in MLCK content may contribute to the differential responses occurred in these two muscle types (Gao et al. 2013).

The activation of MLCK by Ca^{2+}/calmodulin in smooth muscle is modulated by phosphorylation. MLCK is phosphorylated at multiple sites. However, only phosphorylation of the regulatory site at the COOH-terminus of the CaM-binding domain has been found to be associated with changes in the activation constant (K_{CaM}). The phosphorylation of MLCK is suppressed by inhibitors of Ca^{2+}/CaM-dependent protein kinase II (CaMK II), suggesting a pivotal role for this kinase in mediating MLCK phosphorylation. Studies demonstrate that the Ca^{2+} concentrations required for half-maximal RLC phosphorylation are ~400 nM vs. 170 nM when MLCK is phosphorylated compared with when the phosphorylation is inhibited, indicating that MLCK phosphorylation leads to a Ca^{2+} desensitization

for RLC phosphorylation and consequently smooth muscle contraction. It is proposed that Ca^{2+} desensitization due to MLCK phosphorylation would occur when cytosolic Ca^{2+} concentrations rise to high levels, greater than those necessary to initiate myosin RLC phosphorylation. The phosphorylation of MLCK is a reversible process. The dephosphorylation is likely to be mediated by phosphatase PP1 (Gallagher et al. 1997) (Fig. 12.1).

12.4 MLCP

RLC is dephosphorylated by MLCP, a serine/threonine-specific protein phosphatase. The phosphorylation level of RLC and thus the contractility of SMCs are controlled by the activity of MLCK vs. that of MLCP. Protein serine/threonine phosphatases (PSPs) can be divided into three major families: phosphoprotein phosphatases (PPPs), metal-dependent protein phosphatases, and aspartate-based phosphatases. Of these, only the PPPs have characterized roles in smooth muscle contractility. Within the PPP family, there are seven closely related members: PP1, PP2A, PP2B, PP4, PP5, PP6, and PP7. Among these PPPs only PP1 is directly involved in the dephosphorylation of RLC, while PP2A and PP2B may affect SMC contractility through acting on membrane ion channels and other proteins. PP1 has a 35- to 38-kDa catalytic subunit PP1c, which exists as five isoforms: PP1cα1, PP1cα2, PP1cδ, PP1cγ1, and PP1cγ2. At least 100 putative PP1-binding regulatory subunits have been identified. These regulatory subunits modulate the activity of PP1c, target the PP1 catalytic subunit to specific subcellular compartment, modulate substrate specificity, or serve as substrates themselves. PP2A exists as a heterodimers or a heterotrimer. The dimer is made up of a 36-kDa catalytic subunit PP2Ac and a 65-kDa regulatory A subunit PR65. The heterotrimer is formed when PP2Ac-PR65 dimers bind a further regulatory B subunit. PP2B, commonly known as calcineurin, is a Ca^{2+}-dependent phosphatase. It consists of the 60-kDa catalytic subunit calcineurin A and a 19-kDa regulatory subunit calcineurin B. Calcineurin B has four Ca^{2+}-binding sites. The binding of Ca^{2+} results in minimal activation of PP2B and enables Ca^{2+}-bound calmodulin to activate the phosphatase by the relief of the autoinhibition of the catalytic subunit (Shi 2009; Butler et al. 2013).

The phosphatase specifically dephosphorylate RLC consists of a 38-kDa δ isoform of PP1 catalytic subunit (PP1cδ), a 110–130-kDa regulatory subunit termed myosin phosphatase target subunit 1 (MYPT1), and a 20-kDa subunit of unknown function. PP1cδ works by using two manganese ions as catalysts for the dephosphorylation. Once in the proper configuration, both the phosphorylated Ser-19 of RLC of myosin and a free H_2O molecule are stabilized by the hydrogen-bonding residues in the active site, as well as the positively charged ions, which interact strongly with the negative phosphate group. The His-125 on PP1cδ donates a proton to Ser-19 on RLC, and the H_2O molecule attacks the phosphorus atom. After shuffling protons stabilize, the phosphate and alcohol are formed, and both leave the active site (Shi 2009). PP1cδ binds MYPT1 at an RVxF motif at amino

acids 35–38. The ankyrin repeats adjacent to the RVxF motif further anchor the catalytic subunit. A centrally spliced region in MYPT1 produces ≥ five different-sized isoforms of variable length. The physiological significance of these isoforms is unclear. Also, an alternative splicing of a 31-nt exon 24 generates two isoforms, one with and one without a COOH-terminal leucine zipper motif (LZ) that is required for the interaction of cGMP-dependent protein kinase (PKG) with MLCP. In SMCs MLCP is regulated by phosphorylation of MYPT1 at Thr-696 and Thr-853 (human sequence) resulting in reduced activity of MLCP and thus augmented contractility. By contrast, MYPT1 can be phosphorylated of at Ser-695 and Ser-852, which leads to increased MLCP activity and decreased contractility. The phosphorylation of MYPT1 at Ser-668 and Ser-692 has also been suspected to cause increased MLCP activity (Grassie et al. 2011; Butler et al. 2013; Reho et al. 2014).

The phosphorylation of RLC of myosin can be affected indirectly by PP1 and PP2A through acting on a 17-kDa PP1 inhibitor protein, also known as 17-kDa PKC-potentiated inhibitor protein (CPI-17). When CPI-17 is phosphorylated at Thr-38, it specifically inhibits PP1cδ activity and hence results in increased MLC phosphorylation and augmented contraction of SMCs. This effect is attenuated by the dephosphorylation of CPI-17 at Thr-38 by PP1 or PP2A (Eto and Brautigan 2012). In addition to act on RLC,PP1 and PP2A can affect SMC contractility through stimulation or inhibition of L-type voltage-gated Ca^{2+} channels (VGCCs) and large-conductance Ca^{2+}-activated K^+ (BK_{Ca}) channels on cell membrane. PP2A may also influence SMC contractility by acting on caldesmon, calponin, and type 4 phosphodiesterase. Another phosphatase PP2B has been found to inhibit L-type VGCCs and BK_{Ca} channels as well as stimulate Cl^- channels of SMCs. The β isoform of phospholipase C and inositol trisphosphate receptors may also be inhibited by PP2B (Butler et al. 2013).

12.5 Protein Kinase C Signaling

An increased phosphorylation of RLC of myosin occurs not only by the activation of Ca^{2+}/CaM-MLCK signaling, but also by the inhibition of MLCP mediated by PKC-CPI-17 and RhoA-ROCK pathways. Under similar concentrations of cytosolic Ca^{2+}, a higher activity of PKC-CPI-17 or RhoA-ROCK would cause greater phosphorylation of RLC and greater SMC contraction, such a phenomenon is known as Ca^{2+} sensitization. Studies suggest that PKC-mediated Ca^{2+} sensitization is more pronounced during the initiation of rapid development of VSMC contraction. In contrast, ROCK-mediated Ca^{2+} sensitization is more important to sustain the contraction (Dimopoulos et al. 2007).

PKC exists as ten isozymes in humans. They are classified into three types, based on their second messenger requirements: conventional (or classical), novel, and atypical. Conventional PKCs (cPKCs) contain the isoforms α, βI, βII, and γ. Their activation requires diacyl glycerol (DAG) and Ca^{2+}. Novel PKCs (nPKCs) include

the δ, ε, η, and θ isoforms. They require DAG but not Ca^{2+} for activation. Atypical PKCs (aPKCs) have the ζ and ι/λ isoforms; both require neither DAG nor Ca^{2+} for activation. All PKCs consist of an NH_2-terminal regulatory domain and a COOH-terminal catalytic domain. These two domains are tethered together by a hinge region. The catalytic domain is highly conserved containing a C3 region for ATP binding and a C4 region for substrate-binding. In the regulatory domain, the cPKCs each possess tandem C1A and C1B domains that bind to DAG or phorbol esters in membranes and a C2 domain that binds membranes in the presence Ca^{2+}. The nPKCs likewise each contain two tandem C1 domains that bind to DAG or phorbol esters but possess a novel C2 domain that does not bind Ca^{2+} and does not serve as a membrane-targeting module. However, the C1B domain of nPKCs has a 100-fold higher affinity for DAG compared with that of cPKCs. The aPKCs do not respond to either DAG or Ca^{2+}. They contain a single atypical C1 domain that possesses the ability to bind anionic phospholipids and a Phox and Bem1 (PB1) domain that mediates protein–protein interactions. All PKCs contain a pseudosubstrate (PS) sequence that immediately precedes the C1 region. Under resting conditions the PS sequence binds to the substrate-binding cavity in the kinase domain of the COOH-terminus and renders the enzyme inactive (Salamanca and Khalil 2005; Freeley et al. 2011; Wu-Zhang and Newton 2013).

PKC isozymes are activated by a variety of hormones, growth factors, and neurotransmitters. These stimulators, when bound to their respective receptors, activate phospholipase C (PLC), leading to elevated DAG and inositol-1,4,5-trisphosphate (IP_3), followed by an increased Ca^{2+} release from the sarcoplasmic reticulum triggered by IP3. While DAG alone is sufficient to recruit nPKCs to the plasma membrane, both DAG and Ca^{2+} are required for cPKCs to be translocated from the cytosol to the plasma membrane. This interaction of cPKCs or nPKCs with the membrane results in the release of the PS sequence from the catalytic site and activation of the enzyme. The aPKCs are insensitive to second messengers. There is evidence indicating that protein scaffolds may serve as allosteric activators of aPKCs, tethering them in an active conformation near specific substrates (Wu-Zhang and Newton 2013; Igumenova 2015; Tobias and Newton 2016).

For all PKCs in order for them to be activated, they need to be properly folded and in the correct conformation permissive for catalytic action, which is contingent upon phosphorylation of the catalytic region. The cPKCs and nPKCs have three phosphorylation sites, termed the activation loop, the turn motif, and the hydrophobic motif. The atypical PKCs are phosphorylated only on the activation loop and the turn motif. The 3-phosphoinositide-dependent protein kinase-1 (PDK1) is the upstream kinase responsible for initiating the process by transphosphorylation of the activation loop. The aPKCs are insensitive to second messengers. There is evidence indicating that protein scaffolds may serve as allosteric activators of aPKCs, tethering them in an active conformation near specific substrates (Freeley et al. 2011; Tobias and Newton 2016).

PKCs modulate vascular contractility primarily through the phosphorylation of CPI-17 at Thr-38. The phosphorylation increases the affinity of CPI-17 for PP1-MYPT1 by ~1000-fold, resulting in suppressed MLCP activity and thus

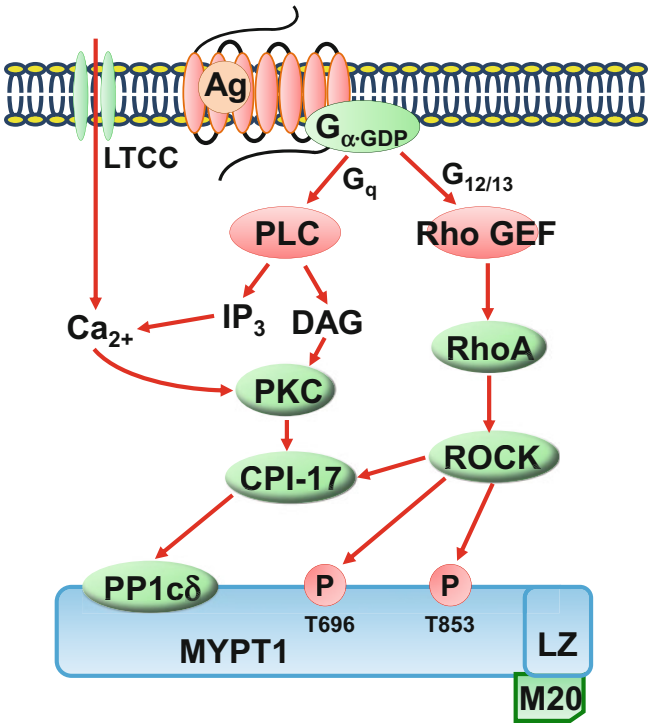

Fig. 12.2 Mechanism for protein kinase C (PKC)- and Rho kinase (ROCK)-mediated the suppression of myosin light chain phosphatase (MLCP) of vascular smooth muscle. PKC is activated by cytosolic Ca^{2+} and diacyl glycerol (DAG). The increased Ca^{2+} results from the influx of extracellular Ca^{2+} through L-type Ca^{2+} channel (LTCC) and Ca^{2+} released from the sarcoplasmic reticulum in response to inositol-1,4,5-trisphosphate (IP_3). Both IP_3 and DAG are generated by phospholipase C (PLC) when the G-protein-coupled receptor (GPCR) is activated by the agonist (Ag). PKC inhibits MLCP via phosphorylation of the 17-kDa PKC-potentiated inhibitor protein (CPI-17), which acts directly on the catalytic subunit PP1cδ of the phosphatase. MLCP is also inhibited by ROCK through the phosphorylation of the regulatory subunit of the enzyme termed myosin phosphatase target subunit 1 (MYPT1) at Thur-696 and Thur-853 (human sequence). ROCK may also inhibit MLCP by the phosphorylation of CPI-17. ROCK is activated by RhoA, a small GTPase protein. RhoA is activated by guanine nucleotide exchange factor (Rho GEF) after the activation of GPCR. MLCP is a heterotrimer. In addition to PP1cδ and MYPT1, MLCP also contains a 20-kDa subunit (M20) of unknown function

enhanced RLC phosphorylation of myosin and augmented vascular tension. CPI-17 is a 147-residue polypeptide in which ~85% of the amino acids are identical in mammalian. The CPI-17 contains an NH_2-terminus, a COOH-terminus, and a central 86-residue PP1 holoenzyme inhibitory (PHIN) domain between residues 35 and 120. Upon phosphorylation at Thr-38, a conformational change leads the exposure of the PP1 inhibitory surface. The phospho-CPI-17 docks at the PP1 active site and simultaneously contacts MYPT1 at the ankyrin-repeat domain and the NH_2-terminal helix domain. The capability of CPI-17 to interact with both PP1

catalytic region and MYPT1 appears to endow it with a high selectivity toward to MLCP (Eto 2009; Eto and Brautigan 2012) (Fig. 12.2).

CPI-17 is expressed predominantly in mature smooth muscle and is more abundant in tonic muscles, such as aortas and femoral arteries (Woodsome et al. 2001). In pig aorta CPI-17 is predominantly activated by PKCα and PKCδ. CPI-17 binds to the regulatory domain of several PKCs, including α, ε, ζ, and λ isoforms. CPI-17 can also be phosphorylated at Thr-38 by ROCK, integrin-linked kinase, protein kinase N1, p21 activated kinase, and zipper-interacting protein kinase. It is believed that PKCs are primarily responsible for fast CPI-17 phosphorylation that occurred during early phase of vasoconstriction, while ROCK is mainly responsible for slow, sustained CPI-17 phosphorylation that occurred during the sustained phase of contractile activity (Butler et al. 2013).

12.6 Rho Kinase Signaling

The RhoA-ROCK pathway plays a central role in the maintenance of the basal and sustained tension of SMCs including VSMCs. It exerts its effect by the phosphorylation of MYPT1, resulting in decreased MLCP activity, increased RLC phosphorylation, and augmented SMC tension. An increased inhibition of the catalytic subunit of MLCP via the inhibition of CPI-17 may also be involved. Moreover, increased expression and activities of RhoA and ROCKs are implicated in exaggerated vascular contractility occurred under pathophysiological conditions (Nagaoka et al. 2004; Tourneux et al. 2008; Chen et al. 2014; Shimokawa et al. 2016).

RhoA (Ras homolog gene family, member A) is a small GTPase protein (~21 kDa) of Rho family. It is composed of an NH_2-terminal containing most of the protein coding for GTP binding and hydrolysis and a COOH-terminal modified via prenylation to anchoring the GTPase into membranes. RhoA exists as inactive GDP-bound and active GTP-bound states. In inactive state, RhoA is bound to GDP existing in the cytosol with its prenylated, hydrophobic tail buried within its partner, GDP dissociation inhibitor (RhoGDI). The activation of membrane receptors coupled to G-proteins ($G_{12/13}\alpha$), membrane depolarization, and/or Ca^{2+} signaling stimulate guanine nucleotide exchange factors (GEFs), leading to the exchange of GTP for GDP on RhoA, RhoGDI dissociation, and the association of GTP-bound RhoA with the plasma membrane where it interacts with ROCK to initiate signaling cascades. The GTP-bound RhoA is hydrolyzed by GTPase-activating proteins (RhoGAPs) and sequestered by RhoGDI which removes the protein from the membrane (Loirand and Pacaud 2010; Butler et al. 2013; Cherfils and Zeghouf 2013).

The ROCK, also known as Rho-associated, coiled-coil-containing protein kinase, is the major downstream effecter of RhoA. It is a serine/threonine kinase of about 160 kDa and existed as two isoforms, ROCK1 and ROCK2. These two isoforms are encoded by two different genes and are ubiquitously expressed.

ROCK1 and ROCK2 share overall amino acid sequence identity of 65% and approximately 92% in the kinase domain. Both isoforms contain an NH_2 terminally located kinase domain, a coiled-coiled region containing the Rho-binding domain (RBD), and a pleckstrin homology (PH) domain with a cysteine-rich C1 domain (CRD). When a substrate is absent, the COOH-terminal region of ROCKs, including the PH domains, acts as an autoinhibitory domain by binding directly to the NH_2-terminal kinase domain. Upon interaction of the RBD domain with GTP-bounded RhoA, the interactions between the NH_2-terminus and the COOH-terminus are disrupted, thus activating the enzyme. ROCK1 can be activated by arachidonic acid or sphingosine phosphorylcholine. These lipids interact with the PH domain disrupting its ability to inhibit ROCK1 (Hartmann et al. 2015; Shimokawa et al. 2016). By contrast, ROCK1 is inhibited by RhoE (Rnd3), an endogenous inhibitor of Rho protein function. RhoE binds to the NH_2-terminal region of ROCK I encompassing the kinase domain (Riento et al. 2003). ROCK1 and ROCK2 can also be cleaved at the C-terminus by caspase-3 and a serine protease granzyme B, respectively. This results in a constitutively active kinase (Sebbagh et al. 2005; Gabet et al. 2011).

ROCKs regulate VSMC contractility mainly by inhibiting the activity of MLCP via the phosphorylation of MYPT1 at Thr-696 and Thr-853 (Fig. 12.2). Phosphorylation of Thr-696 suppresses the catalytic activity of MLCP, and phosphorylation of Thr-853 dissociates MYPT1 from myosin and PP1C (Butler et al. 2013; Khasnis et al. 2014). In rat caudal artery thromboxane A2 mimetic, U-46619-evoked contraction is associated with increased phosphorylation of MYPT1 at Thr-855 (rat sequence equivalent to human Thr-853) and phosphorylation of RLC of myosin. These effects are blunted by the inhibitor of ROCK. However, U-46619 has no effect on Thr-697 (rat sequence equivalent to human Thr-696) (Wilson et al. 2005).In rat cerebral arteries, the myogenic vasoconstriction caused an increase in the intraluminal pressure from 10 to 60 mmHg which is accompanied by increased phosphorylation of MYPT1 at Thr-855 and RLC of myosin but not phosphorylation of MYPT1 at Thr-697. However, an increase in the intraluminal pressure plus 5-HT causes increased phosphorylation of MYPT1 at both Thr-697 and Thr-855, which are diminished by the inhibition of ROCK. Thus, it is likely that the phosphorylation of MYPT1 at Thr-855 occurs at a lower stimulus level than that of Thr-697. Such a mechanism may provide a greater range of increase in the level of Ca^{2+} sensitization and force generation than can be attained by phosphorylation at a single site (Johnson et al. 2009; El-Yazbi et al. 2010). As aforementioned, ROCK may inhibit MLCP activity via phosphorylation of CPI-17 at Thr-38. ROCK may also affect VSMC contractility by acting on many other substrates such as adducin, calponin, ezrin/radixin/moesin (ERM) family, LIM kinases, MLC, and tau. Their physiological significance remains to be determined (Kaneko et al. 2000; Kang et al. 2011; Shimokawa et al. 2016).

References

Brozovich FV, Nicholson CJ, Degen CV, Gao YZ, Aggarwal M, Morgan KG (2016) Mechanisms of vascular smooth muscle contraction and the basis for pharmacologic treatment of smooth muscle disorders. Pharmacol Rev 68:476–532

Butler T, Paul J, Europe-Finner N, Smith R, Chan EC (2013) Role of serine-threonine phosphoprotein phosphatases in smooth muscle contractility. Am J Physiol Cell Physiol 304:C485–C504

Chen Z, Zhang X, Ying L, Dou D, Li Y, Bai Y, Liu J, Liu L, Feng H, Yu X, Leung SWS, Vanhoutte PM, Gao Y (2014) Cyclic IMP-synthesized by sGC as a mediator of hypoxic contraction of coronary arteries. Am J Physiol Heart Circ Physiol 307:H328–H336

Cherfils J, Zeghouf M (2013) Regulation of small GTPases by GEFs, GAPs, and GDIs. Physiol Rev 93:269–309

Dimopoulos GJ, Semba S, Kitazawa K, Eto M, Kitazawa T (2007) Ca^{2+}-dependent rapid Ca^{2+} sensitization of contraction in arterial smooth muscle. Circ Res 100:121–129

Eddinger TJ, Meer DP (2007) Myosin II isoforms in smooth muscle: heterogeneity and function. Am J Physiol Cell Physiol 293:C493–C508

El-Yazbi AF, Johnson RP, Walsh EJ, Takeya K, Walsh MP, Cole WC (2010) Pressure-dependent contribution of rho kinase-mediated calcium sensitization in serotonin-evoked vasoconstriction of rat cerebral arteries. J Physiol 588:1747–1762

Eto M (2009) Regulation of cellular protein phosphatase-1 (PP1) by phosphorylation of the CPI-17 family, C-kinase-activated PP1 inhibitors. J Biol Chem 284:35273–35277

Eto M, Brautigan DL (2012) Endogenous inhibitor proteins that connect Ser/Thr kinases and phosphatases in cell signaling. IUBMB Life 64:732–739

Fisher SA, Ikebe M (1995) Developmental and tissue distribution of expression of nonmuscle and smooth muscle isoforms of myosin light chain kinase. Biochem Biophys Res Commun 217:696–703

Freeley M, Kelleher D, Long A (2011) Regulation of Protein Kinase C function by phosphorylation on conserved and non-conserved sites. Cell Signal 23:753–762

Gabet AS, Coulon S, Fricot A, Vandekerckhove J, Chang Y, Ribeil JA, Lordier L, Zermati Y, Asnafi V, Belaid Z, Debili N, Vainchenker W, Varet B, Hermine O, Courtois G (2011) Caspase-activated ROCK-1 allows erythroblast terminal maturation independently of cytokine-induced Rho signaling. Cell Death Differ 18:678–689

Gallagher PJ, Herring BP, Stull JT (1997) Myosin light chain kinases. J Muscle Res Cell Motil 18:1–16

Gao N, Huang J, He W, Zhu M, Kamm KE, Stull JT (2013) Signaling through myosin light chain kinase in smooth muscles. J Biol Chem 288:7596–7605

Grassie ME, Moffat LD, Walsh MP, MacDonald JA (2011) The myosin phosphatase targeting protein (MYPT) family: a regulated mechanism for achieving substrate specificity of the catalytic subunit of protein phosphatase type 1δ. Arch Biochem Biophys 510:147–159

Hartmann S, Ridley AJ, Lutz S (2015) The function of rho-associated kinases ROCK1 and ROCK2 in the pathogenesis of cardiovascular disease. Front Pharmacol 6:276

Heissler SM, Sellers JR (2016) Various themes of myosin regulation. J Mol Biol 428:1927–1946

Hong F, Haldeman BD, Jackson D, Carter M, Baker JE, Cremo CR (2011) Biochemistry of smooth muscle myosin light chain kinase. Arch Biochem Biophys 510:135–146

Hong F, Brizendine RK, Carter MS, Alcala DB, Brown AE, Chattin AM, Haldeman BD, Walsh MP, Facemyer KC, Baker JE, Cremo CR (2015) Diffusion of myosin light chain kinase on actin: a mechanism to enhance myosin phosphorylation rates in smooth muscle. J Gen Physiol 146:267–280

Igumenova TI (2015) Dynamics and membrane interactions of protein kinase C. Biochemistry 54:4953–4968

Johnson RP, El-Yazbi AF, Takeya K, Walsh EJ, Walsh MP, Cole WC (2009) Ca^{2+} sensitization via phosphorylation of myosin phosphatase targeting subunit at threonine-855 by Rho kinase contributes to the arterial myogenic response. J Physiol 587:2537–2553

Kamm KE, Stull JT (2011) Signaling to myosin regulatory light chain in sarcomeres. J Biol Chem 286:9941–9947

Kaneko T, Amano M, Maeda A, Goto H, Takahashi K, Ito M, Kaibuchi K (2000) Identification of calponin as a novel substrate of rho-kinase. Biochem Biophys Res Commun 273(1): 110–116

Kang JH, Asai D, Tsuchiya A, Mori T, Niidome T, Katayama Y (2011) Peptide substrates for rho-associated kinase 2 (rho-kinase 2/ROCK2). PLoS One 6:e22699

Khasnis M, Nakatomi A, Gumpper K, Eto M (2014) Reconstituted human myosin light chain phosphatase reveals distinct roles of two inhibitory phosphorylation sites of the regulatory subunit, MYPT1. Biochemistry 53:2701–2709

Loirand G, Pacaud P (2010) The role of rho protein signaling in hypertension. Nat Rev Cardiol 7:637–647

Månsson A, Rassier D, Tsiavaliaris G (2015) Poorly understood aspects of striated muscle contraction. Biomed Res Int 2015:245154

Nagaoka T, Morio Y, Casanova N, Bauer N, Gebb S, McMurtry I, Oka M (2004) Rho/Rho kinase signaling mediates increased basal pulmonary vascular tone in chronically hypoxic rats. Am J Physiol Lung Cell Mol Physiol 287:L665–L672

Pfitzer G (2001) Rregulation of myosin phosphorylation in smooth muscle. J Appl Physiol 91:497–503

Reho JJ, Zheng X, Fisher SA (2014) Smooth muscle contractile diversity in the control of regional circulations. Am J Physiol Heart Circ Physiol 306:H163–H172

Riento K, Guasch RM, Garg R, Jin B, Ridley AJ (2003) RhoE binds to ROCK I and inhibits downstream signaling. Mol Cell Biol 23:4219–4229

Salamanca DA, Khalil RA (2005) Protein kinase C isoforms as specific targets for modulation of vascular smooth muscle function in hypertension. Biochem Pharmacol 70:1537–1547

Sebbagh M, Hamelin J, Bertoglio J, Solary E, Bréard J (2005) Direct cleavage of ROCK II by granzyme B induces target cell membrane blebbing in a caspase-independent manner. J Exp Med 201:465–471

Shi Y (2009) Serine/threonine phosphatases: mechanism through structure. Cell 139:468–484

Shimokawa H, Sunamura S, Satoh K (2016) RhoA/Rho-Kinase in the cardiovascular system. Circ Res 118:352–366

Sun YB, Irving M (2010) The molecular basis of the steep force-calcium relation in heart muscle. J Mol Cell Cardiol 48:859–865

Takashima S (2009) Phosphorylation of myosin regulatory light chain by myosin light chain kinase, and muscle contraction. Circ J 73:208–213

Taylor KA, Feig M, Brooks CL 3rd, Fagnant PM, Lowey S, Trybus KM (2014) Role of the essential light chain in the activation of smooth muscle myosin by regulatory light chain phosphorylation. J Struct Biol 185:375–382

Tobias IS, Newton AC (2016) Protein scaffolds control localized protein kinase Cζ activity. J Biol Chem 291:13809–13822

Tourneux P, Chester M, Grover T, Abman SH (2008) Fasudil inhibits the myogenic response in the fetal pulmonary circulation. Am J Physiol Heart Circ Physiol 295:H1505–H1513

Wendt T, Taylor D, Messier T, Trybus KM, Taylor KA (1999) Visualization of head-head interactions in the inhibited state of smooth muscle myosin. J Cell Biol 147:1385–1390

Wilson DP, Susnjar M, Kiss E, Sutherland C, Walsh MP (2005) Thromboxane A2-induced contraction of rat caudal arterial smooth muscle involves activation of Ca^{2+} entry and Ca^{2+} sensitization: Rho-associated kinase-mediated phosphorylation of MYPT1 at Thr-855, but not Thr-697. Biochem J 389:763–774

Woodsome TP, Eto M, Everett A, Brautigan DL, Kitazawa T (2001) Expression of CPI-17 and myosin phosphatase correlates with Ca^{2+} sensitivity of protein kinase C-induced contraction in rabbit smooth muscle. J Physiol 535:553–564

Wu-Zhang AX, Newton AC (2013) Protein kinase C pharmacology: refining the toolbox. Biochem J 452:195–209

Chapter 13
Cyclic AMP Signaling

Abstract Adenosine 3′5′ cyclic monophosphate (cAMP) is the second messenger mediating vasodilatation induced by β_2 adrenergic agonists, vasodilator prostaglandins, histamine, vasoactive intestinal peptide, etc. cAMP exerts its action primarily by the activation of cAMP-dependent kinase (PKA). The effects of cAMP may also be mediated by the exchange proteins directly activated by cAMP and the cyclic nucleotide-gated (CNG) channels. The cytosolic levels of cAMP reflect its synthesis by adenylyl cyclase and its hydrolysis by phosphodiesterases, particularly the type 4 phosphodiesterase. The major mechanisms underlying cAMP-mediated vasodilatation include the activation of potassium channels, the activation of myosin light chain phosphatase, and the inhibition of RhoA/Rho kinase signaling.

Keywords Adenylyl cyclase • cAMP • Phosphodiesterase • PKA • Epac • MLCP • MYPT1 • ROCK

13.1 Introduction

Adenosine 3′5′ cyclic monophosphate (cAMP) is the first second messenger identified and plays fundamental roles in a broad range of responses of various cell types (Sutherland and Rall 1958). It is generated from ATP with a by-product pyrophosphate by adenylyl cyclase (AC). In vascular smooth muscle cells (VSMCs), cAMP mediates vasodilatation response in response to various neurotransmitters and hormones such as β_2 adrenergic agonists, prostacyclin (PGI_2), prostaglandin E_2 (PGE_2), prostaglandin (PGD_2), histamine, and vasoactive intestinal peptide (VIP). cAMP causes vasodilatation primarily by activating cAMP-dependent protein kinase (PKA). It also affects vasoactivity by acting on the exchange protein directly activated by cAMP (Epac) and the cyclic nucleotide-gated (CNG) channels (Biel 2009; Sassone-Corsi 2012; Roberts and Dart 2014; Bob et al.2016; Lezoualc'h et al. 2016).

Y. Gao, *Biology of Vascular Smooth Muscle: Vasoconstriction and Dilatation*,
DOI 10.1007/978-981-10-4810-4_13

13.2 ACs

AC exists as six distinct classes (I-VI), which catalyze the same reaction but represent unrelated gene families with no known sequence or structural homology. All mammalian ACs belong to Class III, defined by a conserved ~200 residue catalytic domain. This class of ACs is divided into two distinct types, nine transmembrane enzymes (tmAC; AC1–9) and one soluble AC (sAC; AC10). Mammalian tmACs are typically made up of two clusters of six transmembrane (TM) domains (TM1 and TM2). TM1 and TM2 are joined by an intracellular loop containing the C1a and C1b regions. A long intracellular tail follows TM2, which contains the C2a and C2b regions before the carboxyl terminus. The C1a and C2a are well conserved and contain all of the catalytic apparatus. The C1a and C2a domains heterodimerize with each other, and an active site is formed at the interface by both C1a and C2. Since the active site is shared between the two domains, association of two catalytic domains in the proper orientation is essential for catalytic activity. The mammalian sAC contains two catalytic domains C_1 and C_2 in tandem followed by a ~1100 residue C-terminal region, which may be an inhibitor of the catalyst. Similar to tmACs, the dimerization of C_1 and C_2 is required for catalytic activity of sAC (Hurley 1999; Steegborn 2014).

The activity of tmACs is regulated by the interaction of various proteins with the catalytic domain of the enzyme, whereas no regulatory proteins have yet been found for sAC. The main regulators of tmACs are heterotrimeric G proteins upon activation of G protein-coupled receptors (GPCRs). All tmAC isoforms are stimulated by the Gsα-subunit, and tmACs 1, 5, and 6 are inhibited by Goα or Giα. The ACs 1, 3, and 8 are stimulated, and ACs 5 and 6 are inhibited by Ca^{2+}/calmodulin (CaM), while ACs 1 and 3 are inhibited by Ca^{2+}/CaM-dependent protein kinase (CaMK) and AC9 is inhibited by calcineurin. Some tmAC isoforms are also stimulated or inhibited by the Gβγ-subunits or protein kinase C (PKC). In addition, all tmACs except AC9 are potently activated by forskolin, a plant diterpene. sAC activity is stimulated by HCO_3^- and Ca^{2+}, and is sensitive to physiologically relevant ATP changes. sAC functions as a physiological sensor for CO_2 and bicarbonate and thus indirectly for pH (Hurley 1999; Linder 2006; Halls and Cooper 2011; Schmid et al. 2014; Steegborn 2014).

VSMCs express multiple AC isoforms, with strongest evidence for ACs 3, 5, and 6. In rat aortic smooth muscle cells (SMCs), the increase in cAMP caused by isoproterenol is reduced by ~60% after selective depletion of AC6 with short interfering RNA sequences, by ~30% after selective depletion of AC3. The activation of PKA and membrane hyperpolarization via activation of K_{ATP} current caused by isoproterenol are markedly suppressed by the depletion of AC6, suggesting that AC6 plays a principal role in β-adrenoceptor-mediated vasodilatation (Nelson et al. 2011). In rat pulmonary arterial SMCs (PASMCs), AC2, AC5/AC6, and, to a lesser extent, AC3 are found being the predominant isoforms in pulmonary arterial SMCs. AC7 and AC8 are present at low levels. The cAMP levels of PASMCs are

stimulated by forskolin or cicaprost, a stable prostacyclin mimetic. These effects are not affected by $G_i\alpha$-coupled receptor agonists carbachol or clonidine. In contrast, A-23187, a Ca^{2+} ionophore, and thapsigargin, which increase the cytosolic Ca^{2+} levels by inhibiting Ca^{2+} uptake of sarcoplasmic reticulum, cause concentration-dependent increase in the intracellular concentration of cAMP. Therefore, it appears that Ca^{2+}-activated AC isoforms are importantly involved in AC-mediated PASMC activity, while $G_i\alpha$ has a minor role in regulating the AC activity (Jourdan et al. 2001).

13.3 cAMP-Hydrolyzing Phosphodiesterases (PDEs)

The intracellular concentration of cAMP is determined as a result of its synthesis by ACs and its hydrolysis by PDEs. PDEs are responsible not only for the termination of cAMP signaling but are also involved in the generation of spatial and temporal varying cAMP changes, controlling distinct cell functions in response to a broad range of extracellular stimuli. PDEs constitute a superfamily of 11 structurally related but functionally distinct gene families (PDE1 to PDE11); some are specific for cAMP (PDEs 4, 7, 8), some for cGMP (PDEs 5, 6, 9), whereas the remainder (PDEs 1–3, 10, 11) catabolize both cAMP and cGMP. Most families contain several PDE genes, which together generate close to 100 PDE isozymes by alternative mRNA splicing or transcriptional processing (Maurice et al. 2014; Bobin et al. 2016).

In VSMCs the cAMP is hydrolyzed primarily by PDE4; PDEs 1 and 3 may also be functionally important. In vascular endothelial cells, PDEs 2–4 are present (Keravis and Lugnier 2012; Maurice et al. 2014). PDEs share a conserved COOH-terminal catalytic domain, with 25–52% amino acid sequence identity, but differ markedly in their NH_2-terminal regulatory domains. The regulatory domains contain diverse elements related to enzyme dimerization, binding of regulatory small molecules, phosphorylation, and localization. The PDE1 family has three isoforms, with PDE1A and PDE1B preferentially hydrolyze cGMP whereas PDE1C hydrolyzes cAMP and cGMP with similar K_m values (0.6–2.2 μM and 0.3–1.1 μM, respectively). PDE1 isoforms are characterized by the existence of two binding sites for CaM in their regulatory domains. They are the only mammalian PDEs that are regulated by Ca^{2+}. PDE1s are predominantly cytosolic, and their catalytic activity is largely determined by cytosolic Ca^{2+} levels. PDE2 hydrolyzes both cAMP and cGMP and exists as PDE2A1, PDE2A2, and PDE2A3, with PDE2A1 as cytosolic and the other two isoforms membrane-associated. The NH_2-terminal domains of the PDE2s have two GAF (cGMP-activated PDE, adenylyl cyclase-, and Fh1A-binding) domains, GAF-A and GAF-B. The GAF-A domain mediates enzyme dimerization, whereas GAF-B domain binds cGMP, resulting in up to a 30-fold increase in cAMP hydrolysis. Therefore, PDE2s are also known as cGMP-stimulated cAMP/cGMP PDEs. It may

represent a mechanism of the cross talk between cAMP and cGMP signalings (Bender and Beavo 2006; Francis et al. 2011; Keravis and Lugnier 2012).

There are two subfamilies for PDE3, PDE3A and PDE3B. PDE3A is mainly present in the heart, platelets, VSMCs, and oocytes. PDE3B is more richly expressed in cells of importance for the regulation of energy homeostasis, such as adipocytes, hepatocytes, and pancreatic β-cells. In tissues, PDE3A has been found being both cytosolic and membrane-bound, whereas PDE3B is predominantly membrane-bound. All these PDEs have similar affinities for cAMP and cGMP (K_m, 0.2 μM and 0.1 μM, respectively). However, the rate of cGMP hydrolysis is only ~10% that of cAMP. cGMP can compete with and inhibit cAMP breakdown at the catalytic site. For this reason, PDE3 is known as cGMP-inhibited PDE. Therefore, changes in cGMP level may affect cAMP signaling through the interference with cAMP breakdown (Bender and Beavo 2006; Francis et al. 2011; Ahmad et al. 2012; Keravis and Lugnier 2012). For instance, acetylcholine (ACh), which elevates cGMP via the activation of endothelial nitric oxide synthase, has no effect on the cAMP level of ovine pulmonary arteries by itself alone. However, the presence of ACh significantly enhances the increase in cAMP level caused by PGE_2. Meanwhile, the vasodilatation caused by the combinatorial treatment of ACh and PGE_2 is greater than the sum of the effects of these agonists when each is used alone (Gao et al. 1998).

The PDE4 family selectively hydrolyzes cAMP (K_m for cAMP, 2 μM; for cGMP >300 μM), so it is also known as cAMP-specific PDE. PDE4 is encoded by four genes, namely, PDE4 A–D. Due to alternative splicing, more than 25 human isoforms (from 50 to 125 kDa) are identified. Long PDE4 isozymes have a unique amino acid signature region known as upstream conserved regions 1 and 2 (UCR1 and UCR2). UCR1 contains a PKA phosphorylation site that upon phosphorylation disrupts the UCR2 inhibitory influence and activates the enzyme. The short PDE4s have no UCR1, and supershort PDE4s contain only half of UCR2. Since the UCR modules mediate dimerization, only long-form PDE4s are dimerized. The COOH-terminal end of the catalytic region of PDE4s contains a phosphorylation site for the extracellular signal-regulated kinase (ERK). Its phosphorylation activates PDE4 short forms but inhibits PDE4 long forms. PDE4s are richly expressed in cardiovascular, neural, immune, and inflammatory systems. In tissues they may be membrane-associated or cytosolic, depending on different isoforms (Francis et al. 2011; Keravis and Lugnier 2012; Maurice et al. 2014).

The intracellular distribution of PDEs is not uniform. Studies suggest that PDE4 activity near the plasma membrane and near CNG channels is lower than total cellular PDE4 activity such that cAMP generated by the tmACs near CNG channels is restricted locally to its effectors (Xin et al. 2015). In rat aorta SMCs, the increase in cAMP evoked by β-adrenergic receptor (β-AR) has been found to be hydrolyzed by PDEs 1, 3, and 4, with PDE4 playing a prominent role. PDE4 and PDE3 act in a synergistic manner to hydrolyze the submembrane cAMP produced by β-AR stimulation (Zhai et al. 2012). PDE4 isoforms can be specifically localized by A-kinase-anchoring proteins (AKAPs) in subcellular compartments nearby PKA, the primary enzyme that mediates cAMP biological responses (Keravis and Lugnier

2012). AKAPs constitute a structurally diverse group of proteins that direct PKA to distinct subcellular sites. In addition to tethering PKA, AKAPs also act as scaffolds to PKA's substrates, ACs, PDEs, and protein phosphatases. In such a way, cAMP signaling is confined to a distinct subcellular microdomain, also known as signalosome, where unique combinations of cAMP effectors and individual or subsets of PDEs form specific complexes via protein–protein interactions (Valsecchi et al. 2013; Lefkimmiatis and Zaccolo 2014; Maurice et al. 2014).

13.4 PKA

PKA is the primary cAMP downstream effector. It is ubiquitously present in mammalian cell. This kinase functions both in the cytoplasm and in the nucleus to regulate a broad range of biological activities, including contractility, differentiation, proliferation, and metabolism of VSMCs. PKA is a tetramer containing two regulatory domains and two catalytic domains. The catalytic subunit contains a small NH_2-terminal lobe (N-lobe), a short linker, and a larger carboxy-terminal lobe (C-lobe) that possesses much of the catalytic machinery and the major substrate docking sites. In addition, the catalytic subunit is flanked by an NH_2-terminal tail (N-tail) and a COOH-terminal tail (C-tail). The regulatory subunit of PKA contains a dimerization and AKAP-docking domain (D/D domain), a linker region with an inhibitor site in the middle and followed by two cAMP-binding domains, CBD-A and CBD-B. In the absence of cAMP, the dimer of the regulatory subunits is bound to the catalytic subunits, and the inhibitor sites of the regulatory subunits dock to the active site clefts of the catalytic subunits and the carboxy-terminal segments of the linkers (C-linkers), whereas the remaining portion of the linkers is involved in defining the quaternary structure of the holoenzyme. When each of the four CBDs of the regulatory subunits is bound to a cAMP molecule, the catalytic subunits are dissociated from the regulatory subunits, resulting in the activation of PKA (Taylor et al. 2012; Boras et al. 2014).

PKA exists as four isoforms of regulatory subunits (RIα, RIβ, RIIα, RIIβ) and three isoforms of catalytic subunits (Cα, Cβ, Cγ). It is generally believed that the catalytic subunits associate freely with the dimers of all the R subunits. There is evidence indicating that PKA-I ($RI\alpha_2C_2$ and $RI\beta_2C_2$) and PKA-II ($RII\alpha_2C_2$ and $RII\beta_2C_2$) holoenzymes have distinct biochemical properties. RIβ-containing holoenzymes are more sensitive to cAMP than are RIα-containing holoenzymes. PKA-Is are more readily dissociated by cAMP than PKA-IIs. Also, the affinity of RI for the type 1 dual-specific A-kinase-anchoring protein (D-AKAP1, a scaffold protein wherein it binds PKA and other signaling proteins and physically tether these multi-protein complexes to specific cellular locations) is two orders of magnitude lower than that of RII. The significance of these variants for vascular contractility remains to be explored (Skalhegg and Tasken 2000).

The activation of PKA may cause vasodilatation through the decrease in the intracellular Ca^{2+} concentration ($[Ca^{2+}]_i$). In rat mesenteric artery, the relaxation

by adrenomedullin is associated with an elevated cAMP level. The vasorelaxant effect is diminished by the inhibition of AC, PKA, and the large-conductance, Ca^{2+}-activated K^+ (BK_{Ca}) channels (Ross and Yallampalli 2006). PKA can also activate ATP-sensitive K^+ (K_{ATP}) channel and two-pore domain acid-sensitive K^+ channel-1 (TASK-1) in VSMCs (Olschewski et al. 2006; Yang et al. 2008; Ford et al. 2011; Foster and Coetzee 2016). The activation of K^+ channels leads to membrane hyperpolarization, resulting in reduced Ca^{2+} influx through voltage-dependent Ca^{2+} channels and consequently vasodilatation. A decrease in $[Ca^{2+}]_i$ may also result from an increased activity of sarco-/endoplasmic reticulum Ca^{2+}-ATPase (SERCA). The activity of SERCA is suppressed by phospholamban (PLB), a protein localized in the sarcoplasmic reticulum (SR). The inhibitory effect of PLB is diminished by the phosphorylation of PLB at Ser-16. In feline aorta the relaxant responses by forskolin (an AC stimulator) and 8-Br-cAMP (a cAMP analog) are accompanied by increased phosphorylation of PLB at Ser-16. The relaxation to forskolin and 8-Br-cAMP is attenuated by the inhibition of SERCA activity. Furthermore, the relaxation to forskolin is attenuated by the inhibition of PKA. Hence, PKA may cause vasodilatation by enhancing the sequestration of cytosolic Ca^{2+} ion resulting from the relief of the inhibitory action of PLB on SERCA (Mundiña-Weilenmann et al. 2000).

In addition to reduction in $[Ca^{2+}]_i$, PKA may cause vasodilatation through a decrease in the Ca^{2+} sensitivity of myofilaments, due to increased dephosphorylation of myosin light chain (MLC) by MLC phosphatase (MLCP). The activity of MLCP can be stimulated by PKA through the phosphorylation of myosin phosphatase target subunit 1 (MYPT1, the regulatory subunit of MLCP) at Ser-695 and Ser-852 (human sequence). In contrast to the stimulatory effect of PKA, MLCP is inhibited by Rho kinase (ROCK) through the phosphorylation of MYPT1 at Thr-696 and Thr-853. These two residues are immediately adjacent to Ser-695 and Ser-852, respectively. The phosphorylation of Ser-695 and Ser-852 by PKA would prevent the phosphorylation of Thr-696 and Thr-853 by ROCK, and vice versa (Wooldridge et al. 2004; Grassie et al. 2012). The effect of ROCK can also be disrupted by PKA through phosphorylation of RhoA at Ser188, which leads to an increased extraction of RhoA from membranes to cytosol by GDP dissociation inhibitor (RhoGDI) and results in reduced activation of ROCK by RhoA, thus reduced inhibition of MLCP, increased MLC dephosphorylation, and vasodilatation (Loirand et al. 2006).

13.5 Epac

Epac is an intracellular sensor for cAMP. It functions as a nucleotide exchange factors for the Rap subfamily of RAS-like small GTPases. The mammalian Epac protein family comprises two members, Epac1 and Epac2, with Epac2 having 3 isoforms that resulted from alternative splicing and differential gene promoters,

namely, Epac2A, Epac2B, and the liver-specific variant Epac2C. Epac1 is richly expressed in VSMCs, whereas Epac2 has only been found at the mRNA level in rat mesenteric arterial SMCs with 200-fold less abundancy than Epac1. Epac1 is expressed in human umbilical vein endothelial cells. Epac proteins consist of an NH_2-terminal regulatory domain and a COOH-terminal catalytic domain. The regulatory domain contains the disheveled/Egl-10/pleckstrin (DEP) domain, responsible for plasma membrane targeting of cAMP-bound Epacs, and the cAMP nucleotide-binding (CNB)-B domain. Epac2A contains a further CNB domain named CNB-A, whereas Epac2C lacks the DEP domain. The catalytic domain contains the Ras-exchange motif (REM) domain that is responsible for the GDP-GTP exchange, the Ras-association (RA) domain that targets Epac1 to the nuclear envelope and Epac2 to the plasma membrane, and the cell division cycle 25 homology domain (CDC25HD) that promotes the exchange of GDP for GTP on Rap (Schmidt et al. 2013; Roberts and Dart 2014).

In the absence of cAMP, Epacs are kept in an auto-inhibitory conformation, in which the regulatory domain folds on top of the catalytic domain, blocking the active site. The binding of cAMP to the CNB-B domain (K_d 2.8 μM) triggers a conformational change causing the regulatory domain to move away from catalytic domain so that the small GTPases Rap proteins can bind to the catalytic domain to be activated to mediate certain cAMP functions. Meanwhile a lipid-binding motif within the regulatory domain is exposed, allowing the proper targeting of Epacs to the plasma membrane (Schmidt et al. 2013; Roberts and Dart 2014).

In α-toxin-permeabilized rabbit pulmonary artery, an Epac-selective cAMP analog 8-pCPT-2′-O-Me-cAMP (8-pCPT-AM) markedly reduces U46619-induced contraction, associated with a decrease in U46619-induced RhoA activity, the phosphorylation of myosin phosphatase target subunit 1 (MYPT1, the regulatory subunit of myosin light chain phosphatase (MLCP)) at Thr-696 and Thr-853, and the phosphorylation of the regulatory myosin light chain (MLC). These effects are insensitive to the inhibition of PKA. The increased Rap1-GTP of rat aortic SMCs by 8-pCPT-AM is not affected by the inhibition of PKA. Moreover, RhoA activity is reduced by 8-pCPT-AM in wide type but not in Rap1B null fibroblasts. These results suggest that cAMP-mediated activation of Epac may lead to a PKA-independent, Ras-related protein 1 (Rap1)-dependent vasodilatation through the inhibition of RhoA activity, enhancement of MLCP activity, and a fall in MLC phosphorylation (Zieba et al. 2011). In rat mesenteric arteries, the relaxation induced by 8-pCPT-AM is suppressed by iberiotoxin, a selective inhibitor of BK_{Ca} channels. 8-pCPT-AM also increases both the frequency and amplitude of spontaneous transient outward currents (STOCs) in isolated mesenteric myocytes in a manner sensitive to iberiotoxin and to ryanodine. In addition, current clamp recordings show that 8-pCPT-AM causes an iberiotoxin-inhibitable hyperpolarization of isolated myocytes. These data suggest that the activation of Epac by cAMP may cause vasodilatation through membrane hyperpolarization and that the hyperpolarization results from the activation of BK_{Ca} due to a Epac-induced increase in localized Ca^{2+} release from ryanodine receptors of

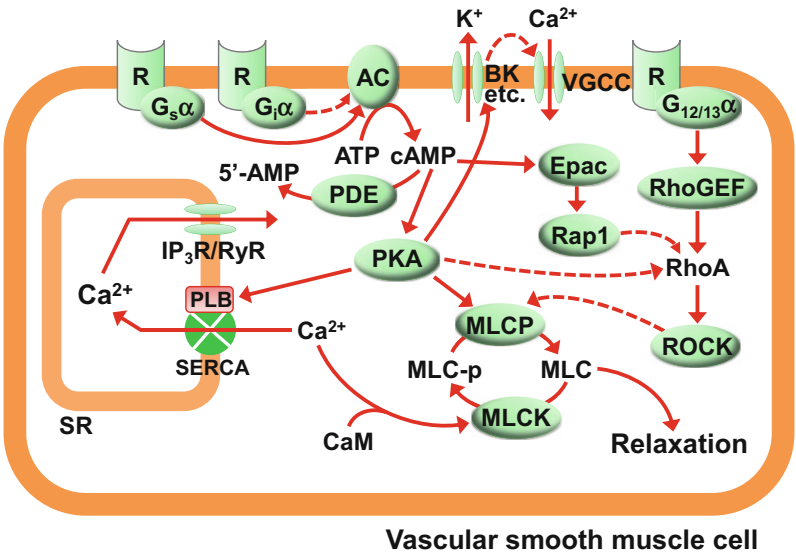

Fig. 13.1 Mechanism underlying cAMP-mediated vasodilatation. cAMP is synthesized by adenylyl cyclase (AC) from ATP. AC is stimulated by $G_s\alpha$ protein but inhibited by $G_i\alpha$ protein. Both $G_s\alpha$ and $G_i\alpha$ proteins are activated upon the binding of agonists to their respective receptors (R). cAMP exerts its action mainly through cAMP-dependent protein kinase (PKA). PKA may reduce the intracellular Ca^{2+} levels by stimulating K^+ channels such as the large-conductance Ca^{2+}-activated K^+ (BK_{Ca}) channels, which leads to membrane hyperpolarization and thus reduced Ca^{2+} influx through the voltage-gated calcium channels (VGCC). PKA also stimulates the sequestration of cytosolic Ca^{2+} into sarcoplasmic reticulum (SR) by the sarco-/endoplasmic reticulum Ca^{2+} ATPase (SERCA) through the phosphorylation of phospholamban (PLB). Since the contraction of vascular smooth muscle (VSM) is caused by Ca^{2+}/calmodulin (CaM)-dependent activation of myosin light chain kinase (MLCK) followed by increased phosphorylation of myosin light chain (MLC-p), a decreased Ca^{2+} level leads to reduced vasocontractility. PKA also causes a decreased Ca^{2+} sensitivity of myofilaments, which results from the stimulatory effect of PKA on myosin light chain (MLC) phosphatase (MLCP). An increased MLCP activity leads to enhanced dephosphorylation of MLC-p and consequently relaxation of VSM. Rho kinase (ROCK) has an inhibitory effect on MLCP. PKA can counteract this effect by the phosphorylation of the regulatory subunit of MLCP (not shown). PKA also attenuates ROCK activity by inhibiting RhoA activity, which is activated by $G_{12/13}\alpha$ protein through Rho guanine nucleotide exchange factor (RhoGEF) when a vasoconstrictor is bound to its receptor. cAMP can also promote relaxation of VSM in a PKA-independent manner by binding to a protein named the exchange protein directly activated by cAMP (Epac). The cAMP-bound Epac inhibits RhoA activity through Ras-related protein 1 (Rap1).). cAMP is hydrolyzed to vasoinactive 5′-AMP by phosphodiesterase (PDE), mainly the cAMP-specific PDE. *IP_3R* inositol 1,4,5-trisphosphate receptor, *RyR* ryanodine receptor. The *solid line arrow*: stimulatory. The *dotted line arrows*: inhibitory

sarcoplasmic reticulum (Roberts et al. 2013) (Fig. 13.1). The activation of Epac by cAMP has also been found to cause vasodilatation through hyperpolarization of VSMCs resulting from the activation of small- and intermediate-conductance Ca^{2+}-activated K^+ channels of the endothelium as well as the activation of endothelial nitric oxide synthase (eNOS) (Roberts et al. 2013).

13.6 CNG Channels

CNG channels are nonselective cation channels that are opened by direct binding of cAMP or cGMP. These channels allow physiological Na^+ and K^+ to pass through without discrimination between them. CNG channels are also permeable to Ca^{2+}, with a relative ion permeability P_{Ca}/P_{Na} ranging from 6.5 to 22. However, Ca^{2+} at high concentrations blocks the monovalent permeation, and the effect is more pronounced at negative potential, peaking at −40 mV. CNG channels are tetramers. Each subunit consists of six membrane-spanning segments, termed S1–S6. A pore region is located between S5 and S6 segments. Both the NH2- and the COOH-termini of CNG channels are intracellular. In the COOH-terminus there resides the cyclic nucleotide-binding domain (CNBD). Upon the binding of cAMP/cGMP to the CNBD, a sequence of allosteric transitions occurs leading to the opening of the ion-conducting pore. The occupation of all four CNBDs of the tetramer by cyclic nucleotides is required for the CNG channel to fully open (Kaupp and Seifert 2002; Wong and Yao 2008; Biel 2009; Gofman et al. 2014).

Mammalian CNGs are classified into two types of subunits, the A subunits (CNGA1-4) and the B subunits (CNGB1 and CNGB3). While the A subunits (except CNGA4) can form functional homotetrameric channels, the A4 and B subunits do not give rise to functional channels when expressed alone and are regarded as modulatory subunits. When coexpressed with CNGA1-3, they form a functional heterotetrameric channel with unique properties (e.g., single channel flickering, increased sensitivity for cAMP) that are characteristic of native CNG channels. CNG channels have long been known expressed in retinal photoreceptors and olfactory neurons and play a critical role in visual and olfactory signal transduction. They are also present at low density in some other tissues such as the brain, testis, and kidney. In the vasculature CNG, A1–A4 and B1 are found to be expressed in various vascular beds of different species (Wong and Yao 2008; Biel 2009).

In mouse aorta the endothelium-dependent relaxation induced by β-adrenoceptor agonist isoproterenol, which elevates cAMP, is reduced by the inhibitors of CNGs. The Ca^{2+} rise of the aortic endothelial cells is also suppressed by the CNG inhibitor. In primary cultured bovine aortic endothelial cells (ECs) and H5V ECs, the cAMP-activated cation current is diminished by the inhibitors of CNGs. The cation current is also markedly reduced by a CNGA2-specific siRNA in H5V ECs. These results suggest that the activation of CNG channels, CNGA2 in particular, mediates β-adrenoceptor agonist-induced endothelial Ca^{2+} influx, which may subsequently activate eNOS and cause a nitric oxide-dependent vasodilatation (Shen et al. 2008; Wong and Yao 2008). Similar phenomenon has also been found when CNG channels are activated by adenosine- and ATP-stimulated cAMP elevation (Cheng et al. 2008; Kwan et al. 2010).

References

Ahmad F, Degerman E, Manganiello VC (2012) Cyclic nucleotide phosphodiesterase 3 signaling complexes. Horm Metab Res 44:776–785

Bender AT, Beavo JA (2006) Cyclic nucleotide phosphodiesterases: molecular regulation to clinical use. Pharmacol Rev 58:488–520

Biel M (2009 Apr 3) Cyclic nucleotide-regulated cation channels. J Biol Chem 284 (14):9017–9021

Bobin P, Belacel-Ouari M, Bedioune I, Zhang L, Leroy J, Leblais V, Fischmeister R, Vandecasteele G (2016) Cyclic nucleotide phosphodiesterases in heart and vessels: a therapeutic perspective. Arch Cardiovasc Dis 109:431–443

Boras BW, Kornev A, Taylor SS, McCulloch AD (2014) Using Markov state models to develop a mechanistic understanding of protein kinase A regulatory subunit RIα activation in response to cAMP binding. J Biol Chem 289:30040–30051

Cheng KT, Leung YK, Shen B, Kwok YC, Wong CO, Kwan HY, Man YB, Ma X, Huang Y, Yao X (2008) CNGA2 channels mediate adenosine adenosine-induced Ca 2+ influx in vascular endothelial cells. Arterioscler Thromb Vasc Biol 28:913–918

Ford CA, Mahajan P, Tabrizchi R (2011) Characterization of β-adrenoceptor-mediated relaxation signals in isolated pulmonary artery of Dahl salt-sensitive hypertensive and normotensive rats. Auton Autacoid Pharmacol 31:1–12

Foster MN, Coetzee WA (2016) K_{ATP} channels in the cardiovascular system. Physiol Rev 96:177–252

Francis SH, Blount MA, Corbin JD (2011) Mammalian cyclic nucleotide phosphodiesterases: molecular mechanisms and physiological functions. Physiol Rev 91:651–690

Gao Y, Tolsa J-F, Shen H, Raj JU (1998) Effect of selective phosphodiesterase inhibitors on the responses of ovine pulmonary veins to prostaglandin E_2. J Appl Physiol 84:13–18

Gofman Y, Schärfe C, Marks DS, Haliloglu T, Ben-Tal N (2014) Structure, dynamics and implied gating mechanism of a human cyclic nucleotide-gated channel. PLoS Comput Biol 10: e1003976

Grassie ME, Sutherland C, Ulke-Lemée A, Chappellaz M, Kiss E, Walsh MP, MacDonald JA (2012) Cross-talk between Rho-associated kinase and cyclic nucleotide-dependent kinase signaling pathways in the regulation of smooth muscle myosin light chain phosphatase. J Biol Chem 287:36356–36369

Halls ML, Cooper DM (2011) Regulation by Ca^{2+}-signaling pathways of adenylyl cyclases. Cold Spring Harb Perspect Biol 3:a004143

Hurley JH (1999) Structure, mechanism, and regulation of mammalian adenylyl cyclase. J Biol Chem 274:7599–7602

Jourdan KB, Mason NA, Long L, Philips PG, Wilkins MR, Morrell NW (2001) Characterization of adenylyl cyclase isoforms in rat peripheral pulmonary arteries. Am J Physiol Lung Cell Mol Physiol 280:L1359–L1369

Kaupp UB, Seifert R (2002) Cyclic nucleotide-gated ion channels. Physiol Rev 82:769–824

Keravis T, Lugnier C (2012) Cyclic nucleotide phosphodiesterase (PDE) isozymes as targets of the intracellular signalling network: benefits of PDE inhibitors in various diseases and perspectives for future therapeutic developments. Br J Pharmacol 165:1288–1305

Kwan HY, Cheng KT, Ma Y, Huang Y, Tang NL, Yu S, Yao X (2010) CNGA2 contributes to ATP-induced noncapacitative Ca2+ influx in vascular endothelial cells. J Vasc Res 47:148–156

Lefkimmiatis K, Zaccolo M (2014) cAMP signaling in subcellular compartments. Pharmacol Ther 143:295–304

Lezoualc'h F, Fazal L, Laudette M, Conte C (2016) Cyclic AMP sensor EPAC proteins and their role in cardiovascular function and disease. Circ Res 118:881–897

Linder JU (2006) Class III adenylyl cyclases: molecular mechanisms of catalysis and regulation. Cell Mol Life Sci 63:1736–1751

Loirand G, Guilluy C, Pacaud P (2006) Regulation of rho proteins by phosphorylation in the cardiovascular system. Trends Cardiovasc Med 16:199–204

Maurice DH, Ke H, Ahmad F, Wang Y, Chung J, Manganiello VC (2014) Advances in targeting cyclic nucleotide phosphodiesterases. Nat Rev Drug Discov 13:290–314

Mundiña-Weilenmann C, Vittone L, Rinaldi G, Said M, de Cingolani GC, Mattiazzi A (2000) Endoplasmic reticulum contribution to the relaxant effect of cGMP- and cAMP-elevating agents in feline aorta. Am J Physiol Heart Circ Physiol 278:H1856–H1865

Nelson CP, Rainbow RD, Brignell JL, Perry MD, Willets JM, Davies NW, Standen NB, Challiss RA (2011) Principal role of adenylyl cyclase 6 in K^+ channel regulation and vasodilator signalling in vascular smooth muscle cells. Cardiovasc Res 91:694–702

Olschewski A, Li Y, Tang B, Hanze J, Eul B, Bohle RM, Wilhelm J, Morty RE, Brau ME, Weir EK, Kwapiszewska G, Klepetko W, Seeger W, Olschewski H (2006) Impact of TASK-1 in human pulmonary artery smooth muscle cells. Circ Res 98:1072–1080

Roberts OL, Dart C (2014) cAMP signalling in the vasculature: the role of Epac (exchange protein directly activated by cAMP). Biochem Soc Trans 42:89–97

Roberts OL, Kamishima T, Barrett-Jolley R, Quayle JM, Dart C (2013) Exchange protein activated by cAMP (Epac) induces vascular relaxation by activating Ca^{2+}-sensitive K^+ channels in rat mesenteric artery. J Physiol 591:5107–5123

Ross GR, Yallampalli C (2006) Endothelium-independent relaxation by adrenomedullin in pregnant rat mesenteric artery: role of cAMP-dependent protein kinase A and calcium-activated potassium channels. J Pharmacol Exp Ther 317:1269–1275

Sassone-Corsi P (2012) The cyclic AMP pathway. Cold Spring Harb Perspect Biol 4. pii:a011148

Schmid A, Meili D, Salathe M (2014) Soluble adenylyl cyclase in health and disease. Biochim Biophys Acta 1842:2584–2592

Schmidt M, Dekker FJ, Maarsingh H (2013) Exchange protein directly activated by cAMP (epac): a multidomain cAMP mediator in the regulation of diverse biological functions. Pharmacol Rev 65:670–709

Shen B, Cheng KT, Leung YK, Kwok YC, Kwan HY, Wong CO, Chen ZY, Huang Y, Yao X (2008) Epinephrine-induced Ca^{2+} influx in vascular endothelial cells is mediated by CNGA2 channels. J Mol Cell Cardiol 45:437–445

Skalhegg BS, Tasken K (2000) Specificity in the cAMP/PKA signaling pathway. Differential expression, regulation, and subcellular localization of subunits of PKA. Front Biosci 5:D678–D693

Steegborn C (2014) Structure, mechanism, and regulation of soluble adenylyl cyclases - similarities and differences to transmembrane adenylyl cyclases. Biochim Biophys Acta 1842:2535–2547

Sutherland EW, Rall TW (1958) Fractionation and characterization of a cyclic adenine ribonucleotide formed by tissue particles. J Biol Chem 232:1077–1091

Taylor SS, Ilouz R, Zhang P, Kornev AP (2012) Assembly of allosteric macromolecular switches: lessons from PKA. Nat Rev Mol Cell Biol 13:646–658

Valsecchi F, Ramos-Espiritu LS, Buck J, Levin LR, Manfredi G (2013) cAMP and mitochondria. Physiology (Bethesda) 28:199–209

Wong CO, Yao X (2008) Cyclic nucleotide-gated channels: a familiar channel family with a new function? Futur Cardiol 4:505–515

Wooldridge AA, MacDonald JA, Erdodi F, Ma C, Borman MA, Hartshorne DJ, Haystead TA (2004) Smooth muscle phosphatase is regulated in vivo by exclusion of phosphorylation of threonine 696 of MYPT1 by phosphorylation of Serine 695 in response to cyclic nucleotides. J Biol Chem 279:34496–34504

Xin W, Feinstein WP, Britain AL, Ochoa CD, Zhu B, Richter W, Leavesley SJ, Rich TC (2015) Estimating the magnitude of near-membrane PDE4 activity in living cells. Am J Physiol Cell Physiol 309:C415–C424

Yang Y, Shi Y, Guo S, Zhang S, Cui N, Shi W, Zhu D, Jiang C (2008) PKA-dependent activation of the vascular smooth muscle isoform of KATP channels by vasoactive intestinal polypeptide

and its effect on relaxation of the mesenteric resistance artery. Biochim Biophys Acta 1778:88–96

Zhai K, Hubert F, Nicolas V, Ji G, Fischmeister R, Leblais V (2012) β-Adrenergic cAMP signals are predominantly regulated by phosphodiesterase type 4 in cultured adult rat aortic smooth muscle cells. PLoS One 7:e47826

Zieba BJ, Artamonov MV, Jin L, Momotani K, Ho R, Franke AS, Neppl RL, Stevenson AS, Khromov AS, Chrzanowska-Wodnicka M, Somlyo AV (2011) The cAMP-responsive Rap1 guanine nucleotide exchange factor, Epac, induces smooth muscle relaxation by down-regulation of RhoA activity. J Biol Chem 286:16681–16692

Chapter 14
Cyclic GMP Signaling

Abstract Guanosine 3′5′ cyclic monophosphate (cGMP) is synthesized by soluble guanylyl cyclase (sGC) when vascular smooth muscle is stimulated with nitric oxide (NO) and nitrovasodilators and by particulate guanylate cyclases (pGC) when stimulated with natriuretic peptides. The intracellular cGMP levels are determined by the balance of the synthesis of this cyclic nucleotide by sGC and pGC and its hydrolysis mainly by the type 5 phosphodiesterase. cGMP exerts its action predominantly through the activation of cGMP-dependent protein kinase (PKG) resulting in reduced cytosolic Ca^{2+} and decreased Ca^{2+} sensitivity of the myofilaments and consequently vasodilatation. In these processes the activation of the large-conductance Ca^{2+}-activated K^+ channel, phosphorylation of IP_3R-associated cGMP kinase substrate, phosphorylation of myosin phosphatase target subunit 1, and counteraction on Rho A/Rho kinase activity may serve as the major mechanisms for the cGMP/PKG signaling.

Keywords Soluble guanylyl cyclase • Particulate guanylate cyclases • cGMP • cIMP • Phosphodiesterase • PKG • IRAG • MLCP • MYPT1 • ROCK

14.1 Introduction

Guanosine 3′5′ cyclic monophosphate (cGMP) was synthesized by Smith et al. in 1960 (Smith et al. 1961), and soon the existence of endogenously produced cGMP was identified in rat urine (Ashman et al. 1963). In late 1970s Murad and colleagues (Kots et al. 2009) and Ignarro and colleagues (Ignarro 1989) separately showed that nitric oxide (NO) stimulated the production of cGMP by activating soluble guanylyl cyclase (sGC). In 1980 Furchgott and Zawadzki found that a diffusible substance is released from the endothelium to cause vasodilatation. The substance was named endothelium-derived relaxing factor (EDRF) (Furchgott and Zawadzki 1980). Seven years late Moncada and colleagues demonstrated that NO is EDRF (Palmer et al. 1987). Since then overwhelming evidence shows that cGMP is the primary secondary messenger mediating a broad range of biological actions including vasodilatation caused by NO and nitrovasodilators (Gao 2010; Vanhoutte et al. 2016).

Y. Gao, *Biology of Vascular Smooth Muscle: Vasoconstriction and Dilatation*,
DOI 10.1007/978-981-10-4810-4_14

In addition to sGC, the activity of guanylyl cyclase was also found in the particulate fraction of various tissue homogenates. This type of enzyme is associated with plasma membrane and termed particulate guanylyl cyclase (pGC) (Hardman and Sutherland 1969; Kuhn 2016). First report on specific stimulation of pGC was obtained in the intestinal tissue by stable toxin of *Escherichia coli* (Hughes et al. 1978). In 1981 De Bold et al. found a natriuretic factor is generated by rat cardiac atria (De Bold et al. 1981). This natriuretic factor was soon known to be an endogenous pGC activator. It is released from atrial-specific granules and secreted into the circulation in response to acute or chronic atrial stretch (Kuhn 2016). It is now well established that cGMP synthesized by both sGC and pGC exerts their actions primarily by activating cGMP-dependent protein kinase (PKG). In vascular smooth muscle, the cGMP-PKG signaling represents a predominant mechanism in the regulation of vasoactivity, in particular vasodilatation (Francis et al. 2010; Gao 2010; Hofmann and Wegener 2013; Vanhoutte et al. 2016).

14.2 sGC

sGC is a ~150 kDa heterodimer existing in two isoforms, α1/β1 and α2/β1. A β2-subunit is identified by homology screening, but it seems to be a pseudogene. The α1/β1 dimer is present in most tissues, whereas the α2/β1 dimer is only found in limited tissues such as the brain, placenta, spleen, and uterus (Budworth et al. 1999). Studies with α1- or α2-subunit knockout mice demonstrate that the α1/β1 isoform represents greater than 90% of sGC activity in the aorta and is the sole sGC dimer in platelets. The α1/β1 and α2/β1 isoforms are equally expressed in the brain (Mergia et al. 2006).

The subunit of sGC, either α or β, is comprised of an NH_2-terminal heme nitric oxide/oxygen (HNOX)-binding domain, a PAS-like (named after the first three proteins in which it was found: period clock protein, ARNT protein, and single minded protein) domain, a coiled-coil domain, and a COOH-terminal catalytic domain. The HNOX domain of the β-subunit contains a prosthetic heme group. In its ferrous form, this heme moiety is the target of NO. Binding of NO leads to the break of the heme from His-105 of the HNOX domain and a conformational change, which is propagated to catalytic domain, resulting in the conversion of GTP to cGMP and a by-product pyrophosphate. Evidence suggests that stoichiometric binding of NO to the heme only leads to partial enzyme activation. The binding of additional NO, either at the heme iron or at a cysteine residue, results in the full activation of the enzyme leading to a 100- to 200-fold increase in sGC activity. The α-subunit does not contain the heme moiety because of the lack of heme-anchoring amino acids. The PAS domain is involved in the heterodimer formation and may have a role in signal propagation from the HNOX domain to the catalytic domain. The catalytic active site of sGC is located at the subunit interface comprising residues from the α- and β-subunits. The α1/β1 heterodimer also contains a proposed pseudosymmetric site, which may act as an allosteric

nucleotide-binding site to communicate with the catalytic nucleotide-binding site. ATP at physiological concentration is inhibitory on sGC via the binding to the pseudosymmetric site (Derbyshire and Marletta 2012; Montfort et al. 2017).

Mice deficient for the β1-subunit of sGC, which resulted in complete loss of the enzyme activity, show a pronounced increase in blood pressure and loss of NO-dependent vasodilatation, indicating a dominant role for sGC in NO-induced vascular response (Friebe et al. 2007; Friebe and Koesling 2009; Potter 2011). It is estimated that sGC is activated in vivo by NO at concentrations ~0.1–5 nM when the heme of sGC in the ferrous state (Hall and Garthwaite 2009). Under oxidative stress the heme may be oxidized to the ferric state rendering the enzyme unresponsible to NO. Moreover, the ferric heme is readily to be dissociated from the apoenzyme. The newly developed NO- and heme-independent sGC activators BAY 58-2667 (cinaciguat) and HMR1766 (ataciguat) are capable of selectively activating the oxidized/heme-free enzyme via binding to the enzyme's heme pocket, causing pronounced vasodilatation. The drugs selectively target a modified state of sGC that is prevalent under disease conditions such as systemic and pulmonary hypertension, heart failure, atherosclerosis, and peripheral arterial occlusive disease (PAOD). HMR1766 is currently in clinical development as an oral therapy for patients with PAOD (Schmidt et al. 2009; Follmann et al. 2013). The activity of sGC is also modulated by intracellular redox status through affecting dynamic equilibrium between the dimeric and monomeric status of sGC. The reductive environment promotes the monomerization of sGC, while oxidative environment facilitates the dimerization of the enzyme. Since the dimer is catalytic active, whereas the monomer is not, the activity of sGC is affected by the encountered redox environments. In porcine coronary and pulmonary arteries, the changes in the dimeric status of sGC in response to reductants and oxidants have been found to be closely related to changes in the intracellular cGMP levels and vasodilatation to NO. Interestingly, hypoxia increases the dimer level and activity of sGC in porcine coronary arteries but reduces the dimer level and activity of sGC in pulmonary arteries (Zheng et al. 2011; Ye et al. 2013). It appears that the different effects of hypoxia on the dimeric status of sGC result from the opposite changes in redox environments occurred between the two vessel types (Dou et al. 2013).

It is widely believed that cGMP is the sole second messenger generated by sGC. However, the possibility that other nucleoside 3′5′ cyclic monophosphates (cNMPs) can also be synthesized by sGC was raised by Garbers et al. in the 1970s (Garbers et al. 1975). Recently, using highly sensitive and selective high-performance liquid chromatography-tandem mass spectrometry technique, Seifert and colleagues (Beste et al. 2012) found that purified recombinant rat sGC synthesized six different cNMPs including cGMP and inosine 3′,5′-cyclic monophosphate (cIMP). Subsequently, an increased production of cIMP in porcine coronary artery has been found under hypoxia when sGC is activated by NO. Moreover, cIMP may mediate the augmented vasoconstriction caused by hypoxia via the activation of Rho kinase (ROCK) (Chen et al. 2014). cIMP is generated from inosine 5′-triphosphate (ITP), which is predominantly derived from ATP deamination. Under normal conditions, ITP is mostly degraded by inosine

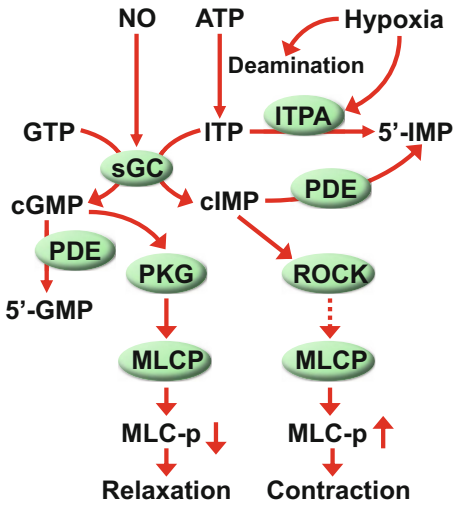

Fig. 14.1 Effect of hypoxia on soluble guanylyl cyclase (sGC)-mediated vascular response. Under normoxic conditions guanosine-5′-triphosphate (GTP) is converted to guanosine 3′5′ cyclic monophosphate (cGMP) when sGC is stimulated by nitric oxide (NO), which activates cGMP-dependent protein kinase (PKG), followed by increased activity of myosin light chain phosphatase (MLCP), decreased phosphorylated regulatory myosin light chain (MLC-p), and relaxation of vascular smooth muscle (VSM). cGMP is hydrolyzed by phosphodiesterase (PDE) to vaso-inactive 5′-GMP. The intracellular inosine 5′-triphosphate (ITP) is mainly derived from the deamination of ATP. Under normoxia ITP is largely degraded to vaso-inactive inosine 5′-monophosphate (5′-IMP) by inosine triphosphatase (ITPA). Under hypoxia ATP deamination is stimulated and/or ITPA is inhibited, resulting in elevated ITP. When sGC is stimulated by NO, ITP is converted to cIMP. cIMP may activate Rho kinase (ROCK), resulting in a reduced activity of MLCP, thus increasing MLC-p and contraction of VSM. cIMP is hydrolyzed by phosphodiesterase (PDE). *Solid line arrows*: activation. *Dotted line arrows*: inhibition

triphosphatase (ITPA) (Sakumi et al. 2010). It is possible that an increased ITP level under hypoxia, resulted from an increased ATP deamination and/or suppressed ITPA activity, promotes the generation of cIMP (Gao 2016; Leung et al. 2016) (Fig. 14.1). In addition to hypoxia, thymoquinone, a biologically active constituent of *Nigella sativa*, has been found to stimulate cIMP production by sGC in isolated porcine coronary arteries, rat aorta, and mesenteric arteries, which is associated with augmentation of vasocontraction (Detremmerie et al. 2016).

14.3 pGCs

The pGCs are transmembrane guanylyl cyclases. Mammalian genome encodes seven pGCs, GC-A to GC-G, which mainly modulate submembrane cGMP microdomains (Piggott et al. 2006). GC-A is activated by A-type natriuretic peptide

(ANP) and B-type natriuretic peptide (BNP) to regulate arterial blood pressure/volume and energy balance. GC-B is stimulated by C-type natriuretic peptide (CNP) and is involved in endochondral ossification. The GC-C is related to the intestinal ion transport and epithelial turnover, whereas GC-E and GC-F are expressed in photoreceptor cells of the retina and their activities are essential for phototransduction. The GC-D and GC-G are pseudogenes in humans. They are involved in olfactory signaling in the rodent (Potter 2011; Kuhn 2016; Sharma et al. 2016).

The pGCs are homodimers, comprising an extracellular ligand-binding domain, a short transmembrane region, and an intracellular COOH-terminal region consisting of a juxtamembranous protein kinase-homology domain (KHD) and a cGMP-synthesizing cyclase domain. These domains are separated by an amphipathic α-helical region that is involved in homodimerization, which is essential for the catalytic activity of pGC. The function of the KHD is not well understood. Its deletion results in a poorly and constitutively active GC-A and renders the receptor unresponsive to ANP. It also participates in the direct interactions of the pGCs with other intracellular proteins such as heat-shock protein 90 (Hsp90), which stabilizes GC-A (Potter 2011; Kuhn 2016; Sharma et al. 2016).

GC-A is richly expressed in vascular smooth muscle cells (VSMCs) and in even higher density in endothelial cells (ECs). SMC-restricted deletion of GC-A in mice eliminates the direct vasodilating effect of ANP. GC-B is abundantly expressed in the heart and at relatively high levels in VSMCs. Within the cardiovascular system, CNP is mainly released from ECs. It is more potent to relax veins than arteries. In contrast, ANP is more potent to relax arteries than veins. The selective disruption of endothelial CNP in mice leads to endothelial dysfunction, hypertension, atherogenesis, and aneurysm (Tolsa et al. 2002; Moyes et al. 2014; Kuhn 2016).

In addition to activate GC-A and GC-B, the natriuretic peptides bind with high affinity to a second receptor, natriuretic peptide receptor-C (NPR-C), with the selectivity ANP > CNP > BNP. NPR-C has a short cytoplasmic domain without guanylyl cyclase activity. NPR-C is expressed in both VSMCs and ECs (Maack 1992). In mice with the NPR-C gene (Npr3) being inactivated the half-life of circulating ANP is two-thirds longer than in the wild type, indicating that NPR-C acts as a clearance receptor (Matsukawa et al. 1999). NPR-C is a homodimer. The intracellular region of each subunit comprises only 37 amino acids forming overlapping Gi/o-binding sequences. The binding of natriuretic peptides to NPR-C may affect vasoactivity via G-protein-linked signaling. A study shows that the administration of specially developed small-molecule agonists for NPR-C promotes relaxation of isolated resistance arteries and reduction in blood pressure in wild-type animals. This effect is diminished in mice lacking NPR-C (Moyes et al. 2014; Kuhn 2016).

14.4 cGMP-Hydrolyzing PDEs

In vasculature the intracellular cGMP is hydrolyzed mainly by the cGMP-binding cGMP-specific PDE known as the type 5 PDE (PDE5 or PDE5A). PDE5 is encoded by a single PDE5A gene which gives rise to three NH_2-terminal variants (PDE5A1, PDE5A2, and PDE5A3). The enzyme is a homodimer. Each monomer is sized ~100 kDa and contains two cGMP-activated PDE, adenylyl cyclase- and Fh1A-binding (GAF) domains (GAF-A and GAF-B domains) in the NH_2-terminal and a COOH-terminal catalytic domain. The GAF-A domain is an allosteric binding site of cGMP, whereas GAF-B has been shown to have a regulatory function and may have weak cGMP-binding activity. In the holoenzyme, binding of cGMP to GAF-A is low. The binding of cGMP to the catalytic site stimulates cGMP binding to GAF-A, leading to an increased affinity of the catalytic site for cGMP. Furthermore, when GAF-A is occupied by cGMP, PDE5 undergoes a conformational change that exposes Ser-102 for rapid phosphorylation by PKG, which in turn increases the affinity of GAF-A for cGMP as well as affinity of the catalytic site for cGMP (Bender and Beavo 2006; Francis et al. 2010; Azevedo et al. 2014).

PDE5 is generally considered to be a cytosolic protein. It is relatively highly expressed in smooth muscle and platelets. PDE5 exists in three isoforms, PDE5A1–PDE5A3. PDE5A1 and PDE5A2 are widely expressed, whereas PDE5A3 expression is restricted to smooth muscle (Bender and Beavo 2006; Azevedo et al. 2014; Maurice et al. 2014). Studies with PDE5 inhibitors have been very useful for elucidating the physiological functions of PDE5, and the most established function of PDE5A is as a regulator of vascular smooth muscle contraction through regulation of cGMP. In porcine coronary arteries, the cGMP-hydrolyzing activity of the vessels is largely eliminated by zaprinast, a PDE5 inhibitor. This is associated with a pronounced potentiation of vasodilatation to DETA NONOate, a NO donor (Liu et al. 2014). PDE5 is highly expressed in pulmonary vasculature (Sanchez et al. 1998; Corbin et al. 2005). Inhibition of PDE5 attenuates pulmonary vasoconstriction, and PDE5 inhibitors have shown to be effective for treatment of pulmonary hypertension (Francis et al. 2010).

In addition to PDE5, there are several other PDE isoforms that are capable of hydrolyzing cGMP, namely, PDE1, PDE2, and PDE3. PDE1 is characterized by the existence of two binding sites for CaM in their regulatory domains and, their catalytic activity is largely determined by cytosolic Ca^{2+} levels. PDE1 has three isoforms, PDE1A–PDE1C. PDE1A and PDE1B is more potent in hydrolyzing cGMP than cAMP, whereas PDE1C hydrolyzes both cyclic nucleotides with equal potency (Bender and Beavo 2006; Francis et al. 2010). In cultured rat aortic VSMCs, the activity of PDE1A1 is stimulated by angiotensin II (Ang II), and ANP-induced cGMP accumulation is reduced by Ang II, indicating that PDE1A1 is activated by vasoconstrictor-induced Ca^{2+} elevation and vasoconstrictor may counteract vasodilatation caused by ANP via enhanced cGMP hydrolysis. PDE1A1 activity is upregulated in nitrate-tolerant blood vessels. Such a mechanism

contributes to the diminished NO-/cGMP-mediated vasodilatation occurred in nitrate tolerance (Kim et al. 2001).

The regulatory region of PDE2 has two GAF domains, GAF-A and GAF-B. The binding of cGMP to GAF-B stimulates the enzyme activity. For this reason, PDE2 is known as cGMP-stimulated cGMP/cAMP PDE. PDE2 hydrolyzes cAMP and cGMP with equal potency (Bender and Beavo 2006; Francis et al. 2010). Studies show that PDE2 inhibition causes pulmonary vasodilatation and ameliorates pulmonary hypertension through the augmentation of cGMP and cAMP signaling (Bubb et al. 2014). PDE3 has two isoforms, PDE3A and PDE3B. The two isoforms have a high degree of amino acid identity (~80% for much of the catalytic region) and very similar kinetic properties. They also have similar affinities for cAMP and cGMP (K_m, 0.2 μM and 0.1 μM, respectively). However, the rate of cAMP hydrolysis is about tenfold of that of cAMP. Since cGMP can compete with and inhibit cAMP hydrolysis at the catalytic site, PDE3s are known as cGMP-inhibited cGMP PDEs (Bender and Beavo 2006; Francis et al. 2010; Keravis and Lugnier 2012). In newborn ovine pulmonary veins, the vasodilatation caused by PGE2 is potentiated by the elevated cGMP caused by endothelium-derived NO. It appears that the suppression cAMP hydrolysis resulted from the inhibition of PDE3 by cGMP is involved (Gao et al. 1998). Inhibition of PDE3 has also been found to enhance relaxant response of pulmonary arteries to prostacyclin in newborn lambs with persistent pulmonary hypertension (Lakshminrusimha et al. 2009).

14.5 PKG

PKG is a serine-/threonine-specific protein kinase that is specifically activated by cGMP. Two types of PKG have been identified in mammal, PKG I and PKG II. They are products of separate genes. The N-terminus (the first ~100 residues) of PKG I is encoded by two alternatively spliced exons resulting in two isoforms, Iα and Iβ. PKG I and PKG II have not been found coexisting in various cell types. PKG I is highly expressed in platelets, the smooth muscle, the lung, and some brain nuclei. PKG Iα predominates in the lung, heart, platelets, and cerebellum. Both type Iα and Iβ are highly expressed in smooth muscle. PKG II is mainly detected in the intestinal mucosa, kidney, chondrocytes, and brain. At the cell level, PKG I is predominantly cytosolic, although it is associated with membranes in some cell types such as platelets. PKG II is anchored to the plasma membrane by N-terminal myristoylation (Francis et al. 2010; Hofmann and Wegener 2013).

All PKGs are homodimers of identical chains arranged in parallel. The monomer of PKG Iα, PKG Iβ, and PKG II subunits are ~77 kDa, ~78 kDa, and ~87 kDa, respectively. They share common structural features. Each monomer is composed of a NH_2-terminal regulatory domain and a COOH-terminal catalytic domain. The regulatory domain includes a dimerization and localization domain provided by an

extended leucine zipper motif, an autoinhibitory domain, and two tandem allosteric CNB domains. The CNB-A shows a high affinity and CNB-B a low affinity for cGMP binding. The catalytic domain contains an Mg^{2+}-/ATP-binding domain and a substrate-binding domain. The leucine zipper motif at the NH_2-terminus of each PKG I monomer is related to homodimerization, selective interaction with particular proteins, and subcellular localization. In the absence of cGMP, the autoinhibitory domain directly contacts the catalytic site residues and suppressed the catalytic activity of the enzyme. Binding of cGMP to CNB domain in the regulatory domain induces conformational changes which release this inhibition, thereby inducing kinase activity. The affinities of the two allosteric cGMP-binding sites on each subunit of PKG Iα differ by ~tenfold, and cGMP-mediated activation exhibits strong positive cooperativity. Binding of cGMP to all four CNB sites of the holoenzyme is required for full activation of the enzyme. PKG I is similar to PKG II in its catalytic rate but differs in substrate specificity. PKG Iα and PKG Iβ do not exhibit either substrate specificity or different catalytic rates. However, PKG Iα affinity for cGMP (K_d ~0.1 μM) is ~tenfold greater than that of PKG Iβ (K_d ~ 0.5–1.0 μM) (Francis et al. 2010; Kim et al. 2016).

In PKG I-deficient mice, the decrease in blood pressure induced by intracarotid bolus application of the NO donor sodium nitroprusside (SNP) is largely abolished. The vasodilatation of arterioles in the cremaster muscle caused by SNP is also reduced by 80%. These observations suggest a dominant role for PKG I in vasodilatation caused by NO/cGMP (Koeppen et al. 2004). PKG I may exert its action by reducing the cytosolic Ca^{2+} through activating the large-conductance Ca^{2+}-activated K^+ (BK_{Ca}) channel, which results in membrane hyperpolarization, reduced extracellular Ca^{2+} entry, and consequently vasodilatation. In human coronary arterioles flow and H_2O_2 induce pressure gradient/concentration-dependent dilation, which is eliminated by iberiotoxin, a BK_{Ca} channel blocker, and markedly attenuated by Rp-8-Br-PET-cGMP, a PKG inhibitor. Treatment of coronary smooth muscle cells (SMCs) with H_2O_2 causes reversible dimerization of PKG Iα. H_2O_2 also increases the probability of BK_{Ca} channel openings in a manner sensitive to PKG Iα inhibitor DT-2. Thus, H_2O_2 may dilate the arterioles through the dimerization and activation of PKG Iα and subsequent opening of smooth muscle BK_{Ca} channels (Zhang et al. 2012). Studies show that PKG I may activate BK_{Ca} channel by phosphorylation of the pore-forming α-subunit of the channel at Ser-1072 (Fukao et al. 1999). There is also evidence suggests that PKG may cause vasodilatation by suppressing the Ca^{2+} influx through the inhibition of voltage-gated Ca^{2+} channels (Ruiz-Velasco et al. 1998; Harraz et al. 2014) and transient receptor potential 1/3 (TRPC1/3) channels (Chen et al. 2009).

The intracellular Ca^{2+} elevation during vasoconstriction results not only from the entry of extracellular Ca^{2+} but also from the release of Ca^{2+} from the sarcoplasmic reticulum (SR) through inositol 1,4,5-trisphosphate receptor (IP_3R) and ryanodine receptor. A 125-kDa PKG substrate, IP_3R-associated cGMP kinase substrate (IRAG), has been found to be associated with IP_3R type Iβ via its coiled-coil domain. IRAG is phosphorylated at Ser-696 by PKG Iβ and the phosphorylation leads to reduced released of Ca^{2+} from the SR (Ammendola et al.

2001). In IRAG-knockout mice, the relaxation of aortas to NO, ANP, and cGMP is significantly attenuated. The inhibition of Ca^{2+} elevation by these vasodilators is also suppressed in IRAG-deficient VSMCs. Therefore, PKG Iβ may mediate NO- and ANP-induced vasodilatation through the inhibition of Ca^{2+} release from the SR by acting on IRAG (Desch et al. 2010; Schlossmann and Desch 2011). PKG I also promotes Ca^{2+} reuptake into the SR by phosphorylation of phospholamban (PLB) at the Ser-16. PLB is a regulator of sarco-/endoplasmic reticulum Ca^{2+}-ATPase (SERCA). In the aorta of PLB knockout mice, the steady level of cytosolic Ca^{2+} after treatment with vasoconstrictor is lower than that of the wild-type aorta. However, there is no significant difference in the relaxant response to the NO donor between the PLB knockout and wild-type aortas. It suggests that PLB may not play a major role in PKG-mediated vasodilatation (Lalli et al. 1999).

PKG may cause vasodilatation by reducing the sensitivity of myofilaments to Ca^{2+}, resulting from the stimulation myosin light chain phosphatase (MLCP) through phosphorylation of myosin phosphatase target subunit 1 (MYPT1, the regulatory subunit of MLCP) at Ser-695 and Ser-852 (human sequence). The increased MLCP activity leads to enhanced dephosphorylation of the regulatory myosin light chain (MLC) and decreased vascular contractility. MYPT1 is also phosphorylated at Thr-696 and Thr-853 (human sequence) by ROCK, which is activated by vasoconstrictors and leads to decreased MLCP activity and thus increased MLC phosphorylation and augmented vasocontractility. The residues Ser-695 and Thr-696 as well as Ser-852 and Thr-853 in MYPT1 are next to each other. The phosphorylation of Ser-695 and Ser-852 by PKG has been shown to prevent the phosphorylation of Thr-696 and Thr-853 by ROCK and vice versa (Wooldridge et al. 2004; Gao et al. 2007, 2008; Somlyo and Somlyo 2003). In addition to counteract ROCK at MYPT1, PKG inhibits the activity of the Rho A by phosphorylation of this ROCK activator at Ser-188, resulting in reduced ROCK activity and enhanced MLCP activity (Sauzeau et al. 2000; Loirand et al. 2006). Moreover, PKG may affect MLCP activity by the phosphorylation of telokin at Ser-13. Telokin is a smooth muscle-specific 17-kDa acidic protein whose sequence is identical to the noncatalytic COOH-terminus of myosin light chain kinase (MLCK) and is independently expressed in smooth muscle. The interaction of phosphorylated telokin with the full-length phospho-MYPT1/PP1 facilitates its binding to phosphomyosin and thus accelerates 20-kDa myosin regulatory light chain dephosphorylation (Choudhury et al. 2004; Khromov et al. 2012) (Fig. 14.2).

In the murine mesenteric and cremaster muscle microcirculation, the vasoconstriction evoked by ANG II (Gq/α-mediated) is inhibited by ANP through PKG-dependent activation of the regulator of G-protein signaling type 2 protein (RGS-2). RGS-2 is a GTPase-activating protein (GAP) for Gq/α. The phosphorylation of RGS-2 by PKG I accelerates the rate that Gα-subunits hydrolyze GTP and consequently deactivate signal transduction (Tang et al. 2003; Osei-Owusu and Blumer 2015). Relaxation of porcine carotid artery caused by nitroglycerine, an intracellular activator of sGC, is associated with a marked increase in the phosphorylation of heat-shock protein 20 (HSP20) on Ser16. HSP20 is a member of a family of proteins known to bind to thin filaments. A short peptide (HSP20 residues

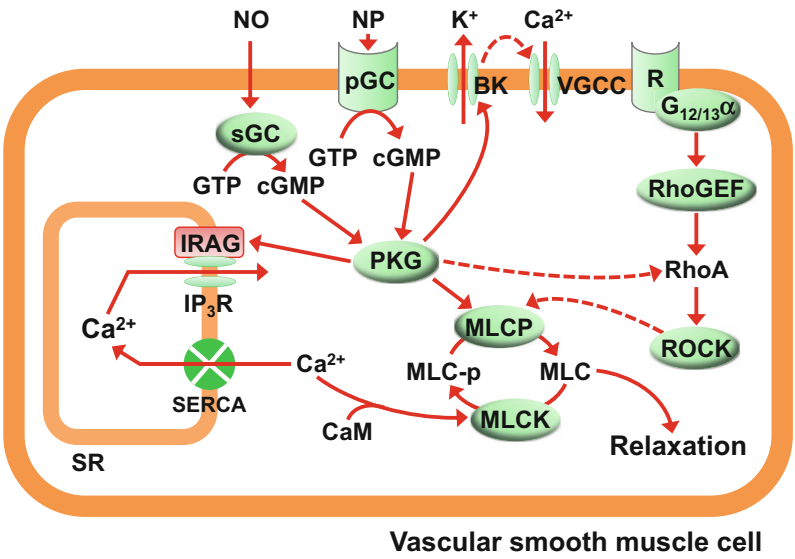

Fig. 14.2 Mechanism underlying cGMP-mediated vasodilatation. cGMP is synthesized by soluble guanylyl cyclase (sGC) and particulate guanylyl cyclase (pGC) from GTP. sGC is stimulated by nitric oxide (NO) and NO-donating agents. pGC is stimulated by natriuretic peptides (NP) such as A-type natriuretic peptide, B-type natriuretic peptide, and C-type natriuretic peptide. cGMP exerts its action primarily via cGMP-dependent protein kinase (PKG). PKG reduces the cytosolic Ca^{2+} levels by stimulating the large-conductance Ca^{2+}-activated K^+ (BK) channels, leading to membrane hyperpolarization and reduced Ca^{2+} influx through the voltage-gated calcium channels (VGCC). PKG also inhibits the release of Ca^{2+} from the sarcoplasmic reticulum (SR) through the inositol 1,4,5-trisphosphate receptor (IP_3R), which results from the phosphorylation of IP_3R-associated cGMP kinase substrate (IRAG) by PKG. An increased cytosolic Ca^{2+} level activates myosin light chain kinase (MLCK) after binding to calmodulin (CaM), which leads to increased phosphorylation of myosin light chain (MLC-p) and vasoconstriction. Therefore, a decreased Ca^{2+} level leads to reduced vasocontractility. PKG also reduces the Ca^{2+} sensitivity of myofilaments by stimulating myosin light chain (MLC) phosphatase (MLCP) resulting from phosphorylation of the regulatory subunit of the enzyme (MYPT1, not shown). The phosphorylation action of PKG could counteract the inhibitory effect of MLCP of Rho kinase (ROCK). PKG also exerts an inhibitory effect on RhoA, the upstream activator of ROCK. RhoA is activated by $G_{12/13}\alpha$ protein through Rho guanine nucleotide exchange factor (RhoGEF) when a vasoconstrictor is bound to its receptor (R). cGMP is hydrolyzed to 5′-GMP by phosphodiesterase (PDE), mainly the cGMP-specific PDE (not shown). *Solid line arrows*: stimulatory. *Dotted line arrows*: inhibitory

110–121, abbreviated HSP20 110-121) binds to actin-containing filaments in the presence of tropomyosin abolishes Ca^{2+}-activated force in skinned porcine carotid artery, accompanied by partially decreased actin-activated myosin ATPase activity. These results raise the possibility that cGMP-/PKG-mediated phosphorylation of HSP20 on Ser16 may have a role in smooth muscle relaxation via binding of HSP20 to the thin filaments of myofilaments and inhibition of cross-bridge cycling (Rembold et al. 2000). More than 30 substrates for PKG I have been

identified. For many of them, their role in the regulation of vasocontractility remains to be elucidated (Schlossmann and Desch 2009).

14.6 CNG Channels

The pivotal roles of CNG channels in the visual and olfactory signalings are well recognized. However, relatively few studies have been conducted regarding the roles of CNG channels in the regulation of vascular activity (Kaupp and Seifert 2002; Wong and Yao. 2008; Biel 2009). CNG channels are nonselective cation channels that are directly activated by cGMP or cAMP allowing physiological Na^+ and K^+ to pass through. Mammalian CNGs are composed of two types of subunits, the A subunits (CNGA1–4) and the B subunits (CNGB1 and CNGB3). The CNGA1–3 subunits can form functional homotetrameric channels. The CNGA4 and CNGB subunits are regarded as modulatory subunits. They can form a functional heterotetrameric channel with CNGA1–3 subunits. In the vasculature CNGA1–4 and CNGB1 are found to be expressed in various vascular beds of several species (Wong and Yao 2008; Biel 2009).

In rat pulmonary artery endothelial cells (PAECs), cGMP and cAMP stimulate a current that is cation permeable and favors Na^+. The current is inhibited by the CNG channel blocker LY83583. Reverse transcriptase-polymerase chain reaction cloning identifies the expression of an olfactory-type CNG channels (heterotetramer consisting of two CNGA2, one CNGA4, and one CNGB1 subunits) in PAECs. The CNG channel is activated by store-operated Ca^{2+} entry accompanied by membrane depolarization of PAECs, suggesting that the CNG channel activity may contribute to feedback inhibition of store-operated calcium entry (Wu et al. 2000). Exposure of porcine PAECs to a high concentration (1 mM) NO donor, NOC-18, for 18 h upregulates the mRNA and protein levels of CNGA2. This effect is associated with prolonged extracellular Ca2+ entry and may be involved in the cytotoxicity of NO (Zhang et al. 2002).

References

Ammendola A, Geiselhöringer A, Hofmann F, Schlossmann J (2001) Molecular determinants of the interaction between the inositol 1,4,5-trisphosphate receptor-associated cGMP kinase substrate (IRAG) and cGMP kinase Iβ. J Biol Chem 276:24153–24159

Ashman DF, Lipton R, Melicow MM, Price TD (1963) Isolation of adenosine 3′,5′-monophosphate and guanosine 3′, 5′-monophosphate from rat urine. Biochem Biophys Res Commun 11:330–334

Azevedo MF, Faucz FR, Bimpaki E, Horvath A, Levy I, de Alexandre RB, Ahmad F, Manganiello V, Stratakis CA (2014) Clinical and molecular genetics of the phosphodiesterases (PDEs). Endocr Rev 35:195–233

Bender AT, Beavo JA (2006) Cyclic nucleotide phosphodiesterases: molecular regulation to clinical use. Pharmacol Rev 58:488–520

Beste KY, Burhenne H, Kaever V, Stasch JP, Seifert R (2012) Nucleotidyl cyclase activity of soluble guanylyl cyclase α1β1. Biochemistry 51:194–204

Biel M (2009) Cyclic nucleotide-regulated cation channels. J Biol Chem 284:9017–9021

Bubb KJ, Trinder SL, Baliga RS, Patel J, Clapp LH, MacAllister RJ, Hobbs AJ (2014) Inhibition of phosphodiesterase 2 augments cGMP and cAMP signaling to ameliorate pulmonary hypertension. Circulation 130:496–507

Budworth J, Meillerais S, Charles I, Powell K (1999) Tissue distribution of the human soluble guanylate cyclases. Biochem Biophys Res Commun 263:696–701

Chen J, Crossland RF, Noorani MM, Marrelli SP (2009) Inhibition of TRPC1/TRPC3 by PKG contributes to NO-mediated vasorelaxation. Am J Physiol Heart Circ Physiol 297:H417–H424

Chen Z, Zhang X, Ying L, Dou D, Li Y, Bai Y, Liu J, Liu L, Feng H, Yu X, Leung SWS, Vanhoutte PM, Gao Y (2014) Cyclic IMP-synthesized by sGC as a mediator of hypoxic contraction of coronary arteries. Am J Physiol Heart Circ Physiol 307:H328–H336

Choudhury N, Khromov AS, Somlyo AP, Somlyo AV (2004) Telokin mediates Ca^{2+}-desensitization through activation of myosin phosphatase in phasic and tonic smooth muscle. J Muscle Res Cell Motil 25:657–665

Corbin JD, Beasley A, Blount MA, Francis SH (2005) High lung PDE5: a strong basis for treating pulmonary hypertension with PDE5 inhibitors. Biochem Biophys Res Commun 334:930–938

De Bold AJ, Borenstein HB, Veress AT, Sonnenberg H (1981) A rapid and potent natriuretic response to intravenous injection of atrial myocardial extract in rats. Life Sci 28:89–94

Derbyshire ER, Marletta MA (2012) Structure and regulation of soluble guanylate cyclase. Annu Rev Biochem 81:533–559

Desch M, Sigl K, Hieke B, Salb K, Kees F, Bernhard D, Jochim A, Spiessberger B, Höcherl K, Feil R, Feil S, Lukowski R, Wegener JW, Hofmann F, Schlossmann J (2010) IRAG determines nitric oxide- and atrial natriuretic peptide-mediated smooth muscle relaxation. Cardiovasc Res 86:496–505

Detremmerie CM, Chen Z, Li Z, Alkharfy KM, Leung SWS, Xu A, Gao Y, Vanhoutte PM (2016) Endothelium-dependent contractions of isolated arteries to thymoquinone require biased activity of sGC with subsequent cIMP production. J Pharmacol Exp Ther 358:558–568

Dou D, Zheng X, Ying L, Ye L, Gao Y (2013) Sulfhydryl-dependent dimerization and cGMP-mediated vasodilatation. J Cardiovasc Pharmacol 62:1–5

Follmann M, Griebenow N, Hahn MG, Hartung I, Mais FJ, Mittendorf J, Schäfer M, Schirok H, Stasch JP, Stoll F, Straub A (2013) The chemistry and biology of soluble guanylate cyclase stimulators and activators. Angew Chem Int Ed Engl 52:9442–9462

Francis SH, Busch JL, Corbin JD, Sibley D (2010) cGMP-dependent protein kinases and cGMP phosphodiesterases in nitric oxide and cGMP action. Pharmacol Rev 62:525–563

Friebe A, Koesling D (2009) The function of NO-sensitive guanylyl cyclase: what we can learn from genetic mouse models. Nitric Oxide 21:149–156

Friebe A, Mergia E, Dangel O, Lange A, Koesling D (2007) Fatal gastrointestinal obstruction and hypertension in mice lacking nitric oxide-sensitive guanylyl cyclase. Proc Natl Acad Sci U S A 104:7699–7704

Fukao M, Mason HS, Britton FC, Kenyon JL, Horowitz B, Keef KD (1999) Cyclic GMP-dependent protein kinase activates cloned BKCa channels expressed in mammalian cells by direct phosphorylation at serine 1072. J Biol Chem 274:10927–10935

Furchgott RF, Zawadzki JV (1980) The obligatory role of endothelial cells in the relaxation of arterial smooth muscle by acetylcholine. Nature 288:373–376

Gao Y (2010) The multiple actions of NO. Pflügers Arch - Eur J Physiol, 2010. 459: 829-839.

Gao Y (2016) Conventional and unconventional mechanisms for soluble guanylyl cyclase signaling. J Cardiovasc Pharmacol 67(367-372):2016

Gao Y, Tolsa J-F, Shen H, Raj JU (1998) Effect of selective phosphodiesterase inhibitors on the responses of ovine pulmonary veins to prostaglandin E_2. J Appl Physiol 84:13–18

Gao Y, Portugal AD, Negash S, Zhou W, Longo LD, Raj JU (2007) Role of Rho kinases in PKG-mediated relaxation of pulmonary arteries of fetal lambs exposed to chronic high altitude hypoxia. Am J Physiol Lung Cell Mol Physiol 292:L678–L684

Gao Y, Portugal AD, Liu J, Negash S, Zhou W, Tian J, Xiang R, Longo LD, Raj JU (2008) Preservation of cGMP-induced relaxation of pulmonary veins of fetal lambs exposed to chronic high altitude hypoxia: role of PKG and Rho kinase. Am J Physiol Lung Cell Mol Physiol 295:L889–L896

Garbers DL, Suddath JL, Hardman JG (1975) Enzymatic formation of inosine 3′, 5′-monophosphate and of 2′-deoxyguanosine 3′, 5′-monophosphate. Inosinate and deoxyguanylate cyclase activity. Biochim Biophys Acta 377:174–185

Hall CN, Garthwaite J (2009) What is the real physiological NO concentration in vivo? Nitric Oxide 21:92–103

Hardman JG, Sutherland EW (1969) Guanyl cyclase, an enzyme catalyzing the formation of guanosine 3′,5′-monophosphate from guanosine trihosphate. J Biol Chem 244:6363–6370

Harraz OF, Brett SE, Welsh DG (2014) Nitric oxide suppresses vascular voltage-gated T-type Ca^{2+} channels through cGMP/PKG signaling. Am J Physiol Heart Circ Physiol 306:H279–H285

Hofmann F, Wegener JW (2013) cGMP-dependent protein kinases (cGK). Methods Mol Biol 1020:17–50

Hughes JM, Murad F, Chang B, Guerrant RL (1978) Role of cyclic GMP in the action of heatstable enterotoxin of *Escherichia coli*. Nature 271:755–756

Ignarro LJ (1989) Endothelium-derived nitric oxide: actions and properties. FASEB J 3:31–36

Kaupp UB, Seifert R (2002) Cyclic nucleotide-gated ion channels. Physiol Rev 82:769–824

Keravis T, Lugnier C (2012) Cyclic nucleotide phosphodiesterase (PDE) isozymes as targets of the intracellular signalling network: benefits of PDE inhibitors in various diseases and perspectives for future therapeutic developments. Br J Pharmacol 165:1288–1305

Khromov AS, Momotani K, Jin L, Artamonov MV, Shannon J, Eto M, Somlyo AV (2012) Molecular mechanism of telokin-mediated disinhibition of myosin light chain phosphatase and cAMP/cGMP-induced relaxation of gastrointestinal smooth muscle. J Biol Chem 287:20975–20985

Kim D, Rybalkin SD, Pi X, Wang Y, Zhang C, Munzel T, Beavo JA, Berk BC, Yan C (2001) Upregulation of phosphodiesterase 1A1 expression is associated with the development of nitrate tolerance. Circulation 104:2338–2343

Kim JJ, Lorenz R, Arold ST, Reger AS, Sankaran B, Casteel DE, Herberg FW, Kim C (2016) Crystal structure of PKG I:cGMP complex reveals a cGMP-mediated dimeric interface that facilitates cgmp-induced activation. Structure 24:710–720

Koeppen M, Feil R, Siegl D, Feil S, Hofmann F, Pohl U, de Wit C (2004) cGMP-dependent protein kinase mediates NO- but not acetylcholine-induced dilations in resistance vessels in vivo. Hypertension 44:952–955

Kots AY, Martin E, Sharina IG, Murad F (2009) A short history of cGMP, guanylyl cyclases, and cGMP-dependent protein kinases. Handb Exp Pharmacol 191:1–14

Kuhn M (2016) Molecular physiology of membrane guanylyl cyclase receptors. Physiol Rev 96:751–804

Lakshminrusimha S, Porta NF, Farrow KN, Chen B, Gugino SF, Kumar VH, Russell JA, Steinhorn RH (2009) Milrinone enhances relaxation to prostacyclin and iloprost in pulmonary arteries isolated from lambs with persistent pulmonary hypertension of the newborn. Pediatr Crit Care Med 10:106–112

Lalli MJ, Shimizu S, Sutliff RL, Kranias EG, Paul RJ (1999) $[Ca^{2+}]_i$ homeostasis and cyclic nucleotide relaxation in aorta of phospholamban-deficient mice. Am J Phys 277:H963–H970

Leung SW, Gao Y, Vanhoutte PM (2016) 3′, 5′-cIMP as potential second messenger in the vascular wall. Handb Exp Pharmacol .2016. [Epub ahead of print]

Liu J, Chen Z, Ye L, Liu H, Dou D, Liu L, Yu X, Gao Y (2014) Preservation of nitric oxide-induced relaxation of porcine coronary artery: roles of the dimers of soluble guanylyl cyclase,

phosphodiesterase type 5, and cGMP-dependent protein kinase. Pflügers Arch Eur J Physiol 466:1999–2008
Loirand G, Guilluy C, Pacaud P (2006) Regulation of rho proteins by phosphorylation in the cardiovascular system. Trends Cardiovasc Med 16:199–204
Maack T (1992) Receptors of atrial natriuretic factor. Annu Rev Physiol 54:11–27
Matsukawa N, Grzesik WJ, Takahashi N, Pandey KN, Pang S, Yamauchi M, Smithies O (1999) The natriuretic peptide clearance receptor locally modulates the physiological effects of the natriuretic peptide system. Proc Natl Acad Sci U S A 96:7403–7408
Maurice DH, Ke H, Ahmad F, Wang Y, Chung J, Manganiello VC (2014) Advances in targeting cyclic nucleotide phosphodiesterases. Nat Rev Drug Discov 13:290–314
Mergia E, Friebe A, Dangel O, Russwurm M, Koesling D (2006) Spare guanylyl cyclase NO receptors ensure high NO sensitivity in the vascular system. J Clin Invest 116:1731–1737
Montfort WR, Wales JA, Weichsel A (2017) Structure and activation of soluble guanylyl cyclase, the nitric oxide sensor. Antioxid Redox Signal 26:107–121
Moyes AJ, Khambata RS, Villar I, Bubb KJ, Baliga RS, Lumsden NG, Xiao F, Gane PJ, Rebstock AS, Worthington RJ, Simone MI, Mota F, Rivilla F, Vallejo S, Peiró C, Sánchez Ferrer CF, Djordjevic S, Caulfield MJ, MacAllister RJ, Selwood DL, Ahluwalia A, Hobbs AJ (2014) Endothelial C-type natriuretic peptide maintains vascular homeostasis. J Clin Invest 124:4039–4051
Osei-Owusu P, Blumer KJ (2015) Regulator of G protein signaling 2: a versatile regulator of vascular function. Prog Mol Biol Transl Sci 133:77–92
Palmer RM, Ferrige AG, Moncada S (1987) Nitric oxide release accounts for the biological activity of endothelium-derived relaxing factor. Nature 327:524–526
Piggott LA, Hassell KA, Berkova Z, Morris AP, Silberbach M, Rich TC (2006) Natriuretic peptides and nitric oxide stimulate cGMP synthesis in different cellular compartments. J Gen Physiol 128:3–14
Potter LR (2011) Guanylyl cyclase structure, function and regulation. Cell Signal 23:1921–1926
Rembold CM, Foster DB, Strauss JD, Wingard CJ, Eyk JE (2000) cGMP-mediated phosphorylation of heat shock protein 20 may cause smooth muscle relaxation without myosin light chain dephosphorylation in swine carotid artery. J Physiol 524:865–878
Ruiz-Velasco V, Zhong J, Hume JR, Keef KD (1998) Modulation of Ca^{2+} channels by cyclic nucleotide cross activation of opposing protein kinases in rabbit portal vein. Circ Res 82:557–565
Sakumi K, Abolhassani N, Behmanesh M, Iyama T, Tsuchimoto D, Nakabeppu Y (2010) ITPA protein, an enzyme that eliminates deaminated purine nucleoside triphosphates in cells. Mutat Res 703:43–50
Sanchez LS, de la Monte SM, Filippov G, Jones RC, Zapol WM, Bloch KD (1998) Cyclic-GMP-binding, cyclic-GMP-specific phosphodiesterase (PDE5) gene expression is regulated during rat pulmonary development. Pediatr Res 43:163–168
Sauzeau V, Le Jeune H, Cario-Toumaniantz C, Smolenski A, Lohmann SM, Bertoglio J, Chardin P, Pacaud P, Loirand G (2000) Cyclic GMP-dependent protein kinase signaling pathway inhibits RhoA-induced Ca^{2+} sensitization of contraction in vascular smooth muscle. J Biol Chem 275:21722–21729
Schlossmann J, Desch M (2009) cGK substrates. Handb Exp Pharmacol 191:163–193
Schlossmann J, Desch M (2011) IRAG and novel PKG targeting in the cardiovascular system. Am J Physiol Heart Circ Physiol n.d.301(3):H672-H682.
Schmidt HH, Schmidt PM, Stasch JP (2009) NO- and haem-independent soluble guanylate cyclase activators. Handb Exp Pharmacol 191:309–339
Sharma RK, Duda T, Makino CL (2016) Integrative signaling networks of membrane guanylate cyclases: biochemistry and physiology. Front Mol Neurosci 9:83. eCollection 2016
Smith M, Drummond GI, Khorana HG (1961) Cyclic phosphates. IV. Ribonucleoside 3,5-cyclic phosphates. A general method of synthesis and some properties. J Am Chem Soc 83:698–706

Somlyo AP, Somlyo AV (2003) Ca^{2+} sensitivity of smooth muscle and nonmuscle myosin II: modulated by G proteins, kinases, and myosin phosphatase. Physiol Rev 83:1325–1358

Tang KM, Wang GR, Lu P, Karas RH, Aronovitz M, Heximer SP, Kaltenbronn KM, Blumer KJ, Siderovski DP, Zhu Y, Mendelsohn ME (2003) Regulator of G-protein signaling-2 mediates vascular smooth muscle relaxation and blood pressure. Nat Med 9:1506–1512

Tolsa J-F, Gao Y, Sander FC, Souici A-C, Moessinger A, Raj JU (2002) Differential responses of pulmonary arteries and veins of newborn lamb to atrial and C-type natriuretic peptides. Am J Physiol Heart Circ Physiol 282:H273–H280

Vanhoutte PM, Zhao Y, Xu A, Leung SW (2016) Thirty years of saying NO: sources, fate, actions, and misfortunes of the endothelium-derived vasodilator mediator. Circ Res 119:375–396

Wong CO, Yao X (2008) Cyclic nucleotide-gated channels: a familiar channel family with a new function? Futur Cardiol 4:505–515

Wooldridge AA, MacDonald JA, Erdodi F, Ma C, Borman MA, Hartshorne DJ, Haystead TA (2004) Smooth muscle phosphatase is regulated in vivo by exclusion of phosphorylation of threonine 696 of MYPT1 by phosphorylation of Serine 695 in response to cyclic nucleotides. J Biol Chem 279:34496–34504

Wu S, Moore TM, Brough GH, Whitt SR, Chinkers M, Li M, Stevens T (2000) Cyclic nucleotide-gated channels mediate membrane depolarization following activation of store-operated calcium entry in endothelial cells. J Biol Chem 275:18887–18896

Ye L, Liu J, Liu H, Ying L, Dou D, Chen Z, Xu X, Raj JU, Gao Y (2013) Sulfhydryl-dependent dimerization of soluble guanylyl cyclase modulates relaxation of porcine pulmonary vessels to nitric oxide. Pflügers Arch Eur J Physiol 465:333–341

Zhang J, Xia SL, Block ER, Patel JM (2002) NO upregulation of a cyclic nucleotide-gated channel contributes to calcium elevation in endothelial cells. Am J Physiol Cell Physiol 283:C1080–C1089

Zhang DX, Borbouse L, Gebremedhin D, Mendoza SA, Zinkevich NS, Li R, Gutterman DD (2012) H_2O_2-induced dilation in human coronary arterioles: role of protein kinase G dimerization and large-conductance Ca^{2+}-activated K^+ channel activation. Circ Res 110:471–480

Zheng X, Ying L, Liu J, Dou D, He Q, Leung SWS, Man RYK, Vanhoutte PM, Gao Y (2011) Role of sulfhydryl-dependent dimerization of soluble guanylyl cyclase in relaxation of porcine coronary artery to nitric oxide. Cardiovasc Res 90:565–572

Part IV
Heterogeneity in Vasoreactivity

Chapter 15
Coronary Vasoreactivity

Abstract The heart has the highest O_2 consumption rate of all of the organs in the body. The resting left ventricle extracts ~70–80% of the O_2 delivered by the coronary circulation. Therefore, an increased myocardial O_2 consumption depends primarily on increased coronary blood flow (CBF). Both under basal conditions and at increased cardiac activity, the CBF and the coronary vascular activities are regulated by coordinately activated mechanisms with the involvement of myogenic response, various endothelium-derived substances, local metabolites, and neuronal influence. The CBF is also constantly affected by the compressive force generated by the systolic and diastolic cycle of the heart, resulting in a predominant diastolic flow in the left ventricle and rendering the endocardium more vulnerable to ischemia. These unique characteristics of coronary circulation and the underlying mechanisms of the related changes in vasoreactivity will be discussed in this chapter.

Keywords Coronary circulation • Phasic flow • Autoregulation • Metabolic factor • Hemodynamic • Endothelium • Neuronal regulation

15.1 Introduction

The term "coronary," which derives from the Latin corona with a meaning of a crown, was first used in the 1670s to describe the vasculature covering the surface of the heart (Tune 2014). The coronary circulation has evolved with some distinct characteristics that are compatible with the cardiac function. The normally functioning heart depends primarily on oxidative phosphorylation, with only ~5% of ATP production resulting from glycolytic metabolism. Moreover, the continuously beating heart even under "resting" conditions consumes a major portion of the O_2 delivered by the coronary circulation leaving very limited O_2 reserve (Duncker and Bache 2008). Therefore a change in myocardial O_2 demand due to increased cardiac output is primarily met by increased coronary blood flow (CBF) via vasodilatation. Indeed, the dynamic range of coronary blood flow can extend approximately tenfold (Wusten et al. 1977; Katz and Feigl 1988). Studies demonstrate that the CBF is closely related to myocardial O_2 consumption, which is regulated by complicated mechanisms in a coordinated and redundant manner.

Y. Gao, *Biology of Vascular Smooth Muscle: Vasoconstriction and Dilatation*,
DOI 10.1007/978-981-10-4810-4_15

Among these mechanisms the myogenic response, metabolic response, endothelium-derived substance, and sympathetic activity are critically involved (Tune 2014; Duncker et al. 2015; Goodwill et al. 2017). In addition to a major role for vasodilatation in meeting the challenge of myocardial O_2 demand, the coronary circulation is featured by its phasic change during the cardiac cycle, resulting from the extravascular compression occurred during systole. It is most pronounced in the coronary flow of the left ventricle. Due to a greater extravascular compression, the autoregulatory mechanism is less effective in endocardial coronary than in epicardial arteries, making the inner layer of the endocardium more prone to ischemic damage (Guyton et al. 1977; Tune 2014; Duncker et al. 2015; Pries et al. 2015). With the key points in mind, we will summarize the current knowledge on coronary anatomy, the characteristics of coronary circulation, and the regulatory mechanisms of coronary vasoreactivity in this chapter.

15.2 Coronary Anatomy

The blood supply to the heart is provided by the left and right coronary arteries, which arise from the aorta above the left and right cusps of the aortic valve, respectively. The left coronary artery passed inferior to the left auricle and divides into the left anterior descending (LAD) and the circumflex (LCX) branches. The LAD runs along the anterior interventricular sulcus and ends at the acute margin of the heart just to the right of the apex. The LCX curves to the left around the heart within anterior atrioventricular sulcus and gives rise to the left marginal arteries as it proceeds toward the posterior surface of the heart. The LCX artery ends at the point where it joins to form the posterior interventricular artery (PIV, or named as posterior descending artery (PDA)) in ~10% of human hearts, known as a left dominant circulation. The right coronary artery (RCA) travels down the right of the anterior atrioventricular sulcus where it gives rise to the right marginal artery. In ~90% of human hearts, the RCA continues down the posterior atrioventricular sulcus and then runs down in the posterior interventricular sulcus to give rise to the PDA, known as a right dominant circulation. Generally speaking, the left coronary artery distributes blood to the left side of the heart, the left atrium and ventricle, and the interventricular septum. The right coronary artery distributes blood to the right atrium, portions of both ventricles, and the heart conduction system (Loukas et al. 2013; Tune 2014).

Coronary arteries that run on the surface of the heart are known as epicardial coronary arteries. These arteries divide over the surface of the heart. After reaching 1–3 mm in diameter, they start to send tributaries (~400–1500 μm in diameter) at right angles into the myocardium from the outer epicardium to the inner endocardium. These transmural arteries are divided in two classes: the class A vessels branch frequently into a fine network in the outer 3/4 to 4/5 of the myocardium; and the class B vessels branch infrequently and maintain similar size diameters until near the endocardium where they subdivide to form a large endocardial plexus.

Myocardial capillary beds run in parallel with the myocardial fibers at a density more than 3000 capillaries per mm^2 in the left ventricle (skeletal muscle has only ~400/mm^2). There is approximately one capillary per mm^2, with a diffusion distance averaged ~8.5 μm. The diameter of cardiac muscle fibers (<20 μm) is less than half that of the skeletal muscle (~50 μm), which facilitates O_2 diffusion into the cardiac cells (Opie and Heusch 2004; Tune 2014).

In a normal heart, almost no large communications exist among the larger coronary arteries. But many anastomoses exist among the smaller arteries, which include (1) small branches of the LAD joined with branches of the posterior interventricular branch of the RCA in the interventricular sulcus, (2) an anastomosis between the LCX and RCA in the atrioventricular sulcus, and (3) an anastomosis between the septal branches of the LCX and RCA in the interventricular septum (Tune 2014). Coronary anastomoses are an alternative source of blood supply to ischemic myocardium. It has been found that the intercoronary anastomoses are more pronounced in arterioles and arteries sized from 10 to 200 μm in normal human hearts whereas in arterioles and arteries sized from 100 to 800 μm in patients with coronary artery disease (Fulton 1963). It is of interest to note that, in comparison with other species including guinea pig, dog, cat, rat, ferret, baboon, rabbit, and pig, the humans possess the most advanced coronary collateral function behind the guinea pig (Maxwell et al. 1987). Moreover, an effective collateral circulation can develop during chronic coronary artery occlusion (Seiler et al. 2013).

The coronary venous system is largely a mirror image of the arterial system, although with more intramyocardial and epicardial anastomoses as compared with the arterial system. The great cardiac vein initially parallels the LAD, then parallels the LCX arteries, and opens into the left extremity of the coronary sinus. It drains ~55% of coronary arterial inflow. Approximately 35% of the cardiac venous drainage, primarily from the right ventricle, drains directly into the right atrium via anterior cardiac veins that parallels the RCA. About 10% of left ventricular venous blood drains directly into the left ventricular cavity via Thebesian veins (Loukas et al. 2009; Tune 2014; Goodwill et al. 2017).

15.3 Characteristics of Coronary Circulation

The coronary circulation exhibits unique characteristics that are both adapted to and essential for a normal cardiac function. Although the heart has the highest O_2 consumption rate of all of the organs in the body, its O_2 needs are adequately met by the regulation of coronary blood flow (CBF) (Feigl 1983; Tune et al. 2004; Duncker and Bache 2008; Goodwill et al. 2017). The CBF is maintained at relative stable levels through autoregulation. Yet, during each cardiac cycle, The CBF shows phasic changes, particularly in the left ventricle (LV), resulting from extravascular compression during systole. Thus the major portion of CBF occurs during the diastole. Since the inner layer of the endocardium has a high O2 consumption and its blood supply is more affected by systolic compressive force, it is more

vulnerable to ischemic insults (Tune et al. 2014; Duncker et al. 2015; Pries et al. 2015).

15.3.1 Coronary Flow at Rest and During Exercise

The resting CBF in the human being averages ~225 ml/min. This is ~5% of the total cardiac output. Myocardial oxygen extraction in the left ventricle (LV) at rest is ~60–80% of arterially delivered O_2. Therefore, the LV O_2 extraction reserve is rather limited, and the increases in O_2 demand must be met primarily by increasing CBF. Indeed, the LV CBF increases threefold to fourfold during exercise, which provides ~80% of the O_2 demand, predominantly (~ 90%) achieved by a decrease in coronary vascular resistance (Tune et al. 2004; Duncker and Bache 2008; Tune 2014; Goodwill et al. 2017).

The resting CBF of the right ventricle (RV) is 0.3–0.6 ml/min/g myocardium, which is less than that of LV (0.5–1.0 ml/min/g). At rest the right ventricle (RV) extracts only ~50% of the O_2 from the coronary flow. The smaller RV O_2 extraction provides a large O_2 extraction reserve for the RV compared with that of LV. Therefore, the RV can meet increases in O_2 demands by increased O_2 extraction and increased coronary flow (Zong et al. 2005; Tune 2014). In conscious dogs the O_2 demands of RV at less strenuous exercise have been found to be met predominantly by increased O_2 extraction, while the O_2 demands of RV at strenuous exercise were met by both a high O_2 extraction and increased coronary flow (Hart et al. 2001). The RV O_2 consumption is less than half that of the LV (4.0 compared with 8.6 ml O_2/min/100 g). This is easy understanding, considering the much lower afterload imposed on the RV (Zong et al. 2005; Tune 2014; Goodwill et al. 2017).

15.3.2 Phasic Changes of Coronary Flow

The LV CBF is characterized by marked phasic variations during the cardiac cycle. The intramyocardial microvessels are compressed by increased LV wall tension during systolic contraction, resulting in reduced coronary arterial inflow and increased coronary venous outflow. During diastole, when the relaxed ventricles no longer compress the left coronary vessels and aortic pressure is still high, left coronary flow rises rapidly. Accordingly, the left ventricle receives ~80% of its blood flow during diastole (Tune 2014). The wall tension developed by the RV is much lower than that of the LV, which pumps against the low resistance of the pulmonary circulation and does not occlude the right coronary vessels during contraction. Therefore, the RV is perfused primarily during systole. The CBF of RV increases as aortic pressure is elevated during systole and tends to wane as pressure falls during diastole (Walker and Buttrick 2013). In a cardiac cycle, the

lengths of systole and diastole vary depending on heart rate. During tachycardia, the fraction of the cardiac cycle for diastole decreases more than that of systole, resulting in reduced time for maximal coronary perfusion. In a healthy heart, the negative effect of the shorter diastole is compensated by vasodilatation elicited by the metabolic signals generated by increased cardiac work. However, a high heart rate could be dangerous when severe coronary artery disease restricts blood flow (Tune 2014; Duncker et al. 2015; Goodwill et al. 2017).

Coronary blood flow not only varies during the cardiac cycle; it also varies with depth in the wall of the heart. During systole the intramuscular pressure is greatest near the endocardium and least near the epicardium. Studies with needle-probe videomicroscopy show that the effects of ventricular systole are greatest in endocardial vessels >100 μm, with average decreases in diameter of ~20%, while microvessels in the epicardium are largely unaffected. A higher extravascular compression could make the endocardium less well perfused vs. the epicardium. Such an inherent disadvantage is compensated for by a higher microvascular density and a higher vessel compliance and thus a lower coronary microvascular resistance in the innermost layer endocardium compared to that of the epicardium. Indeed, the pressure drop across the microcirculation has been found being lower in the endocardium vs. epicardium at perfusion pressures ranging from 40 to 100 mmHg, indicating that coronary microvascular resistance is highest in upstream transmural coronary arteries. In spite of such a compensative mechanism, due to the lower perfusion pressure, greater extravascular compression, and higher O_2 consumption, the endocardium is more vulnerable to ischemia (Hoffman and Buckberg 2014; Tune 2014; Duncker et al. 2015; Goodwill et al. 2017).

15.3.3 Coronary Pressure-Flow Relations

The CBF remains relatively constant within ~60–120 mmHg perfusion pressures, resulting from autoregulation. The coronary autoregulation is largely regulated by local myogenic response and metabolic factors. It is initiated by mechanical stretch of vascular smooth muscle cells (VSMCs), leading to increased cytosolic Ca^{2+} levels and consequently vasoconstriction, whereas the metabolic factors released from the myocardium maintain the blood flow relatively stable (Mosher et al. 1964; Cornelissen et al. 2000; Spaan et al. 2000; Tune 2014; Duncker et al. 2015). Studies show that the degree of coronary myogenic responsiveness is most pronounced in subepicardial arterioles <100 μm in diameter, although modest responses occur in small arteries of up to 400 μm in diameter (Kuo et al. 1988; Kanatsuka et al. 1990; Rajagopalan et al. 1995). When perfusion pressure falls below a critical threshold (<~50–60 mmHg), the autoregulatory response diminishes and coronary arterioles respond passively to further decreases in pressure (Tune 2014; Goodwill et al. 2017).

Studies of transmural pressure-flow relations indicate that autoregulation is more effective in the epicardium than the endocardium. The endocardial blood flows have been found to progressively decline when downstream coronary pressures are reduced below 70 mmHg, whereas epicardial blood flows remain stable until the

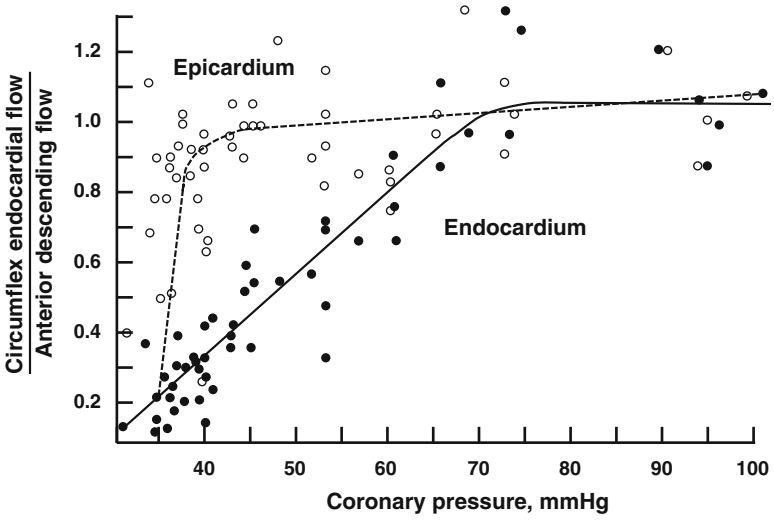

Fig. 15.1 Relationship between coronary pressure and blood flow of the distal left circumflex coronary artery in the epicardium (*open circles* and *dotted line*) and the endocardium (*filled circles* and *solid line*), normalized by dividing the simultaneous flow in the nonischemic area of the left anterior descending coronary artery (This figure is modified from Guyton et al. (1977), with permission)

pressures below 40 mmHg (Guyton et al. 1977) (Fig. 15.1). It is likely that the diminished autoregulation in the endocardium results from the combination of higher extravascular compressive force and higher O_2 consumption in the inner layer of the myocardium (Tune 2014; Duncker et al. 2015). Unlike the LV, there is no clear evidence indicating differences in transmural autoregulation in the right coronary circulation. The endocardial to epicardial (ENDO/EPI) flow ratios of the RV are not affected by perfusion pressures ranging from 30 to 125 mmHg (Yonekura et al. 1988). The similar transmural autoregulation in RV may be due to the lower myocardial oxygen consumption (MVO_2), thinner wall thickness, and lower intraventricular pressure of the RV as compared with that of the RV (Walker and Buttrick 2013).

15.3.4 Myocardial Blood Flow and Myocardial Metabolism

The heart has the highest O_2 consumption rate of all of the organs in the body (~50–100 μl O_2/min/g). Since the resting LV myocardium extracts ~70–80% of the oxygen delivered by the coronary circulation, an increased myocardial O_2 consumption is principally met by increased CBF. Studies suggest that potent vasodilator mechanisms are activated when coronary venous PO_2 falls below ~15–20 mmHg. Strikingly, the myocardial O_2 consumption is closely matched by

myocardial blood flow in a nearly linear relationship. Such a relationship persists in isolated heart preparations, implying that metabolic signals are the primary determinants of O_2 delivery to the myocardium (Feigl 1983; Tune et al. 2004; Duncker and Bache 2008; Tune 2014; Duncker et al. 2015).

In 1963 Berne and Gerlach et al. independently proposed that adenosine may be an important mediator for the changes in CBF elicited by hypoxia (Berne 1963; Gerlach et al. 1963). Subsequent studies found that the blockade of receptors for adenosine has little effect on the CBF during increased myocardial metabolism (Feigl 2004; Tune 2014). Moreover, studies of adenosine kinetics suggest that interstitial adenosine levels are unlikely to be sufficient for adenosine to mediate coronary vasodilation (Kroll and Stepp 1996). It is now recognized that adenosine, while being importantly involved in CBF change during hypoxia, does not play an obligatory role in the coupling of CBF to increased myocardial O_2 consumption (Deussen et al. 2012; Tune 2014). At present, there is no single mediator that has been firmly established to be responsible for the link between CBF and myocardial O_2 consumption (Deussen et al. 2012; Tune 2014; Pries et al. 2015; Goodwill et al. 2017). In 2006 Chilian and colleagues proposed that H_2O_2, a product of cardiac metabolism produced in large quantities proportional to mitochondrial respiration, may act as a mediator to couple myocardial oxygen consumption to CBF via the activation of voltage-gated K^+ (K_v) channels in VSMCs (Saitoh et al. 2006). Their recent in vivo study using a genetic approach further shows blunted metabolic coronary vasodilatation in mice deficient in the redox-sensitive $K_v1.5$ channels. When $K_v1.5$ channel is conditionally restored in VSMCs in knockout mice, the metabolic vasodilatation is restored, implying a requisite role of $K_v1.5$ channels (Ohanyan et al. 2015). It is important to note that, considering the crucial role of metabolic vasodilatation for normal cardiac function, redundant regulatory mechanisms may exist (Chabowski and Gutterman 2015). For instance, a study shows that inhibition of endothelial nitric oxide synthase (eNOS) alone or inhibition of eNOS combined with blockade of adenosine receptors has no effect on the increase in CBF during exercise. Combined blockades of ATP-sensitive K^+ (K_{ATP}) channels and adenosine receptors only modestly reduce exercise-induced increase in CBF. However, the combined blockades of K_{ATP} channels and adenosine receptors plus inhibition of eNOS substantially blunt the coronary vasodilatation during exercise (Ishibashi et al. 1998).

15.4 Coronary Vasoreactivity

Under normal circumstances, the coronary vascular resistance (CVR) resides in small arteries and arterioles of a broad range of vessel sizes (20–400 μm in diameter), in particular those sized 50–200 μm. There is no appreciable pressure drop in the epicardial arteries. However, when the diameters of epicardial arteries are decreased by >50% due to stenosis, the resistance of these vessels contributes significantly to total CVR. When the diameters of epicardial arteries are decreased

by >90%, a reduced resting CBF may occur. There is normally less resistance contributed by capillaries and coronary venules, but the coronary venules and veins possess significant vessel tension and are under active neural and hormonal control (Klassen and Armour 1984; Kuo et al. 1993; Qi et al. 2007; Duncker et al. 2015).

The coronary vasoactivity is determined by the contractile state of the vascular smooth muscle, which is primarily regulated by (A) hemodynamic variations including the tensile stress exerted by blood pressure and the shear stress exerted by blood flow, (B) endothelial cells (ECs) acting as a modulator of signals from the circulation and local, (C) metabolic signals from adjacent tissue, and (D) neuronal influence (Feigl 1983; Duncker and Bache 2008; Deussen et al. 2012; Tune 2014; Duncker et al. 2015; Pries et al. 2015; Goodwill et al. 2017). Considerable heterogeneity exists in vasoreactivity along coronary vasculature. For example, the myogenic response evoked by blood pressure and metabolite-mediated response occurs principally in arterioles, while small arteries tend to more responsible to change in blood flow. The responsiveness of the vessels to metabolites increases as the diameters of arterioles decrease (Fig. 15.2). In contrast, an increase in O_2 consumption elicits a more uniform vasodilation of resistance vessels of all sizes (Jones et al. 1995; Tiefenbacher and Chilian 1998).

15.4.1 Hemodynamic Influence

The coronary vascular activity is constantly influenced by two major hemodynamic variations: the tensile stress perpendicular to the vessel wall resulted from blood pressure and shear stress *parallel to the longitudinal direction of the vessel wall* generated by blood flow. When subject to tensile stress, the mechanical deformations in the cell membrane of *VSMCs* caused by stretch lead to the opening of nonspecific cation channels promoting an inward Na^+ and/or Ca^{2+} current, consequently membrane depolarization, Ca^{2+} influx through voltage-gated Ca^{2+} channels (VGCCs), and vasoconstriction, a phenomenon known as myogenic response (Spassova et al. 2006; Earley and Brayden 2015; Liu and Montell 2015). The myogenic response is an intrinsic property of VSMCs and is independent of the presence of the endothelium (Kuo et al. 1990). It exists across a large range of coronary resistance artery sizes, but in the coronary vasculature in vivo, it is particularly pronounced in arterioles <100 μm. The myogenic response is a key component in coronary autoregulation. It is triggered by increased blood pressure which causes vasoconstriction and thus restores local coronary flow back to the original level (Kanatsuka et al. 1990; Jones et al. 1995; Miller et al. 1997; Duncker et al. 2015).

In contrast to the endothelium independency of myogenic response, the vascular response elicited by shear stress of blood flow is mediated by vasoactive substances released from the endothelial cells (ECs), which include nitric oxide (NO), endothelium-derived hyperpolarizing factor (EDHF), and vasodilator prostaglandins in particular prostaglandin I_2 (PGI_2). The role of NO is more pronounced in

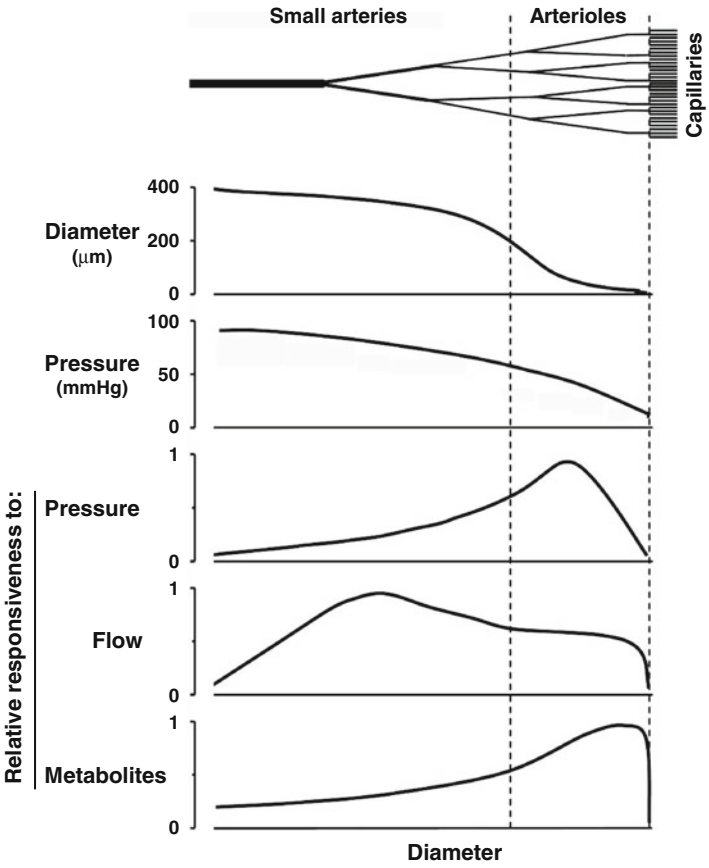

Fig. 15.2 Heterogeneity of coronary arteries and arterioles in the relative responsiveness to pressure, flow, and metabolites (This figure is modified from Tiefenbacher and Chilian (1998), with permission)

conduit arteries, the role of EDHF is more dominant in resistance arteries and arterioles, and the role of PGI_2 is not different among different vessel sizes. There is also evidence implying that when NO function is impaired the effect of EDHF becomes more prominent (Beyer and Gutterman 2012; Shimokawa 2014; Vanhoutte et al. 2016).

EDHF is referred to a group of molecules including epoxyeicosatrienoic acids (EETs), H_2O_2, carbon monoxide, hydrogen sulfide, C-natriuretic peptide, and K^+ itself, which causes vasodilatation by causing membrane hyperpolarization of VSMCs. The precise identity of EDHF varies depending on species, blood vessel types, and physiological/pathophysiological conditions (Beyer and Gutterman 2012; Giles et al. 2012). Studies show that, in human coronary arterioles, EETs and H_2O_2 may act as the mediators for blood flow-induced vasodilatation. The activation of phospholipase A_2 (PLA_2) in response to shear stress leads to

production of arachidonic acid, which is metabolized to EETs by cytochrome P450 (CYP) 2C/2 J isoenzymes. EETs cause VSMC hyperpolarization through activating the large-conductance Ca^{2+}-activated K^+ channels (BK_{Ca}), probably via the putative EET receptor or by activating the subfamily V member 4 transient receptor potential cation channel (TRPV4) to induce localized Ca^{2+} influx that activates sarcoplasmic reticulum (SR) ryanodine receptors (RyR) to trigger local Ca^{2+} sparks and then activate BK_{Ca}. Shear stress can also cause the reduction of molecular O^2 to form superoxide anion ($O_2^{\bullet-}$) by a number of sources, including nicotinamide adenine dinucleotide phosphate oxidase (NOX), mitochondria, and eNOS. $O_2^{\bullet-}$ is then reduced to H_2O_2 by superoxide dismutase. H_2O_2 may trigger the dimerization of PKG 1α monomers via disulfide bridge (−S-S-) formation at cysteine 42, leading to an increased affinity of PKG for BK_{Ca} and thus enhanced membrane hyperpolarization (Beyer and Gutterman 2012; Dou et al. 2012; Ellinsworth et al. 2016).

15.4.2 Endothelium-Derived Vasoactive Factors

Vascular activity is modulated by a number of vasoactive factors derived from ECs, most importantly, NO, EDHFs, and PGI_2 (Shimokawa 2014; Ellinsworth et al. 2016; Vanhoutte et al. 2016). In coronary vasculature the role of NO is most prominent in conduit arteries and resistance arteries >100 μm in diameter (Stepp et al. 2001; Ying et al. 2012). The inhibition of eNOS significantly increases the vasomotor tone of isolated coronary arteries or decreases resting epicardial coronary artery diameter, suggesting a tonic inhibition of coronary activity (Nishikawa and Ogawa 1997; Qi et al. 2007; Qin et al. 2007). Endothelium-derived NO (EDNO) is importantly involved in the responses of coronary vasculature to various circulating and local vasoactive agonists as well as shear stress (Vanhoutte et al. 2016). However, the inhibition of eNOS has limited influence on resting CBF and CBF during increased myocardial metabolism. This may be due to that CBF is largely regulated at small artery and arteriole levels by myogenic response and metabolites where the role of EDNO is not essential (Tune 2014; Duncker et al. 2015).

In healthy human coronary arterioles, EDNO and EDHFs are about equally involved in flow-mediated vasodilatation. In patients with coronary artery disease (CAD), the role of EDNO is diminished, while the role of EDHFs is enhanced (Miura et al. 2001). It is suspected that the production of EDHFs (EETs and H_2O_2) is normally inhibited by EDNO. Early in disease with mild elevation in superoxide, EDNO is quenched and EETs are produced as a compensatory vasodilator. With more severe oxidative stress, H_2O_2 blocks generation of EETs and emerges itself as a compensatory vasodilator (Larsen et al. 2008; Gutterman et al. 2016). Interestingly, BK_{Ca} channels, which are involved in vasodilatation caused by both EETs and H_2O_2, are upregulated in coronary arteries of CAD patients (Wiecha et al. 1997), which in

part contribute to the augmented EDHF-mediated vasodilatations under these diseased conditions.

PGI_2 is the primary prostanoid released from the ECs. It causes vasodilatation by binding to the PGI_2 (IP) receptors and activating cAMP signaling pathway (Baretella and Vanhoutte 2016). In porcine coronary arteries, the inhibition of cyclooxygenase, which blocks the synthesis of prostanoid, results in vasoconstriction at rest, suggesting that the dilator prostanoid, probably PGI_2, exerts a tonic inhibitory action on the resting tone of the coronary artery. Studies also imply that the dilator prostanoid is not mandatory for exercise-induced vasodilation (Merkus et al. 2004). In the remote noninfarcted porcine myocardium after myocardial infarction, the vasodilator effect of EDNO on the coronary resistance arteries is reduced, but the prostanoid vasodilator effect is maintained. The inhibitory effect of the prostanoids on endothelin-mediated vasoconstriction is enhanced. It suggests that under certain pathological conditions when the role of EDNO is compromised the prostanoid vasodilators may serve as a compensatory mechanism (de Beer et al. 2011). In rat aortas under diseased conditions, PGI_2 has been found to evoke vasoconstriction by binding to thromboxane prostanoid (TP) receptors instead of causing vasodilatation by binding to the IP receptors (Baretella and Vanhoutte 2016). It is unclear whether or not such a phenomenon exists in coronary vasculature.

15.4.3 Metabolic Factors

The metabolic factors play a major role in the regulation of CBF not only when myocardial O_2 consumption is increased such as during exercise but also when the myocardium is under hypoxic conditions (Tune 2014; Duncker et al. 2015). Since the heart maintains a high level of O_2 extraction under resting conditions, a further increase in O_2 demand is mainly met by an increase in CBF. The coronary venous pO_2 is at a rather constant level around 20 mmHg under a variety of physiological conditions. It suggests that a change in pO_2 is unlikely to act as a crucial metabolic dilator, although it is well established that hypoxia directly causes coronary vasodilation (Duncker and Bache 2008; Deussen et al. 2012; Pries et al. 2015). CO_2 is produced in proportion to oxidative metabolism. Increased CO_2 results in increased proton concentration, which has been proposed as a mediator for coronary vasodilation (Wexels et al. 1985; Wray and Smith 2004; Deussen et al. 2012). However, during physiologic increases in MVO_2 during exercise, the changes in coronary venous Pco_2 and H^+ concentrations are rather minor and insufficient to elicit increases in CBF (Rooke and Sparks 1980; Tune et al. 2000; Tune 2014). Another metabolite adenosine, as discussed in Chap. 9, could not play a significant role as a metabolic vasodilator but may have an important role in the regulation of CBF under hypoxia (Deussen et al. 2012; Tune 2014). Studies of recent years show that

H_2O_2 generated by myocardial mitochondria may act as a mediator to couple myocardial O_2 consumption to CBF via activation of VSMC K_v channels (Saitoh et al. 2006; Ohanyan et al. 2015). H_2O_2 is produced by myocardial mitochondria proportional to mitochondrial respiration and in large quantities. It is cell membrane permeable and has a sufficiently long half-life to serve as an intercellular signaling molecule to elicit coronary vasodilatation (Chabowski and Gutterman 2015). Many metabolites that are capable of causing vasodilatation can be generated in response to increased myocardial O_2 consumption. It is therefore very likely that more than one of these substances are involved in the metabolic coronary vasodilatation acting coordinately and that redundant regulatory mechanisms are involved (Deussen et al. 2012; Tune 2014; Goodwill et al. 2017).

15.4.4 Neuronal Influences

Coronary circulation is richly innervated by the sympathetic and parasympathetic nerves (Feigl 1998). In humans the α_1-adrenoceptors predominate in conduit coronary arteries, while α_2-adrenoceptors dominate in resistance coronary vessels (Baumgart et al. 1999). For the β-adrenoceptors, the β_1-subtype is more abundant in both the right and left large coronary arteries in humans except that the β_2-adrenoceptors are more dominant in the LAD artery (Amenta et al. 1991). In the dog the large conduit coronary arteries predominantly express β_1-adrenoceptors, a relative equal expression of β_1- and β_2-adrenoceptors in small coronary arteries (100–400 μm in diameter), and β_2-adrenoceptors are mainly located in arterioles sized $<$100 μm in diameter (Murphree et al. 1988). Parasympathetic innervation of both large and small coronary arteries has been demonstrated in a number of species (Feigl 1998). In the dog the degree of cholinergic innervation is LCX $>$ RCA $>$ LAD (Denn and Stone 1976).

The autonomic nervous system has a negligible effect on resting tone in the healthy coronary circulation (Chilian et al. 1981; Griggs et al. 1984). During exercise sympathetic nerve activity affects the CBF through three mechanisms: (1) initiation of local metabolic vasodilation via β-adrenoceptor-mediated increases in heart rate, contractility, and MVO_2; (2) vasodilatation via activation of coronary β-adrenoceptors; and (3) vasoconstriction via activation of coronary α-adrenoceptors (Feigl 1998; Tune 2014). Sympathetic activation increases cardiac function and oxygen consumption while at the same time increases oxygen delivery via β-adrenoceptor-mediated coronary vasodilatation, indicating that sympathetic nervous system regulates the coronary circulation by a feed-forward mechanism. Feed-forward vasodilation improves the speed of CBF regulation and prevents the development of subendocardial ischemia and buildup of local metabolites during sudden increases in demand from exercise (Tune 2014; Duncker et al. 2015; Goodwill et al. 2017). Evidence indicates that ~25% of exercise coronary hyperemia can be attributed to direct β-adrenoceptor-mediated effects of norepinephrine, with little role for circulating epinephrine (Gorman et al. 2000). When β-adrenoceptors are blocked, sympathetic activation unmasks α_1-mediated

coronary vasoconstriction resulting in mild reduction in the CBF. However, O_2 delivery is maintained by increased O_2 extraction, as evident by a reduced coronary venous O_2 tension (Duncker et al. 2015).

The influence of parasympathetic activity on CBF is relatively weak under baseline resting, even when vagal tone is high (Cowan and McKenzie 1990). The blockade of muscarinic receptors elicits a vasodilator response at rest and during mild exercise. It may result from an increased β-adrenergic activity, since it is abolished by the inhibition of β-adrenoceptor. The muscarinic receptor blocker has no effect on CBF at higher levels of exercise (Duncker et al. 1998). It is generally believed that parasympathetic mechanisms are unlikely to significantly contribute to metabolic coronary vasodilation (Feigl 1998; Tune 2014; Duncker et al. 2015; Goodwill et al. 2017).

References

Amenta F, Coppola L, Gallo P, Ferrante F, Forlani A, Monopoli A, Napoleone P (1991) Autoradiographic localization of β-adrenergic receptors in human large coronary arteries. Circ Res 68:1591–1599

Baretella O, Vanhoutte PM (2016) Endothelium-dependent contractions: prostacyclin and endothelin-1, partners in crime? Adv Pharmacol 77:177–208

Baumgart D, Haude M, Gorge G, Liu F, Ge J, Grosse-Eggebrecht C, Erbel R, Heusch G (1999) Augmented alpha-adrenergic constriction of atherosclerotic human coronary arteries. Circulation 99:2090–2097

Berne RM (1963) Cardiac nucleotides in hypoxia: possible role in regulation of coronary blood flow. Am J Phys 204:317–322

Beyer AM, Gutterman DD (2012) Regulation of the human coronary microcirculation. J Mol Cell Cardiol 52:814–821

Chabowski D, Gutterman D (2015) Unveiling the mechanism of coronary metabolic vasodilation: voltage-gated potassium channels and hydrogen peroxide. Circ Res 117:589–591

Chilian WM, Boatwright RB, Shoji T, Griggs DM Jr (1981) Evidence against significant resting sympathetic coronary vasoconstrictor tone in the conscious dog. Circ Res 49:866–876

Cornelissen AJ, Dankelman J, VanBavel E, Stassen HG, Spaan JA (2000) Myogenic reactivity and resistance distribution in the coronary arterial tree: a model study. Am J Physiol Heart Circ Physiol 278:H1490–H1499

Cowan CL, McKenzie JE (1990) Cholinergic regulation of resting coronary blood flow in domestic swine. Am J Phys 259:H109–H115

de Beer VJ, Taverne YJ, Kuster DW, Najafi A, Duncker DJ, Merkus D (2011) Prostanoids suppress the coronary vasoconstrictor influence of endothelin after myocardial infarction. Am J Physiol Heart Circ Physiol 301:H1080–H1089

Denn MJ, Stone HL (1976) Autonomic innervation of dog coronary arteries. J Appl Physiol 41:30–35

Deussen A, Ohanyan V, Jannasch A, Yin L, Chilian W (2012) Mechanisms of metabolic coronary flow regulation. J Mol Cell Cardiol 52:794–801

Dou D, Zheng X, Liu J, Xu X, Ye L, Gao Y (2012) Hydrogen peroxide enhances vasodilatation by increasing dimerization of cGMP-dependent protein kinase type Iα. Circ J 76:1792–1798

Duncker DJ, Bache RJ (2008) Regulation of coronary blood flow during exercise. Physiol Rev 88:1009–1086

Duncker DJ, Stubenitsky R, Verdouw PD (1998) Autonomic control of vasomotion in the porcine coronary circulation during treadmill exercise: evidence for feed-forward beta-adrenergic control. Circ Res 82:1312–1322

Duncker DJ, Koller A, Merkus D, Canty JM Jr (2015) Regulation of coronary blood flow in health and ischemic heart disease. Prog Cardiovasc Dis 57:409–422

Earley S, Brayden JE (2015) Transient receptor potential channels in the vasculature. Physiol Rev 95:645–690

Ellinsworth DC, Sandow SL, Shukla N, Liu Y, Jeremy JY, Gutterman DD (2016) Endothelium-derived hyperpolarization and coronary vasodilation: diverse and integrated roles of epoxyeicosatrienoic acids, hydrogen peroxide, and gap junctions. Microcirculation 23:15–32

Feigl EO (1983) Coronary physiology. Physiol Rev 63:1–205

Feigl EO (1998) Neural control of coronary blood flow. J Vasc Res 35:85–92

Feigl EO (2004) Berne's adenosine hypothesis of coronary blood flow control. Am J Physiol Heart Circ Physiol 287:H1891–H1894

Fulton WFM (1963) Arterial anastomoses in the coronary circulation. I. Anatomical features in normal and diseased hearts demonstrated by stereoarteriography. Scottish Med J 8:420–434

Gerlach E, Deuticke B, Dreisbach RH (1963) Der Nucleotid-Abbau im herzmuskel bei sauerstoffmangel und seine mögliche bedeutung für die coronardurchblutung. Naturwissenschaften 50:228–229

Giles TD, Sander GE, Nossaman BD, Kadowitz PJ (2012) Impaired vasodilation in the pathogenesis of hypertension: focus on nitric oxide, endothelial-derived hyperpolarizing factors, and prostaglandins. J Clin Hypertens (Greenwich) 14:198–205

Goodwill AG, Dick GM, Kiel AM, Tune JD (2017) Regulation of coronary blood flow. Compr Physiol 7:321–382

Gorman MW, Tune JD, Richmond KN, Feigl EO (2000) Quantitative analysis of feedforward sympathetic coronary vasodilation in exercising dogs. J Appl Physiol 89:1903–1911

Griggs DM Jr, Chilian WM, Boatwright RB, Shoji T, Williams DO (1984) Evidence against significant resting alpha-adrenergic coronary vasoconstrictor tone. Fed Proc 43:2873–2877

Gutterman DD, Chabowski DS, Kadlec AO, Durand MJ, Freed JK, Ait-Aissa K, Beyer AM (2016) The human microcirculation: regulation of flow and beyond. Circ Res 118:157–172

Guyton RA, McClenathan JH, Newman GE, Michaelis LL (1977) Significance of subendocardial S-T segment elevation caused by coronary stenosis in the dog. Epicardial S-T segment depression, local ischemia and subsequent necrosis. Am J Cardiol 40:373–380

Hart BJ, Bian X, Gwirtz PA, Setty S, Downey HF (2001) Right ventricular oxygen supply/demand balance in exercising dogs. Am J Physiol Heart Circ Physiol 281:H823–H830

Hoffman JI, Buckberg GD (2014) The myocardial oxygen supply: demand index revisited. J Am Heart Assoc 3:e000285

Ishibashi Y, Duncker DJ, Zhang J, Bache RJ (1998) ATP-sensitive K^+ channels, adenosine, and nitric oxide-mediated mechanisms account for coronary vasodilation during exercise. Circ Res 82:346–359

Jones CJ, Kuo L, Davis MJ, Chilian WM (1995) Regulation of coronary blood flow: coordination of heterogeneous control mechanisms in vascular microdomains. Cardiovasc Re 29:585–596

Kanatsuka H, Lamping KG, Eastham CL, Marcus ML (1990) Heterogeneous changes in epimyocardial microvascular size during graded coronary stenosis. Evidence of the microvascular site for autoregulation. Circ Res 66:389–396

Katz SA, Feigl EO (1988) Systole has little effect on diastolic coronary artery blood flow. Circ Res 62:443–451

Klassen GA, Armour JA (1984) Coronary venous pressure and flow: effects of vagal stimulation, aortic occlusion, and vasodilators. Can J Physiol Pharmacol 62:531–538

Kroll K, Stepp DW (1996) Adenosine kinetics in canine coronary circulation. Am J Phys 270: H1469–H1483

Kuo L, Davis MJ, Chilian WM (1988) Myogenic activity in isolated subepicardial and subendocardial coronary arterioles. Am J Phys 255:H1558–H1562

Kuo L, Chilian WM, Davis MJ (1990) Coronary arteriolar myogenic response is independent of endothelium. Circ Res 66:860–866

Kuo L, Arko F, Chilian WM, Davis MJ (1993) Coronary venular responses to flow and pressure. Circ Res 72:607–615

Larsen BT, Gutterman DD, Sato A, Toyama K, Campbell WB, Zeldin DC, Manthati VL, Falck JR, Miura H (2008) Hydrogen peroxide inhibits cytochrome p450 epoxygenases: interaction between two endothelium-derived hyperpolarizing factors. Circ Res 102:59–67

Liu C, Montell C (2015) Forcing open TRP channels: mechanical gating as a unifying activation mechanism. Biochem Biophys Res Commun 460:22–25

Loukas M, Bilinsky S, Bilinsky E, el-Sedfy A, Anderson RH (2009) Cardiac veins: a review of the literature. Clin Anat 22:129–145

Loukas M, Sharma A, Blaak C, Sorenson E, Mian A (2013) The clinical anatomy of the coronary arteries. J Cardiovasc Transl Res 6:197–207

Maxwell M, Hearse D, Yellon D (1987) Species variation in the coronary collateral circulation during regional myocardial ischaemia: a critical determinant of the rate of evolution and extent of myocardial infarction. Cardiovasc Res 21:737–746

Merkus D, Houweling B, Zarbanoui A, Duncker DJ (2004) Interaction between prostanoids and nitric oxide in regulation of systemic, pulmonary, and coronary vascular tone in exercising swine. Am J Physiol Heart Circ Physiol 286:H1114–H1123

Miller FJ, Dellsperger KC, Gutterman DD (1997) Myogenic constriction of human coronary arterioles. Am J Physiol Heart Circ Physiol 273:H257–H264

Miura H, Wachtel RE, Liu Y, Loberiza FR Jr, Saito T, Miura M, Gutterman DD (2001) Flow-induced dilation of human coronary arterioles: important role of Ca(2+)-activated K(+) channels. Circulation 103:1992–1998

Mosher P, Ross J Jr, McFate PA, Shaw RF (1964) Control of coronary blood flow by an autoregulatory mechanism. Circ Res 14:250–259

Murphree SS, Saffitz JE (1988) Delineation of the distribution of β -adrenergic receptor subtypes in canine myocardium. Circ Res 63:117–125

Nishikawa Y, Ogawa S (1997) Importance of nitric oxide in the coronary artery at rest and during pacing in humans. J Am Coll Cardiol 29:85–92

Ohanyan V, Yin L, Bardakjian R, Kolz C, Enrick M, Hakobyan T, Kmetz J, Bratz I, Luli J, Nagane M, Khan N, Hou H, Kuppusamy P, Graham J, Fu FK, Janota D, Oyewumi MO, Logan S, Lindner JR, Chilian WM (2015) Requisite role of Kv1.5 channels in coronary metabolic dilation. Circ Res 117:612–621

Opie LH, Heusch G (2004) Oxygen supply: coronary flow. In: Heart physiology: from cell to circulation, 4th ed. Opie LH (ed). Lippincott, Williams & Wilkins, Philadelphia, pp 279–305

Pries AR, Badimon L, Bugiardini R, Camici PG, Dorobantu M, Duncker DJ, Escaned J, Koller A, Piek JJ, de Wit C (2015) Coronary vascular regulation, remodelling, and collateralization: mechanisms and clinical implications on behalf of the working group on coronary pathophysiology and microcirculation. Eur Heart J 36:3134–3146

Qi H, Zheng X, Qin X, Dou D, Xu H, Raj JU, Gao Y (2007) PKG regulates the basal tension and plays a major role in nitrovasodilator-induced relaxation of porcine coronary veins. Br J Pharmacol 152:1060–1069

Qin X, Zheng X, Qi H, Dou D, Raj JU, Gao Y (2007) cGMP-dependent protein kinase in regulation of basal tone and in nitroglycerin and nitric oxide induced relaxation in porcine coronary artery. Pflügers Arch Eur J Physiol 454:913–923

Rajagopalan S, Dube S, Canty JM Jr (1995) Regulation of coronary diameter by myogenic mechanisms in arterial microvessels greater than 100 microns in diameter. Am J Phys 268: H788–H793

Rooke T, Sparks HV (1980) Arterial CO_2, myocardial O_2 consumption, and coronary blood flow in the dog. Circ Res 47:217–225

Saitoh S, Zhang C, Tune JD, Potter B, Kiyooka T, Rogers PA, Knudson JD, Dick GM, Swafford A, Chilian WM (2006) Hydrogen peroxide: a feed-forward dilator that couples myocardial metabolism to coronary blood flow. Arterioscler Thromb Vasc Biol 26:2614–2621

Seiler C, Stoller M, Pitt B, Meier P (2013) The human coronary collateral circulation: development and clinical importance. Eur Heart J 34:2674–2682

Shimokawa H (2014) 2014 Williams Harvey lecture: importance of coronary vasomotion abnormalities-from bench to bedside. Eur Heart J 35:3180–3193

Spaan JA, Cornelissen AJ, Chan C, Dankelman J, Yin FC (2010) Dynamics of flow, resistance, and intramural vascular volume in canine coronary circulation. Am J Physiol Heart Circ Physiol 278:H383–H403

Spassova MA, Hewavitharana T, Xu W, Soboloff J, Gill DL (2006) A common mechanism underlies stretch activation and receptor activation of TRPC6 channels. Proc Natl Acad Sci U S A 103:16586–16591

Stepp DW, Merkus D, Nishikawa Y, Chilian WM (2001) Nitric oxide limits coronary vasoconstriction by a shear stress-dependent mechanism. Am J Physiol Heart Circ Physiol 281:H796–H803

Tiefenbacher CP, Chilian WM (1998) Heterogeneity of coronary vasomotion. Basic Res Cardiol 93:446–454

Tune JD (2014) Coronary circulation. Morgan & Claypool Life Sciences, San Francisco, pp 1–175

Tune JD, Richmond KN, Gorman MW, Feigl EO (2000) Role of nitric oxide and adenosine in control of coronary blood flow in exercising dogs. Circulation 101:2942–2948

Tune JD, Gorman MW, Feigl EO (2004) Matching coronary blood flow to myocardial oxygen consumption. J Appl Physiol 97:404–415

Vanhoutte PM, Zhao Y, Xu A, Leung SW (2016) Thirty years of saying NO: sources, fate, actions, and misfortunes of the endothelium-derived vasodilator mediator. Circ Res 119:375–396

Walker LA, Buttrick PM (2013) The right ventricle: biologic insights and response to disease: updated. Curr Cardiol Rev 9:73–81

Wexels JC, Myhre ES, Mjos OD (1985) Effects of carbon dioxide and pH on myocardial blood-flow and metabolism in the dog. Clin Physiol 5:575–588

Wiecha J, Schläger B, Voisard R, Hannekum A, Mattfeldt T, Hombach V (1997) Ca^{2+}-activated K^+ channels in human smooth muscle cells of coronary atherosclerotic plaques and coronary media segments. Basic Res Cardiol 92:233–239

Wray S, Smith RD (2004) Mechanisms of action of pH-induced effects on vascular smooth muscle. Mol Cell Biochem 263:163–172

Wusten B, Buss D, Schaper W (1977) Distribution of left ventricular myocardial blood flow under various loading conditions. Bibl Anat:35–40

Ying L, Xu X, Liu J, Dou D, Yu X, Ye L, He Q, Gao Y (2012) Heterogeneity in relaxation of different sized porcine coronary arteries to nitrovasodilators: role of PKG and MYPT1. Pflügers Arch Eur J Physiol 463:257–268

Yonekura S, Watanabe N, Downey HF (1988) Transmural variation in autoregulation of right ventricular blood flow. Circ Res 62:776–781

Zong P, Tune JD, Downey HF (2005) Mechanisms of oxygen demand/supply balance in the right ventricle. Exp Biol Med (Maywood) 230:507–519

Chapter 16
Cerebral Vasoreactivity

Abstract Cerebral blood flow is regulated by two critical mechanisms, cerebral autoregulation and neurovascular coupling (NVC). Cerebral autoregulation maintains a constant blood flow within the physiological range of systemic pressures, which is primarily conducted through myogenic response. The cerebral microcirculation is supplied by parenchymal arterioles, which form a functional unit with the adjacent nerve terminals, and astrocytes that encase the arterioles, known as neurovascular unit. Such a morphological arrangement ensures rapid spatial and temporal increases in cerebral blood flow in response to neuronal activation, known as NVC. A broad range of metabolic factors, vascular active agents, and neuronal activities are involved in the processes of autoregulation and NVC through affecting vascular reactivity. Among them, the most prominent ones that include O_2, CO_2, adenosine, nitric oxide, prostaglandins, epoxyeicosatrienoic acids, and neuronal regulation will be discussed in this chapter.

Keywords Cerebral circulation • Autoregulation • Neurovascular coupling • Hypoxia • CO_2 • Adenosine • Nitric oxide • Prostaglandin • Epoxyeicosatrienoic acids • Neuronal regulation

16.1 Introduction

The human brain is made up of roughly 100 billion neurons, organized into extensive networks (Herculano-Houzel 2009). It weighs ~2% of the total body mass but consumes ~20% of the O_2 taken up by the whole body at rest. Brain functions are heavily dependent on an uninterrupted O_2 supply. If cerebral O_2 delivery is halted, consciousness could be lost in a few seconds (Lassen 1959; Cipolla 2016).

Under most conditions including sleep, the resting waking state, and during intellectual activities, the total cerebral metabolism is relatively unchanged, and cerebral blood flow (CBF) remains fairly constant. In distinct local areas of the brain, however, an increased neuronal activity and consequently increased metabolic demand and increased blood flow may well occur (Lassen 1959; Heistad and Kontos 2011; Joyner and Casey 2015). To adapt such unique characteristics, the cerebral circulation has developed two key mechanisms to fulfill its function: the

Y. Gao, *Biology of Vascular Smooth Muscle: Vasoconstriction and Dilatation*,
DOI 10.1007/978-981-10-4810-4_16

autoregulatory mechanism and neurovascular coupling (NVC) mechanism. The vascular autoregulation ensures a globally relatively stable perfusion pressure in the face of systemic blood pressure fluctuations (Tzeng and Ainslie 2014; Willie et al. 2014; Cipolla 2016), while NVC ensures sufficient blood flow to the needed brain area with distinct spatial and temporal signatures (Muñoz et al. 2015; Filosa et al. 2016; Lecrux and Hamel 2016). In this chapter, the general anatomy of cerebral vasculature, the characteristics of cerebral autoregulation and NVC, and the various factors involved in the regulation of cerebral vasoreactivities will be discussed.

16.2 The Anatomy of Cerebral Circulation

Blood supply to the brain is provided by the left and right internal carotid and the left and right vertebral arteries. The internal carotid arteries mainly supply the cerebrum, whereas the vertebral arteries supply the cerebellum and brain stem. At the base of the brain, the internal carotid arteries, the anterior communicating artery, anterior cerebral arteries, posterior communicating arteries, and posterior cerebral arteries form a circulatory loop, known as the circle of Willis. Among the participating vessels, the anterior cerebral and anterior communicating arteries are branched from the internal carotid arteries, whereas the posterior cerebral and posterior communicating arteries come from the basilar artery, which is formed by the left and right vertebral arteries. The circle of Willis gives rise to three pairs of main arteries, namely, the anterior, middle, and posterior cerebral arteries. These cerebral arteries split into progressively smaller arteries and arterioles that run along the surface of the brain, known as pial arteries, and then penetrate the brain tissue to supply blood to the corresponding regions of the cerebral cortex (Heistad and Kontos 2011; Cipolla 2016).

The venous drainage of the cerebrum can be separated into two subdivisions: superficial and deep. The superficial system is located between the periosteal and meningeal layers of the dura mater in the brain and known as dural venous sinuses. They drain blood from internal and external veins of the brain, receive cerebrospinal fluid (CSF) from the subarachnoid space via arachnoid granulations, and empty them primarily into the internal jugular vein. The deep venous system is mainly composed of traditional veins inside the deep structures of the brain, which join behind the midbrain to form the great cerebral vein, also known as the vein of Galen. This vein merges with the inferior sagittal sinus to form the straight sinus, which then joins the superficial venous system at the confluence of sinuses (Uddin et al. 2006; Kiliç and Akakin 2008; Heistad and Kontos 2011; Cipolla 2016).

The capillary bed of the brain constitutes a dense network with all capillaries that are constantly perfused with blood (Zlokovic 2008). It is estimated that nearly every neuron in the brain has its own capillary (Zlokovic 2005). The capillaries of the brain are principally made up of one layer of endothelial cells. These endothelial cells are connected by tight junction complexes forming the blood–brain barrier

(BBB) that does not exist in normal circulation. The BBB is impermeable to microscopic objects (e.g., bacteria) and large or hydrophilic molecules but allows the passage of water, some gases, and lipid-soluble molecules by passive diffusion. The cerebral endothelial cells also possess specific transporters apically to actively transport nutrients from the blood into the brain and basolaterally to transport inactivate toxic substances and transfer them into the blood. This barrier also includes a thick basement membrane and astrocytic end-feet (de Vries et al. 1997; Zlokovic 2008). The BBB is absent from the circumventricular organs (CVOs), which are small-sized structures lining the cavity of the third ventricle and of the fourth ventricle. The cerebral endothelium of CVOs is fenestrated so that cross talk between the brain and peripheral blood can carry out, such as the release and transport of hormones. CVOs are not totally without barrier properties. The barrier for CVO lies in the epithelial cells known as tanycytes and ependymal cells such that circulating substances can diffuse into the CVO but not beyond (Duvernoy and Risold 2007; Cipolla 2016).

16.3 Regulation of Cerebral Circulation

In an average adult, CBF is typically 750 ml/min, which equates to an average perfusion of ~50 ml/100 g/min of brain tissue and represents ~15% of the cardiac output. The brain at rest extracts ~20% of the O_2 delivered from the CBF. Under various physiological conditions such as sleep, the resting waking state, and during intellectual effort and exercise, the total cerebral metabolism has been found to remain relatively unchanged. An increased function and thus metabolism of certain local areas of the brain may well occur. However, the distinct neuronal activities normally occurred may exert a limited impact on the global CBF (Lassen 1959; Heistad and Kontos 2011). Therefore, the regulation of cerebral circulation could be fulfilled from two aspects: (1) globally to maintain a relative stable CBF, which is primarily achieved through autoregulation, provided cerebral perfusion pressure (the difference between intra-arterial pressure and the pressure in veins) is within physiological range (Tzeng and Ainslie 2014; Cipolla 2016), and (2) locally to match the blood supply to the metabolic demand suitable for the neuronal activities, which is mainly accomplished through NVC (Muñoz et al. 2015; Filosa et al. 2016; Lecrux and Hamel 2016).

16.3.1 Cerebral Autoregulation

The brain is highly susceptible to hypoxia/ischemic injury. Conversely, overabundant cerebral blood flow can result in the breakdown of the BBB resulting in hyperperfusion syndromes characterized by debilitating neurological sequelae (Tzeng and Ainslie 2014). The classic view of cerebral autoregulation, based on

steady-state cerebral blood flow (CBF) and blood pressure measurements in patients with hypertensive and hypotensive disorders, has long been hold that CBF is maintained at a constant level of perfusion through a broad range of mean arterial pressure of ~60 to 160 mmHg (Lassen 1959; Tzeng and Ainslie 2014; Cipolla 2016). This concept, however, has been found inadequate since the 1980s by studies with the introduction of imaging techniques. These studies reveal that cerebral autoregulation does not maintain constant perfusion across a broad range of mean artery pressure (MAP) as is often believed and that the autoregulation is more effective against acute hypertension than hypotension (Tzeng and Ainslie 2014; Willie et al. 2014). Furthermore, in the cerebral circulation, both large arteries and small arterioles play a critical role in CBF autoregulation. It appears that there exists a hierarchy in vascular responsiveness which forms a basis for more complicated regulation (Heistad et al. 1978; Koller and Toth 2012; Liu et al. 2013).

The myogenic response as the major determinant in CBF autoregulation has been demonstrated under in vitro and in vivo conditions in a number species including humans (Vinall and Simeone 1981; Ngai and Winn 1995; Liu et al. 2013; Willie et al. 2014). Myogenic response is an intrinsic property of vascular smooth muscle cells (VSMCs). It is initiated by pressure-induced VSMC stretch, which leads to membrane depolarization event and increased Ca^{2+} influx through voltage-gated Ca^{2+} channels. Stretch also causes increased Ca^{2+} release from the sarcoplasmic reticulum, increased Ca^{2+} sensitivity of myofilaments, and consequently vasoconstriction (Drummond et al. 2008; Hill and Meininger 2012; Kauffenstein et al. 2012). In isolated rat intracerebral arterioles, at no flow conditions, the increase in pressure from 20 to 100 mmHg results in vasoconstriction, which is greatest at 60 mmHg. Increasing flow rate at a constant pressure of 60 mmHg causes vasodilatation at low flow rates but vasoconstriction at higher flow rates (Ngai and Winn 1995). Under in vivo conditions, changes in pressure are accompanied by changes in flow, and changes in flow may contribute to the autoregulation of CBF evoked by myogenic response (Koller and Toth 2012). It seems that the myogenic response of the large arteries of the neck and cerebrum serves as the first-line defense so that the pial and cortical arterioles subject to minimal changes in pressure and can respond principally to local metabolites (Willie et al. 2014).

16.3.2 Neurovascular Coupling

The cerebral microcirculation is supplied by parenchymal arterioles. These arterioles are innervated from within the brain parenchyma with the nerve terminals that adjoin astrocytes while the end-feet of these astrocytes encase arterioles. To a lesser extent, nerve terminals are also in close vicinity to the arterioles. Such an arrangement, termed "neurovascular unit," forms the morphological basis for the coupling between changes in neurophysiology and hemodynamics, known as NVC (Muñoz et al. 2015; Filosa et al. 2016; Lecrux and Hamel 2016). In the rat, vibrissal

stimulation activates distinct barrel structures in layer IV of the contralateral somatosensory cortex, which is associated with local increases in blood flow in the barrel cortex corresponding to the stimulated whiskers. When the whisker is stimulated, sensory thalamocortical glutamatergic afferents recruit pyramidal cells, some of those containing the type 2 cyclooxygenase (COX-2) directly affect local blood flow by the release of dilatory prostaglandins (PGs), and some affect CBF indirectly by activating astrocytes resulting the release of dilatory epoxyeicosatrienoic acids (EETs), probably via metabotropic glutamate receptors (mGluRs). Some γ-aminobutyric acid (GABA) interneurons are also involved. The parvalbumin-containing GABA interneurons are silenced, which would disinhibit pyramidal cells and augment cortical activity. GABA interneurons may also activate the EET pathway in astrocytes via $GABA_A$ receptor-mediated increase in calcium transients (Lecrux et al. 2011) (Fig. 16.1). Neurons whose cell bodies are from within the subcortical brain regions may project to cortical microvessels to control local blood flow. For instance, basal forebrain stimulation may trigger the release of acetylcholine (ACh) from the nerve terminals in distinct cortex resulting vasodilatation. The vasodilatory effect is also mediated in part by the local release of GABA from cholinoceptive cortical interneurons and indirectly by the release of dilatory EETs from the end-feet of astrocytes that ensheathe parenchymal arterioles (Kocharyan et al. 2008). Distinct cortical interneurons and astrocytes are also activated indirectly by noradrenergic input from locus coeruleus and consequently vasodilatation. These noradrenergic nerve terminals may directly relax parenchymal arterioles via the release of norepinephrine (Toussay et al. 2013).

Some evidence suggests that pericytes may also participate in NVC response (Dalkara and Alarcon-Martinez 2015; Filosa et al. 2016). Pericytes are contractile cells and associated primarily with capillaries. In brain capillaries, pericytes are located between endothelial cells and astrocytes by a thin basal membrane (Peppiatt et al. 2006). These pericytes may regulate the capillary blood flow in response to signaling molecules released from astrocytes and nearby nerve terminals. Pericytes are responsive to vasoconstrictors such as ATP, dopamine, angiotensin II, norepinephrine, and 20-hydroxyeicosatetraenoic acid (20-HETE) and to vasodilators such as nitric oxide (NO), prostaglandin E2 (PGE_2), and adenosine (Filosa et al. 2016). Neuronal activity and the neurotransmitter glutamate have been found to dilate cerebral capillaries by actively relaxing pericytes, which are mediated by PGE_2, but require NO release to suppress vasoconstricting 20-HETE synthesis. Under in vivo conditions, sensory input increases cerebral blood flow, and the capillary dilatation occurs before arterioles, implying that pericytes may act as an initiator for NVC response (Hall et al. 2014). The microglia, in particular a small population of microglia termed juxtavascular microglia, has also been proposed for a role in NVC response. Unlike astrocytes, microglial processes are highly active under physiological conditions. It is suspected that the contribution of microglia toward NVC may occur via the release of small molecular messengers and ligand–receptor interactions (Filosa et al. 2016).

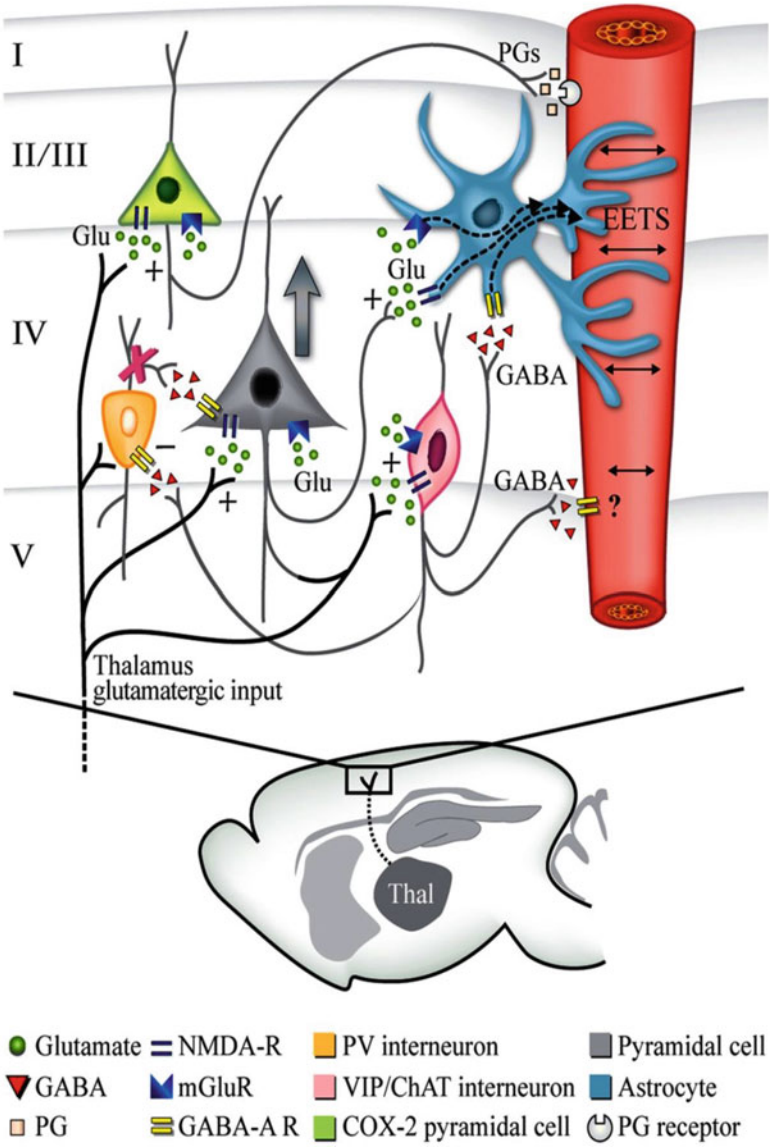

Fig. 16.1 Mechanism underlying the neurovascular coupling (NVC) between neuronal activities evoked by whisker stimulation and blood flow of the local cortex of the rat. Distinct barrel structures in layer IV of the somatosensory cortex are activated by the contralateral vibrissal stimulation, which leads to an increased blood flow in this barrel cortex. When the whisker is stimulated, sensory thalamocortical (Thal) glutamatergic afferents activate pyramidal cells. Some of those containing the type 2 cyclooxygenase (COX-2) directly affect local blood flow by releasing dilatory prostaglandins (PGs), probably PGE_2. The astrocytes that abut on the parenchymal arterioles with their end-feet may release dilatory epoxyeicosatrienoic acids (EETs). The astrocytes are also activated via metabotropic glutamate receptors (mGluRs). Some vasoactive intestinal polypeptide (VIP)/choline acetyltransferase (ChAT)-immunopositive (VIP/ChAT) interneurons may affect vasoactivity by directly acting on the arterioles and indirectly acting on the astrocytes through the release of γ-aminobutyric acid (GABA). The VIP/ChAT interneurons exert

16.4 Regulation of Cerebral Vasoreactivity

In peripheral circulations, the major site of vascular resistance typically resides in small arterioles with diameter <100 μm. In cerebral circulation, however, large arteries contribute importantly to total cerebral vascular resistance. In the rabbit, the arteries upstream to pial arterioles of 100 μm in diameter contribute to about 50% of cerebral arterial resistance. Similar phenomenon has been observed in the cat and primate. The vasoreactivity of large cerebral arteries is an important determinant of microvascular perfusion pressure. For instance, when a focal increase in blood flow to a region occurs, if the resistance of the large artery remains unchanged, a greater drop in pressure would occur in the upstream vascular segment, and consequently a decreased microvascular perfusion pressure ensues, known as vascular "steal." However, a dilatation response of the larger arteries to increased blood flow that normally occurs would lead to a reduced pressure drop in the upstream segment, and thus the proper microvascular perfusion pressure is maintained (Faraci and Heistad 1990; Cipolla 2016).

Cerebral vascular activity is critically affected by a number of local metabolic variants, in particular hypoxia, changes in Pco_2, and adenosine (Willie et al. 2014; Cipolla 2016) At the same time, certain vasoactive agents derived from local neurons, astrocytes, and/or the endothelial cells play an important role in the regulation of cerebral vascular activity, which include nitric oxide (NO), dilator prostaglandins (PGs), and epoxyeicosatrienoic acids (EETs) (Attwell et al. 2010). The entire cerebrovasculature is densely innervated by adrenergic and cholinergic fibers. Their activity may be essential in buffering surges in perfusion pressure and in maintaining the integrity of cerebral vascular functionality (ter Laan et al. 2013; Willie et al. 2014).

16.4.1 Hypoxia

A reduction in Po_2 has no effect on the CBF until it falls below ~50 mmHg, below which CBF increases substantially (Johnston et al. 2003; Masamoto and Tanishita 2009). Cerebral vasodilatation to hypoxia is augmented under hypercapnic conditions and attenuated under hypocapnic conditions (Mardimae et al. 2012). Under isocapnic conditions, hypoxia has been found to increase the CBF by 0.5–2.5% per percentage point reduction in arterial saturation of O_2 (Querido et al. 2013; Willie

Fig. 16.1 (continued) an inhibitory effect on parvalbumin-containing (PV) interneurons. The inhibition of the PV interneurons would disinhibit pyramidal cells and augment cortical activity. The × sign on PV interneurons indicates the silence effect of these interneurons on pyramidal cells. *GABA-A R* $GABA_A$ receptor, *Glu* glutamate, *NMDA-R* N-methyl-d-aspartate receptors (This figure is from Lecrux et al. (2011), with permission)

et al. 2014). For a given severity of isocapnic hypoxia, congruous positron emission tomography (PET) scan reveals that blood flow to the phylogenetically older areas of the brain increases more than that to the cortical regions (Binks et al. 2008; Lewis et al. 2014). The mechanism underlying hypoxia-induced dilatation of cerebral vasculature is multifactorial (Willie et al. 2014; Cipolla 2016), which may include:

1. Stimuli from the neurovascular unit evoked by local tissue hypoxia (Pelligrino et al. 1995; Thompson et al. 2003; Leithner and Royl 2014)
2. Local vasodilatory metabolites such as adenosine and H^+ released from increased anaerobic metabolism (Nolan et al. 1982; Meno et al. 1993)
3. Direct vasodilatory effect of hypoxia resulting in activation of ATP-activated K^+ (K_{ATP}) channels (Taguchi et al. 1994), suppressed Ca^{2+} influx (Pearce et al. 1992), altered activity of sarcoplasmic reticulum Ca^{2+} ATPase (Guibert et al. 2002), and enhanced cGMP activity of the cerebral arteries (Hoiland et al. 2016)

16.4.2 CO_2

CO_2 serves as one of the fundamental regulators of CBF. The cerebral vascular tree, from the internal carotid and vertebral arteries to pial arterioles and parenchymal vessels, exhibits a high sensitivity to Pco_2. The large cerebral arteries show an ~3–6% increase in blood flow per mmHg change in CO_2 above eupnea and ~1–3% decrease in blood flow below eupnea $Paco_2$ (Willie et al. 2014). Different brain regions seem to have a similar sensitivity to changes in $Paco_2$ in the hypercapnic but not hypocapnic range, whereas CO_2 reactivity of the microvasculature is greater in gray matter than in white matter, probably due to relatively less vascularization (Harper and Glass 1965; Mandell et al. 2008; Willie et al. 2012).

It appears that the response of cerebral vasculature to CO_2 results from changes in extracellular fluid pH and that molecular CO_2 does not have independent vasoactivity, as evident by the close relationship between the contractile response of cerebral arteries and arterioles and extracellular pH rather than Pco_2 (Kontos et al. 1977; Toda et al. 1989). In mice, reducing external pH from 7.4 to 7.0 causes dilatation of brain parenchymal arterioles under both normocapnic and hypercapnic conditions, accompanied by dramatically increased Ca^{2+} spark activity. The acidic pH-induced vasodilatation is attenuated by ~60% by the blockers of the large-conductance, calcium-activated K^+ (BK_{Ca}) channels and ryanodine receptors (RyRs) in a nonadditive manner. Similar dilator responses to acidosis were reduced by nearly 60% in arterioles from mice deficient in BK_{Ca} channels. These results suggest that acidification may dilate cerebral arterioles by the activation of BK_{Ca} channels, probably due to enhanced Ca^{2+} sparks resulting from increased luminal Ca^{2+} concentration of the sarcoplasmic reticulum occurred after H^+-dependent inhibition of RyRs (Dabertrand et al. 2012).

16.4.3 Adenosine

Adenosine is a potent dilator of cerebral vasculature. An increased release of adenosine is associated with cerebral vasodilatation during metabolic stress such as neural activation and hypoxia (O'Regan 2005). In adenosine 2A receptor ($A_{2A}R$) knockout mice, the increase in CBF evoked by hypoxia is markedly attenuated compared with that of the wide-type control, suggesting that a significant proportion of the hypoxic vasodilatation is mediated by adenosine via $A_{2A}R$ (Miekisiak et al. 2008). In isolated porcine pial arterioles, adenosine causes vasodilatation by stimulating the release of endothelium-derived NO and by direct binding to the $A_{2A}R$ on VSMCs. Endothelial NO exerts its action through the activation of smooth muscle soluble guanylyl cyclase (sGC), while the direct action of adenosine on VSMCs is mediated by cAMP signaling pathway (Hein et al. 2013).

16.4.4 NO, PGs, and EETs

Substantial evidence suggests that NO, PGs, and EETs are the prominent players in the coupling of neuronal activity to the regional CBF (Attwell et al. 2010). In wide-type mice, the increase in blood flow of unilateral cortical barrel field induced by contralateral whisker stimulation is suppressed by ~45% by NO synthase (NOS) inhibitor nitro-L-arginine. This phenomenon is not observed in neuronal NOS (nNOS) knockout mice, implying an important role for nNOS in NVC (Ma et al. 1996). In neurons, synaptically released glutamate acts on N-methyl-d-aspartate receptors (NMDA-R) resulting in Ca^{2+}-dependent activation of nNOS followed by increased generation of NO, which causes VSMCs to relax via the activation of sGC (Attwell et al. 2010). Studies suggest that endothelial NOS (eNOS) is also activated through the binding of glutamate to NMDA-R on astrocytes in NVC (Stobart et al. 2013). It appears that while both nNOS and eNOS participate in neuronal activity-associated vasodilatory responses, eNOS is more prominent at lower levels of neuronal activity and nNOS dominating at higher neuronal activation levels (de Labra et al. 2009).

Upon stimulation by synaptically released glutamate, both neurons and astrocytes of the neurovascular unit can synthesize vasodilatory PGs, primarily PGE_2, through Ca^{2+}-activated phospholipase A_2 and then the conversion of arachidonic acid to PGs by cyclooxygenase (COX). The vasodilatory PGs exert their action on VSMCs mainly via cAMP signaling. The stimulation by glutamate also causes astrocytes to release EETs resulting from an enhanced activity of epoxygenases on arachidonic acid. EETs cause vasodilatation through hyperpolarization of VSMCs. Arachidonic acid formed in astrocytes may diffuse across cell membranes into the VSMCs where it is converted to 20-hydroxyeicosatetraenoic acid (20-HETE) through cytochrome P450 4A (CYP4A) (Attwell et al. 2010; Muñoz et al. 2015; Lecrux and Hamel 2016). 20-HETE causes vasoconstriction through

depolarization of VSMCs due to the blockade of BK_{Ca} channels. The synthesis of 20-HETE is inhibited by NO (Sun et al. 2000; Roman 2002).

O_2 is required for the synthesis of NO, PGs, EETs, and 20-HETE. The Michaelis constants (K_m values) of O_2 for eNOS and nNOS at 25 °C are ~4 μM and ~350 μM, respectively (Stuehr et al. 2004). The K_m values of O_2 for the synthesis of 20-HETE and EETs at 37 °C are ~55 μM and <10 μM, respectively (Harder et al. 1996), whereas the K_m value for the synthesis of PGs is ~10 μM at 24 °C (Barnett et al. 1994). The concentrations of O_2 in vivo in the cerebral extracellular space range from 20 to 60 μM, which can decrease further during intense synaptic activity (Dings et al. 1998). Therefore, the production of NO derived from nNOS and 20-HETE may be more restricted by the O_2 availability than the production of NO derived from eNOS, PGs, and EETs. In addition, as O_2 concentrations decrease, an increased activity of glycolysis results in increased release of lactate into extracellular space. Extracellular lactate inhibits the uptake of PGE_2 by the prostaglandin transporter, leading to accumulation and subsequent vasodilation. Meanwhile an increased extracellular adenosine under hypoxia can directly dilate parenchymal arterioles (Gordon et al. 2008; Attwell et al. 2010; Gordon et al. 2011) (Fig. 16.2).

16.4.5 Autonomic Regulation of Cerebral Blood Flow

Cerebral vasculature is extensively innervated by adrenergic and cholinergic fibers of extrinsic and intrinsic origins. The extraparenchymal arteries are innervated extrinsically by adrenergic fibers originated in the superior cervical ganglion, cholinergic fibers originated primarily in the sphenopalatine ganglion, and the afferent system originated in the trigeminal ganglion. The intraparenchymal arterioles are innervated intrinsically by nerve terminals projected from brain nuclei such as locus coeruleus, fastigial nucleus, and dorsal raphe nucleus (Edvinsson 1987; ter Laan et al. 2013).

The blockade of sympathetic ganglions with the ganglionic blocker and α-adrenoceptor blocker results in a greater rise in CBF for a given increase in MAP (Kimmerly et al. 2003; Zhang et al. 2004). The tonic sympathetic activity could protect the autoregulation action in buffering surges in perfusion pressure. Such a mechanism seems to operate mainly in larger cerebral arteries. The ability of these larger vessels to maintain flow during changes in perfusion pressure is lost once denervated (ter Laan et al. 2013; Willie et al. 2014). Anatomical studies also reveal rich distribution of cholinergic nerve terminals of cerebral vascular tree (Florence and Bevan 1979; Suzuki and Hardebo 1993; Sato et al. 2004; Hamel 2004; Wu et al. 2014). In isolated cerebral arteries, the stimulation of cholinergic nerves causes vasodilation predominantly via endothelium-derived NO. Moreover, ACh and NO are co-released from the same cholinergic–nitrergic nerves (Lee et al. 2001). In humans the blockade of cholinergic innervation renders the cerebral autoregulation less effective. The evaluation of the relative contributions of

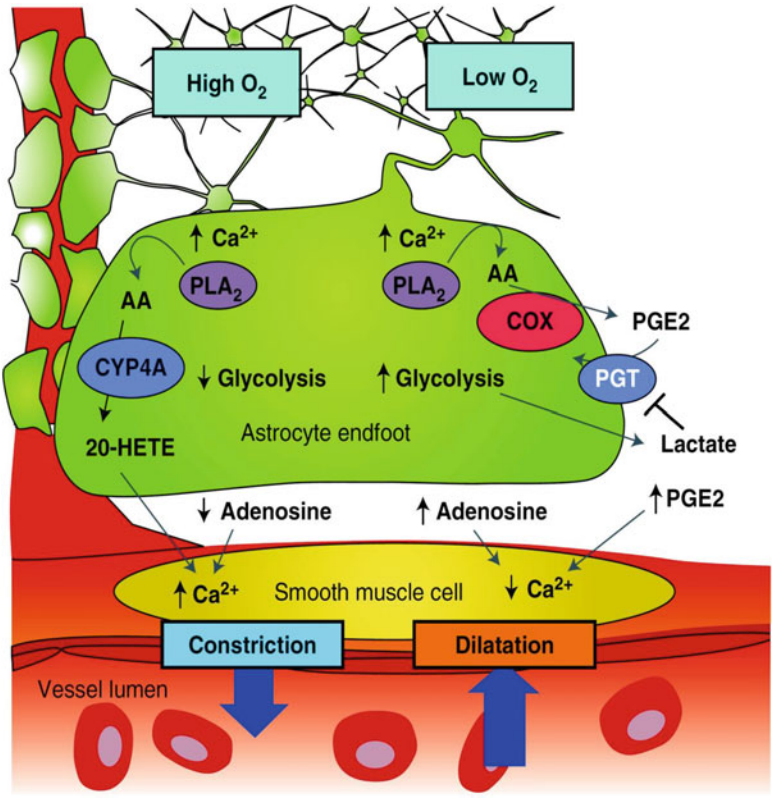

Fig. 16.2 Effect of oxygen tension on astrocyte-mediated vasoactivity. The increase in cytosolic Ca^{2+} activates phospholipase A_2 (PLA_2) resulting in the release of arachidonic acid (AA) from plasma membrane lipids. In high pO_2, AA is converted to 20-hydroxyeicosatetraenoic acid (20-HETE) through cytochrome P450 4A (CYP4A), which causes vasoconstriction via depolarizing the vascular smooth muscle cells (VSMCs) and consequently Ca^{2+} elevation (*left side*). In low pO_2, the synthesis of 20-HETE is inhibited, and AA is converted to prostaglandin E_2 (PGE_2) through cyclooxygenase (COX), which is less sensitive to change in oxygen tension. PGE_2 causes vasodilatation via cAMP signaling pathway involving reducing the cytosolic Ca^{2+} levels. In addition, when pO_2 decreases, glycolysis is enhanced and extracellular lactate is elevated. Increased extracellular lactate may augment vasodilatation by suppressing the prostaglandin transporter (PGT) resulting in increased extracellular PGE_2. In low pO_2, more adenosine is released, which causes vasodilatation via the activation of adenosine A_{2A} receptor (*right side*) (The figure is from Gordon et al. (2011), with permission)

sympathetic, cholinergic, and myogenic mechanisms to cerebral autoregulation suggests that the myogenic response acts as the largest determinant and its effect occur outside the more active region of autoregulation. In contrast, neurogenic influences are largely active within the range of autoregulation, with the sympathetic system playing a larger role than the cholinergic system (Hamner and Tan 2014). The intraparenchymal arterioles are also richly innervated by cholinergic nuclei (Wu et al. 2014). For instance, the basal forebrain cholinergic neurons may

regulate the activity of cortical microvessels by directly acting on the M_5 muscarinic receptors of the VSMCs, through GABA interneurons containing NO or vasoactive intestinal polypeptide (VIP) and through local neurovascular relay neurons containing VIP (Hamel 2004).

References

Attwell D, Buchan AM, Charpak S, Lauritzen M, Macvicar BA, Newman EA (2010) Glial and neuronal control of brain blood flow. Nature 468:232–243

Barnett J, Chow J, Ives D, Chiou M, Mackenzie R, Osen E, Nguyen B, Tsing S, Bach C, Freire J, Chan H, Elliott Sigal E, Ramesha C (1994) Purification, characterization and selective inhibition of human prostaglandin G/H synthase 1 and 2 expressed in the baculovirus system. Biochim Biophys Acta 1209:130–139

Binks AP, Cunningham VJ, Adams L, Banzett RB (2008) Gray matter blood flow change is unevenly distributed during moderate isocapnic hypoxia in humans. J Appl Physiol 104:212–217

Cipolla MJ (2016) The cerebral circulation, 2nd edn. Morgan & Claypool Life Sciences, San Rafael

Dabertrand F, Nelson MT, Brayden JE (2012) Acidosis dilates brain parenchymal arterioles by conversion of calcium waves to sparks to activate BK channels. Circ Res 110:285–294

Dalkara T, Alarcon-Martinez L (2015) Cerebral microvascular pericytes and neurogliovascular signaling in health and disease. Brain Res 1623:3–17

de Labra C, Rivadulla C, Espinosa N, Dasilva M, Cao R, Cudeiro J (2009) Different sources of nitric oxide mediate neurovascular coupling in the lateral geniculate nucleus of the cat. Front Syst Neurosci 3:9

de Vries HE, Kuiper J, de Boer AG, Van Berkel TJ, Breimer DD (1997) The blood-brain barrier in neuroinflammatory diseases. Pharmacol Rev 49:143–155

Drummond HA, Jernigan NL, Grifoni SC (2008) Sensing tension: epithelial sodium channel/acid-sensing ion channel proteins in cardiovascular homeostasis. Hypertension 51:1265–1271

Duvernoy HM, Risold PY (2007) The circumventricular organs: an atlas of comparative anatomy and vascularization. Brain Res Rev 56:119–147

Edvinsson L (1987) Innervation of the cerebral circulation. Ann N Y Acad Sci 519:334–348

Faraci FM, Heistad DD (1990) Regulation of large cerebral arteries and cerebral microvascular pressure. Circ Res 66:8–17

Filosa JA, Morrison HW, Iddings JA, Du W, Kim KJ (2016) Beyond neurovascular coupling, role of astrocytes in the regulation of vascular tone. Neuroscience 323:96–109

Florence VM, Bevan JA (1979) Biochemical determinations of cholinergic innervation in cerebral arteries. Circ Res 45:212–218

Gordon GR, Choi HB, Rungta RL, Ellis-Davies GC, MacVicar BA (2008) Brain metabolism dictates the polarity of astrocyte control over arterioles. Nature 456:745–749

Gordon GRJ, Howarth C, MacVicar BA (2011) Bidirectional control of arteriole diameter by astrocytes. Exp Physiol 96:393–399

Guibert C, Flemming R, Beech DJ (2002) Prevention of a hypoxic Ca^{2+}_i response by SERCA inhibitors in cerebral arterioles. Br J Pharmacol 135:927–934

Hall CN, Reynell C, Gesslein B, Hamilton NB, Mishra A, Sutherland BA, O'Farrell FM, Buchan AM, Lauritzen M, Attwell D (2014) Capillary pericytes regulate cerebral blood flow in health and disease. Nature 508:55–60

Hamel E (2004) Cholinergic modulation of the cortical microvascular bed. Prog Brain Res 145:171–178

Hamner JW, Tan CO (2014) Relative contributions of sympathetic, cholinergic, and myogenic mechanisms to cerebral autoregulation. Stroke 45:1771–1777
Harder DR, Narayanan J, Birks EK, Liard JF, Imig JD, Lombard JH, Lange AR, Roman RJ (1996) Identification of a putative microvascular oxygen sensor. Circ Res 79:54–61
Harper AM, Glass HI (1965) Effect of alterations in the arterial carbon dioxide tension on the blood flow through the cerebral cortex at normal and low arterial blood pressures. J Neurol Neurosurg Psychiatry 28:449–452
Hein TW, Xu W, Ren Y, Kuo L (2013) Cellular signalling pathways mediating dilation of porcine pial arterioles to adenosine A_{2A} receptor activation. Cardiovasc Res 99:156–163
Heistad DD, Kontos HA (2011) Cerebral circulation. Compr Physiol:137–182
Herculano-Houzel S (2009) The human brain in numbers: a linearly scaled-up primate brain. Front Hum Neurosci 3:31
Hill MA, Meininger GA (2012) Arteriolar vascular smooth muscle cells: mechanotransducers in a complex environment. Int J Biochem Cell Biol 44:1505–1510
Hoiland RL, Bain AR, Rieger MG, Bailey DM, Ainslie PN (2016) Hypoxemia, oxygen content, and the regulation of cerebral blood flow. Am J Physiol Regul Integr Comp Physiol 310:R398–R413
Johnston AJ, Steiner LA, Gupta AK, Menon DK (2003) Cerebral oxygen vasoreactivity and cerebral tissue oxygen reactivity. Br J Anaesth 90:774–786
Joyner MJ, Casey DP (2015) Regulation of increased blood flow (hyperemia) to muscles during exercise: a hierarchy of competing physiological needs. Physiol Rev 95:549–601
Kauffenstein G, Laher I, Matrougui K, Guérineau NC, Henrion D (2012) Emerging role of G protein-coupled receptors in microvascular myogenic tone. Cardiovasc Res 95:223–232
Kiliç T, Akakin A (2008) Anatomy of cerebral veins and sinuses. Front Neurol Neurosci 23:4–15
Kimmerly DSDS, Tutungi EE, Wilson TDTD, Serrador JMJM, Gelb AWAW, Hughson RLRL, Shoemaker JKJK (2003) Circulating norepinephrine and cerebrovascular control in conscious humans. Clin Physiol Funct Imaging 23:314–319
Kocharyan A, Fernandes P, Tong XK, Vaucher E, Hamel E (2008) Specific subtypes of cortical GABA interneurons contribute to the neurovascular coupling response to basal forebrain stimulation. J Cereb Blood Flow Metab 28:221–231
Koller A, Toth P (2012) Contribution of flow-dependent vasomotor mechanisms to the autoregulation of cerebral blood flow. J Vasc Res 49:375–389
Kontos HA, Raper AJ, Patterson JL (1977) Analysis of vasoactivity of local pH, PCO2 and bicarbonate on pial vessels. Stroke 8:358–360
Lassen NA (1959) Cerebral blood flow and oxygen consumption in man. Physiol Rev 39:183–238
Lecrux C, Hamel E (2016) Neuronal networks and mediators of cortical neurovascular coupling responses in normal and altered brain states Philos Trans R Soc Lond Ser B Biol Sci 371. pii:20150350
Lecrux C, Toussay X, Kocharyan A, Fernandes P, Neupane S, Lévesque M, Plaisier F, Shmuel A, Cauli B, Hamel E (2011) Pyramidal neurons are "neurogenic hubs" in the neurovascular coupling response to whisker stimulation. J Neurosci 31:9836–9847
Lee TJ, Liu J, Evans MS (2001) Cholinergic-nitrergic transmitter mechanisms in the cerebral circulation. Microsc Res Tech 53:119–128
Leithner C, Royl G (2014) The oxygen paradox of neurovascular coupling. J Cereb Blood Flow Metab 34:19–29
Lewis NC, Messinger L, Monteleone B, Ainslie PN (2014) Effect of acute hypoxia on regional cerebral blood flow: effect of sympathetic nerve activity. J Appl Physiol (1985) 116:1189–1196
Liu J, Zhu YS, Hill C, Armstrong K, Tarumi T, Hodics T, Hynan LS, Zhang R (2013) Cerebral autoregulation of blood velocity and volumetric flow during steady-state changes in arterial pressure. Hypertension 62:973–979

Ma J, Ayata C, Huang PL, Fishman MC, Moskowitz MA (1996) Regional cerebral blood flow response to vibrissal stimulation in mice lacking type I NOS gene expression. Am J Phys 270: H1085–H1090

Mandell DM, Han JS, Poublanc J, Crawley AP, Kassner A, Fisher JA, Mikulis DJ (2008) Selective reduction of blood flow to white matter during hypercapnia corresponds with leukoaraiosis. Stroke 39:1993–1998

Mardimae A, Balaban DY, Machina MA, Battisti-Charbonney A, Han JS, Katznelson R, Minkovich LL, Fedorko L, Murphy PM, Wasowicz M, Naughton F, MeineriM FJA, Duffin J (2012) The interaction of carbon dioxide and hypoxia in the control of cerebral blood flow. Pflugers Arch 464:345–351

Masamoto K, Tanishita K (2009) Oxygen transport in brain tissue. J Biomech Eng 131:74–82

Meno JR, Ngai AC, Winn HR (1993) Changes in pial arteriolar diameter and CSF adenosine concentrations during hypoxia. J Cereb Blood Flow Metab 13:214–220

Miekisiak G, Kulik T, Kusano Y, Kung D, Chen J-F, Winn HR (2008) Cerebral blood flow response in adenosine 2a receptor knockout mice during transient hypoxic hypoxia. J Cereb Blood Flow Metab 28:1656–1664

Muñoz MF, Puebla M, Figueroa XF (2015) Control of the neurovascular coupling by nitric oxide-dependent regulation of astrocytic Ca^{2+} signaling. Front Cell Neurosci 9:59

Ngai AC, Winn HR (1995) Modulation of cerebral arteriolar diameter by intraluminal flow and pressure. Circ Res 77:832–840

Nolan WF, Houck PC, Thomas JL, Davies DG (1982) Ventral medullary extracellular fluid pH and blood flow during hypoxia. Am J Physiol Regul Integr Comp Physiol 242:R195–R198

O'Regan M (2005) Adenosine and the regulation of cerebral blood flow. Neurol Res 27:175–181

Pearce WJ, Ashwal S, Long DM, Cuevas J (1992) Hypoxia inhibits calcium influx in rabbit basilar and carotid arteries. Am J Phys 262:H106–H113

Pelligrino DA, Wang Q, Koenig HM, Albrecht RF (1995) Role of nitric oxide, adenosine, *N*-methyl-D-aspartate receptors, and neuronal activation in hypoxia-induced pial arteriolar dilation in rats. Brain Res 704:61–70

Peppiatt CM, Howarth C, Mobbs P, Attwell D (2006) Bidirectional control of CNS capillary diameter by pericytes. Nature 443:700–704

Querido JS, Ainslie PN, Foster GE, Henderson WR, Halliwill JR, Ayas NT, Sheel AW (2013) Dynamic cerebral autoregulation during and following acute hypoxia: role of carbon dioxide. J Appl Physiol (1985) 114:1183–1190

Roman RJ (2002) P-450 metabolites of arachidonic acid in the control of cardiovascular function. Physiol Rev 82:131–185

Sato A, Sato Y, Uchida S (2004) Activation of the intracerebral cholinergic nerve fibers originating in the basal forebrain increases regional cerebral blood flow in the rat's cortex and hippocampus. Neurosci Lett 361:90–93

Stobart JL, Lu L, Anderson HD, Mori H, Anderson CM (2013) Astrocyte-induced cortical vasodilation is mediated by D-serine and endothelial nitric oxide synthase. Proc Natl Acad Sci U S A 110:3149–3154

Stuehr DJ, Santolini J, Wang ZQ, Wei CC, Adak S (2004) Update on mechanism and catalytic regulation in the NO synthases. J Biol Chem 279:36167–36170

Sun CW, Falck JR, Okamoto H, Harder DR, Roman RJ (2000) Role of cGMP versus 20-HETE in the vasodilator response to nitric oxide in rat cerebral arteries. Am J Physiol Heart Circ Physiol 279:H339–H350

Suzuki N, Hardebo JE (1993) The cerebrovascular parasympathetic innervation. Cerebrovasc Brain Metab Rev 5:33–46

Taguchi H, Heistad DD, Kitazono T, Faraci FM (1994) ATP-sensitive K^+ channels mediate dilatation of cerebral arterioles during hypoxia. Circ Res 74:1005–1008

ter Laan M, van Dijk JM, Elting JW, Staal MJ, Absalom AR (2013) Sympathetic regulation of cerebral blood flow in humans: a review. Br J Anaesth 111:361–367

Thompson JK, Peterson MR, Freeman RD (2003) Single-neuron activity and tissue oxygenation in the cerebral cortex. Science 299:1070–1072
Toda N, Hatano Y, Mori K (1989) Mechanisms underlying response to hypercapnia and bicarbonate of isolated dog cerebral arteries. Am J Phys 257:H141–H146
Toussay X, Basu K, Lacoste B, Hamel E (2013) Locus coeruleus stimulation recruits a broad cortical neuronal network and increases cortical perfusion. J Neurosci 33:3390–3401
Tzeng YC, Ainslie PN (2014) Blood pressure regulation IX: cerebral autoregulation under blood pressure challenges. Eur J Appl Physiol 114:545–559
Uddin MA, Haq TU, Rafique MZ (2006) Cerebral venous system anatomy. J Pak Med Assoc 56:516–519
Vinall PE, Simeone FA (1981) Cerebral autoregulation: an in vitro study. Stroke 12:640–642
Willie CK, Macleod DB, Shaw AD, Smith KJ, Tzeng YC, Eves ND, Ikeda K, Graham J, Lewis NC, Day TA, Ainslie PN (2012) Regional brain blood flow in man during acute changes in arterial blood gases. J Physiol 590:3261–3275
Willie CK, Tzeng YC, Fisher JA, Ainslie PN (2014) Integrative regulation of human brain blood flow. J Physiol 592:841–859
Wu H, Williams J, Nathans J (2014) Complete morphologies of basal forebrain cholinergic neurons in the mouse. elife 3:e02444
Zhang R, Crandall CG, Levine BD (2004) Cerebral hemodynamics during the Valsalva maneuver: insights from ganglionic blockade. Stroke 35:843–847
Zlokovic BV (2005) Neurovascular mechanisms of Alzheimer's neurodegeneration. Trends Neurosci 28:202–208
Zlokovic BV (2008) The blood-brain barrier in health and chronic neurodegenerative disorders. Neuron 57:178–201

Chapter 17
Pulmonary Vasoreactivity

Abstract Pulmonary circulation is characterized by low intravascular arterial pressure and low vascular resistance. As compared with those of systemic circulation, pulmonary arteries have thinner walls with fewer vascular smooth muscles and exhibit a lower basal tone so that modest external forces can exert relatively large hemodynamic effects. The external forces include those resulted from changes in gravity due to postures and changes in lung volume during breathing. The pulmonary circulation accommodates the entire cardiac output. The accommodation of increased output of the right ventricle is mainly achieved by distension and recruitment of pulmonary vessels. Pulmonary vascular activity is regulated by various humoral and neuronal agents including those released from the endothelium. Pulmonary vascular tone is also affected by hypoxia, which causes vasoconstriction. Such a response diverts blood flow from less well-oxygenated to better-oxygenated locations in the lung so that perfusion is better matched to ventilation resulting to a more efficient gas exchange. If the hypoxic stimulus persists, vasoconstriction is accompanied by vascular remodeling, which may lead to the development of pulmonary hypertension.

Keywords Pulmonary circulation • Gravity • Alveolar pressure • Endothelium • Hypoxic vasoconstriction

17.1 Introduction

The pulmonary circulation serves a vital bodily function: gas exchange. To efficiently fulfil this task, it evolves a low intravascular pressure and low vascular resistance system to accommodate the entire output of the right ventricle. For many organs of the systemic circulation, their blood flow remains relatively stable within a broad physiological range of pressure by blood flow autoregulation. This mechanism is not operative in pulmonary circulation. An increased pressure due to increased cardiac output causes pulmonary blood flow to increase, largely a consequence of vessel distension and recruitment. Pulmonary vasculature is thin walled and possesses low tone. Thus, the blood flow in the lung is determined not only by the pressure gradient between arteries and veins but greatly affected by other external factors such as alveolar pressure and lung volume. These

Y. Gao, *Biology of Vascular Smooth Muscle: Vasoconstriction and Dilatation*,
DOI 10.1007/978-981-10-4810-4_17

unique aspects of pulmonary circulation and the regulation of pulmonary vascular activity will be discussed in this chapter. To facilitate the discussion, the anatomic features of pulmonary vasculature will be introduced at the beginning of this chapter (Fishman 2011; Suresh and Shimoda 2016).

17.2 The Anatomy of Pulmonary Vasculature

17.2.1 Pulmonary Artery

The pulmonary artery starts from a single vessel exiting the right ventricle termed pulmonary trunk or main pulmonary artery. It branches into left and right pulmonary arteries, and these vessels further divide to supply each lobe before entering the lung. Within the lung, pulmonary arteries are divided by Elliott and Reid into two populations: conventional and supernumerary vessels. The former proceeds alongside the airway and its branches, whereas the latter does not accompany airways. Supernumerary arteries occur throughout the length of the pulmonary vascular tree to supply the closest pulmonary acinus. The diameter of supernumerary arteries can be quite small compared to that of the parent conventional pulmonary artery and are more numerous toward the lung periphery. It is estimated that the ratio of supernumerary to accompanying terminal arteries is ~2.8:1 (Elliott and Reid 1965; Reid 1965; Burrowes et al. 2005).

In comparison with systemic arteries of similar diameters, pulmonary arteries are much thin walled. Pulmonary arteries with outside diameters greater than 2 mm are elastic arteries primarily comprised of elastic fibers and some smooth muscle. Those with outside diameters less than 2 mm contain less elastic fibers and are prevailed with smooth muscle cells, known as muscular arteries. As the vessels approach capillaries, their diameters reduce to 30–60 μm, and their media contains only 1–2 layers of smooth muscle, known as arterioles. The terminal arterioles break into a network of pulmonary capillaries within the alveolar walls (Elliott and Reid 1965; Reid 1965; Townsley 2012; Suresh and Shimoda 2016).

To quantitatively study the branching of the pulmonary vascular tree, the whole vascular network can be treated as a confluent system of vessels categorized by orders (counting from the periphery) or generations (counting from the lung hilus), with the ordering method more widely used (Horsfield 1984). A study of the human left lung using a diameter-modified Strahler ordering method shows that pulmonary arterial tree comprises 15 branch orders. Order 1 arterioles have an average diameter of 20 μm, whereas the diameter of order 15 arteries averages 14.8 mm (Huang et al. 1996). The analyses of branching orders reveal a linear relationship between order number and mean diameters of pulmonary vessels of each order, where the antilog of the slope defines the diameter ratio. Remarkably, the diameter ratio is fairly well preserved from human lung to pig, dog, cat, and rat lung. Across these species, the diameter ratio averages ~1.65, i.e., the average arterial diameter

increases 65% with each new branch order. The analyses also show that the length of pulmonary arterial segments increases nearly 60% with each successive order, whereas the number of branches increases more than threefold with each successive order moving from the lung hilus to periphery (Townsley 2012).

17.2.2 Pulmonary Capillaries

Pulmonary capillaries may originate from the most distal pulmonary arterial branches. Alternatively, precapillary arterioles branch at right angles from a parent arteriole (30 μm) then give rise to a capillary network. A small arteriole can also abruptly end in a capillary network. In the human and rat lung, extra-alveolar pulmonary arteries 100 μm or more in diameter may give rise directly to capillary networks to supply respiratory bronchioles (Townsley 2012). It appears that small distal pulmonary arteries supply numerous alveoli. Further, numerous septal walls may separate a pulmonary arteriolar inflow point and the pulmonary venule which provides outflow. The path length for flow through the alveolar capillary network has been estimated to range from 250 to 850 μm in several mammalian species (Staub and Schultz 1968; Townsley 2012).

The alveoli are densely wrapped by pulmonary capillaries. A typical pair of adult human lungs contains about 480 million alveoli, with each alveolus having a diameter of ~200 μm. This would produce ~60 m^2 of surface area calculated using the formula for sphere surface area ($S = 4\pi r^2$; r, radius) (Ochs et al. 2004). It is estimated that ~88% of the alveolar surface, i.e., ~53 m^2, is covered by a fine mesh of capillaries (Weibel et al. 2005; Townsley 2012). The gas exchange tissue barrier that separates air and blood is on the order of 1 μm. It is built of three tissue layers: alveolar epithelium and capillary endothelium separated by a thin interstitial layer. For a normal human adult, the physiological diffusing capacity is estimated at ~30 at rest and at ~100 ml O_2 min^{-1} $mmHg^{-1}$ in heavy exercise (Weibel et al. 2005).

17.2.3 Pulmonary Vein

Pulmonary venous system emerges from the capillary bed. As the venous vessels proceed from peripheral to the lung hilus, they merge progressively into larger vessels alongside the pulmonary arteries. After coming out of the lung hilus, pulmonary veins join into four branches entering the right atrium, two from the left and two from the right lung. Similar to arteries, the intrapulmonary veins can be classified as conventional and supernumerary vessels. The venous supernumerary vessels are also much smaller in diameters than parental conventional veins and more numerous toward the lung periphery, with a ratio of ~3.5:1 for supernumerary veins versus the accompanying terminal veins (Elliott and Reid 1965; Reid 1965;

Burrowes et al. 2005). Based on the diameter-modified Strahler ordering system, human pulmonary venous tree consists of 15 branch orders, with order 1 venules having an average diameter of 18 μm, whereas the diameter of order 15 arteries averages 13.0 mm (Huang et al. 1996).

The wall thickness and medial thickness of intrapulmonary veins are much less than those of pulmonary arteries in the same size range. Pulmonary veins are generally characterized by absent internal elastic lamina and containing less smooth muscle but more extracellular matrix. The large pulmonary veins are muscular rather than elastic as compared with large pulmonary arteries (Rhodin 1978; LaBourene et al. 1990; Townsley et al. 1999; Townsley 2012). In various species, pulmonary veins have a coaxial structure, with layers of cardiomyocytes arrayed externally around a subendothelial layer of typical smooth muscle cells (SMCs). In most large mammals, including humans, myocardial layer extends as much as 10–20 mm from the left atrial wall into the large extrapulmonary veins. In the rat, squirrel, and mouse lung, cardiomyocytes are found in pulmonary veins as small as ~30–40 μm in diameter (Paes de Almeida et al. 1975; Hassink et al. 2003; Mueller-Hoecker et al. 2008; Townsley 2012). Studies demonstrate that cardiac myocytes contribute to pulmonary venous tone in a unique manner different from the pulmonary venous SMCs (Michelakis et al. 2001; Cha et al. 2005; Coutu et al. 2006).

17.2.4 Bronchial Vasculature

The bronchial circulation belongs to systemic but not pulmonary circulation. The bronchial arteries take ~1% of cardiac output to supply nutrition and oxygenated blood to the conducting airways, regional lymph nodes, nerves, walls of the pulmonary arteries and veins (vasa vasorum), and the visceral pleura. In humans, there are two bronchial arteries that run to the left lung and one to the right lung. The left bronchial arteries (superior and inferior) usually originate directly from the thoracic aorta. The right bronchial artery may arise from one of the following: (1) the thoracic aorta at a common trunk with the right third posterior intercostal artery, (2) the superior bronchial artery on the left side, and (3) any number of the right intercostal arteries mostly the third right posterior. The intrapulmonary bronchial arteries travel and branch with the bronchi down to the terminal bronchioles resulting in a vast network of capillaries, which form extensive anastomoses with other bronchial arteries as well as the pulmonary vasculature, creating a peribronchial plexus (Baile 1996; Suresh and Shimoda 2016). Much of the oxygenated blood supplied by the bronchial arteries is returned via the pulmonary veins. The bronchial veins only carry ~13% of the blood flow of the bronchial arteries. As a consequence, blood returning to the left heart is slightly less oxygenated than blood found at the level of the pulmonary capillary beds. Venous drainage of the proximal conducting airway follows the same pattern as the arterial supply, with blood being returned to the right heart via the azygos and hemiazygos veins (Charan et al. 2007; Suresh and Shimoda 2016).

17.3 Characteristics of Pulmonary Circulation

In systemic circulation, the amount of blood flow to an organ is affected by its own as well as the global activities. In contrast, the pulmonary circulation has to take the total cardiac output for gas exchange and cannot actively adjust its total blood flow. The mean pressure of pulmonary arteries is about 15 mmHg or about one-sixth that in the systemic arteries. Meanwhile, pulmonary vascular resistance is rather low so that a driving pressure (pulmonary arterial pressure minus left atrial pressure) at rest in humans of ~6–7 cm H_2O elicits a blood flow of ~6 liters/min. During exercise a doubling of the pressure gradient causes the pulmonary blood flow to be tripled (Butler and Paley 1962; Fishman 2011). While the pulmonary circulation accommodates the total cardiac output, the regional distribution of the blood flow in the lung is sensitive to changes in gravity due to different postures, alveolar pressure, and changes in lung volume occurred during respiratory cycle (Fishman 2011; Suresh and Shimoda 2016).

17.3.1 Effects of Gravity and Alveolar Pressure

In the upright human, the pulmonary blood flow increases some ninefold from the apex to the base of the upright lung. Such a flow distribution is not observed when the subject is supine, indicating that gravity is the major factor determining the distribution of blood flow in the lung. According to Pascal's law, the pressure equals the product of gravity, the density of the liquid, and the height of the column. Clearly, the blood pressure in pulmonary vessels increases with distance down the lung. However, the increasing pressure does not explain the increasing flow, since the pulmonary artery pressure (P_a) and pulmonary vein pressure (P_v) increase by the same amount with distance down the lung, and thus the pressure gradients that drive blood flow remain the same. Instead, the increasing blood flow results from the greater intravascular pressures leading to vessel distention and recruitment of vessels. As demonstrated by West and colleagues, the blood flow of the alveolar vessel is determined not only by the difference between P_a and P_v but also by alveolar pressure (P_A) (West et al. 1964; Hughes and West 2008). Based on the relationship between these parameters, the lung can be divided into three regions or zones (Fig. 17.1). In the top region (zone 1), P_A is greater than P_a, the vessel is collapsed, and there is no blood flow. In the bottom region (zone 3), P_a is greater than P_v, and both exceed P_A. The vessel is somewhat distended, and the driving pressure for blood flow is the pressure gradients between P_a and P_v. In the middle region (zone 2), P_a is greater than P_A, but P_A is greater than P_v. The vessel is partly collapsed at the venous end, and the driving pressure for blood flow is the pressure gradients between (P_a–P_A) and P_v. It should be noted that the zone definition is functional, not anatomic. The borders between zones are affected by changes in P_a, P_v, and P_A. They are also altered under many physiological and pathophysiological

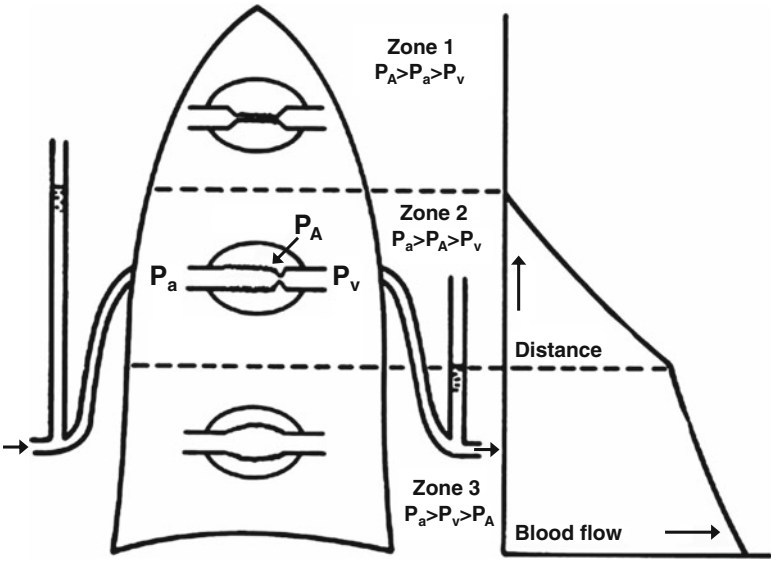

Fig. 17.1 Three-zone model of pulmonary blood flow proposed by West et al. In zone 1, the alveolar pressure (P_A) is greater than pulmonary arterial pressure (P_a) so that the alveolar capillary is collapsed and no blood flow gets through. In zone 2, P_a is greater than P_A so that the blood flow is dictated by the difference between the P_a–P_A gradient and pulmonary venous pressure (P_v). In zone 3, both P_a and P_v are greater than P_A so that the blood flow is determined by the P_a–P_v pressure gradient (This figure is from West et al. (1964), with permission)

conditions, including changes in body position, changes in lung volume, and changes in right ventricular output and left atrial pressure. During normal breathing in a young healthy person, even in the uppermost regions of the lung, P_a is greater than P_A, so there is no zone 1. However, blood loss or other causes of pulmonary hypotension or positive-pressure ventilation can introduce zone 1, resulting in reduced surface area of the lung available for gas exchange (Levitzky 2006; Glenny and Robertson 2011).

17.3.2 Effects of Lung Volume

Respiration affects the pulmonary circulation via venous return, pleural pressure, and the degree of inflation of the lungs. An increase in lung volume during inhalation exerts different effects on alveolar vs. extra-alveolar vessels. Alveolar vessels are capillaries that are contained within the walls separating adjacent alveoli. The alveolar capillaries undergo compression during lung inflation, leading to increased vascular resistance (Mazzone et al. 1978). Extra-alveolar pulmonary vessels are not affected by changes in alveolar pressure. These vessels dilate during lung inflation, which is related to the effects of inflation on the perivascular

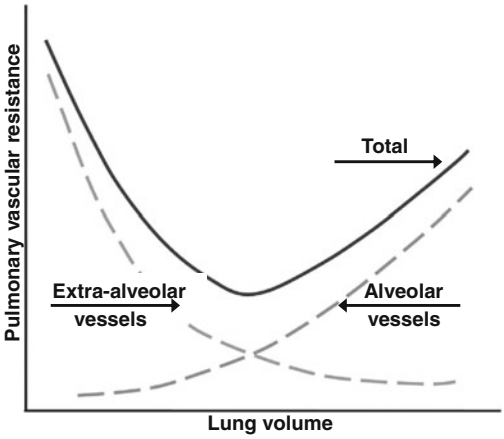

Fig. 17.2 Relationship between pulmonary vascular resistance and lung volume for extra-alveolar pulmonary vessels, alveolar pulmonary vessels, and the total effect of alveolar plus extra-alveolar vessels (The figure is modified from Simmons et al. (1961), with permission)

interstitium surrounding these vessels (Howell et al. 1961; Suresh and Shimoda 2016). The opposing effects of changes in lung volume lead to a U-shaped relationship between lung volume and total pulmonary vascular resistance. The resistance is lowest around normal breathing volume. It increases with both increased and decreased lung volume (Simmons et al. 1961; Fishman 2011; Suresh and Shimoda 2016) (Fig. 17.2). In addition to alveolar and extra-alveolar vessels, there are vessels termed corner vessels in the lung. They are located at sites where three alveoli abut and within pleats in the alveolar walls beneath sharp curvatures in the overlying alveolar film of surfactant. Their location and anatomical arrangement within pleats render them insensitive to fluctuations in alveolar pressure, and blood flow persists in these vessels when alveolar pressure exceeds pulmonary arterial pressure by 10 cm H_2O. These vessels are believed to be preferential channels through which blood flow continues despite wide swings in alveolar pressure (Rosenzweig et al. 1970; Gil 1980; Fishman 2011).

17.3.3 Pulmonary Vascular Pressure and Flow

The mean pulmonary arterial pressure of the human subjects is ~12–15 mmHg. The pressure drop across the pulmonary vascular bed is ~10% of that across the systemic circulation, and pulmonary venous pressure is ~5–10 mmHg (Fishman 2011). A study with dog isolated lung lobes perfused at constant flow found that pulmonary artery pressure averages 20.4 cm H_2O, midcapillary pressure averages 13.3 cm H_2O, and pulmonary vein pressure averages 9.2 cm H_2O. The pulmonary arteries were responsible for 46% of total lobar vascular resistance; the pulmonary capillaries and veins account for 34 and 20% of total lobar vascular resistance, respectively (Brody et al. 1968). A separate study of dog isolated lung lobes perfused at a steady flow rate in zone 3 condition by arterial and venous occlusion

technique shows that the capillary segment contributes a major fraction of the vascular compliance and less than 16% of the total resistance, whereas pulmonary arteries and veins contribute equally to the remaining resistance (Hakim et al. 1982).

The pulmonary arterial pressure varies during each heartbeat. It is ~7–12 mmHg at the end of diastole and rises to 20–30 mmHg during systole (Fishman 2011). Within the physiological ranges, the pressure–flow curve is approximately linear (as in the case of the pressure–volume curve) but becomes nonlinear at very low driving pressures (P_a– P_v; Shoukas 1975). It appears that an increased blood flow induced by pressure may be largely a consequence of vessel distension and recruitment, and the recruitment results from functional shift of the microvessels from zone 2 to zone 3 and from zone 1 to zone 2 (Fishman 2011; Suresh and Shimoda 2016). The mean velocity of blood flow in the human pulmonary artery is ~18 cm/s, a value about the same as that in the large pulmonary veins and aorta. The peak Reynolds numbers in the main pulmonary artery are ~5000–9000, suggesting that the pattern of flow there borders on turbulence. The averaged output of the right ventricle to pulmonary artery and the input of the left ventricle during a respiratory cycle are well matched, excepting that the output of the left ventricle is consistently higher than that of the right ventricle. This is due to the drainage of bronchial veins into the pulmonary veins, which is ~1%–2% of the total left ventricular output (Fishman 2011).

Similar to systemic circulation, the blood flow in the pulmonary circulation is pulsatile. Simultaneous tracings in the dog of pulmonary vascular pressure and blood flow show that variations in pulmonary arterial and venous flow are nearly simultaneous. The maxima and minima in venous flow lag only 0.09 s from corresponding points in arterial flow (Morkin et al. 1965). The pulsatile blood flow in the pulmonary artery remains pulsatile, though with signal attenuation, to approximately the midcapillary region. The drop in pressure pulse appears to be greatest at the entry to the microcirculation. The flow patterns exhibited in venular segment of the pulmonary circulation depend more on left atrial pressures than changes in pulmonary arterial pressure (Wiener et al. 1966; Rajagopalan et al. 1975; Fishman 2011; Mynard and Smolich 2015; Suresh and Shimoda 2016).

17.4 Regulation of Pulmonary Vasoactivity

Although pulmonary circulation is featured by low pressure and low resistance, pulmonary vasculature can exhibit substantial contractile and relaxing responses when exposed to various stimuli. During these responses, the endothelium plays a pivotal role by releasing a number of potent vasoactive substances in particular nitric oxide (NO), prostaglandin I_2 (PGI_2), and endothelin-1 (ET-1) (Barnes and Liu 1995; Suresh and Shimoda 2016). Pulmonary vessels are also richly innervated by sympathetic, parasympathetic, and sensory–motor nerve fibers. It appears that the basal pulmonary vascular tone is limitedly affected by neuronal activity but actively

regulated under various conditions. For instance, sympathetic pulmonary vascular neurons are reflexively activated via arterial chemoreceptors when arterial Po_2 is lowered (Kummer 2011). Pulmonary artery denervation reduces pulmonary artery pressure in acute pulmonary hypertension, indicating an aggregated sympathetic activity development (Rothman et al. 2015). In addition to humoral and neuronal influences, pulmonary vasoactivity is strongly affected by low Po_2 in alveoli and resistance of pulmonary arteries and arterioles. Hypoxia causes systemic vessels to relax but causes pulmonary vessels to contract. Such a unique characteristic serves to maintain high vascular resistance in the fetal lung and match perfusion to ventilation in the adult (Gao and Raj 2010; Sylvester et al. 2012; Dunham-Snary et al. 2017).

17.4.1 Endothelial Regulation

The endothelium exerts profound influence on pulmonary vascular activity by the release of a number of vasoactive agents, in particular, the vasodilators NO and PGI_2 as well as the vasoconstrictor ET-1. In pulmonary vasculature, NO is normally synthesized by the endothelial NO synthase (eNOS) with L-arginine as the substrate. Upon the release, NO can readily diffuse into the underlying vascular smooth muscle cells (VSMCs) to cause vasodilatation via stimulating soluble guanylate cyclase (sGC), resulting in cGMP elevation and cGMP-dependent decreases in intracellular calcium concentration and myofilament Ca^{2+} sensitivity (Gao and Raj 2006; Gao 2010). In resting sheep (Koizumi et al. 1994), pigs (Merkus et al. 2004), horses (Manohar and Goetz 1998), and humans (Stamler et al. 1994; Blitzer et al. 1996), the inhibition of NO synthase leads to increased pulmonary vascular resistance (PVR), indicating a tonic suppression of pulmonary activity by the endothelium-derived NO (EDNO). In fetal and newborn lambs, the increase in fluid shear stress resulting from increased pulmonary blood flow increases EDNO production by phosphorylation of eNOS and by increasing eNOS mRNA and protein expression (Cornfield et al. 1992; Black et al. 1997). In primary cultures of ovine fetal pulmonary arterial endothelial cells, shear stress acutely stimulates NO production via suppressing the phosphorylation of eNOS at Thr-495 and promoting the phosphorylation of eNOS at Ser-1177 (Kumar et al. 2010). Shear stress also upregulates the expression of eNOS through increased phosphorylated c-Jun levels (Wedgwood et al. 2003) and through reduction in binding of STAT3 to eNOS promoter (Sud et al. 2009). The effects of blood flow and shear stress on adult pulmonary vascular activity are not well elucidated. A study shows that blood flow induces vasodilation in the ferret lung in hypoxia but not in normoxia (Chammas et al. 1997). The production of EDNO can be stimulated by various humoral agents and neurotransmitter agents such as acetylcholine, bradykinin, epinephrine, histamine, norepinephrine, serotonin (5-HT), and vasopressin. Some of these agents, in addition to causing vasodilatation via EDNO, can also cause vasoconstriction by directly acting on VSMCs. Under normal conditions, the EDNO-mediated action prevails.

When the endothelium is damaged or the eNOS function is compromised, their direct action on VSMCs is unmasked leading to exaggerated pulmonary vasoconstriction (Barnes and Liu 1995; Suresh and Shimoda 2016).

PGI_2 is the dominant vasodilator prostanoid of pulmonary vasculature synthesized by cyclooxygenases (COX). It is produced mainly by endothelial cells and to a less extent by VSMCs (Brannon et al. 1994; Clapp and Gurung 2015). PGI_2 is synthesized from arachidonic acid (AA) released from the cell membrane following activation of phospholipase A2 (PLA_2) by calcium. Released AA is converted by cyclooxygenases (COX) to 15-OH-prostaglandin-9,11-endoperoxide (PGH_2), which is further converted to PGI_2 by PGI_2 synthases (PGIS). COX is the rate-limiting enzyme for the production of PGI_2 as well as other prostanoids. The enzymes are present as two isoforms, the constitutive isoform is termed COX-1 and the inducible is COX-2. The expression of COX-2 is induced by inflammatory factors (Fitzpatrick and Soberman 2001; Montani et al. 2014). The vasodilator effect of PGI_2 is mediated by binding to cell surface PGI_2 receptors (IP receptors) and binding to nuclear peroxisome proliferator-activated receptors (PPARs). Binding of PGI_2 to IP receptors causes vasodilatation via elevation of intracellular cAMP by activating G-protein-coupled adenylate cyclase (Clapp and Gurung 2015). In human pulmonary arteries, the binding of PGI_2 to the nuclear receptor PPARβ/δ may cause vasodilatation via the activation of Ca^{2+}-dependent K^+ channels (Li et al. 2012). The inhibition of COX has been found to increase pulmonary arterial pressure in a number species including rabbits (Tan et al. 1997), piglets (Redding et al. 1984), dogs (Lindenfeld et al. 1983), and sheep (Newman et al. 1986), suggesting that basal production of a vasodilator prostanoid, likely PGI_2, exerts an inhibitory effect on pulmonary vasomotor tone. In fetal goats and lambs, ventilation-induced pulmonary vasodilatation is associated with increased production of PGI_2. These changes are prevented by the inhibition of COX, suggesting that PGI_2 is involved in the reduction in PVR at birth (Gao and Raj 2010). In patients with pulmonary arterial hypertension (PAH), the PGIS is reduced in pulmonary arteries, implying that a decreased PGI_2 production may contribute to the increased PVR (Tuder et al. 1999). In agreement with these findings, the administration PGI_2 analogs has been shown to be effective in the treatment of pulmonary arterial hypertension (PAH) (Ataya et al. 2016).

While NO and PGI_2 exert an inhibitory effect on pulmonary vascular activity, ET-1, a peptide produced primarily by endothelial cells, causes profound pulmonary vasoconstriction. ET-1 belongs to a family of bicyclic 21-amino acid peptides consisting of three isoforms: ET-1, ET-2, and ET-3. ET-1 is the major isoform with vasoactive properties and has been found to be the most potent endogenous vasoconstrictor. In endothelial cells ET-1 is stored in Weibel–Palade bodies and released by exocytosis in response to Ca^{2+} elevation elicited by stimuli such as mechanical stretch, hypoxia, growth factors, cytokines, and adhesion molecules. ET-1 is also shuttled continuously from the trans-Golgi network to the cell surface in secretory vesicles via the constitutive secretory pathway, which contributes to the basal vascular tone under physiological conditions. ET-1 is released from endothelial cells predominantly (~80%) toward the abluminal side where it binds to two receptor types, ET_A and ET_B receptors, which are present in VSMCs and induce

vasoconstriction by the inhibition of Ca^{2+} influx and Ca^{2+} release from the sarcoplasmic reticulum and by the interference with RhoA–Rho kinase signaling. ET-1 also causes vasodilatation by stimulating the release of NO and PGI_2 after binding to endothelial ET_B receptors. The endothelial ET_B receptors also mediate the pulmonary clearance of circulating ET-1 (Davenport et al. 2016; Gao et al. 2016).

In the lung of humans and rats, ET_A receptors are more abundant in the proximal, whereas ET_B receptors are more abundant in the distal pulmonary arterial SMCs. The expression of ET_B receptors in the endothelium is higher in proximal than in distal vessels (Gao and Raj 2010). In porcine pulmonary arterial SMCs, ET-1 at a low concentration (10^{-10} M) that does not affect the intracellular Ca^{2+} nor the cell length markedly augments hypoxic vasocontraction, suggesting that ET-1 exerts a priming effect (Sham et al. 2000). In isolated porcine distal pulmonary arteries, the vasoconstriction evoked by hypoxia is largely abolished by BQ-123, an ET_A receptor antagonist, or endothelial denudation and restored in endothelium-denuded pulmonary arteries pretreated with ET-1 (10^{-10} M). Hence, it appears that the full in vivo expression of hypoxic pulmonary vasoconstriction (HPV) requires basal release of ET-1 from the endothelium to facilitate the hypoxic reactivity of the underlying pulmonary arterial smooth muscle (Liu et al. 2001). An increased ET-1 level in the blood and in pulmonary vessels is a common feature of PAH of both the newborn and the adult. Persistent and excessive pulmonary vasoconstriction and vascular remodeling caused by ET-1 are clearly critically involved (Gao and Raj 2010; Sylvester et al. 2012; Suresh and Shimoda 2016).

17.4.2 Autonomic Nervous Influence

The pulmonary vasculature is innervated by sympathetic, parasympathetic, and sensory–motor nerve fibers. The sympathetic nerves arise from the first five thoracic ganglia, the satellite ganglia, and middle and inferior cervical ganglia. Postganglionic fibers from these ganglia intermix with parasympathetic nerve fibers arising from vagus nerves to form anterior and posterior plexus at the tracheal bifurcation and a periarterial plexus and a peribronchial plexus at the lung hilus. The former innervates the pulmonary vascular tree, whereas the latter innervates the bronchial tree. The periarterial plexus starts as bundles of large nerve trunks but diminishes in size so that it exists only as a single fiber at the level of arterioles. In most organs, arterioles have the highest level of sympathetic innervation; in contrast, the highest density of sympathetic innervation is in extrapulmonary vessels. Intrapulmonary veins are also innervated by autonomic sensory nerve fibers, although to a lesser extent than the arterial network. The innervation density varies substantially among species, and in general, adrenergic innervation is more extensive than cholinergic fiber density (Barnes and Liu 1995; Tan et al. 2007; Kummer 2011; Townsley 2012; Suresh and Shimoda 2016).

Sympathetic activation increases PVR via the release of norepinephrine, which causes vasoconstriction by binding to α-adrenergic receptors (α-ARs), primarily α_1-

ARs. The stimulation of sympathetic nerve also causes pulmonary vasodilation by binding to β-adrenergic receptors (β-ARs) (Barnes and Liu 1995). Under physiological conditions, there is limited basal sympathetic influence on pulmonary vascular tone. During exercise the blockade of α-ARs decreases PVR, whereas the blockade of β-ARs increases PVR compared with the control in pigs. In the presence of both α-AR and β-AR blockers, the PVR is not different from the control. Thus, although the sympathetic activity is increased during exercise, its effect on PVR is neutral due to the opposing effects of α-ARs and β-ARs (Kane et al. 1993). In an acute porcine model of pulmonary hypertension, the denervation of pulmonary artery reduces pulmonary artery pressure and PVR, suggesting that the contractile influence of sympathetic innervation is more dominate and that the suppression of sympathetic activity may be an effective mean to prevent the excessive α-AR activity under certain condition such as pulmonary hypertension (Porcelli and Bergofsky 1973; Rothman et al. 2015).

Parasympathetic stimulation causes release of acetylcholine (ACh). Vagally released ACh may cause pulmonary arteries of the cat to dilate via EDNO (McMahon et al. 1992). ACh causes human pulmonary arteries to relax in vessels with endothelium. When the endothelium is removed, ACh induces a small contractile response due to direct action on the SMCs (Greenberg et al. 1987). The functional role of cholinergic innervation in pulmonary circulation is not very clear. In conscious dogs cholinergic blockade has no effect on basal pulmonary arterial pressure and PVR, indicating that these nerves may not have a major role in the maintenance of low pulmonary vascular tone (Murray et al. 1986; Barnes and Liu 1995). In addition to the classic neurotransmitters, neuropeptide Y and ATP can be co-released from sympathetic nerve varicosities, vasoactive intestinal peptide and NO can be co-released from parasympathetic nerve varicosities, and also calcitonin gene-related peptide (CGRP) and substance P can be co-released from sensory–motor nerve varicosities. These neurotransmitters may modulate the activity of autonomic nervous system (Burnstock 2009; Burnstock and Ralevic 2013). Their role in pulmonary circulation remains to be elucidated.

17.4.3 Hypoxic Pulmonary Vasoconstriction

Hypoxic vasoconstriction is a unique feature of the pulmonary circulation as hypoxia causes vasodilatation of systemic vessels. The contractile response of pulmonary vasculature evoked by hypoxia is first noticed by Beutner in 1852 (Beutner 1852). It is characterized in detail by von Euler and Lillestrand in 1946 (Von Euler and Liljestrand 1946). The main site of HPV is located in small muscular arterioles. When alveolar oxygen tension is reduced, a constrictive response of pulmonary arteries and arterioles occurs within a few minutes resulting in increased PVR. The response reaches its maximum within 5 min and is maintained for the duration of the hypoxic exposure. Upon reoxygenation, HPV rapidly reverses, and PVR returns to normal levels within minutes. It is generally

believed that under physiological conditions, a localized HPV diverts blood flow from poorly oxygenated to better-oxygenated portions of the lung so that the blood perfusion and ventilation can be more efficiently matched. However, a more global and sustained HPV may lead to vascular remodeling and the development of PAH (Sylvester et al. 2012; Sommer et al. 2016; Suresh and Shimoda 2016).

Although HPV has been demonstrated in various species, the mechanism underlying this phenomenon is still not well understood. It is generally recognized that HPV is an intrinsic property of pulmonary VSMCs. However, the full expression of HPV depends on the presence of the endothelium, probably due to a priming effect exerted by some factor(s) released from the endothelium or cross talk between endothelial cells and VSMCs via myoendothelial gap junctions (Ward and Aaronson 1999; Wang et al. 2012; Gao et al. 2016). Currently, there are two major hypotheses regarding HPV, the redox hypothesis (Archer et al. 1993; Dunham-Snary et al. 2017) and the reactive oxygen species (ROS) hypothesis (Leach et al. 2001; Waypa et al. 2001; Waypa et al. 2016). Both hypotheses propose that the mitochondria in pulmonary arterial SMCs act as the oxygen sensor. However, the redox hypothesis believes that hypoxia causes a reduced generation of ROS, while the ROS hypothesis believes that hypoxia causes an increased generation of ROS by mitochondria (Sylvester et al. 2012). The discrepancy in the measured changes in ROS may result from the artefacts due to nonspecificity and autoxidation of fluorescent ROS probes, re-oxygenation during the measurement, time dependency of ROS release and detoxification, and extra- and intracellular compartmentalization of ROS signaling (Waypa et al. 2010; Griendling et al. 2016; Sommer et al. 2016).

According to the redox hypothesis, ROS generation under normoxia occurs at mitochondrial electron transport chain (ETC) complexes I and III. The superoxide ($O_2^{\cdot -}$) produced is converted to H_2O_2 by superoxide dismutase. H_2O_2, along with the oxidized redox couples (e.g., oxidized and reduced nicotinamide adenine dinucleotide (NAD^+/NADH), oxidized and reduced glutathione (GSSG/GSH)), maintains $K_v1.5$ sulfhydryl group oxidation and channel in an open state, resulting in the resting membrane potential of the pulmonary arterial SMCs at −60 mV and thus inhibition of voltage-gated Ca^{2+} channels (VGCCs). During hypoxia, the limited availability of O_2 leads to diminished H_2O_2 generation by ETC and decreased ratio of oxidized/reduced redox couples. Consequently, the sulfhydryl groups on voltage-dependent K^+ channel $K_V1.5$ is reduced causing the K_V channels to close, membrane potential depolarization to −20 mV, the opening of VGCCs, and activation of the contractile apparatus. In addition, the altered redox status may stimulate the release of Ca^{2+} from sarcoplasmic reticulum (SR) into the cytosol and promote extracellular Ca^{2+} entry through store-operated Ca^{2+} channels (SOCCs) (Sylvester et al. 2012; Dunham-Snary et al. 2017). For the ROS hypothesis, it is proposed that hypoxia stimulates mitochondrial ETC complex III to generate $O_2^{\cdot -}$ at the Q_0 ubiquinone binding site within the inner membrane. $O_2^{\cdot -}$ generated there is ejected into the intermembrane space by the strong electrical field across the membrane resulting from the electrical gradient (−180 mV) and then diffuses into the cytosol. In the process, $O_2^{\cdot -}$ is also converted to H_2O_2. ROS may stimulate the nonselective

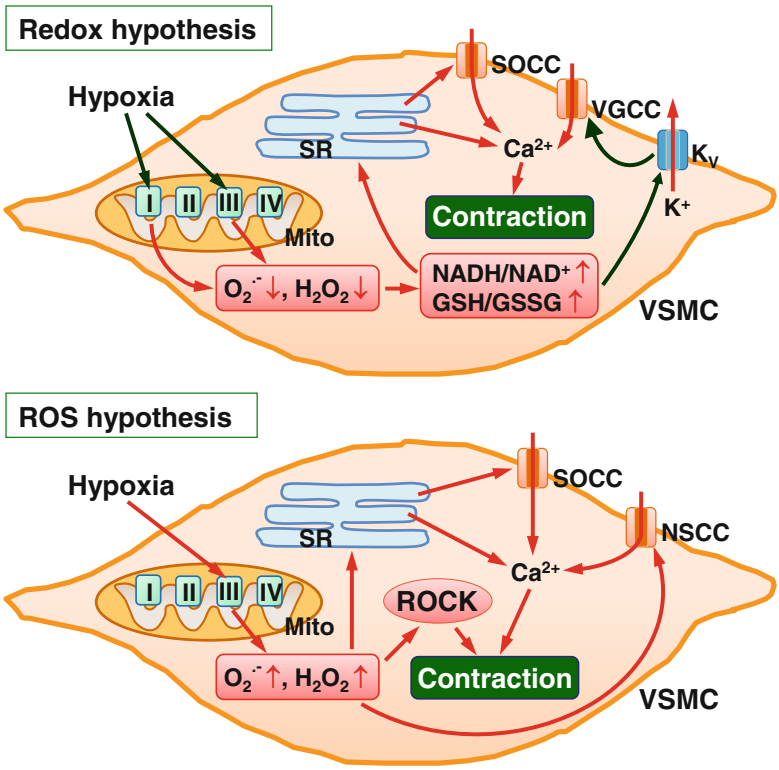

Fig. 17.3 Comparison of the two hypotheses proposed for hypoxic pulmonary vasoconstriction (HPV): the redox hypothesis (the *upper panel* of the figure) and reactive oxygen species (ROS) hypothesis (the *lower panel* of the figure). The redox hypothesis proposes that hypoxia inhibits the generation of ROS by mitochondrial electron transport chain (ETC) complexes I and III, leading to decreased cytosol levels of superoxide ($O_2^{\cdot-}$) and H_2O_2 and increased ratio of reduced to oxidized nicotinamide adenine dinucleotide ($NADH/NAD^+$) and reduced to oxidized glutathione (GSH/GSSG). Consequently, the voltage-gated K^+ channels (K_V) are reduced causing them to close, leading to membrane potential depolarization, opening of voltage-gated Ca^{2+} channels (VGCCs), and activation of the contractile apparatus. Meanwhile, the altered redox status may stimulate the release of Ca^{2+} from sarcoplasmic reticulum (SR) and promote Ca^{2+} entry through store-operated Ca^{2+} channels (SOCCs). All these events promote HPV. The ROS hypothesis proposes that hypoxia causes increased production of superoxide ($O_2^{\cdot-}$) and H_2O_2 by mitochondrial ETC complex III. ROS causes vasoconstriction through activation of nonselective cation channels (NSCC) resulting in increased extracellular Ca^{2+} influx. ROS also activates Rho kinase (ROCK) leading to sensitization of myofilaments to Ca^{2+} and thus augmented contractility. Additionally, an increased Ca^{2+} release from SR and increased Ca^{2+} entry through SOCC channels may also be involved resulted from the actions of ROS. *Red arrow lines* indicate a stimulatory effect, and *green arrow lines* indicate inhibitory effect. *Mito* mitochondria, *VSMC* vascular smooth muscle cell

cation channels (NSCC), promote Ca^{2+} release from sarcoplasmic reticulum through ryanodine-sensitive channels, and increase Ca^{2+} entry through SOCC channels. These events lead to increased intracellular levels of the Ca^{2+} ions and

thus vasoconstriction. ROS also activates Rho kinase (ROCK) leading to sensitization of myofilaments to Ca^{2+} and thus augmented contractility (Sylvester et al. 2012; Waypa et al. 2013; Sommer et al. 2016) (Fig. 17.3).

References

Archer SL, Huang J, Henry T, Peterson D, Weir EK (1993) A redox-based O_2 sensor in rat pulmonary vasculature. Circ Res 73:1100–1112

Ataya A, Cope J, Alnuaimat H (2016) A review of targeted pulmonary arterial hypertension-specific pharmacotherapy. J Clin Med 5.pii: E114

Baile EM (1996) The anatomy and physiology of the bronchial circulation. J Aerosol Med 9:1–6

Barnes PJ, Liu SF (1995) Regulation of pulmonary vascular tone. Pharmacol Rev 47:87–131

Beutner A (1852) Ueber die Strom- und Druckkräfte des Blutes in der Arteria pulmonalis. Z Rationelle Med 2:97–138

Black SM, Johengen MJ, Ma ZD, Bristow J, Soifer SJ (1997) Ventilation and oxygenation induce endothelial nitric oxide synthase gene expression in the lungs of fetal lambs. J Clin Invest 100:1448–1458

Blitzer ML, Loh E, Roddy MA, Stamler JS, Creager MA (1996) Endothelium derived nitric oxide regulates systemic and pulmonary vascular resistance during acute hypoxia in humans. J Am Coll Cardiol 28:591–596

Brannon TS, North AJ, Wells LB, Shaul PW (1994) Prostacyclin synthesis in ovine pulmonary artery is developmentally regulated by changes in cyclooxygenase-1 gene expression. J Clin Invest 93:2230–2235

Brody JS, Stemmler EJ, DuBois AB (1968) Longitudinal distribution of vascular resistance in the pulmonary arteries, capillaries, and veins. J Clin Invest 47:783–799

Burnstock G (2009) Autonomic neurotransmission: 60 years since sir Henry Dale. Annu Rev Pharmacol Toxicol 49:1–30

Burnstock G, Ralevic V (2013) Purinergic signaling and blood vessels in health and disease. Pharmacol Rev 66:102–192

Burrowes KS, Hunter PJ, Tawhai MH (2005) Anatomically based finite element models of the human pulmonary arterial and venous trees including supernumerary vessels. J Appl Physiol 99:731–738

Butler J, Paley HW (1962) Lung volume and pulmonary circulation. Med Thorac 19:261–267

Cha TJ, Ehrlich JR, Zhang L, Chartier D, Leung TK, Nattel S (2005) Atrial tachycardia remodeling of pulmonary vein cardiomyocytes: comparison with left atrium and potential relation to arrhythmogenesis. Circulation 111:728–735

Chammas JH, Rickaby DA, Guarin M, Linehan JH, Hanger CC, Dawson CA (1997) Flow-induced vasodilation in the ferret lung. J Appl Physiol 83:495–502

Charan NB, Thompson WH, Carvalho P (2007) Functional anatomy of bronchial veins. Pulm Pharmacol Ther 20:100–103

Clapp LH, Gurung R (2015) The mechanistic basis of prostacyclin and its stable analogues in pulmonary arterial hypertension: role of membrane versus nuclear receptors. Prostaglandins Other Lipid Mediat 120:56–71

Cornfield DN, Chatfield BA, McQueston JA, McMurtry IF, Abman SH (1992) Effects of birth-related stimuli on L-arginine-dependent pulmonary vasodilation in ovine fetus. Am J Physiol Heart Circ Physiol 262:H1474–H1481

Coutu P, Chartier D, Nattel S (2006) Comparison of Ca^{2+}-handling properties of canine pulmonary vein and left atrial cardiomyocytes. Am J Physiol Heart Circ Physiol 291:H2290–H2300

Davenport AP, Hyndman KA, Dhaun N, Southan C, Kohan DE, Pollock JS, Pollock DM, Webb DJ, Maguire JJ (2016) Endothelin. Pharmacol Rev 68:357–418

Dunham-Snary KJ, Wu D, Sykes EA, Thakrar A, Parlow LR, Mewburn JD, Parlow JL, Archer SL (2017) Hypoxic pulmonary vasoconstriction: from molecular mechanisms to medicine. Chest 151:181–192

Elliott FM, Reid LM (1965) Some new facts about the pulmonary artery and its branching pattern. Clin Radiol 16:193–198

Fishman AP (2011) Pulmonary circulation. Compr Physiol:93–165

Fitzpatrick FA, Soberman R (2001) Regulated formation of eicosanoids. J Clin Invest 107:1347–1351

Gao Y (2010) The multiple actions of NO. Pflügers Arch Eur J Physiol 459:829–839

Gao Y, Raj JU (2006) cGMP-dependent protein kinase in regulation of the pulmonary circulation. Curr Resp Med Rev 2:373–381

Gao Y, Raj JU (2010) Regulation of the pulmonary circulation in the fetus and newborn. Physiol Rev 90:1291–1335

Gao Y, Chen T, Raj JU (2016) Endothelial and smooth muscle cell interactions in the pathobiology of pulmonary hypertension. Am J Respir Cell Mol Biol 54:451–460

Gil J (1980) Organization of microcirculation in the lung. Annu Rev Physiol 42:177–186

Glenny R, Robertson HT (2011) Distribution of perfusion. Compr Physiol 1:245–262

Greenberg B, Rhoden K, Barnes PJ (1987) Endothelium-dependent relaxation of human pulmonary arteries. Am J Phys 252:H434–H438

Griendling KK, Touyz RM, Zweier JL, Dikalov S, Chilian W, Chen YR, Harrison DG, Bhatnagar A, American Heart Association Council on Basic Cardiovascular Sciences (2016) Measurement of reactive oxygen species, reactive nitrogen species, and redox-dependent signaling in the cardiovascular system: a scientific statement from the American Heart Association. Circ Res 119:e39–e75

Hakim TS, Michel RP, Chang HK (1982) Partitioning of pulmonary vascular resistance in dogs by arterial and venous occlusion. J Appl Physiol Respir Environ Exerc Physiol 52:710–715

Hassink RJ, Aretz HT, Ruskin J, Keane D (2003) Morphology of atrial myocardium in human pulmonary veins: a postmortem analysis in patients with and without atrial fibrillation. J Am Coll Cardiol 42:1108–1114

Horsfield K (1984) Axial pathways compared with complete data in morphological studies of the lung. Respir Physiol 55:317–324

Howell JB, Permutt S, Proctor DF, Riley RL (1961) Effect of inflation of the lung on different parts of pulmonary vascular bed. J Appl Physiol 16:71–76

Huang W, Yen RT, McLaurine M, Bledsoe G (1996) Morphometry of the human pulmonary vasculature. J Appl Physiol 81:2123–2133

Hughes M, West JB (2008) Point: gravity is the major factor determining the distribution of blood flow in the human lung. J Appl Physiol 104:1531–1533

Kane DW, Tesauro T, Newman JH (1993) Adrenergic modulation of the pulmonary circulation during strenuous exercise in sheep. Am Rev Respir Dis 147:1233–1238

Koizumi T, Gupta R, Banerjee M, Newman JH (1994) Changes in pulmonary vascular tone during exercise. Effects of nitric oxide (NO) synthase inhibition, L-arginine infusion and NO inhalation. J Clin Invest 94:2285–2282

Kumar S, Sud N, Fonseca FV, Hou Y, Black SM (2010) Shear stress stimulates nitric oxide signaling in pulmonary arterial endothelial cells via a reduction in catalase activity: role of protein kinase C. Am J Physiol Lung Cell Mol Physiol 298:L105–L116

Kummer W (2011) Pulmonary vascular innervation and its role in responses to hypoxia: size matters! Proc Am Thorac Soc 8:471–476

LaBourene JI, Coles JG, Johnson DJ, Mehra A, Keeley FW, Rabinovitch M (1990) Alterations in elastin and collagen related to the mechanism of progressive pulmonary venous obstruction in a piglet model. A hemodynamic, ultrastructural, and biochemical study. Circ Res 66:438–456

Leach RM, Hill HM, Snetkov VA, Robertson TP, Ward JP (2001) Divergent roles of glycolysis and the mitochondrial electron transport chain in hypoxic pulmonary vasoconstriction of the rat: identity of the hypoxic sensor. J Physiol 536:211–224

Levitzky MG (2006) Teaching the effects of gravity and intravascular and alveolar pressures on the distribution of pulmonary blood flow using a classic paper by West et al. Adv Physiol Educ 30:5–8

Li Y, Connolly M, Nagaraj C, Tang B, Bálint Z, Popper H, Smolle-Juettner FM, Lindenmann J, Kwapiszewska G, Aaronson PI, Wohlkoenig C, Leithner K, Olschewski H, Olschewski A (2012) Peroxisome proliferator-activated receptor-β/δ, the acute signaling factor in prostacyclin-induced pulmonary vasodilation. Am J Respir Cell Mol Biol 46:372–379

Lindenfeld J, Reeves JT, Horwitz LD (1983) Low exercise pulmonary resistance is not dependent on vasodilator prostaglandins. J Appl Physiol 55:558–561

Liu Q, Sham JS, Shimoda LA, Sylvester JT (2001) Hypoxic constriction of porcine distal pulmonary arteries: endothelium and endothelin dependence. Am J Physiol Lung Cell Mol Physiol 280:L856–L865

Manohar M, Goetz TE (1998) L-NAME does not affect exercise-induced pulmonary hypertension in thoroughbred horses. J Appl Physiol 84:1902–1908

Mazzone RW, Durand CM, West JB (1978) Electron microscopy of lung rapidly frozen under controlled physiological conditions. J Appl Physiol Respir Environ Exerc Physiol 45:325–333

McMahon TJ, Hood JS, Kadowitz PJ (1992) Pulmonary vasodilator response to vagal stimulation is blocked by N omega-nitro-L-arginine methyl ester in the cat. Circ Res 70:364–369

Merkus D, Houweling B, Zarbanoui A, Duncker DJ (2004) Interaction between prostanoids and nitric oxide in regulation of systemic, pulmonary and coronary vascular tone in exercising swine. Am J Phys 286:H1114–H1123

Michelakis ED, Weir EK, Wu X, Nsair A, Waite R, Hashimoto K, Puttagunta L, Knaus HG, Archer SL (2001) Potassium channels regulate tone in rat pulmonary veins. Am J Physiol Lung Cell Mol Physiol 280:L1138–L1147

Montani D, Chaumais MC, Guignabert C, Günther S, Girerd B, Jaïs X, Algalarrondo V, Price LC, Savale L, Sitbon O, Simonneau G, Humbert M (2014) Targeted therapies in pulmonary arterial hypertension. Pharmacol Ther 141:172–191

Morkin E, Collins JA, Goldman HS, Fishman AP (1965) Pattern of blood flow in the pulmonary veins of the dog. J Appl Physiol 20:1118–1128

Mueller-Hoecker J, Beitinger F, Fernandez B, Bahlmann O, Assmann G, Troidl C, Dimomeletis I, Kaab S, Deindl E (2008) Of rodents and humans: a light microscopic and ultrastructural study on cardiomyocytes in pulmonary veins. Int J Med Sci 5:152–158

Murray PA, Lodato RF, Michael JR (1986) Neural antagonists modulate pulmonary vascular pressure-flow plots in conscious dogs. J Appl Physiol 60:1900–1907

Mynard JP, Smolich JJ (2015) One-dimensional haemodynamic modeling and wave dynamics in the entire adult circulation. Ann Biomed Eng 43:1443–1460

Newman JH, Butka BJ, Brigham KL (1986) Thromboxane A2 and prostacyclin do not modulate pulmonary hemodynamics during exercise in sheep. J Appl Physiol 61:1706–1711

Ochs M, Nyengaard JR, Jung A, Knudsen L, Voigt M, Wahlers T, Richter J, Gundersen HJ (2004) The number of alveoli in the human lung. Am J Respir Crit Care Med 169:120–124

Paes de Almeida O, Bohm CM, de Paula Carvalho M, Paes de Carvalho A (1975) The cardiac muscle in the pulmonary vein of the rat: a morphological and electrophysiological study. J Morphol 145:409–433

Porcelli RJ, Bergofsky EH (1973) Adrenergic receptors in pulmonary vasoconstrictor responses to gaseous and humoral agents. J Appl Physiol 34:483–488

Rajagopalan B, Friend JA, Stallard T, Lee GD (1975) Blood flow in pulmonary veins: II. The influence of events transmitted from the right and left sides of the heart. Cardiovasc Res 13:677–683

Redding GJ, McMurtry I, Reeves JT (1984) Effects of meclofenamate on pulmonary vascular resistance correlate with postnatal age in young piglets. Pediatr Res 18:579–583

Reid L (1965) The angiogram and pulmonary artery structure and branching (in the normal and with reference to disease). Proc Royal Soc Med 58:681–684

Rhodin JA (1978) Microscopic anatomy of the pulmonary vascular bed in the cat lung. Microvasc Res 15:169–193

Rosenzweig DY, Hughes JM, Glazier JB (1970) Effects of transpulmonary and vascular pressures on pulmonary blood volume in isolated lung. J Appl Physiol 28:553–560

Rothman AM, Arnold ND, Chang W, Watson O, Swift AJ, Condliffe R, Elliot CA, Kiely DG, Suvarna SK, Gunn J, Lawrie A (2015) Pulmonary artery denervation reduces pulmonary artery pressure and induces histological changes in an acute porcine model of pulmonary hypertension. Circ Cardiovasc Interv 8:e002569

Sham JS, Crenshaw BR Jr, Deng LH, Shimoda LA, Sylvester JT (2000) Effects of hypoxia in porcine pulmonary arterial myocytes: roles of K_V channel and endothelin-1. Am J Physiol Lung Cell Mol Physiol 279:L262–L272

Shoukas AA (1975) Pressure-flow and pressure-volume relations in the entire pulmonary vascular bed of the dog determined by two-port analysis. Circ Res 37:809–818

Simmons DH, Linde LM, Miller JH, O'Reilly RJ (1961) Relation between lung volume and pulmonary vascular resistance. Circ Res 9:465–471

Sommer N, Strielkov I, Pak O, Weissmann N (2016) Oxygen sensing and signal transduction in hypoxic pulmonary vasoconstriction. Eur Respir J 47:288–303

Stamler JS, Loh E, Reddy MA, Creager MA (1994) Nitric oxide regulates basal systemic and pulmonary vascular resistance in healthy humans. Circulation 89:2035–2040

Staub NC, Schultz EL (1968) Pulmonary capillary length in dogs, cat and rabbit. Respir Physiol 5:371–378

Sud N, Kumar S, Wedgwood S, Black SM (2009) Modulation of PKC signaling alters the shear stress-mediated increases in endothelial nitric oxide synthase transcription: role of STAT3. Am J Physiol Lung Cell Mol Physiol 296:L519–L526

Suresh K, Shimoda LA (2016) Lung circulation. Compr Physiol 6:897–943

Sylvester JT, Shimoda LA, Aaronson PI, Ward JP (2012) Hypoxic pulmonary vasoconstriction. Physiol Rev 92:367–520

Tan JZ, Kaley G, Gurtner GH (1997) Nitric oxide and prostaglandins mediate vasodilation to 5,6-EET in rabbit lung. Adv Exp Med Biol 407:561–566

Tan AY, Chen PS, Chen LS, Fishbein MC (2007) Autonomic nerves in pulmonary veins. Heart Rhythm 4(3 suppl):S57–S60

Townsley MI (2012) Structure and composition of pulmonary arteries, capillaries, and veins. Compr Physiol 2:675–709

Townsley MI, Snell KS, Ivey CL, Culberson DE, Liu DC, Reed RK, Mathieu-Costello O (1999) Remodeling of lung interstitium but not resistance vessels in canine pacing-induced heart failure. J Appl Physiol 87:1823–1830

Tuder RM, Cool CD, Geraci MW, Wang J, Abman SH, Wright L, Badesch D, Voelkel NF (1999) Prostacyclin synthase expression is decreased in lungs from patients with severe pulmonary hypertension. Am J Respir Crit Care Med 159:1925–1932

von Euler US, Liljestrand G (1946) Observations on the pulmonary arterial blood pressure of the cat. Acta Physiol Scand 12:301–320

Wang L, Yin J, Nickles HT, Ranke H, Tabuchi A, Hoffmann J, Tabeling C, Barbosa-Sicard E, Chanson M, Kwak BR, Shin HS, Wu S, Isakson BE, Witzenrath M, de Wit C, Fleming I, Kuppe H, Kuebler WM (2012) Hypoxic pulmonary vasoconstriction requires connexin 40-mediated endothelial signal conduction. J Clin Invest 122:4218–4230

Ward JPT, Aaronson PI (1999) Mechanisms of hypoxic pulmonary vasoconstriction: can anyone be right? Respir Physiol 115:261–271

Waypa GB, Chandel NS, Schumacker PT (2001) Model for hypoxic pulmonary vasoconstriction involving mitochondrial oxygen sensing. Circ Res 88:1259–1266

Waypa GB, Marks JD, Guzy R, Mungai PT, Schriewer J, Dokic D, Schumacker PT (2010) Hypoxia triggers subcellular compartmental redox signaling in vascular smooth muscle cells. Circ Res 106:526–535

Waypa GB, Marks JD, Guzy RD, Mungai PT, Schriewer JM, Dokic D, Ball MK, Schumacker PT (2013) Superoxide generated at mitochondrial complex III triggers acute responses to hypoxia in the pulmonary circulation. Am J Respir Crit Care Med 187:424–432

Waypa GB, Smith KA, Schumacker PT (2016) O_2 sensing, mitochondria and ROS signaling: the fog is lifting. Mol Asp Med 47–48:76–89

Wedgwood S, Mitchell CJ, Fineman JR, Black SM (2003) Developmental differences in the shear stress-induced expression of endothelial NO synthase: changing role of AP-1. Am J Physiol Lung Cell Mol Physiol 284:L650–L662

Weibel ER, Sapovale B, Filoche M (2005) Design of peripheral airways for efficient gas exchange. Respir Physiol Neurobiol 148:3–21

West JB, Dollery CT, Naimark A (1964) Distribution of blood flow in isolated lung; relation to vascular and alveolar pressures. J Appl Physiol 19:713–724

Wiener F, Morkin E, Skalak R, Fishman AP (1966) Wave propagation in the pulmonary circulation. Circ Res 19:834–850

Chapter 18
Hypoxic Vasoreactivity

Abstract Hypoxia may affect vascular activity by directly acting on the vasculature and indirectly through circulating humoral agents, neuronal transmitters, and metabolites released from the perfused tissues. In response to hypoxia, the systemic blood vessels contract, predominantly due to the metabolites from the perfused tissues but not the vasculature per se so that blood flow is matched to the tissue metabolism. In contrast, hypoxia causes pulmonary blood vessels to contract, largely due to the direct effect of hypoxia on vasculature so that blood flow is diverted to the locations where the alveoli are better oxygenated. The focus of this chapter is on the mechanisms underlying the direct effect of hypoxia on vasculature, including the roles of reactive oxygen species, redox modulation, and 5′-adenosine monophosphate-activated protein kinase. The influence of erythrocytes, in particular the hemoglobin, and hypoxia-inducible factor on hypoxic vascular activity is also being focused.

Keywords Reactive oxygen species • Redox • AMPK • Erythrocyte • Hypoxia-inducible factor

18.1 Introduction

Hypoxia is referred to reduced oxygen availability caused by systemic or local blood circulation alternations. Naturally speaking, the reduced oxygen availability would decrease ATP generation and thus suppress vasoactivity. Such a scenario is often unlikely to be true. The Po_2 for the half maximal activity of oxidative metabolism in mitochondria is less than 1 mmHg, which represents a much severe hypoxic condition than required for evoking a hypoxic vascular response (Gnaiger 2001; Wenger et al. 2015). Studies demonstrate that hypoxia affects vascular activity more often though altering the related signaling activities other than ATP production. Since the enzymes that generate the messengers may have different sensitivity to Po_2, hypoxia could affect vasoactivity by acting on different enzymes depending on the extent of reduction of Po_2. O_2 is required for the synthesis of vasoactive agents nitric oxide (NO), prostaglandins (PGs), epoxyeicosatrienoic acids (EETs), and 20-hydroxyeicosatetraenoic acid (20-HETE). The Michaelis constants (K_m values) of O_2 for endothelial NO synthase (eNOS) and neuronal

Y. Gao, *Biology of Vascular Smooth Muscle: Vasoconstriction and Dilatation*,
DOI 10.1007/978-981-10-4810-4_18

NO synthase (nNOS) are ~4 μM and ~350 μM, respectively (Stuehr et al. 2004). The K_m values of O_2 for the synthesis of 20-HETE and EETs are ~55 μM and <10 μM, respectively (Harder et al. 1996); whereas the K_m value for the synthesis of PGs is ~10 μM (Barnett et al. 1994). Hence, the production of NO derived from nNOS and 20-HETE may be more sensitive to O_2 availability than the production of NO derived from eNOS, PGs, and EETs. Also, hypoxia may exert opposing effects on different cellular targets. In pulmonary artery smooth muscle cells (PASMCs), hypoxia stimulates nonselective cation channels (NSCC) but inhibits voltage-dependent K^+ channels (Shimoda and Polak 2011).

When exposed to hypoxia, the vasculature recruits complex mechanisms to preserve its functionality and to minimize adverse hypoxic effect. The responses evoked by the reduction in oxygen availability have been found to be based on a range of oxygen-sensing signal cascades including changes in the production of reactive oxygen species (ROS), in particular those generated from the electron carrier units of the mitochondrial (Sommer et al. 2016; Waypa et al. 2016), and changes in the redox status of subcellular compartments (Dou et al. 2013; Byon et al. 2016). 5′-Adenosine monophosphate-activated protein kinase (AMPK), the key player in maintaining cellular energy homeostasis, is implicated in the modulation of hypoxic responses (Evans et al. 2015). The roles of these oxygen sensors in vascular vasoactivities will be the major focus in this chapter. Hypoxia also modulates the response of the blood vessels in an erythrocyte-dependent manner (Kulandavelu et al. 2015; Zhang et al. 2015; Wan et al. 2008 Hoiland et al. 2016). The related mechanism will be discussed. Hypoxia can evoke an acute and reversible vascular response within minutes of stimulation by mobilizing existing cellular mechanisms. The acute hypoxic response may be of important physiological significance. As is known, hypoxic vasodilatation of systemic vessels serves to ameliorate tissue underperfusion, while hypoxic vasoconstriction of pulmonary vessels helps to optimize ventilation–perfusion ratio. If hypoxic stimulation is persistent and prolonged, an exaggerated vasoconstriction along with vascular remodeling may develop which leads to dysfunctional vascular activity. The chronic hypoxic response is orchestrated, to a large extent, by hypoxia-inducible factors (HIFs), which are the master transcription factors that regulate cellular responses to hypoxia. The focus of the present chapter is not chronic hypoxic vascular activity. However, there is evidence indicating the involvement of HIFs in the maintenance of normal pulmonary vascular tone (Kim et al. 2013). Therefore, the role of HIFs in the regulation of hypoxic vasoactivity will also be discussed.

18.2 ROS and Hypoxic Vasoactivity

ROS are chemically reactive chemical species containing O_2. In vasculature the ROS of functional importance includes superoxide ($O_2^{\cdot-}$), peroxides (H_2O_2), and hydroxyl radical ($^{\bullet}OH$). Among them, $O_2^{\cdot-}$ is the precursor of many ROS. The

dismutation of $O_2^{\cdot -}$ by superoxide dismutase (SOD) produces H_2O_2, which in turn may be fully reduced to water by catalase or partially reduced to $^{\bullet}OH$ through Fenton reaction using ferrous ion as the catalyst. The hydroxyl radical is the strongest oxidants known, with a very short in vivo half-life of approximately 10^{-9} s and high nonspecific reactivities with nearly diffusion-controlled rate constants. It can damage virtually all types of macromolecules in the vicinity resulting in tissue damage. This makes it unsuitable to be a signaling molecule (Grek et al. 2013). By contrast, $O_2^{\cdot -}$ and H_2O_2 are less reactive. These ROS, in particular H_2O_2, due to its stability, intracellular and transcellular mobility, and its specificity for protein thiols, have been found to be involved in a plethora of biological processes (DeLeon et al. 2016). Under normal conditions, ROS is constantly generated and maintained within a physiological range by a broad range of antioxidant enzymes as well as no-enzymatic mechanisms. An impaired ROS scavenge which occurs under pathological conditions may lead to dysfunctional cardiovascular activity (Forman et al. 2010; Panth et al. 2016; Sies 2017).

In the cardiovascular system, the enzymatic sources of ROS include mitochondrial electron transport chain, NAD(P)H oxidase, lipoxygenase, cyclooxygenase, cytochrome P450s, xanthine oxidase, uncoupled eNOS, and other hemoproteins. Among these sources, the former two are the major ROS generator. Mitochondria can generate $O_2^{\cdot -}$ at complexes I, II, or III, through the escape of electrons from iron–sulfur groups, flavin-containing proteins, or from the ubisemiquinone in the Q cycle of complex III. The $O_2^{\cdot -}$-formed in mitochondria is quickly dismutated to H_2O_2 and diffuse into the cytosol. The peroxide, by attacking nucleophilic cysteine residues, can serve as a powerful and reversible modifier of protein structure and function (Waypa et al. 2016). Another important source of ROS is the NAD(P)H oxidase, which is found in two types: one in neutrophils and the other in non-neutrophilic cells. In mammalian there are seven isoforms of the enzyme being identified. Among them, Nox1, Nox2, Nox4, and Nox5 are expressed in the cardiovascular system. NAD(P)H oxidase oxidizes NADPH to reduce oxygen to $O_2^{\cdot -}$, of which most is converted to H_2O_2. For $O_2^{\cdot -}$, it can rapidly react with NO and thereby reduces the bioavailability of this gaseous transmitter and produces peroxynitrite (ONOO−), a potent oxidant. $O_2^{\cdot -}$ also reacts with iron–sulfur clusters and reduces Fe^{3+} in hemes. For instance, $O_2^{\cdot -}$ may inactivate the Fe–S cluster containing aconitase, resulting in suppressed progression of tricarboxylic acids through the citric acid cycle and altered cellular energy state (Bedard and Krause 2007; Brandes et al. 2014).

It is well recognized that hypoxia dilates systemic arteries to increase blood flow to the O_2-needed tissues but constricts pulmonary arteries to optimize the perfusion–ventilation ratio (Sylvester et al. 2012). Studies show that hypoxia increases the intracellular ROS levels in freshly isolated mouse pulmonary artery smooth muscle cells (PASMCs) but not in mesenteric artery smooth muscle cells (SMCs). During hypoxia an increased mitochondrial ROS generation leads to activation of NOX1 by PKCε, with consequent enhancement of the elevation in ROS, rise in the intracellular Ca^{2+} level ($[Ca^{2+}]_i$), and the shortening of PASMCs (Rathore et al. 2006; Rathore et al. 2008; Wang and Zheng 2010). In isolated rat

arteries constricted with U46619 (a thromboxane A_2 mimetic), $O_2^{\cdot-}$ generated with 6-anilino-5,8-quinolinequinone (LY83583) causes constriction in pulmonary and relaxation in mesenteric arteries, which is prevented by superoxide dismutase and catalase. LY83583 causes Rho kinase (ROCK)-dependent constriction in α-toxin-permeabilized pulmonary but not mesenteric arteries. LY83583 causes increases in pulmonary but decreases in mesenteric arteries in the intracellular Ca^{2+} level ($[Ca^{2+}]_i$) and in phosphorylation of the 20-kDa myosin light chain (MLC_{20}). The inhibition of K_V channels abolishes LY83583-induced relaxation in the mesenteric artery without affecting constriction in the pulmonary artery. When these arteries are constricted with 30 mM K^+ instead of U46619, LY83583 constricts both artery types with no effect on $[Ca^{2+}]_i$. These observations suggest that $O_2^{\cdot-}$ causes ROCK-mediated Ca^{2+} sensitization as well as the activation of K_V channels in the pulmonary artery. The net effect is vasoconstriction. In mesenteric arteries $O_2^{\cdot-}$ only opens K_V channels, resulting in vasodilatation (Knock et al. 2008; Snetkov et al. 2011). An augmented RhoA–ROCK signaling caused by $O_2^{\cdot-}$ has also been associated with chronic hypoxia-induced pulmonary vasoconstriction (Broughton et al. 2010). Acute hypoxia has been found to decrease ROS levels in both human pulmonary and coronary artery SMCs. However, chronic exposure to hypoxia markedly increases ROS levels in PASMCs but decreases ROS production in coronary artery SMCs (Wu et al. 2007). It should be noted that although substantial evidence suggests that ROS contributes to the vascular responses evoked by hypoxia, the changes in ROS caused by hypoxia reported in literatures are still inconsistent, at least in part due to the ephemeral nature and rapid reactivity of ROS and the technical challenge in the measurement of ROS (Griendling et al. 2016; Waypa et al. 2016).

18.3 Redox Modulation of Hypoxic Vasoactivity

The signaling transduction of ROS, especially H_2O_2, is often through the redox modulation of the thiol (-SH) and disulfide status of specific cysteine residues. The sulfur atom in cysteine residues is sensitive to oxidation by H_2O_2. In its reduced state, it exists as a thiol (-SH). Upon encounter with H_2O_2, it reacts to form sulfenic acid (-SOH). Sulfenic acid is unstable and can easily react with other cysteine thiols to form intra- or intermolecular disulfides (-S-S-) (Fig. 18.1). Alternatively, sulfenic acids react with GSH, leading to *S*-glutathionylation. The rate of protein thiols reacting with oxidants depends on the oxidant as well as on the reactivity of the respective cysteine. The formation of disulfide bond or *S*-glutathionylation leads to conformational changes within proteins or protein complexes and consequently changes in cellular signaling. The above reactions are reversible. The disulfides can be reduced back to thiols by the oxidoreductases thioredoxin and glutaredoxin, whereas the S-glutathionylated protein can be reduced back to thiols by the glutaredoxin. The resultant oxidized thioredoxin and glutaredoxin are maintained as the reduced forms at the expense of NADPH,

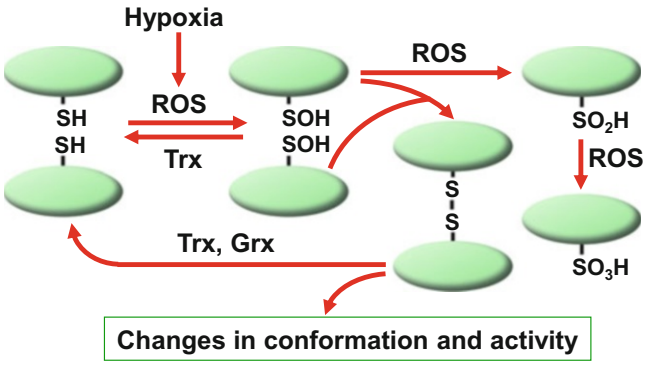

Fig. 18.1 Redox modulation of protein or enzyme activity. Under hypoxic conditions an increased production of reactive oxygen species (ROS) causes oxidation of cysteine thiol (-SH), resulting in the formation of sulfenic acid (-SOH), which can react with another thiol to form an intermolecular disulfide bond (-SS-), or an intramolecular disulfide (not shown), and consequently leading to changes in conformation and activity of the protein or enzyme. These oxidative modifications are reversible, and reduction is catalyzed by the thioredoxin (Trx) and/or glutaredoxin (Grx). When exposed to high ROS level, sulfenic acid may be further oxidized to sulfinic acid ($-SO_2H$) and sulfonic acid ($-SO_3H$). These reactions are generally irreversible and lead to altered activity of protein or enzyme

which is generated from the pentose phosphate pathway, a metabolic pathway parallel to glycolysis. When H_2O_2 levels are sufficiently high (>μM), sulfenic acid is oxidized, often irreversibly, to sulfinic acid ($-SO_2H$) and sulfonic acid ($-SO_3H$), resulting in permanently altered protein function (Berndt et al. 2007; Go and Jones 2011; Bindoli and Rigobello 2013; Putker et al. 2014).

The thiol-dependent redox modulation is highly specific. For instance, a single α-subunit of human voltage-gated K^+ channel Kv1.5 has six intracellular cysteines divided among the NH_2- and COOH-termini. Sulfenic acid modification of COOH-terminal C581 alone is sufficient to result in internalization and protein degradation of the channel (Svoboda et al. 2012). Also, for example, cAMP-dependent protein kinase (PKA) is a tetramer consisting of two regulatory subunits and two catalytic subunits; and the activation of PKA requires the dissociation of the catalytic subunits from regulatory subunits. In type II PKA, upon exposure to H_2O_2, a disulfide bond forms between Cys-97 in regulatory α- or β-subunit and Cys-199 in the catalytic α-subunit, resulting in diminished enzyme activity. However, in type I PKA, the formation of a disulfide bond between its two regulatory subunits (Cys-17 and Cys-38) causes a subcellular translocation and activation of the kinase (Brennan et al. 2006; de Piña et al. 2008; Burgoyne et al. 2013). Most reactions of thiols in biochemical systems are strongly dependent on the pKa of the cysteine side chain. In free cysteine, the pKa of the thiol is 8.3–8.5. The pKa values of cysteine thiols in proteins can be substantially reduced by their local environment so that the active-site cysteines become more sensitive to redox modulation. This is likely primarily due to stabilizing hydrogen bonds between the cysteine sulfur and the polypeptide backbone or nearby side chains: the higher the number of stabilizing

hydrogen bonds, the lower the pKa of the cysteine. Positively charged amino acids in close vicinity to the cysteine may also play a role in reducing the cysteine pKa. Moreover, the coordination of metal ions such as Zn^{2+} and $Fe^{2+/3+}$, which stabilize the negatively charged thiolate anions, may substantially decrease the pKa of cysteines. In addition, the local concentrations of ROS vs. antioxidants, the accessibility for oxidant action, and the influence of the redox modulation on protein function are all important factors related to redox modulation (Winterbourn and Hampton 2008; Lo Conte and Carroll 2013; Byon et al. 2016).

Soluble guanylyl cyclase (sGC) is the primary enzyme for nitric oxide (NO). When stimulated by endogenous or exogenous NO, it converts GTP to cGMP, which causes vasodilatation by activating cGMP-dependent protein kinase (PKG). sGC is a heterodimer, and the dimerization is obligatory for the catalytic activity of enzyme (Gao 2016). In porcine coronary arteries, the dimer level of sGC is decreased by thiol reductants, associated with diminished enzymatic activity and decreased vasodilatation to NO. In contrast, the dimer level of sGC is increased by ROS, indicating that the dimeric status of the enzyme as well as its catalytic activity is redox modulated by formation and dissociation of the disulfide bond between its two subunits. Similar phenomenon has also been observed in the porcine pulmonary artery. Interestingly, hypoxia increases the dimer level of sGC of coronary arteries, accompanied by enhanced sGC activity and augmented vasodilatation to NO. However, hypoxia decreases the dimer level of sGC of pulmonary arteries, accompanied by reduced sGC activity and attenuated vasodilatation to NO. It appears that hypoxia leads to opposite changes in the redox status in coronary vs. pulmonary arteries, resulting in opposite changes in the dimerization of sGC via disulfide bond formation and thus different responses of the vessels to NO (Zheng et al. 2011; Dou et al. 2013; Ye et al. 2013).

PKG is the primary effector enzyme for cGMP. It exists as two types: PKG I and PKG II. In the vascular system, only PKG I is expressed, which exists as two isoforms: PKG Iα and PKG Iβ. All types of PKGs are homodimer. Each monomer contains a regulatory domain and a catalytic domain. The monomer of PKG preserves the salient properties of dimeric PKG, including cGMP binding and kinase activity. However, the dimerization increases sensitivity of the kinase for cGMP and the affinity of PKG for its substrate, resulting in better efficacy of signal transduction. Disulfide dimerization is specific to the PKG Iα isoforms resulting in the formation of disulfide bond by the Cys-42 residues of two Iα isoforms, whereas the Iβ isoforms are not redox modulated (Dou et al. 2013; Prysyazhna and Eaton 2015). Studies show that exposure to H_2O_2 increases inter-monomer disulfide bond formation in PKGIα, associated with increased kinase activity and enhanced vasodilatation to NO and cGMP (Burgoyne et al. 2007; Dou et al. 2012). Hypoxia has been found to cause the bovine coronary artery to relax and pulmonary artery to contract, coincident with increased and decreased dimerization of PKG, respectively. The dimerization of PKG is prevented by the thiol reductant dithiothreitol, suggesting thiol-dependent dimer formation (Neo et al. 2011). The divergent responses between the coronary and pulmonary artery may in part result from the opposing effects of these two vessel types on glucose-6-phosphate

dehydrogenase (G6PD), a rate-limiting enzyme for NADPH formation. Hypoxia suppresses G6PD activity of the coronary artery, resulting in a decreased ratio of $NADPH/NADP^+$ and thus leading to a more oxidized cytosolic environment and increased disulfide bond formation of PKG. In contrast, G6PD activity of the pulmonary artery is stimulated by hypoxia, leading to an increased ratio of $NADPH/NADP^+$, a more reduced cytosolic environment, and decreased PKG dimerization (Gupte and Wolin 2006; Gupte et al. 2010).

18.4 AMPK and Hypoxic Vasoactivity

AMPK is a ubiquitously expressed serine/threonine kinase identified as the key player in maintaining cellular energy homeostasis. It is a heterotrimeric protein complex containing one catalytic α-subunit and two regulatory β- and γ-subunits, of which there are multiple isoforms conferring at least 12 different subunit combinations and thus the capacity for the modulation of both substrate- and cell-specific functions (Ross et al. 2016b). The γ-subunit of AMPK contains four cystathionine β-synthase (CBS) motifs, which act in pairs to form the binding sites for adenine nucleotides. Binding of AMP increases AMPK activity by allosteric activation and by promoting phosphorylation and inhibiting dephosphorylation at Thr-172 on the α-subunit. The binding of ADP also leads to the inhibition of dephosphorylation at Thr-172 but to a less extent than that of AMP. Thr-172 is primarily phosphorylated by liver kinase B1 (LKB1). LKB1 is constitutively active, but its ability to phosphorylate Thr-172 is markedly enhanced by conformational changes in its substrate, AMPK, caused by binding of AMP to the γ-subunit. ATP competitively inhibits the binding of both AMP and ADP to the γ-subunit. Hence, AMPK activity is closely regulated by the cellular AMP/ATP and ADP/ATP ratios. AMPK can also be activated by increases in cytosolic Ca^{2+}, which triggers direct phosphorylation of Thr-172 by Ca^{2+}/calmodulin-dependent protein kinase kinase 2 (Gowans et al. 2013; Hardie and Ashford 2014; Jeon 2016; Ross et al. 2016a).

It is well recognized that metabolic conditions associated with an increased AMP/ATP ratio are primary factors in the activation of AMPK. However, there is evidence suggesting that AMPK activity can also be redox modulated. Exposure of HEK 293 cells to H_2O_2 causes oxidative modification of cysteine residues, including *S*-glutathionylation, and increase in AMPK activity. The change in AMPK activity occurs without a decrease in cellular levels of ATP and is abolished by the mutation of Cys-304 of the α-subunit. Activation of the α-subunit of AMPK has been observed in the lungs of acatalasemic mice or mice treated with the catalase inhibitor, conditions in which intracellular H_2O_2 levels are increased (Zmijewski et al. 2010). Studies also show that the reducing status of Cys130/Cys174 in the α-subunit of AMPK is essential for activation of AMPK during energy starvation and the antioxidant enzyme thioredoxin may serve as an important cofactor for AMPK activation by the cleavage of disulfides formed by Cys130/Cys174. When the function of thioredoxin is compromised, glucose deprivation may lead to

oxidation of Cys130 and Cys174, which interferes with the interaction between AMPK and its upstream activator LKB1 and leads to diminished activation of AMPK (Shao et al. 2014). In addition to direct redox modulation, ROS also indirectly affect the activity of AMPK. For instance, hypoxia may activate AMPK through the action of mitochondria-derived ROS on LKB1 (Emerling et al. 2009).

As mentioned earlier, AMPK is a heterotrimer made up of different isoforms of the α-, β-, and γ-subunits. It appears that the predominant AMPK subunit composition in small PASMCs is α1β2γ1. The AMPK-α1 activity is inversely related to pulmonary artery diameter, as is the magnitude of pulmonary artery constriction by hypoxia. Moreover, the AMPK-α1 activity was much higher in second- and third-order branches of the pulmonary arterial tree compared with systemic (mesenteric) arteries, which dilate rather than constrict when stimulated with hypoxia. The exposure of pulmonary arterial smooth muscle to hypoxia increases the activity of AMPK with concomitant increase in $[Ca^{2+}]_i$, whereas the inhibition of AMPK suppresses hypoxic pulmonary vasoconstriction. Hence, hypoxia may cause pulmonary vasoconstriction through AMPK-dependent elevation of $[Ca^{2+}]_i$ (Evans et al. 2005; Robertson et al. 2008; Evans et al. 2015). The increase in $[Ca^{2+}]_i$ may result from the suppression of Kv1.5 K^+ channels, which are the predominant Kv expressed in resistant pulmonary arteries. The treatment with AMPK activator A769662 or intracellular dialysis of the activated human AMPK results in the inhibition of recombinant currents carried by Kv1.5 channels, consistent with the finding that Kv1.5 channels are inhibited by hypoxia in PASMCs (Moral-Sanz et al. 2016). Currently, evidence available supports the postulation that hypoxic pulmonary vasoconstriction may in part be due to activation of LKB1–AMPK signaling pathway resulting from the inhibition of mitochondrial oxidative phosphorylation, which leads to diminished activity of Kv1.5 channels and elevated $[Ca^{2+}]_i$ (Evans et al. 2015; Sommer et al. 2016).

18.5 Erythrocyte-Dependent Hypoxic Vasoactivity

In addition to delivering O_2 to the body tissues, the red blood cells, also known as erythrocytes, promote hypoxic vasodilatation through three possible mechanisms: (1) ATP release and subsequent acting on the endothelial cells resulting in the release of NO, (2) nitrite reduction to NO by deoxyhemoglobin (deoxy-Hb), and (3) release of S-nitrosothiol (SNO) from S-nitrosohemoglobin (SNO-Hb) (Hoiland et al. 2016). The release of ATP from erythrocytes occurs in milliseconds when exposed to low O_2 tension, making it a physiologically relevant mediator of microvascular blood flow (Dietrich et al. 2000). It appears that the release of ATP evoked by hypoxia is linked to the oxygenation state of the hemoglobin molecule via alterations in its conformation (Jagger et al. 2001). The released ATP binds to endothelial $P2Y_2$ purinergic receptors to stimulate the production of NO and potentially prostaglandin I_2 (PGI_2). ATP breaks down into AMP and subsequently

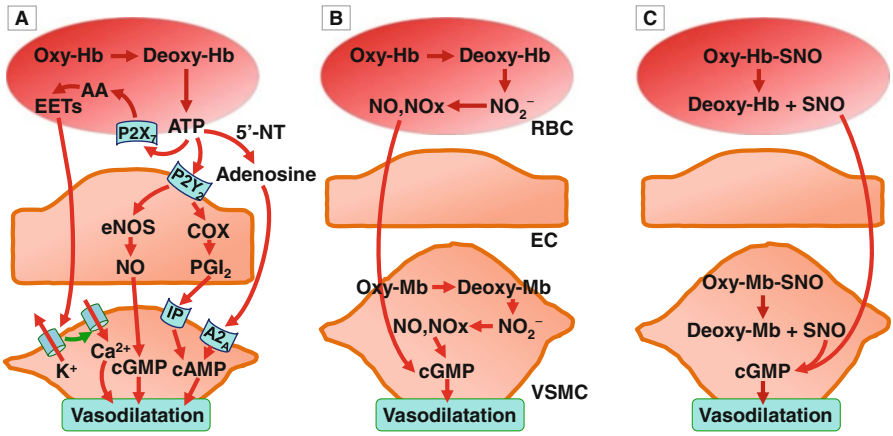

Fig. 18.2 Possible mechanisms for erythrocyte (RBC)-dependent hypoxic vasodilatation: (**a**) Oxygenated hemoglobin (Oxy-Hb) is converted to deoxygenated hemoglobin (deoxy-Hb) under reduced oxygen tension. Deoxy-Hb promotes ATP release from RBCs through acting on the $P2Y_7$ purinergic receptors on endothelial cells (ECs) resulting in activation of endothelial nitric oxide synthase (eNOS) to release nitric oxide (NO) and activation of cyclooxygenase (COX) to release prostaglandin I_2 (PGI_2), which causes vasodilatation by elevating cGMP and cAMP, respectively. ATP can also bind to $P2X_7$ purinergic receptors to cause RBCs to release epoxyeicosatrienoic acids (EETs), resulting in activation of membrane K^+ channels of the vascular smooth muscle cells (VSMCs). The released ATP can also be converted to adenosine by 5′-nucleotidase (5′-NT) leading to elevated intracellular cAMP levels of VSMCs and thus vasodilatation. (**b**) Deoxy-Hb may act as a nitrite reductase to generate NO, which could be further converted to bioactive metabolites of NO (Nox) to cause vasodilatation via cGMP signaling. NO and NOx are also generated by deoxygenated myoglobin (deoxy-Mb) expressed in VSMCs. (**c**). Under normoxic conditions (such as in the lung), a Cys within the β-chain of Hb, βCys93, undergoes oxidative modification by NO to form S-nitrosohemoglobin (SNO-Hb). When oxygen tension is reduced (such as in arterioles and capillaries), SNO-Hb reacts with RBC thiols, such as GSH and anion exchanger-1, to release S-nitrosothiol (SNO) leading to cGMP-mediated vasodilatation. Whether or not a similar reaction occurs for deoxy-Mb in VSMCs remains to be determined. $A2_A$, adenosine $A2_A$ receptor; IP, PGI_2 receptor; Oxy-Mb, oxygenated myoglobin. *Red line* and *arrow* indicate stimulatory action; *green line* and *arrow* indicate inhibitory action

adenosine, which causes vasodilatation through binding to adenosine A_{2A} receptors on vascular smooth muscle cells (VSMCs). ATP can also bind to the erythrocyte $P2X_7$ purinergic receptor to induce the release of EETs, which cause VSMCs to relax via the activation of membrane K^+ channels (Burnstock 2015; Hoiland et al. 2016) (Fig. 18.2). Increased ATP release from erythrocytes is also evoked by other factors including shear stress. During hypoxia, the increased local blood velocity would lead to increased shear stress and thus increased ATP release. Studies both in vivo and in vitro show that significant amounts of ATP are released from erythrocytes in response to hypoxia and shear stress at the same time (Mairbäurl et al. 2013).

Oxygenated hemoglobin (Oxy-Hb) acts as a nitrite oxidase producing nitrate, whereas deoxy-Hb acts as a nitrite reductase leading to the production of

NO. Hence, hypoxia may cause vasodilatation via erythrocyte-derived NO resulting from the action of deoxy-Hb on nitrite (Cantu-Medellin et al. 2011; Omar and Webb 2014). Consistent with such a notion, studies show that in the presence of erythrocytes, nitrite at physiologically relevant concentrations is considerably more potent in relaxing rabbit or rat aortas at low oxygen tensions than at high oxygen tensions (Crawford et al. 2006). In humans erythrocytes in the blood are the major intravascular storage sites of nitrite (Dejam et al. 2005). The majority (~70%) of circulating and stored nitrite is derived from the oxidation of endogenous NO synthesized by NO synthase, and the remainder is acquired through dietary intake (Omar and Webb 2014). Besides hemoglobin (Hb) in erythrocytes, myoglobin expressed in VSMCs may have a significant role in nitrite-dependent hypoxic vasodilation in vivo and ex vivo (Totzeck et al. 2012). Nitrite may exert its vasodilatory effect via NO metabolites rather than free NO through multiple heme, iron–sulfur cluster, and molybdenum-based reductases distributed among distinct subcellular compartments (Umbrello et al. 2014).

In all mammals and birds, three amino acids in Hb are strictly conserved: a His and a Phe are required to carry oxygen, and the third, a Cys within the β-chain, βCys93, undergoes oxidative modification by NO to form SNO-Hb that retains NO bioactivity in blood and is involved in hypoxic vasodilatation. Mice with a βCys93Ala mutation are deficient in hypoxic vasodilatation. In these mutant mice, peripheral blood flow and tissue oxygenation are reduced at basal conditions and decline excessively during hypoxia (Kulandavelu et al. 2015; Zhang et al. 2015). Hb exists as two alternative conformations, named R-state (for relaxed, high O_2 affinity) and T-state (for tense, low O_2 affinity). Thiol affinity for NO is high in the R-state and low in the T-state. The formation of SNO-Hb is through covalent bonding of NO with βCys93 of the Hb molecule, which occurs most effectively in the R-state in the lungs. When oxygen tension is reduced such as in peripheral circulation, NO is released upon the deoxygenation and transition to the T-state of Hb. The released NO reacts with thiols in erythrocytes, such as GSH and anion exchanger-1, to form SNO, which causes cGMP-mediated vasodilatation. SNO provides the chemical stability required for NO to reach VSMCs as free NO would be scavenged too quickly to elicit vasodilation (Jia et al. 1996; Stamler et al. 1997; Hoiland et al. 2016).

18.6 HIFs and Hypoxic Vasoactivity

HIFs are the master transcription factors that respond to insufficient O_2 supply, i.e., hypoxia, for the cellular activity. Within any given cell, hypoxia may regulate the expression of hundreds of mRNAs via HIFs, including those involved in regulation of vascular tone, mitogen, and metabolism. HIF functions as a heterodimer comprised of an α-subunit (HIF-1α, HIF-2α, HIF-3α) and a β-subunit (HIF-1β, HIF-2β, HIF-3β). Both α- and β-subunits are continuously transcribed and translated. Under normoxic conditions, the α-subunit is rapidly degraded, resulting from prolyl

hydroxylation (Pro-402 and Pro-564 in human HIF-1α) by the dioxygenases prolyl hydroxylase domain protein 2 (PHD2) with O_2 and α-ketoglutarate as substrates, followed by the binding of the von Hippel–Lindau (VHL) protein, polyubiquitination, and proteosomal degradation. The asparagine residue (Asp-803) in the α-subunit can also be hydroxylated by the asparaginyl hydroxylase factor inhibiting HIF-1 (FIH-1) in an O_2- and α-ketoglutarate-dependent manner, resulting in disruption of the interaction between HIF and the p300 transcriptional coactivator and preventing transcription of the target gene. During hypoxia, degradation of the α-subunit is progressively inhibited as the Po_2 decreases, leading to the accumulation of HIF-α and translocation into the nucleus, where it binds to HIF-β, forms a transcriptional complex with coactivators, binds to the HIF binding site within the hypoxia response element (HRE), and thus modulates the transcription of various target genes (Shimoda and Laurie 2014; Prabhakar and Semenza 2015; Duan 2016; Waypa et al. 2016).

In rat PASMCs, the expression of peroxiredoxin-5 (Prdx5), a H_2O_2 scavenger, in the intermembrane space of the mitochondria, attenuates hypoxia-induced HIF-1α stabilization and activity (Sabharwal et al. 2013). Studies have also shown that hypoxic stabilization of HIF-1α can be prevented by site-specific inhibitors of mitochondrial complex III to inhibit superoxide generation (Orr et al. 2015). These findings suggest that mitochondrial ROS signals have an important role in the regulation of HIF-1α stabilization during hypoxia. Current evidence indicates that ROS may act on HIF-1α through the modulation of PHD/FIH activities, either by oxidizing cysteine residues or by attacking the coordinated iron atom. Alternatively, ROS may affect the interaction between PHD/FIH and other proteins (Waypa et al. 2016). Interestingly, HIF prolyl hydroxylation has been found to be more sensitive to hypoxia than HIF asparaginyl hydroxylation, whereas the reverse is true when cells are exposed to H_2O_2. These findings imply that hypoxia and oxidant stress represent separate regulatory inputs to the HIF hydroxylase pathways (Tian et al. 2011; Masson et al. 2012; Ratcliffe 2013).

HIF-1α is likely to be involved in both the maintenance of normal pulmonary vascular tone and the development of pulmonary artery hypertension (PAH). Mice with SMC specific deletion of HIF-1α (SM22α-HIF-1α$^{-/-}$) exhibit higher right ventricular systolic pressure (RVSP) compared with wild-type littermates under normoxia and during exposure to hypoxia. The elevated RVSP indicates an exaggerated pulmonary vascular contractility, which is in line with the finding that the phosphorylation of myosin light chain (MLC), a determinant of SMC tone, is greater in PASMCs isolated from SM22α-HIF-1α$^{-/-}$ mice compared with that of PASMCs from wild-type mice. Hence, under normoxia and hypoxia, PASMC HIF-1α may maintain low pulmonary vascular tone by reducing MLC phosphorylation (Kim et al. 2013). In PASMCs from patients with PAH, the expression of HIF-1α is decreased, whereas prolyl hydroxylase activity is increased compared with controls. Moreover, a decreased expression of Kv1.5 K^+ channels, an enhanced elevation of $[Ca^{2+}]_i$ in response to hypoxia, and increased MLC phosphorylation occur in PASMCs of PAH patients. PASMC contractility has been found to be inversely correlated with HIF-1α activity. Therefore, compromised

PASMC HIF-1α expression may underlie augmented pulmonary vascular contractility that characterizes pulmonary hypertension (Barnes et al. 2017).

References

Barnes EA, Chen CH, Sedan O, Cornfield DN (2017) Loss of smooth muscle cell hypoxia inducible factor-1α underlies increased vascular contractility in pulmonary hypertension. FASEB J 31:650–662

Barnett J, Chow J, Ives D, Chiou M, Mackenzie R, Osen E, Nguyen B, Tsing S, Bach C, Freire J, Chan H, Elliott Sigal E, Ramesha C (1994) Purification, characterization and selective inhibition of human prostaglandin G/H synthase 1 and 2 expressed in the baculovirus system. Biochim Biophys Acta 1209:130–139

Bedard K, Krause KH (2007) The NOX family of ROS-generating NADPH oxidases: physiology and pathophysiology. Physiol Rev 87:245–313

Berndt C, Lillig CH, Holmgren A (2007) Thiol-based mechanisms of the thioredoxin and glutaredoxin systems: implications for diseases in the cardiovascular system. Am J Physiol Heart Circ Physiol 292:H1227–H1236

Bindoli A, Rigobello MP (2013) Principles in redox signaling: from chemistry to functional significance. Antioxid Redox Signal 18:1557–1593

Brandes RP, Weissmann N, Schröder K (2014) Redox-mediated signal transduction by cardiovascular Nox NADPH oxidases. J Mol Cell Cardiol 73:70–79

Brennan JP, Bardswell SC, Burgoyne JR, Fuller W, Schröder E, Wait R, Begum S, Kentish JC, Eaton P (2006) Oxidant-induced activation of type I protein kinase A is mediated by RI subunit interprotein disulfide bond formation. J Biol Chem 281:21827–21836

Broughton BR, Jernigan NL, Norton CE, Walker BR, Resta TC (2010) Chronic hypoxia augments depolarization-induced Ca^{2+} sensitization in pulmonary vascular smooth muscle through superoxide-dependent stimulation of RhoA. Am J Physiol Lung Cell Mol Physiol 298:L232–L242

Burgoyne JR, Madhani M, Cuello F, Charles RL, Brennan JP, Schröder E, Browning DD, Eaton P (2007) Cysteine redox sensor in PKGIα enables oxidant-induced activation. Science 317:1393–1397

Burgoyne JR, Oka S, Ale-Agha N, Eaton P (2013) Hydrogen peroxide sensing and signaling by protein kinases in the cardiovascular system. Antioxid Redox Signal 18:1042–1052

Burnstock G (2015) Blood cells: an historical account of the roles of purinergic signalling. Purinergic Signal 11:411–434

Byon CH, Heath JM, Chen Y (2016) Redox signaling in cardiovascular pathophysiology: a focus on hydrogen peroxide and vascular smooth muscle cells. Redox Biol 9:244–253

Cantu-Medellin N, Vitturi DA, Rodriguez C, Murphy S, Dorman S, Shiva S, Zhou Y, Jia Y, Palmer AF, Patel RP (2011) Effects of T- and R-state stabilization on deoxyhemoglobin-nitrite reactions and stimulation of nitric oxide signaling. Nitric Oxide 25:59–69

Crawford JH, Isbell TS, Huang Z, Shiva S, Chacko BK, Schechter AN, Darley-Usmar VM, Kerby JD, Lang JD Jr, Kraus D, Ho C, Gladwin MT, Patel RP (2006) Hypoxia, red blood cells, and nitrite regulate NO-dependent hypoxic vasodilation. Blood 107:566–574

de Piña MZ, Vázquez-Meza H, Pardo JP, Rendón JL, Villalobos-Molina R, Riveros-Rosas H, Piña E (2008) Signaling the signal, cyclic AMP-dependent protein kinase inhibition by insulin-formed H_2O_2 and reactivation by thioredoxin. J Biol Chem 283:12373–12386

Dejam A, Hunter CJ, Pelletier MM, Hsu LL, Machado RF, Shiva S, Power GG, Kelm M, Gladwin MT, Schechter AN (2005) Erythrocytes are the major intravascular storage sites of nitrite in human blood. Blood 106:734–739

DeLeon ER, Gao Y, Huang E, Arif M, Arora N, Divietro A, Patel S, Olson KR (2016) A case of mistaken identity: are reactive oxygen species actually reactive sulfide species? Am J Physiol Regul Integr Comp Physiol 310:R549–R560

Dietrich HH, Ellsworth ML, Sprague RS, Dacey RG Jr (2000) Red blood cell regulation of microvascular tone through adenosine triphosphate. Am J Physiol Heart Circ Physiol 278: H1294–H1298

Dou D, Zheng X, Liu J, Xu X, Ye L, Gao Y (2012) Hydrogen peroxide enhances vasodilatation by increasing dimerization of cGMP-dependent protein kinase type Iα. Circ J 76:1792–1798

Dou D, Zheng X, Ying L, Ye L, Gao Y (2013) Sulfhydryl-dependent dimerization and cGMP-mediated vasodilatation. J Cardiovasc Pharmacol 62:1–5

Duan C (2016) Hypoxia-inducible factor 3 biology: complexities and emerging themes. Am J Physiol Cell Physiol 310:C260–C269

Emerling BM, Weinberg F, Snyder C, Burgess Z, Mutlu GM, Viollet B, Budinger GR, Chandel NS (2009) Hypoxic activation of AMPK is dependent on mitochondrial ROS but independent of an increase in AMP/ATP ratio. Free Radic Biol Med 46:1386–1391

Evans AM, Mustard KJ, Wyatt CN, Peers C, Dipp M, Kumar P, Kinnear NP, Hardie DG (2005) Does AMP-activated protein kinase couple inhibition of mitochondrial oxidative phosphorylation by hypoxia to calcium signaling in O2-sensing cells? J Biol Chem 280:41504–41511

Evans AM, Lewis SA, Ogunbayo OA, Moral-Sanz J (2015) Modulation of the LKB1-AMPK signalling pathway underpins hypoxic pulmonary vasoconstriction and pulmonary hypertension. Adv Exp Med Biol 860:89–99

Forman HJ, Maiorino M, Ursini F (2010) Signaling functions of reactive oxygen species. Biochemistry 49:835–842

Gao Y (2016) Conventional and unconventional mechanisms for soluble guanylyl cyclase signaling. J Cardiovasc Pharmacol 67:367–372

Gnaiger E (2001) Bioenergetics at low oxygen: dependence of respiration and phosphorylation on oxygen and adenosine diphosphate supply. Respir Physiol 128:277–297

Go YM, Jones DP (2011) Cysteine/cystine redox signaling in cardiovascular disease. Free Radic Biol Med 50:495–509

Gowans GJ, Hawley SA, Ross FA, Hardie DG (2013) AMP is a true physiological regulator of AMP-activated protein kinase by both allosteric activation and enhancing net phosphorylation. Cell Metab 18:556–566

Grek CL, Zhang J, Manevich Y, Townsend DM, Tew KD (2013) Causes and consequences of cysteine S-glutathionylation. J Biol Chem 288:26497–26504

Griendling KK, Touyz RM, Zweier JL, Dikalov S, Chilian W, Chen YR, Harrison DG, Bhatnagar A, American Heart Association Council on Basic Cardiovascular Sciences (2016) Measurement of reactive oxygen species, reactive nitrogen species, and redox-dependent signaling in the cardiovascular system: a scientific statement from the American Heart Association. Circ Res 119:e39–e75

Gupte SA, Wolin MS (2006) Hypoxia promotes relaxation of bovine coronary arteries through lowering cytosolic NADPH. Am J Physiol Heart Circ Physiol 290:H2228–H2238

Gupte RS, Rawat DK, Chettimada S, Cioffi DL, Wolin MS, Gerthoffer WT, McMurtry IF, Gupte SA (2010) Activation of glucose-6-phosphate dehydrogenase promotes acute hypoxic pulmonary artery contraction. J Biol Chem 285:19561–19571

Harder DR, Narayanan J, Birks EK, Liard JF, Imig JD, Lombard JH, Lange AR, Roman RJ (1996) Identification of a putative microvascular oxygen sensor. Circ Res 79:54–61

Hardie DG, Ashford ML (2014) AMPK: regulating energy balance at the cellular and whole body levels. Physiology (Bethesda) 29:99–107

Hoiland RL, Bain AR, Rieger MG, Bailey DM, Ainslie PN (2016) Hypoxemia, oxygen content, and the regulation of cerebral blood flow. Am J Physiol Regul Integr Comp Physiol 310:R398–R413

Jagger JE, Bateman RM, Ellsworth ML, Ellis CG (2001) Role of erythrocyte in regulating local O2 delivery mediated by hemoglobin oxygenation. Am J Physiol Heart Circ Physiol 280:H2833–H2839

Jeon SM (2016) Regulation and function of AMPK in physiology and diseases. Exp Mol Med 48: e245

Jia L, Bonaventura C, Bonaventura J, Stamler JS (1996) S-nitrosohaemoglobin: a dynamic activity of blood involved in vascular control. Nature 380:221–226

Kim YM, Barnes EA, Alvira CM, Ying L, Reddy S, Cornfield DN (2013) Hypoxia-inducible factor-1α in pulmonary artery smooth muscle cells lowers vascular tone by decreasing myosin light chain phosphorylation. Circ Res 112:1230–1233

Knock GA, Snetkov VA, Shaifta Y, Connolly M, Drndarski S, Noah A, Pourmahram GE, Becker S, Aaronson PI, Ward JP (2008) Superoxide constricts rat pulmonary arteries via Rho-kinase-mediated Ca^{2+} sensitization. Free Radic Biol Med 46:633–642

Kulandavelu S, Balkan W, Hare JM (2015) Regulation of oxygen delivery to the body via hypoxic vasodilation. Proc Natl Acad Sci U S A 112:6254–6255

Lo Conte M, Carroll KS (2013) The redox biochemistry of protein sulfenylation and sulfinylation. J Biol Chem 288:26480–26488

Mairbäurl H, Ruppe FA, Bärtsch P (2013) Role of hemolysis in red cell adenosine triphosphate release in simulated exercise conditions in vitro. Med Sci Sports Exerc 45:1941–1947

Masson N, Singleton RS, Sekirnik R, Trudgian DC, Ambrose LJ, Miranda MX, Tian YM, Kessler BM, Schofield CJ, Ratcliffe PJ (2012) The FIH hydroxylase is a cellular peroxide sensor that modulates HIF transcriptional activity. EMBO Rep 13:251–257

Moral-Sanz J, Mahmoud AD, Ross FA, Eldstrom J, Fedida D, Hardie DG, Evans AM (2016) AMP-activated protein kinase inhibits Kv 1.5 channel currents of pulmonary arterial myocytes in response to hypoxia and inhibition of mitochondrial oxidative phosphorylation. J Physiol 594:4901–4915

Neo BH, Kandhi S, Wolin MS (2011) Roles for redox mechanisms controlling protein kinase G in pulmonary and coronary artery responses to hypoxia. Am J Physiol Heart Circ Physiol 301: H2295–H2304

Omar SA, Webb AJ (2014) Nitrite reduction and cardiovascular protection. J Mol Cell Cardiol 73:57–69

Orr AL, Vargas L, Turk CN, Baaten JE, Matzen JT, Dardov VJ, Attle SJ, Li J, Quackenbush DC, Goncalves RL, Perevoshchikova IV, Petrassi HM, Meeusen SL, Ainscow EK, Brand MD (2015) Suppressors of superoxide production from mitochondrial complex III. Nat Chem Biol 11:834–836

Panth N, Paudel KR, Parajuli K (2016) Reactive oxygen species: a key Hallmark of cardiovascular disease. Adv Med 2016:9152732

Prabhakar NR, Semenza GL (2015) Oxygen sensing and homeostasis. Physiology (Bethesda) 30:340–348

Prysyazhna O, Eaton P (2015) Redox regulation of cGMP-dependent protein kinase Iα in the cardiovascular system. Front Pharmacol 6:139

Putker M, Vos HR, Dansen TB (2014) Intermolecular disulfide-dependent redox signalling. Biochem Soc Trans 42:971–978

Ratcliffe PJ (2013) Oxygen sensing and hypoxia signalling pathways in animals: the implications of physiology for cancer. J Physiol 591:2027–2042

Rathore R, Zheng YM, Li XQ, Wang QS, Liu QH, Ginnan R, Singer HA, Ho YS, Wang YX (2006) Mitochondrial ROS-PKCepsilon signaling axis is uniquely involved in hypoxic increase in $[Ca^{2+}]_i$ in pulmonary artery smooth muscle cells. Biochem Biophys Res Commun 351:784–790

Rathore R, Zheng YM, Niu CF, Liu QH, Korde A, Ho YS, Wang YX (2008) Hypoxia activates NADPH oxidase to increase $[ROS]_i$ and $[Ca^{2+}]_i$ through the mitochondrial ROS-PKCε signaling axis in pulmonary artery smooth muscle cells. Free Radic Biol Med 45:1223–1231

Robertson TP, Mustard KJ, Lewis TH, Clark JH, Wyatt CN, Blanco EA, Peers C, Hardie DG, Evans AM (2008) AMP-activated protein kinase and hypoxic pulmonary vasoconstriction. Eur J Pharmacol 595:39–43

Ross FA, Jensen TE, Hardie DG (2016a) Differential regulation by AMP and ADP of AMPK complexes containing different gamma subunit isoforms. Biochem J 473:189–199

Ross FA, MacKintosh C, Hardie DG (2016b) AMP-activated protein kinase: a cellular energy sensor that comes in 12 flavours. FEBS J 283:2987–3001

Sabharwal SS, Waypa GB, Marks JD, Schumacker PT (2013) Peroxiredoxin-5 targeted to the mitochondrial intermembrane space attenuates hypoxia-induced reactive oxygen species signalling. Biochem J 456:337–346

Shao D, Oka S, Liu T, Zhai P, Ago T, Sciarretta S, Li H, Sadoshima J (2014) A redox-dependent mechanism for regulation of AMPK activation by Thioredoxin1 during energy starvation. Cell Metab 19:232–245

Shimoda LA, Laurie SS (2014) HIF and pulmonary vascular responses to hypoxia. J Appl Physiol (1985) 116:867–874

Shimoda LA, Polak J (2011) Hypoxia. 4. Hypoxia and ion channel function. Am J Physiol Cell Physiol 300:C951–C967

Sies H (2017) Hydrogen peroxide as a central redox signaling molecule in physiological oxidative stress: oxidative eustress. Redox Biol 11:613–619

Snetkov VA, Smirnov SV, Kua J, Aaronson PI, Ward JP, Knock GA (2011) Superoxide differentially controls pulmonary and systemic vascular tone through multiple signalling pathways. Cardiovasc Res 89:214–224

Sommer N, Strielkov I, Pak O, Weissmann N (2016) Oxygen sensing and signal transduction in hypoxic pulmonary vasoconstriction. Eur Respir J 47:288–303

Stamler JS, Jia L, Eu JP, McMahon TJ, Demchenko IT, Bonaventura J, Gernert K, Piantadosi CA (1997) Blood flow regulation by S-nitrosohemoglobin in the physiological oxygen gradient. Science 276:2034–2037

Stuehr DJ, Santolini J, Wang ZQ, Wei CC, Adak S (2004) Update on mechanism and catalytic regulation in the NO synthases. J Biol Chem 279:36167–36170

Svoboda LK, Reddie KG, Zhang L, Vesely ED, Williams ES, Schumacher SM, O'Connell RP, Shaw R, Day SM, Anumonwo JM, Carroll KS, Martens JR (2012) Redox-sensitive sulfenic acid modification regulates surface expression of the cardiovascular voltage-gated potassium channel Kv1.5. Circ Res 111:842–853

Sylvester JT, Shimoda LA, Aaronson PI, Ward JP (2012) Hypoxic pulmonary vasoconstriction. Physiol Rev 92:367–520

Tian Y, Yeoh KK, Lee MK, Ericsson T, Kessler BM, Kramer HB, Edelmann MJ, William C, Pugh CW, Schofield CJ, Ratcliffe PJ (2011) Differential sensitivity of HIF hydroxylation sites to hypoxia and hydroxylase inhibitors. J Biol Chem 286:13041–13051

Totzeck M, Hendgen-Cotta UB, Luedike P, Berenbrink M, Klare JP, Steinhoff HJ, Semmler D, Shiva S, Williams D, Kipar A, Gladwin MT, Schrader J, Kelm M, Cossins AR, Rassaf T (2012) Nitrite regulates hypoxic vasodilation via myoglobin-dependent nitric oxide generation. Circulation 126:325–334

Umbrello M, Dyson A, Pinto BB, Fernandez BO, Simon V, Feelisch M, Singer M (2014) Short-term hypoxic vasodilation in vivo is mediated by bioactive nitric oxide metabolites, rather than free nitric oxide derived from haemoglobin-mediated nitrite reduction. J Physiol 592:1061–1075

Wan J, Ristenpart WD, Stone HA (2008) Dynamics of shear-induced ATP release from red blood cells. Proc Natl Acad Sci U S A 105(43):16432–16437

Wang YX, Zheng YM (2010) Role of ROS signaling in differential hypoxic Ca2+ and contractile responses in pulmonary and systemic vascular smooth muscle cells. Respir Physiol Neurobiol 174:192–200

Waypa GB, Smith KA, Schumacker PT (2016) O_2 sensing, mitochondria and ROS signaling: the fog is lifting. Mol Asp Med 47-48:76–89

Wenger RH, Kurtcuoglu V, Scholz CC, Marti HH, Hoogewijs D (2015) Frequently asked questions in hypoxia research. Hypoxia (Auckl) 3:35–43

Winterbourn CC, Hampton MB (2008) Thiol chemistry and specificity in redox signaling. Free Radic Biol Med 45:549–561

Wu W, Platoshyn O, Firth AL, Yuan JX (2007) Hypoxia divergently regulates production of reactive oxygen species in human pulmonary and coronary artery smooth muscle cells. Am J Physiol Lung Cell Mol Physiol 293:L952–L959

Ye L, Liu J, Liu H, Ying L, Dou D, Chen Z, Xu X, Raj JU, Gao Y (2013) Sulfhydryl-dependent dimerization of soluble guanylyl cyclase modulates relaxation of porcine pulmonary vessels to nitric oxide. Pflügers Arch Eur J Physiol 465:333–341

Zhang R, Hess DT, Qian Z, Hausladen A, Fonseca F, Chaube R, Reynolds JD, Stamler JS (2015) Hemoglobin βCys93 is essential for cardiovascular function and integrated response to hypoxia. Proc Natl Acad Sci U S A 112:6425–6430

Zheng X, Ying L, Liu J, Dou D, He Q, Leung SWS, Man RYK, Vanhoutte PM, Gao Y (2011) Role of sulfhydryl-dependent dimerization of soluble guanylyl cyclase in relaxation of porcine coronary artery to nitric oxide. Cardiovasc Res 90:565–572

Zmijewski JW, Banerjee S, Bae H, Friggeri A, Lazarowski ER, Abraham E (2010) Exposure to hydrogen peroxide induces oxidation and activation of AMP-activated protein kinase. J Biol Chem 285:33154–33164

Chapter 19
Aging and Vasoreactivity

Abstract Increasing deterioration of the vasculature, both structurally and functionally, occurs with aging. Although these changes are a natural process, they can be accelerated or decelerated by altering various factors including the activity of telomerase and several metabolism-related pathways mediated by signaling molecules such as silent mating type information regulation 2 homolog 1, adenosine 5′-monophosphate-activated protein kinase, and mechanistic target of rapamycin. The aging of the vasculature is also critically affected by mitochondrial activities, in particular the production of mitochondria-derived reactive oxygen species, mitochondria biogenesis, and certain mitochondrial retrograde signalwings. In this chapter the current understanding of the above aspects will be discussed. Furthermore, the structural characteristics and functional changes of aging vasculature will be examined. While aging is not a disease, aging makes the vasculature more vulnerable to various vascular risk factors. Therefore, a better knowledge of the activities of aged blood vessels and the underlying mechanisms is clearly of therapeutic importance.

Keywords Telomere • Metabolism • Mitochondria • Structural characteristics • Endothelium • Nitric oxide • Prostanoids

19.1 Introduction

Aging is a natural process characterized by irreversible loss of physiological integrity, compromised organ functionality, and increased vulnerability to diseases. It is affected by a variety of factors including telomere attrition, genomic instability, epigenetic modification, metabolism, and mitochondrial functionality (López-Otín et al. 2013, 2016). In vasculature, the aging process is regulated in a complicated manner at the genetic, biochemical, cellular, histologic, and organismal levels. In particular, vascular aging is affected by the shortening telomeres, changes in metabolism-related signaling pathways, and the mitochondrial functionality (Kovacic et al. 2011a; Mikhed et al. 2015; Costantino et al. 2016). The aged vasculature is structurally featured by its thickened and stiffened vessel wall as well as enlarged vessel diameter, which leads to an increased cardiac workload and impaired end organ perfusion (Kovacic et al. 2011b). The aberrant endothelial activities are the hallmark

Y. Gao, *Biology of Vascular Smooth Muscle: Vasoconstriction and Dilatation*,
DOI 10.1007/978-981-10-4810-4_19

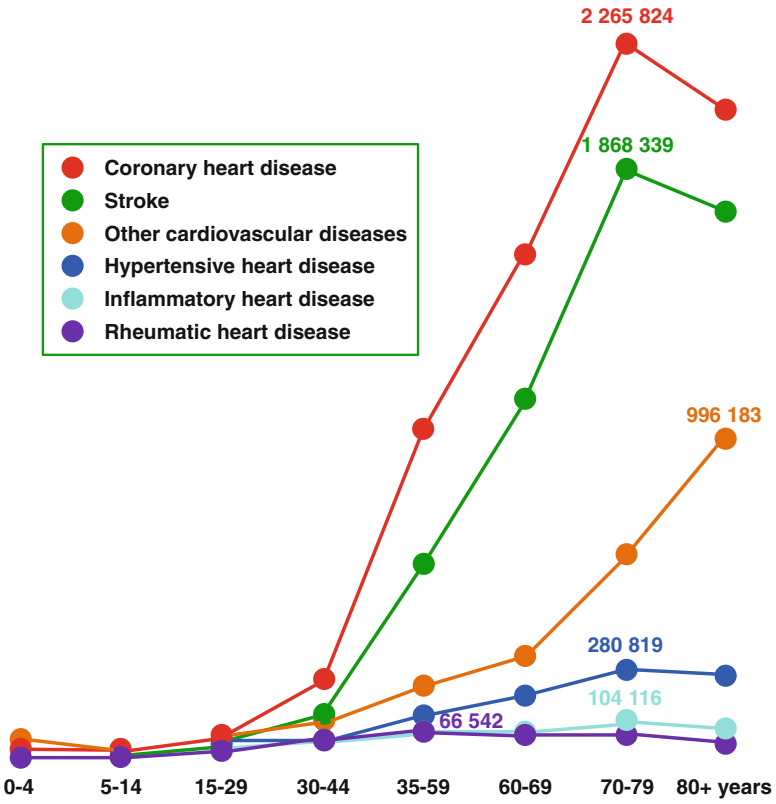

Fig. 19.1 Number of deaths globally per year from different types of cardiovascular disease by age. Highest numbers shown, 2002 (This figure is modified from the figure of World Health Organization (http://www.who.int/cardiovascular_diseases/resources/atlas/en/))

of vascular aging, which are manifested by a diminished endothelial-dependent vasodilatory activity and an exaggerated vasoconstrictive activity. The dysfunction in the endothelial activities often occurs as the very early event which leads to various cardiovascular diseases (Thijssen et al. 2015; Vanhoutte et al. 2017). According to the World Health Organization, the mortality of cardiovascular diseases increases at a staggering speed for people at age 45 years and up (Fig. 19.1) (http://www.who.int/cardiovascular_diseases/resources/atlas/en/). Clearly, cardiovascular diseases are strongly related to aging. Therefore, a better understanding of vascular aging will be of great interest not only for the treatments of cardiovascular diseases of the elderly but also for the maintenance of as healthy as possible vascular functionality during aging. Sir William Osler probably had it correct saying that "you're only as old as your arteries" (Nandish et al. 2011).

19.2 Telomere and Vascular Aging

A telomere is a region consisting of a tract of tandemly repeated short DNA repeats and associated protective proteins at the end of a chromosome. Its name is derived from the Greek nouns telos (end) and meros (part). The telomere protects the end of the chromosome from deterioration or from fusion with neighboring chromosomes. During replication, the enzymes that duplicate DNA cannot operate all the way to the end of a chromosome due to the synthesis of Okazaki fragments which requires RNA primers attaching ahead on the lagging strand. Therefore DNA sequences are lost every time a cell/DNA replicates until the loss reaches a critical level that causes cell division to end. In eukaryotes the attrition of chromosome ends can be replenished through the addition of telomeric repeat sequences by the cellular ribonucleoprotein enzyme telomerase, also known as terminal transferase. In humans the levels of telomerase or the action of telomerase of many cell types are limiting, and telomeres shorten throughout the life span. The average telomere length of humans declines from about 11 kilobases at birth to less than 4 kilobases in old age, with average rate of decline being greater in men than in women (Okuda et al. 2002; Arai et al. 2015; Blackburn et al. 2015; Dalgård et al. 2015).

Although the telomere length is a function of age, considerable difference exists among various cell types and even similar cell type of different locations. In humans the telomere length of the intima of human iliac arteries is less than that of iliac veins, reflecting a higher telomere loss in arteries resulting from greater hemodynamic stress. The rate of telomere loss is greater in the intima of iliac arteries compared to that of the internal thoracic arteries, a region of the arterial tree subject to less hemodynamic stress. However, there is no significant difference in the rates of telomere loss between the medial tissue of the iliac and internal thoracic arteries, suggesting that chronic stress leading to cellular senescence is more pronounced in the intima than in the media (Chang and Harley 1995). Some other factors such as oxidative stress and inflammation can also lead to telomere shortening. In patients with atherosclerosis, the atherosclerotic plaques show markedly shorter telomeres than normal vessels, and telomere shortening is closely correlated to increasing severity of atherosclerosis. In vivo, vascular smooth muscle cells (VSMCs) in plaques exhibit oxidative DNA damage. Furthermore, oxidants induce premature senescence in vitro, with accelerated telomere shortening and reduced telomerase activity. Reactive oxygen species (ROS) may promote telomere loss during replication, in part, by damage to telomeric DNA and reduction in telomerase activity (Matthews et al. 2006). Chronic inflammatory exposure may play a key role in pathogenesis of a number of vascular diseases. In adolescents, inflammatory markers, including C-reactive protein and fibrinogen, have been found to be inversely associated with short leukocyte telomere length (LTL), a surrogate indicator of the senescent status of the tissues. Cardiovascular diseases normally do not appear before middle age. The study suggests that an accelerated shortening of telomeres caused by inflammation in adolescence may account for atherosclerosis seen in adult studies (Masi et al. 2012).

The major enzyme that counteracts telomere shortening is telomerase, which consists of the catalytic subunit telomerase reverse transcriptase (TERT) and the telomerase RNA component (TERC). By using TERC as a template, TERT can add a six-nucleotide repeating sequence, 5′-TTAGGG, to the 3′ strand of chromosomes thus reversing telomere shortening. These TTAGGG repeats (with their various protein binding partners) are known as telomeres (Ait-Aissa et al. 2016; Yeh and Wang 2016). Human umbilical vein endothelial cells (HUVECs) have been found to go through a progressing decrease in the activity of telomerase during cell passages which proceeds cell senescence. This phenomenon is mitigated by the treatment of nitric oxide (NO) donor but exacerbated by the inhibition of endothelial NO synthase (eNOS), suggesting that endogenous NO may prevent age-related downregulation of telomerase activity and delay cell senescence (Vasa et al. 2000). In HUVECs the decrease in the mRNA levels of TERT, the catalytic subunit of telomerase, and enzyme activity occurred during cell senescence can be reversed by fibroblast growth factor-2 (Kurz et al. 2003). In addition, Akt, also known as protein kinase B, has been implicated in the activation of endothelial TERT by posttranscriptional modification (Breitschopf et al. 2001). In VSMCs, increased telomerase activity is correlated with cell proliferation, whereas the inhibition of telomerase suppresses the growth of VSMCs. It is proposed that telomerase is first activated in the cytoplasm with the involvement of phosphorylation of TERT, followed by nuclear translocation, and consequently cell growth (Minamino and Kourembanas 2001). These studies raise the possibility that the senescent phenotype of aged vascular cells may be delayed or even reversed through pharmacological intervention of telomerase activity. However, our current understanding on the related mechanism is rather limited, and much more has to be done to make such a possibility a reality. Encouragingly, emerging evidence indicates that the maintenance of telomerase activity and telomere length and thus normal vascular activity is correlated with healthy lifestyle and exercise (Werner et al. 2009; Kovacic et al. 2011a; Ait-Aissa et al. 2016; Yeh and Wang 2016).

19.3 Metabolism-Related Signalings and Vascular Aging

Increasing evidence indicates that adverse alternation in metabolism can accelerate vascular aging leading to detrimental consequences. Conversely, caloric restriction exerts beneficial effects on vascular aging and functionality. These processes are regulated by several signaling pathways related to metabolic homoestasis with the involvements of various signaling messengers such as SIRT1 (silent mating type information regulation 2 homolog 1), adenosine 5′-monophosphate-activated protein kinase (AMPK), and mechanistic target of rapamycin (mTOR) (Costantino et al. 2016; López-Otín et al. 2016; Uryga and Bennett 2016).

SIRT1 is the human homolog of the yeast Sir2 that is known for its antiaging activities. SIRT1 is originally classified as a NAD-dependent deacetylase. It is clear

now that SIRT1 also exerts its action without the involvement of protein deacetylation (Cencioni et al. 2015; Kida and Goligorsky 2016). SIRT1 is activated in caloric restriction. Mice overexpressing SIRT1 show characteristics similar to that of calorie-restricted mice: leaner, metabolically more active, more glucose tolerant, and with reduced levels of blood cholesterol, adipokines, insulin, and fasting glucose. Moreover, resveratrol, a putative SIRT1 activator, extends the life span of lower-order species and mice fed with a high-calorie diet (Kovacic et al. 2011a). In senescent porcine aortic endothelial cells (PAECs), the expression of SIRT1 is downregulated. In contrast, the protein levels of LKB1, a serine/threonine kinase, and the phosphorylation at Thr-172 of its downstream target AMPK are increased. Overexpression of LKB1 promotes cellular senescence, which is blocked by increasing SIRT1 levels. Hyperactivation of AMPK induces endothelial senescence. These results indicate that SIRT1 and LKB1/AMPK are critically involved in the regulation of endothelial senescence (Zu et al. 2010). In addition to LKB1/AMPK, studies suggest that SIRT1 protects ECs from premature senescence by directly and indirectly modulating the activity and expression of several key endothelial homeostatic factors, which include p53, Notch intracellular domain (NICD), forkhead transcription factor FOXO1, plasminogen activator inhibitor-1 (PAI-1), and eNOS. SIRT1 also exerts an inhibitory action on nuclear factor κB (NF-κB) resulting in suppressed vascular inflammation (Kida and Goligorsky 2016). During aging, miR-217 expression is induced in ECs, resulting in reduced expression of SIRT1 expression and the development of endothelial senescence (Potente 2010).

mTOR is a serine/threonine protein kinase which serves as intracellular sensor for energy, nutrients, and stress. mTOR links with other proteins and serves as a the catalytic subunit of two structurally distinct complexes, mTORC1and mTORC2. mTORC1 is inhibited by rapamycins through binding to the FK506-binding protein FKBP12, whereas mTORC2 is not directly affected by rapamycin. However, chronic rapamycin exposure can sequester mTOR from mTORC2, resulting in the inhibition of mTORC2 activity. Studies of gene deletion, mutation, and RNA interference (RNAi) as well as utilizing rapamycin demonstrate that the suppression of mTOR signaling increases life span in yeast, nematodes, fruit flies, and mice, establishing mTORC1 as a central, evolutionarily conserved regulator of longevity and that its effect may be in part mediated by the ribosomal protein S6 kinase beta-1 (S6K1). Evidence also suggests that mTORC2 may have anti-longevity by the inhibition of forkhead transcription factor FOXO3a through Akt (Ming et al. 2012; Johnson et al. 2013).

The expression and activity of senescence-associated β-galactosidase (SA-β-gal) is greater, but the proliferation and the activity of telomerase are lower in aging human VSMCs obtained by extended passages as compared with young VSMCs. These senescence-related changes are prevented by the treatment of VSMCs with the inhibitor of phosphatidylinositol-4,5-bisphosphate 3-kinase (PI3K), rapamycin, or silencing of mTOR expression, co-incident with reduced phosphorylation of mTOR at Ser-2448 and Thr-2446 and S6K1. These observations suggest that the PI3K/Akt/mTORC1/S6K1 pathway plays a pivotal role in the senescence process

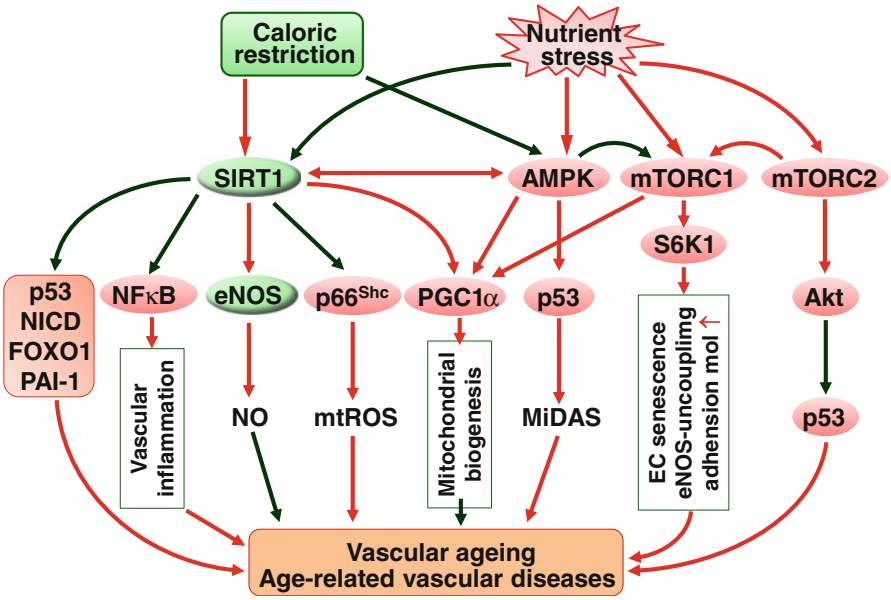

Fig. 19.2 Possible mechanisms underlying the influence of metabolism-related signaling on vascular aging and age-related vascular diseases. SIRT1 is activated by caloric restriction, whereas adenosine 5′-monophosphate-activated protein kinase (AMPK) and mechanistic target of rapamycin (mTOR) complexes mTORC1 and mTORC2 are activated by nutrient stress. SIRT1 may exert its action via (1) the inhibition of p53, Notch intracellular domain (NICD), forkhead transcription factor FOXO1, and plasminogen activator inhibitor-1 (PAI-1); (2) inhibition of vascular inflammation via nuclear factor κB (NF-κB); and (3) stimulation of the production of nitric oxide (NO) via endothelial NO synthase (eNOS). SIRT1 can also exert its action by inhibiting the production of mitochondria-derived reactive oxygen species (mtROS) via mitochondrial adaptor protein $p66^{Shc}$ and by preserving the mitochondrial biogenesis via peroxisome proliferator-activated receptor γ coactivator-1α (PGC-1α). PGC-1α activity is also stimulated by AMPK and mTORC1. AMPK may accelerate vascular aging through promoting mitochondrial dysfunction-associated senescence (MiDAS) via p53. The pro-aging effect of mTORC1 is mediated by ribosomal protein S6 kinase beta-1 (S6K1) resulting in endothelial cell (EC) senescence, eNOS uncoupling, and elevated levels of adhesion molecule (mol). In contrast, mTORC2 may exert an antiaging effect through the inhibition of p53 by Akt protein. *Red arrow line* indicates a stimulatory action, and *green arrow line* indicates an inhibitory action

of human VSMCs (Tan et al. 2016). While mTORC1 may exert a pro-aging effect on VSMCs, mTORC2 may exert an antiaging effect on ECs. In rat mesenteric arterial ECs, 14,15-epoxyeicosatrienoic acid (14,15-EET), a cytochrome P450 epoxygenase-derived arachidonic acid metabolite, inhibits cell senescence in a manner not sensitive to rapamycin but is attenuated by Akt inhibitor. The effect is abolished by reducing the expression of Rictor, a protein component of mTORC2 complex. The nuclear translocation of TERT, a catalytic subunit of telomerase, and the nuclear telomerase activity are also enhanced by treatment with 14,15-EET. Hence, 14,15-EET may inhibit EC senescence through activation of mTORC2/Akt signaling pathway (Johnson et al. 2013; Yang et al. 2014) (Fig. 19.2).

19.4 Mitochondria and Vascular Aging

Mitochondria are endowed with many important cellular functions. In addition to the production of ATP, their involvement in the generation of intermediary metabolites needed in the biosynthesis of many macromolecules, cellular redox homeostasis, oxygen sensing, inflammation, cell proliferation, and apoptosis gives mitochondria wide-ranging roles in cellular homoestasis (Smith et al. 2012; Chandel 2014). Substantial evidence indicates that mitochondria exert significant influence on vascular activity during aging and on the development of age-related vascular diseases, which largely resulted from the aberrant changes in ROS production, mitochondrial biogenesis, and mitochondrial signalings (Ungvari et al. 2010; Mikhed et al. 2015). Although anomalous mitochondrial activity may lead to molecular damages and a shortened life span, an early response of mitochondria to stress is the induction of the mitochondrial unfolded protein response (UPRmt). This leads to a signaling cascade to the nucleus and the syntheses of chaperones, which are then transported to the mitochondria where their function is required to the adaptational response of the mitochondria. Growing evidence demonstrates that mild perturbations of mitochondrial function can exert cytoprotective effects and extend longevity (Yang and Hekimi 2010; Baker et al. 2012; Runkel et al. 2014; López-Otín et al. 2016).

19.4.1 Mitochondrial ROS and Vascular Aging

Mitochondria are the most abundant cellular source of ROS. The steady-state concentration of superoxide in the mitochondrial matrix is about five- to tenfold higher than that in cytosol and nucleus. Such a high rate of ROS formation correlates well with the greater susceptibility of mitochondrial DNA (mtDNA) to oxidative damage as compared with that of nuclear DNA. Since mtDNA mainly encodes for proteins of the mitochondrial respiration chain, which is the major site for ROS production, the impaired mtDNA translation could lead to mitochondrial uncoupling with further increase in ROS formation (Cadenas and Davies 2000; Brand 2010; Mikhed et al. 2015). Studies show that the production of mitochondrial ROS is increasing with age, accompanied by increased oxidative lesions of mtDNA and diminished endothelium-dependent vasodilatation. Judged by the results obtained from mice deficient in aldehyde dehydrogenase-2 (ALDH-2) and manganese superoxide dismutase (Mn-SOD), the increase of mitochondrial ROS appears to significantly contribute to age-dependent endothelial dysfunction (Wenzel et al. 2008).

The mitochondrial adaptor protein $p66^{Shc}$ is a key player in the homoestasis of mitochondrial redox status. $P66^{Shc}$ promotes ROS production by controlling the partition of ATP generation in the cell, by participating to the electron flow chain in the mitochondria and by opening the mitochondrial permeability transition pore

(PTP) (Camici et al. 2015). In mice deficient in $p66^{Shc}$ ($p66^{shc-/-}$), the levels of ROS are reduced and the life span is extended by 30% (Migliaccio et al. 1999). The endothelium-dependent relaxation is age-dependently impaired in wild-type mice but not in $p66^{shc-/-}$ mice. Coincidently, an age-related decline of NO release and increase in ROS production occur in wild type but not $p66^{shc-/-}$ mice. These findings imply a critical role for $p66^{shc}$ in ROS-mediated endothelial dysfunction in aging vasculature. Furthermore, the inactivation of the $p66^{shc}$ may represent a unique target to prevent vascular aging (Francia et al. 2004). Studies demonstrate that the expression of $p66^{Shc}$ is inhibited by SIRT1, resulting in reduced oxidative stress, ameriolated endothelial senescence, and endothelial dysfunction (Chen et al. 2013).

19.4.2 Mitochondrial Biogenesis and Vascular Aging

Mitochondrial biogenesis is the process by which cells increase the mitochondrial mass and copy number. It constitutes a dynamic mechanism with mitochondrial autophagy (mitophagy), a process to degrade the defective mitochondria, for the maintenance of mitochondrial homeostasis. A decrease in mitochondrial biogenesis can reduce turnover of specific mitochondrial components resulting in the accumulation of oxidized lipids, proteins, and damaged DNA, which would lead to a gradual deterioration of various mitochondrial functions (Ungvari et al. 2010; Diot et al. 2016; Whitaker et al. 2016). Studies show that, with age, mitochondrial biogenesis is impaired in both ECs and VSMCs (Burns et al. 1979, 1981; Ungvari et al. 2008; Chalmers et al. 2016).

Mitochondrial biogenesis is primarily regulated by peroxisome proliferator-activated receptor γ coactivator-1α (PGC-1α), which is activated by the upstream signaling molecules such as NO and AMPK (Suliman and Piantadosi 2016). In aged vasculature, PGC-1α is downregulated in part due to diminished NO production and bioavailability (Ungvari et al. 2008, 2010). In the human brain, the senescence of VSMCs induced by angiotensin has been found to be suppressed by fibroblast growth factor 21 (FGF21). FGF21 suppresses cerebrovascular aging via improving mitochondrial biogenesis and inhibiting p53, a crucial factor mediating cellular senescence, in an AMPK-dependent manner (Wang et al. 2016). In addition to mitochondrial biogenesis, other mechanisms include mitochondrial fission and fusion, which permit a constant remodeling of mitochondrial architecture, and mitophagy. Coordinated regulation of these processes, known as mitochondrial quality control (mQC), is essential for mitochondrial homoestasis. By fusion of damaged mitochondrial sections with healthy organelles, damage can be compensated. Alternatively, damaged mitochondrial sections are isolated via fission and removed by mitophagy. If mitochondrial function cannot be repaired, a death signal is released from the mitochondria resulting in the apoptotic removal of the entire cell (Ungvari et al. 2010; Runkel et al. 2014; Suliman and Piantadosi 2016). In aged human umbilical vein ECs, both fusion and fission activities are decreased with

distinct alterations in overall morphology and fine structure as well as loss of mitochondrial membrane potential (Jendrach et al. 2005). In the aortas of C57BL6 mice, aging is associated with impaired mQC, greater activation of $p66^{shc}$, elevated superoxide production, and increased arterial stiffness. These aberrant changes are normalized by the enhancement of mitophagy, implying a pivotal role of mitophagy in mQC (LaRocca et al. 2014; Diot et al. 2016).

19.4.3 Mitochondrial Retrograde Signaling and Vascular Aging

Signal transduction from the cytosol to mitochondria is referred to as anterograde signaling and signal transduction from mitochondria to cytosol as retrograde signaling (Chandel 2014). Evidence shows that mitochondria-derived ROS may serve as a retrograde signal to modulate the activities of a number of redox-sensitive transcription factors including NF-κB, activator protein 1 (AP-1), NF-E2-related factor 2 (Nrf-2), and p53 (Ungvari et al. 2010). NF-κB plays a central role in vascular inflammatory response. In aged rat arterial vessels, NF-κB activity is increased, which is prevented by scavenging H_2O_2 and by carbonyl cyanide-4-(trifluoromethoxy) phenylhydrazone (FCCP), an oxidative phosphorylation uncoupler. Moreover, the inhibition of NF-κB attenuates inflammatory gene expression and monocyte adhesiveness. These results suggest that mitochondria-derived H_2O_2 may contribute to NF-κB activation, resulting in the proinflammatory phenotypic alterations in the aged vasculature (Ungvari et al. 2007). Defective mitochondria have also been found to release a retrograde signal to activate the nuclear localization of the Rtg1/3 complex that affects the expression of genes encoding for enzymes in mitochondrial metabolism, peroxisomal biogenesis, and stress response pathways (Hill and Van Remmen 2014).

In response to stress, mitochondria can release some small signaling peptides such as humanin, mitokines, and mitochondrial damage-associated molecular patterns (mitDAMPs) (Hill and Van Remmen 2014; da Cunha et al. 2015; López-Otín et al. 2016). Among the mitochondrial-derived peptides, humanin is better studied. It is a 24-amino acid peptide that is originally shown to have an anti-apoptotic function against neuronal cell death caused by Alzheimer's disease. Subsequent studies show that it preserves endothelial function and prevents atherosclerotic plaque progression in mouse models of accelerated vascular aging (Bachar et al. 2010; Oh et al. 2011; Gong et al. 2014). Humanin acts intracellularly to inhibit apoptosis. It also acts extracellularly to exert its cytoprotective, anti-inflammatory, and metabolic-protective effects (Hill and Van Remmen 2014). Humanin expression declines with age both in humans and mice (Muzumdar et al. 2009). Studies show that long-lived, growth hormone (GH)-deficient Ames mice display elevated circulating humanin levels, while short-lived GH-transgenic mice have reduced humanin levels. GH or insulin-like growth factor-1 (IGF-I) can reduce circulating

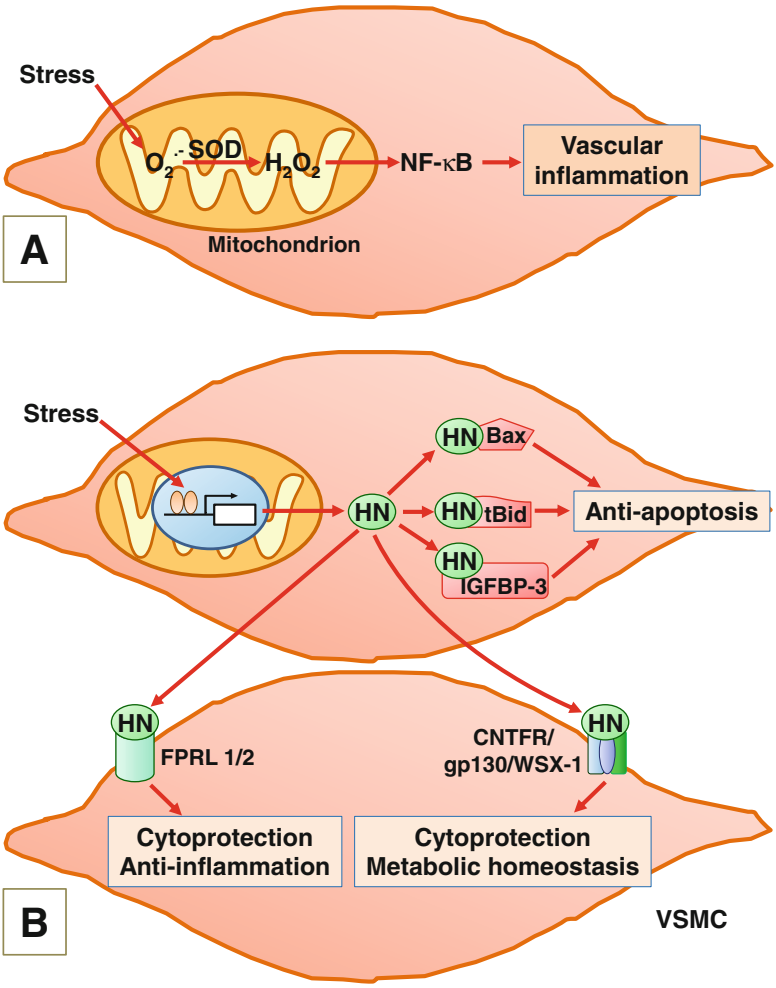

Fig. 19.3 Mechanisms for mitochondrial H_2O_2 (**a**) and humanin (**b**) to act as retrograde signaling molecules to induce pro-aging and antiaging effects in vascular smooth muscle cells (VSMCs). (**a**) Under stress the production of superoxide ion in mitochondria is increased. It is converted to the cell membrane-permeable H_2O_2 by superoxide dismutase (SOD), resulting in the activation of the nuclear factor κB (NF-κB) and consequently increased expression of proinflammatory molecules and augmented vascular inflammation. (**b**) Humanin (HN) is generated within the mitochondrial genome in response to stress. It can act intracellularly as well as extracellularly. In the cytosol, HN inhibits apoptosis through binding to and inactivating proapoptotic proteins Bcl-2- associated X protein (Bax), the truncated form of BH3 interacting domain death agonist (tBid), and insulin-like growth factor (IGF)-binding protein-3 (IGFBP-3). HN can be released into the extracellular space and into the circulation. It exerts its cytoprotection and anti-inflammatory actions through binding to human G-protein-coupled formyl peptide receptor-like-1 (FPRL-1) or its murine counterpart FPRL-2. It can also bind to a tripartite cytokine-like receptor complex comprising the ciliary neurotrophic factor (CNTF) receptor, glycoprotein (gp)130, and the IL-27 receptor WSX1, which promotes cytoprotection and metabolic homeostasis

humanin levels in both mice and human subjects. Hence, it appears that humanin levels can be regulated by GH and IGF-I and that humanin levels correlate with life span in mice (Gong et al. 2014; Hill and Van Remmen 2014; Lee et al. 2014) (Fig. 19.3).

19.5 Structural Characteristics of Aging Blood Vessels

The thickening and stiffening of the vessel wall as well as the enlargement of vessel diameters are the most prominent characteristics of aging blood vessels (Kovacic et al. 2011b; Thijssen et al. 2015). In both men and women, the increase in carotid artery intima-media thickness (IMT) occurs linearly ($\sim$5 μm year^{-1}) with aging (Homma et al. 2001; Engelen et al. 2013). The magnitude of age-related thickening is comparable between central and peripheral arteries, indicating that the thickening of the vascular wall is likely to represent a systemic effect of aging per se. The thickening of the vessel wall seems to be a consequence of elevated blood pressure, as systolic blood pressure has been found to be positively correlated to brachial, superficial femoral, and popliteal IMT (van den Munckhof et al. 2012). Indeed, the carotid IMT is reduced by antihypertensive treatment. The magnitude of reduction in IMT is closely related to the decrease in carotid pulse pressure (Boutouyrie et al. 2000; Thijssen et al. 2015).

Both conduit and peripheral arteries exhibit an age-dependent increase in the vessel diameter, and the relative increase in diameter with aging is comparable between central and peripheral vessels (van den Munckhof et al. 2012). Cross-sectional analysis of the common carotid artery shows that each year of older age is associated with 0.017 mm larger diameter among persons with no pre-existing disease but 0.03 mm larger diameter among persons with stroke and/or coronary heart disease (Eigenbrodt et al. 2006). Among individuals aged from 25 to 67 years old, the diameters of popliteal and femoral diameter have been found to increase by $\sim$0.5% per year (Sandgren et al. 1998, 1999). Several factors may contribute to the age-related enlargement of vessel diameter, including loss of elastic fibers, fracturing of the elastic lamellae, and adaptation to stiffening of the vasculature. Among these factors, the loss of elastic fibers may be of particular importance. With the loss of elastic fibers, the vasculature would rely more on the stiffer collagen in the vessel wall, and consequently the vessel diameter is enlarged (Fritze et al. 2012; Aquaro et al. 2013; Thijssen et al. 2015).

The arteries, both large and smaller sized, mainly of the intima, become increasingly stiff with advancing age. Some important changes occurring in the vessel wall may be causally related to arterial stiffening, such as increased calcium deposition, decreased elastin content, increased elastin fragmentation, and increased collagen content (Virmani et al. 1991; Kovacic et al. 2011b; Thijssen et al. 2015). With aging the elastic lamellae undergo fragmentation and thinning, and thus, an increased ratio of collagen to elastin ensues. Collagen is 100- to 1000-fold stiffer than elastin, rendering the vessel wall increasingly resistant to stretching (Greenwald 2007). An

age-related increase in the formation of advanced glycation end products (AGEs) may also contribute to vascular stiffening. AGEs are the end product of a nonenzymatic reaction with sugar derivatives that lead to irreversible cross-links with proteins (Brownlee 1995). AGE-linked collagen is stiffer and less amenable to normal turnover (Verzijl et al. 2000). Similarly, elastin in the aortic wall is also susceptible to glycation (Konova et al. 2004).

The arterial stiffness can be evaluated by the arterial pulse wave velocity (PWV). Pulse waves generated by the heart travel forward in the arteries and undergo partial reflections at sites of impedance mismatch (such as the junction of the artery and smaller high-resistance arterioles). Innumerable reflections effectively merge into a discrete reflected wave. In the healthy human, the reflected pulse wave arrives at the aortic root during diastole. In older people, the stiffening of the arteries results in greater forward and reflected PWVs, with the reflected pulse wave arriving at the aortic root in late systole. Consequently, the late systolic pressure is augmented, which causes an increased systolic workload for the heart, reduced coronary perfusion during diastole, and the transmission of higher pressures to end organs such as the brain and kidneys, translating into increased probability in ventricular hypertrophy, renal impairment, and cerebrovascular events. It is now generally recognized that arterial PWV is an independent predictor of adverse cardiovascular events and mortality (Willum-Hansen et al. 2006; Lim and Townsend 2009; Kovacic et al. 2011b; Townsend et al. 2015; Phan et al. 2016).

19.6 Functional Changes of Aging Blood Vessels

The delicate balance between vasodilatory activity and vasoconstrictive activity maintains vascular homeostasis. In aging vasculature, the vasodilatory activity is often diminished while vasoconstrictive activity is aggravated, predominantly due to abnormal endothelial functions such as altered balance between the availability of endothelium-derived relaxing messengers and that of endothelium-derived contracting messengers. Many age-related factors contribute to the functional changes of vascular activity, such as telomere attrition, DNA damage, pro-ageing protein accumulation, and cellular senescence. These changes have profound influence on vascular activity. Consequently, increased levels of ROS, chronical existence of unsterile inflammation, and aberrant signaling activities ensue, which lead to the manifestation of unfavorable vascular activities and development of vascular diseases (Kovacic et al. 2011a, b; Thijssen et al. 2015; Costantino et al. 2016; Vanhoutte et al. 2016, 2017).

19.6.1 Diminished Vasodilatory Activity

Endothelium-derived NO (EDNO), vasodilator prostanoids in particular prostaglandin I_2 (PGI_2), and endothelium-dependent hyperpolarization (EDH) are the primary factors that drive the vasodilatory response (Vanhoutte et al. 2016, 2017). An impaired EDNO-dependent vasodilatation in aging arteries has been documented ranging from coronary arteries to peripheral conduit, resistance, and microvessels. This can be ascribed to downregulated expression of eNOS resulting mainly from increased NF-κB activity, reduced eNOS activity resulting from reduced dimerization and coupling of the enzyme, increased arginase activity competing with eNOS for L-arginine, and increased inactivation of NO by ROS (Thijssen et al. 2015; Vanhoutte et al. 2016). NO causes vasodilatation mainly by the stimulation of soluble guanylyl cyclase (sGC) resulting in increased generation of cGMP while cGMP is degraded by phosphodiesterase (PDE) (Gao 2010). In arteries of aged rats, the expression of sGC and NO-induced relaxation are decreased (Chen et al. 2000; Klöss et al. 2000). In senescent human VSMCs, the expression of type 1 PDE is increased (Bautista Niño et al. 2015).

The endothelium-dependent vasodilatation induced by acetylcholine (ACh) is less in old mice as compared with that in young mice. Such a difference is absent when cyclooxygenase (COX) is inhibited. The diminished vasodilatation that occurred in old mice is associated with decreased expressions of SIRT1 and inducible cyclooxygenase (COX-2). The restoration of SIRT1 by SRT1720, a SIRT1 activator, leads to the normalization of COX-2 expression as well as the endothelium-dependent vasodilatation. These results suggest that a reduced production of vasodilator prostanoids may contribute to reduced endothelium-dependent vasodilatation and that this phenomenon may be due to a decreased expression of COX-2 resulting from aging-related downregulation of SIRT1 (Gano et al. 2014). An altered EDH-dependent vasodilatation has also been documented. Among the two components that constitute EDH in rat mesenteric arteries, the activity of small-conductance calcium-activated potassium (SK_{Ca}) channels is decreased with aging, while the activity of intermediate-conductance calcium-activated potassium (IK_{Ca}) channels is less susceptible to the effect of aging (Kong et al. 2015; Leung and Vanhoutte 2017).

19.6.2 Augmented Vasoconstrictive Activity

The vasoconstrictive activity is increasingly exaggerated with aging. These changes are often originated from aberrant activities of endothelium-derived constrictors, mainly endothelin-1 (ET-1) and COX products (Thijssen et al. 2015; Vanhoutte et al. 2017). ET-1 is rapidly synthesized and released from the endothelial cells (ECs) upon stimulation. It causes vasoconstriction via

ET_A receptors on VSMCs. Meanwhile it also causes vasodilatation via ET_B receptors on ECs resulting from the release of EDNO and PGI_2. ET_B receptors also possess "clearance" function: once ET-1 binds the receptors, the ligand-occupied receptors are internalized and degraded by endosomes/lysosomes (Oksche et al. 2000; Davenport et al. 2016; Vanhoutte et al. 2017). The blockade of $ET_{A/B}$ receptors increases leg blood flow more in older men (67–76 years old) compared with younger individuals (19–50 years old), indicating that ET-1 exerts a greater constrictive action in older men (Thijssen et al. 2007). The increased constrictive activity of ET-1 is at least in part due to an increased expression of ET-1 in ECs of older men, as revealed by Western blotting (Donato et al. 2009). Animal studies demonstrate that exaggerated vasoconstrictive response of aged arteries to ET-1 may also result from enhanced ET_A receptor signaling (Donato et al. 2005) or impaired ET_B receptor endothelium-dependent vasodilatation (Asai et al. 2001).

Although ET-1 is the most potent vasoconstrictor known so far, the available evidence suggests that under most circumstances including aging (except in the case of insulin resistance), prostanoids produced by COX in the endothelium might explain endothelium-dependent contractions (Félétou et al. 2010; Vanhoutte et al. 2017). In hamster aortas, endothelium-dependent contraction is evoked by ACh after inhibition of nitric oxide production. The contraction is abolished by the COX-2 inhibitor or by the thromboxane (TP) receptor antagonists. The ACh-evoked contraction is accompanied by an increased production of prostaglandin $F_{2\alpha}$ ($PGF_{2\alpha}$). Western blotting shows that COX-2 is mainly expressed in the endothelium. COX-2 expression, vascular sensitivity to $PGF_{2\alpha}$, and ACh-stimulated contractions are augmented in aortas of aged hamsters. Thus, $PGF_{2\alpha}$ synthesized by the constitutively expressed COX-2 in ECs may act as an age-dependent vasoconstrictor via the TP receptors (Wong et al. 2009). COX-2 has also been found to be expressed constitutively in the endothelium of the rat pulmonary and human renal arteries. In situations where endothelial COX-2 is present, the prostanoids synthesized by this isoform can evoke endothelium-dependent contractions (Vanhoutte et al. 2017).

In the aorta of Wistar Kyoto (WKY) and spontaneously hypertensive (SHR) rats, both the constitutive and inducible COXs, COX-1 and COX-2, respectively, are expressed in ECs and VSMCs, with COX-1 dominant. Moreover, the expression of COX-1 is upregulated by aging and hypertension. COXs convert arachidonic acid to prostaglandin H_2, which is further converted to various prostanoids by their own synthases. In vasculature, prostanoids are mainly synthesized in ECs and the predominant prostanoid is PGI_2 (Fitzpatrick and Soberman 2001; Gluais et al. 2005; Tang and Vanhoutte 2008; Félétou et al. 2010). Interestingly, although it is well known that PGI_2 is a potent vasodilator, it causes relaxation of aortas in WKY rats aged less than 15 weeks but contraction of the vessels in WKY rats aged greater than 7 months. Meanwhile, the capacity for PGI_2 release increases with aging. These changes are greater in SHR than in WKY (Rapoport and Williams 1996). Moreover, the magnitudes of endothelium-dependent contractions evoked by ACh of the aged aortas of WKY and SHR rats are closely correlated with increase in the release of PGI_2 caused

by this muscarinic agonist. The production of PGI_2 and the contraction induced by ACh are significantly reduced by NS 398, a preferential COX-2 inhibitor, and largely abolished by valeryl salicylate, a preferential COX-1 inhibitor (Gluais et al. 2005). The contraction of the aged aortas evoked by ACh or by carbacyclin, a PGI_2 analogue, is markedly suppressed by the thromboxane A_2 (TXA_2)/prostaglandin H_2 (PGH_2) receptor antagonist SQ29548 (Rapoport and Williams 1996). These results suggest that PGI_2 synthetized by endothelial COXs, mainly COX-1, is the principle endothelium-derived contracting factor (EDCF) in the aged or hypertensive rat aortas in response to ACh. Furthermore, PGI_2 appear to cause vasoconstriction largely by bonding to the TP receptors on VSMCs (Félétou et al. 2010; Vanhoutte et al. 2017).

References

Ait-Aissa K, Ebben JD, Kadlec AO, Beyer AM. Friend or foe? (2016) Telomerase as a pharmacological target in cancer and cardiovascular disease. Pharmacol Res 111:422–433

Aquaro GD, Cagnolo A, Tiwari KK, Todiere G, Bevilacqua S, Di Bella G, Ait-Ali L, Festa P, Glauber M, Lombardi M (2013) Age-dependent changes in elastic properties of thoracic aorta evaluated by magnetic resonance in normal subjects. Interact Cardiovasc Thorac Surg 17:674–679

Arai Y, Martin-Ruiz CM, Takayama M, Abe Y, Takebayashi T, Koyasu S, Suematsu M, Hirose N, von Zglinicki T (2015) Inflammation, but not telomere length, predicts successful ageing at extreme old age: a longitudinal study of semi-supercentenarians. EBioMedicine 2:1549–1558

Asai K, Kudej RK, Takagi G, Kudej AB, Natividad F, Shen YT, Vatner DE, Vatner SF (2001) Paradoxically enhanced endothelin-B receptor-mediated vasoconstriction in conscious old monkeys. Circulation 103:2382–2386

Bachar AR, Scheffer L, Schroeder AS, Nakamura HK, Cobb LJ, Oh YK, Lerman LO, Pagano RE, Cohen P, Lerman A (2010) Humanin is expressed in human vascular walls and has a cytoprotective effect against oxidized LDL-induced oxidative stress. Cardiovasc Res 88:360–366

Baker BM, Nargund AM, Sun T, Haynes CM (2012) Protective coupling of mitochondrial function and protein synthesis via the eIF2alpha kinase GCN-2. PLoS Genet 8:e1002760

Bautista Niño PK, Durik M, Danser AH, de Vries R, Musterd-Bhaggoe UM, Meima ME, Kavousi M, Ghanbari M, Hoeijmakers JH, O'Donnell CJ, Franceschini N, Janssen GM, De Mey JG, Liu Y, Shanahan CM, Franco OH, Dehghan A, Roks AJ (2015) Phosphodiesterase 1 regulation is a key mechanism in vascular aging. Clin Sci (Lond) 129:1061–1075

Blackburn EH, Epel ES, Lin J (2015) Human telomere biology: a contributory and interactive factor in aging, disease risks, and protection. Science 350:1193–1198

Boutouyrie P, Bussy C, Hayoz D, Hengstler J, Dartois N, Laloux B, Brunner H, Laurent S (2000) Local pulse pressure and regression of arterial wall hypertrophy during long-term antihypertensive treatment. Circulation 101:2601–2606

Brand MD (2010) The sites and topology of mitochondrial superoxide production. Exp Gerontol 45:466–472

Breitschopf K, Zeiher AM, Dimmeler S (2001) Pro-atherogenic factors induce telomerase inactivation in endothelial cells through an Akt-dependent mechanism. FEBS Lett 493:21–25

Brownlee M (1995) Advanced protein glycosylation in diabetes and aging. Annu Rev Med 46:223–234

Burns EM, Kruckeberg TW, Comerford LE, Buschmann MT (1979) Thinning of capillary walls and declining numbers of endothelial mitochondria in the cerebral cortex of the aging primate, *Macaca nemestrina*. J Gerontol 34:642–650

Burns EM, Kruckeberg TW, Gaetano PK (1981) Changes with age in cerebral capillary morphology. Neurobiol Aging 2:283–291

Cadenas E, Davies KJ (2000) Mitochondrial free radical generation, oxidative stress, and aging. Free Radic Biol Med 29:222–230

Camici GG, Savarese G, Akhmedov A, Lüscher TF (2015) Molecular mechanism of endothelial and vascular aging: implications for cardiovascular disease. Eur Heart J 36:3392–3403

Cencioni C, Spallotta F, Mai A, Martelli F, Farsetti A, Zeiher AM, Gaetano C (2015) Sirtuin function in aging heart and vessels. J Mol Cell Cardiol 83:55–61

Chalmers S, Saunter CD, Girkin JM, McCarron JG (2016) Age decreases mitochondrial motility and increases mitochondrial size in vascular smooth muscle. J Physiol 594:4283–4295

Chandel NS (2014) Mitochondria as signaling organelles. BMC Biol 12:34

Chang E, Harley CBJ (1995) Telomere length and replicative aging in human vascular tissues. Proc Natl Acad Sci U S A 92:11190–11194

Chen L, Daum G, Fischer JW, Hawkins S, Bochaton-Piallat ML, Gabbiani G, Clowes AW (2000) Loss of expression of the beta subunit of soluble guanylyl cyclase prevents nitric oxide-mediated inhibition of DNA synthesis in smooth muscle cells of old rats. Cir Res 86:520–525

Chen HZ, Wan YZ, Liu DP (2013) Cross-talk between SIRT1 and $p66^{Shc}$ in vascular diseases. Trends Cardiovasc Med 23:237–241

Costantino S, Paneni F, Cosentino F (2016) Ageing, metabolism and cardiovascular disease. J Physiol 594:2061–2073

da Cunha FM, Torelli NQ, Kowaltowski AJ (2015) Mitochondrial retrograde signaling: triggers, pathways, and outcomes. Oxidative Med Cell Longev 2015:482582

Dalgård C, Benetos A, Verhulst S, Labat C, Kark JD, Christensen K, Kimura M, Kyvik KO, Aviv A (2015) Leukocyte telomere length dynamics in women and men: menopause vs age effects. Int J Epidemiol 44:1688–1695

Davenport AP, Hyndman KA, Dhaun N, Southan C, Kohan DE, Pollock JS, Pollock DM, Webb DJ, Maguire JJ (2016) Endothelin. Pharmacol Rev 68:357–418

Diot A, Morten K, Poulton J (2016) Mitophagy plays a central role in mitochondrial ageing. Mamm Genome 27:381–395

Donato AJ, Lesniewski LA, Delp MD (2005) The effects of aging and exercise training on endothelin-1 vasoconstrictor responses in rat skeletal muscle arterioles. Cardiovasc Res 66:393–401

Donato AJ, Gano LB, Eskurza I, Silver AE, Gates PE, Jablonski K, Seals DR (2009) Vascular endothelial dysfunction with aging: endothelin-1 and endothelial nitric oxide synthase. Am J Physiol Heart Circ Physiol 297:H425–H432

Eigenbrodt ML, Bursac Z, Rose KM, Couper DJ, Tracy RE, Evans GW, Brancati FL, Mehta JL (2006) Common carotid arterial interadventitial distance (diameter) as an indicator of the damaging effects of age and atherosclerosis, a cross-sectional study of the Atherosclerosis Risk in Community Cohort Limited Access Data (ARICLAD), 1987–89. Cardiovasc Ultrasound 4:1

Engelen L, Ferreira I, Stehouwer CD, Boutouyrie P, Laurent S, Reference values for arterial measurements C (2013) Reference intervals for common carotid intima-media thickness measured with echotracking: relation with risk factors. Eur Heart J 34:2368–2380

Félétou M, Huang Y, Vanhoutte PM (2010) Vasoconstrictor prostanoids. Pflugers Arch 459:941–950

Fitzpatrick FA, Soberman R (2001) Regulated formation of eicosanoids. J Clin Invest 107:1347–1351

Francia P, delli Gatti C, Bachschmid M, Martin-Padura I, Savoia C, Migliaccio E, Pelicci PG, Schiavoni M, Lüscher TF, Volpe M, Cosentino F (2004) Deletion of p66shc gene protects against age-related endothelial dysfunction. Circulation 110:2889–2895

Fritze O, Romero B, Schleicher M, Jacob MP, Oh DY, Starcher B, Schenke-Layland K, Bujan J, Stock UA (2012) Age-related changes in the elastic tissue of the human aorta. J Vasc Res 49:77–86

Gano LB, Donato AJ, Pasha HM, Hearon CM Jr, Sindler AL, Seals DR (2014) The SIRT1 activator SRT1720 reverses vascular endothelial dysfunction, excessive superoxide production, and inflammation with aging in mice. Am J Physiol Heart Circ Physiol 307:H1754–H1763

Gao Y (2010) The multiple actions of NO. Pflügers Arch-Eur J Physiol 459:829–839

Gluais P, Lonchampt M, Morrow JD, Vanhoutte PM, Feletou M (2005) Acetylcholine-induced endothelium-dependent contractions in the SHR aorta: the Janus face of prostacyclin. Br J Pharmacol 146:834–845

Gong Z, Tas E, Muzumdar R (2014) Humanin and age-related diseases: a new link? Front Endocrinol (Lausanne) 5:210

Greenwald SE (2007) Ageing of the conduit arteries. J Pathol 211:157–172

Hill S, Van Remmen H (2014) Mitochondrial stress signaling in longevity: a new role for mitochondrial function in aging. Redox Biol 2:936–944

Homma S, Hirose N, Ishida H, Ishii T, Araki G (2001) Carotid plaque and intima-media thickness assessed by B-mode ultrasonography in subjects ranging from young adults to centenarians. Stroke 32:830–835

Jendrach M, Pohl S, Voth M, Kowald A, Hammerstein P, Bereiter-Hahn J (2005) Morphodynamic changes of mitochondria during ageing of human endothelial cells. Mech Ageing Dev 126:813–821

Johnson SC, Rabinovitch PS, Kaeberlein M (2013) mTOR is a key modulator of ageing and age-related disease. Nature 493:338–345

Kida Y, Goligorsky MS (2016) Sirtuins, cell senescence, and vascular aging. Can J Cardiol 32:634–641

Klöss S, Bouloumié A, Mülsch A (2000) Aging and chronic hypertension decrease expression of rat aortic soluble guanylyl cyclase. Hypertension 35:43–47

Kong BW, Man RY, Gao Y, Vanhoutte PM, Leung SW (2015) Reduced activity of SKC a and Na-K ATPase underlies the accelerated impairment of EDH-type relaxations in mesenteric arteries of aging spontaneously hypertensive rats. Pharmacol Res Perspect 3:e00150

Konova E, Baydanoff S, Atanasova M, Velkova A (2004) Age-related changes in the glycation of human aortic elastin. Exp Gerontol 39:249–254

Kovacic JC, Moreno P, Hachinski V, Nabel EG, Fuster V (2011a) Cellular senescence, vascular disease, and aging: Part 1 of a 2-part review. Circulation 123:1650–1660

Kovacic JC, Moreno P, Nabel EG, Hachinski V, Fuster V (2011b) Cellular senescence, vascular disease, and aging: part 2 of a 2-part review: clinical vascular disease in the elderly. Circulation 123:1900–1910

Kurz DJ, Hong Y, Trivier E, Huang HL, Decary S, Zang GH, Lüscher TF, Erusalimsky JD (2003) Fibroblast growth factor-2, but not vascular endothelial growth factor, upregulates telomerase activity in human endothelial cells. Arterioscler Thromb Vasc Biol 23:748–754

LaRocca TJ, Hearon CM Jr, Henson GD, Seals DR (2014) Mitochondrial quality control and age-associated arterial stiffening. Exp Gerontol 58:78–82

Lee C, Wan J, Miyazaki B, Fang Y, Guevara-Aguirre J, Yen K, Longo V, Bartke A, Cohen P (2014) IGF-I regulates the age-dependent signaling peptide humanin. Aging Cell 13:958–961

Leung SW, Vanhoutte PM (2017) Endothelium-dependent hyperpolarization: age, gender and blood pressure, do they matter? Acta Physiol (Oxf) 219:108–123

Lim MA, Townsend RR (2009) Arterial compliance in the elderly: its effect on blood pressure measurement and cardiovascular outcomes. Clin Geriatr Med 25:191–205

López-Otín C, Blasco MA, Partridge L, Serrano M, Kroemer G (2013) The hallmarks of aging. Cell 153:1194–1217

López-Otín C, Galluzzi L, Freije JM, Madeo F, Kroemer G (2016) Metabolic control of longevity. Cell 166:802–821

Masi S, Nightingale CM, Day IN, Guthrie P, Rumley A, Lowe GD, von Zglinicki T, D'Aiuto F, Taddei S, Klein N, Salpea K, Cook DG, Humphries SE, Whincup PH, Deanfield JE (2012)

Inflammation and not cardiovascular risk factors is associated with short leukocyte telomere length in 13- to 16-year-old adolescents. Arterioscler Thromb Vasc Biol 32:2029–2034
Matthews C, Gorenne I, Scott S, Figg N, Kirkpatrick P, Ritchie A, Goddard M, Bennett M (2006) Vascular smooth muscle cells undergo telomere-based senescence in human atherosclerosis: effects of telomerase and oxidative stress. Circ Res 99:156–164
Migliaccio E, Giorgio M, Mele S, Pelicci G, Reboldi P, Pandolfi PP, Lanfrancone L, Pelicci PG (1999) The p66shc adaptor protein controls oxidative stress response and life span in mammals. Nature 402:309–313
Mikhed Y, Daiber A, Steven S (2015) Mitochondrial oxidative stress, mitochondrial DNA damage and their role in age-related vascular dysfunction. Int J Mol Sci 16:15918–15953
Minamino T, Kourembanas S (2001) Mechanisms of telomerase induction during vascular smooth muscle cell proliferation. Circ Res 89:237–243
Ming XF, Montani JP, Yang Z (2012) Perspectives of targeting mTORC1-S6K1 in cardiovascular aging. Front Physiol 3:5
Muzumdar RH, Huffman DM, Atzmon G, Buettner C, Cobb LJ, Fishman S, Budagov T, Cui L, Einstein FH, Poduval A, Hwang D, Barzilai N, Cohen P (2009) Humanin: a novel central regulator of peripheral insulin action. PLoS One 4:e6334
Nandish S, Oliveros R, Chilton R (2011) Keeping your arteries young: vascular health. J Clin Hypertens (Greenwich) 13:706–707
Oh YK, Bachar AR, Zacharias DG, Kim SG, Wan J, Cobb LJ, Lerman LO, Cohen P, Lerman A (2011) Humanin preserves endothelial function and prevents atherosclerotic plaque progression in hypercholesterolemic apoe deficient mice. Atherosclerosis 219:65–73
Oksche A, Boese G, Horstmeyer A, Furkert J, Beyermann M, Bienert M, Rosenthal W (2000) Late endosomal/lysosomal targeting and lack of recycling of the ligand-occupied endothelin B receptor. Mol Pharmacol 57:1104–1113
Okuda K, Bardeguez A, Gardner JP, Rodriguez P, Ganesh V, Kimura M, Skurnick J, Awad G, Aviv A (2002) Telomere length in the newborn. Pediatr Res 52:377–381
Phan TS, Li JK, Segers P, Reddy-Koppula M, Akers SR, Kuna ST, Gislason T, Pack AI, Chirinos JA (2016) Aging is associated with an earlier arrival of reflected waves without a distal shift in reflection sites. J Am Heart Assoc 5:pii:e003733
Potente M (2010) An energy-sensor network takes center stage during endothelial aging. Circ Res 106:1316–1318
Rapoport RM, Williams SP (1996) Role of prostaglandins in acetylcholine-induced contraction of aorta from spontaneously hypertensive and Wistar-Kyoto rats. Hypertension 28:64–75
Runkel ED, Baumeister R, Schulze E (2014) Mitochondrial stress: balancing friend and foe. Exp Gerontol 56:194–201
Sandgren T, Sonesson B, Ahlgren AR, Lanne T (1998) Factors predicting the diameter of the popliteal artery in healthy humans. J Vasc Surg 28:284–289
Sandgren T, Sonesson B, Ahlgren R, Lanne T (1999) The diameter of the common femoral artery in healthy human: influence of sex, age, and body size. J Vasc Surg 29:503–510
Smith RA, Hartley RC, Cochemé HM, Murphy MP (2012) Mitochondrial pharmacology. Trends Pharmacol Sci 33:341–352
Suliman HB, Piantadosi CA (2016) Mitochondrial quality control as a therapeutic target. Pharmacol Rev 68:20–48
Tan P, Wang YJ, Li S, Wang Y, He JY, Chen YY, Deng HQ, Huang W, Zhan JK, Liu YS (2016) The PI3K/Akt/mTOR pathway regulates the replicative senescence of human VSMCs. Mol Cell Biochem 422:1–10
Tang EH, Vanhoutte PM (2008) Gene expression changes of prostanoid synthases in endothelial cells and prostanoid receptors in vascular smooth muscle cells caused by aging and hypertension. Physiol Genomics 32:409–418
Thijssen DH, Rongen GA, van Dijk A, Smits P, Hopman MT (2007) Enhanced endothelin-1-mediated leg vascular tone in healthy older subjects. J Appl Physiol (1985) 103:852–857

Thijssen DH, Carter SE, Green DJ (2015) Arterial structure and function in vascular ageing: are you as old as your arteries? J Physiol 594:2275–2284

Townsend RR, Wilkinson IB, Schiffrin EL, Avolio AP, Chirinos JA, Cockcroft JR, Heffernan KS, Lakatta EG, McEniery CM, Mitchell GF, Najjar SS, Nichols WW, Urbina EM, Weber T (2015) Recommendations for improving and standardizing vascular research on arterial stiffness: a scientific statement from the American Heart Association. Hypertension 66:698–722

Ungvari Z, Orosz Z, Labinskyy N, Rivera A, Xiangmin Z, Smith K, Csiszar A (2007) Increased mitochondrial H_2O_2 production promotes endothelial NF-kappaB activation in aged rat arteries. Am J Physiol Heart Circ Physiol 293:H37–H47

Ungvari ZI, Labinskyy N, Gupte SA, Chander PN, Edwards JG, Csiszar A (2008) Dysregulation of mitochondrial biogenesis in vascular endothelial and smooth muscle cells of aged rats. Am J Physiol Heart Circ Physiol 294:H2121–H2128

Ungvari Z, Sonntag WE, Csiszar A (2010) Mitochondria and aging in the vascular system. J Mol Med (Berl) 88:1021–1027

Uryga AK, Bennett MR (2016) Ageing induced vascular smooth muscle cell senescence in atherosclerosis. J Physiol 594:2115–2124

van den Munckhof I, Scholten R, Cable NT, Hopman MT, Green DJ, Thijssen DH (2012) Impact of age and sex on carotid and peripheral arterial wall thickness in humans. Acta Physiol (Oxf) 206:220–228

Vanhoutte PM, Zhao Y, Xu A, Leung SW (2016) Thirty years of saying no: sources, fate, actions, and misfortunes of the endothelium-derived vasodilator mediator. Circ Res 119:375–396

Vanhoutte PM, Shimokawa H, Feletou M, Tang EH (2017) Endothelial dysfunction and vascular disease - a 30th anniversary update. Acta Physiol (Oxf) 219:22–96

Vasa M, Breitschopf K, Zeiher AM, Dimmeler S (2000) Nitric oxide activates telomerase and delays endothelial cell senescence. Circ Res 87:540–542

Verzijl N, DeGroot J, Thorpe SR, Bank RA, Shaw JN, Lyons TJ, Bijlsma JW, Lafeber FP, Baynes JW, TeKoppele JM (2000) Effect of collagen turnover on the accumulation of advanced glycation end products. J Biol Chem 275:39027–39031

Virmani R, Avolio AP, Mergner WJ, Robinowitz M, Herderick EE, Cornhill JF, Guo SY, Liu TH, Ou DY, O'Rourke M (1991) Effect of aging on aortic morphology in populations with high and low prevalence of hypertension and atherosclerosis: comparison between occidental and Chinese communities. Am J Pathol 139:1119–1129

Wang XM, Xiao H, Liu LL, Cheng D, Li XJ, Si LY (2016) FGF21 represses cerebrovascular aging via improving mitochondrial biogenesis and inhibiting p53 signaling pathway in an AMPK-dependent manner. Exp Cell Res 346:147–156

Wenzel P, Schuhmacher S, Kienhöfer J, Müller J, Hortmann M, Oelze M, Schulz E, Treiber N, Kawamoto T, Scharffetter-Kochanek K, Münzel T, Bürkle A, Bachschmid MM, Daiber A (2008) Manganese superoxide dismutase and aldehyde dehydrogenase deficiency increase mitochondrial oxidative stress and aggravate age-dependent vascular dysfunction. Cardiovasc Res 80:280–289

Werner C, Furster T, Widmann T, Poss J, Roggia C, Hanhoun M, Scharhag J, Buchner N, Meyer T, Kindermann W, Haendeler J, Bohm M, Laufs U (2009) Physical exercise prevents cellular senescence in circulating leukocytes and in the vessel wall. Circulation 120:2438–2447

Whitaker RM, Corum D, Beeson CC, Schnellmann RG (2016) Mitochondrial biogenesis as a pharmacological target: a new approach to acute and chronic diseases. Annu Rev Pharmacol Toxicol 56:229–249

Willum-Hansen T, Staessen JA, Torp-Pedersen C, Rasmussen S, Thijs L, Ibsen H, Jeppesen J (2006) Prognostic value of aortic pulse wave velocity as index of arterial stiffness in the general population. Circulation 113:664–670

Wong SL, Leung FP, Lau CW, Au CL, Yung LM, Yao X, Chen ZY, Vanhoutte PM, Gollasch M, Huang Y (2009) Cyclooxygenase-2-derived prostaglandin F2alpha mediates endothelium-dependent contractions in the aortae of hamsters with increased impact during aging. Circ Res 104:228–235

Yang W, Hekimi S (2010) A mitochondrial superoxide signal triggers increased longevity in *Caenorhabditis elegans*. PLoS Biol 8:e1000556

Yang C, Pan S, Yan S, Li Z, Yang J, Wang Y, Xiong Y (2014) Inhibitory effect of 14,15-EET on endothelial senescence through activation of mTOR complex 2/Akt signaling pathways. Int J Biochem Cell Biol 50:93–100

Yeh JK, Wang CY (2016) Telomeres and telomerase in cardiovascular diseases. Genes (Basel) 7: E58

Zu Y, Liu L, Lee MY, Xu C, Liang Y, Man RY, Vanhoutte PM, Wang Y (2010) SIRT1 promotes proliferation and prevents senescence through targeting LKB1 in primary porcine aortic endothelial cells. Circ Res 106:1384–1393